Environmental Chemistry for a Sustainable World

Mu. Naushad
Saravanan Rajendran
Francisco Gracia *Editors*

Advanced Nanostructured Materials for Environmental Remediation

Springer

Environmental Chemistry for a Sustainable World

Volume 25

Other Publications by the Editors

Books
Environmental Chemistry
http://www.springer.com/978-3-540-22860-8

Organic Contaminants in Riverine and Groundwater Systems
http://www.springer.com/978-3-540-31169-0

Sustainable Agriculture
Volume 1: http://www.springer.com/978-90-481-2665-1
Volume 2: http://www.springer.com/978-94-007-0393-3

Book series
Environmental Chemistry for a Sustainable World
http://www.springer.com/series/11480

Sustainable Agriculture Reviews
http://www.springer.com/series/8380

Journals
Environmental Chemistry Letters
http://www.springer.com/10311

Agronomy for Sustainable Development
http://www.springer.com/13593

More information about this series at http://www.springer.com/series/11480

Mu. Naushad • Saravanan Rajendran
Francisco Gracia
Editors

Advanced Nanostructured Materials for Environmental Remediation

Springer

Editors
Mu. Naushad
Department of Chemistry, College of Science
King Saud University
Riyadh, Saudi Arabia

Saravanan Rajendran
Faculty of Engineering, Department of Mechanical Engineering
University of Tarapacá
Arica, Chile

Francisco Gracia
Department of Chemical Engineering, Biotechnology and Materials
Universidad de Chile
Santiago, Chile

ISSN 2213-7114 ISSN 2213-7122 (electronic)
Environmental Chemistry for a Sustainable World
ISBN 978-3-030-04476-3 ISBN 978-3-030-04477-0 (eBook)
https://doi.org/10.1007/978-3-030-04477-0

Library of Congress Control Number: 2019930038

This Springer imprint is published by the registered company Springer Nature Switzerland AG.
The registered company address is: Gewerbestrasse 11, 6330 Cham, Switzerland

Preface

Albert Einstein said, “The environment is everything that isn’t me”. The environment is everything that surrounds us which can be living or nonliving things. But nowadays, environmental pollution is one of the major problems that affects biodiversity, ecosystems, and human health worldwide by contaminating air, soil, and water. Public concern about environmental pollution has increased extensively since the beginning of the twentieth century with growing awareness of the stresses being placed on the environment due to activities arising from both industrial activity and intensive agriculture, and as a consequence of high-profile incidents that have highlighted the risks of pollution for human health. The limitation in the conventional method of materials used in water remediation for organic, inorganic, and microbial contaminants and efficacy of these materials makes the research community to shift toward nanotechnology aid for environmental needs. Richard Feynman said, “For a successful technology, reality must take precedence over public relations, for Nature cannot be fooled.” Nanomaterials represent a promising new technology for rapid environmental clean-up and pollution control. Environmental nanotechnology would offer an innovative mechanism to remediate and treat the contaminants to the acceptable level. This book provides a wide-range exploration on the ongoing research and development events in environmental nanotechnology. We anticipate that this book will make noteworthy appeal to scientist and researchers working in the field of nanotechnology for environmental sciences.

Riyadh, Saudi Arabia — Mu. Naushad
Arica, Chile — Saravanan Rajendran
Santiago, Chile — Francisco Gracia

Acknowledgments

First and foremost, we thank God Almighty for the blessings He has bestowed upon us and for giving us the strength to complete this task.

Our deep sense of gratitude and heartfelt thanks go to the series editor, Eric Lichtfouse, for his encouragement, mentoring, and useful discussions during the preparation of this book. We sincerely express our gratitude to the publisher, Springer, for accepting this book as part of the series Environmental Chemistry for a Sustainable World. We also extend our thanks to contributing authors and reviewers for their valuable involvement throughout this book. We express our heartfelt gratitude to researchers and publisher for permitting us the copyright to use their figures and tables. Even though every effort has been made to obtain the copyright permissions from the respective owners to include citations with the reproduced materials, we would still like to offer our deep apologies to any copyright holder if unknowingly their right is being infringed.

Mu. Naushad would like to express his sincere thanks to the chairman, Department of Chemistry, College of Science, King Saud University, Saudi Arabia, for his valuable suggestions and constant inspiration. He also extends his heartfelt gratitude to the Deanship of Scientific Research at King Saud University for the financial support.

Saravanan Rajendran is thankful for the financial support from the SERC (CONICYT/FONDAP/15110019), FONDECYT, Government of Chile (Project No.: 11170414), and Faculty of Engineering, Department of Mechanical Engineering, University of Tarapacá, Arica, Chile. He also extends deep gratitude to Prof. Lorena Cornejo Ponce (EUDIM, Universidad de Tarapacá) and Prof. Rodrigo Palma (director, SERC) for their constant support and encouragement which helped him to complete the task.

Francisco Gracia gratefully acknowledges financial support from the Conicyt-Fondecyt (Project 1171193) and MINECON-Chile through project Millennium Nucleus MULTIMAT – ICM/MINECON.

Contents

Contributors

Jesudas Balasubramanian Department of Pharmacology and Environmental Toxicology, Dr. ALM PGIBMS, University of Madras, Chennai, India

Abdulhakeem Bello Department of Materials Science and Engineering, African University of Science and Technology (AUST), Abuja, Nigeria

Marcela P. Bernardo Department of Chemistry, Federal University of São Carlos, São Carlos, SP, Brazil

National Nanotechnology Laboratory for Agribusiness, Embrapa Instrumentação, São Carlos, SP, Brazil

Arulvasu Chinnasamy Department of Zoology, University of Madras, Chennai, India

Moo Hwan Cho Department of Chemical Engineering and Technology, BCC, Jazan University, Jazan, Saudi Arabia

Raghunath Das Department of Applied Chemistry, University of Johannesburg, Johannesburg, South Africa

Selvaraj Devi Department of Inorganic Chemistry, University of Madras, Guindy, Chennai, India

D. Duraibabu The Key Laboratory of Low-Carbon Chemistry & Energy Conservation of Guangdong Province/State Key Laboratory of Optoelectronic Materials and Technologies, School of Materials Science and Engineering, Sun Yat-Sen University, Guangzhou, People's Republic of China

D. Durgalakshmi Department of Medical Physics, Anna University, Chennai, India

Mohamed I. Fadlalla Department of Chemical Engineering, Institute for Catalysis Research and c*change (DST-NRF Centre of Excellence in Catalysis), University of Cape Town, Cape Town, South Africa

Babu Gajendran Department of Biology and Chemistry, The Key Laboratory of Chemistry for Natural Products of Guizhou Province and Chinese Academy of Sciences, Guizhou, China

State Key Laboratory of Functions and Applications of Medicinal Plants, Guizhou Medical University, Guiyang, China

S. Ganesh Babu Department of Chemical Engineering, Institute for Catalysis Research and c*change (DST-NRF Centre of Excellence in Catalysis), University of Cape Town, Cape Town, South Africa

Mounika Gudeppu Department of Pharmacology and Environmental Toxicology, Dr. ALM PGIBMS, University of Madras, Chennai, India

Mpitloane J. Hato Department of Chemistry, School of Physical and Mineral Sciences, University of Limpopo (Turfloop), Polokwane, South Africa

Department of Environmental Sciences, College of Agriculture and Environmental Sciences, University of South Africa (UNISA), Pretoria, South Africa

Kamdem Paumo Hugues Department of Applied Chemistry, University of Johannesburg, Johannesburg, South Africa

Sankar Jagadeeshan Cell Biology Division, Memorial Sloan Kettering Cancer Center, New York, NY, USA

Ealisha Jha Department of Physics and Physical Oceanography, Memorial University of Newfoundland, St. John's, NL, Canada

Mohammad Ehtisham Khan Department of Chemical Engineering and Technology, BCC, Jazan University, Jazan, Saudi Arabia

Vignesh Kumaravel Department of Environmental Science, School of Science, Institute of Technology Sligo, Sligo, Republic of Ireland

Yanmei Li Department of Biology and Chemistry, The Key Laboratory of Chemistry for Natural Products of Guizhou Province and Chinese Academy of Sciences, Guizhou, China

State Key Laboratory of Functions and Applications of Medicinal Plants, Guizhou Medical University, Guiyang, China

Arjun Maity Department of Applied Chemistry, University of Johannesburg, Johannesburg, South Africa

DST/CSIR National Center for Nanostructured Materials, Council for Scientific and Industrial Research (CSIR), Pretoria, South Africa

Katlego Makgopa Department of Chemistry, Faculty of Science, Tshwane University of Technology (Acardia Campus), Pretoria, South Africa

R. Manjumeena Center for Advanced Studies in Botany, University of Madras, Chennai, India

Devaraj Manoj Department of Physical Chemistry, University of Madras, Chennai, India

Present Address: Key laboratory of Material Chemistry for Energy Conversion and Storage, Ministry of Education, School of Chemistry and Chemical Engineering, Huazhong University of Science and Technology, Wuhan, China

Thabiso C. Maponya Department of Chemistry, School of Physical and Mineral Sciences, University of Limpopo (Turfloop), Polokwane, South Africa

DST/CSIR Innovation Centre, National Centre for Nanostructured Materials, CSIR Material Science and Manufacturing, Pretoria, South Africa

Luiz H. C. Mattoso National Nanotechnology Laboratory for Agribusiness, Embrapa Instrumentação, São Carlos, SP, Brazil

Kwena D. Modibane Department of Chemistry, School of Physical and Mineral Sciences, University of Limpopo (Turfloop), Polokwane, South Africa

Gobeng R. Monama Department of Chemistry, School of Physical and Mineral Sciences, University of Limpopo (Turfloop), Polokwane, South Africa

Francys K. V. Moreira Department of Materials Engineering – DEMa, Federal University of São Carlos – UFSCar, São Carlos, SP, Brazil

National Nanotechnology Laboratory for Agribusiness, Embrapa Instrumentação, São Carlos, SP, Brazil

Mu. Naushad Department of Chemistry, College of Science, King Saud University, Riyadh, Saudi Arabia

Pritam Kumar Panda Division of Pediatrics, Hematology and Oncology, University of Freiburg, Freiburg, Germany

Rajesh Parsanathan Department of Endocrinology, Dr. ALM PG IBMS, University of Madras, Chennai, Tamilnadu, India

Present Address: Department of Pediatrics, Louisiana State University Health Science Centre, Shreveport, LA, USA

Sebastian Raja National Nanotechnology Laboratory for Agribusiness, Embrapa Instrumentação, São Carlos, SP, Brazil

Saravanan Rajendran Faculty of Engineering, Department of Mechanical Engineering, University of Tarapacá, Arica, Chile

Kabelo E. Ramohlola Department of Chemistry, School of Physical and Mineral Sciences, University of Limpopo (Turfloop), Polokwane, South Africa

J. Santhanalakshmi Department of Physical Chemistry, University of Madras, Chennai, India

V. Selvam Department of Chemistry, The M.D.T. Hindu College, Tirunelveli, Tamilnadu, India

P. Senthil Kumar Department of Chemistry, School of Advanced Sciences, VIT University, Vellore, Tamilnadu, India

Sivaraman Somasundaram Department of Chemistry, Kongju National University, Gongju, Republic of Korea

Mrutyunjay Suar School of Biotechnology, KIIT University, Bhubaneswar, India

Sumathi Thangarajan Department of Medical Biochemistry, Dr. ALM PGIBMS, University of Madras, Chennai, India

Vairaperumal Tharmaraj Department of Analytical Chemistry, National Chung-Hsing University, Taichung, Taiwan

Arun Thirumurugan Advanced Materials Laboratory, Department of Mechanical Engineering, University of Chile, Santiago, Chile

Krishnapriya Madhu Varier Department of Medical Biochemistry, Dr. ALM PGIBMS, University of Madras, Chennai, India

Department of Zoology, University of Madras, Chennai, India

Suresh K. Verma School of Biotechnology, KIIT University, Bhubaneswar, India

About the Editors

Mu. Naushad is presently working as an associate professor in the Department of Chemistry, College of Science, King Saud University (KSU), Riyadh, Kingdom of Saudi Arabia. He obtained his MSc and PhD degrees in analytical chemistry from Aligarh Muslim University, Aligarh, India, in 2002 and 2007, respectively. He has a vast research experience in the multidisciplinary fields of analytical chemistry, materials chemistry, and environmental science. He holds several US patents, over 250 publications in the international journals of repute, 20 book chapters, and several books published by renowned international publishers. He has >6000 citations with a Google Scholar H-Index of >47. He has successfully run several research projects funded by National Plan for Science, Technology, and Innovation (NPST) and King Abdulaziz City for Science and Technology (KACST), Kingdom of Saudi Arabia. He is the editor/editorial member of several reputed journals like *Scientific Report* (Nature), *Process Safety and Environmental Protection* (Elsevier), *Journal of Water Process Engineering* (Elsevier), and *International Journal of Environmental Research and Public Health* (MDPI). He is also the associate editor for *Environmental Chemistry Letters* (Springer) and *Desalination and Water Treatment* (Taylor & Francis). He has been awarded the Scientist of the Year Award 2015 from National Environmental Science Academy, Delhi, India, and Almarai Award 2017, Saudi Arabia.

Saravanan Rajendran has received his PhD in physics-material science in 2013 from the Department of Nuclear Physics, University of Madras, Chennai, India. He was awarded the University Research Fellowship (URF) during 2009–2011 by the University of Madras. After working as an assistant professor in Dhanalakshmi College of Engineering, Chennai, India, during 2013–2014, he was awarded SERC and CONICYT-FONDECYT postdoctoral fellowship (2014–2017) by the University of Chile, Santiago. He has worked (2017–2018) in the research group of Professor John Irvine, School of Chemistry, University of St Andrews, United Kingdom, as a postdoctoral research fellow within the framework of a EPSRC-Global Challenges Research Fund for the removal of blue-green algae and their

toxins. Currently, he is working as a research associate in the Faculty of Engineering, Department of Mechanical Engineering, University of Tarapacá, Arica, Chile. He has published several international peer-reviewed journals and book chapters. His work interest includes nanoporous- and nanomaterial-based catalysts for renewable energy and wastewater purification.

Francisco Gracia received a PhD in chemical engineering from the University of Notre Dame, USA. He is currently associate professor at ChEBM Department, Universidad de Chile, and deputy director at the Multifunctional Materials Millennium Nucleus (MultiMat). His research interests are in the area of heterogeneous catalysis, nanostructured functional materials, gas-solid interphase reactivity with emphasis on CO_2 activation and utilization, H_2 generation, photocatalysis, and energy-related applications. He is a co-author of 50+ research publications and a book chapter and edited a book in subjects related to nanotechnology and photo- and environmental catalysis.

Chapter 1
Current Role of Nanomaterials in Environmental Remediation

D. Durgalakshmi, Saravanan Rajendran, and Mu. Naushad

Contents

Abstract Natural causes of pollution are unavoidable; however, man-made pollution is increasing and causing alarming health issues, declining availability of clean water, and a lesser supply of good food. The limitations of conventional methods and materials used in water remediation to eliminate organic, inorganic, and microbial contaminants have prompted the research community to pursue nanotechnological aids for environmental needs. Nanomaterials have great advantages over bulk materials because of their greater surface area, higher reactivity, and hence better performance. The size effect of nanomaterialas is more of realistic perspective; thus, future technologies will be more focused on product development of nanotechnology for low cost but could extend to high-end users. In this chapter, we discuss nanostructured materials in the carbon family and the importance of metal oxides and magnetic materials in environmental remediation. We also outline the present need for

D. Durgalakshmi (✉)
Department of Medical Physics, Anna University, Chennai, India

S. Rajendran
Faculty of Engineering, Department of Mechanical Engineering, University of Tarapacá, Arica, Chile

Mu. Naushad
Department of Chemistry, College of Science, King Saud University, Riyadh, Saudi Arabia

Mu. Naushad et al. (eds.), *Advanced Nanostructured Materials for Environmental Remediation*, Environmental Chemistry for a Sustainable World 25,
https://doi.org/10.1007/978-3-030-04477-0_1

nanomaterials in environmental applications and the nanomaterials currently being used for water remediation, antibacterial coatings, and biosensor applications.

Keywords Nanomaterials · Environment · Water treatment · Photocatalysis · Sensors · Antimicrobial

1.1 The Need for a Sustainable Environment

The Brundtland Commission (formerly known as the World Commission on the Environment and Development) united all countries to pursue sustainable development together. In the commission's report in 1987, it was stated that "sustainable development is a development, that needs of the present without compromising the ability of future generations to meet their own needs" (Wood 1993). In this millennium, there is growing concern that life on earth is imperiled by the destruction of nature, wrought by human intervention. The hole in the ozone layer, the prospect of global warming, loss of biodiversity, and the dangers of radioactive and hazardous wastes create a problem for current and future generations. The Earth Summit in Rio de Janeiro in 1992 issued a declaration on the environment and development, which articulated that "to achieve sustainable development, environmental protection shall constitute an integral part of the development process and cannot be considered in isolation from it" (United Nations 1992). At the 2012 Rio Earth Summit, four main issues were addressed: (1) systematic scrutiny of the production of toxic and radioactive chemicals, (2) need for development of renewable energy resources as a replacement for fossil fuels, (3) health problems caused by air pollution due to vehicle emissions, and (4) scarcity of noncontaminated water and growing need for drinking water (Tollefson and Gilbert 2012; Cardinale et al. 2012; Haines et al. 2012). Although the human population growth rate is decreasing, the world's population is expected to increase from the present 7.4 billion to 9.2 billion by 2040 (Roser and Ortiz-Ospina 2017). This will create immense pressure on the scarcity of energy, food, and medicine, with diminishing forests and natural resources.

The quality of surface water or groundwater depends on both natural influences and human influences. Organic chemicals and pathogens potentially can enter wherever surface water makes its way into groundwater. The presence of emerging pollutants in water bodies traditionally could be the result of point (mainly urban and industrial) pollution or diffuse (agricultural) pollution. Nonpoint-source pollution usually involves large areas and may cause a larger impact on groundwater quality than point-source pollution. The World Health Organization (WHO) directs global efforts to prevent transmission of waterborne disease and also advises governments on the development of health-based targets and regulations (WHO 2018). Contaminated water and poor sanitation are linked to transmission of diseases such as cholera, diarrhea, dysentery, hepatitis A, typhoid, and polio. The WHO has reported that by 2025, half of the world's population will be living in water-stressed areas. In low- and middle-income countries, 38% of health care facilities lack improved water sources, 19% do not have improved sanitation, and 35% lack water and soap for hand washing.

Drinking water may reasonably be expected to contain at least small amounts of some contaminants (see Table 1.1). Although some contaminants may be harmful if consumed at certain levels in drinking water, the presence of contaminants does not necessarily indicate that the water poses a health risk (EPA 2016). Drinking water contaminants are generally categorized as physical, chemical, radiological, or biological (World Health Organization 2004; Faust and Aly 2018), and these categories are used in the definition of contaminants given in the US Safe Drinking Water Act (SDWA) (EPA 2016). Physical contaminantions are mostly the first indicator, indicating that water has become contaminated. Sediment and organic material suspended in the water of lakes, rivers, and streams, from soil erosion, are examples of physical contaminants. Chemical contaminants include elements or compounds that may occur naturally or may be man made. Examples of chemical contaminants include nitrogen, bleach, salts, pesticides, metals, toxins produced by bacteria, and human or animal drugs. Chemical contaminants can be categorized as organic or inorganic. Organic contaminants in the environment are more prevalent than inorganic contaminants. The main organic water contaminants are listed in Table 1.2 (Lamastra et al. 2016). Organic contaminants can be further subdivided into halogenated, nonhalogenated, and pharmaceutical contaminants (Pan and Zhang 2013; Jobst et al. 2013; Li et al. 2014; Adeleye et al. 2016). The compounds that compose the inorganic fraction of groundwater are heavily influenced by interactions between source water and soils. As source water moves through a soil, a chemical reaction takes place in the soil: water interface will change the composition of both phases. Inorganic chemicals that occur naturally in soils, sediments, rocks, and dissolved mineral matter can also degrade the quality of groundwater. This classification of inorganic pollutants includes metal cations and some anions. Among the metal cations that have been found to pollute water and soils are Pb, Cr, Cu, Zn, Co, Mn, Ni, Hg, and Cd, while radioactive isotopes of Pu, Cs, and Sr, among others, pose potential threats as pollutants. In some situations, some anionic species such as phosphates, arsenate, borate, and nitrates are also considered pollutants (Manahan 2017).

Microbiological organisms in water are generally referred to as biological contaminants. Examples include viruses, bacteria, protozoans, and parasites (Ashbolt 2015). Radiological contaminants are chemical elements with unstable atoms that can emit ionizing radiation. Because the presence of ionizing radiation is one of the standard features of the earth's surface, the adverse effects on health that may be ascribed to radioactive contaminants in drinking water have been assessed in relation to the average background radiation dose, from all sources, of 100 mrem per year (NRC 2016). Examples of radiological contaminants include cesium, plutonium, and uranium.

1.2 Nanomaterial Aids for Water Treatment

Many current problems involving water quality could be resolved or greatly ameliorated using nanosorbents, nanocatalysts, bioactive nanoparticles, and nanostructured catalytic membranes (Savage and Diallo 2005; Mohmood et al. 2013; Gehrke et al. 2015).

Table 1.1 Drinking water contaminants

Organic contaminants			Inorganic contaminants	Radio nuclei	Particulates and microbial
Halogenated	Nonhalogenated	Pharmaceutical			
1,1,2-Trichloroethane	Acetonitrile	Atenolol	Aluminum	Cesium-137	Viruses:
1,1,1-Trichloroethane	Atrazine	Bisphenol A	Antimony	Iodine-131	Adenoviruses
1,2-Dibromo-3-chloropropane	Bis/tris solutions, cyclohexane	Carbamazepine	Arsenic	Lead-210	Caliciviruses
1,2-Dibromoethane	Butylated hydroxytoluene	Chloramphenicol	Barium	Radium-226	Enteroviruses (including polioviruses, coxsackieviruses, and echoviruses)
2-Chlorophenol	Caffeine	Chlorhexadine	Beryllium	Radium-228	Hepatitis A virus
Alachlor	DAPI	Clofibric acid	Cadmium	Strontium-90	Bacteria:
Benzalkonium chloride	DEET	D-gluconic succinic acid	Chloride	Thorium-228	*Campylobacter jejuni*
Bromodichloromethane	DEP	Diazinon	Chromium	Tritium	*Helicobacter pylori*
Bromophenol blue	DMSO	Diclofenac	Copper		*Legionella pneumophila*
Carbon tetrachloride	DOCDD	Doxycycline	Cyanide		*Mycobacterium avium*
Chloroform		Gemfibrozil	Dissolved solids		*Salmonella enterica* (nontyphoid)
Crystal violet	EDTA	Ibuprofen	Fluoride		*Shigella sonnei*
DCB	Ethyl ether	Iopamidol	Hardness		Protozoans:
Endrin	Fluorescein	Ketoprofen	Iron		*Naegleria fowleri*
Eosin	Hematoxylin	Lincomycin	Lead		
Heptachlor	HEPES	Norfloxacin	Manganese		

Hexachlorobenzene	Hexanes	Ofloxacin	Mercury		
Hexachlorocyclohexane (lindane)	Hybridization buffer (sodium dodecyl sulfate/sodium phosphate dibasic buffer)	Oxytetracycline	Nickel		
Hexachlorocyclopentadiene	Isopropyl acetate	Paracetamol (acetaminophen)	Nitrates (as nitrogen)		
Methoxychlor	Methyl orange	Phenazone	Nitrite (combined nitrate/nitrite)		
Methylene blue	Naphthalene	Primidone	Selenium		
Methylene chloride	NBBS	Propyphenazone	Silver		
PBDEs	Oil Red O, petroleum ether (mineral spirits)	Salicylic acid	Sodium		
PCBs	Phenol 2-propanol ≥24%	Sulfametazine (sulfamethazine)	Sulfate		
Rhodamine B	Simazine	Sulfamethoxazole	Thallium		
Safranin	TAE	Tetrabromobisphenol A	Zinc		
TCB	TBE	Tetracycline			
TCE	TEMED	Triclosan			
Tetrachloroethylene	Tert-butanol				
Trichloroethylene	Tetrahydrofuran				
	Toluene				
	Tris base				
	Xylene cyanol				

DAPI 4′,6-diamidino-2-phenylindole, *DCB* dichlorobenzene, *DEET* *N*,*N*-diethyl-*m*-toluamide, *DEP* diethyl phthalate, *DMSO* dimethyl sulfoxide, *DOCDD* 1,6-dioxacyclododecane-7,12-dione, *EDTA* ethylenediaminetetraacetic acid, *HEPES* 4-(2-hydroxyethyl)-1-piperazineethanesulfonic acid, *NBBS* *N*-butyl benzenesulfonamide, *PBDE* polybrominated diphenyl ether, *PCB* polychlorinated biphenyl, *TAE* mixture of tris base, acetic acid, and EDTA, *TBE* tris-borate, *TCB* trichlorobenzene, *TCE* trichloroethylene, *TEMED* tetramethylethylenediamine

Table 1.2 Main organic contaminants in water (Lamastra et al. 2016)

Compound group	Compound class
Pharmaceuticals	Veterinary and human antibiotics, analgesics, anti-inflammatories, steroids and hormones, antidiabetic agents, antidepressants, stimulants, x-ray contrast agents, lipid regulators, blood viscosity–affecting agents
Personal care products	Fragrances, sunscreen agents, insect repellents, antiseptics, surfactants
Pesticides	Insecticides, fungicides, herbicides, nematocides, biocides
Food additives	Antioxidants, sweeteners
Manufacturing additives	Corrosion inhibitors, flame retardants, gas propellants, plasticizers, plastic additives, stain repellents, surfactants, antioxidants, solvents, paraffin

Advances in nanoscale science and engineering suggest that nanoparticles can enhance filtration among other materials, and innovations in the development of novel technologies to desalinate water are among the most exciting and promising advances. Nanotechnology-derived products can potentially reduce the concentrations of toxic compounds to sub–part per billion levels and assist in the attainment of water quality standards as prescribed by health advisories (Savage and Diallo 2005). This ability may be due to the particle size of the contaminants observed in water bodies, as shown in Fig. 1.1 (Stumm 1977). Innovations in the development of novel technologies to desalinate water are among the most exciting and promising advances due to the size effect, as nanoparticles can interact one to one with the targeted particulates. Figure 1.2 illustrates some distinctive environmental nanocomposites and their properties (Zhang et al. 2016). Use of specific nanoparticles, either embedded in membranes or on other structural media, can rapidly purify contaminants in unusable water. In addition to the obvious advantages for industrialized nations, the benefits for developing countries would also be enormous (Kharisov et al. 2016). Innovative use of nanoparticles for treatment of industrial wastewater is another potentially useful application.

1.2.1 Carbon-Based Nanostructures

With increasing interest in nanotechnology, many types of metallic and carbon-based nanomaterials have emerged. Graphene (G), graphene oxide (GO), single-walled carbon nanotubes (SWNTs), and multiwalled carbon nanotubes (MWNTs) have been investigated as potential advanced water purification agents (Smith and Rodrigues 2015; Perreault et al. 2015; Al-Othman et al. 2012). Properties such as a large surface area, ease of chemical or physical modification, tuning of properties for particular applications, and excellent capacity for microbial disinfection and removal of both organic and inorganic contaminants mean that carbon-based nanomaterials and their respective nanocomposites offer many possibilities for novel applications in water treatment (Fig. 1.3) (Smith and Rodrigues 2015). These

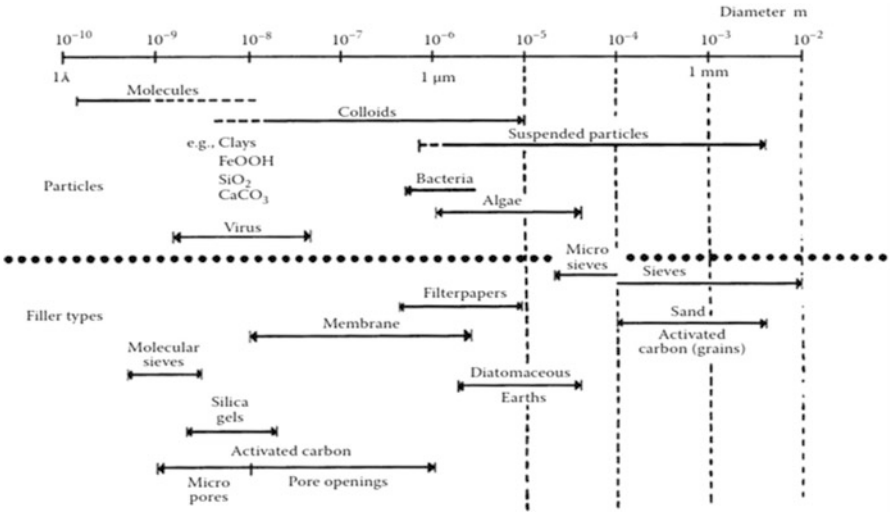

Fig. 1.1 Spectrum of particle sizes that may be observed in natural waters and in groundwater. The conventional physical process of separation of particles is also indicated. (Adapted from Stumm (1977) with permission. Copyright (1977) American Chemical Society)

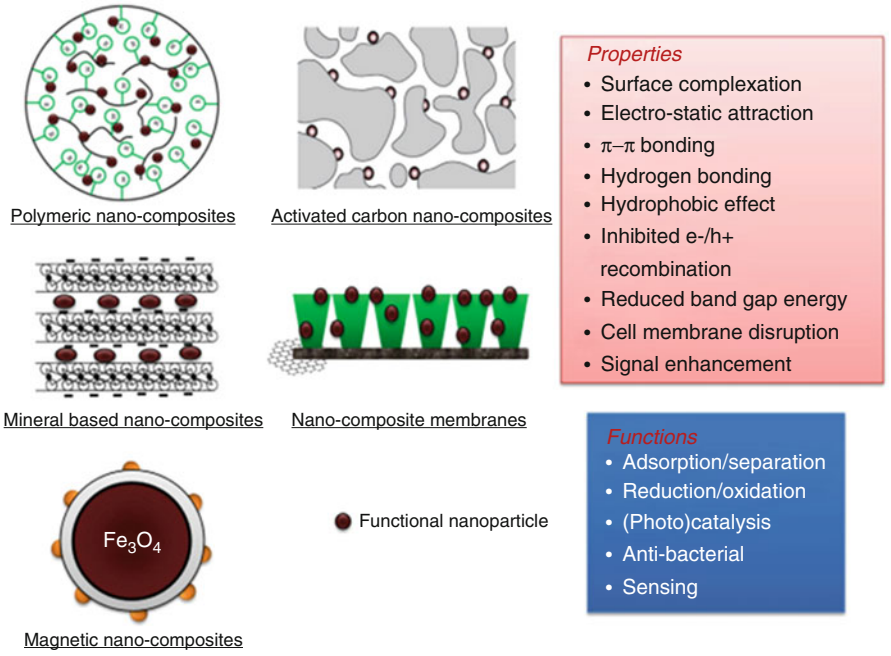

Fig. 1.2 Distinctive environmental nanocomposites and their properties (Zhang et al. 2016)

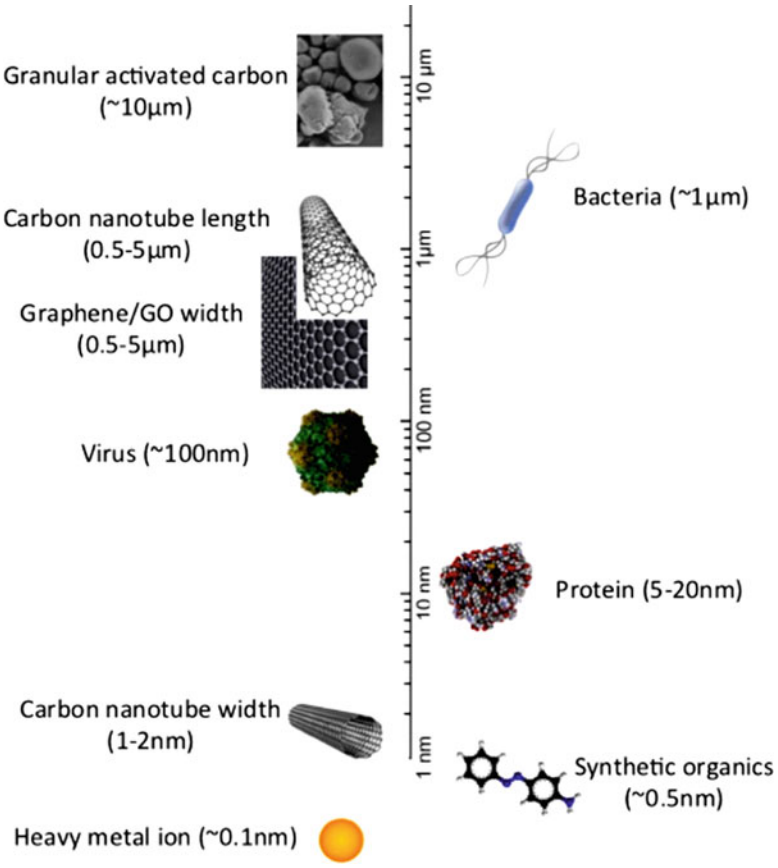

Fig. 1.3 Relative sizes of major classes of carbon nanomaterials and common water contaminants (Smith and Rodrigues 2015)

materials are seldom applied in their pure forms; however, graphene has been incorporated into a variety of composite materials because of its extremely large specific surface area and ease of broad functionalization, which offers abundant "anchoring" sites for various functional nanoparticles, including magnetic Fe_3O_4, photoreactive TiO_2, antimicrobial Ag and Au, and multifunctional nanocomposites such as graphene–TiO_2–magnetite and graphene–Au–magnetite (Jiang et al. 2016; Rakkesh et al. 2014, 2015). Carbon-based nanomaterials, such as graphene and carbon nanotubes (CNTs), can be found in functionalized or nonfunctionalized forms. For instance, graphene or CNTs can be functionalized with –OH and –COOH groups via chemical oxidation methods to produce graphene oxide and functionalized CNTs, which are highly dispersible in water in comparison with their pristine counterparts (Vardharajula et al. 2012).

The functionalization of carbon-based nanomaterials serves two major purposes (Hebbar et al. 2017). First, it improves the hydrophilicity of CNTs and graphene,

improving their dispersion in aqueous media. Better dispersion increases the available surface of each nanoparticle and thus its exposure to microbial and chemical contaminants. Second, depending on the surface charge properties of the target contaminant, nanomaterial surfaces can be modified to maximize electrostatic interactions between the sorbent and sorbate to improve sorption capacity. Electrostatic interaction has been found to be the main driving force behind adsorption of positively charged compounds (i.e., heavy metals) by negatively charged functionalized CNTs or graphene oxide. In addition, aggregated forms of carbon nanomaterials contain more mesopores than many conventional carbon-based adsorbents such as granular activated carbon (GAC), which has more microscale pores. Mesopores provide easier access to both large and small fractions of contaminant compounds on the adsorbent surface (Smith and Rodrigues 2015).

In conventional treatment plants, GAC filters are frequently used to remove heavy metals by adsorption. However, this method often fails to meet regulatory requirements because of its poor removal efficiency at low concentrations of heavy metals and its slow adsorption rates. Recent studies have shown that CNTs and graphene oxide, in particular, are capable of removing significant amounts of heavy metals from aqueous solutions. In most studies involving nanotubes, SWNTs have been able to successfully remove Pb^{2+}, Zn^{2+}, Cd^{2+}, and Cu^{2+} from aqueous solutions (Sadegh et al. 2016; Suárez-Iglesias et al. 2017). The results from studies investigating the affinity order of heavy metal ions for CNTs have been contradictory. Furthermore, these studies have demonstrated that the adsorption capacity of CNTs is highly dependent on the pH of the solution. A common point in all of these studies is that these nanomaterials exhibit significantly higher adsorption capacities than any other conventional adsorbents in similar experimental conditions. Another attractive feature of graphene is its intrinsic antimicrobial properties, which have led to applications in antimicrobial coatings and antifouling membranes. The postulated mechanisms of bacterial inactivation/cell membrane damage include physical disruption, oxidative stress, and extraction of phospholipids from cell membranes (Jiang et al. 2016).

1.2.2 Metal and Metal Oxide Nanomaterials

Nanosized metals and metal oxides have received ever-increasing attention because of their high performance and low cost for contaminant removal (Saravanan et al. 2011). Nanomaterials, especially inorganic nanomaterials (metals, metal oxides, metal sulfates, quantum dots, etc.) with fundamental properties have attracted considerable interest in the development of biomedicine, catalysis, fuel cells, sensors, and magnetic data storage (Wu et al. 2016). In comparison with the simple isotropic morphologies of inorganic NPs, novel anisotropic morphologies of inorganic NPs give rise to new features and unique physicochemical properties due to the number of step edges and kink sites on the surface and the high surface area to volume ratios in the nanoscale regime (see Figs. 1.4 and 1.5) (Tran and Lu 2011;

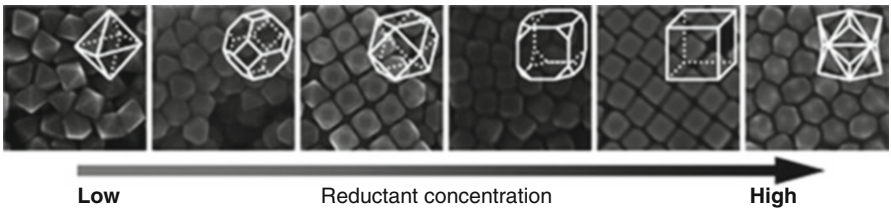

Fig. 1.4 Scanning electron microscopy images of monodispersed polyhedral Au nanoparticles. (Adapted from Eguchi et al. (2012), with permission. Copyright (2012) American Chemical Society)

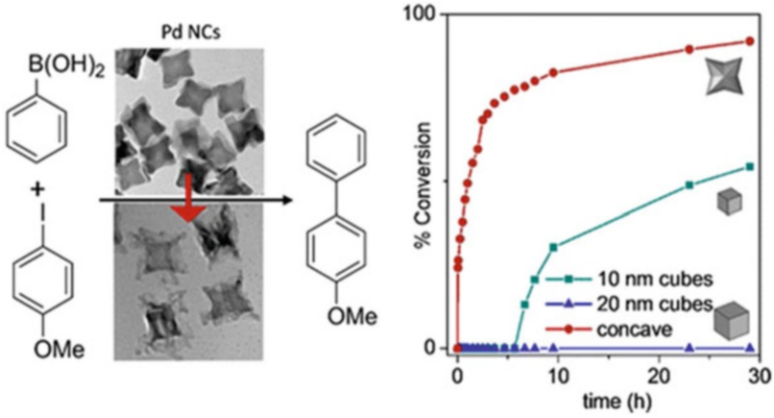

Fig. 1.5 Structure–property relationship of palladium nanocrystals (*Pd NCs*), showing the effects of different shapes on their reactivity. (Adapted from Collins et al. (2014), with permission. Copyright (2014) American Chemical Society)

Jing et al. 2014; Eguchi et al. 2012). For instance, polyhedral Au NPs with high-index facets exhibit excellent optical and catalytic properties. Nanosized metals and metal oxides mainly include nanosized zero-valent iron, ferric oxides, aluminum oxides, manganese oxides, titanium oxides, magnesium oxides, and cerium oxides (Chen et al. 2014; Zhang et al. 2013; Dasgupta et al. 2017). Alumina is a classical adsorbent, and its γ-alumina form is anticipated to be more adsorptive than α-alumina (Afkhami et al. 2010). Recently, nanosized ZnO was found to be capable of removing various contaminants, with high performance and selectivity. The synthesized ZnO featured a small crystallite size, abundant surface defects, a wide band gap, and capability to hinder electron–hole pair recombination (Kumar and Rao 2015). It also exhibited significant photocatalytic and antibacterial activity. Furthermore, some studies have pointed out that by doping of nanosized metal oxides with Fe, N, Cu, Zr, Co, or Ce, the photocatalytic activity and stability of the metal oxide nanoparticles could be significantly enhanced (Hernández-Alonso et al. 2009;

Nagaveni et al. 2004; Narayana et al. 2011). During the last decade, titanium dioxide (TiO_2) nanoparticles have emerged as promising photocatalysts for water purification (Rakkesh and Balakumar 2013). TiO_2 particles are very versatile; they can serve as both oxidative and reductive catalysts for organic and inorganic pollutants (Hernández-Alonso et al. 2009; Nakata and Fujishima 2012).

1.2.3 Magnetic Nanoparticles

Nanomaterials in combination with polymers or other nanomaterials, such as magnetic particles, have great potential in the development of advanced functional materials for water treatment. These nanohybrid materials will allow safer use of these nanomaterials for water treatment since it will be possible to recover 100% of the nanomaterials and avoid other adverse environmental impacts that might occur from release of these materials into the environment. It will be important, however, to investigate the removal efficiency of these nanocomposites for diverse biological and chemical contaminants, as well as their potential for reusability prior to applications in water treatment. This would tremendously reduce the cost of this technology.

Zero-valent iron (ZVI) is an effective tool for water remediation. Its reactivity has been largely improved by the development of nanoscale ZVI (nZVI) (Fu et al. 2014; Tosco et al. 2014). nZVI possesses many specific positive features such as high reactivity toward a broad range of contaminants due to its large specific area and diminutive size, which help to promote effective subsurface dispersion and injection into aqueous slurries for remediation of contaminated areas. Studies have shown that by manipulating the size of ZVI from the micron scale to the nanoscale, the rate constant for pentavalent arsenate (As(V)) removal could be improved by 1–3 orders of magnitude (Tosco et al. 2014). This outstanding reactivity of nZVI was presumed to result from its significantly increased surface area and active sites, in comparison with bulk ZVI. nZVI was also capable of removing other contaminants such as nitrate, dyes, environmentally persistent toxic contaminants, and antibiotics through adsorption, oxidation, reduction, and coprecipitation (Zhang et al. 2016).

Growing interest in the use of nanosized iron oxides for wastewater treatment has resulted from their strong sorption capability, operational simplicity, and resourceful. The phases of iron oxides discussed here are nonmagnetic goethite (a-FeOOH) and hematite (α-Fe_2O_3), magnetic magnetite (Fe_3O_4) and maghemite (γ-Fe_2O_3), and hydrous ferric oxides (HFOs) (Mu et al. 2017; Poulton et al. 2004). Goethite and hematite incorporate a range of geochemically and environmentally important oxy-anions and cations in their complex matrices (Mohapatra et al. 2010). They have been considered efficient and low-cost absorbents for the mitigation of various contaminants. A schematic representation of a water purification system with a multilayered nanomaterial-based matrix—which could remove organic, inorganic, and microbial contamination—is shown in Fig. 1.6.

Fig. 1.6 Nanomaterial-packed layer for purification of water contaminants

1.3 Nanomaterials in Chemosensors and Biosensors

To date, the use of CNTs (CNTs) and graphene, and their related species, has received the greatest interest for use in sensing applications. In addition to pristine graphene, several surface-treated forms such as photoluminescent graphene oxide and reduced graphene oxide (RGO) have been used in sensing

applications (Chen et al. 2012; Baptista et al. 2015; Peik-See et al. 2014). The purity of synthesized carbon nanostructures is an essential consideration for any possible sensing application. Two key issues are the presence of (1) impurities, which may interfere with the detection of analytes; and (2) a polydisperse sample, which influences both the optical properties and the ability to form ordered assemblies (Baptista et al. 2015). In general, carbon nanostructures display poor solubility in aqueous solvents, where they are prone to aggregation due to hydrophobic interactions. However, this can be addressed through surface functionalization by covalent or noncovalent methods. Surface modification is also used to introduce receptor sites for sensing. The diverse intrinsic properties of carbon nanomaterials give rise to a range of sensing mechanisms, the most common of which are (1) electrical, where binding of the analyte changes the dielectric environment; (2) electrochemical, due to a redox process at the CNT surface; and (3) optical, such as fluorescence quenching, where there is a loss of emission due to the interaction between the carbon nanomaterials and the analyte (Holzinger et al. 2014). The sensing of small molecules—including drugs, metal ions, gaseous analytes, and biomolecules—is vitally important in the areas of health, the environment, food, and safety (Yang et al. 2010). The sensing of metal ions such as Fe^{2+}, Zn^{2+}, Ca^{2+}, Na^{+}, K^{+}, and Mg^{2+} is very important in the area of health (Baptista et al. 2015). Other important analytes for health include glucose, neurotransmitters such as dopamine, gene sequences for disease diagnosis, and illegal drug molecules. Sensors are also required for environmental monitoring of metal ion pollutants and toxins; the detection of these pollutants in trace amounts, especially mercury, is critically important (Baptista et al. 2015).

In addition to electrode materials, functional nanomaterials can not only produce a synergic effect involving catalytic activity, conductivity, and biocompatibility to accelerate signal transduction but also amplify biorecognition events with specifically designed signal tags, leading to highly sensitive biosensing. Extensive research has led to advances in the construction of functional electrode materials coupled with numerous electrochemical methods (Jiang et al. 2012). Besides that, a wide variety of strategies are being used to improve the efficacy of sensing for various electrochemical applications (Zhang and Li 2012; Jiang et al. 2012). Signal amplification can be achieved by utilizing NPs as carriers or tracers, catalysts, and electronic conductors and produce a synergic effect among catalytic activity, conductivity, and biocompatibility. New developments in nanotechnology and material science, as well as in custom engineering of biorecognition components, have advanced the progress of useful and reliable electrochemical sensors and biosensors. Materials and biomaterials with rich nanostructures not only improve electronic properties and increase the effective electrode surface for transferring electrochemical signals but also produce detectable signals for indirect detection of targets. Thus, the resulting methods possess high sensitivity and good specificity. An illustration of electrochemical sensors and biosensors based on nanomaterials and nanostructures is given in Fig. 1.7.

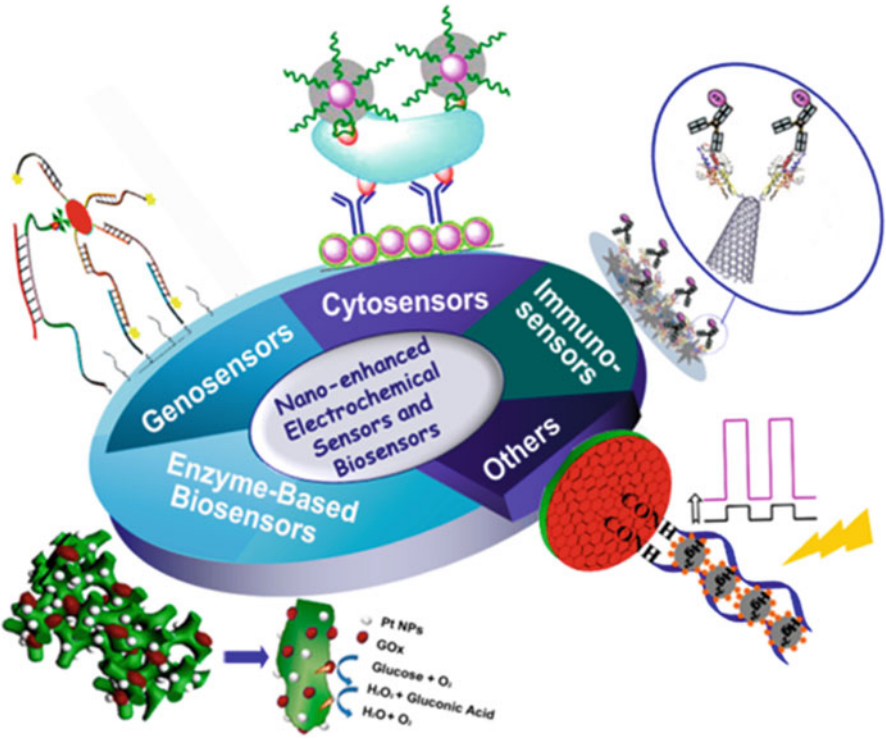

Fig. 1.7 Electrochemical sensors and biosensors based on nanomaterials and nanostructures, in which electrochemical sensors for small-molecular, enzyme-based biosensors, genosensors, immunosensors, and cytosensors are demonstrated. *GOx* glucose oxidase, *Pt NPs* platinum nanoparticles. (Adapted from Zhu et al. (2014), with permission. Copyright (2014) American Chemical Society)

1.4 Nanomaterials as Effective Antimicrobial Agents

Antibacterial activity is related to compounds that locally kill bacteria or slow down their growth, without being toxic to surrounding tissue in general. Use of antibacterial agents is paramount to fight infectious diseases. Resistance is most often based on evolutionary processes taking place during—for example—antibiotic therapy, and leads to inheritable resistance. In addition, horizontal gene transfer by conjugation, transduction, or transformation can be a possible way for resistance to build up. Drug resistance leads to high-dose administration of antibiotics, often generating intolerable toxicity. This has prompted the development of alternative strategies to treat bacterial diseases. Among them, nanoscale materials have emerged as novel antimicrobial agents (Hajipour et al. 2012). In particular, several classes of antimicrobial nanoparticles and nanosized carriers for antibiotic delivery have proved their effectiveness for treating infectious diseases, including antibiotic-resistant ones, in vitro as well as in animal models (Campoccia et al. 2013; Herman and Herman 2014).

Species sensitivity is not only related to the structure of the cell wall in Gram-positive (+) and Gram-negative (−) bacteria. Several additional factors can influence bacterial susceptibility to or tolerance of NPs (Dinesh et al. 2012). For example, *Escherichia coli* (−) is highly susceptible to CuO NPs, whereas *Staphylococcus aureus* (+) and *Bacillus subtilis* (+) are less susceptible. The antibacterial effect of Ag NPs is greater than that of Cu NPs against *E. coli* (−) and *S. aureus* (+) bacteria. *S. aureus* (+) and *B. subtilis* (+) are more susceptible to NiO and ZnO NPs than *E. coli* (−) (Hajipour et al. 2012; Sirelkhatim et al. 2015).

One of the major shortcomings of antibacterial drugs is their failure to fight bacteria (e.g., *S. aureus* (+)) that have the capability to produce biofilms. Exposure to Ag NPs may prevent colonization of new bacteria on biofilm and decrease the development and succession of the biofilm. MgF_2 NPs have antimicrobial activity and are able to prevent biofilm formation by common pathogens such as *E. coli* and *S. aureus* (Lellouche et al. 2012). Furthermore, MgF_2 NP–modified catheters are able to restrict biofilm formation by these bacteria significantly. Moreover, glass surfaces coated with ZnO NPs are able to produce reactive oxygen species (ROS) that interfere with *E. coli* and *S. aureus* biofilm formation.

When compared with various types of NPs, gold and silver surface–coated superparamagnetic iron oxide NPs (SPIONs) show the highest antibacterial activity against biofilms (Franci et al. 2015; Martinez-Gutierrez et al. 2013). Figure 1.8 illustrates the mechanism of action of silver ring–coated and gold-coated SPIONs against bacterial biofilms (Hajipour et al. 2012). The figure shows that monodisperse SPIONs, silver ring–coated SPIONs, and silver ring–coated, gold-coated SPIONs have strong toxic effects by penetration into the biofilms. Both the SPION core and the intermediate gold shell have the capability to induce heat with application of alternative magnetic and laser fields. The produced heat can be used as an additional means to escalate bacterial death using these NPs. The magnified section in the center of Fig. 1.8 illustrates the irreversible effects of NPs and their ions on the various parts of the bacteria (e.g., the cell wall, DNA, and mitochondria). It is notable that magnetic NPs have considerable capability to penetrate into biofilms with use of external magnetic fields.

1.5 Summary

Every person on earth deserves a sustainable lifestyle that includes clean water, unpolluted air, good food, and health care. Clean water is not only essential for human health but also critical in a variety of key industries including the electronics, pharmaceutical, and food industries. In the current scenario, our world is facing alarming challenges in meeting rising demands for clean water, due to (i) extended droughts, (ii) population growth, (iii) more stringent health-based regulations, and (iv) competing demands from a variety of users. Developments in nanoscience and nanotechnology offer potential alternatives to conventional water-purifying systems, due to the versatile size-mediated properties and efficacy of nanoparticles. With

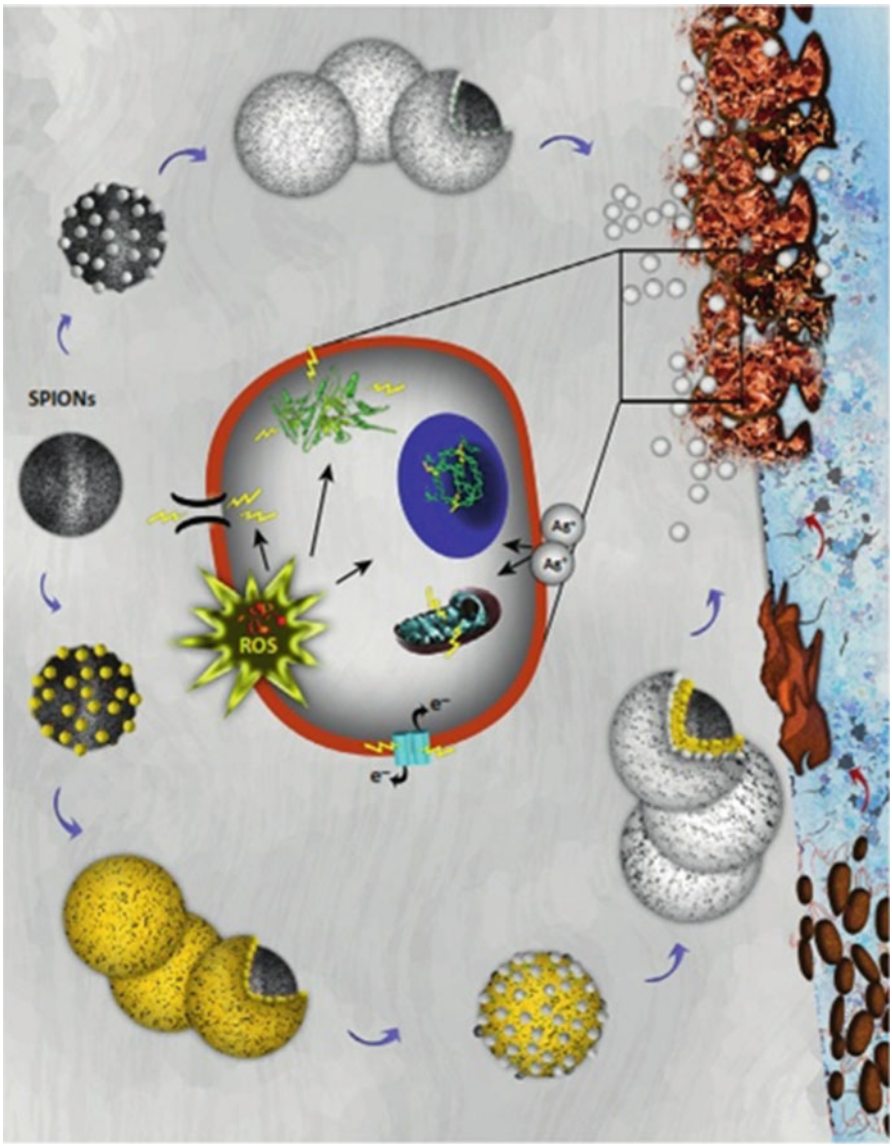

Fig. 1.8 Toxicological effects of multifunctional nanoparticles on bacterial biofilms (Hajipour et al. 2012). The *black spheres* denote superparamagnetic iron oxide nanoparticles (*SPIONs*), the *gray shells* denote silver ring–coated SPIONs, and the *yellow shells* denote gold-coated SPIONs. *ROS* reactive oxygen species

scaling up of this technology for use on a wider scale, nanomaterials are highly recommendable because of their higher antibacterial efficacy and greater efficiency for water purification and even for sensing applications, in comparison with bulk

particles. Because of the large surface area properties of nanomaterials, only very small quantities are required to meet environmental needs and they can also be of low cost.

This book provides a compilation of extensive discussions on emerging nanomaterials for use in environmental applications and in wastewater treatment by photocatalysis, nanomaterial coatings for use in antibacterial applications, and the role of nanomaterials as chemosensors and biosensors.

Acknowledgements D. Durgalakshmi gratefully acknowledges financial support from a Department of Science & Technology (Government of India)–Innovation in Science Pursuit for Inspired Research (DST-INSPIRE) faculty fellowship (no. 04/2016/000845). R. Saravanan gratefully acknowledges financial support from the Chilean Solar Energy Research Center (SERC; CONICYT/FONDAP/15110019); the National Fund for Scientific and Technological Development (FONDECYT), Government of Chile (project no. 11170414); and Faculty of Engineering, Department of Mechanical Engineering, University of Tarapacá, Arica, Chile.

References

Adeleye AS, Conway JR, Garner K, Huang Y, Su Y, Keller AA (2016) Engineered nanomaterials for water treatment and remediation: costs, benefits, and applicability. Chem Eng J 286:640–662

Afkhami A, Saber-Tehrani M, Bagheri H (2010) Simultaneous removal of heavy-metal ions in wastewater samples using nano-alumina modified with 2,4-dinitrophenylhydrazine. J Hazard Mater 181(1–3):836–844

Al-Othman ZA, Ali R, Naushad M (2012) Hexavalent chromium removal from aqueous medium by activated carbon prepared from peanut shell: adsorption kinetics, equilibrium and thermodynamic studies. Chem Eng J 184:238–247

Ashbolt NJ (2015) Microbial contamination of drinking water and human health from community water systems. Curr Environ Health Rep 2(1):95–106

Baptista FR, Belhout S, Giordani S, Quinn S (2015) Recent developments in carbon nanomaterial sensors. Chem Soc Rev 44(13):4433–4453

Campoccia D, Montanaro L, Arciola CR (2013) A review of the biomaterials technologies for infection-resistant surfaces. Biomaterials 34(34):8533–8554

Cardinale BJ, Duffy JE, Gonzalez A, Hooper DU, Perrings C, Venail P, Narwani A, Mace GM, Tilman D, Wardle DA (2012) Biodiversity loss and its impact on humanity. Nature 486 (7401):59

Chen D, Feng H, Li J (2012) Graphene oxide: preparation, functionalization, and electrochemical applications. Chem Rev 112(11):6027–6053

Chen L, Xin H, Fang Y, Zhang C, Zhang F, Cao X, Zhang C, Li X (2014) Application of metal oxide heterostructures in arsenic removal from contaminated water. J Nanomater 2014:Article ID 793610. https://doi.org/10.1155/2014/793610. Accessed 3 Oct 2018

Collins G, Schmidt M, O'Dwyer C, McGlacken G, Holmes JD (2014) Enhanced catalytic activity of high-index faceted palladium nanoparticles in Suzuki–Miyaura coupling due to efficient leaching mechanism. ACS Catal 4(9):3105–3111

Dasgupta N, Ranjan S, Ramalingam C (2017) Applications of nanotechnology in agriculture and water quality management. Environ Chem Lett 15(4):591–605

Dinesh R, Anandaraj M, Srinivasan V, Hamza S (2012) Engineered nanoparticles in the soil and their potential implications to microbial activity. Geoderma 173:19–27

Eguchi M, Mitsui D, Wu H-L, Sato R, Teranishi T (2012) Simple reductant concentration-dependent shape control of polyhedral gold nanoparticles and their plasmonic properties. Langmuir 28(24):9021–9026

EPA [US Environmental Protection Agency] (2016) Contaminant candidate list (CCL) and regulatory determination: definition of "contaminant". https://www.epa.gov/ccl/definition-contaminant. Accessed 3 Oct 2018

Faust SD, Aly OM (2018) Chemistry of water treatment. CRC, Boca Raton

Franci G, Falanga A, Galdiero S, Palomba L, Rai M, Morelli G, Galdiero M (2015) Silver nanoparticles as potential antibacterial agents. Molecules 20(5):8856–8874

Fu F, Dionysiou DD, Liu H (2014) The use of zero-valent iron for groundwater remediation and wastewater treatment: a review. J Hazard Mater 267:194–205

Gehrke I, Geiser A, Somborn-Schulz A (2015) Innovations in nanotechnology for water treatment. Nanotechnol Sci Appl 8:1

Haines A, Alleyne G, Kickbusch I, Dora C (2012) From the Earth Summit to Rio+ 20: integration of health and sustainable development. Lancet 379(9832):2189–2197

Hajipour MJ, Fromm KM, Ashkarran AA, de Aberasturi DJ, de Larramendi IR, Rojo T, Serpooshan V, Parak WJ, Mahmoudi M (2012) Antibacterial properties of nanoparticles. Trends Biotechnol 30(10):499–511

Hebbar RS, Isloor AM, Asiri AM (2017) Carbon nanotube- and graphene-based advanced membrane materials for desalination. Environ Chem Lett 15(4):643–671

Herman A, Herman AP (2014) Nanoparticles as antimicrobial agents: their toxicity and mechanisms of action. J Nanosci Nanotechnol 14(1):946–957

Hernández-Alonso MD, Fresno F, Suárez S, Coronado JM (2009) Development of alternative photocatalysts to TiO_2: challenges and opportunities. Energy Environ Sci 2(12):1231–1257

Holzinger M, Le Goff A, Cosnier S (2014) Nanomaterials for biosensing applications: a review. Front Chem 2:63

Jiang J, Li Y, Liu J, Huang X, Yuan C, Lou XW (2012) Recent advances in metal oxide–based electrode architecture design for electrochemical energy storage. Adv Mater 24(38):5166–5180

Jiang Y, Biswas P, Fortner JD (2016) A review of recent developments in graphene-enabled membranes for water treatment. Environ Sci Water Res Technol 2(6):915–922

Jing H, Zhang Q, Large N, Yu C, Blom DA, Nordlander P, Wang H (2014) Tunable plasmonic nanoparticles with catalytically active high-index facets. Nano Lett 14(6):3674–3682

Jobst KJ, Shen L, Reiner EJ, Taguchi VY, Helm PA, McCrindle R, Backus S (2013) The use of mass defect plots for the identification of (novel) halogenated contaminants in the environment. Anal Bioanal Chem 405(10):3289–3297

Kharisov BI, Kharissova OV, Ortiz-Mendez U (2016) CRC concise encyclopedia of nanotechnology. CRC, Boca Raton

Kumar SG, Rao KK (2015) Zinc oxide based photocatalysis: tailoring surface-bulk structure and related interfacial charge carrier dynamics for better environmental applications. RSC Adv 5 (5):3306–3351

Lamastra L, Balderacchi M, Trevisan M (2016) Inclusion of emerging organic contaminants in groundwater monitoring plans. MethodsX 3:459–476

Lellouche J, Friedman A, Lellouche J-P, Gedanken A, Banin E (2012) Improved antibacterial and antibiofilm activity of magnesium fluoride nanoparticles obtained by water-based ultrasound chemistry. Nanomedicine 8(5):702–711

Li Y, Zhu G, Ng WJ, Tan SK (2014) A review on removing pharmaceutical contaminants from wastewater by constructed wetlands: design, performance and mechanism. Sci Total Environ 468:908–932

Manahan S (2017) Environmental chemistry. CRC, New York

Martinez-Gutierrez F, Boegli L, Agostinho A, Sánchez EM, Bach H, Ruiz F, James G (2013) Antibiofilm activity of silver nanoparticles against different microorganisms. Biofouling 29 (6):651–660

Mohapatra M, Rout K, Gupta S, Singh P, Anand S, Mishra B (2010) Facile synthesis of additive-assisted nano goethite powder and its application for fluoride remediation. J Nanopart Res 12 (2):681–686

Mohmood I, Lopes CB, Lopes I, Ahmad I, Duarte AC, Pereira E (2013) Nanoscale materials and their use in water contaminants removal—a review. Environ Sci Pollut Res 20(3):1239–1260

Mu Y, Jia F, Ai Z, Zhang L (2017) Iron oxide shell mediated environmental remediation properties of nano zero-valent iron. Environ Sci Nano 4(1):27–45

Nagaveni K, Hegde M, Madras G (2004) Structure and photocatalytic activity of $Ti_{1-x}M_xO_{2\pm\delta}$ (M = W, V, Ce, Zr, Fe, and Cu) synthesized by solution combustion method. J Phys Chem B 108(52):20204–20212

Nakata K, Fujishima A (2012) TiO_2 photocatalysis: design and applications. J Photochem Photobiol C: Photochem Rev 13(3):169–189

Narayana RL, Matheswaran M, Aziz AA, Saravanan P (2011) Photocatalytic decolourization of basic green dye by pure and Fe, Co doped TiO_2 under daylight illumination. Desalination 269 (1–3):249–253

NRC [US Nuclear Regulatory Commission] (2016) Backgrounder on tritium, radiation protection limits, and drinking water standards. https://www.nrc.gov/reading-rm/doc-collections/fact-sheets/tritium-radiation-fs.html. Accessed 3 Oct 2018

Pan Y, Zhang X (2013) Four groups of new aromatic halogenated disinfection byproducts: effect of bromide concentration on their formation and speciation in chlorinated drinking water. Environ Sci Technol 47(3):1265–1273

Peik-See T, Pandikumar A, Ngee LH, Ming HN, Hua CC (2014) Magnetically separable reduced graphene oxide/iron oxide nanocomposite materials for environmental remediation. Cat Sci Technol 4(12):4396–4405

Perreault F, De Faria AF, Nejati S, Elimelech M (2015) Antimicrobial properties of graphene oxide nanosheets: why size matters. ACS Nano 9(7):7226–7236

Poulton SW, Krom MD, Raiswell R (2004) A revised scheme for the reactivity of iron (oxyhydr) oxide minerals towards dissolved sulfide. Geochim Cosmochim Acta 68(18):3703–3715

Rakkesh RA, Balakumar S (2013) Facile synthesis of ZnO/TiO_2 core–shell nanostructures and their photocatalytic activities. J Nanosci Nanotechnol 13(1):370–376

Rakkesh RA, Durgalakshmi D, Balakumar S (2014) Efficient sunlight-driven photocatalytic activity of chemically bonded GNS–TiO_2 and GNS–ZnO heterostructures. J Mater Chem C 2 (33):6827–6834

Rakkesh RA, Durgalakshmi D, Balakumar S (2015) Nanostructuring of a GNS-V_2O_5–TiO_2 core–shell photocatalyst for water remediation applications under sun-light irradiation. RSC Adv 5 (24):18633–18641

Roser M, Ortiz-Ospina E (2017) World population growth. Our World in Data. https://ourworldindata.org/world-population-growth/. Accessed 3 Oct 2018

Sadegh H, Shahryari Ghoshekandi R, Masjedi A, Mahmoodi Z, Kazemi M (2016) A review on carbon nanotubes adsorbents for the removal of pollutants from aqueous solutions. Int J Nano Dimens 7(2):109–120

Saravanan R, Shankar H, Prakash T, Narayanan V, Stephen A (2011) ZnO/CdO composite nanorods for photocatalytic degradation of methylene blue under visible light. Mater Chem Phys 125(1–2):277–280

Savage N, Diallo MS (2005) Nanomaterials and water purification: opportunities and challenges. J Nanopart Res 7(4–5):331–342

Sirelkhatim A, Mahmud S, Seeni A, Kaus NHM, Ann LC, Bakhori SKM, Hasan H, Mohamad D (2015) Review on zinc oxide nanoparticles: antibacterial activity and toxicity mechanism. Nano Micro Lett 7(3):219–242

Smith SC, Rodrigues DF (2015) Carbon-based nanomaterials for removal of chemical and biological contaminants from water: a review of mechanisms and applications. Carbon 91:122–143

Stumm W (1977) Chemical interaction in particle separation. Environ Sci Technol 11 (12):1066–1070

Suárez-Iglesias O, Collado S, Oulego P, Díaz M (2017) Graphene-family nanomaterials in wastewater treatment plants. Chem Eng J 313:121–135

Tollefson J, Gilbert N (2012) Rio report card: the world has failed to deliver on many of the promises it made 20 years ago at the Earth Summit in Brazil. Nature 486(7401):20–24

Tosco T, Papini MP, Viggi CC, Sethi R (2014) Nanoscale zerovalent iron particles for groundwater remediation: a review. J Clean Prod 77:10–21

Tran TT, Lu X (2011) Synergistic effect of Ag and Pd ions on shape-selective growth of polyhedral Au nanocrystals with high-index facets. J Phys Chem C 115 (9):3638–3645

United Nations (1992) Rio declaration on environment and development. United Nations, New York

Vardharajula S, Ali SZ, Tiwari PM, Eroğlu E, Vig K, Dennis VA, Singh SR (2012) Functionalized carbon nanotubes: biomedical applications. Int J Nanomedicine 7:5361–5374. https://doi.org/10.2147/IJN.S35832. Accessed 3 Oct 2018

World Health Organization (2004) Guidelines for drinking-water quality. Volume 1: recommendations. World Health Organization, Geneva

World Health Organization (2018) Drinking-water. http://www.who.int/news-room/fact-sheets/detail/drinking-water. Accessed 3 Oct 2018

Wood C (1993) Planning for a sustainable environment: a report by the Town and Country Planning Association. In: Blowers A (ed). Earthscan, London 38–39

Wu Z, Yang S, Wu W (2016) Shape control of inorganic nanoparticles from solution. Nanoscale 8 (3):1237–1259

Yang W, Ratinac KR, Ringer SP, Thordarson P, Gooding JJ, Braet F (2010) Carbon nanomaterials in biosensors: should you use nanotubes or graphene? Angew Chem Int Ed 49(12):2114–2138

Zhang J, Li CM (2012) Nanoporous metals: fabrication strategies and advanced electrochemical applications in catalysis, sensing and energy systems. Chem Soc Rev 41(21):7016–7031

Zhang Q, Du Q, Hua M, Jiao T, Gao F, Pan B (2013) Sorption enhancement of lead ions from water by surface charged polystyrene-supported nano-zirconium oxide composites. Environ Sci Technol 47(12):6536–6544

Zhang Y, Wu B, Xu H, Liu H, Wang M, He Y, Pan B (2016) Nanomaterials-enabled water and wastewater treatment. NanoImpact 3:22–39

Zhu C, Yang G, Li H, Du D, Lin Y (2014) Electrochemical sensors and biosensors based on nanomaterials and nanostructures. Anal Chem 87(1):230–249

Chapter 2
Recent Advances in Nanomaterials for Wastewater Treatment

Mohamed I. Fadlalla, P. Senthil Kumar, V. Selvam, and S. Ganesh Babu

Contents

Abstract Developing an efficient wastewater treatment technique is one of the major necessities of the twenty-first century, owing to the scarcity of water resources. Besides, it is of paramount important to find appropriate methodologies to economically treat wastewater. Recent advances in nanotechnology have attracted the attention of many researchers for wastewater treatment. The major advantages of such nanomaterial-based systems are that they can be reused and have been found to be very effective. Though many research works have been reported in this regard, there is very limited collective information. Hence, the major objective of this work is to describe recent achievements in nanomaterial-based systems for wastewater

M. I. Fadlalla · S. Ganesh Babu (✉)
Department of Chemical Engineering, Institute for Catalysis Research and c*change (DST-NRF Centre of Excellence in Catalysis), University of Cape Town, Cape Town, South Africa

P. Senthil Kumar
Department of Chemistry, School of Advanced Sciences, VIT University, Vellore, Tamilnadu, India

V. Selvam
Department of Chemistry, The M.D.T. Hindu College, Tirunelveli, Tamilnadu, India

Mu. Naushad et al. (eds.), *Advanced Nanostructured Materials for Environmental Remediation*, Environmental Chemistry for a Sustainable World 25,
https://doi.org/10.1007/978-3-030-04477-0_2

treatment. This chapter critically reviews and lists the uses of nanomaterials in wastewater treatment. This comprises the utilization of semiconducting nanoparticles either alone or combined with ozonation, the Fenton process, or sonolysis for effective degradation/removal of organic pollutants. Furthermore, the effectiveness of nanotechnology in antimicrobial activity to produce pure water via an eco-friendly route is discussed. Similarly, the role of nanomaterials in adsorption techniques (specifically, carbon-based nanoadsorbents) to remove heavy metal contamination from industrial wastewater is also discussed in detail.

Keywords Nanomaterials · Ozonation · Fenton process · Sonolysis · Antimicrobial · Adsorption · Wastewater treatment

2.1 Introduction

Water is one of the major ingredients for all living bodies in the universe and is available in abundance (Grey et al. 2013). However, unfortunately only about 1% of it is readily accessible for consumption by human beings (Adeleye et al. 2016). According to an estimation from the World Health Organization (WHO) in 2015, more than 1.1 billion people are struggling to obtain pure drinking water worldwide. This is mainly the consequence of growing populations and growing industrialization (Adeleye et al. 2016). One of the major challenges is to purify the wastewater from industrial processes by removing the organic and inorganic pollutants to obtain water with permissible quality (Naushad et al. 2018; Schwarzenbach et al. 2006). Most of the current technologies possess some limitations—namely, high-energy prerequisites, incomplete removal of pollutants, and production of toxic sludge during the wastewater purification process (Ferroudj et al. 2013; Qu et al. 2012). Furthermore, these systems are expensive, which, in turn, increases the price of potable water (Ferroudj et al. 2013).

The available biological techniques for the purification of wastewater suffer from the drawback of being very slow processes, and sometimes they increase the toxicity by releasing microorganisms into drinking water (Naushad et al. 2017; Zelmanov and Semiat 2008). Moreover, the application of these biological systems is inefficient for wastewater that contains nonbiodegradable impurities (Zelmanov and Semiat 2008). Similarly, it is difficult to achieve 100% purification by physical filtration methods, and these methods generate toxic sludge, which is extremely problematic for disposal (Catalkaya et al. 2003; Bali et al. 2003). Hence, development of an efficient technology is highly desired for the complete removal of contaminants from wastewater (Parsons and Jefferson 2006). This can also be achieved by either improving or modifying existing technologies (Burkhard et al. 2000). In addition, it is worth trying combinations of two or more techniques to increase the activity and overcome the drawbacks of individual

systems (Ferroudj et al. 2013). In this regard, several technologies are emerging to address the drawbacks of the present methodologies for wastewater treatment (Gupta et al. 2015). On the other hand, nanotechnology has been shown to be a potential tool for addressing several environmental issues, including wastewater remediation (Zare et al. 2013; Sadegh et al. 2014).

Various publications have reported the utilization of nanomaterials for wastewater treatment (Kyzas and Matis 2015; Zhang et al. 2014). The role of nanomaterials in treatment of industrial and municipal wastewater is vastly diversified, viz., nanoadsorbents (Tang et al. 2014; Shamsizadeh et al. 2014; Kyzas and Matis 2015; El Saliby et al. 2008), semiconducting nanocatalysts (Babu et al. 2015a; Kumar et al. 2016), electrocatalysts (Dutta et al. 2014), antimicrobial materials (Chaturvedi et al. 2012), and nanomembranes (Lau and Ismail 2009; Ouyang et al. 2013; Blanco et al. 2012; Petrinic et al. 2007; Hilal et al. 2004; Babursah et al. 2006; Rashidi et al. 2015; El Saliby et al. 2008). Besides, combination of nanomaterials with other existing technologies improves the performance of the systems. For instance, semiconducting nanomaterials significantly increase the degradation ability of the Fenton process (Kurian et al. 2014; Ma et al. 2015), ozonolysis (Babu et al. 2016a), sonolysis (Babu et al. 2016b), and so on.

Several research works have been reported in which nanomaterials have been applied for purification of wastewater (Leshuk and Gu 2014; Palit 2017; Savage and Diallo 2005; Theron et al. 2008; Santhosh et al. 2016; Zhang et al. 2016; Ghasemzadeh et al. 2016; Baruah et al. 2016). This chapter focuses on the use of semiconducting nanomaterials for organic pollutant degradation and the utilization of nanocatalysts in combination with some important existing technologies—namely, sonolysis, ozonolysis, and the Fenton process. This chapter also highlights the role of nanomaterials as nanoadsorbents and nanomembranes. Furthermore, the influence of nanomaterials on antimicrobial activity is discussed in detail.

2.2 Nanomaterials for Wastewater Treatment

Nanotechnology is one of the interesting fields that deals with particles less than 100 nm in size (Amin et al. 2014). Because of their small size, their surface to volume ratio is relatively high; in other words, these particles possess numerous active sites, which, in turn, significantly improve their activity (Chaturvedi et al. 2012). Several types of nanomaterials such as nanotubes, quantum dots, nanowires, nanocolloids, nanoparticles, and nanofilms have been reported in the literature for various applications (Lubick and Betts 2008; Edelstein and Cammaratra 1998). In terms of removal of organic and inorganic pollutants from water, nanomaterials play a vital role owing to the unique functionalities of nanoparticles (Brumfiel 2003; Theron et al. 2008; Gupta et al. 2015).

2.2.1 Semiconducting Nanomaterials

The industrialized society discharges a wide variety of environmental contaminants from residential, commercial, and industrial sources (Shannon et al. 2008; Schwarzenbach et al. 2006). There are approximately 30,000 commercially available chemicals, and not much is known regarding their occurrence and fate in the environment (Munir et al. 2006). The greater challenge lies with the treatment of newly emerging micropollutants (e.g., pharmaceuticals, antibiotics, and pathogens), which are being detected more often as analytical methods improve. Advanced oxidation processes (AOPs) such as UV/H_2O_2, ozonation, the photo-Fenton process (Titus et al. 2004), γ-radiolysis, sonolysis, electrochemical oxidation (Park et al. 2008), and photocatalysis (Demeestere et al. 2007) have been widely and extensively explored to mitigate a vast variety of pollutants present in various environmental media. They are initiated primarily from the formation of reactive and short-lived oxygen-containing radicals (e.g., •OH, HOO•, and $O_2^{\bullet-}$). Among them, the hydroxyl radical (•OH) is the most reactive and powerful oxidant ($E^0 = 2.7$ V), which reacts with most organic compounds at diffusion-limited rates. AOPs have been considered as alternatives to conventional water treatment technologies (Liu et al. 2009). However, they have yet to overcome the challenges of energy efficiency and cost competitiveness (Jones et al. 2007).

Photocatalysis is a green technology, which offers numerous applications and a best method for energy-related problems, as illustrated in Fig. 2.1 (Kuwahara and Yamashita 2011). The word "photocatalysis" is of Greek origin and is composed of two parts: the prefix "photo-" (*photos*, "light") and the word "catalysis" (*katalyo*, "break apart" or "decompose"). Although there is no consensus in the scientific community as to a proper definition of photocatalysis, the term can be generally used to describe a process in which light is used to active a substance—the photocatalyst—which modifies the rate of a chemical reaction without being involved in the chemical transformation (Herrmann 2005).

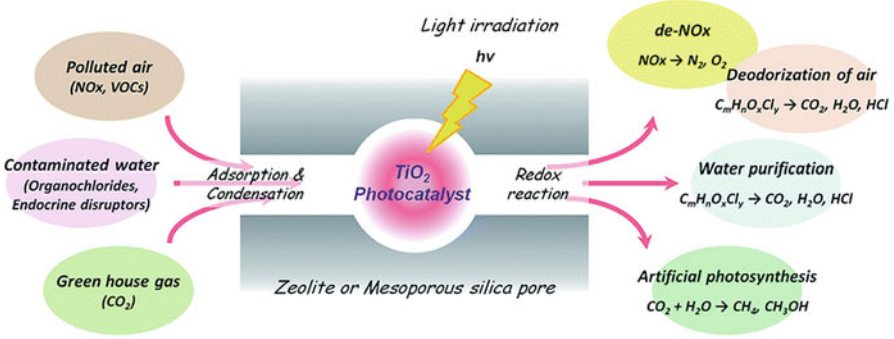

Fig. 2.1 Applications of photocatalysis. *hv* photon energy, *NOx* nitrogen oxide, *VOC* volatile organic compound. (Reproduced from Kuwahara and Yamashita (2011), with permission)

A light-absorbing substance is added to a reaction, which facilitates the reaction while remaining unchanged at the end of the reaction. When light strikes a semiconductor, electrons within the particle become excited, creating a higher state of energy within the electrons. Thus, the main difference between a conventional thermal catalyst and a photocatalyst is that the former is activated by heat whereas the latter is activated by photons of appropriate light energy. Recently, nanomaterials have been widely used as photocatalysts in the presence of light (Table 2.1). The photocatalytic activity of nanoparticles (NPs) represents a rich resource for chemical processes, employed both in industry and in academia (Senanayake et al. 2013).

The use of CuO nanoparticles as a photocatalyst for the degradation of different kinds of dye solutions has been reported (Kumar et al. 2017). The energy gap of the CuO was altered by modifications of the experimental protocols, and a significant variation from 2.2 to 2.7 eV was observed. The oxygen defects may have affected the crystal lattice, which was reflected in the energy gap value. Moreover, the CuO with the tailored energy gap exhibited enhanced photocatalytic efficiency toward the degradation of organic dye solutions. The reaction kinetics, degradation mechanism, and catalyst stability, as well as the roles of bandgap tailoring in the photoreaction, were comprehensively studied. The prevention of electron–hole pair recombination was strongly evidenced by photoluminescence studies. The species responsible for the degradation was identified by trapping experiments. The crucial role of bandgap tailoring in the improved photocatalytic activity was attributed to superior electron transfer ability, enhanced light harvesting, and boosted catalytic active sites.

Photocatalytic degradation of methyl orange (MO) dye solution was performed by Babu et al. using a reduced graphene oxide (rGO)–supported CuO–TiO_2 nanocomposite (Babu et al. 2015b), as illustrated in Fig. 2.2. The authors provided a detailed discussion of the role of rGO in the photocatalytic process. The energy gap of the CuO–TiO_2 nanocomposite was not altered/affected even after the rGO doping, and this suggested that the role of the rGO was only that of a solid support. Photoluminescence (PL) analysis of the CuO–TiO_2 and loaded rGO clearly suggested that the rGO not only acted as a solid support but also facilitated fast transport of electrons and thereby hindered the rate of charge carrier recombination. Moreover, the role of rGO was strongly evidenced by the photoelectrical response, which could clearly explain the electron transfer performance. Hence, this provided solid evidence that the rGO-loaded nanocomposite might exhibit greater photocatalytic activity.

Use of diffused sunlight–assisted photocatalytic mineralization of methyl orange dye solution in the presence of different photocatalysts (viz., CuO, TiO_2, CuO–TiO_2, and rGO-loaded CuO–TiO_2 nanocomposites) was evaluated. The results suggested that the rGO-loaded CuO–TiO_2 nanocomposites exhibited enhanced photocatalytic efficiency in comparison with that of the other photocatalysts, since the characterization results were unique. Moreover, the photocatalytic reaction was also performed under different conditions, viz., darkness, light alone, ultrasound, diffused sunlight, and use of both ultrasound and diffused sunlight in the same reaction. The results that were observed suggested that the combination of ultrasound and diffused sunlight provided higher efficiency. The total organic carbon (TOC)

Table 2.1 List of photocatalysts reported for degradation of organic pollutants and heavy metal reduction

Photocatalyst	Synthetic method	Particle size	Pollutant/heavy metal reduction	Degradation (%)	Reference
$CuO–TiO_2$/rGO	Sonochemical synthesis	13 nm	Methyl orange	89	Babu et al. (2015b)
SnS_2/rGO	Precipitation method		Methyl orange	92	Babu et al. (2015a)
α-Fe_2O_3	Precipitation method	35 nm	Rhodamine B and methylene blue	96	Dutta et al. (2014)
γ-Fe_2O_3/SiO_2	Emulsion solvent evaporation	100 nm	Methyl orange, methylene blue, and p-nitrophenol	95	Ferroudj et al. (2013)
Ti–SBA-15	Grafting method	100 nm	Eriochrome black T	89	Gobara et al. (2016)
MoS_2/Fe_3O_4	Solution processing method	50 nm	Rhodamine B	90	Han et al. (2017)
TiO_2–2-naphthol complex	Simple condensation method	1 μM	Cr(VI) reduction	100	Karthik et al. (2015)
Dye-sensitized TiO_2	Sonochemical synthesis	–	Reactive red 198	80	Kaur and Singh (2007)
Zn-doped Fe_3O_4	One-pot solvothermal route	120 nm	Rhodamine B and cephalexin	97	Nguyen et al. (2017)
CuO/ZnO	Precipitation method	50 nm	Congo red and rhodamine B	90	Kumar et al. (2017)

rGO reduced graphene oxide, *SBA* mesoporous silica

analysis suggested that the complete mineralization of the methyl orange dye solution in the presence of rGO-loaded $CuO–TiO_2$ nanocomposites and the photocatalyst possessed significant stability even after its third run.

2.2.2 *Fenton Process*

It is well known that the Fenton process and semiconductor nanophotocatalysts, when used individually, have some drawbacks that limit their effectiveness in the degradation of organic pollutants. Photocatalysis is a relatively slow process because

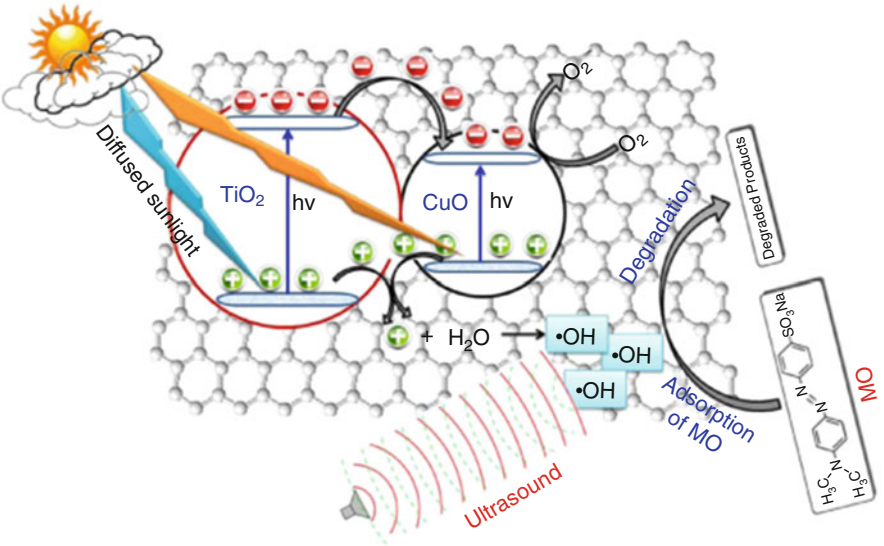

Fig. 2.2 Plausible mechanism for ultrasound-assisted photocatalytic degradation of methyl orange (*MO*) under diffused sunlight. *hv* photon energy. (Reproduced from Babu et al. (2015b), with permission)

of its low oxidation rate, whereas the Fenton process is selective, resulting in only partial oxidation of organic compounds. Partial oxidation leads to the formation of carboxylic acids as end products that cannot be further oxidized; therefore, complete mineralization is not achieved.

The degradation of an aqueous solution of glycerol via a photocatalytic Fenton technique has been reported (Cheng et al. 2015). Ultraviolet–visible (UV–Vis) diffuse reflectance spectroscopy results demonstrated that the $CuFe_2O_4$ might be active in the visible region, since the energy gap was 1.58 eV. The $CuFe_2O_4$ possessed a Brunauer–Emmett–Teller (BET) specific surface area of 104 m^2/g, which was also further evidenced by a field emission scanning electron microscopy (FE-SEM) micrograph showing a highly porous structure. The glycerol was subjected to adsorption and direct photolysis; the results suggested that there was no significant degradation (only 4% and 17%, respectively, in 4 h) in the absence of a catalyst as well as light. This was because of the splitting of H_2O_2 into hydroxyl (●OH) radicals. In addition, in the presence of the photocatalyst, the photo-Fenton process occurred, and the degradation percentage was 40% at a catalyst loading of 5.0 g/L. Significantly, from the power law modeling, the order of the reaction with respect to the glycerol (0.20) and H_2O_2 (0.80) was found to be fractional—a typical representation of chemical kinetics expression. Moreover, via the Langmuir–Hinshelwood model, the adsorption constant for H_2O_2 (0.033 mM^{-1} min^{-1}) was found to be much lower than that for glycerol (1.010 mM^{-1} min^{-1}). This indicated that the H_2O_2 splitting into hydroxyl radicals occurred in the bulk phase, while the glycerol substrate needed to chemisorb on the catalyst surface before being attacked by the

hydroxyl radicals. This demonstrated that the $CuFe_2O_4$ could generate additional hydroxyl radicals to attack the glycerol molecule.

In the photo-Fenton reaction, it is possible that metal nanoparticles may be leached and deposited in an aquatic environment. Hence, to prevent metal leaching and deposition in an aquatic environment from a photo-Fenton system, Yue et al. (2018) developed a carbon-based visible-light-active photo-electro-Fenton-like (PEF) cell, as shown in Fig. 2.3. The PEF preferentially generated highly active •OH radicals for environmental remediation. In this cell, the mesoporous carbon–coated graphite felt (MesoC/GF) cathode effectively generated H_2O_2 by electrochemical reduction of oxygen. Graphitic carbon nitride (g-C_3N_4) could provide a platform for metal-free visible-light photocatalytic activities, acting as an efficient metal-free Fenton catalyst for H_2O_2 activation to produce •OH radicals under visible-light irradiation. Optimization of the different operational parameters such as the applied voltage, photocatalyst dosage, and pH condition was investigated for mineralization of a phenol solution. This metal-free visible-light-active PEF cell exhibited excellent mineralization efficiency toward stubborn phenol with high stability, and its performance against phenol was much higher than that of a g-C_3N_4-only photocatalysis cell and a MesoC/GF-only electrolysis cell. Moreover, this PEF cell presented Fenton catalytic activities that were comparable to, or even better than, those of the similar electro-Fenton cell using MesoC/GF and homogeneous Fe^{2+} ions.

Medicinal waste (viz., drugs and wastewater) is considered a threat to aquatic life, and the photocatalytic Fenton process is an effective choice for mineralization of such pollutants. Hence, Moussavi et al. (2018) reported the effect of Fe^{2+} on

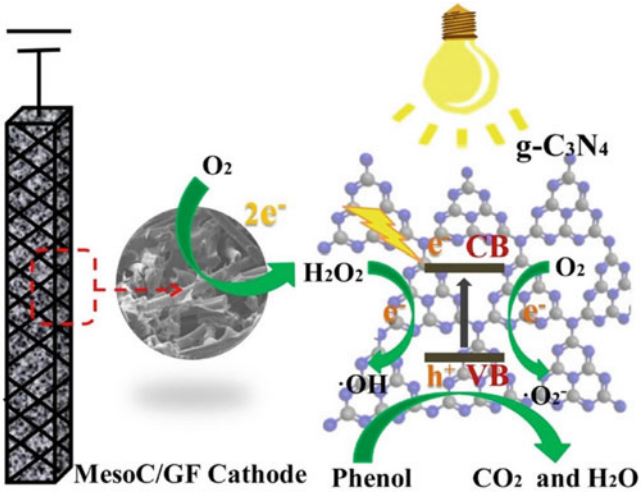

Fig. 2.3 Photoelectrochemical Fenton process. *CB* conduction band, *g-C_3N_4* graphitic carbon nitride, *MesoC/GF* mesoporous carbon–coated graphite felt, *VB* valence band. (Reproduced from Yue et al. (2018), with permission)

degradation of cloxacillin (CLX) in a vacuum ultraviolet (VUV) photoreactor, and the effects of the reaction parameters were optimized for maximum efficiency. The rate of CLX degradation in the VUV photoreactor was considerably improved by the presence of a low concentration of Fe^{2+}.

The photo-Fenton reaction accelerated by a water homolysis process and photo-oxidation of water molecules by VUV photons, as well as the photo-Fenton reaction, were the main mechanisms of CLX degradation in the VUV/Fe^{2+} process. The optimized condition for maximum CLX degradation was a solution at an acidic pH. Eighty percent of the CLX was mineralized within 60 min of irradiation, and almost 99% of it was degraded at a hydraulic retention time of 5 min in the continuous-flow VUV/Fe^{2+} process. The intermediates formed during the degradation were analyzed using a liquid chromatography–mass spectrometry (LC–MS) technique, and it was noted that the C–N, C–S, and C–Cl bonds were completely mineralized, and the smaller aliphatic compounds were the remaining organic by-products of the CLX degradation. In addition, the VUV/Fe^{2+} process was more energy effective than the VUV process. Accordingly, the VUV/Fe^{2+} process is a technically efficient and energy-effective process for high-rate degradation and mineralization of such emerging water contaminants as antibiotics.

The surface morphology and crystal structure of the synthesized nanophotocatalyst usually play vital roles in enhancing the photocatalytic properties and activity of catalysts. Sulfate-functionalized Fe_2O_3/TiO_2 nanotubes utilized as visible-light-active heterogeneous photo-Fenton catalysts were synthesized by a solvothermal and acid impregnation method, as shown in Fig. 2.4 (Han et al. 2017). The authors reported that the temperature maintained in the hydrothermal process in the synthetic process produced an obvious effect on the morphology and structure of prepared samples with transformation from nanotubes to nanowires. Substantial dispersion of Fe_2O_3 nanoparticles into the highly porous TiO_2 nanotubes

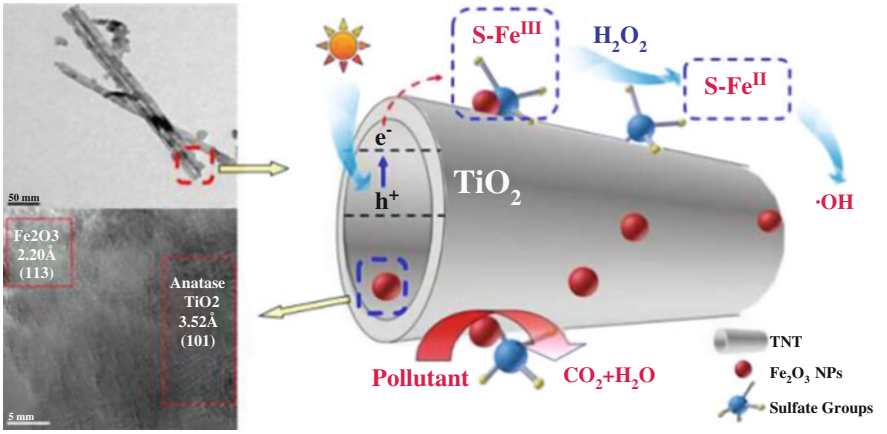

Fig. 2.4 Use of sulfate-functionalized Fe_2O_3/TiO_2 nanotubes as visible-light-active heterogeneous photo-Fenton catalysts. *e–* electron, *h+* hole, *NP* nanoparticle, *TNT* 2,4,6-trinitrotoluene. (Reproduced from Xu et al. (2015), with permission)

was successfully achieved, which was beneficial to the transfer of photogenerated electrons between the (101) planes in anatase TiO_2 and (113) planes in α-Fe_2O_3. With the sulfate group functionalized into the structure of the Fe_2O_3/TiO_2 nanotubes, the photocatalytic efficacy was significantly enhanced by the increases in light absorption and surface acidity. The prepared sulfated Fe_2O_3/TiO_2 nanotubes, with strong synergistic effects, had remarkable catalytic activity in a wide pH range of 4.0–10.0 and exhibited excellent stability and reusability, presenting good potentiality for application in environmental and energy fields.

Fe_3O_4 NPs have been considered a promising and efficient photo-Fenton agent for various kinds of pollutants. Moreover, they have been coupled with diverse kinds of nanoparticles and utilized as a photo-Fenton catalyst. The main objective of a study by Xu et al. was to compare the effectiveness of a MoS_2/Fe_3O_4 nanocomposite for visible-light photocatalytic, Fenton-like catalytic, and photo-Fenton-like catalytic degradation of a rhodamine B (RhB) dye solution. The authors reported that the magnetic nanocomposite magnetite nanoparticles (Fe_3O_4 NPs) and molybdenum disulfide microspheres (MoS_2) were successfully synthesized by a hydrothermal route. The effects of the Fe_3O_4 to MoS_2 ratio and the reaction time on the shape and properties of the magnetic nanocomposite were investigated in detail (Xu et al. 2015). The photocatalytic activity results demonstrated that the Fe_3O_4 nanoparticles could bind well to the MoS_2 microspheres when the concentration of Fe_3O_4 NPs was about 10 mg/L and the reaction time was about 18 h. The visible-light photocatalytic, Fenton-like catalytic, and photo-Fenton-like catalytic performances of the as-prepared MoS_2/Fe_3O_4 nanocomposite were comparatively evaluated by degradation of RhB. It was found that the MoS_2/Fe_3O_4 nanocomposite exhibited excellent photo-Fenton-like catalytic degradation performance. The ease of synthesis and separation, coupled with the excellent removal of organic dyes, make the MoS_2/Fe_3O_4 nanocomposite an attractive catalyst for the purification of contaminated water.

Ferrite nanoparticles play a phenomenal role in the photocatalytic Fenton-type reaction for the degradation of organic pollutants. A series of copper oxide (CuOx)–decorated $ZnFe_2O_4$ samples were synthesized by a hydrothermal method and investigated as a catalyst for the photocatalytic and Fenton-like degradation of orange II (Zhao et al. 2017). The active species and catalyst active sites in the two processes were also studied. It was found that the introduction of CuOx significantly enhanced the photocatalytic and Fenton-like performance of $ZnFe_2O_4$. More specifically, $ZnFe_2O_4$–Cu_3 synthesized with a Cu to Zn ratio of 3:7 exhibited very high Fenton-like activity in the pH range of 5–9. The excellent photocatalytic efficacy of $ZnFe_2O_4$–Cu_3 may be due to formation of heterojunction between $ZnFe_2O_4$ and Cu_2O, which could possibly improve the charge separation efficiency of the photogenerated charge carriers. Complete degradation of orange II dye was mainly attributed to slower recombination of the photogenerated charge carriers. The main active reactive oxygen species (ROS) in the Fenton-like reaction was $O_2^{-}\bullet$, and the surface $\equiv Cu^{2+}$ with higher redox ability should have been the active site for H_2O_2 activation despite its lower surface content than those of $\equiv Cu^{+}$, $\equiv Fe^{2+}$, and $\equiv Fe^{3+}$. Finally, a possible pathway for orange II degradation was proposed according to the LC–MS result.

The Fenton catalysts H_2O_2 and Fe^{2+} have been well known for a long time and are employed for environmental remediation through a Fenton mechanism involving ROS. The logistics of storage and transportation of H_2O_2 limits its applications. Moreover, semiconductor photocatalysts have been utilized extensively for environmental remediation involving ROS through irradiation of light. There is a need to develop a single catalyst that combines both Fenton and photocatalytic mechanisms. With this objective, we designed and synthesized a new catalyst, based on ZnO_2/Fe^{2+}, that is useful for environmental remediation. This single catalyst, which exhibits simultaneous Fenton–photocatalytic reactions, produces H_2O_2 in situ from the peroxide of ZnO_2 (solid), thus avoiding storage and transportation issues. This new catalyst works in the dark (a Fenton-like mechanism), under visible light (a photo-Fenton mechanism), and under UV light (a photocatalytic mechanism). Further, its performance is better than that of the known Fenton catalyst (Prasanna and Vijayaraghavan 2017).

The possibilities of recyclability of the photo-Fenton catalyst have been considered for long-term use/runs against organic dyes and pollutants. Uniform and magnetic recyclable mesocrystalline Zn–doped Fe_3O_4 hollow submicrospheres (HSMSs) were successfully synthesized via a simple one-pot solvothermal route and used as an efficient heterogeneous photo-Fenton catalyst (Nguyen et al. 2017). The physical characterization demonstrated highly porous magnetite nanocrystal building blocks assembled by oriented attachment with Zn-rich surfaces. Fe_3O_4 mesocrystals were assembled by oriented nanocrystals and a Zn-rich amorphous shell grew on the surfaces. Then, the Zn gradually diffused into the Fe_3O_4 crystals to form Zn-doped Fe_3O_4 due to the Kirkendall effect with an increase in the reaction time. Meanwhile, the inner nanocrystals dissolved and the outer particles grew larger, owing to the Ostwald ripening process, leading to formation of a hollow structure with a porous shell. The Zn-doped Fe_3O_4 HSMSs exhibited high and stable photo-Fenton activity for degradation of RhB and cephalexin under visible-light irradiation in the presence of H_2O_2, which resulted from their hollow mesocrystal structure and Zn doping. They could be easily separated and reused through application of an external magnetic field. The results suggested that the as-obtained magnetite hollow mesocrystals could be a promising catalyst in the photo-Fenton process.

2.2.3 *Ozonation*

Photocatalysis and ozonation processes have remarkable potential in wastewater treatment, though use of photocatalysis alone for wastewater treatment is considered a slow process, and ozonation is highly selective. Therefore, combination of these two processes might overcome these drawbacks.

Hence, a photocatalytic ozonation process was developed for complete mineralization of organic pollutants with potential practical applicability. Metal ion (Ag, Cu, and Fe)–doped titanium dioxide (TiO_2) nanoparticles were employed for

photocatalytic ozonation of phenol solutions and secondary municipal wastewater under visible-light illumination (Mecha et al. 2016). An extensive product analysis confirmed the complete degradation, and different concentrations of phenol in the degradation were monitored using dissolved organic carbon (DOC), chemical oxygen demand (COD), and UV absorbance (UV254), with the data modeled using pseudo-first-order kinetics. Synergy index values between 1.03 and 4.31 were obtained between ozonation and photocatalysis, resulting in faster degradation of organic contaminants by use of UV–Vis and solar photocatalytic ozonation than by photocatalysis and ozonation alone. The treated water satisfied South African water treatment standards in terms of COD, phenol, and DOC levels. The use of solar radiation makes the process environmentally benign and less costly, and therefore it is of major significance.

Radwan et al. (2016) developed a fixed-bed flow-through ultraviolet A/light-emitting diode (UVA-LED) photoreactor for comparison of the efficiency of ozone, photocatalysis, and photocatalysis–ozone degradation and mineralization of two pure pesticides—2,4-dichlorophenoxyacetic acid (2,4-D) and 2-methyl-4-chlorophenoxyacetic acid (MCPA)—and a commercial one, Killex. For the degradation of the parent compounds, ozone-based processes were more effective, whereas for mineralization, photocatalytic processes were more effective. Photocatalytic ozonation was very effective for the processes of both degradation and mineralization of the parent compounds. The rates of photocatalytic ozonation and mineralization were higher than the summation of the corresponding rates achieved by ozonation alone and photocatalysis alone, indicating a symbiotic relationship. Overall, the photocatalytic ozonation process with fixed-bed TiO_2 reduces the time needed for the degradation and mineralization of the pesticides, reduces the costs of powder catalyst separation, and overcomes the reduced efficiency of immobilized catalysts, making the process quite attractive for practical applications.

The efficiencies of AOPs—viz., electron beam radiolysis in the presence of $K_2S_2O_8$, gamma radiolysis in the presence of $K_2S_2O_8$, photocatalysis, photocatalysis in the presence of $K_2S_2O_8$, ozonolysis, and ozonolysis in the presence of $K_2S_2O_8$—were systematically investigated for the treatment of modified (pH adjusted with H_2SO_4) simulated textile dye wastewater (MSTDWW) containing reactive red 120. The efficiencies of these AOPs were investigated in terms of their oxygen-equivalent chemical oxidation capacity, and the costs of energy and other ancillary inputs. The smallest amount of oxidant was required by electron beam radiolysis, in comparison with the other AOPs studied here, to achieve the same extent of mineralization of MSTDWW. To the best of our knowledge, this study was the first to report an approach to calculate the equivalent cost of gamma radiolysis in comparison with other AOPs consuming electrical energy. Among these AOPs, electron beam treatment of MSTDWW in the presence of $K_2S_2O_8$ had the lowest effective cost.

The main objective of this work was extensive investigation of *N*,*N*-diethyl-meta-toluamide (DEET) degradation by a photocatalytic ozonation process, using WO_3 in suspension and visible-light radiation (wavelength $\geq$390 nm), as illustrated in Fig. 2.5 (Mena et al. 2017). This combined process has been shown to be an efficient treatment for the complete mineralization of organic contaminants; HO• radicals

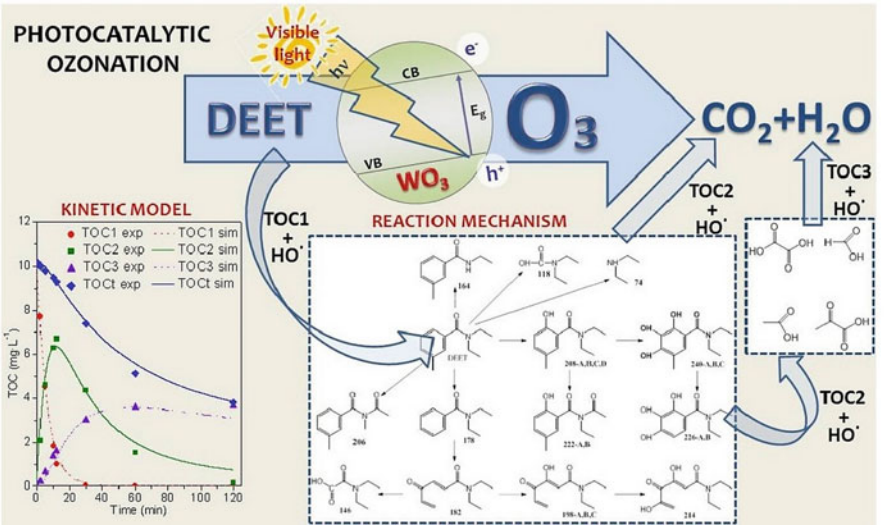

Fig. 2.5 Photocatalytic ozonation. *DEET N,N*-diethyl-meta-toluamide, *exp* experimental, *sim* simulated, *TOC1* total organic carbon. (Reproduced from Mena et al. (2017), with permission)

were the active main species involved. Moreover, it was observed that different oxidation products were identified by LC–MS and ion chromatography analyses, and the evolution of their relative abundances with the reaction time was established. The efficiency of photocatalytic ozonation treatment was demonstrated not only by the DEET depletion rate but also by the evolution of the main intermediate species and mineralization.

It was well known that intermediates may be formed during the photo-Fenton reaction, but all of the large intermediates that initially formed were completely removed within a 60 min reaction time. Only short-chain organic acids with much lower toxicity remained in the solution at concentrations in agreement with the mineralization degree achieved (up to 60% in 2 h). A reaction mechanism of photocatalytic ozonation of DEET involving different chemical reaction steps, with the final formation of short-chain organic acids and mineralization to CO_2, was proposed. A lumped kinetic model based on TOC and a hydroxyl radical reaction was developed to simulate the evolution of DEET, the intermediates, and the short-chain organic acids in terms of TOC to provide a simplified approach for this process.

2.2.4 Sonolysis

The textile industry is currently manufacturing around 30 million tons of products annually. This production is accompanied by 700,000 tons of different dyes. The use of dyes has generated environmental challenges downstream, and the current

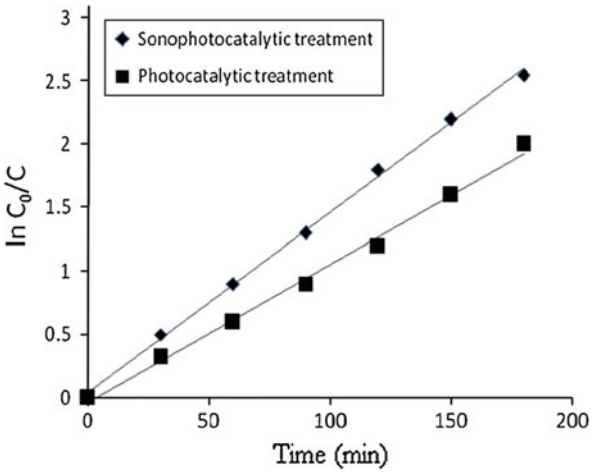

Fig. 2.6 Sonophotocatalytic and photocatalytic kinetics in the degradation of alizarin. (Reproduced from Verma et al. (2014), with permission)

methods used in water treatment (e.g., biological treatment) are inefficient for dye degradation. Therefore, different approaches are being implemented, such as AOPs for the treatment of toxins and bioresistant organic pollutants (Legrini et al. 1993; Mills et al. 1993).

Verma et al. studied the degradation of alizarin (a model reactive dye), using photocatalytic and photochemical oxidation processes (Verma et al. 2014). The effect of sonochemical processing on the dye degradation was also investigated. The authors highlighted the effects of pH, TiO_2 loading, and oxidant dose, where the trends agreed with those reported in the literature (Hachem et al. 2001). The degradation levels were 88% and 94% with the photocatalyst and sonophotocatalyst treatments, respectively, under optimum testing conditions. This was accompanied by a decrease in the COD. This study highlighted the synergic effect of sonophotocatalysts for the degradation of dyes (Fig. 2.6). This approach could be used in conjunction with biological treatment of organic pollutants in water.

Kaur and Singh investigated the degradation of reactive red 198 dye by dye-sensitized TiO_2 (Kaur and Singh 2007). The rate of dye degradation varied as a function of the photocatalysis, sonocatalysis, and sonolysis under visible light. The authors also investigated the effects of different reaction conditions (i.e., the pH, concentration of substrate, and catalyst loading). Ultrasonic activation is responsible for splitting of H_2O_2 produced by photocatalysis and sonolysis, resulting in the production of high-oxidation species such as superoxide (O_2^-) and singlet oxygen ($^1O_2$). The synergic effect of sonophotocatalysis could be attributed to the ultrasound breaking the catalyst particles, in which the surface area increases, leading to an increase in the number of reactive radicals. The increase in radical species thus increases the degradation rate over dye-sensitized TiO_2 (Lu et al. 2002; Shirgaonkar and Pandit 1998).

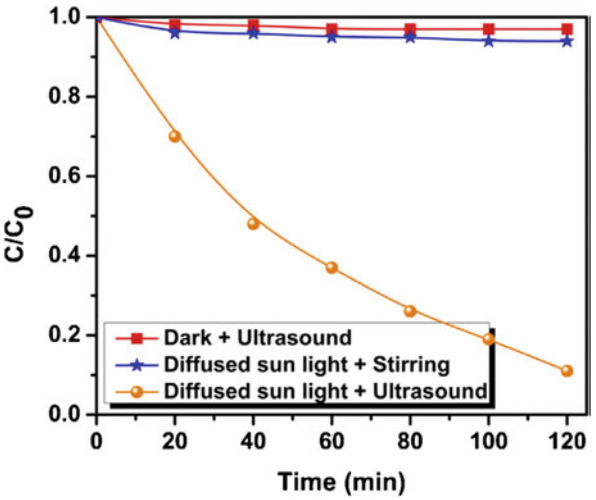

Fig. 2.7 Degradation of methyl orange by different processes, showing the synergic effect of the combination of sonophotocatalysis. (Reproduced from Babu et al. (2015b), with permission)

Babu et al. studied the degradation and mineralization of methyl orange over CuO–TiO_2 supported on an rGO photocatalyst (Babu et al. 2015b). The study showed synergy in the combination of sonochemical and photocatalyst treatment, with a tenfold increase in degradation under sunlight, as shown in Fig. 2.7. The inclusion of rGO doubled the activity of CuO–TiO_2; this was attributed to the ability of rGO to facilitate transfer, storage, and shuttling of electrons, leading to separation of electron–hole pairs. This was confirmed by photoluminescence. Furthermore, the authors highlighted the degradation of methyl orange mediated by hydroxyl radicals, as confirmed by LC–MS. Moreover, similar degradation results were obtained with methyl blue and 4-chlorophenol; these results suggested versatility of the system.

The enhanced activity of sonophotocatalysis versus sonocatalysis was also highlighted by Gobara et al., who studied the degradation of erichrome black T dye with a titanium-modified mesoporous silica (Ti–SBA-15) catalyst (Fig. 2.8) (Gobara et al. 2016). The results obtained showed 88.7% degradation of erichrome black T dye after 70 min. Furthermore, the kinetic studies showed that the process had a pseudo-first-order reaction mechanism with a 27.4×10^{-3} rate constant. An increase in the concentration of TiO_2 in the catalyst also led to improved activity of the catalyst in sonocatalysis and sonophotocatalysis. This was further confirmed by the low activity of a pure SBA-15 catalyst in the degradation of erichrome black T dye.

Mosleh et al. used a novel photocatalyst (Ag_3PO_4/Bi_2S_3–HKUST-1–MOF) for the sonophotocatalytic degradation of two dyes: trypan blue (TB) and vesuvine (VS). The study investigated the reaction parameters (i.e., the dye concentration, irradiation time and sonication, flow rate, photocatalyst dosage, and pH) (Mosleh et al. 2016). These parameters were optimized using central composite design (CCD) along with desirability function (DF). Under optimum conditions the sonophotocatalyst degradation rates were 98.44% for TB and 99.36% for VS. Moreover, a kinetic model of the system clearly showed the synergic effect of sonophotocatalysis in comparison with sonocatalysis and photocatalysis (Fig. 2.9).

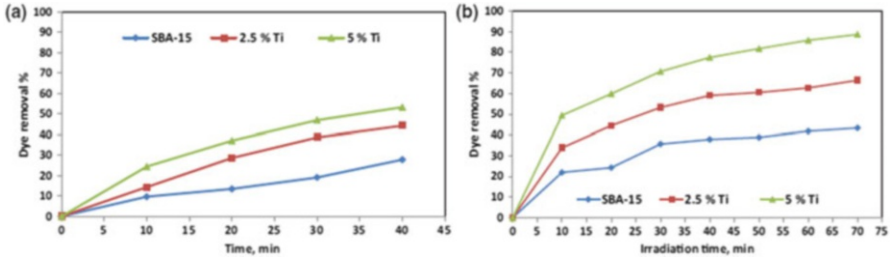

Fig. 2.8 Effect of Ti loading on mesoporous silica (*SBA-15*) on dye removal in an aqueous solution by sonocatalysis (**a**) and sonophotocatalysis (**b**). (Reproduced from Gobara et al. (2016), with permission)

2.2.5 Sono-Fenton Systems

Barrera-Salgado et al. used Fe_2O_3/Al_2O_3 as a catalyst for the degradation of acid green 50 (AG50) textile dye (Barrera-Salgado et al. 2016). The study focused on using coupled Fenton processes such as Fenton, photo-Fenton, sono-Fenton, and sono-photo-Fenton processes, in addition, to optimize the reaction conditions (e.g., the iron content, annealing temperature, pH, and initial AG50 concentration). The degradation of organic pollutants by the Fenton process involves formation of hydroxyl radicals by activation of H_2O_2 (as shown in Eqs. 2.1, 2.2, 2.3, 2.4, 2.5 and 2.6), and the coupling of the Fenton process with photo- and sono- processes results in increases in radical species (as shown by Eqs. 2.7 and 2.8). The results of the study (Fig. 2.10) showed the synergic effect of the coupled photo-sono-Fenton process for TOC removal. The most influential reaction parameter was the reaction pH.

$$Fe^{2+} + H_2O_2 \rightarrow Fe^{3+} + OH^- + OH^{\bullet} \tag{2.1}$$

$$Fe^{2+} + OH^{\bullet} \rightarrow Fe^{3+} + OH^- \tag{2.2}$$

$$OH^{\bullet} + H_2O_2 \rightarrow H_2O + OOH^{\bullet} \tag{2.3}$$

$$Fe^{3+} + H_2O_2 \rightarrow Fe^{2+} + H^+ + OOH^{\bullet} \tag{2.4}$$

$$Fe^{3+} + R^{\bullet} \rightarrow Fe^{2+} + R^+ \tag{2.5}$$

$$Fe^{3+} + OOH^{\bullet} \rightarrow Fe^{2+} + H^+ + O_2 \tag{2.6}$$

$$Fe^{III}(OH)^{2+} \xrightarrow{h\nu} Fe^{2+} + OH^{\bullet} \tag{2.7}$$

$$H_2O +))) \rightarrow OH^{\bullet} + H^{\bullet} \tag{2.8}$$

Chitra et al. studied the degradation of ethylenediaminetetraacetic acid (EDTA), using sono-, photo- and sono-photo-Fenton processes (Chitra et al. 2013). The degradation of EDTA is key in liquid waste treatment for several reasons such as

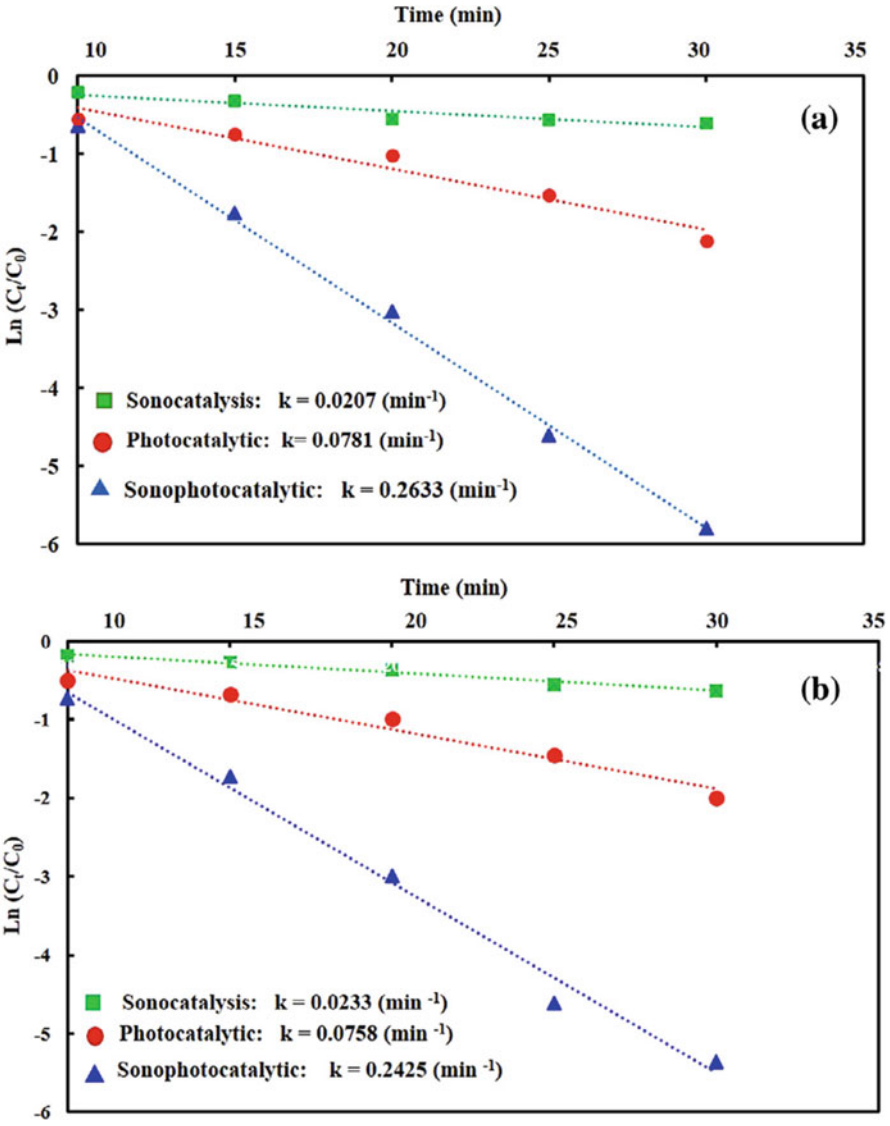

Fig. 2.9 Effects of sonocatalysis, photocatalysis, and sonophotocatalysis processes on the rate constant (in the Langmuir–Hinshelwood kinetics model) in optimum conditions. (Reproduced from Mosleh et al. (2016), with permission)

EDTA complexation with cations that negatively affect their removal, and leachability of the cations from immobilized waste. The results obtained (Fig. 2.11) showed the synergic effect of the combination of sono- and photo-Fenton processes in the degradation of EDTA. The photo-Fenton process increases the

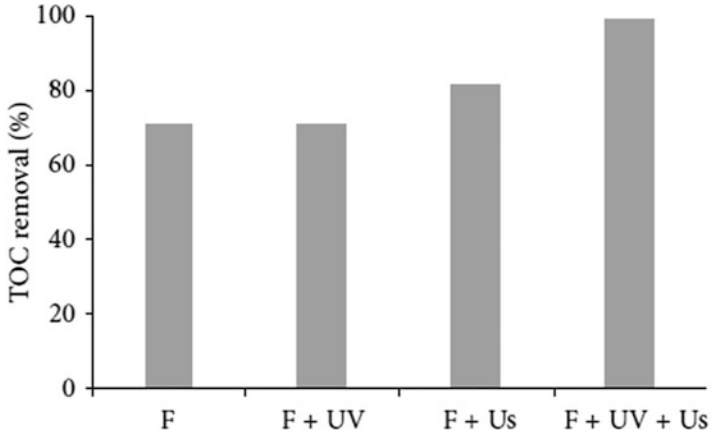

Fig. 2.10 Effects of different catalytic processes for removal of total organic carbon (*TOC*). *F* Fenton, *Us* ultrasound, *UV* ultraviolet. (Reproduced from Barrera-Salgado et al. (2016), with permission)

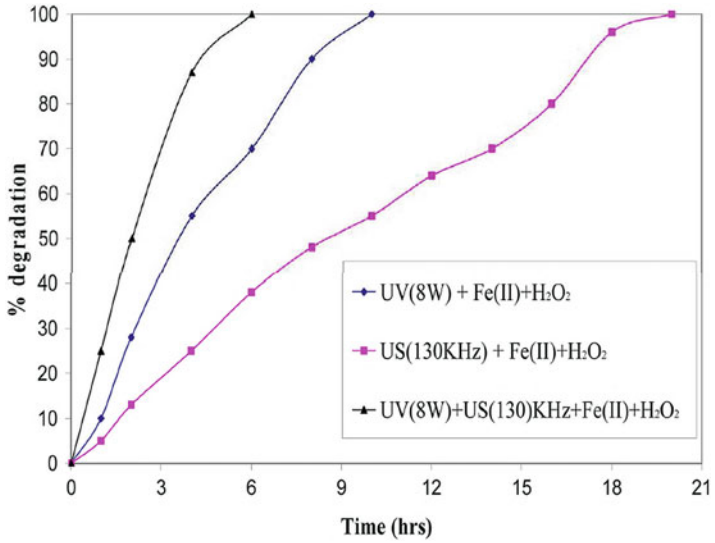

Fig. 2.11 Ethylenediaminetetraacetic acid (*EDTA*) degradation via different catalytic processes as a function of time. *US* ultrasound, *UV* ultraviolet. (Reproduced from Chitra et al. (2013), with permission)

numbers of hydroxyl radicals formed and the development of a recycle mechanism in which Fe^{3+} is photoreduced to Fe^{2+}, which, in turn, reacts with H_2O_2 to form the hydroxyl radicals. Furthermore, UV liquid forms hydroxyl radicals by direct photolysis of $Fe(OH)^{2+}$. In the case of the sono-Fenton process, radicals (e.g.,

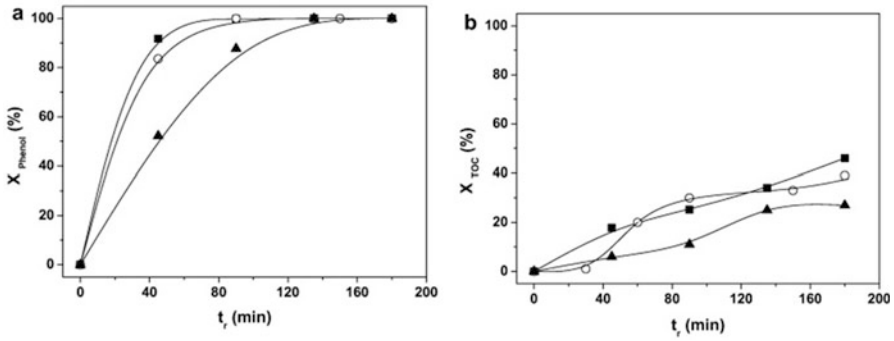

Fig. 2.12 Effects of different reaction parameters on phenol degradation by different catalytic processes. *TOC* total organic carbon. (Reproduced from Segura et al. (2009), with permission)

H•, •OH, and HOO•) are formed by the sonolysis of water, and these radicals are utilized in the degradation of organic pollutants (Adewuyi 2001). Therefore, the combination of photo- and sono-Fenton processes results in an increase in the number of active radicals and results in a higher level of EDTA degradation, leading to the synergic effect of combined sono- and photo-Fenton processes.

Segura et al. investigated the degradation of a phenolic aqueous solution over a H_2O_2/Fe_2O_3–SBA-15 catalyst, utilizing separate and combined sono- and/or photo-Fenton processes (Segura et al. 2009). The results (Fig. 2.12) showed that the phenol degradation and TOC conversion obtained during the sono-photo-Fenton process were superior to those achieved by the separate sono-Fenton and photo-Fenton processes. The surface area of the particles was increased by the ultrasound cavitation effect. Such an increase in the particle surface area results in an increase in the number of active sites for the production of radicals during the photo-Fenton process (Li Puma et al. 2007; Nikolopoulos et al. 2006). Therefore, sequential use of sono- and photo-Fenton processes led to a synergic effect with improved phenol degradation and TOC conversion. These results were in agreement with those described by Babuponnusami and Muthulukumar (Babuponnusami and Muthukumar 2011) for the degradation of phenol by sono-, photo-, and sono-photo-Fenton processes. The latter study showed the synergic effect of the sono-photo-Fenton process in different reaction conditions that were reported to affect the catalyst activity, such as the H_2O_2 concentration (Guo et al. 2005), Fe^{2+} concentration (Guo et al. 2005), pH (Ranjit et al. 2008), and phenol concentration (Wang et al. 1999). The synergic effect led to a reduction in the Fe^{2+} and H_2O_2 concentrations by 30–50% and 12.5%, respectively. Furthermore, a satisfactory correlation between the experimental data and the data predicted by the kinetics model was shown.

The synergic effect of the photo-sono-Fenton process for organic pollutant removal was further highlighted by a study carried out by Dukkanci (Dukkanci 2016). The study used a perovskite $LaFeO_3$ catalyst for photo-sono-Fenton degradation of bisphenol A (BPA), since the presence of Fe^{3+} results in production of

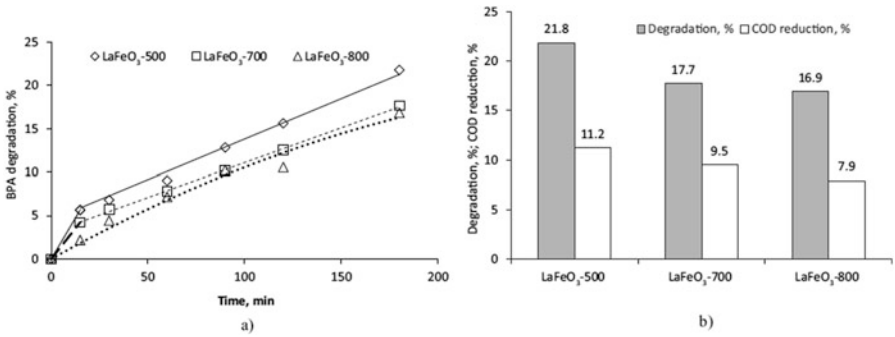

Fig. 2.13 Effects of $LaFeO_3$ calcination temperature on bisphenol A (*BPA*) degradation time (**a**) and chemical oxygen demand (*COD*) (**b**). (Reproduced from Dukkanci (2016), with permission)

radicals; therefore, the catalyst acts as a Fenton-like catalyst (Ünnü et al. 2016). The effect of the calcination temperature on the catalyst activity is shown in Fig. 2.13. Calcination at 500 °C provided the highest activity, which was explained by changes in the particle size and surface area. An increase in the calcination temperature led to an increase in particle size, which led to a decrease in surface area. This, in turn, decreased BPA degradation and the COD because of the decrease in the numbers of accessible catalyst particles resulting from the decrease in surface area and the increase in particle size.

2.2.6 Antimicrobial Activity

The importance of effective and environmentally friendly disinfection methods or processes is immense because of the large number of deaths associated with, or resulting from, infected water and other sources (Ganguly et al. 2018; Shannon et al. 2008). Therefore, research has been focused on development and optimization of effective and eco-friendly disinfection processes. Photocatalytic disinfection is one of the most promising processes because of the greenness of this process (Jiang et al. 2017; Ravelli et al. 2009). Ganguly et al. (2018) reviewed key aspects of photocatalysis as a disinfectant, such as its fundamentals, mechanisms, kinetics, and advances. The different mechanisms of inactivation of microorganisms by the photocatalyst include generation of ROS, which leads to degradation of enzymes (e.g., coenzyme A) (Matsunaga et al. 1985); destruction of cell membranes or walls, which leads to leakage of key components (e.g., K^+ ions) (Saito et al. 1992); and destruction of the phospholipid component in the cell wall by ROS interaction. Also highlighted are the different kinetic models (e.g., the Chick–Watson, Chick's, and delayed Chick–Watson models) available for this process and how different reaction parameters (Fig. 2.14) influence the kinetics and the activity of antimicrobial activity by photocatalysis.

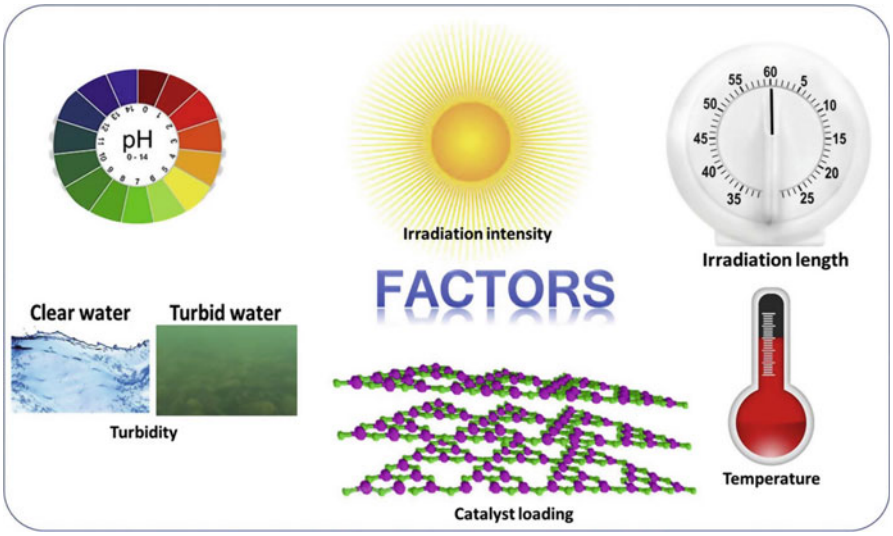

Fig. 2.14 Process parameters influencing the mechanism of antimicrobial activity. (Reproduced from Ganguly et al. (2018), with permission)

Dhanasekar et al. investigated the antimicrobial activity of copper-doped TiO_2 nanoparticles/rGO (Dhanasekar et al. 2018). The study used two Gram-positive bacteria (*Staphylococcus aureus* and *Streptococcus oralis*) and two Gram-negative bacteria (*Escherichia coli* and *Pseudomonas aeruginosa*). The introduction of copper improved the activity in visible light and antimicrobial activity, and the inclusion of rGO enhanced the charge transfer during microbial degradation through photocatalysis, in comparison with TiO_2 alone. These results were determined by minimum inhibitory concentration and zone of inhibition analyses (Fig. 2.15). Furthermore, the introduction of Cu_2O–TiO_2 into polyvinyl alcohol (PVA) polymer showed superior antimicrobial activity (Figs. 2.16 and 2.17) in comparison with TiO_2 alone; this makes the material a suitable candidate for packaging material to replace the less effective TiO_2.

Ananpattarachai et al. investigated inactivation of *E. coli* and *S. aureus* by a photocatalytic process using undoped, Ni-doped, and N-doped TiO_2 as photocatalysts (Ananpattarachai et al. 2016). The study showed the superior antibacterial activity of N-doped TiO_2, which stemmed from N-doping (in comparison with Ni-doping) decreasing the energy gap, leading to more absorption of visible light, which, in turn, produced more radical OH groups and ROS. This system was shown to be more effective against Gram-positive bacteria (*S. aureus*) than against Gram-negative bacteria (*E. coli*). This conclusion was drawn from analysis of the time required for complete inactivation of *S. aureus* and *E. coli* (360 and 420 min, respectively, in the presence of visible light). Moreover, the inactivation rates also followed a similar trend. These results highlighted the importance of visible light and materials capable of visible-light absorption in bacterial degradation.

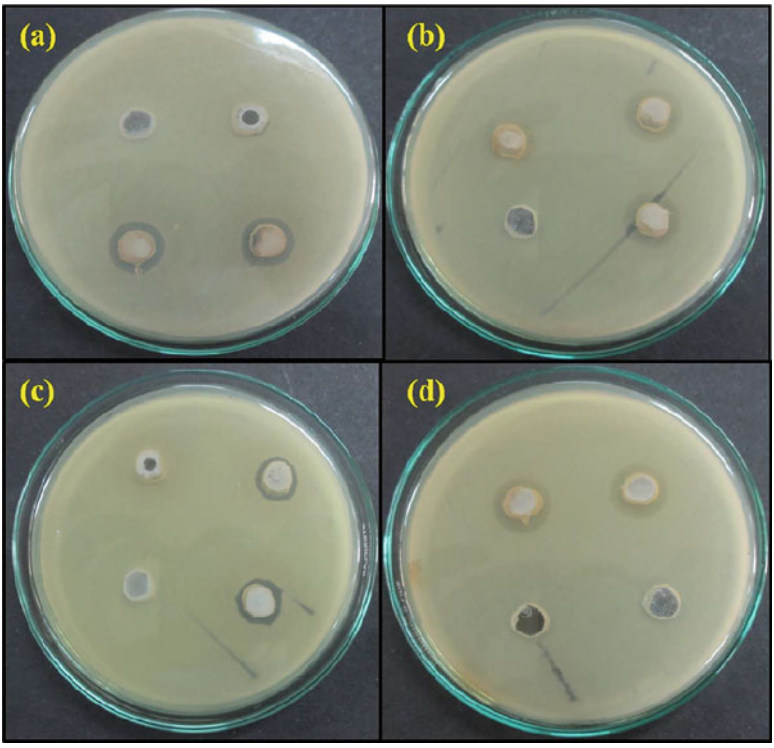

Fig. 2.15 Zones of inhibition with use of a Cu_2O–TiO_2/rGO nanocomposite (**a**) and (**b**) versus TiO_2 nanoparticles alone (**c**) and (**d**) against *Staphylococcus aureus* (**a**, **c**) and *Pseudomonas aeruginosa* (**b**, **d**). *rGO* reduced graphene oxide. (Reproduced from Dhanasekar et al. (2018), with permission)

Joost et al. used a nano-TiO_2 film for inactivation of *E. coli*. Their study used two techniques to investigate the efficiency of the photocatalytic nano-TiO_2 film: viable bacterial cells and crucial fatty acids in the bacteria plasma membrane. The nano-TiO_2 film and a UVA light source resulted in total inactivation of *E. coli* within 20 min (Fig. 2.17) (Joost et al. 2015). SEM images showed changes in the bacterial structure/morphology and the appearance of a halo surrounding the bacterial cell, which could have been due to leakage of organic material or ions (e.g., K^+) from the bacteria cell (Foster et al. 2011; Leung et al. 2008; Sunada et al. 2003). In addition, the study showed a clear correlation between the crucial fatty acid decomposition and bacterial inactivation, which could be key for morphological changes and crucial component leakage from the bacterial cell (*E. coli*). These two factors could lead to cell death, and this is supported by the fact that fatty acid decomposition starts after 10 min of UVA exposure.

Khan et al. reported a novel and environmentally friendly synthesis method for silver nanoparticles (Ag NPs) in which a reductant and nanoparticle stabilizer was extracted from *Caruluma edulis* (Khan et al. 2016). The antibacterial study of the

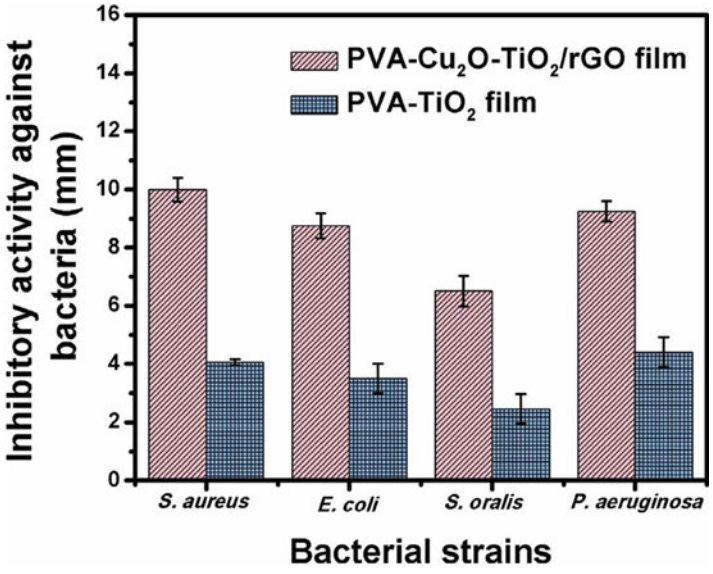

Fig. 2.16 Inhibitory activity of PVA–TiO_2 and PVA–Cu_2O–TiO_2/rGO nanocomposites against *Staphylococcus aureus*, *Escherichia coli*, *Streptococcus oralis*, and *Pseudomonas aeruginosa*. *PVA* polyvinyl alcohol, *rGO* reduced graphene oxide. (Reproduced from Dhanasekar et al. (2018), with permission)

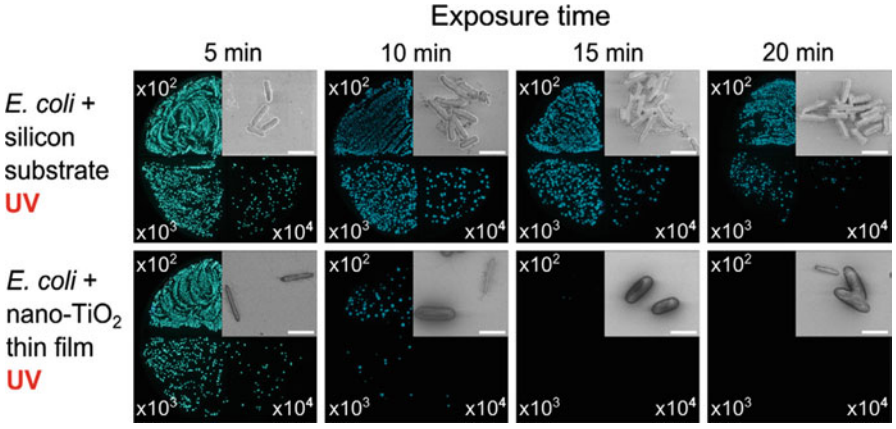

Fig. 2.17 Effect of nano-TiO_2 on bacteria as a function of time. *UV* ultraviolet. (Reproduced from Joost et al. (2015), with permission)

Ag NPs was carried out using zone of inhibition and minimum inhibitory concentration analyses of inactivation of *S. aureus, Bacillus subtilis*, and *E. coli.* The zone of inhibition study (Table 2.2) showed that Ag NPs have a larger zone of inhibition than the standard antibacterial agent cefalexin. This superior antibacterial activity could be due to the positively charged silver nanoparticles reacting with the

Table 2.2 Zone of inhibition effects of silver nanoparticles on different microorganisms

Microorganism	Zone of inhibition (mm)	
	Silver nanoparticles (± SD)	Standard (± SD)
Staphylococcus aureus	17 ± 0.3	10 ± 0.5
Bacillus subtilis	19 ± 0.4	11 ± 0.6
Escherichia coli	16 ± 0.2	9 ± 0.3

Reproduced from Khan et al. (2016), with permission
Standard = cefalexin; 35 °C; 20–24 h; 50 μL of 8 mg/mL
SD standard deviation

Table 2.3 Minimum inhibitory concentrations (*MICs*) of silver nanoparticles for different microorganisms

Bacterial strain	MIC (μg)
Staphylococcus aureus	125
Bacillus subtilis	125
Escherichia coli	250

Reproduced from Khan et al. (2016), with permission
35 °C; 20–24 h

negatively charged biomacromolecular bacteria cell component (e.g., phosphate in enzymes) and with the bacteria's nucleic acid. These interactions would lead to structural changes in the bacterial membrane and cell wall, resulting in the death of the bacterial cell (Nirmala et al. 2011). The minimum inhibition concentration study (Table 2.3) showed the lethality of silver nanoparticles for the different bacterial types. This lethality was attributable to silver particles interfering with the electron transport chain, DNA replication, and expression of ribosomal and other proteins (Gao et al. 2002; Saikia et al. 2010; Yamanaka et al. 2005).

2.2.7 Nanoadsorbents

Heavy metals pose risks for human beings and animals even at low levels of exposure. Most heavy metals are highly soluble in water and can spread into the ecosystem without difficulty. They bind with essential cellular components such as proteins, enzymes, and nucleic acids, and restrict the functioning of living organisms and the human body (Khan et al. 2010). Therefore, heavy metals must be removed completely, but this is a challenging task for researchers and scientists (Awual et al. 2015). Important sources of heavy metals are the mining industry, metal plating industry, sewage irrigation, electronics industry, and production of fertilizers, pesticides, and a variety of plastics (Ahmad et al. 2015). With increases in industrialization, the amounts of heavy metals in ecosystems also increase.

Recently, a number of methods have been used for efficient removal of heavy metals from ecosystems, such as chemical precipitation, ion exchange, coagulation, reverse osmosis, electrochemical processes, solvent extraction, and adsorption (Fu and Wang 2011). Among these methods, adsorption offers reversibility, low

costs, ease of operation, and high efficiency. Therefore, the adsorption process is an important technique for the removal of heavy metals from ecosystems.

For this purpose, various adsorbents are available, such as nanosized metal oxides (NMOs), including nanosized ferric oxides, manganese oxides, aluminum oxides, titanium oxides, magnesium oxides, and cerium oxides. Uses of carbon nanotubes (CNTs) (Ihsanullah et al. 2016), chitosan (Ahmad et al. 2016), modified iron oxide (Sigdel et al. 2016), graphene oxide (GO) (Tadjarodi et al. 2016), complexing membranes (Guan et al. 2016), and other novel adsorbents have been reported for heavy metal removal. Sigdel et al. observed that As(III) and As(V) can be effectively removed by hydrous iron oxide–impregnated alginate beads (Sigdel et al. 2016). Thanawatpoontawee et al. reported that 90% of As(V) can be removed by iron-loaded zein beads (Thanawatpoontawee et al. 2016). However, although the developed adsorbents have high efficiency for removal of heavy metals, it can be reduced by the presence of competing ions. Because of their surface area, structure, and mechanical properties, graphene-based materials are excellent adsorbents for heavy metal removal (Chowdhury and Balasubramanian 2014; Cortés-Arriagada et al. 2016). Rao et al. (2009) observed that the synthesis of graphene-based adsorbents presents a significant challenge but also represents considerable progress for removal of heavy metals.

However, in many applications, surface modification is necessary, as pristine graphene may be ineffective in some specific applications such as adsorption of heavy metal ions (Cao and Li 2014). Consequently, graphene has been modified using various means such as oxides/hydroxides (Ren et al. 2013), chitosan-functionalized GO (Kumar and Jiang 2016), zinc peroxide–functionalized graphite (Uppal et al. 2016), and aluminum and iron–doped graphene (Cortés-Arriagada and Toro-Labbé 2016). In any application, consideration must be given to the available functional groups in the graphene that hold the active sites. Peng et al. (2017) reviewed graphene-based composites and highlighted the adsorption mechanisms and the operational parameters. So, use of graphene-based composites for removal of heavy metals or any other application is based on the available functional group in the graphene that hold the active sites (Fig. 2.18).

2.2.8 Inorganic Pollutant Removal

The photocatalytic reduction of heavy metals using nanophotocatalysts is of paramount important for reduction of heavy metal contamination in aquatic environments. Karthik et al. (2015) formularized a new kind of catalyst, 2-naphthol–functionalized TiO_2 nanoparticles, for photocatalytic reduction of Cr(IV) in an aquatic environment. The 2-naphthol–functionalized TiO_2 nanoparticles exhibited superior photocatalytic reduction efficiency in comparison with that of bare TiO_2. The enhancement of the photocatalytic efficacy might have been due to the extension of optical absorption caused by functionalization of 2-naphthol, resulting in a 400- to 500-nm peak on UV–Vis spectroscopy.

Fig. 2.18 Diethylenetriaminepentaacetic acid–modified magnetic graphene oxide. (Reproduced from Li et al. (2017), with permission)

Moreover, the highly porous nature of the 2-naphthol–functionalized TiO_2 nanoparticles could induce the adsorption of the substrate and improve the activity on BET analysis. In addition, the photogenerated electron transfer from 2-naphthol to TiO_2 (ligand-to-metal transfer) could significantly improve the photocatalytic performance in comparison with the bare TiO_2 counterpart. The photocatalytic reduction of Cr(IV) to Cr(III) using 2-naphthol–functionalized TiO_2 nanoparticles was strongly evidenced by atomic absorption spectroscopy (AAS); the initial and final solutions were tested using AAS to estimate the Cr concentrations, which were found to be 19.72 and 18.68 parts per million (ppm), respectively.

The use of sulfur (S)–decorated MoO_3 (S@MoO_3) nanorods for photocatalytic reduction of Cr(IV) to Cr(III) was described by Prabavathi et al. (2018), as represented in Fig. 2.19. Transmission electron microscopy (TEM) images of the S@MoO_3 nanorods clearly indicated that the S particles were deposited on the surface of the MoO_3 nanorods. Moreover, morphology is the one of the important parameters for the improvement of photocatalytic activity. Among various percentages of S-loaded MoO_3 nanorods, 1% S@MoO_3 nanorods exhibited excellent efficiency of visible-light photocatalytic activity in comparison with pure MoO_3, S, and other S@MoO_3 nanocomposites.

The enhanced effect of the photocatalytic reduction efficacy might have been due to the surface morphology and slow electron–hole recombination. Moreover, complete photocatalytic reduction was observed within 60 min of irradiation. The influence of the different inorganic salts/ions was investigated. The actively participating ROS were identified using a trapping experiment, which suggested that the superoxide radical anion was actively participating in the photocatalytic reduction reaction.

Photocatalytic reduction is not focused only on heavy metals; transition metals are also considered toxic in aquatic environments. Hence, an attempt has been made to treat polluted water containing a combination of inorganic contaminants by taking advantage of solar photocatalytic redox reactions (Singh and Chaudhary 2013). The

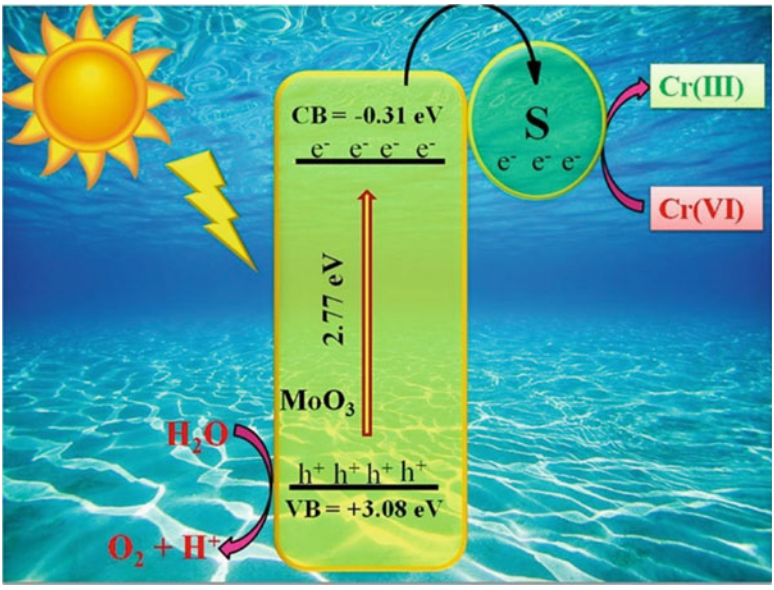

Fig. 2.19 Photocatalytic reduction of Cr(VI) to Cr(III) in the presence of sulfur-decorated MoO_3 ($S@MoO_3$) nanorods under visible-light irradiation. *CB* conduction band. (Reproduced from Prabavathi et al. (2018), with permission)

wastewater released from industries may contain substantial heavy metals, providing an opportunity to achieve simultaneous reduction of both of these wastewater components. Photocatalytic reduction reactions have also been attempted at different pH values to optimize the best reaction conditions. The toxic metals in the waste water were Cr, Ni, Zn, and Cu.

Dark adsorption reactions were performed by Singh and Chaudhary (2013), along with sunlight irradiation, to understand the process in detail. The results showed relatively good reductions of chromium and copper in comparison with the other two metals. Chromium was reduced slowly in the acidic pH range, while the other metals were reduced in the alkaline and neutral pH ranges. The results provided a cost-effective method for the removal of organic and inorganic pollutants simultaneously from polluted industrial wastewater through a photocatalytic reduction process.

Indirect photocatalytic reduction of arsenate to arsenite in an aqueous solution in the presence of TiO_2 as a photocatalyst under light illumination was investigated (Samad et al. 2018). Moreover, various hole scavengers (viz., methanol, ethanol, 2-propanol, formaldehyde, acetone, formic acid, and acetic acid) were utilized for detection of active participation of reactive oxidative species, as shown in Fig. 2.20.

Though direct photocatalytic reduction of arsenate to arsenite in the presence of TiO_2 was impossible, indirect reduction of As(V) was possible in the presence of sacrificial electron donors to form strongly reductive radicals. The addition of ethanol was very effective for indirect photocatalytic reduction of As(V) in an aqueous solution with a TiO_2 photocatalyst. The indirect photocatalytic reduction

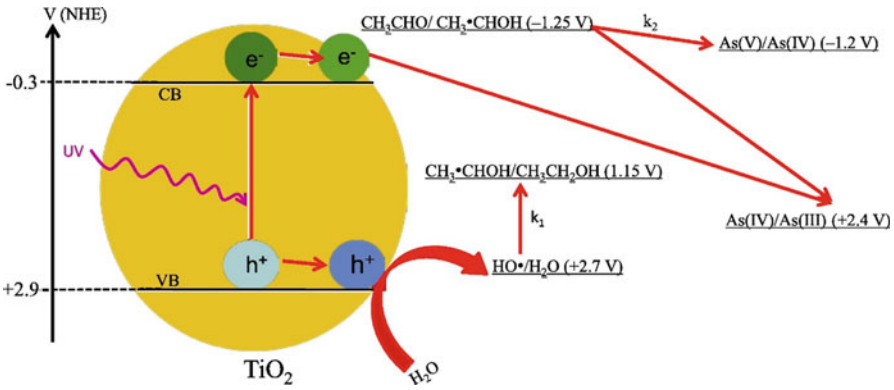

Fig. 2.20 Photocatalytic reduction of As(V) to As(IV) to As(III). *CB* conduction band, *NHE* normal hydrogen electrode, *VB* valence band. (Reproduced from Samad et al. (2018), with permission)

rate of As(V) may have been related to both the reaction rate constants of the hydroxyl radicals with the hole scavenger and the reactivities for the M^{-} radicals produced by the reaction of ^{-}OH with the hole scavenger.

The possibility of simultaneous recovery of heavy metals from wastewater and production of electricity was demonstrated by a novel photoelectrochemical cell (PEC) (Fig. 2.21). A photo anode of the cell was constructed that bore a nanoparticulate titania (TiO_2) film capped with a block copolymer [poly(ethylene glycol)-*b*-poly(propylene glycol)-*b*-poly(ethylene glycol)] hole scavenger, which consumed photogenerated holes, while the photogenerated electrons were transferred to a copper cathode, reducing the dissolved metal ions and producing electricity (Wang et al. 2017). Dissolved silver (Ag^{+}), copper (Cu^{2+}), hexavalent chromium (as dichromate $Cr_2O_7^{2-}$), and lead (Pb^{2+}) ions in a mixture (0.2 mM each) were removed at different rates, according to their reduction potentials.

Reduced Ag^{+}, Cu^{2+}, and Pb^{2+} ions produced metal deposits on the cathode electrode, which were mechanically recovered, while $Cr_2O_7^{2-}$ was reduced to the less toxic Cr^{3+} in solution. The cell produced a current density (J_{sc}) of 0.23 mA/cm^2, an open circuit voltage (V_{oc}) of 0.63 V, and a maximum power density of 0.084 mW/cm^2. A satisfactory performance of this PEC for the treatment of lead-acid battery wastewater was observed. The cathodic reduction of heavy metals was limited by the rate of electron–hole generation at the photoanode. The PEC performance decreased by 30% after nine consecutive runs, caused by progressive degradation of the photoanode.

2.2.9 Nanomembranes

It is well known that membrane fouling is one of the most severe problems restricting membrane-based separation technology for the treatment of wastewater. A photocatalytic nanofiltration membrane (NFM) with a self-cleaning property,

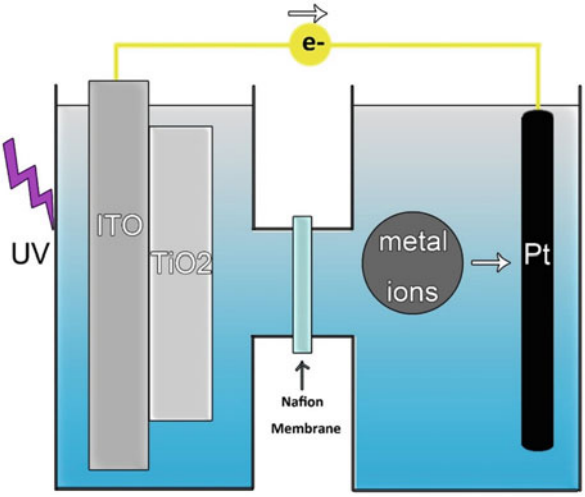

Fig. 2.21 Photoelectrochemical reduction of metal ions. *ITO* indium tin oxide, *UV* ultraviolet. (Reproduced from Wang et al. (2017), with permission)

fabricated using a facile biomimetic mineralization process, was described by Lv et al. (2017). In this strategy, fabrication of the ultrafiltration membrane was achieved using a polydopamine (PDA)/polyethyleneimine (PEI) intermediate layer by a codeposition method followed by mineralization of a photocatalytic layer consisting of β-FeOOH nanorods. The PDA–PEI layer acted as a nanofiltration-selective layer, as well as an intermediate layer for anchoring the β-FeOOH nanorods via strong coordination complexes between Fe^{3+} and catechol groups. In the presence of visible light, the β-FeOOH layer exhibited efficient photocatalytic activity for degrading dye solution through the photo-Fenton reaction in the presence of hydrogen peroxide, resulting in effective nanofiltration performance and self-cleaning capability. Moreover, the stability under simultaneous filtration and photocatalysis processing was satisfactory, showing immense potential for advanced wastewater treatment.

It is important for both the activity and the stability of the photocatalyst to be improved in a heterogeneous Fenton reaction, with no limitation in the working pH and no production of sludge. A combination of a catalyst (Cu_2O) and pores-channel-dispersed H_2O_2 was proposed to treat pulp wastewater. The degradation degree of COD in the wastewater was up to 77% in a ceramic membrane reactor using Cu_2O powder ($2.0\ g \cdot L^{-1}$) and membrane-feeding H_2O_2 ($0.8\ mL \cdot L^{-1}$) within 60 min. Evolution of •OH radical formation in the advanced oxidation process was analyzed with a fluorescent method. The utilization efficiency of H_2O_2 was successfully enhanced by 10% with the membrane distributor. Further on, the catalyst recyclability was evaluated in a five-cycle test. The concentration of copper ions being dissolved in the treated water was monitored with inductively coupled plasma (ICP). After Cu_2O/H_2O_2 (membrane) treatment the effluent was qualified for discharge with a COD concentration lower than $15\ mg \cdot L^{-1}$, in accordance with the Chinese national standard GB25467–2010.

The electro-Fenton process is a promising advanced oxidation process for water treatment, consisting of a series of redox reactions. An electrochemical filter was designed and assessed for sequential electro-Fenton reactions to optimize the treatment process. The CNT membrane stack (thickness ~200 μm) used here consisted of (1) a CNT network cathode for O_2 reduction to H_2O_2; (2) a CNT–$COOFe^{2+}$ cathode for chemical reduction of H_2O_2 to •OH and HO^-, and to regenerate Fe^{2+} in situ; (3) a porous polyvinylidene fluoride (PVDF) or polytetrafluoroethylene (PTFE) insulating separator; and 4) a CNT filter anode for the remaining intermediate oxidation intermediates. The sequential electro-Fenton process was compared with individual electrochemical and Fenton processes using oxalate (a persistent organic compound) as a target molecule. Synergism was observed during the sequential electro-Fenton process. For example, when $[DO]_{in} = 38 \pm 1$ mg L^{-1}, $J = 1.6$ mL min^{-1}, neutral pH, and $E_{cell} = 2.89$ V, the sequential electro-Fenton oxidation rate was 206.8 ± 6.3 mgC m^{-2} h^{-1}, which was four times greater than the sum of the individual electrochemistry (16.4 ± 3.2 mgC m^{-2} h^{-1}) and Fenton (33.3 ± 1.3 mgC m^{-2} h^{-1}) reaction fluxes, and the energy consumption was 45.8 kWh $kgTOC^{-1}$. The sequential electro-Fenton process was also challenged with the refractory trifluoroacetic acid (TFA) and trichloroacetic acid (TCA), and they could be transferred at removal rates of 11.3 ± 1.2 and 21.8 ± 1.9 mmol m^{-2} h^{-1}, respectively, with different transformation mechanisms.

2.3 Conclusions and Future Perspectives

In the present era, significant techniques are necessary for wastewater purification technology to eliminate chemical and biological pollutants from industrial effluent. In this context, nanomaterial-based wastewater purification technologies are essential. Furthermore, from the above illustrations, it is very clear that nanomaterials have great impact in wastewater treatment. The contribution of semiconducting nanomaterials in wastewater treatment for degradation is extremely substantial. However, combination of these nanomaterials with other purification techniques (ozonation, sonolysis, the Fenton process, etc.) synergistically improves these processes. Nanomaterials also play a vital role in removal of pollutants via adsorption or filtration approaches. Furthermore, the role of nanomaterials in antimicrobial activity is very important. Hence, the use of nanomaterials in the purification of wastewater is very efficient, without any doubt. However, the release/leaching of nanoparticles into the water system during these processes poses serious risk. Besides, the cost of making the nanomaterials makes these wastewater treatments very expensive, which limits the application of nanotechnology in these fields. Hence, tremendous efforts are required in the synthesis of cost-effective nanomaterials and restriction of leaching of nanoparticles into aqueous environments. Nevertheless, because of their effectiveness, nanomaterials will certainly play a key role in wastewater treatment on an industrial scale.

References

Adeleye AS, Conway JR, Garner K, Huang Y, Su Y, Keller AA (2016) Engineered nanomaterials for water treatment and remediation: costs, benefits, and applicability. Chem Eng J 286:640–662. https://doi.org/10.1016/j.cej.2015.10.105

Adewuyi YG (2001) Sonochemistry: environmental science and engineering applications. Ind Eng Chem Res 40:4681–4715. https://doi.org/10.1021/ie010096l

Ahmad M, Ahmed S, Swami BL, Ikram S (2015) Adsorption of heavy metal ions: role of chitosan and cellulose for water treatment. Int J Phcog 2:280–289. https://doi.org/10.13040/IJPSR.0975-8232.IJP

Ahmad M, Manzoor K, Venkatachalam P, Ikram S (2016) Kinetic and thermodynamic evaluation of adsorption of Cu(II) by thiosemicarbazide chitosan. Int J Biol Macromol 92:910–919. https://doi.org/10.1016/j.ijbiomac.2016.07.075

Amin MT, Alazba AA, Manzoor U (2014) A review of removal of pollutants from water/wastewater using different types of nanomaterials. Adv Mater Sci Eng 2014:825910. https://doi.org/10.1155/2014/825910

Ananpattarachai J, Boonto Y, Kajitvichyanukul P (2016) Visible light photocatalytic antibacterial activity of Ni-doped and N-doped TiO_2 on *Staphylococcus aureus* and *Escherichia coli* bacteria. Environ Sci Pollut Res 23:4111–4119. https://doi.org/10.1007/s11356-015-4775-1

Awual R, Eldesoky GE, Yaita T et al (2015) Schiff based ligand containing nano-composite adsorbent for optical copper(II) ions removal from aqueous solutions. Chem Eng J 279:639–647. https://doi.org/10.1016/j.cej.2015.05.049

Babu SG, Neppolian B, Ashokkumar M (2016a) Ultrasound assisted synthesis of nanoparticles for energy and environmental applications. Handbook of ultrasonics and sonochemistry. Springer, Singapore, pp 423–456. https://doi.org/10.1007/978-981-287-470-2_16-1

Babu SG, Neppolian B, Ashokkumar M (2016b) The role of ultrasound on advanced oxidation processes. Top Curr Chem 374:75. https://doi.org/10.1007/s41061-016-0072-9

Babu SG, Vijayan AS, Neppolian B, Ashokkumar M (2015a) SnS_2/rGO: an efficient photocatalyst for the complete degradation of organic contaminants. Mater Focus 4:272–276. https://doi.org/10.1166/mat.2015.1247

Babu SG, Vinoth R, Neppolian B, Dionysiou DD, Ashokkumar M (2015b) Diffused sunlight driven highly synergistic pathway for complete mineralization of organic contaminants using reduced graphene oxide supported photocatalyst. J Hazard Mater 291:83–92. https://doi.org/10.1016/j.jhazmat.2015.02.071

Babuponnusami A, Muthukumar K (2011) Degradation of phenol in aqueous solution by Fenton, sono-Fenton and sono-photo-Fenton methods. Clean Soil Air Water 39:142–147. https://doi.org/10.1002/clen.201000072

Babursah SC, Akmakci M, Kinaci C (2006) Analysis and monitoring: costing textile effluent recovery and reuse. Filtr Separat 43:26–30. https://doi.org/10.1016/S0015-1882(06)70889-8

Bali U, Catalkaya EC, Sengul F (2003) Photochemical degradation and mineralization of phenol: a comparative study. J Environ Sci Health A 38:2259–2275. https://doi.org/10.1081/ESE-120023373

Barrera-Salgado KE, Ramírez-Robledo G, Álvarez-Gallegos A, Pineda-Arellano CA, Sierra-Espinosa FZ, Hernández-Pérez JA, Silva-Martínez S (2016) Fenton process coupled to ultrasound and UV light irradiation for the oxidation of a model pollutant. J Chemother 1:1–7. https://doi.org/10.1155/2016/4262530

Baruah S, Khan N, Dutta M (2016) Perspectives and applications of nanotechnology in water treatment. J Environ Chem Lett 14:1. https://doi.org/10.1007/s10311-015-0542-2

Blanco J, Torrades F, De la Varga M, Garcia-Montano J (2012) Fenton and biological–Fenton coupled processes for textile wastewater treatment and reuse. Desalination 286:394–399. https://doi.org/10.1016/j.desal.2011.11.055

Brumfiel G (2003) Nanotechnology: a little knowledge. Nature 424:246–248. https://doi.org/10.1038/424246a

Burkhard R, Deletic A, Craig A (2000) Techniques for water and wastewater management: a review of techniques and their integration in planning. Urban Water 2:197–221. https://doi.org/10.1016/S1462-0758(00)00056-X

Cao Y, Li X (2014) Adsorption of graphene for the removal of inorganic pollutants in water purification: a review. Adsorption 20:713–727. https://doi.org/10.1007/s10450-014-9615-y

Catalkaya EC, Bali U, Sengul F (2003) Photochemical degradation and mineralization of 4-chlorophenol. Environ Sci Pollut Res Int 10:113–120. https://doi.org/10.1065/espr2002.10

Chaturvedi S, Dave PN, Shah NK (2012) Applications of nanocatalysts in new era. J Saudi Chem Soc 16:307–325. https://doi.org/10.1016/j.jscs.2011.01.015

Cheng CK, Kong ZY, Khan MR (2015) Photocatalytic–Fenton degradation of glycerol solution over visible light-responsive $CuFe_2O_4$. Water Air Soil Pollut 226:327. https://doi.org/10.1007/s11270-015-2592-2

Chitra S, Paramasivan K, Sinha PK (2013) Sono-photo Fenton treatment of liquid waste containing ethylenediaminetetraacetic acid (EDTA). Int J Nonferrous Met 2:89–94. https://doi.org/10.4236/ijnm.2013.22012

Chowdhury S, Balasubramanian R (2014) Recent advances in the use of graphene-family nanoadsorbents for removal of toxic pollutants from wastewater. Adv Colloid Interf Sci 204:35–56. https://doi.org/10.1016/j.cis.2013.12.005

Cortés-Arriagada D, Toro-Labbé A (2016) Aluminum and iron doped graphene for adsorption of methylated arsenic pollutants. Appl Surf Sci 386:84–95. https://doi.org/10.1016/j.apsusc.2016.05.154

Demeestere K, Dewulf J, Langenhove HV (2007) Heterogeneous photocatalysis as an advanced oxidation process for the abatement of chlorinated, monocyclic aromatic and sulfurous volatile organic compounds in air: state of the art. Environ Sci Technol 37:489–538. https://doi.org/10.1080/10643380600966467

Dhanasekar M, Jenefer V, Nambiar RB, Babu SG, Selvam SP, Neppolian B, Bhat SV (2018) Ambient light antimicrobial activity of reduced graphene oxide supported metal doped TiO_2 nanoparticles and their PVA based polymer nanocomposite films. Mater Res Bull 97:238–243. https://doi.org/10.1016/j.materresbull.2017.08.056

Dukkanci M (2016) Degradation of bisphenol-A using a sonophoto Fenton-like hybrid process over a $LaFeO_3$ perovskite catalyst and a comparison of its activity with that of a TiO_2 photocatalyst. Turk J Chem 40:784–801. https://doi.org/10.3906/kim-1602-59

Dutta AK, Maji SK, Adhikary B (2014) α-Fe_2O_3 nanoparticles: an easily recoverable effective photo-catalyst for the degradation of rose bengal and methylene blue dyes in the waste-water treatment plant. Mater Res Bull 49:28–34. https://doi.org/10.1016/j.materresbull.2013.08.024

Edelstein AS, Cammaratra RC (1998) Nanomaterials: synthesis, properties and applications. CRC Press, Boca Raton

El Saliby IJ, Shon H, Kandasamy J, Vigneswaran S (2008) Nanotechnology for wastewater treatment: in brief. In: Water and wastewater treatment technologies. In: Encyclopedia of Life Support Systems (EOLSS). EOLSS, Paris

Ferroudj N, Nzimoto J, Davidson A, Talbot D, Briot E, Dupuis V, Abramson S (2013) Maghemite nanoparticles and maghemite/silica nanocomposite microspheres as magnetic Fenton catalysts for the removal of water pollutants. Appl Catal B Environ 136:9–18. https://doi.org/10.1016/j.apcatb.2013.01.046

Foster HA, Ditta IB, Varghese S, Steele A (2011) Photocatalytic disinfection using titanium dioxide: spectrum and mechanism of antimicrobial activity. Appl Microbiol Biotechnol 90:1847–1868. https://doi.org/10.1007/s00253-011-3213-7

Fu FL, Wang Q (2011) Removal of heavy metal ions from wastewaters: a review. J Environ Manag 92:407–418. https://doi.org/10.1016/j.jenvman.2010.11.011

Ganguly P, Byrne C, Breen A, Pillai SC (2018) Antimicrobial activity of photocatalysts: fundamentals, mechanisms, kinetics and recent advances. Appl Catal B 225:51–75. https://doi.org/10.1016/j.apcatb.2017.11.018

Gao X, Zhang J, Zhang L (2002) Hollow sphere selenium nanoparticles: their in-vitro anti hydroxyl radical effect. Adv Mater 14:290–293. https://doi.org/10.1002/1521-4095(20020219)14:4<290::AID-ADMA290>3.0.CO;2-U

Ghasemzadeh G, Momenpour M, Omidi F, Hosseini MR, Ahani M, Barzegari A (2016) Applications of nanomaterials in water treatment and environmental remediation. Front Environ Sci Eng 8:471–482. https://doi.org/10.1007/s11783-014-0654-0

Gobara HM, Elsalamony RA, Hassan SA (2016) Sonophotocatalytic degradation of eriochrome black-T dye in water using Ti grafted SBA-15. J Porous Mater 23:1311–1318. https://doi.org/10.1007/s10934-016-0190-3

Grey D, Garrick D, Blackmore D, Kelman J, Muller M, Sadoff C (2013) Water security in one blue planet: twenty-first century policy challenges for science. Philos Trans Roy Soc London A: Math, Phys Eng Sci 371:20120406. https://doi.org/10.1098/rsta.2012.0406

Guan Z, Lv J, Bai P, Guo X (2016) Boron removal from aqueous solutions by adsorption. Rev Desalin 383:29–37. https://doi.org/10.1016/j.desal.2015.12.026

Guo Z, Zheng Z, Zheng S, Hu W, Feng R (2005) Effect of various sono-oxidation parameters on the removal of aqueous 2,4-dinitrophenol. Ultrason Sonochem 12:461–465. https://doi.org/10.1016/j.ultsonch.2004.07.006

Gupta VK, Tyagi I, Sadegh H, Shahryari-Ghoshekand R, Makhlouf ASH, Maazinejad B (2015) Nanoparticles as adsorbent; a positive approach for removal of noxious metal ions: a review. Sci Technol Dev 34:195–214. https://doi.org/10.3923/std.2015.195.214

Hachem C, Bocquillon F, Zahraa O, Bouchy M (2001) Decolourization of textile industry wastewater by the photocatalytic degradation process. Dyes Pigments 49:117–125. https://doi.org/10.1016/S0143-7208(01)00014-6

Han C, Huang G, Zhu D, Hu K (2017) Facile synthesis of MoS_2/Fe_3O_4 nanocomposite with excellent photo-Fenton-like catalytic performance. Mater Chem Phys 200:16–22. https://doi.org/10.1016/j.matchemphys.2017.07.065

Herrmann JM (2005) Heterogeneous photocatalysis: state of the art and present applications. Top Catal 34:49–65. https://doi.org/10.1007/s11244-005-3788-2

Hilal N, Al-Zoubi H, Darwish NA, Mohamma AW, Arabi MA (2004) A comprehensive review of nanofiltration membranes: treatment, pre-treatment, modelling, and atomic force microscopy. Desalination 170:281–308. https://doi.org/10.1016/j.desal.2004.01.007

Ihsanullah AA, Al-amer AM, Laoui T, Al-marri MJ, Nasser MS, Khraisheh MAIM (2016) Heavy metal removal from aqueous solution by advanced carbon nanotubes: critical review of adsorption applications. Sep Purif Technol 157:141–161. https://doi.org/10.1016/j.seppur.2015.11.039

Jiang L, Yuan X, Pan Y, Liang J, Zeng G, Wu Z, Wang H (2017) Doping of graphitic carbon nitride for photocatalysis: a review. Appl Catal B 217:388–406. https://doi.org/10.1016/j.apcatb.2017.06.003

Jones OAH, Green PG, Voulvoulis N, Lester JN (2007) Questioning the excessive use of advanced treatment to remove organic micropollutants from wastewater. Environ Sci Technol 41:5085–5089. https://doi.org/10.1021/es0628248

Joost U, Juganson K, Visnapuu M, Mortimer M, Kahru A, Nõmmiste E, Joost U, Kisand V, Ivask A (2015) Photocatalytic antibacterial activity of nano-TiO_2 (anatase)-based thin films: effects on *Escherichia coli* cells and fatty acids. J Photochem Photobiol B 142:178–185. https://doi.org/10.1016/j.jphotobiol.2014.12.010

Karthik P, Vinoth R, Babu SG, Wen M, Kamegawa T, Yamashita H, Neppolian B (2015) Synthesis of highly visible light active TiO_2-2-naphthol surface complex and its application in photocatalytic chromium(VI) reduction. RSC Adv 5:39752–39759. https://doi.org/10.1039/C5RA03831F

Kaur S, Singh V (2007) Visible light induced sonophotocatalytic degradation of reactive red dye 198 using dye sensitized TiO_2. Ultrason Sonochem 14:531–537. https://doi.org/10.1016/j.ultsonch.2006.09.015

Khan S, Cao Q, Zheng YM, Huang YZ, Zhu YG (2010) Health risks of heavy metals in contaminated soils and food crops irrigated with wastewater in Beijing, China. Environ Pollut 152:686–692. https://doi.org/10.1016/j.envpol.2007.06.056

Khan ZUH, Khan A, Shah A, Chen Y, Wan P, Khan AU, Tahir K, Muhamma N, Khan FU, Shah HU (2016) Photocatalytic, antimicrobial activities of biogenic silver nanoparticles and electrochemical degradation of water soluble dyes at glassy carbon/silver modified past electrode using

buffer solution. J Photochem Photobiol B 156:100–107. https://doi.org/10.1016/j.jphotobiol.2016.01.016

Kumar KAS, Jiang S (2016) Chitosan-functionalized graphene oxide: a novel adsorbent an efficient adsorption of arsenic from aqueous solution. J Environ Chem Eng 4:1698–1713. https://doi.org/10.1016/j.jece.2016.02.035

Kumar PS, Selvakumar M, Babu SG, Induja S, Karuthapandian S (2017) CuO/ZnO nanorods: an affordable efficient p-n heterojunction and morphology dependent photocatalytic activity against organic contaminants. J Alloys Compd 701:562–573. https://doi.org/10.1016/j.jallcom.2017.01.126

Kumar PS, Selvakumar M, Babu SG, Karuthapandian S (2016) Veteran cupric oxide with new morphology and modified bandgap for superior photocatalytic activity against different kinds of organic contaminants (acidic, azo and triphenylmethane dyes). Mater Res Bull 83:522–533. https://doi.org/10.1016/j.materresbull.2016.06.043

Kurian M, Nair DS, Rahnamol AM (2014) Influence of the synthesis conditions on the catalytic efficiency of $NiFe_2O_4$ and $ZnFe_2O_4$ nanoparticles towards the wet peroxide oxidation of 4-chlorophenol. React Kinet Mech Catal 111:591–604. https://doi.org/10.1007/s11144-013-0667-x

Kuwahara Y, Yamashita H (2011) Efficient photocatalytic degradation of organics diluted in water and air using TiO_2 designed with zeolites and mesoporous silica materials. J Mater Chem 21:2407–2416. https://doi.org/10.1039/C0JM02741C

Kyzas GZ, Matis KA (2015) Nanoadsorbents for pollutants removal: a review. J Mol Liq 203:159–168. https://doi.org/10.1016/j.molliq.2015.01.004

Lau WJ, Ismail A (2009) Polymeric nanofiltration membranes for textile dye wastewater treatment: preparation, performance evaluation, transport modelling, and fouling control—a review. Desalination 245:321–348. https://doi.org/10.1016/j.desal.2007.12.058

Legrini O, Oliveros E, Braun AM (1993) Photochemical processes for water treatment. Chem Rev 93:671–698. https://doi.org/10.1021/cr00018a003

Leshuk T, Gu F (2014) Nanotechnology for water treatment and purification, Lecture notes in nanoscale science and technology, vol 22. Springer, Cham. https://doi.org/10.1007/978-3-319-06578-6_7

Leung TY, Chan CY, Hu C, Yu JC, Wong PK (2008) Photocatalytic disinfection of marine bacteria using fluorescent light. Water Res 42:4827–4837. https://doi.org/10.1016/j.watres.2008.08.031

Li Puma G, Toepfer B, Gora A (2007) Photocatalytic oxidation of multicomponent systems of herbicides: scale-up of laboratory kinetics rate data to plant scale. Catal Today 124:124–132. https://doi.org/10.1016/j.cattod.2007.03.047

Li X, Wang S, Liu Y, Jiang L, Song B, Li M, Zeng G, Tan X, Cai X, Ding Y (2017) Adsorption of Cu(II), Pb(II), and Cd(II) ions from acidic aqueous solutions by diethylenetriaminepentaacetic acid-modified magnetic graphene oxide. J Chem Eng Data 62:407–416. https://doi.org/10.1021/acs.jced.6b00746

Liu ZH, Kanjo Y, Mizutani S (2009) Removal mechanisms for endocrine disrupting compounds (EDCs) in wastewater treatment—physical means, biodegradation, and chemical advanced oxidation: a review. Sci Total Environ 407:731–748. https://doi.org/10.1016/j.scitotenv.2008.08.039

Lu Y, Riyanto N, Weavers LK (2002) Sonolysis of synthetic sediment particles: particle characteristics affecting particle dissolution and size reduction. Ultrason Sonochem 9:181–188. https://doi.org/10.1016/S1350-4177(02)00076-7

Lubick N, Betts K (2008) Silver socks have cloudy lining court bans widely used flame retardant. Environ Sci Technol 42:3910–3910. https://doi.org/10.1021/es0871199

Lv Y, Zhang C, He C, Yang SJ, Darling SB, Xu ZK (2017) Photocatalytic nanofiltration membranes with self-cleaning property for wastewater treatment. Adv Funct Mater 27:1700251. https://doi.org/10.1002/adfm.201700251

Ma H, Wang H, Na C (2015) Microwave-assisted optimization of platinum-nickel nanoalloys for catalytic water treatment. Appl Catal B Environ 163:198–204. https://doi.org/10.1016/j.apcatb.2014.07.062

Matsunaga T, Tomoda R, Nakajima T, Wake H (1985) Photoelectrochemical sterilization of microbial cells by semiconductor powders. FEMS Microbiol Lett 29:211–214. https://doi.org/10.1111/j.1574-6968.1985.tb00864.x

Mecha AC, Onyango MS, Ochieng A, Fourie CJS, Momba MNB (2016) Synergistic effect of UV–vis and solar photocatalytic ozonation on the degradation of phenol in municipal wastewater: a comparative study. J Catal 341:116–125. https://doi.org/10.1016/j.jcat.2016.06.015

Mena E, Rey A, Rodríguez EM, Beltrán FJ (2017) Reaction mechanism and kinetics of DEET visible light assisted photocatalytic ozonation with WO_3 catalyst. Appl Catal B Environ 202:460–472. https://doi.org/10.1016/j.apcatb.2016.09.029

Mills A, Davies RH, Worsley D (1993) Water purification by semiconductor photocatalysis. Chem Soc Rev 22:417–425. https://doi.org/10.1039/CS9932200417

Mosleh S, Rahimi MR, Ghaedi M, Dashtian K (2016) Sonophotocatalytic degradation of trypan blue and vesuvine dyes in the presence of blue light active photocatalyst of Ag_3PO_4/Bi_2S_3-HKUST-1-MOF: central composite optimization and synergistic effect study. Ultrason Sonochem 32:387–397. https://doi.org/10.1016/j.ultsonch.2016.04.007

Moussavi G, Rezaei M, Porakbar M (2018) Comparing VUV and VUV/Fe^{2+} processes for decomposition of cloxacillin antibiotic: degradation rate and pathways, mineralization and by-product analysis. Chem Eng J 332:140–149. https://doi.org/10.1016/j.cej.2017.09.057

Naushad M, Ahamad T, Al-Maswari BM et al (2017) Nickel ferrite bearing nitrogen-doped mesoporous carbon as efficient adsorbent for the removal of highly toxic metal ion from aqueous medium. Chem Eng J 330:1351. https://doi.org/10.1016/j.cej.2017.08.079

Naushad M, Sharma G, Kumar A et al (2018) Efficient removal of toxic phosphate anions from aqueous environment using pectin based quaternary amino anion exchanger. Int J Biol Macromol 106:1–10. https://doi.org/10.1016/j.ijbiomac.2017.07.169

Nguyen XS, Zhang G, Yang X (2017) Mesocrystalline Zn-doped Fe_3O_4 hollow submicrospheres: formation mechanism and enhanced photo-Fenton catalytic performance. ACS Appl Mater Interfaces 9:8900–8909. https://doi.org/10.1021/acsami.6b16839

Nikolopoulos AN, Igglessi-Markopoulou O, Papayannakos N (2006) Ultrasound assisted catalytic wet peroxide oxidation of phenol: kinetics and intraparticle diffusion effects. Ultrason Sonochem 13:92–97. https://doi.org/10.1016/j.ultsonch.2004.10.001

Nirmala R, Sheikh FA, Kanjwal MA, Lee JH, Park S-J, Navamathavan R, Kim HY (2011) Synthesis and characterization of bovine femur bone hydroxyapatite containing silver nanoparticles for the biomedical applications. J Nanopart Res 13:1917–1927. https://doi.org/10.1007/s11051-010-9944-z

Ouyang X, Li W, Xie S, Zhai T, Yu M, Gan J, Lu X (2013) Hierarchical CeO_2 nanospheres as highly-efficient adsorbents for dye removal. New J Chem 37:585–588. https://doi.org/10.1039/C3NJ41095A

Palit S (2017) Nanomaterials for industrial wastewater treatment and water purification. In: Martínez L, Kharissova O, Kharisov B (eds) Handbook of ecomaterials. Springer, Cham. https://doi.org/10.1007/978-3-319-48281-1_9-1

Park H, Vecitis CD, Hoffmann MR (2008) Solar-powered electrochemical oxidation of organic compounds coupled with the cathodic production of molecular hydrogen. J Phys Chem A 112:7616–7626. https://doi.org/10.1021/jp802807e

Parsons S, Jefferson B (2006) Introduction to potable water treatment processes. Wiley-Blackwell, Hoboken. https://doi.org/10.1002/9781444305470

Peng W, Li H, Liu Y, Song S (2017) A review on heavy metal ions adsorption from water by graphene oxide and its composites. J Mol Liq 230:496–504. https://doi.org/10.1016/j.molliq.2017.01.064

Petrinic I, Andersen NPR, Sostar-Turk S, Le Marechal AM (2007) The removal of reactive dye printing compounds using nanofiltration. Dyes Pigments 74:512–518. https://doi.org/10.1016/j.dyepig.2006.11.003

Prabavathi SL, Kumar PS, Saravanakumar K, Muthuraj V, Karuthapandian S (2018) A novel sulphur decorated 1-D MoO_3 nanorods: facile synthesis and high performance for photocatalytic

reduction of hexavalent chromium. J Photochem Photobio A 356:642–651. https://doi.org/10.1016/j.jphotochem.2018.02.007

Prasanna VL, Vijayaraghavan R (2017) Simultaneous Fenton–photocatalytic reactions through a new single catalyst (Nano ZnO_2/Fe^{2+}) for dye degradation. J Phys Chem C 121:18557–18563. https://doi.org/10.1021/acs.jpcc.7b04092

Qu X, Brame J, Li Q, Alvarez PJ (2012) Nanotechnology for a safe and sustainable water supply: enabling integrated water treatment and reuse. Acc Chem Res 46:834–843. https://doi.org/10.1021/ar300029v

Radwan EK, Yu L, Achari G, Langford CH (2016) Photocatalytic ozonation of pesticides in a fixed bed flow through UVA–LED photoreactor. Environ Sci Pollut Res 23:21313–21318. https://doi.org/10.1007/s11356-016-7346-1

Ranjit PJD, Palanivelu K, Lee C-S (2008) Degradation of 2,4-dichlorophenol in aqueous solution by sono-Fenton method. Korean J Chem Eng 25:112–117. https://doi.org/10.1007/s11814-008-0020-7

Rao CNR, Sood AK, Subrahmanyam KS, Govindaraj A (2009) Graphene: the new twodimensional nanomaterial. Angew Chem Int Ed 48:7752–7777. https://doi.org/10.1002/anie.200901678

Rashidi HR, Sulaiman NMN, Hashim NA, Hassan CRC, Ramli MR (2015) Synthetic reactive dye wastewater treatment by using nanomembrane filtration. Desalin Water Treat 55:86–95. https://doi.org/10.1080/19443994.2014.912964

Ravelli D, Dondi D, Fagnoni M, Albini A (2009) Photocatalysis. A multi-faceted concept for green chemistry. Chem Soc Rev 38:1999–2011. https://doi.org/10.1039/B714786B

Ren X, Li J, Tan X, Wang X (2013) Comparative study of graphene oxide, activated carbon and carbon nanotubes as adsorbents for copper decontamination. Dalton Trans 42:5266–5274. https://doi.org/10.1039/c3dt32969k

Sadegh H, Shahryari-Ghoshekandi R, Kazemi M (2014) Study in synthesis and characterization of carbon nanotubes decorated by magnetic iron oxide nanoparticles. Int Nano Lett 4:129–135. https://doi.org/10.1007/s40089-014-0128-1

Saikia JP, Paul S, Konwar BK, Samdarshi SK (2010) Nickel oxide nanoparticles: a novel antioxidant. Colloids Surf B: Biointerfaces 78:146–148. https://doi.org/10.1016/j.colsurfb.2010.02.016

Saito T, Iwase T, Horie J, Morioka T (1992) Mode of photocatalytic bactericidal action of powdered semiconductor TiO_2 on mutans streptococci. J Photochem Photobiol B 14:369–379. https://doi.org/10.1016/1011-1344(92)85115-B

Samad A, Ahsan S, Tateishi I, Furukawa M, Katsumata H, Suzuki T, Kaneco S (2018) Indirect photocatalytic reduction of arsenate to arsenite in aqueous solution with TiO_2 in the presence of hole scavengers. Chin J Chem Eng 23:529–533. https://doi.org/10.1016/j.cjche.2017.05.019

Santhosh C, Velmurugan V, Jacob G, Jeong SK, Grace AN, Bhatnagar A (2016) Role of nanomaterials in water treatment applications: a review. Chem Eng J 306:1116–1137. https://doi.org/10.1016/j.cej.2016.08.053

Savage N, Diallo MS (2005) Nanomaterials and water purification: opportunities and challenges. J Nanopart Res 7:331. https://doi.org/10.1007/s11051-005-7523-5

Schwarzenbach RP, Escher BI, Fenner K, Hofstetter TB, Johnson CA, Gunten UV, Wehrli B (2006) The challenge of micropollutants in aquatic systems. Science 313:1072–1077. https://doi.org/10.1126/science.1127291

Segura Y, Molina R, Martínez F, Melero JA (2009) Integrated heterogeneous sono–photo Fenton processes for the degradation of phenolic aqueous solutions. Ultrason Sonochem 16:417–424. https://doi.org/10.1016/j.ultsonch.2008.10.004

Senanayake SD, Stacchiola D, Rodriguez JA (2013) Unique properties of ceria nanoparticles supported on metals: novel inverse ceria/copper catalysts for CO oxidation and the water-gas shift reaction. Acc Chem Res 46:1702–1711. https://doi.org/10.1021/ar300231p

Shannon MA, Bohn PW, Elimelech M, Georgiadis JG, Marinas BJ, Mayes AM (2008) Science and technology for water purification in the coming decades. Nature 452:301–310. https://doi.org/10.1038/nature06599

Shirgaonkar IZ, Pandit AB (1998) Sonophotochemical destruction of aqueous solution of 2,4,6-trichlorophenol. Ultrason Sonochem 5:53–61. https://doi.org/10.1016/S1350-4177(98)00013-3

Sigdel A, Park J, Kwak H, Park P (2016) Arsenic removal from aqueous solutions by adsorption onto hydrous iron oxide-impregnated alginate beads. J Ind Eng Chem 35:277–286. https://doi.org/10.1016/j.jiec.2016.01.005

Singh C, Chaudhary R (2013) Visible light induced photocatalytic reduction of metals (Cr, Cu, Ni, and Zn) and its synergism with different pH, TiO_2, and H_2O_2 doses in simulated wastewater. J Renew Sustain Energy 5:053102. https://doi.org/10.1063/1.4818899

Sunada K, Watanabe T, Hashimoto K (2003) Studies on photokilling of bacteria on TiO_2 thin film. J Photochem Photobiol A 156:227–233. https://doi.org/10.1016/S1010-6030(02)00434-3

Tadjarodi A, Moazen S, Zare-dorabei R, Barzin A (2016) Highly efficient ultrasonic assisted removal of Hg(II) ions on graphene oxide modified with 2-pyridinecarboxaldehyde thiosemicarbazone: adsorption isotherms and kinetics studies. Ultrason Sonochem 33:118–128. https://doi.org/10.1016/j.ultsonch.2016.04.030

Tang X, Zhang Q, Liu Z, Pan K, Dong Y, Li Y (2014) Removal of Cu(II) by loofah fibers as a natural and low-cost adsorbent from aqueous solutions. J Mol Liq 199:401–407. https://doi.org/10.1016/j.molliq.2014.09.033

Thanawatpoontawee S, Imyim A, Praphairaksit N (2016) Iron-loaded zein beads as a biocompatible adsorbent for arsenic(V) removal. J Ind Eng Chem 43:127–132. https://doi.org/10.1016/j.jiec.2016.07.058

Theron J, Walker JA, Cloete TE (2008) Nanotechnology and water treatment: applications and emerging opportunities. Crit Rev Microbiol 34:43–69. https://doi.org/10.1080/10408410701710442

Titus MP, Molina VG, Banos MA, Gimenez J, Esplugas S (2004) Degradation of chlorophenols by means of advanced oxidation processes: a general review. Appl Catal B 47:219–256. https://doi.org/10.1016/j.apcatb.2003.09.010

Ünnü BA, Gündüz G, Dükkancı M (2016) Heterogeneous Fenton-like oxidation of crystal violet using an iron loaded ZSM-5 zeolite. Desalin Water Treat 57:11835–11849. https://doi.org/10.1080/19443994.2015.1044915

Uppal H, Tawale J, Singh N (2016) Zinc peroxide functionalized synthetic graphite: an economical and efficient adsorbent for adsorption of arsenic(III) and (V). J Environ Chem Eng 4:2964–2975. https://doi.org/10.1016/j.jece.2016.05.038

Verma A, Sangwan P, Dixit D (2014) Sonophotocatalytic degradation studies of alizarin reactive red dye. Arab J Sci Eng 39:7477–7482. https://doi.org/10.1007/s13369-014-1309-y

Wang TH, Kang SF, Lin YH (1999) Comparison among Fenton-related processes to remove 2,4-dinitrophenol. J Environ Sci Health A 34:1267–1281. https://doi.org/10.1080/10934529909376895

Wang D, Li Y, Puma GL, Lianos P, Wang C, Wang P (2017) Photoelectrochemical cell for simultaneous electricity generation and heavy metals recovery from wastewater. J Hazard Mater 323:681–689. https://doi.org/10.1016/j.jhazmat.2016.10.037

Xu Z, Huang C, Wang L, Pan X, Qin L, Guo X, Zhang G (2015) Sulfate functionalized Fe_2O_3 nanoparticles on TiO_2 nanotube as efficient visible light-active photo-Fenton catalyst. Ind Eng Chem Res 54:4593–4602. https://doi.org/10.1021/acs.iecr.5b00335

Yamanaka M, Hara K, Kudo J (2005) Bactericidal actions of a silver ion solution on *Escherichia coli*, studied by energy-filtering transmission electron microscopy and proteomic analysis. Appl Environ Microbiol 71:7589–7593. https://doi.org/10.1128/AEM.71.11.7589-7593.2005

Yue D, Qian X, Kan M, Fang M, Jia J, Yang X, Zhao Y (2018) A metal-free visible light active photo-electro-Fenton-like cell for organic pollutants degradation. Appl Catal B Environ 229:211–217. https://doi.org/10.1016/j.apcatb.2018.02.033

Zare K, Najafi F, Sadegh H (2013) Studies of ab initio and Monte Carlo simulation on interaction of fluorouracil anticancer drug with carbon nanotube. J Nanostruct Chem 3:1–8. https://doi.org/10.1186/2193-8865-3-71

Zelmanov G, Semiat R (2008) Phenol oxidation kinetics in water solution using iron (3)-oxide-based nano-catalysts. Water Res 42:3848–3856. https://doi.org/10.1016/j.watres.2008.05.009

Zhang Q, Xu R, Xu P, Chen R, He Q, Zhong J, Gu X (2014) Performance study of ZrO_2 ceramic micro-filtration membranes used in pretreatment of DMF wastewater. Desalination 346:1–8. https://doi.org/10.1016/j.desal.2014.05.006

Zhang Y, Wu B, Xu H, Liu H, Wang M, He Y, Pan B (2016) Nanomaterials-enabled water and wastewater treatment. Nano Impact 3–4:22–39. https://doi.org/10.1016/j.impact.2016.09.004

Zhao W, Liang C, Wang B, Xing S (2017) Enhanced photocatalytic and Fenton-like performance of CuO_x-decorated $ZnFe_2O_4$. ACS Appl Mater Interfaces 9:41927–41936. https://doi.org/10.1021/acsami.7b14799

Chapter 3
Nano-metal Oxides for Antibacterial Activity

Sankar Jagadeeshan and Rajesh Parsanathan

Contents

Author contributed equally with all other contributors.Sankar Jagadeeshan and Rajesh Parsanathan

S. Jagadeeshan
Cell Biology Division, Memorial Sloan Kettering Cancer Center, New York, NY, USA

R. Parsanathan (✉)
Department of Endocrinology, Dr. ALM PG IBMS, University of Madras, Chennai, Tamilnadu, India

Present Address: Department of Pediatrics, Louisiana State University Health Science Centre, Shreveport, LA, USA
e-mail: rparsa@lsuhsc.edu

Mu. Naushad et al. (eds.), *Advanced Nanostructured Materials for Environmental Remediation*, Environmental Chemistry for a Sustainable World 25,
https://doi.org/10.1007/978-3-030-04477-0_3

Abstract Metal oxide nanoparticles (MeO-NPs) represent a field of material chemistry which attracts considerable interest due to the potential technological applications such as medicine, information technology, catalysis, energy storage and sensing and developing synthetic tailored nanostructures. Many nanomaterials can be used as metal oxides (Ag, Al, Ca, Ce, Cu, Mg, Ti, Yt, Zn). Certain MeO-NPs have strong antimicrobial properties, and its mechanism of actions involved in eliminating bacteria has been studied.

In this chapter we review the methods by which MeO-NPs are synthesized such as sonochemical, electrochemical, co-precipitation, solvothermal, sol-gel, microwave, wet chemical, microemulsion, laser ablation, chemical vapour-based, combustion and template/surface-mediated synthesis methods and biological mycosynthesis, as well as crucial factors (size, shape, roughness, zeta potential, doping modifications and environmental conditions) which affect the antibacterial mechanisms of MeO-NPs. The link between energy-efficient preparation of huge new variety of MeO-NP preparations and its final structural morphology can be exploited for use in a whole range of technologically important areas including efficient antimicrobial properties.

Previous studies have shown that the antimicrobial properties and the mechanism of action of different MeO-NPs that play a wide role as antimicrobial agents such as cell membrane damage by electrostatic interaction, metal/metal ion homeostasis disturbance, reactive oxygen species production, protein enzyme dysfunction, genotoxicity and signal transduction inhibition and photokilling are also reviewed in this chapter. Evidence suggests that in general some nanomaterials can be more toxic than their macro-scale counterparts and therefore caution is warranted on human health. Previous in vitro studies indicated that in comparison with a material's

larger (parent) counterpart, nanomaterials can move easily through cell membranes and can cause severe toxic effects on human health. We will also provide some examples of the features and applications of few known MeO-NPs (TiO_2, Ag_2O, ZnO, CuO, MgO, CaO, CeO_2, Y_2O_3, Al_2O_3 and bimetallic oxide nanoparticles). Indeed, the application of MeO-NPs with the minimized toxicity possibly will be extensively used in the near future for eradicating several infectious conditions as alternative of traditional antibiotics to overcome antimicrobial resistance.

Keywords Antimicrobial · Antibacterial activity · Doping · Metal oxide · Nanomaterials · Nano-metal oxides · Reactive oxygen species · Zeta potential

3.1 Introduction

Nanomaterials have wide range of applications due to their increased reactivity in comparison to their micro-sized counterparts. Nanoscaled materials exhibit larger surface-to-volume ratio which provides unsaturated and, thus, more reactive surface atoms. To consider nanoparticles for any biological therapeutic applications, many key features have to be fulfilled, such as composition, size, crystallinity, morphology, stability, non-agglomeration and finally biocompatibility. One such class of biologically relevant nanomaterials is metal oxide (MeO) nanoparticles (NPs). MeO-NPs possess unique physical and chemical characteristics linked to their nanometre size, thus offering versatility.

Most of the biochemical reactions within a body occur at the atomic level. Therefore, it is safe to assume that the collaborative synergy between nanotechnology and basic life sciences could solve many issues faced by fundamental biologists. Infectious diseases are one such issue which is the main cause of mortality in the world, and the hunt for antimicrobial agents without resistance is warranted. The emergence of multidrug resistance (MDR) and antibiotic resistance has been reported, and it is a public health concern. Such emergence of resistance is due to indiscriminate use of antibiotics, leading to the evolution of new antibiotic-resistant strains at a faster pace. Presently, microbial resistance to antibiotics has been reaching a critical level. In exploring various options to address this problem, inorganic nanomaterials, like metal oxide nanoparticles (MeO-NPs), have emerged as promising candidates since they possess greater durability, lower toxicity and higher stability and selectivity when compared to organic ones. The availability of many different MeO-NPs with diverse physicochemical and functional properties offers promise as antimicrobial agents. In this chapter, we summarize the general synthesis procedures, microbicidal mechanisms, safety concerns and future prospects of MeO-NPs.

3.2 Synthesis Methods of Metal Oxide Nanoparticles

The choice of synthesis method determines the physicochemical characteristics of the metal oxide nanoparticle, such as the size, dispersity, type of intrinsic and/or extrinsic defects, morphology and crystal structure (Stankic et al. 2016). Some of the common synthesis procedures for MeO-NPs are given below.

3.2.1 Sonochemical Method

In sonochemical methods, solution of the starting material (e.g. metallic salts) is subjected to a stream of intensified ultrasonic vibrations, which breaks the chemical bonds of the compounds leading to the creation of a localized cavitational implosion hotspots (Gedanken 2004). This method has been used to synthesize a wide range of nanomaterials as metals, alloys, metal oxides, metal sulphides, metal nitrides, metal-polymer composites, metal chalcogenides, metal carbides, etc. Examples of reported metal oxides synthesized by this method include TiO_2, ZnO, CeO_2, MoO_3, V_2O_5, In_2O_3 and Eu/Dy-doped In_2O_3, $ZnFe_2O_4$, $PbWO_4$, $BiPO_4$, $ZnAl_2O_4$ and $ZnGa_2O_4$—pure and doped with varying combinations of Dy^{+3}, Tb^{+3}, Eu^{+3} and Mn^{+2}, Fe_3O_4, $BaFe_{12}O_{19}$ (Shafi et al. 1999) and Mn-doped γ-Fe_2O_3 (Lai et al. 2003). The advantages associated with sonochemical methods include uniform size distribution, a higher surface area, faster reaction time and improved phase purity of the metal oxide nanoparticles (Fig. 3.1a).

3.2.2 Electrochemical

This method uses electrolyte solutions with two-electrode setup where the bulk metal will be kept in anode and transformed into metal clusters (Pandey et al. 2012). To stabilize the metal clusters, tetra alkyl ammonium salts are used as supporting electrolyte (Fig. 3.1c). Electrolysis is carried out in a nitrogen atmosphere to remove the dissolved oxygen, and the metal cations migrate to the cathode, whereas the bulk metal is oxidized at the anode. The residual oxygen in the electrolytic bath oxidizes the metal into respective MeOs. Added, ammonium stabilizers prevent agglomeration with metal powders. The current density controls the cluster size. Chromium(III) oxide (Cr_2O_3), CuO and CuO multi-armed NPs have been synthesized, and their toxic effects on micro-organisms have been validated (Reyes et al. 2015).

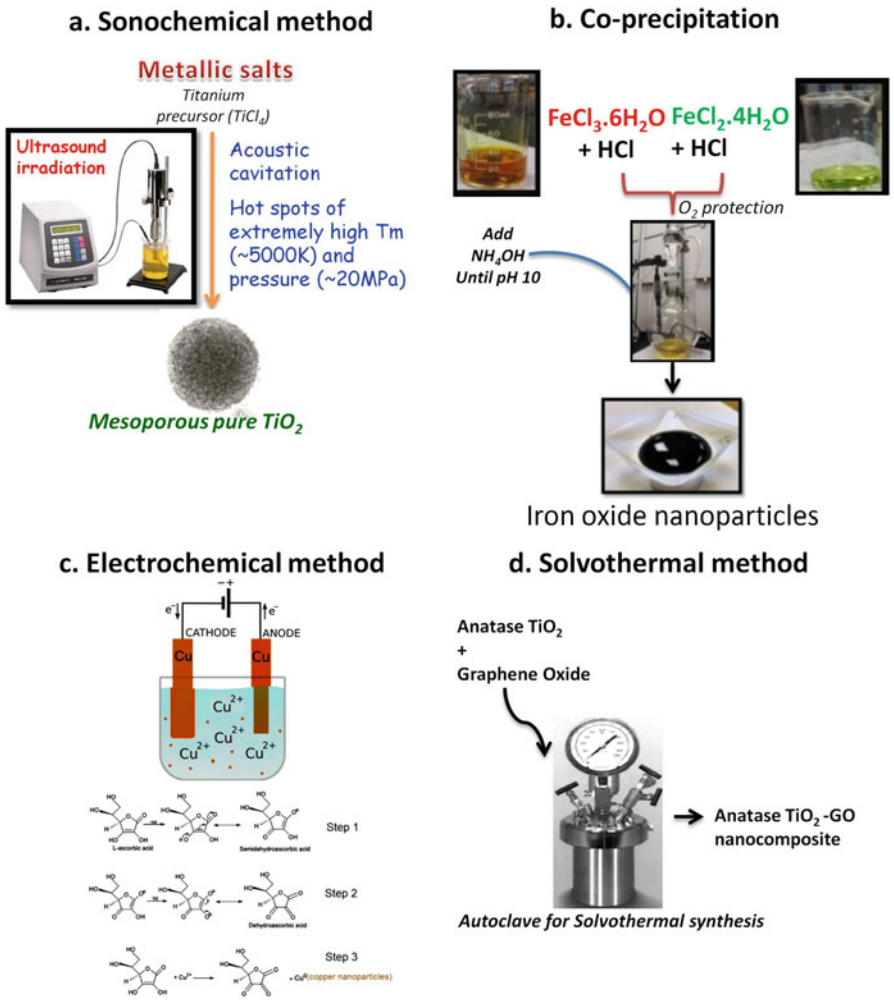

Fig. 3.1 Synthesis methods of metal oxide nanoparticles: (**a**) sonochemical method, (**b**) co-precipitation method, (**c**) electrochemical method *from* https://ninithi.wordpress.com/ and (**d**) solvothermal method

3.2.3 Co-precipitation Method

The co-precipitation method involves precipitating the oxohydroxide form from a solution of a salt precursor (metal salts like nitrates or chlorides) in a solvent (like water) by using a precipitating medium. The chloride salts obtained are washed,

whilst hydroxides are removed by heating to obtain the desired MeOs. Once a critical concentration of species in solution is reached, a short burst of nucleation occurs followed by growth phase (Fig. 3.1b). This method has been employed in synthesizing metal oxides like ZnO, MnO_2, $BiVO_4$, MgO, $Ni_{1-x}Zn_xFe_2$ O4, SnO_2, Cu-doped ZnO, $MgFe_2O_4$, Ni-$CeZrO_2$ and Y_2O_3:Eu^{+3}. Co-precipitation is commonly used for preparing magnetic nanoparticles such as magnetite by using a base, usually NaOH and NH_4OH, for alkaline co-precipitation of ferrous and ferric salts dissolved in water in stoichiometric amounts (Colombo et al. 2012; Kumar et al. 2013b; Mascolo et al. 2013). The advantages of this method are low cost, mild reaction conditions like low synthesis temperature, the possibility to perform direct synthesis in water, simplicity of processing, the ease of scale-up, flexibility in modulation of core and surface properties (Mascolo et al. 2013; Sujatha et al. 2016).

3.2.4 Solvothermal Method

These methods are employed to prepare a variety of nanomaterials by dispersing the starting material in a suitable solvent and subjecting it to moderately high temperature and pressure conditions which lead to product formation. An organometallic complex of titanium and orthobutoxide was used for the synthesis of TiO_2 nanoparticles (Gopalakrishnan et al. 2011). When the reaction is performed using water as the solvent, the method is called hydrothermal synthesis. Chemical parameters (type, composition and concentration of the reactants, ratio-solvent/reducing agent) and thermodynamic parameters (temperature, pressure and reaction time) affect the final particle formation (Fig. 3.1d). It was also observed that basicity and hydrolysis ratio of the reacting medium together with the steric or electrostatic stabilization of the reactive molecules affects the nucleation and growth steps, which in turn control the particle size, shape, composition and crystal structure of particles. For instance, varying the hydrolysis ratio allows to synthesize either metal, (oxy)hydroxide or oxide nanoparticles (Feldmann and Jungk 2001). Nanoparticles of Nb_2O_5, MgO, TiO_2, $MnFe_2O_4$, $CoFe_2O_4$ and Fe_3O_4 have been synthesized using polyol as the solvent (Feldmann and Jungk 2001; Wan et al. 2007). An advantage of this technique is the use of suitable surfactants that can tune the particle characteristics and limit their agglomeration.

3.2.5 Sol-Gel Method

The main steps of sol-gel method include the hydrolysis of metal organic compound precursors, like alcoxysilane (Corr et al. 2008), to produce the corresponding oxohydroxide, followed by condensation to form a network of the metal hydroxide. After hydroxide polymerizes, it forms a dense porous gel and the subsequent drying and heating of which leads to the production of ultrafine porous oxides in the desired

crystal phase. The method has been used to synthesize a variety of metal oxide nanoparticles, like TiO_2, ZnO (Caglar and Ruzgar 2015), MgO, CuO, ZrO_2 and Nb_2O_5 and nanocomposites, like $LiCoO_2$ thin film, Cu-doped ZnO nanoparticles, CuO/Cu_2O nanocomposites (Mallick 2014), Ce-doped ZrO_2, oxides of Hf, Ta and Nb. This technique has also been used to prepare novel nanocomposites such as $InNbO_4$, a photocatalytically active ternary metal oxides semiconductor. Sol-gel method, moreover, allows for a formation of multi-metal oxides instead of a mixture of the individual binary oxides, as shown for SnO_2-doped In_2O_3. Also sol-gel provides the particle size to be tuned by simply varying the gelation time (Fig. 3.2a). In addition, it has been reported that supercritical fluids can be used to synthesize nanoparticles like TiO_2, ZrO_2, Al_2O_3, TiO_2-SiO_2, SiO_2-Al_2O_3 and ZrO_2/TiO_2 hybrid oxide nanotubes (Sui and Charpentier 2012).

3.2.6 Microwave

In this simple benchtop method, the precursors are dissolved in deionized water separately and are made into a mixture of 100 mL solution followed by stirring continuously for 10 min at room temperature until it turns into a white gel (Roy and Bhattacharya 2011). The mixture is then irradiated with microwave energy and is cooled naturally at room temperature. The precipitate is vacuum-filtered, washed with deionized water and absolute ethanol and dried in a vacuum at 80 °C for 1 h (Fig. 3.2b). Microwave-assisted methods involve quick and uniform heating of the reaction medium with no temperature gradients through two mechanisms: dipolar polarization and ionic conduction. Highly crystalline nanoparticles of MnO, Fe_3O_4, CeO_2, CaO, $BaTiO_3$, ZnO, Cr_2O_3, CoO, Mn_2O_3 and MgO have been successfully synthesized using microwave-assisted routes (Roy and Bhattacharya 2011).

3.2.7 Wet Chemical

The wet chemical route is a simple and cost-efficient method that employs any surface irrespective of shapes and curves with wide applicability (Wu et al. 2005). The precursors are mixed in ultrapure water and are stirred for 30 min, combined and heated for 45 min and collected by centrifugation. CuO nanorods, Fe_3O_4 and ZnO NPs have been produced and tested against micro-organisms (Fig. 3.2c).

3.2.8 Microemulsion Method

This method comprises two immiscible phases (oil and water) which are separated by a monolayer of surfactant molecules forming two binary systems—water/

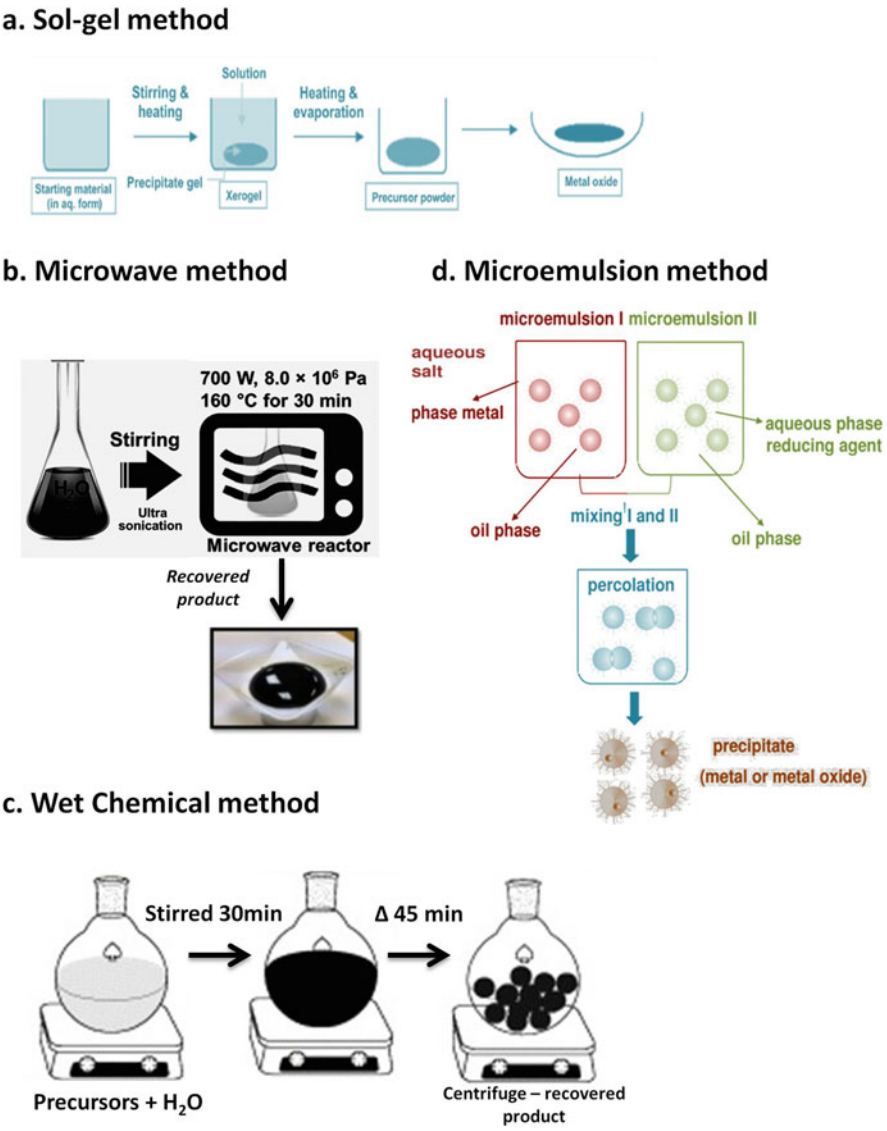

Fig. 3.2 Synthesis methods of metal oxide nanoparticles: (**a**) sol-gel method, (**b**) microwave method, (**c**) wet chemical method and (**d**) microemulsion method

surfactant and oil/surfactant—such that the hydrophobic tails of the surfactant molecules are dissolved in the oil phase and the hydrophilic head groups in the aqueous phase. The microemulsions act as nanoreactors for synthesis of the nanoparticles. This is then followed by centrifugation, wash cycles and drying/calcinations (Fig. 3.2d). Shape and size can be manipulated in these methods by affecting the various self-assembled structures formed in the binary systems (Jaiswal

et al. 2015). This method was used to synthesize iron oxide nanoparticles (Wu et al. 2008), NiO (Jaiswal et al. 2015), CeO_2, TiO_2, ZnO and CuO (Kumar et al. 2013a), and nanocomposites like $BaAlO_2$ and iron oxide-doped alumina nanoparticles. The ability to control the formation of different kinds of core-shell structures with sub-nanometric resolution is seen as a major benefit of this technique (Stankic et al. 2005). Additionally, the method also provides the possibility to manipulate size and morphology of nanoparticles by adjusting parameters such as concentration and type of surfactant, the type of continuous phase, the concentration of precursors and molar ratio of water to surfactant. The disadvantage associated with this method involves the necessity of several washing processes and further stabilization treatment due to aggregation of the produced nanoparticles (Wu et al. 2008).

3.2.9 Laser Ablation Method

This method is used to generate nanoparticles by laser irradiation of immersed targets of colloidal solutions generated from bulk materials immersed in aqueous or nonaqueous solvents (Dolgaev et al. 2002). The method has been used to synthesize ZnO, NiO, SnO_2, ZrO_2, iron oxide and Al_2O_3 but also ternary metal oxides like Au-SnO_2 and Cu/Cu_2O (Fig. 3.3a). The size of the nanoparticles can be controlled by manipulating two parameters: laser fluence and the nature of the liquid media. Some of the drawbacks associated with laser ablation are related to propensity for nanoparticle agglomeration, lack of long-term stabilization in solution and the need for capping (Zamiri et al. 2012).

3.2.10 Chemical Vapour-Based Methods

In chemical vapour deposition, substrates are heated to high temperatures and exposed to precursor materials in the gaseous state. The precursors react or decompose on the substrate surface to form nanomaterial (Fig. 3.3b). In this approach, within the flow reactor, pure metal or its organic salts are heat transformed into the vapour phase and then introduced into a hot-wall reactor, where they react with the oxidizing agent under conditions that favour the chemical nucleation (Chen et al. 2015). Usually an inert gas, such as argon, is used to carry the gaseous reactants to the reaction zone where nucleation and crystal growth occur. Finally, the product that is also in the gas phase is carried to a much cooler zone where, due to such temperature gradient, it transforms into a solid state and can get collected. These techniques are extensively employed to produce uniform and contamination-free metal oxide nanoparticles and films, such as ZnO nanowires and films (Terasako et al. 2007) and defect-free ZnO nanoparticles, nanocubes and nanospheres of magnetite, Cu_2O, MgO and CaO, SnO_2, SrO, CoO and Co_3O_4 and boron-doped ZnO (Yadav and Uplane 2012).

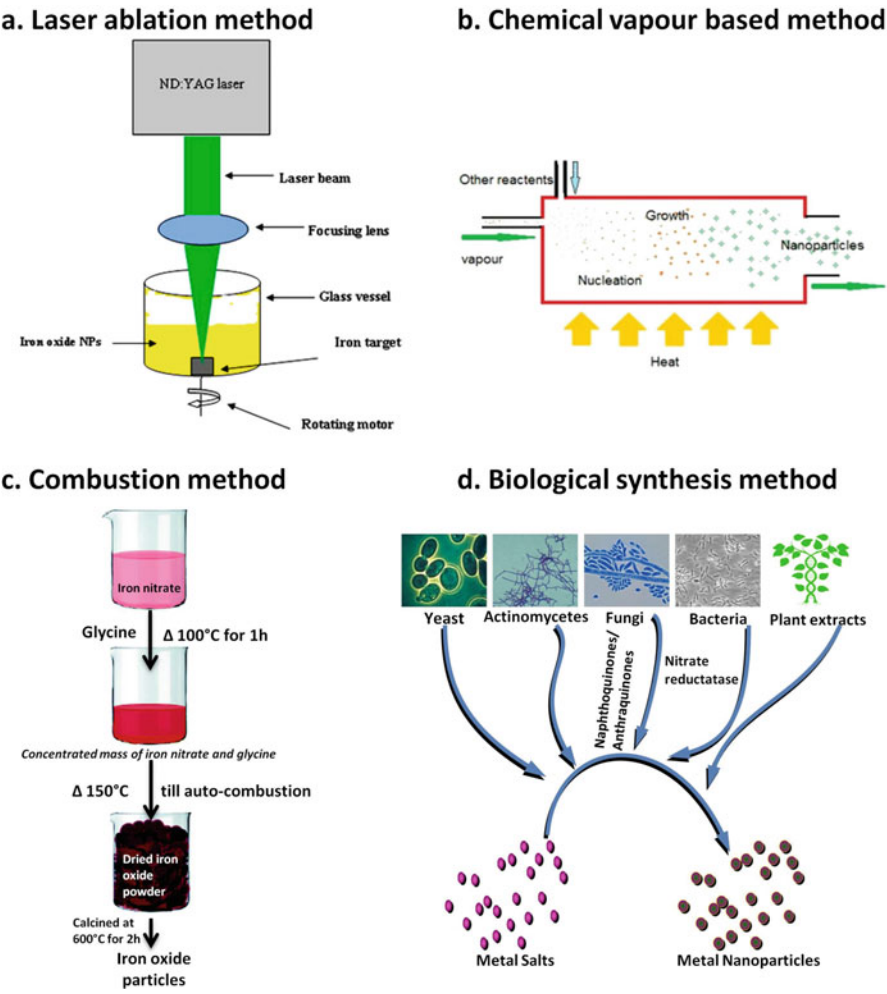

Fig. 3.3 Synthesis methods of metal oxide nanoparticles: (**a**) laser ablation method, (**b**) chemical vapour-based method *from* https://ninithi.wordpress.com/, (**c**) combustion method and (**d**) biological synthesis

3.2.11 Combustion Method

In this synthesis method, pure metallic precursor is heated by different techniques to evaporate it into a background gas in which the second reactant, i.e. oxidizing agent, is admixed (Fig. 3.3c). The synthesis starts with an initialization in which the metal is only partially heated for the oxidation reaction to start. Thereafter, the heat required for the following metal evaporation is produced in situ by the combustion reaction itself. Nanoparticles of ZnO (Assi et al. 2014), FeO, CuO, Mn_2O_3, MgO, CdO and Co_3O_4 or Ag supported on MgO surface, Co_3O_4 on CuO nanowire arrays

(Co_3O_4@CuO) (Feng et al. 2012) and $La_{0.82}Sr_{0.18}MnO_3$ (Epherre et al. 2011) are a few examples of combustion-based method.

3.2.12 Template/Surface-Mediated Synthesis

The major strategies employed in this type of fabrication are electrochemical, electroless depositions and sol-gel (Hulteen and Martin 1997), chemical polymerization (Martin 1996) and chemical vapour deposition (Cepak et al. 1997). Consequently, as the reaction between metal and oxidizing agent may take place in a different medium, this method can be attributed to both of the previously listed classes of synthesis. The method is based on fabrication of the desired nanomaterial within the pores or channels of a nanoporous template. Depending on the properties of the template, various morphologies of nanomaterial, such as rods, fibrils and tubules, can be prepared. This method can be used to synthesize self-assembly systems with tubular and fibrillary-like nanostructures with small diameters (D'Souza and Richards 2007). Highly monodispersed nanostructures with enhanced activities, uniform morphology and a high specific surface area can be obtained using this synthesis method. Examples are mesoporous MoO_2 nanoparticles with improved electrochemical properties, α-Fe_3O_4 and Co_3O_4, Fe_2O_3 and mesoporous $NiMn_2O_x$.

3.2.13 Biological Synthesis

Nature is able to synthesize a variety of metal oxide nanomaterials under ambient conditions (Deravi et al. 2010). Biocompatibility is one of the most important requirements for any nanomaterial used in the field of nanomedicine; extensive research for synthesis techniques using micro-organisms is currently explored. For instance, magnetite nanocrystals have been synthesized in magnetotactic bacteria as a part of their magnetic navigation device (Lang et al. 2007). ZnO nanoparticles were synthesized from leaf extracts (Rajiv et al. 2013). Raliya and Tarafdar have synthesized ZnO, MgO and TiO_2 nanoparticles by using fungus (Raliya and Tarafdar 2014). In these syntheses, an enzymatic reaction replaces the chemical process which eliminates the production of toxic wastes and is more eco-friendly. In addition, a biological synthesis is less energy intensive than its physicochemical counterparts. The particles generated by these processes have higher catalytic reactivity and greater specific surface area, if not coated with a lipid layer. In some cases, nanoparticles produced in micro-organisms are purified and coated with protein corona which confers their physiological solubility and stability. These may be critical for biomedical applications and are the bottleneck of some purification methods. The biological synthesis is supported by the fact that the majority of the bacteria inhabit ambient conditions of varying temperature, pH and pressure. By

varying parameters like micro-organism type and strain, its growth phase, culture growth medium, pH, substrate concentrations, temperature, reaction time, addition of nontarget ions and a source compound of the wanted nanoparticle, it is possible to control size of particle and their monodispersity (Li et al. 2011). Compared to chemical and physical methods, the main drawback associated with biological synthesis is the inability to obtain desired size and/or shape of nanoparticles along with a low yield. Slow in general, this process may take several hours and even a few days. Moreover, the decomposition of formed nanoparticles may take place after a certain period of time. Due to its biocompatibility, however, this process remains very attractive when it comes to the production of potential antibacterial agents (Fig. 3.3d).

3.2.13.1 Mycosynthesis

The precursor compound is added to a fungal filtrate and is stirred continuously for 4–6 h at 80 °C. A white precipitate will be formed after a yellowish brown precipitate on constant stirring. The MeO nanopowder precipitate can be obtained on calcination for 2 h at 350 °C and 400 °C (Gopinath et al. 2015). CeO_2 NPs have been made, and their antibacterial efficacy has been tested (dos Santos et al. 2014).

3.3 Crucial Factors Affecting the Antibacterial Mechanisms of Metal NPs

The physicochemical properties of NPs include their size, charge, zeta potential, surface morphology and crystal structure, which are significant elements that regulate the actions of NPs on bacterial cells. Moreover, environmental conditions, the bacterial strain and the exposure time are other major factors that influence the antibacterial effects of NPs. Many data suggested that a large specific surface area, high surface energy and atomic ligand deficiency lead to the aggregation of metal oxide NPs (Raghunath and Perumal 2017). Therefore, it is important to discuss the main factors influencing the antibacterial activity of metal oxide NPs (Fig. 3.4).

3.3.1 Size

Bacterial adhesion is a well-known process in the formation of bacterial biofilms that makes the individual organisms much more resistant or invulnerable to conventional antibiotics. Current research has shown that the size of a metal NP can greatly affect its antibacterial activity. Smaller NPs have larger specific surface areas, which result in a higher probability of being in touch with and passing through the bacterial cell membrane than with larger NPs or polymers (Gurunathan et al. 2014).

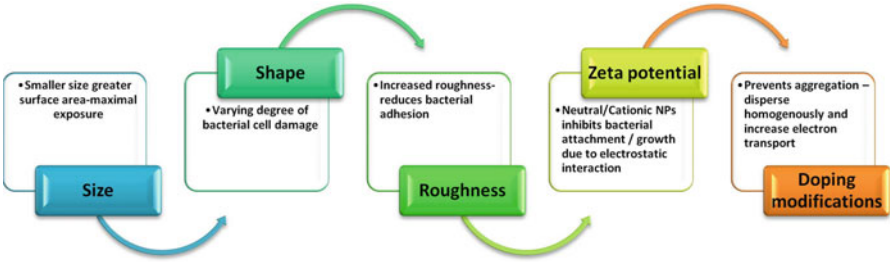

Fig. 3.4 Crucial physiochemical properties affecting the antibacterial mechanisms of metal nanoparticles

3.3.2 Shape

Shape is an important factor related to antimicrobial activity. NPs with different shapes can cause varying degrees of bacterial cell damage through interactions with periplasmic enzymes (Cha et al. 2015). A comparison of pyramid-, plate-, and sphere-shaped ZnO NPs showed that the combination of β-galactosidase and shape-specific ZnO NPs produced photocatalytic activity via obstruction and restructuring of the enzyme. Pyramid-shaped n-ZnO has also been shown to prevent the degradation of enzymes. Y_2O_3 is widely used as an antibacterial agent with broad-spectrum antimicrobial activity. Prismatic-shaped Y_2O_3 NPs have shown greater antibacterial activity against *Pseudomonas desmolyticum* and *S. aureus*. Therefore, the shape of Y_2O_3 NPs may influence their antibacterial activity, which may be due to the direct interaction between prismatic Y_2O_3 NPs and the surface of the bacterial cell membrane, leading to breakage of the bacterial cell membrane. Ag NPs were first applied in the field of biomedicine as sustained-release bactericidal agents. Cube-shaped Ag NPs exhibit stronger antibacterial activity than sphere-shaped and wire-shaped Ag NPs with similar diameters, suggesting that the shape effect on antibacterial activity is due to the specific surface area and facet reactivity (Actis et al. 2015).

3.3.3 Roughness

In contrast to the extensive research regarding the effects of different NP characteristics on bacterial cells, few studies have addressed the effect of roughness. TiO_2 and copper nanoparticles for antimicrobial surface properties were shown previously. As the roughness of NPs increases, the size and the surface area-to-mass ratio promote the adsorption of bacterial proteins, followed by a reduction in bacterial adhesion (Sukhorukova et al. 2015).

3.3.4 Zeta Potential

Recent studies have demonstrated that the zeta potential of NPs has a strong influence on bacterial adhesion. Because the electrostatic attraction between positively charged NPs and the bacterial cell membrane, which is negatively charged, is prone to being adsorbed on the bacterial surface and is closely connected with bacteria, in contrast to their negatively charged counterparts, the potential of NPs to selectively gather at sites of bacterial infection increases vascular permeability (Bian et al. 2011). Accumulation of cationic NPs is beneficial to inhibiting bacterial growth by limiting bacterial attachment. Slight penetration of NPs into the outer regions of the *S. aureus* envelope somehow provides high germicidal efficacy, possibly because the NPs can reach key structures through ion exchange. Compared with negatively charged and neutral NPs, positively charged counterparts have been believed to enhance reactive oxygen species (ROS) production. A recent study showed that negatively charged NPs do not adhere to bacteria due to the negative potential on both. However, at higher concentrations, negatively charged NPs have a certain level of antibacterial activity due to molecular crowding, which leads to interactions between the NPs and the bacterial surface (Arakha et al. 2015).

3.3.5 Doping Modification

The NPs currently used in clinical settings are limited by aggregation. Many studies have employed doping modifications to prevent the aggregation of NPs and to allow NPs to disperse in aqueous environments or other hydrophilic media. Doping modification is also one of the most effective methods to regulate and control the interaction of NPs and bacteria. Lately, the combination of ZnO NPs with Au to form ZnO/Au nanocomposites has been used to improve photocatalytic activity and enhance ROS generation. These effects are a result of the following factors: improved light absorption due to the surface plasmon resonance wavelength of Au; an altered band gap width of ZnO, which enhances the reactivity of photoinduced charge carriers; and increased efficiency of electron transport and charge carrier separation. The activity of antibacterial ZnO can be altered by doping modification (Mehmood et al. 2015). For example, in orthopaedic and dental implants to reduce the formation of biofilms, doped nano-TiO_2 improve the photocatalytic activity by extending the active to visible spectrum (Sangari et al. 2015).

3.3.6 Environmental Conditions

A range of studies have indicated that different environmental conditions cause significant differences in antimicrobial activity. For example, the temperature of

the environment has a potent influence on antibacterial activity due to its effect on the ROS generation rate. When ZnO NPs are stimulated by temperature, electrons are captured at the active sites. Afterwards, the electrons interact with oxygen (O_2) to produce ROS, thereby enhancing the antimicrobial effectiveness of ZnO NPs. Moreover, the pH of the environment influences in vitro antimicrobial activity. A decrease in the pH increases the dissolution rate of ZnO NPs, which results in greater antimicrobial properties (Saliani et al. 2015). pH was specifically found to be associated with a 3.5 ± 0.2 to 5.8 ± 0.1-fold increase in NP adhesion to the bacterial surface. In addition, the loss of efficacy of poly(lactic-co-glycolic acid) (PLGA)-poly (l-histidine) (PLH)-poly(ethylene glycol) (PEG)-encapsulated vancomycin decreased under acidic conditions. The results suggested that selective protonation of the imidazole groups of PLH under acidic conditions strongly influenced NP surface charge switching. At low pH, the surfaces of the NPs were positively charged, which is beneficial to the interaction with the negatively charged groups of the bacterial cell barrier, inducing strong multivalent electrostatic regulation (Radovic-Moreno et al. 2012). The characteristics of the medium, such as the pH and osmotic pressure, can influence the aggregation, surface charge and solubility of NPs (Peretyazhko et al. 2014). Antibacterial tests of ZnO NPs in five types of media demonstrated that the antimicrobial activity of ZnO NPs is mainly due to free Zn ions and zinc complexes. Furthermore, the medium can supply nutrients to bacteria to improve their tolerance to NPs (Li et al. 2011). Finally, a study has shown that preparation of ZnO NPs under different stirring conditions can affect their antibacterial activity against Gram-positive (*B. subtilis*) and Gram-negative (*E. coli*) bacteria and a fungus (*C. albicans*) (Khan et al. 2016).

3.4 Mechanisms of Metal Oxide Nanoparticle (MeO-NP) Antimicrobial Activity

With their unique physical, chemical, electrical, magnetic, optical and biological properties, MeO-NPs are of immense interest to scientists as antimicrobial agents. Molecular mechanisms of antimicrobial activity of MeO-NPs are still in its infancy, and its mechanistic elucidation is a topic that demands in-depth research. Although the mechanisms are not fully understood, research has revealed that retardation/killing of bacterial growth is brought about by the interplay of one or more mechanisms and it varies with the MeO-NP nature and chemistry. The principal mode of antimicrobial activity is the generation of ROS. Besides ROS production, damage to cell membranes by electrostatic interaction, disturbance in metal/metal ion homeostasis, protein and enzyme dysfunction, genotoxicity and photokilling are other modes of action (Fig. 3.5).

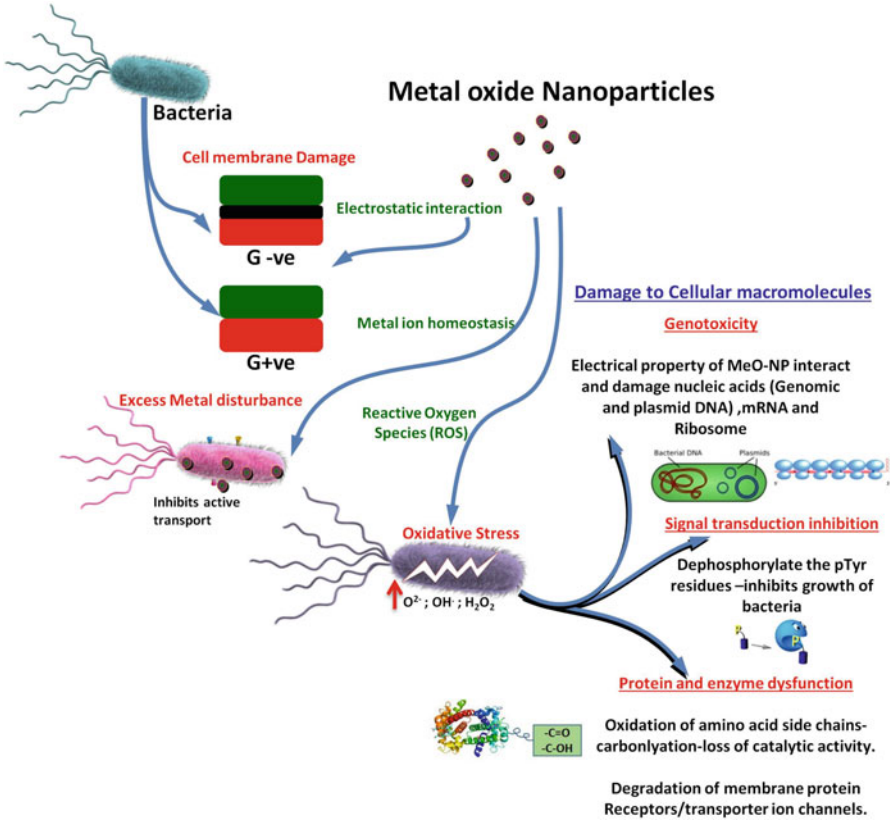

Fig. 3.5 Mechanisms of metal oxide nanoparticle (MeO-NP) antimicrobial activity

3.4.1 Cell Membrane Damage by Electrostatic Interaction

The electronegative chemical groups of the polymers on bacterial membranes are sites of metal cation attraction. The negative charge is carried on the surface of both bacteria and spores at biological pH because of the carboxylic acid groups in the proteins. The charge difference between bacterial membranes and MeO-NPs leads to electrostatic attraction, and thus MeO-NPs accumulate on the cell surface and ultimately allow entry into the bacteria. This co-ordination of membrane polymers with cationic MeO-NPs exerts toxicity to micro-organisms. Gram-negative bacteria have a greater negative charge than Gram-positive bacteria (Chung et al. 2004), and hence the electrostatic interaction will be stronger in Gram-negative strains. Lipo-polysaccharide (LPS) in the outer leaflet of the lipid bilayer has more charge per unit surface than other phospholipids in Gram-negative bacteria, thus rendering them highly negative in charge. The electrostatic force of attraction depends on the surface area available for interaction, which is extensively offered by MeO-NPs compared with their native large-sized particles, thus imparting cytotoxicity. The ratio of

particle size to surface area (smaller particle size with the larger surface area) determines greater the efficacy of MeO-NPs in inhibiting the growth of bacteria. Attachment of MeO-NPs alters the structure and permeability of the cell membrane. Positively charged MeO-NPs make a strong bond with membranes, resulting in the disorganization of cell walls. This membrane disruption in turn increases permeability, eventually pulling more MeO-NPs into the microbial system with simultaneous leakage of cellular contents (cellular factors, LPS and membrane proteins). The pores on the membranes are in the order of nanometres, whereas the bacterial size is in the micrometre range, which makes the entry of MeO-NPs into bacterial cells possible. The zeta potential exhibited by MeO-NPs elevates the interaction with bacterial membranes causing membrane disruption and loss of intracellular contents. Accumulation of MeO-NPs within the cell dissipates the proton motive force, thus disrupting the chemiosmotic potential of the membranes and causing leakage of protons. Growth is inhibited as an after-effect of the electrostatic interaction between MeO-NPs and the cell surface. In some cases, formation of pits is observed in the cell walls of bacteria exposed to aluminium oxide (Al_2O_3) NPs. In addition to cell membrane binding, MeO-NPs bind with mesosomes and hence alter cellular respiration, cell division and DNA replication. Although multiple mechanisms of microbial cell membrane damage have been revealed from different studies (Chung et al. 2004), further investigation is warranted.

3.4.2 Disturbance in Metal/Metal Ion Homeostasis

Metal ion homeostasis is essential for microbial survival as it regulates metabolic functions by assisting coenzymes, cofactors and catalysts. An excess metal or metal ion within a bacterium causes metabolic functional disorders. Metal ions bind with DNA and disrupt the helical nature by cross-linking between and within DNA strands. This has been reported on exposure of micro-organisms to copper oxide (CuO) NPs. Metal ions released from the MeO-NPs carry a positive charge, bringing electrostatic interactions into play. The metal ions neutralize the charges on LPS and increase permeabilization of the outer membrane. Bacterial growth is slowed down as the membranes become disorganized, with increased permeability contributing to the accumulation of MeO-NPs in the cells. ZnO NPs and silver (Ag) NPs were shown to disrupt the porins and LPS in the outer membrane. Strong binding of MeO-NPs to the outer membrane inhibits active transport and the activities of dehydrogenase and periplasmic enzymes, as evidenced from the treatment of *Escherichia coli* with TiO_2 and CdONPs (Rezaei-Zarchi et al. 2010). Long-chain polycations coated onto cell surfaces are reported to efficiently kill both Gram-positive and Gram-negative bacteria (Tiller et al. 2001). Released metal ions from MeO-NPs in cells are reduced to metal atoms by thiol (–SH) groups in enzymes and proteins, thus inactivating the essential metabolic proteins by blocking respiration and leading to cell death. Metal ions can also interact with –SH groups in the peptidoglycan layer and cause cell wall destruction. MeO-NPs slowly release

metal ions through adsorption, dissolution and hydrolysis (Wang et al. 2016); they are toxic and abrasive to bacteria and hence lyse the cells. The abrasive nature of MeO-NPs causes surface defects, thus bringing physical damage to the cell wall.

3.4.3 Production of Reactive Oxygen Species (ROS) and Oxidative Stress

Once MeO-NPs enter into bacteria, they induce the generation of ROS [superoxide anion (O^{2-}), hydroxyl radicals (OH•), hydrogen peroxide (H_2O_2) and organic hydroperoxides] that are pernicious to bacteria, causing damage to almost all organic biomolecules (amino acids, carbohydrates, lipids, nucleic acids and proteins) and eventually causing microbial death. Three key features play a role in the generation of ROS: active redox cycling, pro-oxidant functional groups on the MeO-NP surface and cell-particle interactions (Nel et al. 2006). The change in electronic properties and reduction in particle size produce reactive groups on the surface of the particles. These reactive sites are the centre of interaction between molecular oxygen and electron donor/acceptor active sites and result in the formation of $O^{2\bullet-}$. This $O^{2\bullet-}$ will further produce more ROS through Fenton-type reactions (Nel et al. 2006). The physicochemical properties of MeO-NPs, such as surface area, diffusibility and electrophilic nature, determine the amount of ROS produced in the bacteria. ROS production by MeO-NPs primarily inhibits respiratory enzymes (Thekkae Padil and Cernik 2013). $O^{2\bullet-}$ generates damaged iron-sulphur (Fe-S) clusters in the electron transport chain, releasing more ferrous ions, thus decreasing ATP production. These electrostatic interactions lead to morphological changes in bacterial cells, causing distortion and damage to the bacterial cell membrane on treatment with MeO-NPs. These ferrous ions are oxidized by the Fenton reaction, generating more OH• and eventually damaging DNA, proteins and lipids. H_2O_2, a potent oxidant lethal to cells, harms DNA and proteins in micro-organisms. In fungi, ROS exhibited anticandidal activity through cytotoxicity and apoptotic cell death on exposure to ZnO NPs. ZnO NPs are shown to inhibit fungal growth by impeding cell function and the formation of fungal hyphae (He et al. 2011). These increased free radicals will initiate the peroxidation of unsaturated phospholipids in the membranes, thus producing more peroxyl radical intermediates, leading to severe damage. The membrane architecture becomes damaged due to lipid peroxidation, thus causing conformational changes in membrane proteins and altering membrane fluidity, integrity and lateral organization, ultimately affecting membrane properties and functions. Ion imbalance occurs as more ions leak due to membrane damage. Malondialdehyde (MDA), an index of cell membrane damage, is increased due to lipid peroxidation by ROS. TiO_2 NPs increased the production of MDA in bacterial cells. Being reactive, MDA alters proteins through carbonylation or forms protein-MDA adducts. ROS production damages phospholipids in the membranes, lipoproteins and nucleic acids, causing oxidative stress eventually destroying the microbe.

Glutathione, a non-enzymatic antioxidant, protects bacteria from oxidative stress. Metal ions discharged from MeO-NPs oxidize cellular glutathione leading to excessive ROS. In addition, oxidized glutathione increases lipid peroxidation in the bacterial membrane leading to damage to bacterial cells. The antioxidant enzyme activities are disrupted by excessive generation of ROS within the bacterial cell. This imbalance in oxidants and antioxidants causes oxidative stress within the microbes. Generation of ROS eventually leading to oxidative stress is one of the mechanisms mediated by MeO-NPs against micro-organisms to kill them.

3.4.4 Protein and Enzyme Dysfunction

Protein dysfunction is another mode of antibacterial activity exhibited by MeO-NPs (Aggarwal et al. 2009). Metal ions catalyse the oxidation of amino acid side chains resulting in protein-bound carbonyls. The levels of carbonylation within the protein molecule serve as a marker for oxidative protein damage. This protein carbonylation will lead to loss of catalytic activity in the case of enzymes, ultimately triggering protein degradation. In addition, these ions react with the –SH groups of many proteins and enzymes and render them inactive. Some metals, such as Ag in particular, may act as a weak acid and have a tendency to react with soft bases such as sulphur and phosphorus, which are the main constituents of proteins and DNA, respectively. Metals released can interact with these soft bases and damage DNA, thus leading to cell death. In addition, bacterial Fe-S dehydratases are prone to inactivation by MeO-NPs. In *E. coli*, Cu depleted Fe-S dehydratases and eventually triggered bacteriostasis. Metalloid oxyanion tellurium(IV) generated ROS and oxidized Fe-S clusters (Calderon et al. 2009). Besides obstructing the catalytic site, MeO-NPs are also capable of binding to non-catalytic sites, thereby hindering enzyme activity.

3.4.5 Genotoxicity and Signal Transduction Inhibition

Due to their electrical properties, MeO-NPs interact with nucleic acids, particularly genomic and plasmid DNA (Giannousi et al. 2014). MeO-NPs suppress the cell division of microbes by disrupting the replication processes both of chromosomal and plasmid DNA. Iron oxide (IO) NPs mediated DNA damage by hydrogen peroxide in aerobic micro-organisms (Arakha et al. 2015). In rare cases, metal ions bind to the 30s ribosomal subunit, thus stalling movement of the ribosome complex and blocking the translation of proteins from mRNA. Signal transduction in bacteria is known to be affected by MeO-NPs. Phosphotyrosine is an essential component of the signal transduction mechanism in bacteria; MeO-NPs dephosphorylate the phosphotyrosine residues, thus inhibiting signal transduction and ultimately obstructing the growth of bacteria (Shrivastava et al. 2007).

3.4.6 Photokilling

Photokilling occurs when MeO-NPs are exposed to microbes in the presence of light. Only transition MeOs can be photosensitized, not all MeOs (Chen and Wang 2014). The effect of light will lead to photochemical alteration of the cell membrane, Ca^{2+} permeability, diminution in superoxide dismutase (SOD) activity, damage to proteins/DNA and abnormal cell division. Generation of O^{2-} is the primary reason wherein the generation and release of electrons occur through light. These electrons are grabbed by MeO-NPs, thus generating more ROS. The growth of nosocomial bacteria was suppressed via photochemical reactions exhibited by Fe_3O_4 NPs. Under 50 min of UV light, complete killing of micro-organisms occurred in the presence of TiO_2.

3.4.7 Other Mechanisms

Yet another mechanism found to be effective against *E.coli* occurs when Ag-TiO_2 acts as a photocatalyst under solar light illumination. The surface plasmon resonance effect under solar light sustains the generation of photoinduced electrons, eventually leading to the production of ROS within bacterial cells, thus killing them (Gomathi Devi and Nagaraj 2014). Biofilms are the most difficult to tackle with antibiotics. MeO-NPs offer a great advantage against biofilm formation. A study with superparamagnetic iron oxide nanoparticles (SPIONs) alone and in conjugation with iron and zinc showed antibiofilm efficacy against methicillin-resistant *Staphylococcus aureus* (MRSA) when supplemented with fructose metabolites. The fructose might facilitate increased uptake of SPIONs by biofilms, and in addition it might reduce the toxicity of NP treatments. ZnO NPs in combination with ultrasound stimulus (5 W/cm^2) decreased the *S. aureus* populations efficaciously. Agglomeration of MeO-NPs plays a major role in the interaction with micro-organisms where ultrasound stimulation agitates the clumped bacteria and prevents aggregation of NPs, thus improving the interaction between the particles and microbes. Production of H_2O_2 upon ultrasound stimulus in combination with ZnO NPs was enhanced. Although this ultrasound stimulation is found to be effective, the stimulus will enhance its entry into the systemic circulation. The photothermal killing of MRSA and vancomycin-resistant enterococci using Van-Fe_3O_4@Au nanoeggs was demonstrated (Huang et al. 2009). Van-Fe_3O_4@Au nanoeggs acted as photothermal agents under near-infrared light illuminated at 808 nm, ca. 250 mW/cm^2 exhibited magnetic properties and enhanced photothermal killing of both Gram-positive and Gram-negative bacteria and some antibiotic-resistant strains. The major setback is that this photothermal killing has been demonstrated in a dispersed solution but not in in vitro and in vivo systems (Stankic et al. 2016; Wang et al. 2017). The different mechanisms through which the different MeO-NPs exert their antimicrobial action have not been completely understood. A thorough understanding of how MeO-NPs act on microbes is the need of the hour. Further studies are warranted to determine

whether simple MeO-NPs, the conjugated forms, doped forms functionalization or surface modifications are the best for antimicrobial action and whether all the forms exhibit the same mechanism or do the modifications bring in a change in the mechanism.

3.5 Features and Applications of Few Known MeO-NPs

3.5.1 TiO_2 Nanoparticles

Currently, reports indicate that TiO_2 NPs can be used for many industrial applications and can act as a multifunctional material. These nanoparticles are very durable and work on a wide spectrum of bacteria as antimicrobial agents (Al Othman et al. 2013). The photocatalytic properties of TiO_2 are especially useful in the eradication of bacteria (Al Othman et al. 2013). This property, along with its size and surface characteristics, determines the industrial applications of TiO_2 NPs. These NPs are used in paints, cosmetics, antibacterial agents, sunscreens, treatment of waste water, water treatment for drinking purposes, self-cleaning applications, antifogging agents, gasoline detectors as well as for a large number of biomedical applications. The photocatalytic property of TiO_2 depends on its nanostructure, size along with the purity of the metal oxide used. It has been reported previously that oxidative stress after the formation of ROS could play a very important role in the antimicrobial mechanism of TiO_2 NPs. The generated ROS causes damage to the molecular structure of the cell, including DNA, lipid and protein damage. TiO_2 irradiation by lighting or UV produces band gaps or electron holes and free electrons that allow redox reactions to take place on the surface of the TiO_2 semiconductor. Thus, when the TiO_2 absorbs a high-energy photon, electrons in TiO_2 are excited, which then bounce from the valence band to the conduction band, creating an energy hole and a free electron which, along with an oxidant, reduce the product. In the case of reductive reactions, these electrons combine with an oxygen molecule to form O^{2-} which, along with water, generate hydroxyl radicals. The photocatalytic activity of titanium dioxide is very useful in the degradation of hydrocarbons and organic contaminants in the soil and water. Moreover, this activity also enables the metal oxide to degrade noxious chemicals along with inhibiting biofilms and resisting bacterial growth (Lampimäki et al. 2015; Sahoo et al. 2015). TiO_2 NPs can be used in a wide variety of applications. Some of these include the use of these NPs as antibacterial agents, self-cleaning, UV protection, super-hydrophilic as well as ultra-hydrophobic coats on houses and dye degradation in effluent water along with forming a nano-catalyst when the metal oxide is coupled to cellulose and polycarboxylic acids (Karimi et al. 2010). As mentioned above, the photocatalytic properties of TiO_2 NPs play a major role in the eradication of microbes. The NPs produce reactive oxygen molecules in the presence of UV light. This photocatalytic activity resulted in lipid peroxidation that caused an increase in the membrane fluidity and disrupted the cell structure (Niazi and Gu 2009). However, TiO_2 NPs

could cause considerable damage to the DNA and other biomolecules in human cells and tissues (Fang et al. 2015). TiO_2 thus possesses strong antimicrobial properties due to its mechanism of ROS generation; however, it can prove to be very toxic to human health.

3.5.2 Silver Oxide (Ag_2O) Nanoparticles

Many reports in literature state that Ag NPs are one of the most popular inorganic NPs to be used for inhibition of microbes (El-Batal et al. 2014). Since ancient times, silver has been used in homes and industries as a preferred antimicrobial agent to deal with the microbial attack and avoid spoilage. Currently, scientists are exploring various other applications of Ag NPs along with its bactericidal properties (You et al. 2012). Ag NPs can be produced on a preparatory scale by various techniques (Peters et al. 2014), such as photocatalysis, matrix biochemistry, photochemical or radiochemical, photoreduction, sonolysis, wire explosion, polyols, micelle-based and biological synthesis (Attarchi et al. 2013). As mentioned above, though silver has strong antimicrobial properties (Griffith et al. 2015), it can have an adverse effect on the human body (Ahamed et al. 2010). Silver has an 'oligodynamic' effect, i.e. it is able to exert a bactericidal effect on the containers that are coated with it, e.g. silver pots that store water. This is could be on account of the inherent antimicrobial property by the silver metal (Mousavi et al. 2015). The efficacy of Ag NPs has been tested against a wide range of bacteria. Ag NPs, even in low concentrations, have shown a positive effect on more than 650 disease-causing microbes, including bacteria, algae and fungi, present in the human body. The basic bactericidal mechanism of Ag_2O NPs can be explained in brief: generally, inorganic ions destroy the cell structure by disrupting the membrane and the disulphide linkages present on the various protein in the transmembrane layer (Chichiriccò and Poma 2015). The destruction of this membrane eventually leads to a slowdown in the metabolic processes, leading to cell death. The metal ions further catalyse the formation of free radicals, which oxidize various macromolecules in the cell. There is no contact between the metal ion and the microbes in the body, as the free radicals can travel through the bloodstream and diffuse in the body which inhibits the microbial cell population. As the microbes are not exposed to the radicals for long durations, they are not capable of developing resistance to it. However, in spite of the many advantages, silver ions can affect the biomolecules and lead to cell disruption. They have an affinity for the nucleophile amino acid residues on the proteins and can even react with the sulfhydryl, imidazole, amino, carboxy and phosphate residues in the proteins and the various cellular components (Griffith et al. 2015). Silver also combines with an oxygen molecule and reacts with the sulfhydryl groups, to form R-S-S-R bonds, thus hindering respiratory activities and resulting in cell death (Ikegami et al. 2015). Silver NPs inhibit many oxidative enzymes, including alcohol dehydrogenase, and inhibit the uptake of succinate by the membrane vesicles. They cause oxidative DNA damage and interfere with DNA replication

processes (Hackenberg et al. 2011) and mitochondrial functioning and destroy the cellular membrane structure (Balakumaran et al. 2016; Griffith et al. 2015). Ionic forms of silver or Ag NPs can interact with the bacterial cell wall by electrostatic interactions and form small pits on the cell wall. Generally, low concentrations of Ag + can lead to loss of protons from the cell membrane, resulting in the destruction of cellular structure. The antimicrobial action of Ag NPs was due to the formation of free radicals, which disrupted cell membranes. Furthermore, these free radicals on the membrane surface result in electron spin resonance (ESR), which is another bactericidal effect. The Ag_2O nanoparticles might be demonstrated as a novel antibiotic. These nanoparticles can damage the DNA of *E. coli*, and it can terminate the cell cycle at the G2/M phase due to the DNA damage. The mechanism of this action is through oxidative stress. Therefore, these nanoparticles demonstrated strong antimicrobial activity with high toxicity (Sathyanarayanan et al. 2013).

3.5.3 ZnO Nanoparticles

ZnO NPs are very effective antimicrobial agents and are efficient against both, Gram-positive and Gram-negative bacteria, in addition to the thermophilic and barophilic spores (Raghupathi et al. 2011). The metal oxide, ZnO, has many applications involving their use as solar cells, detectors, displays, gasoline detectors, piezoelectric units, varistors, electro-acoustic transducers, sunscreens, antireflection films, photodiodes accompanied by UV light emitters, UV absorbers and photocatalysts (Montes et al. 2014). The structural formations of ZnO are as nanowires, nanotubes, nanobelts and nanocages. The ZnO NPs are effective antimicrobial agents as they reduce the microbial viability. The exact mechanism of this activity is not understood yet. However, one theory proposes the formation of a strong oxidant, hydrogen peroxide (H_2O_2). Another hypothesis for antibacterial activity of ZnO NPs involves their accumulation on the bacterial cell membrane, with the help of electrostatic attractive forces. Some other possible mechanisms that involve cell membrane disruption include generation of ROS on the NP surface, the release of zinc ion in the cell, membrane dysfunction or internalization of NPs, which could aid in its antimicrobial activity (Li et al. 2012). Besides, ZnO NPs also possess very high photocatalytic properties, which help its role as an antibacterial and antifungal agent. ZnO NPs are capable of forming ROS even under the presence of UV light (Mehmood et al. 2015).

3.5.4 CuO Nanoparticles

Due to their unique physicochemical and biological properties along with their wide antibacterial properties, Cu nanoparticles have become very popular amongst the scientific community (Lee et al. 2013; Li et al. 2012). Copper nanoparticles set

directly into submicron contaminants connected with sepiolite particles and compared the bactericidal efficacy of this mixture with the known antibacterial agent, triclosan. Cu NPs were also deposited on polypropylene by magnetron sputter, to improve its resistance to UV radiation. The improvement in the electromechanical conductivity of the material after deposition of Cu NPs in the form of a thin film was also investigated (Habibi and Rezvani 2015). Cu NPs can easily penetrate across the cell membrane and bring considerable damage to the enzymatic processes of the cell. This property makes them very effective antimicrobial agents (Reyes et al. 2015).

3.5.5 *MgO Nanoparticles*

Magnesium oxide NPs are very stable and biocompatible and are very efficient antibacterial agents. Microbes are capable of developing resistance to any chemical that is added to their natural environment. MgO NPs, being a relatively new ceramic antimicrobial agent, have very effective bactericidal properties. The high alkalinity and presence of oxygen gaps on the MgO NPs also add to their antibacterial property. When used in combination with the other antibacterial agents, they can bring about complete eradication of the pathogenic microbes (Hahn et al. 2012; Sawai 2003). According to published reports, MgO NPs damage the cell membrane and cause lipid peroxidation, leading to the leakage of intracellular contents, which results in cell death (Yamamoto et al. 2010).

3.5.6 *CaO Nanoparticles*

The CaO NPs demonstrated the strong antimicrobial activity due to alkalinity and ROS. The antimicrobial mechanism of these nanoparticles is related to the generation of ROS and increase of pH due to the hydration of this nanoparticle in water. The CaO NPs showed antimicrobial activity against both Gram-negative and Gram-positive bacteria such as *E. coli* and *S. aureus*. The antimicrobial mechanism of CaO NPs was due to the ROS generation. Therefore, it can damage the cell membrane and then leading to the leakage of intracellular contents which can cause cell death. Therefore, CaO nanoparticles indicated excellent antimicrobial activity, but it shows toxicity due to the generation of ROS free radicals (Sawai 2003; Yamamoto et al. 2010).

3.5.7 *CeO_2 Nanoparticles*

Cerium oxide (CeO_2) is a nonstoichiometric compound. The cerium (Ce) atom is characterized by three and four oxidation states (Ce4+, Ce3+). There are oxygen gaps present in the oxidation states of these two CeO_2 NPs. The creation of an

oxygen vacancy is accompanied by the reduction of the Ce4+ form to the Ce3+, resulting in the loss of an oxygen molecule. This unique radical scavenging property of ceria makes them an attractive option in wound healing. CeO_2 nanoparticles have a good antimicrobial activity, as they can act as radical scavengers and block the ROS production to eliminate bacteria (dos Santos et al. 2014).

3.5.8 Y_2O_3 Nanoparticles

Yttrium oxide (Y_2O_3) has a cubic structural composition. The metal oxide, yttrium oxide, is important due to its highest value for free energy released from the formation of its oxide form, from its elemental form. Yttrium oxide (Y_2O_3) does not deviate from its stoichiometry under the normal temperature and pressure conditions or by the effect of atmospheric CO_2 and H_2O. The antioxidant properties of these NPs also prevent the cell death due to excessive oxidative stress. The properties of NPs are dependent on its structure but not on its size, with similar activity seen in the size range of 6–1000 nm. These nanoparticles are able to rescue cells from oxidation cell death induced by stress in a way that seems to be dependent on the structure of the particle but independent to its size in the range of 6–1000 nm. The yttria NPs are relatively non-toxic to macrophages and neutrophils. This is a very useful wound healing property (Becker et al. 2002).

3.5.9 Al_2O_3 Nanoparticles

Alumina forms stable NPs which are resistant to temperature changes and have a hexagonal close packing structure, comprising of the oxygen and the Al^{3+} ions that fill 65% of all the octahedral sites present in the structural network. Alumina NPs act as antioxidants and block the production of ROS, indirectly blocking apoptosis, which initiates the ROS defence system, before completing the cell death programme (Sadiq et al. 2009).

3.5.10 Bimetallic Oxide Nanoparticles

Bimetallic oxides are new materials containing dual active metal oxide NPs (Fe, Ni, Mg, Zn and Ag) that has been considered to have special properties such as high antimicrobial activity. The previously published study reported antimicrobial activity of different bimetallic oxides against Gram-negative and Gram-positive bacteria. ZnMgO NPs are one of the bimetallic oxide NPs that showed antimicrobial activity against Gram-negative (*E. coli*) and Gram-positive (*B. subtilis*) bacteria. The ZnMgO NPs also showed high antibacterial activity against *B. subtilis* bacteria. The Fe-Ag NPs showed high antimicrobial activity against Gram-negative bacteria

(*E. coli*). The antimicrobial mechanism of both might the ROS generation and cell wall damaged. Therefore, the combination of this metal oxide can be improved only antimicrobial activity (Parham et al. 2016; Vidic et al. 2013).

3.6 Limitations of the Current Research and Future Prospects

The antibacterial mechanisms of NPs are still unclear. For instance, many studies attribute the antibacterial activity to oxidative stress or ROS, whereas for other NPs, such as MgO NPs, the antibacterial mechanism may not be associated with the regulation of bacterial metabolism. Therefore, the antibacterial mechanisms of NPs are worth addressing in future research. The lack of unified standards is one limitation of the existing studies on the antibacterial mechanisms of NPs. In particular, different bacterial strains, action times and NP characteristics have been examined in different studies, which make it difficult to compare antibacterial activity. Moreover, no single method fulfils all the conditions for obtaining information about the antibacterial mechanisms of NPs. Because different types of NPs exhibit different antibacterial effects, a comprehensive analysis is often proposed to study the potential antibacterial mechanisms. Sensitive bacterial strains are also often used to exactly determine the antibacterial activity of NPs. Other limitations are the complex structure of the bacterial cell membrane and the lack of research approaches for in vitro studies. Furthermore, in vitro models cannot fully simulate the in vivo condition to accurately duplicate cellular interactions in the body. Therefore, it is impossible to estimate the antibacterial action of NPs through in vitro bacterial cell culture alone. There are still many unanswered questions regarding nanoneurotoxicity, such as how NPs cross the bacterial cell membrane. The bacterial cell membrane is both a barrier and a channel for the inward and outward movement of substances. In Gram-negative bacteria cell membranes, porins, which generally allow the passage of molecules, 600 Da, are the main channels for the movement of foreign molecules into and out of the bacterial cell body. Therefore, the transport of nearly NPs will be limited due to their size. However, certain scholars have proposed that porins can mediate the passage of NPs with diameters in the range of 1–9 nm through the bacterial cell membrane (Huang et al. 2009). Endocytosis of bacteria, similar to what is observed for eukaryotic cells, may be considered as another mechanism of NP movement (Wang et al. 2017). However, no results have been presented on this topic. Currently, the most reasonable mechanism is that bacterial cell exposure to lower concentrations of NPs causes the complete disintegration of the cells and removal of the LPS layer, which protrudes from the cell surface in the form of vesicles. Such membrane protrusions bind to NPs, which then enter the cell by electrostatic attraction. Furthermore, studies addressing the intracellular inhibitory mechanisms remain limited. The oxidative stress induced by NPs deserves attention, and few

studies have considered the action of NPs on the gene expression, protein synthesis and metabolism of bacterial cells.

The next hurdle in the use of MeO-NPs as antimicrobials is their potential toxicity in humans. Although MeO-NPs can be an alternative to conventional antibiotics, the disruption of beneficial microflora is a concern in addition to the systemic toxicity, and effective delivery has to be explored. The need of the hour is knowledge of the interaction of MeO-NPs with human cells and organs, such as their ability to cross the blood-brain barrier and blood-testis barrier. Such knowledge acquired through studies in the coming years will explore MeO-NPs in agriculture, environmental sciences, food science, medicine and veterinary science. Microbes expel conventional antibiotics and acquire resistance through ATP-binding cassette (ABC) transporters. The importing of divalent metal ions into the cell through ABC transporters has not yet been explored by scientists.

3.7 Conclusion

Finally it may be concluded that the metal oxide nanoparticles with the minimized toxicity possibly will be extensively used in the near future for eradicating several infectious conditions. We believe that development of the simple and low-cost inorganic antimicrobial agents such as metal and metal oxide nanoparticles as alternative of traditional antibiotics might be promising for the future of pharmaceutics and medicine to overcome antimicrobial resistance.

Acknowledgements The authors acknowledge Mr. William McLean for critical proofreading and excellent editing of this book chapter.

References

Actis L, Srinivasan A, Lopez-Ribot JL, Ramasubramanian AK, Ong JL (2015) Effect of silver nanoparticle geometry on methicillin susceptible and resistant Staphylococcus aureus, and osteoblast viability. J Mater Sci Mater Med 26:215. https://doi.org/10.1007/s10856-015-5538-8

Aggarwal P, Hall JB, McLeland CB, Dobrovolskaia MA, McNeil SE (2009) Nanoparticle interaction with plasma proteins as it relates to particle biodistribution, biocompatibility and therapeutic efficacy. Adv Drug Deliv Rev 61:428–437. https://doi.org/10.1016/j.addr.2009.03.009

Ahamed M, Alsalhi MS, Siddiqui MK (2010) Silver nanoparticle applications and human health. Clin Chim Acta 411:1841–1848. https://doi.org/10.1016/j.cca.2010.08.016

Al Othman ZA, Alam MM, Naushad M, Inamuddin, Khan MF (2013) Inorganic nanoparticles and nanomaterials based on titanium (Ti): applications in medicine. Mater Sci Forum 754:21–87. https://doi.org/10.4028/www.scientific.net/MSF.754.21

Arakha M et al (2015) Antimicrobial activity of iron oxide nanoparticle upon modulation of nanoparticle-bacteria interface. Sci Rep 5:14813. https://doi.org/10.1038/srep14813

Assi N, Mohammadi A, Sadr Manuchehri Q, Walker RB (2014) Synthesis and characterization of ZnO nanoparticle synthesized by a microwave-assisted combustion method and catalytic activity for the removal of ortho-nitrophenol. Desalin Water Treat 54:1939–1948. https://doi.org/10.1080/19443994.2014.891083

Attarchi N, Montazer M, Toliyat T (2013) Ag/TiO2/β-CD nano composite: preparation and photo catalytic properties for methylene blue degradation. Appl Catal A Gen 467:107–116. https://doi.org/10.1016/j.apcata.2013.07.018

Balakumaran MD, Ramachandran R, Balashanmugam P, Mukeshkumar DJ, Kalaichelvan PT (2016) Mycosynthesis of silver and gold nanoparticles: optimization, characterization and antimicrobial activity against human pathogens. Microbiol Res 182:8–20. https://doi.org/10.1016/j.micres.2015.09.009

Becker S, Soukup JM, Gallagher JE (2002) Differential particulate air pollution induced oxidant stress in human granulocytes, monocytes and alveolar macrophages. Toxicol in Vitro 16:209–218. https://doi.org/10.1016/s0887-2333(02)00015-2

Bian S-W, Mudunkotuwa IA, Rupasinghe T, Grassian VH (2011) Aggregation and dissolution of 4 nm ZnO nanoparticles in aqueous environments: influence of pH, ionic strength, size, and adsorption of humic acid. Langmuir 27:6059–6068. https://doi.org/10.1021/la200570n

Caglar M, Ruzgar S (2015) Influence of the deposition temperature on the physical properties of high electron mobility ZnO films by sol–gel process. J Alloys Compd 644:101–105. https://doi.org/10.1016/j.jallcom.2015.04.167

Calderon IL et al (2009) Tellurite-mediated disabling of [4Fe-4S] clusters of Escherichia coli dehydratases. Microbiology 155:1840–1846. https://doi.org/10.1099/mic.0.026260-0

Cepak VM et al (1997) Chemical strategies for template syntheses of composite micro- and nanostructures. Chem Mater 9:1065–1067. https://doi.org/10.1021/cm970014c

Cha S-H, Hong J, McGuffie M, Yeom B, VanEpps JS, Kotov NA (2015) Shape-dependent biomimetic inhibition of enzyme by nanoparticles and their antibacterial activity. ACS Nano 9:9097–9105. https://doi.org/10.1021/acsnano.5b03247

Chen H, Wang L (2014) Nanostructure sensitization of transition metal oxides for visible-light photocatalysis. Beilstein J Nanotechnol 5:696–710. https://doi.org/10.3762/bjnano.5.82

Chen Y, Tian X, Zeng W, Zhu X, Hu H, Duan H (2015) Vapor-phase preparation of gold nanocrystals by chloroauric acid pyrolysis. J Colloid Interface Sci 439:21–27. https://doi.org/10.1016/j.jcis.2014.10.017

Chichiriccò G, Poma A (2015) Penetration and toxicity of nanomaterials in higher plants. Nanomaterials 5:851–873. https://doi.org/10.3390/nano5020851

Chung YC, Su YP, Chen CC, Jia G, Wang HL, Wu JC, Lin JG (2004) Relationship between antibacterial activity of chitosan and surface characteristics of cell wall. Acta Pharmacol Sin 25:932–936

Colombo M et al (2012) Biological applications of magnetic nanoparticles. Chem Soc Rev 41:4306–4334. https://doi.org/10.1039/c2cs15337h

Corr SA, Gun'ko YK, Douvalis AP, Venkatesan M, Gunning RD, Nellist PD (2008) From nanocrystals to nanorods: new iron oxide−silica nanocomposites from metallorganic precursors. J Phys Chem C 112:1008–1018. https://doi.org/10.1021/jp076871d

D'Souza L, Richards R (2007) Synthesis of metal-oxide nanoparticles: liquid–solid transformations. Synthesis, properties, and applications of oxide nanomaterials. John Wiley & Sons, Hoboken

Deravi L, Swartz J, Wright D (2010) The biomimetic synthesis of metal oxide nanomaterials vol 2. Nanomaterials for the life sciences vol. 2: nanostructured oxides. WILEY-VCH Verlag GmbH & Co. KGaA, Weinheim

Dolgaev SI, Simakin AV, Voronov VV, Shafeev GA, Bozon-Verduraz F (2002) Nanoparticles produced by laser ablation of solids in liquid environment. Appl Surf Sci 186:546–551. https://doi.org/10.1016/s0169-4332(01)00634-1

dos Santos C, Passos Farias I, Reis Albuquerque A, e Silva P, Costa One G, Sampaio F (2014) Antimicrobial activity of nano cerium oxide (IV) (CeO2) against Streptococcus mutans. BMC Proc 8(Suppl 4):P48. https://doi.org/10.1186/1753-6561-8-s4-p48

El-Batal A, Haroun B, Farrag A, Baraka A, El-Sayyad G (2014) Synthesis of silver nanoparticles and incorporation with certain antibiotic using gamma irradiation. Br J Pharm Res 4:1341–1363

Epherre R et al (2011) Manganite perovskite nanoparticles for self-controlled magnetic fluid hyperthermia: about the suitability of an aqueous combustion synthesis route. J Mater Chem 21:4393–4401. https://doi.org/10.1039/c0jm03963b

Fang Q, Shi X, Zhang L, Wang Q, Wang X, Guo Y, Zhou B (2015) Effect of titanium dioxide nanoparticles on the bioavailability, metabolism, and toxicity of pentachlorophenol in zebrafish larvae. J Hazard Mater 283:897–904. https://doi.org/10.1016/j.jhazmat.2014.10.039

Feldmann C, Jungk HO (2001) Polyol-mediated preparation of nanoscale oxide particles we thank Jacqueline Merikhi and Gerd Much for carrying out the scanning electron microscopy (SEM) and the atomic force microscopy (AFM) investigations, respectively. Angew Chem Int Ed Eng 40:359–362

Feng Y, Cho IS, Rao PM, Cai L, Zheng X (2012) Sol-flame synthesis: a general strategy to decorate nanowires with metal oxide/noble metal nanoparticles. Nano Lett 13:855–860. https://doi.org/10.1021/nl300060b

Gedanken A (2004) Using sonochemistry for the fabrication of nanomaterials. Ultrason Sonochem 11:47–55. https://doi.org/10.1016/j.ultsonch.2004.01.037

Giannousi K, Lafazanis K, Arvanitidis J, Pantazaki A, Dendrinou-Samara C (2014) Hydrothermal synthesis of copper based nanoparticles: antimicrobial screening and interaction with DNA. J Inorg Biochem 133:24–32. https://doi.org/10.1016/j.jinorgbio.2013.12.009

Gomathi Devi L, Nagaraj B (2014) Disinfection of Escherichia coli Gram negative bacteria using surface modified TiO2: optimization of Ag metallization and depiction of charge transfer mechanism. Photochem Photobiol 90:1089–1098. https://doi.org/10.1111/php.12308

Gopalakrishnan K, Joshi HM, Kumar P, Panchakarla LS, Rao CNR (2011) Selectivity in the photocatalytic properties of the composites of TiO2 nanoparticles with B- and N-doped graphenes. Chem Phys Lett 511:304–308. https://doi.org/10.1016/j.cplett.2011.06.033

Gopinath K, Karthika V, Sundaravadivelan C, Gowri S, Arumugam A (2015) Mycogenesis of cerium oxide nanoparticles using Aspergillus niger culture filtrate and their applications for antibacterial and larvicidal activities. J Nanostruct Chem 5:295–303. https://doi.org/10.1007/s40097-015-0161-2

Griffith M, Udekwu KI, Gkotzis S, Mah T-F, Alarcon EI (2015) Anti-microbiological and anti-infective activities of silver. In: Silver nanoparticle applications. Engineering materials, pp 127–146. https://doi.org/10.1007/978-3-319-11262-6_6

Gurunathan S, Han JW, Kwon DN, Kim JH (2014) Enhanced antibacterial and anti-biofilm activities of silver nanoparticles against gram-negative and gram-positive bacteria. Nanoscale Res Lett 9:373. https://doi.org/10.1186/1556-276X-9-373

Habibi MH, Rezvani Z (2015) Photocatalytic degradation of an azo textile dye (C.I. Reactive Red 195 (3BF)) in aqueous solution over copper cobaltite nanocomposite coated on glass by Doctor Blade method. Spectrochim Acta A Mol Biomol Spectrosc 147:173–177. https://doi.org/10.1016/j.saa.2015.03.077

Hackenberg S et al (2011) Silver nanoparticles: evaluation of DNA damage, toxicity and functional impairment in human mesenchymal stem cells. Toxicol Lett 201:27–33. https://doi.org/10.1016/j.toxlet.2010.12.001

Hahn A, Fuhlrott J, Loos A, Barcikowski S (2012) Cytotoxicity and ion release of alloy nanoparticles. J Nanopart Res 14:1–10. https://doi.org/10.1007/s11051-011-0686-3

He L, Liu Y, Mustapha A, Lin M (2011) Antifungal activity of zinc oxide nanoparticles against Botrytis cinerea and Penicillium expansum. Microbiol Res 166:207–215. https://doi.org/10.1016/j.micres.2010.03.003

Huang WC, Tsai PJ, Chen YC (2009) Multifunctional Fe3O4@Au nanoeggs as photothermal agents for selective killing of nosocomial and antibiotic-resistant bacteria. Small 5:51–56. https://doi.org/10.1002/smll.200801042

Hulteen JC, Martin CR (1997) A general template-based method for the preparation of nanomaterials. J Mater Chem 7:1075–1087. https://doi.org/10.1039/a700027h

Ikegami T et al (2015) Two novel motifs of watermelon silver mottle virus NSs protein are responsible for RNA silencing suppression and pathogenicity. PLoS One 10(5):e0126161. https://doi.org/10.1371/journal.pone.0126161

Jaiswal M, Dudhe R, Sharma PK (2015) Nanoemulsion: an advanced mode of drug delivery system. 3 Biotech 5:123–127. https://doi.org/10.1007/s13205-014-0214-0

Karimi L, Mirjalili M, Yazdanshenas ME, Nazari A (2010) Effect of nano TiO2 on self-cleaning property of cross-linking cotton fabric with succinic acid under UV irradiation. Photochem Photobiol 86:1030–1037. https://doi.org/10.1111/j.1751-1097.2010.00756.x

Khan MF et al (2016) Sol-gel synthesis of thorn-like ZnO nanoparticles endorsing mechanical stirring effect and their antimicrobial activities: potential role as nano-antibiotics. Sci Rep 6:27689. https://doi.org/10.1038/srep27689

Kumar A, Saxena A, De A, Shankar R, Mozumdar S (2013a) Facile synthesis of size-tunable copper and copper oxide nanoparticles using reverse microemulsions. RSC Adv 3:5015–5021. https://doi.org/10.1039/c3ra23455j

Kumar H, Manisha, Sangwan P (2013b) Synthesis and characterization of MnO2 nanoparticles using co-precipitation technique. Int J Chem Chem Eng 3:155–160

Lai J, Shafi KL, Ulman A, Lee Y, Vogt T, Estournès C (2003) Doping γ-Fe2O3 nanoparticles with Mn(III) suppresses the transition to the α-Fe2O3 structure. J Am Chem Soc 125:11470–11471. https://doi.org/10.1021/ja035409d

Lampimäki M et al (2015) Exploring the environmental photochemistry on the TiO2(110) surface in situ by near ambient pressure X-ray photoelectron spectroscopy. J Phys Chem C 119:7076–7085. https://doi.org/10.1021/jp511340n

Lang C, Schuler D, Faivre D (2007) Synthesis of magnetite nanoparticles for bio- and nanotechnology: genetic engineering and biomimetics of bacterial magnetosomes. Macromol Biosci 7:144–151. https://doi.org/10.1002/mabi.200600235

Lee H-J, Song JY, Kim BS (2013) Biological synthesis of copper nanoparticles using Magnolia kobus leaf extract and their antibacterial activity. J Chem Technol Biotechnol 88:1971–1977. https://doi.org/10.1002/jctb.4052

Li X, Xu H, Chen Z-S, Chen G (2011) Biosynthesis of nanoparticles by microorganisms and their applications. J Nanomater 2011:1–16. https://doi.org/10.1155/2011/270974

Li Y, Zhang W, Niu J, Chen Y (2012) Mechanism of photogenerated reactive oxygen species and correlation with the antibacterial properties of engineered metal-oxide nanoparticles. ACS Nano 6:5164–5173. https://doi.org/10.1021/nn300934k

Mallick P (2014) Synthesis of copper oxide nanocomposite (Cu2O/CuO) by sol–gel route. Proc Natl Acad Sci, India Sect A: Phys Sci 84:387–389. https://doi.org/10.1007/s40010-014-0131-y

Martin CR (1996) Membrane-based synthesis of nanomaterials. Chem Mater 8:1739–1746. https://doi.org/10.1021/cm960166s

Mascolo MC, Pei Y, Ring TA (2013) Room temperature co-precipitation synthesis of magnetite nanoparticles in a large pH window with different bases. Materials (Basel) 6:5549–5567. https://doi.org/10.3390/ma6125549

Mehmood S, Rehman MA, Ismail H, Mirza B, Bhatti AS (2015) Significance of postgrowth processing of ZnO nanostructures on antibacterial activity against gram-positive and gram-negative bacteria. Int J Nanomedicine 10:4521–4533. https://doi.org/10.2147/IJN.S83356

Montes V et al (2014) Synthesis of different ZnO-supported metal systems through microemulsion technique and application to catalytic transformation of glycerol to acetol and 1,2-propanediol. Catal Today 223:129–137. https://doi.org/10.1016/j.cattod.2013.09.021

Mousavi FP, Pour HH, Nasab AH, Rajabalipour AA, Barouni M (2015) Investigation into shelf life of fresh dates and pistachios in a package modified with nano-silver glob. J Health Sci 8:134–144. https://doi.org/10.5539/gjhs.v8n5p134

Nel A, Xia T, Madler L, Li N (2006) Toxic potential of materials at the nanolevel. Science 311:622–627. https://doi.org/10.1126/science.1114397

Niazi JH, Gu MB (2009) Toxicity of metallic nanoparticles in microorganisms- a review. In: Atmospheric and biological environmental monitoring, pp 193–206. https://doi.org/10.1007/978-1-4020-9674-7_12

Pandey P, Merwyn S, Agarwal GS, Tripathi BK, Pant SC (2012) Electrochemical synthesis of multi-armed CuO nanoparticles and their remarkable bactericidal potential against waterborne bacteria. J Nanopart Res 14:709–721. https://doi.org/10.1007/s11051-011-0709-0

Parham S, Wicaksono DHB, Bagherbaigi S, Lee SL, Nur H (2016) Antimicrobial treatment of different metal oxide nanoparticles: a critical review. J Chin Chem Soc 63:385–393. https://doi.org/10.1002/jccs.201500446

Peretyazhko TS, Zhang Q, Colvin VL (2014) Size-controlled dissolution of silver nanoparticles at neutral and acidic pH conditions: kinetics and size changes. Environ Sci Technol 48:11954–11961. https://doi.org/10.1021/es5023202

Peters RJB, Rivera ZH, van Bemmel G, Marvin HJP, Weigel S, Bouwmeester H (2014) Development and validation of single particle ICP-MS for sizing and quantitative determination of nano-silver in chicken meat. Anal Bioanal Chem 406(16):3875–3885. https://doi.org/10.1007/s00216-013-7571-0

Radovic-Moreno AF, Lu TK, Puscasu VA, Yoon CJ, Langer R, Farokhzad OC (2012) Surface charge-switching polymeric nanoparticles for bacterial cell wall-targeted delivery of antibiotics. ACS Nano 6:4279–4287. https://doi.org/10.1021/nn3008383

Raghunath A, Perumal E (2017) Metal oxide nanoparticles as antimicrobial agents: a promise for the future. Int J Antimicrob Agents 49:137–152. https://doi.org/10.1016/j.ijantimicag.2016.11.011

Raghupathi KR, Koodali RT, Manna AC (2011) Size-dependent bacterial growth inhibition and mechanism of antibacterial activity of zinc oxide nanoparticles. Langmuir 27:4020–4028. https://doi.org/10.1021/la104825u

Rajiv P, Rajeshwari S, Venckatesh R (2013) Bio-fabrication of zinc oxide nanoparticles using leaf extract of Parthenium hysterophorus L. and its size-dependent antifungal activity against plant fungal pathogens. Spectrochim Acta A Mol Biomol Spectrosc 112:384–387. https://doi.org/10.1016/j.saa.2013.04.072

Raliya R, Tarafdar JC (2014) Biosynthesis and characterization of zinc, magnesium and titanium nanoparticles: an eco-friendly approach. Int Nano Lett 4(1):93. https://doi.org/10.1007/s40089-014-0093-8

Reyes VC, Opot SO, Mahendra S (2015) Planktonic and biofilm-grown nitrogen-cycling bacteria exhibit different susceptibilities to copper nanoparticles. Environ Toxicol Chem 34:887–897. https://doi.org/10.1002/etc.2867

Rezaei-Zarchi S, Javed A, Javeed G, Soufian S, Barzegari F, Bayanduri M (2010) Comparative study of antimicrobial activities of TiO2 and CdO nanoparticles against the pathogenic strain of Escherichia coli. Iran J Pathol 5:83–89

Roy A, Bhattacharya J (2011) Microwave-assisted synthesis and characterization of CaO nanoparticles. Int J Nanosci 10:413–418. https://doi.org/10.1142/s0219581x11008150

Sadiq IM, Chowdhury B, Chandrasekaran N, Mukherjee A (2009) Antimicrobial sensitivity of Escherichia coli to alumina nanoparticles. Nanomedicine 5:282–286. https://doi.org/10.1016/j.nano.2009.01.002

Sahoo DP, Rath D, Nanda B, Parida KM (2015) Transition metal/metal oxide modified MCM-41 for pollutant degradation and hydrogen energy production: a review. RSC Adv 5:83707–83724. https://doi.org/10.1039/c5ra14555d

Saliani M, Jalal R, Kafshdare Goharshadi E (2015) Effects of pH and temperature on antibacterial activity of zinc oxide nanofluid against Escherichia coli O157: H7 and Staphylococcus aureus. Jundishapur J Microbiol 8:e17115. https://doi.org/10.5812/jjm.17115

Sangari M, Umadevi M, Mayandi J, Pinheiro JP (2015) Photocatalytic degradation and antimicrobial applications of F-doped MWCNTs/TiO2 composites. Spectrochim Acta A Mol Biomol Spectrosc 139:290–295. https://doi.org/10.1016/j.saa.2014.12.061

Sathyanarayanan MB, Balachandranath R, Genji Srinivasulu Y, Kannaiyan SK, Subbiahdoss G (2013) The effect of gold and iron-oxide nanoparticles on biofilm-forming pathogens. ISRN Microbiol 2013:272086. https://doi.org/10.1155/2013/272086

Sawai J (2003) Quantitative evaluation of antibacterial activities of metallic oxide powders (ZnO, MgO and CaO) by conductimetric assay. J Microbiol Methods 54:177–182

Shafi K, Felner I, Mastai Y, Gedanken A (1999) Olympic ring formation from newly prepared barium hexaferrite nanoparticle suspension. J Phys Chem B 103:3358–3360. https://doi.org/10.1021/jp9846911

Shrivastava S, Bera T, Roy A, Singh G, Ramachandrarao P, Dash D (2007) Characterization of enhanced antibacterial effects of novel silver nanoparticles. Nanotechnology 18(22):225103. https://doi.org/10.1088/0957-4484/18/22/225103

Stankic S, Sterrer M, Hofmann P, Bernardi J, Diwald O, Knözinger E (2005) Novel optical surface properties of Ca2+-doped MgO nanocrystals. Nano Lett 5:1889–1893. https://doi.org/10.1021/nl0511418

Stankic S, Suman S, Haque F, Vidic J (2016) Pure and multi metal oxide nanoparticles: synthesis, antibacterial and cytotoxic properties. J Nanobiotechnol 14:73. https://doi.org/10.1186/s12951-016-0225-6

Sui R, Charpentier P (2012) Synthesis of metal oxide nanostructures by direct sol–gel chemistry in supercritical fluids. Chem Rev 112:3057–3082. https://doi.org/10.1021/cr2000465

Sujatha K, Seethalakshmi T, Shanmugasundaram O (2016) Synthesis, characterization of nano tin oxide via co-precipitation method. Nanotechnol Res Pract 11(3):98–105. https://doi.org/10.13187/nrp.2016.11.98

Sukhorukova IV et al (2015) Toward bioactive yet antibacterial surfaces. Colloids Surf B: Biointerfaces 135:158–165. https://doi.org/10.1016/j.colsurfb.2015.06.059

Terasako T, Yagi M, Ishizaki M, Senda Y, Matsuura H, Shirakata S (2007) Growth of zinc oxide films and nanowires by atmospheric-pressure chemical vapor deposition using zinc powder and water as source materials. Surf Coat Technol 201:8924–8930. https://doi.org/10.1016/j.surfcoat.2007.04.017

Thekkae Padil VV, Cernik M (2013) Green synthesis of copper oxide nanoparticles using gum karaya as a biotemplate and their antibacterial application. Int J Nanomedicine 8:889–898. https://doi.org/10.2147/IJN.S40599

Tiller JC, Liao CJ, Lewis K, Klibanov AM (2001) Designing surfaces that kill bacteria on contact. Proc Natl Acad Sci U S A 98:5981–5985. https://doi.org/10.1073/pnas.111143098

Vidic J et al (2013) Selective antibacterial effects of mixed ZnMgO nanoparticles. J Nanopart Res 15(5):1595. https://doi.org/10.1007/s11051-013-1595-4

Wan J, Cai W, Meng X, Liu E (2007) Monodisperse water-soluble magnetite nanoparticles prepared by polyol process for high-performance magnetic resonance imaging. Chem Commun (Camb) 2007:5004–5006. https://doi.org/10.1039/b712795b

Wang D, Lin Z, Wang T, Yao Z, Qin M, Zheng S, Lu W (2016) Where does the toxicity of metal oxide nanoparticles come from: the nanoparticles, the ions, or a combination of both? J Hazard Mater 308:328–334. https://doi.org/10.1016/j.jhazmat.2016.01.066

Wang L, Hu C, Shao L (2017) The antimicrobial activity of nanoparticles: present situation and prospects for the future. Int J Nanomedicine 12:1227–1249. https://doi.org/10.2147/IJN.S121956

Wu X, Zheng L, Wu D (2005) Fabrication of superhydrophobic surfaces from microstructured ZnO-based surfaces via a wet-chemical route. Langmuir 21:2665–2667. https://doi.org/10.1021/la050275y

Wu W, He Q, Jiang C (2008) Magnetic iron oxide nanoparticles: synthesis and surface functionalization strategies. Nanoscale Res Lett 3:397–415. https://doi.org/10.1007/s11671-008-9174-9

Yadav S, Uplane M (2012) Synthesis and properties of boron doped ZnO thin films by spray CVD technique at low substrate temperature. Int J Eng Sci Technol 4:4893–4898

Yamamoto O, Ohira T, Alvarez K, Fukuda M (2010) Antibacterial characteristics of CaCO3–MgO composites. Mater Sci Eng B 173:208–212. https://doi.org/10.1016/j.mseb.2009.12.007

You C, Han C, Wang X, Zheng Y, Li Q, Hu X, Sun H (2012) The progress of silver nanoparticles in the antibacterial mechanism, clinical application and cytotoxicity. Mol Biol Rep 39:9193–9201. https://doi.org/10.1007/s11033-012-1792-8

Zamiri R, Zakaria A, Ahangar HA, Darroudi M, Zak AK, Drummen GPC (2012) Aqueous starch as a stabilizer in zinc oxide nanoparticle synthesis via laser ablation. J Alloys Compd 516:41–48. https://doi.org/10.1016/j.jallcom.2011.11.118

Chapter 4
Nanomaterials for Advanced Analytical Applications in Chemo- and Biosensors

Selvaraj Devi and Vairaperumal Tharmaraj

Contents

Abstract Nanomaterials with unique optical properties and biocompatibility have been widely employed for designing and fabricating highly selective and sensitive nanosensors for the detection of various chemical and biological species. The development of nanomaterial-based chemo- and biosensors is studied usually under direct spectroscopic and reagent-mediated sensor platforms using both unmodified and surface-functionalized nanomaterials. This chapter mainly focuses on selective sensing of chemical and biological molecules using various types of nanomaterials. The main readouts are absorption (colorimetric, UV-visible), fluorescence, Raman/SERS spectroscopic, and electrochemical sensing techniques. The detailed discussion on the design of nanomaterial-based sensing systems, sensing

S. Devi
Department of Inorganic Chemistry, University of Madras, Guindy, Chennai, India

V. Tharmaraj (✉)
Department of Analytical Chemistry, National Chung-Hsing University, Taichung, Taiwan

Mu. Naushad et al. (eds.), *Advanced Nanostructured Materials for Environmental Remediation*, Environmental Chemistry for a Sustainable World 25,
https://doi.org/10.1007/978-3-030-04477-0_4

principle, sensing method, and their signaling mechanisms has been provided. The sensing systems can also be ideally utilized for real-time applications.

Keywords Nanomaterials · Chemosensors · Biosensors · Absorption · Fluorescence · SERS and electrochemical sensors

4.1 Introduction

The recognition and sensing of chemical and biologically important species have emerged as significant goals in the field of nanosensors in recent years (Quang and Kim 2010; Zhou et al. 2011; Kim et al. 2011). Nanostructured materials are of great interest due to their size- and shape-dependent physical and chemical properties (Ferrando et al. 2008; Huynh et al. 2002; Kumar et al. 2016). There is also an increased interest in the synthesis of more complex nanostructures such as core-shell and hollow particles for advanced applications in chemical and biological sensing (Liang et al. 2009; Taton et al. 2000). The design and fabrication of nanomaterial-based sensors have generated great interest in detection of chemical and biological important target species with high precision and accuracy (Awual et al. 2015; Borisov and Wolfbeis 2008; Jung et al. 2010). The detection of the targeted species typically occurs through a controlled binding event and is then transmitted as a readable signal. A variety of signaling procedures are used for nanoparticle-based sensor with light absorption or either through fluorescence (Descalzo et al. 2005; Doleman et al. 2007) or scattering or current and potential changes (Zhan and Bard 2007).

Several analytical techniques, such as resonance Rayleigh scattering (Wen et al. 2013; Zhan et al. 2012), atomic absorption spectrometry (AAS) (Gao et al. 2012), inductively coupled plasma mass spectrometry (ICP-MS) (Chen et al. 2010), cold vapor atomic fluorescence spectrometry (Zhang et al. 2010), attenuated total reflectance Fourier-transform infrared spectroscopy (ATR-FTIR) (Vigano et al. 2005), etc., have been developed for sensing chemical and biological molecules. Most of the analytical techniques are more expensive and time-consuming processes. Consequently, high selectivity and sensitivity with simple instruments and easy operation have received much attention in recent years. Absorption spectroscopy (colorimetric/UV-visible), fluorescence spectroscopy, Raman spectroscopy, and electrochemistry are powerful analytical techniques for qualitative and quantitative sensing of chemical and biological molecules, as they offer simple handling, easy interpretation, moderate cost, portability, and fast analysis of the samples.

In general, sensors involve interaction between the target molecule (analyte) and a receptor (chemical or biological) that is signaled by an easily detectable change (Fabbrizzi and Poggi 1995). Most sensors depend on the binding mechanism or a chemical reaction to change the reporter characteristics (De Silva et al. 1997). All the

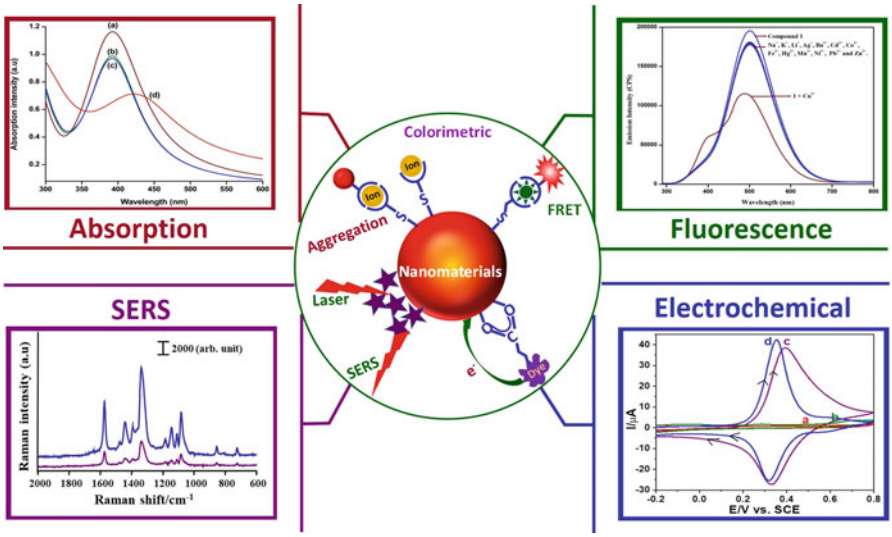

Fig. 4.1 Schematic illustration of signal amplification strategies using unmodified and surface-functionalized nanomaterials for sensing via absorption, fluorescence, SERS and electrochemical methods

sensors have been synthesized along these strategies for the detection of chemical and biological important analytes. According to the current IUPAC's definition "A chemical or bio-sensor is a device that transforms chemical information, ranging from the concentration of a specific sample component to total composition analysis, into an analytically useful signal." Optical reporter absorption (colorimetric and UV-visible), fluorescence, Raman spectroscopy, and electrochemical sensing have been widely used in this context (De Silva et al. 2009; Nguyen and Anslyn 2006), owing to a usually fast and convenient implementation. The instrumentation required for the use of such techniques is relatively simple and cheap which makes the quite attraction of sensors. However, the development of sensors is not trivial; materials science, molecular recognition, and device implementation are some of the aspects that play a significant role in the design of sensors.

In order to obtain the excellent selectivity and high sensitivity of chemical and biosensing, specific recognition and/or signal triggering elements are introduced which should be functionalized on the surface of nanomaterials with appropriate methods. The various approaches (Fig. 4.1) for the functionalization of nanoparticles (NPs) usually include noncovalent interaction such as physical adsorption, specific affinity interaction, and entrapment of chemical or biomolecules around the nanoparticles and covalent interaction of chemical or biomolecules with the functional groups on the nanoparticle surface (Veiseh et al. 2010). In signal amplification strategies, the nanomaterials usually act as catalysts to trigger the detectable signal or carriers for high loading of signal tags.

4.2 Principle and Operation Stages of a Sensor (Fig. 4.2)

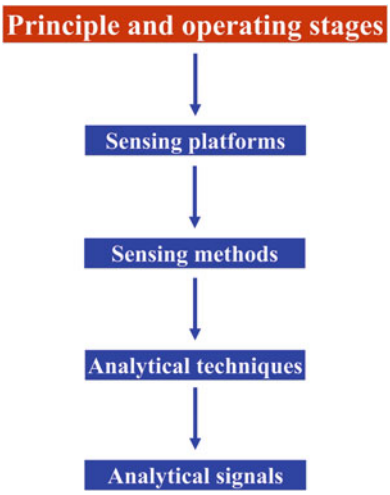

Fig. 4.2 Sensors principle and operation stages of a sensing system

4.3 Structure Adopted for Nanomaterial-Based Chemo- and Biosensors

The development of nanomaterial-based chemical and biological sensors is typically under direct spectroscopic and reagent-mediated sensors using both unmodified and surface-functionalized nanomaterials. This chapter exclusively deals with powerful analytical techniques such as absorption spectroscopy (colorimetric/UV-visible), fluorescence spectroscopy, Raman spectroscopy, and electrochemistry. The detection of analyte is directly based on some fundamental optical or electrical property via color changes/absorption, emission, scattering, or current and/or potential changes. The whole structure of this chapter is shown in Fig. 4.3.

4.4 Nanomaterials as Sensing Platforms

The development of nanomaterial-based sensors is usually achieved either in unmodified or in functionalized nanoparticles.

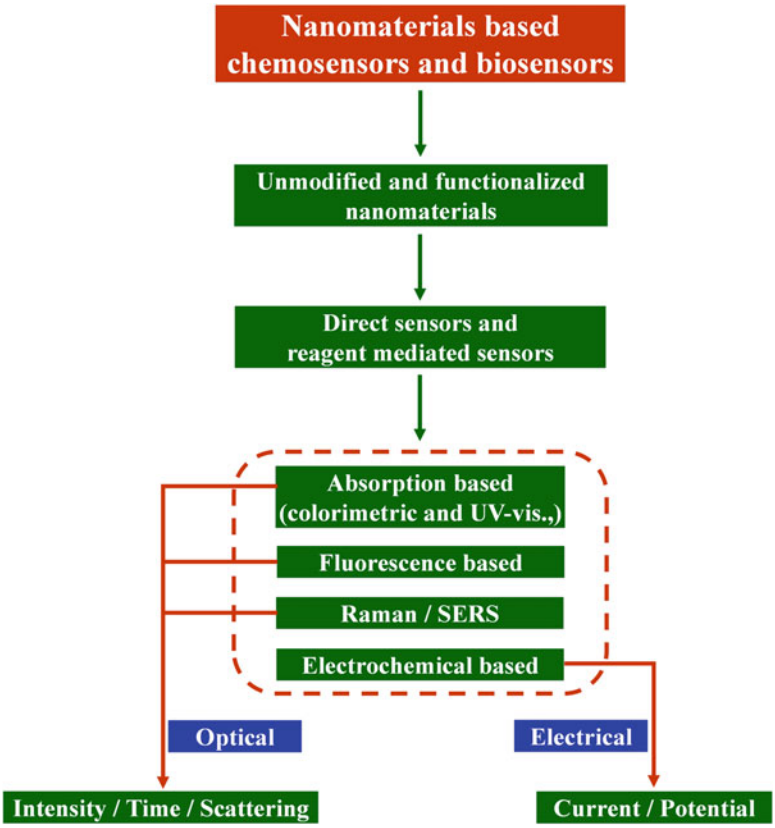

Fig. 4.3 Sensing platform for nanomaterial-based chemo- and biosensors

4.4.1 Unmodified Nanoparticles

Unmodified metallic nanoparticle surface has positive charge with flexible high affinity toward negatively charged ones. This affinity differences offer many advantages; since different sizes and shapes of metallic nanoparticle solution have different stability, they give various color signals.

4.4.2 Functionalized Nanoparticles

Nanoparticles can be converted into powerful nanoscale chemo- and biosensors by functionalizing their surface with specific binding receptors and/or reporter molecules such as nucleic acids, proteins, dyes, and fluorescent tags. In addition, many

other specific organic compounds which introduce new functionality will enhance their selectivity and sensitivity of target molecules.

4.5 Sensing Methods

In general, chemo- and biosensors may be categorized under two types: (i) direct sensors and (ii) reagent-mediated sensors.

4.5.1 Direct Spectroscopy Sensing

In a direct sensor, the analyte is detected directly via the basic phenomenon; localized surface plasmon resonance (LSPR) is responsible for the brilliant colors exhibited by the metal nanoparticles under illumination. Various direct sensor techniques are widely used, but this chapter exclusively deals with UV-visible and fluorescence spectroscopic methods and Raman/surface-enhanced Raman spectroscopy (SERS) measurements.

4.5.2 Reagent-Mediated Sensing

In a reagent-mediated sensing system, the change in analytical response is coming from the intermediate reagent. For example, analyte concentration is monitored from the analyte sensitive dye molecule or catalyst. This chapter mainly deals about only two types of reagent-mediated sensors, namely, colorimetric sensing and electrochemical sensors.

4.6 Analytical Techniques and Signals

4.6.1 UV-Visible Absorption-Based Sensors

UV-visible absorption spectroscopy is an important analytical technique for sensor application, as it offers simple handling, easy interpretation, moderate cost, portability, and fast analysis of the samples. To design nanomaterial-based sensing platform for the detection of environmental pollution materials (heavy and biological essential metal ions) and biomolecules, researchers have utilized the nanoparticle aggregation- or disaggregation-induced color change that reflects a redshift in the extinction spectrum (Polavarapu et al. 2014; Zhai et al. 2014). Based on this principle, simple and rapid colorimetric detection of Cu^{2+} ions in aqueous medium

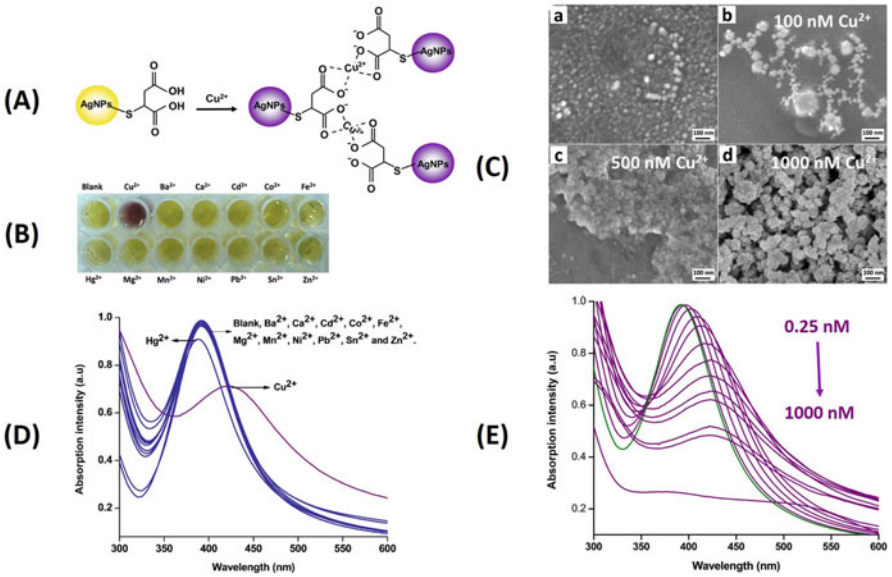

Fig. 4.4 (**A**) Schematic diagram for the interaction of TMA-AgNPs with Cu^{2+}. (**B**) Photograph of TMA-AgNPs (0.25 mM) in presence of Cu^{2+} and various metal ions (500 nM). (**C**) SEM images of TMA-AgNPs (a), TMA-AgNPs in the presence of 100 nM (b), 500 nM (c), and 1000 nM (d) of Cu^{2+} ions. (**D**) UV-visible spectra of TMA-AgNPs (0.25 mM) in the presence of Cu^{2+} and various other metal ions (100 nM) in aqueous medium. (**E**) UV-visible spectra of TMA-AgNPs (0.25 mM) upon addition of Cu^{2+} from 0.25 to 1000 nM in aqueous medium

via aggregation of thiomalic acid-functionalized Ag nanoparticles (TMA-AgNPs) has been developed as shown in Fig. 4.4A (Tharmaraj and Jyisy 2014). A visually detectable color change from yellow to purple in the presence of Cu^{2+} ion over other metal ions was observed (Fig. 4.4B). The aggregation behavior was confirmed by SEM images of TMA-AgNPs and TMA-AgNPs in the presence of 100 nM, 500 nM, and 1000 nM Cu^{2+} which is shown in Fig. 4.4C. TMA-AgNPs can be aggregated only in the presence of Cu^{2+} that cause a redshift of SPR band from 392 to 423 nm as observed in UV-visible spectra (Fig. 4.4D). Sensitivity response of TMA-AgNPs to Cu^{2+} was estimated in the concentration ranges of Cu^{2+} from 0.25 nM to 1000 nM, and their corresponding UV-visible spectra are shown in Fig. 4.4E. This chemosensor has excellent selectivity and sensitivity for Cu^{2+}, and the detection limit is as low as 0.25 nM and also successfully applied for the detection of copper ion in real water samples.

A simple, selective, and sensitive colorimetric detection of Hg^{2+} was achieved in aqueous medium using soaproot plant-stabilized silver nanoparticles by biologically green synthesis (Farhadi et al. 2012). In the presence of Hg^{2+}, the yellow AgNP solution was turned to colorless, accompanying the broadening and blueshifting of SPR band. This sensing method has been applied for real sample analysis, and the detection limit is as low as 2.2 μM. The selective detection of Co^{2+} ion on different

Table 4.1 List of UV-visible absorption-based colorimetric sensors

Nanomaterial probes	Analyte	Mechanisms	Limit of detection	Linear range	References
Tripolyphosphate-modified AgNPs	Mn^{2+}	Aggregation	0.1 μM	0.05–20 μM	Gao et al. (2013)
Ascorbic acid-capped AgNPs	Cr_6^{2+}	Aggregation	0.5 nM	0.07–1.84 μM	Wu et al. (2013)
Dendrimer-stabilized AgNPs	Hg^{2+}	Aggregation	10 ppb	10 ppb–10 ppm	Yuan et al. (2013)
Starch-stabilized AgNPs	Cu^{2+}	Aggregation	0.5 μM	0.1–10 μM	Miao et al. (2013)
Unmodified AuNPs	Cysteine	Aggregation	0.01 ppm	0.1–0.6 ppm	Jongjinakool et al. (2014)
Valine-capped AgNPs	Pb^{2+}	Aggregation	30.5 μM	0–100 ppm	Priyadarshini and Pradhan (2017)
Peptide-capped AuNP	Ni^{2+}	Aggregation	34 nM	60–160 nM	Parnsubsakula et al. (2018)
Mercaptosuccinic acid-modified AuNPs	Cr^{3+}	Aggregation	0.04 μM	0.6–1.4 μM	Yu et al. (2017)
Ligand-stabilized AuNPs	Pd^{2+}	Aggregation	4.23 μM	1–100 μM	Anwar et al. (2018)
Functionalized AgNPs	Ni^{2+}	Aggregation	0.6 μM	4.0–60 μM	Feng et al. (2017)

shapes of (nanosphere, nanoplate, and nanorod) glutathione-modified silver nanoparticles (GSH-AgNPs) is based on aggregation by the formation of chelating complex between Co^{2+} ion and COO^{-} groups of glutathione (Sung et al. 2013). Selective colorimetric detection for Cu^{2+}- and lidocaine hydrochloride (LC-HCl)-based sensor was developed by the aggregation of homocysteine-functionalized silver nanoparticles (Dou et al. 2013) that result in the color change from deep brown to bright yellow, and the SPR intensity characterized at 571 nm was found to be proportional to the concentration of Cu^{2+} ions, and the detection limit is as low as 3.2 nM. "Mix-and-detect" rapid virtual colorimetric ultrasensitive detection of Hg^{2+} ion using label-free cysteamine-capped AgNPs has been developed (Bhattacharjee and Chakraborty 2014). In the presence of Hg^{2+} ion, thiophillic Hg^{2+} would lead to partial exchange of cysteamine ligand with the detection limit of 275 pM. Some recent reports for UV-visible absorption method-based sensing systems are listed in Table 4.1.

4.6.2 Fluorescence-Based Sensors

Fluorescence spectroscopy is one of the most powerful ultrasensitive analytical techniques when compared to other analytical methods which make the detection

of single molecules. Also this approach provides a limit of detection (LOD = 3.3σ/S, where σ is standard deviation of the response and S is the slope of the calibration curve) at a signal-to-noise (S/N) ratio for the detection up to parts-per-trillion level with good precision and accuracy (Wang et al. 2014; Nolan and Lippard 2008). Design of nanomaterial-based fluorescent sensors for quick detection of targets molecules has been developed either by fluorescent enhancement (turn on) or quenching (turn off) that controls the response through both energy and electron transfer processes (Liu et al. 2014; Jia et al. 2014).

Alginate-stabilized silver nanocubes (AgNCbs) bound to rhodamine 6G (Rh6G) composite as selective sensor for Hg^{2+} ion in aqueous solution have been developed (Tharmaraj and Pitchumani 2011) with the detection limit as low as 0.1 nM. Rh6G dye molecules bound to AgNCbs surface were observed in quenching the fluorescence; when there is presence of Hg^{2+} ion, bound Rh6G is released from the alginate-AgNCb surfaces which indicate a large fluorescence restoration with a concomitant color change from yellow to purple. Ratiometric fluorescence probe is designed and developed (Niu et al. 2015) by linking with two parts, positively charged aggregation-induced emission (AIE) organic fluorescence nanoparticles (OFNPs) as the reference and negatively charged Au nanoclusters (Au NCs) as the response. This probe can be used to detect Hg^{2+} and also melamine, since red fluorescence of Au NCs can be quenched by mercury ions and recovered by melamine, due to the strong affinity between metallophilic Hg^{2+}–Au and Hg^{2+}–N. This dual-emission ratiometric fluorescence probe has good biocompatibility; hence it is applicable for biological imaging and detection.

Thiol-DNA-functionalized gold nanoparticles (AuNPs) as a simple fluorescence spectrometric sensor for Hg^{2+} detection in aqueous solution were developed (Wang et al. 2015). Hg^{2+} is selectively induced conformational change of single-stranded DNA (ssDNA) with an enhanced fluorescence resonance energy transfer (FRET) process between the energy donor (fluorescein, FAM) and the energy acceptor (AuNPs). The assay enables the detection limit as low as 8 nM and also applied to monitor Hg^{2+} in tap water samples. Noncross-linking aggregation of fluorosurfactant-capped silver nanoparticles for colorimetric sensing of cysteine was developed (Chen et al. 2014). High specificity toward cysteine was observed as the nonionic fluorosurfactant ligand thiol-silver interaction prohibited the binding of other functional groups on the surface of AgNPs. This sensing probe can be successfully applied for the determination of cysteine in human urine and plasma samples with the detection limit as low as 0.05 μM.

Dansyl fluorophore-functionalized thiol-stabilized AgNPs containing 2-aminothiophenol units with excellent selective binding sites for Cu^{2+} ion were developed, and energy transfer (ET) from the dansyl moiety to the copper complex occurs that causes the fluorescent ratiometric response as seen in Fig. 4.5A (Tharmaraj and Pitchumani 2013). High-resolution transmission electron microscopy (HRTEM) images of highly dispersed thiol-stabilized silver nanoparticles, 2D lattice fringe spacing image, and selected area electron diffraction (SAED) pattern are shown in Fig. 4.5B(a-d). The particle size and lattice fringes of AgNP were 5.5 nm and 0.2 nm, respectively. The lattice planes of nano silver were observed in

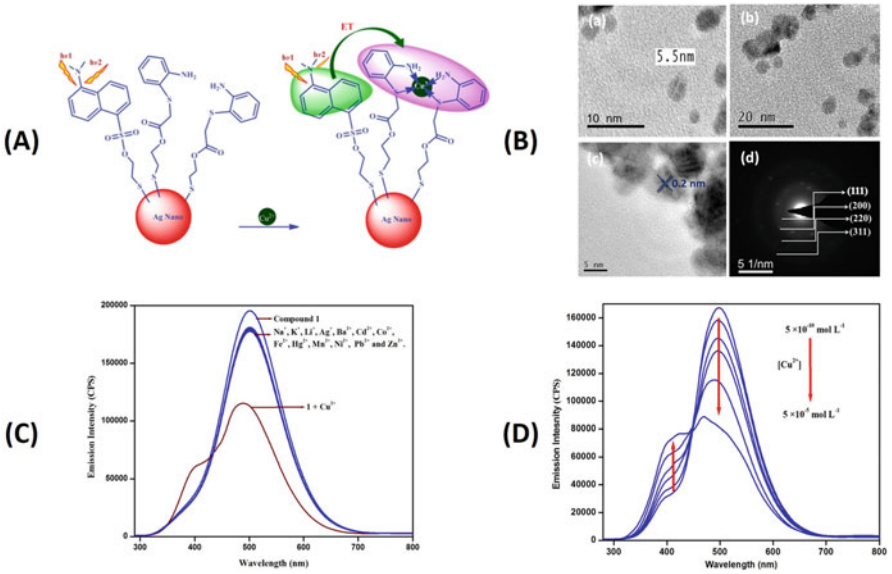

Fig. 4.5 (**A**) Schematic diagram proposed binding mechanisms for dansyl-AgNPs with Cu^{2+} ion. (**B**) (a), (b) HRTEM images of highly dispersed thiol-stabilized AgNPs. (c) The 2D lattice fringes of HRTEM image. (d) Selected area diffraction pattern is showing the corresponding planes. (**C**) Fluorescence spectra of dansyl-AgNPs (1 mg mL^{-1}) in the presence of Cu^{2+} and various other metal ions (0.5 μM). (**D**) Fluorescence spectra of dansyl-AgNPs (1 mg mL^{-1}) upon addition of Cu^{2+} from 0.5 nM to 0.5 μM

SAED pattern. Selectivity of fluorescent ratiometric response for the decrease in fluorescence at 497 nm and an increase in fluorescence at 410 nm with an isoemissive point at 445 nm was favored only in the presence of Cu^{2+} ions, whereas other metal ions led to no fluorescence ratiometric change as seen in Fig. 4.5C. Sensitivity response of dansyl-AgNPs to Cu^{2+} was evaluated in the concentration ranges of Cu^{2+} from 0.5 nM to 0.5 μM, and their corresponding fluorescence spectra is shown in Fig. 4.5D.

Some recent reports for fluorescence method-based sensing systems are listed in Table 4.2.

4.6.3 Raman/Surface-Enhanced Raman Spectroscopy (SERS) Sensors

Raman spectroscopy is one of the important analytical techniques used in the field of sensors for identification of specific molecules. But traditional Raman spectroscopy has very poor efficiency of inelastic scattering processes with relatively weak signal. In recent years these problems are overcome by developing advanced method like

Table 4.2 List of fluorescence sensors based on nanomaterials

Nanomaterial probes	Sensing strategy	Analyte	Mechanisms	Limit of detection	References
3-Mercaptopropionic acid-capped CdS quantum dots	Turn off-on	Lysozyme	Displacement	6.3 nM	Liu et al. (2016)
AuNPs and porous silicon nanoparticles	Turn off-on	L-Cysteine	FRET	35 μM	Zhang and Jia (2017)
Gold nanoparticles	Electrostatic interaction	Melamine	FRET	0.18 μg L^{-1}	Cao et al. (2014)
Carbon dots	Quenching effect	Hydroquinone (H_2Q)	Electron transfer	0.1 μM	Ni et al. (2015)
BODIPY-functionalized AuNPs	Turn on	Cysteine	Displacement	1.2 μM	Lo et al. (2015)

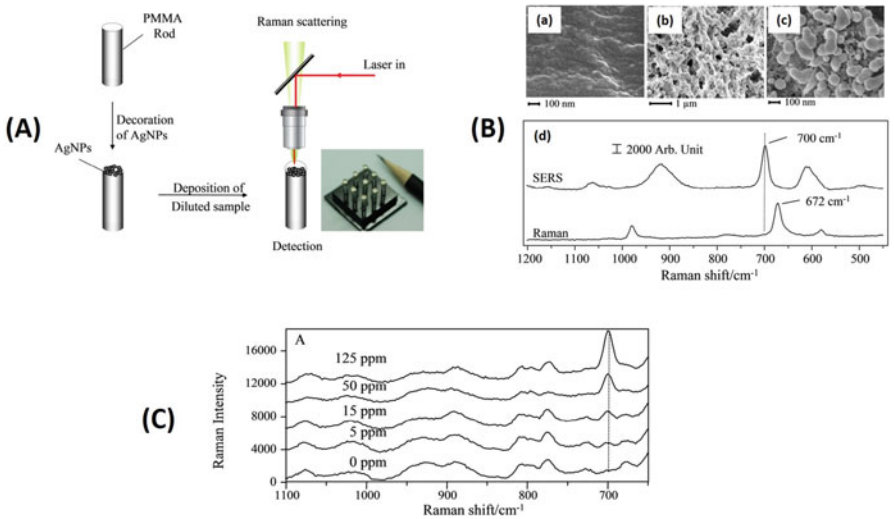

Fig. 4.6 (**A**) Schematic diagram of SERS detection of target molecules using droplet-based method. (**B**) SEM images of bare PMMA rod (a), PVDF-coated rod (b), and AgNPs decorated on PVDF-coated rod (c). Raman spectra of solid melamine and SERS spectra of melamine in water (400 ppb) detected by cylindrical substrate (d). (**C**) SERS spectra of melamine in milk liquid at 0, 5, 15, 50 and 125 ppm

surface-enhanced Raman spectroscopy (SERS). In SERS, the target molecule is brought into close proximity to a metallic (typically Ag, Au, or Cu) surface with nanoscopically defined features or in solution next to a nanoparticle with a diameter much smaller than the wavelength of the excitation light.

Silver nanoparticle decorated on filter paper as a highly sensitive surface-enhanced Raman scattering (SERS) substrate was fabricated for detection of tyrosine in aqueous solution (Cheng et al. 2011) with the detection limit as low as 625 nM. The Raman labels to use for detection of protein and protein concentration assay were developed (Han et al. 2010) which uses the SERS signal of Coomassie Brilliant Blue dye adsorbed nonspecifically to silver colloids for monitoring the total protein concentration.

Silver nanoparticles decorated on a cylindrical support was developed (Rajapandiyan et al. 2011) for the detection of melamine in milk liquid and powder samples by surface-enhanced Raman spectroscopy (SERS) technique. Figure 4.6A illustrates the detection procedures in the cylindrical SERS substrate. Cylindrical SERS substrate was prepared by decoration of silver nanoparticles (AgNPs) on a solid support of polymethyl methacrylate (PMMA) rod by silver mirror reaction. SEM images show the PMMA surface roughness was increased after treating with PVDF solution. Also, the size of the formed AgNPs was around 200 nm in diameter with the Raman spectra of solid melamine and SERS spectra of melamine as shown in Fig. 4.6B. Sensitivity response of AgNP cylindrical substrate to the melamine

Table 4.3 List of SERS sensors based on nanomaterials

Nanomaterials probes	Analyte	Limit of detection	References
Silver nanoparticles	Rhodamine 6G	Single molecule	Nie and Emery (1997)
Au electrode	Adenine	0.01 pM	Cho et al. (2009)
Au-SiO_2 core-shell NPs	Nile blue A, toluidine blue O, and methylene blue	NA	Fernandez-Lopez et al. (2009)
Ag-Au core-shell NPs	Adenosine triphosphate, hemoglobin, and myoglobin	NA	Kumar et al. (2007)
Star-shaped AuNPs	1-Naphthalenethiol, Alexa Fluor 750, and phenol	NA	Rodriguez-Lorenzo et al. (2010)
AgNPs	Yeast cells W303-1A	Subcellular level	Sujith et al. (2009)
Au-Ag core-shell NPs on Fe_3O_4 hybrid nanospheres	4-Aminothiophenol	NA	Guo et al. (2009a, b)
TiO_2 NPs	4-Mercaptobenzoic acid	0.1 μM	Yang et al. (2009)
AuNPs	2,4,6-TNT	$<1 \times 10^{-10}$ g	
Au-Ag core-shell NPs on multiwalled carbon nanotube	Adenine and 4-aminothiophenol	NA	Guo et al. (2009a, b)

concentration ranges was tested up to 125 ppm, and their corresponding SERS spectra are shown in Fig. 4.6C.

Some recent reports for SERS method-based sensing systems are listed in Table 4.3.

4.6.4 Electrochemical-Based Sensors

Electrochemical methods have been used extremely in analysis of biological and environmental interest compounds due to their advantages such as quick response, wide linear dynamic range, simplicity, reliability, reproducibility, inherent miniaturization, low cost, low-power requirements, and high selectivity and sensitivity. The type of electrical signal used for quantitation distinguishes the various electroanalytical techniques. For example, in case of voltammetry, the current is measured as a function of changing potential that can be applied in different ways (linear, cyclic, anodic stripping voltammetry). Amperometric measurements are performed by maintaining a constant potential at the working electrode with respect to reference electrode and measuring the generated current. The generated potentials or currents are related to the contents of analyte in the test solution (Zoski 2007). The researchers first tried to detect compounds using carbon and metal electrodes without

any chemical modification. But the problems such as oxidation or reduction occur at high over potential, suffer from interferences and kinetically sluggish. Therefore, the development of electrochemical sensor based on chemically modified electrodes for estimating biologically important compounds is a rapidly growing area of electrochemistry to overcome the problems associated with bare electrodes. Particularly, the chemically modified electrodes have been fabricated using nanomaterials such as metal nanoparticles, metal oxide nanomaterials, and carbon nanomaterials.

Silver nanoparticles incorporated within the mesoporous silicate framework of zeolite Y-modified glassy carbon electrode-based electrochemical sensor were developed for the simultaneous detection of dopamine (DA) and uric acid (UA) (Meenakshi et al. 2016). The oxidation of DA and UA was obtained at +0.31 V and +0.43 V (vs. Ag/AgCl) using AgNPs/Zeo-Y/GCE under the optimum experimental condition. A well-resolved peak potential window (~120 mV) for the oxidation of both DA and UA was observed at AgNPs/Zeo-Y/GCE system. This is due to the strong electrostatic interaction between the positively charged DA and negatively charged silver nanoparticles embedded in zeolite Y which facilitates the electron transfer process is favorable and the oxidation peak potential of DA is resolved against UA. The detection limits of DA and UA were found to be 1.6×10^{-8} M and 2.51×10^{-8} M in the linear range of 0.02×10^{-6} to 0.18×10^{-6} M ($R^2 = 0.9899$) and 0.05×10^{-6} to 0.7×10^{-6} M ($R^2 = 0.9996$) by using differential pulse voltammetry (DPV) method.

The electrochemical oxidation of paracetamol (PAR) and caffeine (CAF) using nickel hexacyanoferrate-decorated titanium nanotube (TNT)-modified glassy carbon electrode was developed (Fig. 4.7A) (Devi and Pandian 2014). The SEM image of TNT shows the formation of tube-like structure with the external diameter of 10–80 nm ranges and several micrometers in length. The TEM image shows that the TNT wall consists of two layers with an average external diameter of 28 nm. After surface modification with NiHCF, the size and shape of TNT become expanded with the uniform deposition of NiHCF on both inner and outer surfaces (Fig. 4.7B). DPV experiment was carried out for the simultaneous detection of PAR and CAF with well-separated peak potentials. The determination of PAR has been done separately in the concentration ranges of 1.3–10.7 μM with the solution containing 6 μM CAF (Fig. 4.7C). Similarly, the determination of CAF has been studied in the concentration ranges of 7.3–18.7 μM in presence of PAR at a fixed concentration of 1.3 μM (Fig. 4.7D). The detection limits of PAR and CAF are found to be 29.5 and 18.2 nM, respectively. Some recent reports for electrochemical method-based sensing systems are listed in Table 4.4.

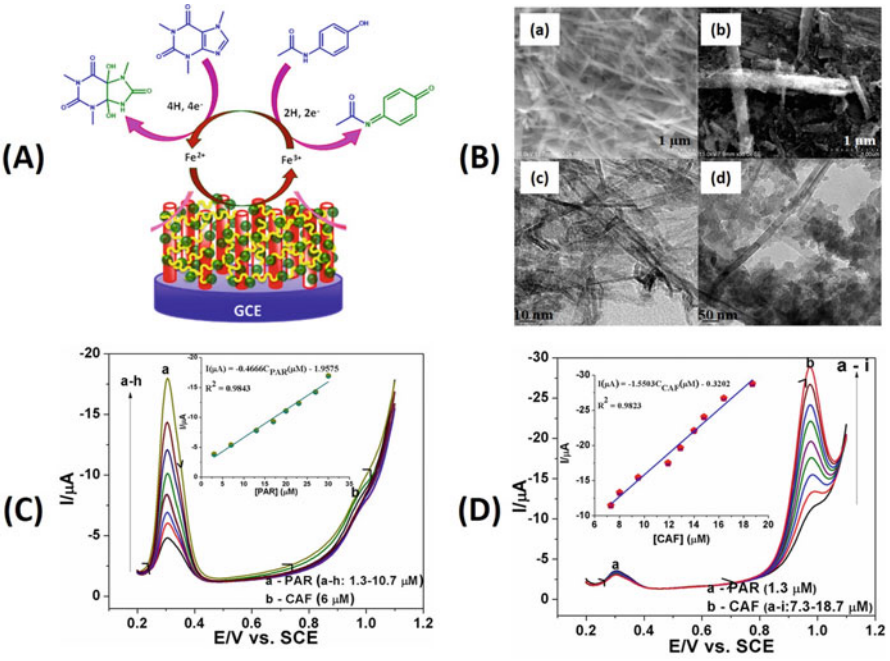

Fig. 4.7 (**A**) Mechanisms for the oxidation of paracetamol and caffeine at NiHCF/TNT@GCE. (**B**) FE-SEM and HR-TEM images of TNT (a and c) and NiHCF/TNT (b and d). (**C**) DPV of CS-NiHCF@TNT/GCE at concentration of PAR (a–h, 1.3–10.7 μM) and 6 μM of CAF. (**D**) DPV of CS-NiHCF@TNT/GCE at concentration of CAF (a–i, 7.3–18.7 μM) and 1.3 μM of PAR. The inset shows the calibration plot

Table 4.4 List of electrochemical sensors based on nanomaterials

Nanomaterial probes	Analyte	Method	Limit of detection	References
CS@PPY/CS_2	Hg^{2+}	DPV	1.8 μM	Devi et al. (2014)
DNA-SWCNT	Pb^{2+}	DPV	0.4 nM	Lian et al. (2014)
AgNPs-GO	As^{3+}	SW-ASV	0.24 nM	Dar et al. (2014)
Aptamer-AuNPs	Cu^{2+}	SWV	0.1 pM	Noroozifar et al. (2011)
NiHCF@TiO_2/GCE	Nitrites	DPV	0.11 μM	Sophia et al. (2012)
Ag nanostructure/gold electrode	Ascorbic acid	DPV	0.01 mM	Zheng et al. (2013)
Au/Pt/Pd/TiO_2 NTs	Dopamine	DPV	0.03 μM	Mahshid et al. (2011)
Manganese vanadate nanorods/GCE	Cysteine	CV	0.026 μM	Pei et al. (2013)

4.7 Conclusions

Remarkable progress in the development of simple and efficient methods for sensing of chemical and biomolecules utilizing nanomaterials has been made over the past several years. The successful development of sensors with high selectivity and sensitivity for specific, toxic, heavy/biologically essential metal ions and biomolecules to detect in real-time monitoring was clearly demonstrated. In this chapter, we believed that most promising results and remarkable sensing system in terms of high selectivity and sensitivity have been discussed. However, many of the absorption- and fluorescence-based sensing systems were operated in aqueous medium, and some other system using nonaqueous solvents was applied for real sample analysis. Fluorescence sensors based on surface-functionalized nanomaterials have been widely used in biological and environmental sample analysis, due to their high sensitivity, low cost, and commercial availability. SERS technique has great promise for chemical and biosensing applications based on design of paper, and also fiber-based SERS active substrates have very high surface area with flexibility for efficient analysis of biological live samples. Electrochemical techniques are coupled with nanomaterials that have been used for the development of electrochemical sensors. The attractive design and fabrication of nanomaterial-based electrochemical sensing systems can offer a highly selective increase in sensitivity and reproducibility. Most of the sensing systems with a very low detection limits (in the range of ppb) were thus achieved and applied for the real sample analysis.

References

Anwar A, Minhaz A, Khan NA, Kalantari K, Afifi ABM, Shah MR (2018) Synthesis of gold nanoparticles stabilized by a pyrazinium thioacetate ligand: a new colorimetric nanosensor for detection of heavy metal Pd(II). Sensors Actuators B 257:875–881. https://doi.org/10.1016/j.snb.2017.11.040

Awual MR, Hasan MM, Naushad M et al (2015) Preparation of new class composite adsorbent for enhanced palladium(II) detection and recovery. Sensors Actuators B Chem 209:790–797. https://doi.org/10.1016/j.snb.2014.12.053

Bhattacharjee Y, Chakraborty A (2014) Label-free cysteamine-capped silver nanoparticle-based colorimetric assay for hg(ii) detection in water with subnanomolar exactitude. ACS Sustain Chem Eng 2:2149–2154. https://doi.org/10.1021/sc500339n

Borisov SM, Wolfbeis OS (2008) Optical biosensors. Chem Rev 108(2):423–461. https://doi.org/10.1021/cr068105t

Cao X, Shen F, Zhang M, Guo J, Luo Y, Xu J, Li Y, Sun C (2014) Highly sensitive detection of melamine based on fluorescence resonance energy transfer between rhodamine B and gold nanoparticles. Dyes Pigments 111:9–107. https://doi.org/10.1016/j.dyepig.2014.06.001

Chen B, Heng S, Peng H, Hu B, Yu X, Zhang Z, Pang D, Yue X, Zhu Y (2010) Magnetic solid phase microextraction on a microchip combined with electrothermal vaporization-inductively coupled plasma mass spectrometry for determination of Cd, Hg and Pb in cells. Anal At Spectrom 25:1931–1938. https://doi.org/10.1039/C0JA00003E

Chen S, Gao H, Shen W, Lu C, Yuan Q (2014) Colorimetric detection of cysteine using noncrosslinking aggregation of fluorosurfactant-capped silver nanoparticles. Sens Actuators B Chem 190:673–678. https://doi.org/10.1016/j.snb.2013.09.036

Cheng ML, Tsai BC, Yang J (2011) Silver nanoparticle-treated filter paper as a highly sensitive surface-enhanced Raman scattering (SERS) substrate for detection of tyrosine in aqueous solution. Anal Chim Acta 708(1–2):89–96. https://doi.org/10.1016/j.aca.2011.10.013

Cho HS, Lee B, Liu GL, Agarwal A, Lee LP (2009) Label-free and highly sensitive biomolecular detection using SERS and electrokinetic preconcentration. Lab Chip 9:3360–3363. https://doi.org/10.1039/B912076A

Dar RA, Khare NG, Cole DP, Karna SP, Srivastava AK (2014) Green synthesis of a silver nanoparticle–graphene oxide composite and its application for As(III) detection. RSC Adv 4:14432–14440. https://doi.org/10.1039/C4RA00934G

De Silva AP, Gunaratne HQN, Gunnlaugsson T, Huxley AJM, McCoy CP, Rademacher JT, Rice TE (1997) Signaling recognition events with fluorescent sensors and switches. Chem Rev 97 (5):1515–1566. https://doi.org/10.1021/cr960386p

De Silva AP, Moody TS, Wright GD (2009) Fluorescent PET (photoinduced electron transfer) sensors as potent analytical tools. Analyst 134(12):2385–2393. https://doi.org/10.1039/b912527m

Descalzo AB, Rurack K, Weisshoff H, Martınez-Manez R, Marcos MD, Amoros P, Hoffmann K, Soto J (2005) Rational design of a chromo- and fluorogenic hybrid chemosensor material for the detection of long-chain carboxylates. J Am Chem Soc 127(1):184–200. https://doi.org/10.1021/ja045683n

Devi S, Pandian K (2014) Synthesis of chitosan protected nickel hexacyanoferrate modified titanium oxide nanotube and study its application on simultaneous s electrochemical detection of paracetamol and caffeine. Adv Mater Res 938(2014):192–198. https://doi.org/10.4028/www.scientific.net/AMR.938.192

Devi S, Devasena T, Saratha S, Tharmaraj P, Pandian K (2014) Dithiocarbamate post functionalized polypyrrole modified carbon sphere for the selective and sensitive detection of mercury by voltammetry method. Int J Electrochem Sci 9:670–683

Doleman L, Davies L, Rowe L, Moschou EA, Deo S, Daunert S (2007) Bioluminescence DNA hybridization assay for Plasmodium falciparum based on the photoprotein aequorin. Anal Chem 79(11):4149–4153. https://doi.org/10.1021/ac0702847

Dou Y, Yang X, Liu Z, Zhu S (2013) Homocysteine-functionalized silver nanoparticles for selective sensing of Cu^{2+} ions and lidocaine hydrochloride. Colloids Surf A Physicochem Eng Asp 423:20–26. https://doi.org/10.1016/j.colsurfa.2013.01.027

Fabbrizzi L, Poggi A (1995) Sensors and switches from supramolecular chemistry. Chem Soc Rev 24:197–202. https://doi.org/10.1039/CS9952400197

Farhadi K, Forougha M, Molaei R, Hajizadeha S, Rafipour A (2012) Highly selective Hg^{2+} colorimetric sensor using green synthesized and unmodified silver nanoparticles. Sensors Actuators B Chem 161:880–885. https://doi.org/10.1016/j.snb.2011.11.052

Feng J, Jin W, Huang P, Wu F (2017) Highly selective colorimetric detection of Ni^{2+} using silver nanoparticles cofunctionalized with adenosine monophosphate and sodium dodecyl sulfonate. J Nanopart Res 19:306. https://doi.org/10.1007/s11051-017-3998-0

Fernandez-Lopez C, Mateo-Mateo C, Alvarez-Puebla RA, Perez-Juste J, Pastoriza-Santos I, Liz-Marzan LM (2009) Highly controlled silica coating of PEG-capped metal nanoparticles and preparation of SERS-encoded particles. Langmuir 25(24):13894–13899. https://doi.org/10.1021/la9016454

Ferrando R, Jellinek J, Johnston RL (2008) Nanoalloys: from theory to applications of alloy clusters and nanoparticles. Chem Rev 108(3):845–910. https://doi.org/10.1021/cr040090g

Gao Y, Shi Z, Long Z, Wu P, Zheng C, Hou X (2012) Determination and speciation of mercury in environmental and biological samples by analytical atomic spectrometry. Microchem J 103:1–14. https://doi.org/10.1016/j.microc.2012.02.001

Gao YX, Xin JW, Shen ZY, Pan W, Li X, Wu AG (2013) A new rapid colorimetric detection method of Mn^{2+} based on tripolyphosphate modified silver nanoparticles. Sensors Actuators B 181:288–293. https://doi.org/10.1016/j.snb.2013.01.079

Guo S, Dong S, Wang E (2009a) A general route to construct diverse multifunctional Fe_3O_4/metal hybrid nanostructures. Chem Eur J 15(10):2416–2424. https://doi.org/10.1002/chem.200801942

Guo SJ, Li J, Ren W, Wen D, Dong SJ, Wang EK (2009b) Carbon nanotube/silica coaxial nanocable as a three-dimensional support for loading diverse ultra-high-density metal nanostructures: facile preparation and use as enhanced materials for electrochemical devices and SERS. Chem Mater 21(11):2247–2257. https://doi.org/10.1021/cm900300v

Han XX, Xie Y, Zhao B, Ozaki Y (2010) Highly sensitive protein concentration assay over a wide range via surface-enhanced Raman scattering of Coomassie brilliant blue. Anal Chem 82 (11):4325–4328. https://doi.org/10.1021/ac100596u

Huynh WU, Dittmer JJ, Alivisatos AP (2002) Hybrid nanorod-polymer solar cells. Science 295 (5564):2425–2427. https://doi.org/10.1126/science.1069156

Jia J, Wu A, Luan S (2014) Synthesis and investigation of the imprinting efficiency of ion imprinted nanoparticles for recognizing copper. Phys Chem Chem Phys 16:16158–16165. https://doi.org/10.1039/C4CP01858C

Jongjinakool S, Palasak K, Bousod N, Teepoo S (2014) Gold nanoparticles-based colorimetric sensor for cysteine detection. Energy Procedia 56:10–18. https://doi.org/10.1016/j.egypro.2014.07.126

Jung JH, Park M, Shinkai S (2010) Fabrication of silica nanotubes by using self-assembled gels and their applications in environmental and biological fields. Chem Soc Rev 39:4286–4302. https://doi.org/10.1039/C002959A

Kim HN, Guo Z, Zhu W, Yoon J, Tian H (2011) Recent progress on polymer-based fluorescent and colorimetric chemosensors. Chem Soc Rev 40:79–93. https://doi.org/10.1039/C0CS00058B

Kumar GVP, Shruthi S, Vibha B, Reddy BAA, Kundu TK, Narayana C (2007) Hot spots in Ag Core−Au shell nanoparticles potent for surface-enhanced Raman scattering studies of biomolecules. J Phys Chem C 111(11):4388–4392. https://doi.org/10.1021/jp068253n

Kumar A, Guo C, Sharma G et al (2016) Magnetically recoverable ZrO2/Fe3O4/chitosan nanomaterials for enhanced sunlight driven photoreduction of carcinogenic Cr(VI) and dechlorination & mineralization of 4-chlorophenol from simulated waste water. RSC Adv 6:13251–13263. https://doi.org/10.1039/C5RA23372K

Lian Y, Yuan M, Zhao H (2014) DNA wrapped metallic single-walled carbon nanotube sensor for Pb (II) detection. Fullerenes, Nanotubes, Carbon Nanostruct 22(5):510–518. https://doi.org/10.1080/1536383X.2012.690462

Liang CH, Wang CC, Lin YC, Chen CH, Wong CH, Wu CY (2009) Iron oxide/gold core/shell nanoparticles for ultrasensitive detection of carbohydrate−protein interactions. Anal Chem 81 (18):7750–7756. https://doi.org/10.1021/ac9012286

Liu J, Zuo W, Zhang W, Liu J, Wang Z, Yang Z, Wang B (2014) Europium(III) complex-functionalized magnetic nanoparticle as a chemosensor for ultrasensitive detection and removal of copper(II) from aqueous solution. Nanoscale 6:11473–11478. https://doi.org/10.1039/C4NR03454F

Liu X, Na W, Qua Z, Su X (2016) Turn-off–on fluorescence probe based on 3-mercaptopropionic acid-capped CdS quantum dots for selective and sensitive lysozyme detection. RSC Adv 6:85795–85801. https://doi.org/10.1039/C6RA14420A

Lo SH, Wu MC, Wu SP (2015) A turn-on fluorescent sensor for cysteine based on BODIPY functionalized Au nanoparticles and its application in living cell imaging. Sensors Actuators B Chem 221:1366–1371. https://doi.org/10.1016/j.snb.2015.08.015

Mahshid S, Li C, Mahshid SS, Askari M, Dolati A, Yang L, Luo S, Cai Q (2011) Sensitive determination of dopamine in the presence of uric acid and ascorbic acid using TiO_2 nanotubes modified with Pd, Pt and Au nanoparticles. Analyst 136(11):2322–2329. https://doi.org/10.1039/c1an15021a

Meenakshi S, Devi S, Pandian K, Devendiran R, Selvaraj M (2016) Sunlight assisted synthesis of silver nanoparticles in zeolite matrix and study of its application on electrochemical detection of dopamine and uric acid in urine samples. Mater Sci Eng C 69:85–94. https://doi.org/10.1016/j.msec.2016.06.037

Miao LJ, Xin JW, Shen ZY, Zhang YJ, Wang HY, Wu AG (2013) Exploring a new rapid colorimetric detection method of Cu^{2+} with high sensitivity and selectivity. Sensors Actuators B 176:906–912. https://doi.org/10.1016/j.snb.2012.10.070

Nguyen BT, Anslyn EV (2006) Indicator-displacement assays. Coord Chem Rev 250 (23–24):3118–3127. https://doi.org/10.1016/j.ccr.2006.04.009

Ni P, Dai H, Li Z, Sun Y, Hu J, Jiang S, Wang Y, Li Z (2015) Carbon dots based fluorescent sensor for sensitive determination of hydroquinone. Talanta 144:258–262. https://doi.org/10.1016/j.talanta.2015.06.014

Nie SM, Emery SR (1997) Probing single molecules and single nanoparticles by surface-enhanced Raman scattering. Science 275(5303):1102–1106

Niu C, Liu Q, Shang Z, Zhaoa L, Ouyang J (2015) Dual-emission fluorescent sensor based on AIE organic nanoparticles and Au nanoclusters for the detection of mercury and melamine. Nanoscale 7:8457–8465. https://doi.org/10.1039/C5NR00554J

Nolan EM, Lippard SJ (2008) Tools and tactics for the optical detection of mercuric ion. Chem Rev 108(9):3443–3480. https://doi.org/10.1021/cr068000q

Noroozifar M, Khorasani-Motlagh M, Taheri A (2011) Determination of cyanide in wastewaters using modified glassy carbon electrode with immobilized silver hexacyanoferrate nanoparticles on multiwall carbon nanotube. J Hazard Mater 185(1):255–261. https://doi.org/10.1016/j.jhazmat.2010.09.02

Parnsubsakula A, Oaewb S, Surareungchai W (2018) Zwitterionic peptide-capped gold nanoparticles for colorimetric detection of Ni^{2+}. Nanoscale 10:5466–5473. https://doi.org/10.1039/C7NR07998B

Pei LZ, Pei YQ, Xie YK, Fan CG, Yu HY (2013) Synthesis and characterization of manganese vanadate nanorods as glassy carbon electrode modified materials for the determination of L-cysteine. Cryst Eng Comm 15:1729–1738. https://doi.org/10.1039/C2CE26592C

Polavarapu L, Perez-Juste J, Xu QH, Liz-Marzan LM (2014) Optical sensing of biological, chemical and ionic species through aggregation of plasmonic nanoparticles. J Mater Chem C 2:7460–7476. https://doi.org/10.1039/C4TC01142B

Priyadarshini E, Pradhan N (2017) Metal-induced aggregation of valine capped gold nanoparticles: an efficient and rapid approach for colorimetric detection of Pb^{2+} ions. Sci Rep 7:9278. https://doi.org/10.1038/s41598-017-08847-5

Quang DT, Kim SJ (2010) Fluoro- and chromogenic chemodosimeters for heavy metal ion detection in solution and biospecimens. Chem Rev 110(10):6280–6301. https://doi.org/10.1021/cr100154p

Rajapandiyan P, Tang WL, Yang J (2011) Rapid detection of melamine in milk liquid and powder by surface-enhanced Raman scattering substrate array. Food Control 56:155–160. https://doi.org/10.1016/j.foodcont.2015.03.028

Rodriguez-Lorenzo L, Alvarez-Puebla RA, de Abajo FJG, Liz-Marzan LM (2010) Surface enhanced Raman scattering using star-shaped gold colloidal nanoparticles. J Phys Chem C 114(16):7336–7340. https://doi.org/10.1021/jp909253w

Sophia SJ, Devi S, Pandian K (2012) Electrocatalytic oxidation of hydrazine based on NiHCF@TiO_2 core- shell nanoparticles modified GCE. Int J Electrochem Sci 7:6580–6598

Sujith A, Itoh T, Abe H, Yoshida KI, Kiran MS, Biju V, Ishikawa M (2009) Imaging the cell wall of living single yeast cells using surface-enhanced Raman spectroscopy. Anal Bioanal Chem 394 (7):1803–1809. https://doi.org/10.1007/s00216-009-2883-9

Sung HK, Oh SY, Park C, Kim Y (2013) Colorimetric detection of Co^{2+} ion using silver nanoparticles with spherical, plate, and rod shapes. Langmuir 29:8978–8982. https://doi.org/10.1021/la401408f

Taton TA, Mirkin CA, Letsinger RL (2000) Scanometric DNA array detection with nanoparticle probes. Science 289(5485):1757–1760

Tharmaraj V, Jyisy Y (2014) Sensitive and selective colorimetric detection of Cu^{2+} in aqueous medium via aggregation of thiomalic acid functionalized Ag nanoparticles. Analyst 139:6304–6309. https://doi.org/10.1039/c4an01449a

Tharmaraj V, Pitchumani K (2011) Alginate stabilized silver nanocube–Rh6G composite as a highly selective mercury sensor in aqueous solution. Nanoscale 3:1166–1170. https://doi.org/10.1039/C0NR00749H

Tharmaraj V, Pitchumani K (2013) A highly selective ratiometric fluorescent chemosensor for Cu (II) based on dansyl-functionalized thiol stabilized silver nanoparticles. J Mater Chem B 1:1962–1967. https://doi.org/10.1039/C3TB00534H

Veiseh O, Gunn JW, Zhang MQ (2010) Design and fabrication of magnetic nanoparticles for targeted drug delivery and imaging. Adv Drug Deliv Rev 62(3):284–304. https://doi.org/10.1016/j.addr.2009.11.002

Vigano C, Ruysschaert JM, Goormaghtigh E (2005) Sensor applications of attenuated total reflection infrared spectroscopy. Talanta 65(5):1132–1142. https://doi.org/10.1016/j.talanta.2004.07.052

Wang F, Wang L, Chen X, Yoon J (2014) Recent progress in the development of fluorometric and colorimetric chemosensors for detection of cyanide ions. Chem Soc Rev 43:4312–4324. https://doi.org/10.1039/C4CS00008K

Wang G, Lu Y, Yan C, Lu Y (2015) DNA-functionalization gold nanoparticles based fluorescence sensor for sensitive detection of Hg^{2+} in aqueous solution. Sensors Actuators B Chem 211:1–6. https://doi.org/10.1016/j.snb.2015.01.051

Wen G, Lin C, Tang M, Liu G, Liang A, Jiang Z (2013) A highly sensitive aptamer method for Ag+ sensing using resonance Rayleigh scattering as the detection technique and a modified nanogold probe. RSC Adv 3:1941–1946. https://doi.org/10.1039/C2RA22542E

Wu X, Xu Y, Dong Y, Jiang X, Zhu N (2013) Colorimetric determination of hexavalent chromium with ascorbic acid capped silver nanoparticles. Anal Methods 5:560. https://doi.org/10.1039/c2ay25989c

Yang LB, Jiang X, Ruan WD, Zhao B, Xu WQ, Lombardi JR (2009) Adsorption study of 4-MBA on TiO2 nanoparticles by surface-enhanced Raman spectroscopy. J Raman Spectrosc 40:2004–2008. https://doi.org/10.1002/jrs.2358

Yu Y, Hong Y, Wang Y, Sun X, Liu B (2017) Mercaptosuccinic acid modified gold nanoparticles as colorimetric sensor for fast detection and simultaneous identification of Cr^{3+}. Sensors Actuators B 239:865–873. https://doi.org/10.1016/j.snb.2016.08.043

Yuan X, Wen S, Shena M, Shi X (2013) Dendrimer-stabilized silver nanoparticles enable efficient colorimetric sensing of mercury ions in aqueous solution. Anal Methods 5:5486. https://doi.org/10.1039/c3ay41331d

Zhai D, Xu W, Zhang L, Chang YT (2014) The role of "disaggregation" in optical probe development. Chem Soc Rev 43:2402–2411. https://doi.org/10.1039/C3CS60368G

Zhan W, Bard AJ (2007) Electrogenerated chemiluminescence. Immunoassay of human C-reactive protein by using $Ru(bpy)_3^{2+}$-encapsulated liposomes as labels. Anal Chem 79(2):459–463. https://doi.org/10.1021/ac061336f

Zhan S, Wu Y, He L, Wang F, Zhan X, Zhou P, Qiu S (2012) Measuring the size and density of nanoparticles by centrifugal sedimentation and flotation. Anal Methods 4:3997–4002. https://doi.org/10.1039/C8AY00237A

Zhang H, Jia Z (2017) Development of fluorescent FRET probes for "off-on" detection of L-cysteine based on gold nanoparticles and porous silicon nanoparticles in ethanol solution. Sensors 17(3):520. https://doi.org/10.3390/s17030520

Zhang WB, Su ZF, Chu XF, Yang XA (2010) Evaluation of a new electrolytic cold vapour generation system for mercury determination by AFS. Talanta 80(5):2106–2112. https://doi.org/10.1016/j.talanta.2009.11.016

Zheng Y, Huang Z, Zhao C, Weng S, Zheng W, Lin X (2013) A gold electrode with a flower-like gold nanostructure for simultaneous determination of dopamine and ascorbic acid. Microchim Acta 180(7–8):537–544. https://doi.org/10.1007/s00604-013-0964-0

Zhou Y, Xu Z, Yoon J (2011) Fluorescent and colorimetric chemosensors for detection of nucleotides, FAD and NADH: highlighted research during 2004–2010. Chem Soc Rev 40:2222–2235. https://doi.org/10.1039/C0CS00169D

Zoski CG (2007) Handbook of electrochemistry. Elsevier, Oxford

Chapter 5
Surface-Modified Conducting Polymer-Based Nanostructured Materials for the Removal of Toxic Heavy Metals from Wastewater

Raghunath Das, Kamdem Paumo Hugues, and Arjun Maity

Contents

Abstract In the last few decades, there has been a significant escalation in the level of toxic heavy metals in water bodies due to their exponential industrial usage. These hazardous water and soil pollutants have been broadly investigated for their serious effects on human health and other life systems, and their lethal concentrations have been reviewed by well-established international bodies, including the WHO and US EPA. Therefore, efficient remediation of toxic heavy metals from wastewater represents a major burden for the environmentalists. Amongst other numerous techniques reported for that purpose, adsorption technology has been established as one of the conventional and promising procedures for effective application at relatively low

R. Das · K. P. Hugues
Department of Applied Chemistry, University of Johannesburg, Johannesburg, South Africa

A. Maity (✉)
Department of Applied Chemistry, University of Johannesburg, Johannesburg, South Africa

DST/CSIR National Center for Nanostructured Materials, Council for Scientific and Industrial Research (CSIR), Pretoria, South Africa
e-mail: amaity@csir.co.za

Mu. Naushad et al. (eds.), *Advanced Nanostructured Materials for Environmental Remediation*, Environmental Chemistry for a Sustainable World 25,
https://doi.org/10.1007/978-3-030-04477-0_5

cost. Recent data show that conducting polymers and their functionalised derivatives as adsorbents have received substantial attention for As(III), As(V), Cr(VI), Pb(II), Zn(II), Hg(II) and Cu(II) remediation from polluted streams (i.e. industrial effluents, mine wastewaters, landfill leachate and groundwater). The common goal of the research behind these fascinating adsorbents is to develop supported nanostructures with enhanced performance for wastewater treatment systems. Nanostructured materials of different shape and morphology exhibit better performance in environmental remediation than their macromolecular counterparts, owing to large surface area associates with high surface reactivity. The current chapter reviews the synthesis and adsorption studies (isotherm, kinetics, maximum capacities and thermodynamics) of recently reported nanostructured conducting polymer-based materials for treatment of As(III)-, As(V)-, Cr(VI)- and Hg(II)-contaminated water medium.

Keywords Conducting polymer nanocomposites · Heavy metal ions · Wastewater treatment · Adsorption kinetics · Adsorption isotherms · Adsorption thermodynamics · Breakthrough adsorption modelling

5.1 Introduction

Environmental pollution has become a solemn problem affecting human health and other life systems, as a result of the exponential development of industries and technologies (Meena et al. 2018; Huang et al. 2018; Eyrikh et al. 2017). Healthcare services in developed as well as underdeveloped countries are struggling under the rise of diseases associated with water pollution (Akpalu and Normanyo 2017). This hypothetically avoidable situation is surely evolving into a global disaster. Safe water paucity is now seen as a critical challenge. Owing to the variations in natural and anthropogenic activities that lead to adulteration of both terrestrial and aquatic ecosystem with toxic heavy metals and metalloids, approximately 80% of the world population is at serious risk from threats to water security (Vörösmarty et al. 2010). Uncontrolled discharges of untreated sewage and industrial wastewater as well as the use of fertilizers and agricultural pesticides are some of the major contributors. In that regard, existing freshwater resources are progressively becoming polluted and unavailable. In a remedial action, the hazardous heavy metals of greatest concern consist of arsenic, chromium, mercury, cadmium, nickel, lead, zinc and copper.

Significant efforts have been made to remove or reduce the level of heavy metals to allowable limits in the environment. Traditional methods that have been employed include biological treatment, reverse osmosis, extraction, precipitation, dissolved air flotation, sedimentation, electrolysis, membrane filtration, ion exchange and many more (Santhosh et al. 2016; Adeleye et al. 2016). However, most of these approaches are plagued with numerous limitations that impede their practical and effective application. Production of sludge as secondary pollutant in precipitation, limited

potential in biological treatment, high-energy requirements in membrane filtration, sophisticated equipment in dissolved air flotation and high operational costs in electrolysis can be mentioned. Adsorption technology, on the other hand, has often been regarded as a relatively superior process owing to the simple design, ease of operation and cost-effectiveness (Ali et al. 2016; Burakov et al. 2018; He et al. 2016; Zhou et al. 2015; Yu et al. 2012).

A variety of materials are reported in the literature for heavy metal adsorption, and these comprise biomaterials, industrial wastes, activated carbon, clay minerals, zeolites, metal oxides and conducting polymer-based nanomaterials (Sud et al. 2008; Nguyen et al. 2013; Ahmed and Ahmaruzzaman 2016; Wong et al. 2018; Uddin 2017; Reeve and Fallowfield 2018; Zare et al. 2018). Conducting polymers, as highly π-conjugated polymeric systems, have established themselves as suitable materials for potential application in water treatment. These conjugated organic materials, also identified as synthetic metals, exhibit vast surface area, high conductivity, outstanding optical properties, unique electrochemical characteristic and remarkable biocompatibility (Nguyen and Yoon 2016). Moreover, their synthetic ease, nontoxicity, relatively low cost as well as modifiable surface chemistry are of particular attention. Because of the presence of heteroatom with good affinity towards heavy metals in their chemical structure, polypyrrole (PPy), polyaniline (PANI) and polythiophene (PTh) appear to be the most promising candidates for the adsorption of metal cations (Balint et al. 2014). Conducting polymer surface modification with appropriate organic or inorganic constituent serves as a means for further enhancing their valuable properties, providing the prospect to tailor the materials for a particular application (Hackett et al. 2017).

Parameters that influence the adsorption efficiency of heavy metals on to conducting polymer-based nanostructure materials include solution pH, contact time, adsorbent dose, temperature and initial concentration in batch mode as well as flow rate, bed height and initial pollutant concentration with regard to column dynamic study.

Solution pH directly influences speciation of ions in solution, surface charge and complexation of adsorbent during sorption. Change in pH denotes variation of H^+ and OH^- present in the test solution. These ions can easily interact with the adsorbent and thereby impact the adsorption efficiency. Contact time, on the other hand, is a factor directly affecting the kinetics of adsorption as it assists in establishing the likely speed of diffusion and binding at the surface of the material. Generally, metal ion removal is high at longer contact time up until equilibrium. The adsorbent dose makes provision of the ability of a metal to be adsorbed with the least quantity of the adsorbent at a particular operating condition. An increase in adsorbent dose results in increased active adsorption sites, hence improved in adsorption capacity. Further, a decrease in temperature is usually accompanied with a decline in heavy metal adsorption onto the adsorbent.

The main focus of this chapter is to review the recent developments in the synthesis, characterization and sorption performance of hybrid conducting polymer-based nanostructured materials for the remediation of selected toxic metal cation As(III)-, As(VI)-, Hg(II)- or Cr(VI)-contaminated water under various

experimental conditions. The mechanism involved during the adsorption process is also highlighted.

5.2 Synthesis and Modification of Nanostructured Conducting Polymers

Numerous techniques including template-based, template-free and electrospinning processes have been reported for the synthesis of nanostructured conducting polymer.

Template-based synthesis of nanostructured materials entails three main steps, namely, preparation of the template, synthesis of the target material with the prepared template and removal of the template. Hard template is the most frequently used approach for the preparation of conducting polymer nanostructure. This technique requires porous membrane that ushers the growth of nanostructure within the pores, resulting in controlled size and morphology of the prepared material. Templates such as polyester, polycarbonate and anodic aluminium oxide membranes have been employed for the fabrication of PPy and PANI nanostructures (Ghosh et al. 2016; Esman and Lellouche 2010). Moreover, materials such as nanoporous zeolites and mesoporous silica and carbons have also been identified to serve as host in a guest–host inclusion process for the synthesis of conducting polymers with well-defined structure (Chen et al. 2018; Li et al. 2018). For example, in their interest for cyclodextrin structure, Gu and co-workers achieved the synthesis of controlled rectangle- or square pore-shaped PANI nanotubes via solution polymerization of aniline (ANI) in the presence of β-cyclodextrin (Gu et al. 2014). The obtained powder was thoroughly washed with ethanol to get rid of the template. β-Cyclodextrin is a hydrophilic seven-membered molecule with hydrophobic cavities. Relatively low concentration of aniline monomer and β-cyclodextrin generated the square pore-shaped nanostructures.

Soft template, usually described as relatively cheap and simple technique for the fabrication of nanostructured conducting polymers, is based upon a self-assemble process. Selective control of noncovalent bonding interactions such as hydrogen bonding, π-π stacking, metal-ligand coordination and Van der Waals forces during the polymerization process can also serve as systematic procedure for preparation of nanostructured particles with specific geometry (Sommer et al. 2015). Chemical oxidative polymerization in the presence of adsorbed surfactant molecules as well as chiral dopant organic acids has been reported for the synthesis of PPy and PANI nanostructures. For example, Zhang et al. reported the synthesis of nanostructured polypyrrole with ribbon-, wire- and sphere-like morphologies by solution chemistry methodology using surfactants (Zhang et al. 2006). Nonionic poly(ethylene glycol) mono-p-nonylphenyl ether or cationic short-chain octyltrimethylammonium bromide yielded PPy nanoparticles with spherical morphology. Cationic cetyltrimethylammonium bromide or dodecyltrimethylammonium bromide as

long-chain aliphatic surfactant, on the other hand, afforded the wire- and ribbon-like nanostructures. The use of anionic sodium dodecyl sulphate generated undefined geometrical nanofeature. Dai and Lu reported the use of fibrillar methyl orange for the synthesis of PPy as well as PANI nanotubes (Dai and Lu 2007). Likewise, the acid red 1 dopant in place of fibrillar methyl orange afforded the rectangular-sectioned PPy nanotubes (Yan and Han 2007). Swollen liquid crystals, obtained through mixing of either sodium dodecyl sulphate or cetyltrimethylammonium bromide with aniline hydrochloride followed by the addition of cyclohexane and 1-pentanol, yielded PANI particles with morphology that depends on initiator and mesophase reaction mode (Dutt and Siril 2014). Mixing mode afforded spherical morphology, while diffusion approach generated rod-like shape. Chiral organic acids have also been reported as soft templates for the synthesis of PPy and PANI nanofibres. Yan et al. reported the fabrication of PANI nanofibres with helical conformation using D- and L-camphorsulphonic acid (CSA) enantiomers (Yan et al. 2007). CSA acted to prevent overgrowth and induce optical activity of the PANI fibres. Clockwise and anticlockwise helical configurations were accomplished in the presence of D-CSA and L-CSA, respectively. However, taking into consideration that the complete removal of template after polymerization process in template-based synthesis remains a key challenge, template-free procedures have equally attracted considerable interest and are discussed below.

A facile chemical technique to obtain pure polyaniline nanofibres without the need for any template has been reported using aqueous/organic interfacial polymerization (Huang and Kaner 2004). In this case, the reactants (ANI monomer and oxidant) are both dissolved in immiscible solvent system, and the oxidative polymerization occurs only at the interface between the solvents, leading to nanofibres with relatively identical diameters. Although the solvent interface does not directly affect the formation of nanofibres, it assists in avoiding overgrowth of the already formed nanofibres. Another template-free approach for the fabrication of PANI nanofibres (Fig. 5.1) is the self-assemble strategy through rapid-mixing polymerization. Monomer and initiator are forced to consume instantly for primary nanofibre growth, exclusively (Deng et al. 2017; Bhaumik et al. 2016a, b). In a different type

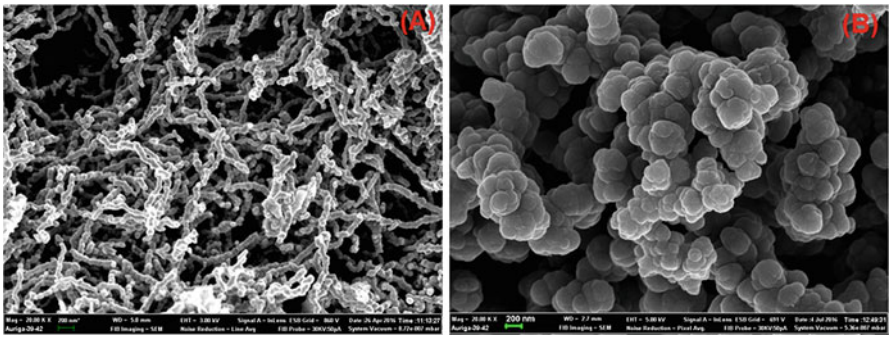

Fig. 5.1 SEM images of synthesized pure PANI nanofibres (**a**) and PPy (**b**)

of study, Wang et al. equally developed a template-free and site-specific electrochemical polymerization methodology to fabricate individually addressable PANI nanowires on microelectrode junctions (Wang et al. 2004). Electrospinning is a nanofibre fabrication technique that makes use of high voltage to charge the surface of a polymer solution and hence instigate the ejection of liquid jet through a small orifice. The nanofibre size prepared using this method can be controlled by changing the following parameters: voltage, flow rate, solution conductivity, size of the orifice and distance between the orifice and the collector. Electrospinning has been employed to synthesize continuous conductive PPy and PANI nanofibres with uniform morphology and physical stability (Moutsatsou et al. 2015).

Conducting polymer functionalization can also improve their valuable properties further. These hybrid materials have attracted significant research interest in the field of environmental remediation owing to their distinctive physicochemical properties that the individual constituents do not display. PPy matrix modification with clay minerals or their organically modified derivatives, for example, was achieved in situ, through polymerization of monomer pyrrole (Py) with dispersed clay or modified clay particles, and found to exhibit high adsorption capacity towards Cr(VI) in batch study (Ballav et al. 2014; Setshedi et al. 2013). Graphene oxide dispersion, on the other hand, afforded highly active PPy-graphene oxide nanocomposite with impressive performance regarding Cr(VI) uptake both in batch and column dynamic studies (Setshedi et al. 2015). Graphene oxide is a monomolecular sheet-bearing oxygen functional group such as hydroxyl, carboxyl and epoxide at the edges. Next, taking into consideration the ability of cyclodextrins to self-assemble with various pollutants via inclusion complexation (Chen and Jiang 2011), Chauke and co-workers reported the oxidative synthesis of PPy functionalized with both graphene oxide and α-cyclodextrin (Chauke et al. 2015). Moreover, anion and cation containing nanostructured materials possessing high ion-exchange proficiency have also captivated significant consideration (Asiabi et al. 2017). Zwitterionic glycine-doped PPy (Fig. 5.2A), for example, was fabricated by chemical oxidative polymerization of Py in the presence of glycine and reported as highly efficient material for the uptake of toxic chromium(VI), more so than PPy homopolymer (Ballav et al. 2012). Similarly, with the purpose of improving only the anionic exchange potential of PPy for Cr(VI) adsorption, incorporation of 2,5-diaminobenzene sulphonic acid (DABSA) during polymerization process has been reported as shown in Fig. 5.2B

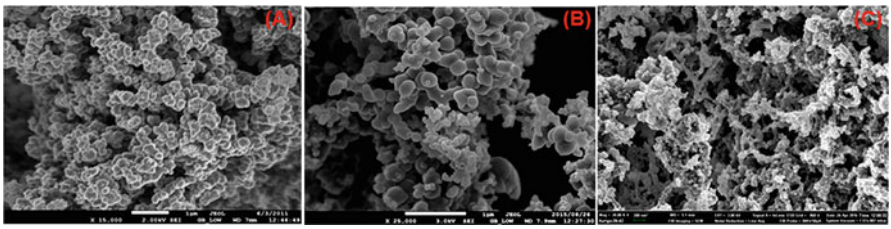

Fig. 5.2 SEM images of glycine- (**a**) and DABSA- (**b**) modified PPy; Fe^0- deposited PANI nanocomposites (**c**)

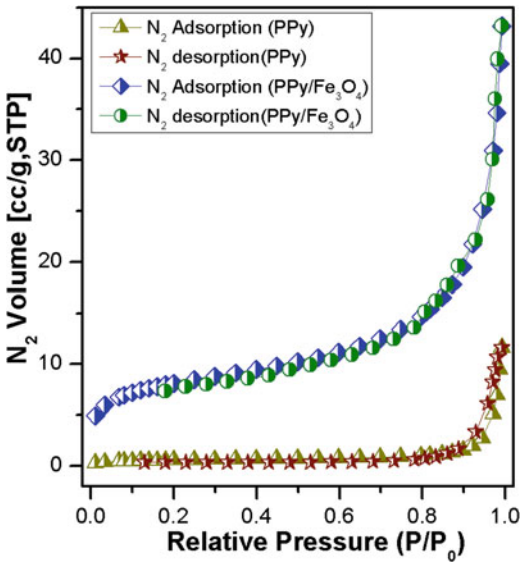

Fig. 5.3 BET surface area of PPy and PPy/Fe_3O_4

(Kera et al. 2016). Sulphur-containing entities are also well employed as dopant for mercury-selective adsorption as a result of strong metal-ligand complex stability (Ballav et al. 2018; Das et al. 2017a, b, c; Oveisi et al. 2017).

Furthermore, incorporation or deposition of inorganic nanoparticles such as carbon nanotube, Fe_3O_4, Fe^0 and SiO_2 onto conducting polymer supports has been found to increase their chemical, thermal and mechanical stabilities (Ng et al. 2013; Ghaemi and Daraei 2016; Zare et al. 2018). The resultant nanocomposites have also revealed superior adsorption capacities as well as better selectivity for toxic heavy metal remediation (Peng et al. 2017; Kumar et al. 2013; Burakov et al. 2018). For example, Das and co-workers reported the synthesis of PANI/Fe^0 nanocomposite (see Fig. 5.2C) via reductive insertion of nanosized iron zero onto support of PANI nanofibres (Das et al. 2017a, b, c). $FeCl_2$/$FeCl_3$ by-products were used as source of Fe^0 in the presence of sodium borohydride. The as-prepared adsorbent demonstrated As(V) removal efficacy of up to 99.9%. In a cognate study, PPy- and PANI-maghemite nanocomposites were fabricated through in situ polymerization of Py and aniline monomers with γ-Fe_2O_3, obtained by $FeCl_2$/$FeCl_3$ chemical co-precipitation (Chávez-Guajardo et al. 2015). These maghemite nanomaterials were found to act as efficient adsorbent towards Cu(II) and Cr(VI) species from aqueous solution. Aigbe and co-workers described the synthesis of PPy magnetic nanocomposite with fast adsorptive capacity towards Cr(VI) ions in unsteady electromagnetic field, through Py polymerization with Fe_3O_4-suspended nanoparticles (Aigbe et al. 2018). The BET surface area increased after incorporation of Fe_3O_4 nanoparticle on to the PPy matrix as illustrated in Fig. 5.3. Magnetism is a distinctive physical property that was established recently to ease the treatment of water by directing the adsorbate pollutant orientation towards the adsorbent pores. Magnetic field meaningfully impacts the size distribution of the nanoparticles as well as the

zeta potential in sorption process (Zaidi et al. 2014). Ternary PPy graphene/SiO_2 adsorbent prepared by chemical polymerization of pyrrole in dispersed silica-intercalated graphene nanocomposite, developed using a sol-gel procedure, was reported to exhibit high surface area as well as prodigious Cr(VI) removal ability (Fang et al. 2018). PPy-decorated Fe_3O_4/reduced graphene oxide nanoparticles (PPy-Fe_3O_4/rGO) were synthesized by in situ polymerization of pyrrole monomer in hexadecyltrimethylammonium bromide solution containing Fe_3O_4/rGO nanoparticles generated using post-oxidation methodology (Wang et al. 2015). Comprehensive assay on the uptake of Cr(VI) using PPy/Fe_3O_4/rGO in batch adsorption mode revealed that this ternary hybrid nanocomposite performed much better than the binary Fe_3O_4/rGO sub-nanocomponent.

5.3 Separation of Toxic Pollutants from Water Through Adsorption Process

Adsorption process involves the transfer and adhesion of ions, atoms or molecules of the adsorbates to the surface sites provided by an adsorbent. The adsorbent surface binds the upcoming adsorbate molecules through physical adsorption (physisorption) and/or chemical adsorption (chemisorption). Physisorption mainly takes place through driven forces like hydrogen bond, Van der Waals forces, static, dipole-dipole and π-π interactions (Kim and Lee 2014; Li et al. 2005; Cao et al. 2012). In chemical adsorption, pollutants get accumulated through chemical bonds at the surface of the adsorbent due to electron exchange. Adsorption being a surface phenomenon, the extent of the process is built upon the surface characteristics of the adsorbent, and these include charges, particle size and molecular structure (Jia et al. 2002; Chen and Lin 2001). In adsorption technology, the removal of pollutant by solid adsorbent is typically addressed either in batch or column mode. These are detailed in the next sections.

5.3.1 Batch Adsorption Technique

In batch operation experiment, a fixed quantity of solid adsorbent is mixed all at once with a definite amount of adsorbate-containing solution. The adsorbate-adsorbent system is kept in agitation for a certain period of time on a thermostated orbital shaker (Ghorai et al. 2014; Bhaumik et al. 2014a, b; Patra et al. 2017). As the adsorption progresses, an equilibrium adsorption stage is attained between solute adsorbate in solution and adsorbent. The separation of subsequent solution is accomplished either by filtration or centrifugation. The adsorbate concentration at the end is determined through UV-Vis spectrophotometer or ICP-MS techniques (Xiong et al. 2013; Wang et al. 2014a, b). Numerous adsorption parameters including solution pH, experimental temperature, adsorbent dose, adsorbate concentration

and contact time are varied to acquire the ideal adsorption conditions. The adsorption capacity (% removal) for the subtraction of pollutants from aqueous medium is calculated following eq. (5.1). The quantity of adsorbed metal cations over adsorbent mass at equilibrium (q_e) and at any time t (q_t) is calculated through the following eqs. (5.2) and (5.3), respectively (Liu et al. 2015; Zhang et al. 2017).

$$Adsorption\ efficiency = \frac{C_0 - C_e}{C_0} \times 100 \tag{5.1}$$

$$q_e = (C_0 - C_e) \times \frac{V}{m} \tag{5.2}$$

$$q_t = (C_0 - C_t) \times \frac{V}{m} \tag{5.3}$$

The solution concentrations initially at time t and at equilibrium time are represented as C_0, C_t and C_e (mg/L), respectively. V (L) and m (g) denote the volume of adsorbate solution and the amount of adsorbent used. The duration of contact time of solid/liquid in adsorption predicts the rate of uptake of the solute pollutants from liquid medium.

Adsorption Kinetics

The affinity between the initial adsorbate concentration and the adsorption rate has been established to explore the adsorption mechanism as well as the rate-determining steps. Kinetics study is regularly performed by taking different initial concentrations of adsorbate solution at fixed pH, temperature and adsorbent dosage (Das et al. 2017a, b, c). After a certain time interval, an aliquot is taken, and the outstanding adsorbate concentration is measured. Aiming to elucidate the rate of adsorption and rate-determining step of adsorbate onto the adsorbent surface with respect to time, adsorption kinetic models including the pseudo-first-order (Legergren 1898), pseudo-second-order (Ho and McKay 1999), second-order (Ho 2006) and intraparticle diffusion (Weber and Morris 1963) are frequently applied.

The integrated mathematical linear forms of Legergren pseudo-first-order, Ho and McKay pseudo-second-order and Ho second-order kinetic models are articulated using Eqs. (5.4), (5.5) and (5.6), respectively.

$$log(q_e - q_t) = logq_e - \frac{K_1}{2.303}\, t \tag{5.4}$$

$$\frac{t}{q_t} = \frac{1}{K_2 q_e^2} + \frac{t}{q_e} \tag{5.5}$$

$$\frac{1}{(q_e - q_t)} = \frac{1}{q_e} + K_3 t \tag{5.6}$$

q_e and q_t (mg/g) represent the quantity of uptake adsorbates at equilibrium and time t, respectively. K_1 (min^{-1}), K_2 (g/mg.min) and K_3 (g/mg.min) are the pseudo-first-order, pseudo-second-order and second-order rate constant, respectively. In pseudo-first-order, the rate constants and adsorption capacities are obtained from the linear graph of $\log(q_e\text{-}q_t)$ against t. However, pseudo-second-order and second-order kinetics parameters are determined using the graphs of t/q_t against t and $1/(q_e\text{-}q_t)$ against t, respectively.

Moreover, to figure out the probability of intraparticle diffusion of adsorbed metal ions, Weber and Morris have introduced the intraparticle diffusion (IDP) model transcribed by the following expression (Weber and Morris 1963):

$$q_t = K_{id} t^{1/2} + C \tag{5.7}$$

where k_{id} ($mg/g.min^{1/2}$) represents the IDP constant, which can be obtained from the slope of the graph q_t vs $t^{1/2}$, and C is a constant related to the thickness of the boundary layer.

Adsorption Isotherm

The equilibrium adsorption isotherm predicts the adsorbent-adsorbate interaction and the mathematical relation of the amount (mg) of adsorbates uptake per gram of adsorbent to the solution concentration at a constant temperature (Afkhami and Moosavi 2010; Ghaedi et al. 2014). Therefore, to understand the interaction between adsorbate and adsorbent, it is necessary to correlate the experimental adsorption data with some well-known adsorption isotherm models. The obtained equilibrium adsorption data are frequently fitted into well-known adsorption isotherm, namely, the Langmuir and Freundlich (Langmuir 1918; Freundlich 1906). Langmuir isotherm is based on the physical supposition that the adsorbent surface has a fixed number of equivalent active sites and the maximum adsorptive capacity consists of a monolayer process (Langmuir 1918; Reed and Matsumoto 1993) and can be expressed as:

$$q_e = \frac{b.Q_0.C_e}{1 + b.C_e} \tag{5.8}$$

where C_e (mg/L) stands as the equilibrium adsorbate concentration and q_e (mg/g) denotes the quantity of adsorbed adsorbate. Q_0 (mg/g), the Langmuir constant, signifies the maximum monolayer adsorption capacity, and b (L/mg) value connects to the energy of adsorption. The linearized Langmuir equation is given as follows:

$$\frac{C_e}{q_e} = \frac{1}{b.Q_0} + \frac{C_e}{Q_0} \tag{5.9}$$

Q_0 and b values are estimated from the slope and intercept of the plot of C_e/q_e against C_e.

The separation factor of the Langmuir adsorption isotherm R_L is an essential feature to determine the favourability and applicability of an adsorption process (Hall et al. 1966). The equation can be expressed as:

$$R_L = \frac{1}{1 + b.C_0} \tag{5.10}$$

where C_0 (mg/L) is the initial adsorbate concentration and b is the Langmuir constant. The type of isotherm strongly correlates with obtained R_L values. Values within the range $0 < R_L < 1$ for each of the different initial concentrations indicate favourable adsorption, whereas $R_L = 1$, $R_L = 0$ and $R_L > 1$ suggest linear, irreversible and unfavourable adsorption process, respectively.

The Freundlich isotherm model is employed for the description of reversible and complex adsorption process. It assumes that the binding sites on the surface of the adsorbent are occupied by adsorbate in multilayer adsorption manner, and this model is represented as follows:

$$q_e = K_F C_e^{1/n} \tag{5.11}$$

The linearized Freundlich model can be represented as the logarithms of Eq. (5.11).

$$\ln q_e = \ln K_f + \frac{1}{n} \ln C_e \tag{5.12}$$

where K_F and n are the constants associated to the adsorption capacity and intensity of adsorption, respectively, and their values can be acquired from the slope and intercept of the graph lnq_e against lnC_e. The higher the K_f value, the greater will be the adsorption efficiency. Moreover, n values within the range 0 and 10 indicate favourable adsorption process (Gong et al. 2011; Meng et al. 2015).

Adsorption Thermodynamics

The amount of pollutants adsorbed on the adsorbent surface depends upon the temperature of the adsorption medium. Thermodynamic variable characteristics including the Gibbs free energy change (ΔG), change in enthalpy (ΔH) and change in entropy (ΔS) of the adsorption experiments are determined using the following equation (Tang et al. 2015; Attallah et al. 2016):

$$\Delta G^0 = -RTlnK \tag{5.13}$$

$$\Delta G^0 = \Delta H^0 - T\Delta S^0 \tag{5.14}$$

$$K = \frac{q_e}{C_e} \tag{5.15}$$

$$lnK = \frac{\Delta S^0}{R} - \frac{\Delta H^0}{RT} \tag{5.16}$$

where K, R, T (K), q_e (mg/g) and C_e (mg/L) symbolize the equilibrium constant, the universal gas constant (8.314 J/K·mol), the temperature, the quantity of the adsorbed pollutants and the equilibrium concentration, respectively. The enthalpy change (ΔH°) and entropy change (ΔS°) of the adsorption are estimated from the slope and intercept of the van 't Hoff plot of ln$K$ alongside 1/T, respectively. A negative free energy change value (ΔG°) specifies the achievability and spontaneity of the process. More negative ΔG values with increasing temperatures suggest stronger interaction adsorbent/adsorbate molecule as well as elevated degree of spontaneity. In addition, the magnitude of ΔG° value reflects the nature of adsorption process. ΔG° values in the range −20 and 0 kJ/mol signify physisorption process, while values in between −80 and −400 kJ/mol suggest chemisorption process (Salam et al. 2012). Positive ΔH° value indicates the endothermic nature of an adsorption process (Xu et al. 2011; Zhang and Ou 2013). Positive values of ΔS° reflect increased disorder and randomness of the adsorption system (Paşka et al. 2014; Dong et al. 2011).

5.3.2 Fixed Bed Column Experiments

The aim of a column sorption test is to quantify the parameters which are required to design industrial scale fixed bed water treatment. The performance of a fixed bed column is evaluated using the theoretical breakthrough curves (BTC). The shape and appearance of the breakthrough point in fixed bed column experiment serve as key indicator to assess the effective applicability of the used adsorbent. The breakthrough point defines the time at which the concentration of effluent surpasses the maximum acceptable release concentration of a particular contaminant. This can be estimated by plotting Ct/Co against time t. The initial adsorbate concentration, flow rate of effluent and bed mass/bed height are parameters influencing the shape of the breakthrough curves. The breakthrough capacity of the packed column is estimated as follows:

$$q_b = \frac{C_0}{m} \int_0^{V_b} \left(1 - \frac{C_t}{C_0}\right) dV \tag{5.17}$$

where q_b (mg/g), C_t (mg/L), m (g) and V_b (L) represent the bed capacity at breakthrough point, the concentration of outlet solution at time t, the bed mass and the volume processed at breakthrough point, respectively. For a particular bed height (adsorbent mass), the performance of a packed bed column is depending on the number of bed volumes (BV) processed before the breakthrough point is attained (Onyango et al. 2009). BV can be expressed through the following equation.

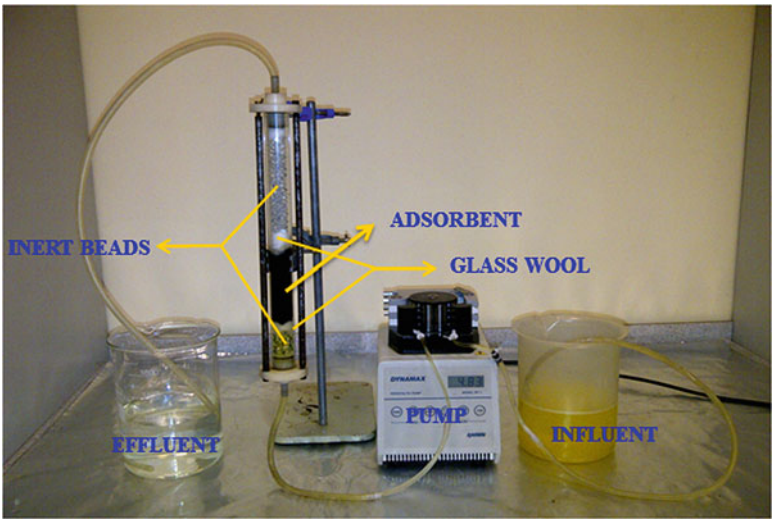

Fig. 5.4 Picture of a fixed bed packed column adsorption experiment

$$\mathrm{BV} = \frac{\text{Volume of solution processed at break through point(L)}}{\text{Volume of adsorbent bed (L)}} \tag{5.18}$$

During a continuous flow adsorption investigation, the adsorbent become exhausted after certain runs. The adsorbent exhaustion rate (AER) described the mass of adsorbent deactivated per volume of solution processed at breakthrough point. Lesser values of AER imply better column performance. AER is expressed by the following equation.

$$\mathrm{AER} = \frac{\text{mass of adsorbent (g) in column}}{\text{volume of solution processed (L)}} \tag{5.19}$$

Continuous flow adsorption experiments for Cr(VI) uptake in a packed bed perspex glass cylindrical pipe of 2 cm inner diameter and 30 cm height using PPy/Fe_3O_4-developed adsorbent as shown in Fig. 5.4 have been reported (Bhaumik et al. 2013). A known quantity of PPy/Fe_3O_4 (2, 4 and 6 g) was packed into the above described column, where the top and bottom ends of the adsorbent bed were concealed by a deposit of glass wool, with the purpose of avoiding any loss of adsorbent as well as giving mechanical support to the adsorbent bed. In addition, glass beads were sited on top of the column bed to preclude the adsorbent from being dragged with the outflow. A peristaltic pump was used to maintain the desired flow rate of the effluent samples in an upwards mode. The effluent samples were collected at a certain time intermission, and the concentration of the adsorbates was assessed. The volumes of Cr(VI)-contaminated water processed at breakthrough point (2.8; 7.2; 12.6 L) as well as the numbers of bed volumes (183; 286; 364) were found to increase with the

bed mass. In addition, the estimated values of AER decrease (from 0.69 to 0.47 g/L) with increased adsorbent mass. The time required to attain breakthrough point was reported to decrease (from 2400 to 420 min) with increased flow rate (3–7 mL/min). On the other hand, column study for Cr(VI) uptake using PPy/graphene oxide as adsorbent revealed that V_b at breakthrough point (5.13; 22.32; 33.12 L) improved with adsorbent mass (1, 2 and 3 g) (Setshedi et al. 2015). Furthermore, increased concentration of Cr(VI) (from 10 to 50 mg/L) led to a decrease in breakthrough time thus declined in V_b values (from 64.08 to 7.2 L).

Modelling of Column Dynamic Adsorption

To successfully design a fixed bed column, several mathematical models have been established. The mathematical modelling of breakthrough curves acquired from a series of experiments is very crucial as it provides insight of the conditions for an optimum performance of the column. Thomas, Yoon-Nelson and Bohart-Adams models are widely applied to fit the experimental data.

Thomas Model

This model follows the Langmuir kinetics of adsorption, and the rate driving force obeys the second-order reversible reaction kinetics (Thomas 1944). In this case, the chemical reaction is not the rate-limiting step; rather the process is governed by the mass transfer at the interface of the adsorbent (Suksabye et al. 2008; Malkoc and Nuhoglu 2006). Its linearized form is represented as follows:

$$\ln\left(\frac{C_0}{C_t}-1\right)=\frac{K_{Th}q_0m}{Q}-K_{Th}C_0t \tag{5.20}$$

where K_{Th} (mL/min.mg) and q_0 (mg/g) denote the Thomas rate constant and the equilibrium adsorbate uptake, respectively. The plot of $ln(C_0/C_t-1)$ against time t provides the K_{Th} and q_0 values.

The Yoon-Nelson Model

Yoon and Nelson have reported a simple theoretical model to predict the breakthrough activities (Yoon and Nelson 1984). This model is founded on the hypothesis that the rate at which the probability of adsorption of adsorbate molecules decreases is proportional to the probability of adsorbate adsorption as well as the probability of adsorbent breakthrough on the adsorbent bed (Chen et al. 2012). This model can be linearized using the following expression:

$$\ln\left(\frac{C_t}{C_0-C_t}\right)=K_{YN}t-K_{YN}\tau \tag{5.21}$$

where K_{YN} (min^{-1}), τ and t (min) symbolize the Yoon and Nelson rate constant, the time required for 50% adsorbate breakthrough and the processing time, respectively. A linear plot of $ln[C_t/(C_0-C_t)]$ vs sampling time t can then be exploited to obtain K_{YN} and τ values from the slope and intercept, respectively.

Bohart-Adams Model

The Bohart and Adams model is based on the assumption that the adsorption equilibrium is not prompt and the rate of adsorption is directly related to the remaining capacity of the adsorbent as well as the concentration of the adsorbate species (Bohart and Adams 1920). The mathematical equation for Bohart-Adams model can be expressed as:

$$\ln\left(\frac{C_t}{C_0}\right) = K_{BA}C_0 t - K_{BA}N_0\left(\frac{Z}{U_0}\right) \tag{5.22}$$

where K_{BA} (L/mg.min) is the Bohart-Adams rate constant and N_0 (mg/L) is the maximum saturation concentration of the adsorbates. Z (cm) stands for bed depth of the fixed bed column, and U_0 (cm/min) is the linear velocity defined as the ratio of

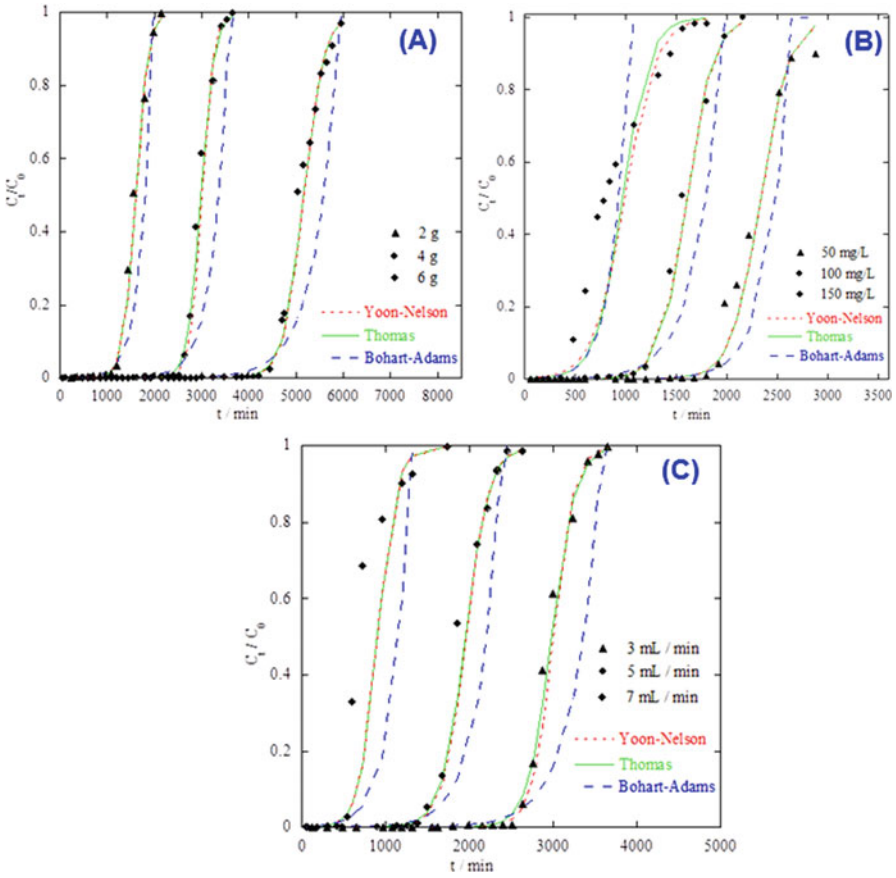

Fig. 5.5 Breakthrough curves for Cr(VI) removal onto PPy/Fe_3O_4 nanocomposite at different adsorbent mass (**a**), initial Cr(VI) concentrations (**b**) and flow rates (**c**)

volumetric flow rate (mL/min) to the cross-sectional area (cm^2) of the bed. A linear plot of $ln(C_t/C_0)$ against t gives the value of K_{BA} and N_0. It is evident from this model that the breakthrough data can well describe the initial part of a column dynamic experiment.

Thomas and Yoon-Nelson theoretical models were found to better depict the experimental breakthrough curves for Cr(VI) removal using PPy/Fe_3O_4, PPy/graphene oxide and PPy/organically modified montmorillonite clay nanocomposites as examples (Setshedi et al. 2015; Bhaumik et al. 2013; Setshedi et al. 2014). Figure 5.5 illustrates the suitability of the breakthrough curves with the above-described mathematical models for toxic chromium uptake onto PPy/Fe_3O_4 adsorbent at various column parameters (Bhaumik et al. 2013).

5.4 Application of Modified Conducting Polymers for Heavy Metal Ion Remediation

5.4.1 Removal of Cr(VI)

Chromium, as one the most abundant metal in Earth's crust (Shahid et al. 2017), mainly exists in the environment in the form of hexavalent chromium Cr (VI) and trivalent chromium Cr (III). Though chromium compounds serve as vital micronutrient for sugar and lipid metabolism in humans (Hua et al. 2012), long-term exposure to considerable Cr(VI) concentration has been reported as cancer-initiating. Soluble Cr(VI) derivatives, as compared to Cr(III), are strong oxidizing agents that can permeate cell membranes. Their toxicity pledges with the formation of unstable and highly reactive intermediates which are responsible for cellular components and DNA damages (Holmes et al. 2006). Chromium-contaminated soil and slag have also been reported as poisonous in plants even at low Cr (VI) concentration through seed germination inhibition, pigment status degradation and oxidative stress induction (Patra et al. 2018). The maximum contaminant level for chromium set by the US Environmental Protection Agency EPA has been promulgated as 0.1 mg/L for water surface, 0.05 mg/L for drinking water and 0.25 mg/L for industrial water (Aigbe et al. 2018). Table 5.1 reports the recent investigations of conducting polymer nanocomposites, used as adsorbent for the removal of Cr(VI) ions from water medium. As evidenced, PPy-intercalated graphene oxide (PPy/GO) nanocomposite was the most potent adsorbent with maximum uptakes of 625 mg/g at 25 °C. The Cr(VI) adsorption onto PPy/GO was dictated by chemisorption, taking into consideration the valence forces involving sharing or exchange of electrons. Moreover, the PPy/GO adsorptive capacity was able to treat 64.08 L of 25 mg/L toxic aqueous solution of Cr(VI) using 2 g of PPy/GO nanocomposite at a flow rate of 3 mL/min in column dynamic setup (Setshedi et al. 2015). Likewise, H_2SO_4-doped poly-diaminopyridine/GO also showed remarkable performance towards Cr(VI) in aqueous solution with a maximum adsorption capacity of 609.76 at pH 1 (Dinda and Saha 2015). This conducting

Table 5.1 Modified conducting polymer materials for chromium(VI) remediation

Adsorbent	Chromium species	Operating conditions	Adsorption isotherm	Adsorption kinetics	Adsorption capacity (mg/g)	Adsorption thermodynamics (KJ/mol)	References
Polyaniline/graphene (PANI/graphene)	Cr(VI)	$T = 30\ °C$; $C_{Ads} = 0.25$ g/L; $C_{Cr} = 100$ ppm; pH = 6.5	Langmuir	Pseudo-second-order	192	Not reported	Harijan and Chandra (2016)
Polyaniline/silica gel (PANI/SiO_2)	Cr(VI)	$T = 30\ °C$; $C_{Ads} = 2$ g/L; $C_{Cr} = 50$ mg/L; pH = 4.2	Freundlich	Pseudo-second-order	63.41	$\Delta G^0 = -8.30$ $\Delta H^0 = 15.51$ $\Delta S^0 = 0.02$	Karthik and Meenakshi (2014)
Polyaniline/Fe^0 (PANI/Fe^0)	Cr(VI)	$C_{Ads} = 0.5$ g/L; $C_{Cr} = 100$ mg/L; pH = 2	Langmuir	Not reported	434.78	Not reported	Bhaumik et al. (2014a, b)
*p*TSA-doped polyaniline/multiwalled carbon nanotube/graphene oxide (*p*TSA/PANi/CNT/GO)	Cr(VI)	$T = 30\ °C$; $C_{Ads} = 1$ g/L; $C_{Cr} = 200$ mg/L; pH = 2	Freundlich	Pseudo-second-order	142.85	$\Delta G^0 = -6.30$ $\Delta H^0 = 346.65$ $\Delta S^0 = 1.16$	Ansari et al. (2017)
Polypyrrole-polypyrrole/Fe_3O_4 magnetic nanocomposite (PPy/Fe_3O_4)	Cr(VI)	$T = 25\ °C$; $C_{Ads} = 2$ g/L; $C_{Cr} = 200$ mg/L; pH = 2	Langmuir	Pseudo-second-order	169.5	$\Delta G^0 = -0.56$ $\Delta H^0 = 43.40$ $\Delta S^0 = 0.15$	Bhaumik et al. (2011)
Fe_3O_4/PPy microspheres	Cr(VI)	$T = 25\ °C$; $C_{Ads} = 1$ g/L; $C_{Cr} = 200$ mg/L; pH = 2	Langmuir	Not reported	209.2	Not reported	Wang et al. (2012)
Polypyrrole-polyaniline/iron oxide (PPy-PANI/Fe_3O_4)	Cr(VI)	$T = 25\ °C$; $C_{Ads} = 1$ g/L; $C_{Cr} = 100$ mg/L; pH = 2	Langmuir	Pseudo-second-order	303	$\Delta G^0 = -1.79$ $\Delta H^0 = 47.41$ $\Delta S^0 = 0.16$	Kera et al. (2017)
Polyaniline/magnetic mesoporous silica	Cr(VI)	$T = 35\ °C$; $C_{Ads} = 0.8$ g/L; $C_{Cr} = 100$ mg/L; pH = 2	Langmuir	Pseudo-second-order	193.85	$\Delta G^0 = -1.20$ $\Delta H^0 = -16.23$ $\Delta S^0 = -0.05$	Tang et al. (2014)

(continued)

Table 5.1 (continued)

Adsorbent	Chromium species	Operating conditions	Adsorption isotherm	Adsorption kinetics	Adsorption capacity (mg/g)	Adsorption thermodynamics (KJ/mol)	References
Glycine-doped polypyrrole (PPy-gly)	Cr(VI)	T = 25 °C; C_{Ads} = 2 g/L; C_{Cr} = 100 mg/L; pH = 2	Langmuir	Pseudo-second-order	217.39	Not reported	Ballav et al. (2012)
Polypyrrole/halloysite nanotube (PPy/HNTs)	Cr(VI)	T = 25 °C; C_{Ads} = 1.5 g/L; C_{Cr} = 100 mg/L; pH = 2	Langmuir	Pseudo-second-order	149.25	$\Delta G^0 = -0.14$ $\Delta H^0 = 71.75$ $\Delta S^0 = 0.24$	Ballav et al. (2014)
H_2SO_4-doped poly diaminopyridine/graphene	Cr(VI)	C_{Ads} = 1 g/L; C_{Cr} = 500 mg/L; pH = 1	Langmuir	Pseudo-second-order	609.76	Not reported	Dinda and Saha (2015)
Polypyrrole/titanium (IV) phosphate	Cr(VI)	T = 30 °C C_{Ads} = 10 g/L; C_{Cr} = 200 mg/L; pH = 2	Langmuir	Pseudo-second-order	175	$\Delta G^0 = -2.42$ $\Delta H^0 = 18.61$ $\Delta S^0 = 0.08$	Baig et al. (2015)
Polypyrrole/reduced graphene oxide/Fe_3O_4 (PPy/rG/Fe_3O_4)	Cr(VI)	T = 30 °C; C_{Ads} = 0.25 g/L; C_{Cr} = 48.4 mg/L; pH = 3	Langmuir	Not reported	293.3	$\Delta G^0 = -24.31$ $\Delta H^0 = 22.97$ $\Delta S^0 = 0.16$	Wang et al. (2015)
Polypyrrole/graphene/Fe_3O_4 (PPy/graphene /Fe_3O_4)	Cr(VI)	T = 30 °C; C_{Ads} = 0.16 g/L; C_{Cr} = 120 mg/L; pH = 2	Langmuir	Pseudo-second-order	348.4	Not reported	Yao et al. (2014)
Polypyrrole/graphene oxide (PPy/GO)	Cr(VI)	T = 25 °C; C_{Ads} = 0.5 g/L; C_{Cr} = 100 mg/L; pH = 2	Langmuir	Pseudo-second-order	625	$\Delta G^0 = -7.29$ $\Delta H^0 = 78.42$ $\Delta S^0 = 0.28$	Setshedi et al. (2015)
Polypyrrole wrapped oxidized multiwalled carbon nanotubes (PPy/OMWCNTs)	Cr(VI)	T = 25 °C; C_{Ads} = 0.5 g/L; C_{Cr} = 200 mg/L; pH = 2	Langmuir	Pseudo-second-order	294	$\Delta G^0 = -0.24$ $\Delta H^0 = 13.24$ $\Delta S^0 = 0.04$	Bhaumik et al. (2016a, b)
Polypyrrole/2,5-diaminobenzene sulphonic acid (PPy/DABSA)	Cr(VI)	T = 25 °C; C_{Ads} = 1 g/L; C_{Cr} = 100 mg/L; pH = 2	Langmuir	Pseudo-second-order	303	$\Delta G^0 = -2.65$ $\Delta H^0 = 41.50$ $\Delta S^0 = 0.15$	Kera et al. (2016)

Polypyrrole-coated Fe_3O_4 (PPy/Fe_3O_4))	Cr(VI)	C_{Ads} = 0.8 g/L; 50.4% Fe_3O_4 loaded; C_{Cr} = 100 mg/L; pH = 2	Not reported	Not reported	119	Not reported	Muliwa et al. (2016)
Exfoliated polypyrrole/organically modified montmorillonite clay (PPy-OMMT)	Cr(VI)	T = 25 °C; C_{Ads} = 3 g/L; C_{Cr} = 250 mg/L; pH = 2	Langmuir	Pseudo-second-order	119.34	$\Delta G^0 = -0.59$ $\Delta H^0 = 64.55$ $\Delta S^0 = 0.22$	Setshedi et al. (2013)
Polypyrrole/graphene oxide/alpha cyclodextrin (PPy/GO/α-CD)	Cr(VI)	T = 25 °C; C_{Ads} = 0.5 g/L; C_{Cr} = 200 ppm; pH = 2	Langmuir	Pseudo-second-order	606	Not reported	Chauke et al. (2015)
Polypyrrole/maghemite (PPy/γ-Fe_2O_3)	Cr(VI)	T = 25 °C; C_{Ads} = 0.2 g/L; C_{Cr} = 100 mg/L; pH = 2	Langmuir	Pseudo-second-order	209	Not reported	Chávez-Guajardo et al. (2015)
Polyaniline/maghemite (PPy/γ-Fe_2O_3)	Cr(VI)	T = 25 °C; C_{Ads} = 0.2 g/L; C_{Cr} = 100 mg/L; pH = 2	Langmuir	Pseudo-second-order	196	Not reported	Chávez-Guajardo et al. (2015)
Polyaniline-coated ethyl celluloses (PANI/ECs)	Cr(VI)	Room temperature; C_{Ads} = 3 g/L; 20 wt % PANi loadings; C_{Cr} = 2 mg/L; pH = 1	Langmuir	Pseudo-second-order	38.76	Not reported	Qiu et al. (2014)
Polypyrrole/chitin	Cr(VI)	T = 30 °C; C_{Ads} = 2 g/L; C_{Cr} = 50 mg/L; pH = 4.8	Langmuir Freundlich	Pseudo-second-order	28.92	$\Delta G^0 = -8.30$ $\Delta H^0 = 15.51$ $\Delta S^0 = 0.02$	Karthik and Meenakshi (2014)
Polyaniline/humic acid (PANI/HA)	Cr(VI)	T = 25 °C; C_{Ads} = 0.5 g/L; C_{Cr} = 15 mg/L; pH = 5	Freundlich	Pseudo-second-order	150	Not reported	Li et al. (2011)
Phytic acid-doped polyaniline/cellulose acetate (PANI-PA/CA)	Cr(VI)	T = 30 °C; 3 cm × 3 cm membrane; C_{Cr} = 67.28 mg/L; pH = 2	Langmuir	Pseudo-second-order	94.34	Not reported	Li et al. (2014)

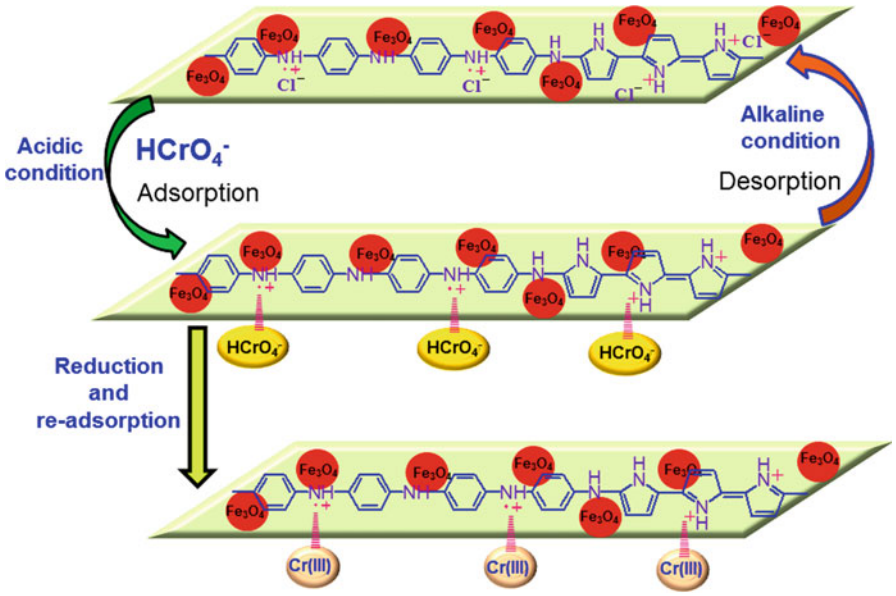

Scheme 5.1 Mechanism of Cr(VI) removal using Fe_3O_4-incorporated PPy-PANI adsorbent

polymer composite was reported as rapid and effective adsorbent even at relatively high concentration (500 mg/L) of toxic chromium. Further, the Cr(VI) removal process using H_2SO_4-doped poly-diaminopyridine/GO followed a reduction mechanism at lower acidic pH medium and an anion exchange between SO_4^{2-} ions of the dopant and $CrO_4^{2-}/Cr_2O_7^{-}$ species at higher pH. Conducting polymer-incorporated superparamagnetic iron oxide magnetite and maghemite nanoparticles, on the other hand, have equally been employed as efficient adsorbent for the removal of Cr(VI), essentially because of their unique characteristics that include high saturation magnetization, multiple active binding sites and large surface area. Also, the magnetic properties allow the removal of contaminant-adsorbed materials from the aqueous media with ease by simple application of a suitable magnetic field. Fe_3O_4-incorporated PPy-PANI nanoparticles, for example, exhibited improved adsorption efficiency towards Cr(VI) from 227 mg/g to 303 mg/g at 25 °C and pH 2 (Kera et al. 2017). The adsorption process was found to proceed via ion exchange $HCrO_4^-$ vs Cl^- and subsequent reduction of adsorbed Cr(VI) to less toxic Cr(III), as shown in Scheme 5.1. Remarkably, the treatment of Cr(VI)-loaded Fe_3O_4-incorporated PPy-PANI nanoparticles in alkaline medium regenerated the adsorbent for multiple uses. A step further, the magnetic nanocomposite could be easily isolated from the aqueous solution using an external magnet.

5.4.2 Removal of As(III)/As(V)

Arsenic a metalloid dispersed in the environment in several species is well known for its application in electronics, agriculture as well as wood preservation. Usually, surface and groundwater source contamination by arsenic and its compounds occurs in our environments from both natural and manmade factors. The main source of arsenical in groundwater, wherein arsenite As(III) and arsenate As(V) species are always co-existing, is frequently the natural deposits in sediments, rocks and soil (Saldaña-Robles et al. 2017). Moreover, the dissolution of arsenic-bearing iron wastes has also been recognized as a new source of arsenical in groundwater (Clancy et al. 2015). Alternatively, industrial effluent containing arsenical is of significant anthropogenic impact. A recent assessment by the World Health Organization revealed that approximately 200 million people globally are exposed to arsenic-contaminated water higher than the recommended maximum acceptable limit 10 μg/L (Zhang et al. 2018). Short-term human exposure to significant amount of arsenicals was found to lead to sterility and miscarriages in women (Lei et al. 2015). Cases of DNA as well as brain damages have also been reported in both men and women. Prolonged exposure to trace amount, on the other hand, can lead to lung, kidney, skin, liver and bladder cancers (Yin et al. 2017). Table 5.2 displays the reported studies for the removal of arsenic species by modified conducting polymer-based nanostructured materials. The highest maximum adsorption capacity [232.5 mg/g for As(III) and 227.3 mg/g for As(V)] at pH 7 was achieved through embedment of metallic iron of average diameter 6.4 nm onto the PANI nanofibre support (Bhaumik et al. 2015). Electrostatic interaction and complexation taking place at the surface of PANI/Fe^0 adsorbent between arsenic species and surface binding sites were identified as possible mechanisms involved during the removal process. In aqueous environment, nanosized Fe^0 particles react with H_2O and dissolved O_2 molecules to yield oxides/hydroxides of iron, and subsequently, arsenic cations adsorption occurs by substitution of OH^- surface bond and formation of arsenate complex. Similarly, nano-hydrous zirconium oxide-deposited polystyrene exhibited noteworthy As(V) uptake of 88.74 mg/g at pH value 7 through both electrostatic attraction with positively charge nitrogen of polystyrene matrix and hydroxyl ion exchange of hydrated zirconium oxides. Relative to incorporated organic entities, nanosized inorganic particles within conducting polymer nanostructure cast seem more efficient for arsenic remedial from contaminated water.

5.4.3 Removal of Hg(II)

Mercury (Hg) is well-documented as the most notorious metal pollutant in aquatic ecosystem (Walters et al. 2011). Coal and petrochemical oil combustion, release of wastewaters from mining, chlor-alkali as well as battery production are some of the anthropogenic notable sources of mercury pollution in waterway. Mercury occurs in the environment in various species: elemental (Hg^0), oxidized inorganic (Hg^{2+}, Hg_2^{2+})

Table 5.2 Modified conducting polymer materials for arsenic species As(III)/As(V) remediation from aqueous milieu

Adsorbent	Arsenic species	Operating conditions	Isotherm model	Adsorption kinetics	Adsorption capacity (mg/g)	Adsorption thermodynamics	References
Polyaniline/polyvinyl alcohol (PANI/PVA)	As(III)	$C_{Ads} = 2$ g/L; $C_{As} = 10$ mg/L; pH = 11	Langmuir	Pseudo-second-order	27.25	Not reported	Roghani et al. (2016)
Polyaniline/Fe^0 (PANI/Fe^0)	As(III)	$C_{Ads} = 0.1$ g/L; $C_{As} = 1$ mg/L; pH = 7	Langmuir	Pseudo-second-order	232.5 for As (III)	Not reported	Bhaumik et al. (2015)
	As(V)				227.3 for As (V)		
Polyaniline/polystyrene and hydroxypropyl cellulose (PANI/PS/HPC)	As(III)	T = 25 °C; $C_{Ads} = 10$ g/L; pH = 8	Langmuir Freundlich	Not reported	56 for As(III)	$\Delta G^0 = -4.08$	Davodi and Jahangiri (2014)
	As(V)				52 for As (V)	$\Delta H^0 = -32.11$	
						$\Delta S^0 = -0.09$	
Polystyrene/hydrous zirconium oxide (PS/HZO)	As(V)	$C_{Ads} = 0.2$ g/L $C_{As} = 20$ mg/L; pH = 7	Freundlich	Pseudo-first-order	88.74	Not reported	Pan et al. (2014)

and organic (alkylated mercury) (Syversen and Kaur 2012). At room temperature, gaseous Hg^0 can be deposited in far-off regions from pollution sources. Inorganic containing Hg^{2+} species have been established to be a severe contaminant owing to high solubility and stability. Hg^{2+} can easily undergo biological methylation by bacteria to generate highly toxic organometallic CH_3Hg derivative (Klapstein and O'Driscoll 2018). Aquatic animals such as fish and shellfish bioaccumulate high amount of this mercury form through feeding. Acute consumption of significant amounts of these Hg-contaminated animals could negatively impact on the human central nervous system and other key tissues (Jaishankar et al. 2014). Based on the best available science to prevent potential health-related problems, the World Health Organization and US Environmental Protection Agency have recommended 0.001 and 0.002 mg/L as the lethal doses for mercury in drinking water. Table 5.3 shows a survey for the removal of Hg (II) from aqueous solution using nanostructure-modified conducting polymer as adsorbent. Accordingly, the incorporation of reduced graphene oxide within the matrix of conducting polymers (PANI or PPy) was found to significantly increase their mercury adsorptive performances. PANI/rGO and PPy/rGO exhibited relatively the highest adsorption capacities. As compared to pristine PANI, the maximum Hg(II) uptake on PANI/rGO was improved from 515.46 mg/g to 1000.00 mg/g (Li et al. 2013). Likewise, Freundlich and Langmuir isotherm models revealed the maximum adsorption capacities of 400 and 980 mg/g for PPy and PPy/rGO nanocomposites, respectively (Chandra and Kim 2011). The increase in adsorption capacities was ascribed to large surface area of inserted rGO, leading to increased number of active adsorption sites. Similar interpretation also defined the high adsorption capacity of PANI/attapulgite for the removal of Hg (II). Attapulgite is a crystal-like hydrated magnesium aluminium phyllosilicate mineral with a fibrous morphology and large surface area.

5.4.4 Effect of Adsorbent Morphology on Their Performance

The adsorption efficiency of an adsorbent appears to vary with the morphology, and this can be controlled during the preparation procedure. For example, interconnected-chain PANI NFs, obtained through fast mixing oxidative polymerization of ANI with $FeCl_3$ at room temperature, exhibited a maximum Cr (VI) removal capacity of 345 mg/g at pH 2.0 (Bhaumik et al. 2014a, b). However, previous investigation on Cr(VI) uptake from wastewater using short-chain PANI revealed a maximum adsorption capacity of 63 mg/g at pH 3.0 (Kumar et al. 2008). This short-chain PANI adsorbent was prepared via chemical oxidative polymerization of ANI with ammonium persulphate (APS) in the presence of chain terminator 1,4-phenylenediamine at 5 °C. Recently, Wang and co-workers also reported the synthesis of nanostructured PANI with different morphologies, based on the change in the protonic acids during sono-assisted preparation process (Wang et al. 2014a, b). Four protonic acids, namely, HCl, sulphamic acid (SA), citric acid (CA) and 2-aminoethanesulphonic acid (TA) were used. The use of strong acid HCl yielded

Table 5.3 Modified conducting polymer materials for the removal of mercury species Hg(II)

Adsorbent	Mercury species	Operating conditions	Isotherm model	Adsorption kinetics	Adsorption capacity (mg/g)	Adsorption thermodynamics (KJ/mol)	References
Polyaniline	Hg(II)	$C_{Ads} = 0.2$ g/L; $C_{Hg} = 43$ mg/L; pH = 5.5	Not reported	Not reported	600	Not reported	Wang et al. (2009)
Polypyrrole/cellulose	Hg(II)	$C_{Ads} = 10$ g/L; $C_{Hg} = 250$ ppm; pH = 6	Langmuir Freundlich	Pseudo-second-order	31.69	Not reported	Hanif et al. (2016)
Polypyrrole/mesoporous silica (PPy/SBA-15)	Hg(II)	T = 25 °C; $C_{Ads} = 1$ g/L; $C_{Hg} = 40$ mg/L; pH = 8	Langmuir	Pseudo-second-order	200	$\Delta G^0 = -3.93$ $\Delta H^0 = 19.82$ $\Delta S^0 = 0.08$	Shafiabadi et al. (2016)
Polypyrrole/thiol-functionalized zeolite Beta/mesoporous silica (PPy/SH-Beta/MCM-41)	Hg(II)	T = 25 °C; $C_{Ads} = 2.2$ g/L; $C_{Hg} = 400$ mg/L; pH = 8	Freundlich	Pseudo-second-order	157.43	$\Delta G^0 = -4.62$ $\Delta H^0 = 22.73$ $\Delta S^0 = 0.09$	Javadian and Taghavi (2014)
Polyaniline/attapulgite (PANI/ATP)	Hg(II)	T = 25 °C; $C_{Ads} = 0.25$ g/L; $C_{Hg} = 50$ mg/L; pH = 6	Langmuir	Pseudo-second-order	800	Not reported	Cui et al. (2012)
Polypyrrole/reduced graphene oxide(PPy/rGO)	Hg(II)	T = 20 °C; 15 wt % GO loadings; $C_{Ads} = 0.2$ g/L; $C_{Hg} = 50$ ppm; pH = 3	Langmuir Freundlich	Pseudo-second-order	980	Not reported	Chandra and Kim (2011)
Polyaniline and reduced graphene oxide (PANI/rGO)	Hg(II)	T = 32 °C; $C_{Ads} = 0.2$ g/L; $C_{Hg} = 165.88$ mg/L; pH = 4	Langmuir Freundlich	Pseudo-second-order	1000	Not reported	Li et al. (2013)
Polyaniline/graphene oxide (PANI/GO)	Hg(II)	T = 25 °C $C_{Ads} = 0.1$ g/L; $C_{Hg} = 10$ mg/L; pH = 5	Langmuir	Pseudo-second-order	80.7	Not reported	Fan et al. (2015)
Polyaniline/humic acid (PANI/HA)	Hg(II)	T = 25 °C; $C_{Ads} = 0.5$ g/L; $C_{Hg} = 50$ mg/L; pH = 5	Langmuir	Pseudo-second-order	671	Not reported	Zhang et al. (2010)
Phytic acid-doped polyaniline/cellulose acetate (PANI-PA/CA)	Hg(II)	T = 30 °C; 3 cm × 3 cm membrane; $C_{Hg} = 223.33$ mg/L; pH = 5	Langmuir	Pseudo-second-order	280.11	Not reported	Li et al. (2014)

aggregated particles. Polymerization in SA, on the other hand, generated nanoparticles with approximately 100 nm diameters. Weak organic acid CA afforded straight and smooth-like nanoparticles with average diameters and length of 150–250 nm and 2.5 μm, respectively. Flexible and relatively smaller nanoparticles of 80–100 nm in diameter were obtained with polymerization in TA. With regard to their performance in Cr(VI) adsorption process, PANI-HCl presented the highest maximum adsorption capacity of 182 mg/g at pH 4.0 and 25 °C, as compared to PANI-SA (164 mg/g), PANI-CA (145 mg/g) and PANI-TA (111 mg/g). Moreover, aggregated spherical-like PPy/Fe_3O_4 nanocomposite, fabricated by in situ chemical oxidative polymerization of Py in the presence of Fe_3O_4 NPs in deionized water at ambient temperature, showed a maximum adsorption capacity of 169.5 mg/g towards Cr(VI) at pH 2 (Bhaumik et al. 2011). A year later, the corresponding orange-like microspheres were reported to uncover higher maximum adsorption capacity of 209.2 mg/g under similar condition (Wang et al. 2012). The identical Fe_3O_4/PPy composite microspheres were obtained via in situ oxidative polymerization of Py in the presence of Fe_3O_4 microspheres in deionized water/alcohol/HCl mixtures under sonication.

5.5 Conclusion

Herein, we present the recent studies performed on synthesized conducting polymer containing nanostructured materials for the removal of selected highly toxic Cr(VI), As(III), As(V) and Hg(II) from aqueous medium using adsorption technology. PANI and PPy matrixes were the most explored supports for high adsorption owing to their ion-exchange ability under specific conditions at nitrogen atoms, which serve as active binding sites. Incorporation of nanosized inorganic particles with high surface area as well as large number of active sites was found to lead to materials with outstanding adsorption capacities. Generally, kinetics study revealed that the adsorption process of Cr(VI), As(III), As(V) and Hg(II) onto the surface-modified conducting polymer nanostructured materials followed the Ho and McKay pseudo-second-order rate model and the removal efficiency could be best described using Freundlich and Langmuir isotherms. Ion exchange, electrostatic attraction and surface complexation were reported as the most plausible mechanisms in that regard. Moreover, the process was strongly dependent on the key factors such as temperature, adsorbent dosage, initial concentration of metal ion pollutant and solution pH. Efficient uptake of As(III)/As(V) was achieved at alkaline pH, while Cr (VI) and Hg(II) removal was mostly favourable under acidic conditions. The data compiled in the current review can serve as valuable template for the design and fabrication of potential and effective adsorbent for heavy metal ion-contaminated water treatment systems. Next, advanced investigation on the reusability of heavy metal-adsorbed waste materials in catalysis, medicine or gas sensing remains an area that needs special attention so as to limit the risk of secondary pollution.

References

Adeleye AS, Conway JR, Garner K, Huang Y, Su Y, Keller AA (2016) Engineered nanomaterials for water treatment and remediation: costs, benefits, and applicability. Chem Eng J 286:640–662. https://doi.org/10.1016/j.cej.2015.10.105

Afkhami A, Moosavi R (2010) Adsorptive removal of Congo red, a carcinogenic textile dye, from aqueous solutions by maghemite nanoparticles. J Hazard Mater 174:398–403. https://doi.org/10.1016/j.jhazmat.2009.09.066

Ahmed MJ, Ahmaruzzaman M (2016) A review on potential usage of industrial waste materials for binding heavy metal ions from aqueous solutions. J Water Process Eng 10:39–47. https://doi.org/10.1016/j.jwpe.2016.01.014

Aigbe UO, Das R, Ho WH, Srinivasu V, Maity A (2018) A novel method for removal of Cr (VI) using polypyrrole magnetic nanocomposite in the presence of unsteady magnetic fields. Sep Purif Technol 194:377–387. https://doi.org/10.1016/j.seppur.2017.11.057

Akpalu W, Normanyo AK (2017) Gold mining pollution and the cost of private healthcare: the case of Ghana. Ecol Econ 142:104–112. https://doi.org/10.1016/j.ecolecon.2017.06.025

Ali RM, Hamad HA, Hussein MM, Malash GF (2016) Potential of using green adsorbent of heavy metal removal from aqueous solutions: adsorption kinetics, isotherm, thermodynamic, mechanism and economic analysis. Ecol Eng 91:317–332. https://doi.org/10.1016/j.ecoleng.2016.03.015

Ansari MO, Kumar R, Ansari SA, Ansari SP, Barakat MA, Alshahrie A, Cho MH (2017) Anion selective pTSA doped polyaniline@ graphene oxide-multiwalled carbon nanotube composite for Cr (VI) and Congo red adsorption. J Colloid Interface Sci 496:407–415. https://doi.org/10.1016/j.jcis.2017.02.034

Asiabi H, Yamini Y, Shamsayei M (2017) Highly selective and efficient removal of arsenic(V), chromium(VI)and selenium(VI) oxyanions by layered double hydroxide intercalated with zwitterionic glycine. J Hazard Mater 339:239–247. https://doi.org/10.1016/j.jhazmat.2017.06.042

Attallah OA, Al-Ghobashy MA, Nebsen M, Salem MY (2016) Removal of cationic and anionic dyes from aqueous solution with magnetite/pectin and magnetite/silica/pectin hybrid nanocomposites: kinetic, isotherm and mechanism analysis. RSC Adv 6:11461–11480. https://doi.org/10.1039/c5ra23452b

Baig U, Rao RA, Khan AA, Sanagi MM, Gondal MA (2015) Removal of carcinogenic hexavalent chromium from aqueous solutions using newly synthesized and characterized polypyrrole–titanium (IV) phosphate nanocomposite. Chem Eng J 280:494–504. https://doi.org/10.1016/j.cej.2015.06.031

Balint R, Cassidy NJ, Cartmell SH (2014) Conductive polymers: towards a smart biomaterial for tissue engineering. Acta Biomater 10:2341–2353. https://doi.org/10.1016/j.actbio.2014.02.015

Ballav N, Maity A, Mishra SB (2012) High efficient removal of chromium(VI) using glycine doped polypyrrole adsorbent from aqueous solution. Chem Eng J 198–199:536–546. https://doi.org/10.1016/j.cej.2012.05.110

Ballav N, Choi HJ, Mishra SB, Maity A (2014) Polypyrrole-coated halloysite nanotube clay nanocomposite: synthesis, characterization and Cr(VI) adsorption behaviour. Appl Clay Sci 102:60–70. https://doi.org/10.1016/j.clay.2014.10.008

Ballav N, Das R, Giri S, Muliwa AM, Pillay K, Maity A (2018) L-cysteine doped polypyrrole (PPy@L-Cyst): a super adsorbent for the rapid removal of Hg^{+2} and efficient catalytic activity of the spent adsorbent for reuse. Chem Eng J 345:621–630. https://doi.org/10.1016/j.cej.2018.01.093

Bhaumik M, Maity A, Srinivasu VV, Onyango MS (2011) Enhanced removal of Cr(VI) from aqueous solution using polypyrrole/Fe_3O_4 magnetic nanocomposite. J Hazard Mater 190:381–390. https://doi.org/10.1016/j.jhazmat.2011.03.062

Bhaumik M, Setshedi K, Maity A, Onyango MS (2013) Chromium(VI) removal from water using fixed bed column of polypyrrole/Fe_3O_4 nanocomposite. Sep Purif Technol 110:11–19. https://doi.org/10.1016/j.seppur.2013.02.037

Bhaumik M, Choi HJ, McCrindle RI, Maity A (2014a) Composite nanofibers prepared from metallic iron nanoparticles and polyaniline: high performance for water treatment applications. J Colloid Interface Sci 425:75–82. https://doi.org/10.1016/j.jcis.2014.03.031

Bhaumik M, Choi HJ, Seopela MP, McCrindle RI, Maity A (2014b) Highly effective removal of toxic Cr(VI) from wastewater using sulfuric acid-modified avocado seed. Ind Eng Chem Res 53:1214–1224. https://doi.org/10.1021/ie402627d

Bhaumik M, Noubactep C, Gupta VK, McCrindle RI, Maity A (2015) Polyaniline/Fe^0 composite nanofibers: an excellent adsorbent for the removal of arsenic from aqueous solutions. Chem Eng J 271:135–146. https://doi.org/10.1016/j.cej.2015.02.079

Bhaumik M, Agarwal S, Gupta VK, Maity A (2016a) Enhanced removal of Cr (VI) from aqueous solutions using polypyrrole wrapped oxidized MWCNTs nanocomposites adsorbent. J Colloid Interface Sci 470:257–267. https://doi.org/10.1016/j.jcis.2016.02.054

Bhaumik M, McCrindle RI, Maity A, Agarwal S, Gupta VK (2016b) Polyaniline nanofibers as highly effective re-usable adsorbent for removal of reactive black 5 from aqueous solutions. J Colloid Interface Sci 466:442–451. https://doi.org/10.1016/j.jcis.2015.12.056

Bohart GS, Adams EQ (1920) Some aspects of the behaviour of charcoal with respect to chlorine. J Am Chem Soc 42:523–544. https://doi.org/10.1021/ja01448a018

Burakov AE, Galunin EV, Burakova IV, Kucherova AE, Agarwal S, Tkachev AG, Gupta VK (2018) Adsorption of heavy metals on conventional and nanostructured materials for wastewater treatment purposes: a review. Ecotoxicol Environ Saf 148:702–712. https://doi.org/10.1016/j.ecoenv.2017.11.034

Cao CY, Qu J, Yan WS, Zhu JF, Wu ZY, Song WG (2012) Low-cost synthesis of flowerlike α-Fe_2O_3 nanostructures for heavy metal ion removal: adsorption property and mechanism. Langmuir 28:4573–4579. https://doi.org/10.1021/la300097y

Chandra V, Kim KS (2011) Highly selective adsorption of Hg^{2+} by a polypyrrole–reduced graphene oxide composite. Chem Comm 47(13):3942–3944. https://doi.org/10.1039/c1cc00005e

Chauke VP, Maity A, Chetty A (2015) High-performance towards removal of toxic hexavalent chromium from aqueous solution using graphene oxide-alpha cyclodextrin-polypyrrole nanocomposites. J Mol Liq 211:71–77. https://doi.org/10.1016/j.molliq.2015.06.044

Chávez-Guajardo AE, Medina-Llamas JC, Maqueira L, Andrade CAS, Alves KGB, de Melo CP (2015) Efficient removal of Cr (VI) and Cu (II) ions from aqueous media by use of polypyrrole/maghemite and polyaniline/maghemite magnetic nanocomposites. Chem Eng J 281:826–836. https://doi.org/10.1016/j.cej.2015.07.008

Chen G, Jiang M (2011) Cyclodextrin-based inclusion complexation bridging supramolecular chemistry and macromolecular self-assembly. Chem Soc Rev 40:2254–2266. https://doi.org/10.1039/C0CS00153H

Chen JP, Lin M (2001) Surface charge and metal ion adsorption on an H-type activated carbon: experimental observation and modeling simulation by the surface complex formation approach. Carbon 39:1491–1504. https://doi.org/10.1016/S0008-6223(00)00277-3

Chen C, Yue Q, Gao B, Li Q, Xu X, Fu K (2012) Adsorption of hexavalent chromium from aqueous solution by modified cornstalk: a fixed-bed column study. Bioresour Technol 113:114–120. https://doi.org/10.1016/j.biortech.2011.11.110

Chen M, Qin L, Liu Y, Zhang F (2018) Controllable preparation of polymer brushes from mesoporous silica SBA-15 via surface-initiated ARGET ATRP. Microporous Mesoporous Mater 263:158–164. https://doi.org/10.1016/j.micromeso.2017.12.019

Clancy TM, Snyder KV, Reddy R, Lanzirotti A, Amrose SE, Raskin L, Hayes KF (2015) Evaluating the cement stabilization of arsenic-bearing iron wastesfrom drinking water treatment. J Hazard Mater 300:522–529. https://doi.org/10.1016/j.jhazmat.2015.07.051

Cui H, Qian Y, Li Q, Zhang Q, Zhai J (2012) Adsorption of aqueous Hg (II) by a polyaniline/attapulgite composite. Chem Eng J 211:216–223. https://doi.org/10.1016/j.cej.2012.09.057

Dai T, Lu Y (2007) Water-soluble methyl orange fibrils as versatile templates for the fabrication of conducting polymer microtubules. Macromol Rapid Commun 28(5):629–633. https://doi.org/10.1002/marc.200600697

Das R, Bhaumik M, Giri S, Maity A (2017a) Sonocatalytic rapid degradation of Congo red dye from aqueous solution using magnetic Fe^0/polyaniline nanofibers. Ultrason Sonochem 37:600–613. https://doi.org/10.1016/j.ultsonch.2017.02.022

Das R, Giri S, Abia ALK, Dhonge B, Maity A (2017b) Removal of noble metal ions (Ag+) by mercapto group-containing polypyrrole matrix and reusability of its waste material in environmental applications. ACS Sustain Chem Eng 5(3):2711–2724. https://doi.org/10.1021/acssuschemeng.6b03008

Das R, Giri S, Muliwa AM, Maity A (2017c) High-performance Hg(II) removal using thiol-functionalized polypyrrole (PPy/MAA) composite and effective catalytic activity of Hg(II)-adsorbed waste material. ACS Sustain Chem Eng 5(9):7524–7536. https://doi.org/10.1021/acssuschemeng.7b00477

Davodi B, Jahangiri M (2014) Determination of optimum conditions for removal of As (III) and As (V) by polyaniline/polystyrene nanocomposite. Synth Met 194:97–101. https://doi.org/10.1016/j.synthmet.2014.04.020

Deng J, Guo J, Liu P (2017) Growth of polyaniline nanomaterials in rapid-mixing polymerization. Colloids Surf A Physicochem Eng Asp 521:247–250. https://doi.org/10.1016/j.colsurfa.2016.09.016

Dinda D, Saha SK (2015) Sulfuric acid doped poly diaminopyridine/graphene composite to remove high concentration of toxic Cr (VI). J Hazard Mater 291:93–101. https://doi.org/10.1016/j.jhazmat.2015.02.065

Dong Z, Ye T, Zhao Y, Yu J, Wang F, Zhang L, Wang X, Guo S (2011) Perovskite $BaZrO_3$ hollow micro- and nanospheres: controllable fabrication, photoluminescence and adsorption of reactive dyes. J Mater Chem 21:5978–5984. https://doi.org/10.1039/C0JM04534A

Dutt S, Siril PF (2014) A novel approach for the synthesis of polyaniline nanostructures using swollen liquid crystal templates. Mater Lett 124:50–53. https://doi.org/10.1016/j.matlet.2014.03.068

Esman N, Lellouche JP (2010) Fabrication of functional polypyrrole (PolyPyr)-nanotubes using anodized aluminium oxide (AAO) template membranes. Compromising between effectiveness and mildness of template dissolution conditions for a safe release of PolyPyr-nanotubes. Polymer Chem 1(2):158–160. https://doi.org/10.1039/b9py00206e/

Eyrikh S, Eichler A, Tobler L, Malygina N, Papina T, Schwikowski M (2017) A 320 year ice-core record of atmospheric Hg pollution in the Altai, Central Asia. Environ Sci Technol 51:11597–11606. https://doi.org/10.1021/acs.est.7b03140

Fan Q, Yang Y, Hao Y, Zhao X, Feng Y (2015) Preparation of three-dimensional PANI/GO for the separation of Hg (II) from aqueous solution. J Mol Liq 212:557–562. https://doi.org/10.1016/j.molliq.2015.10.008

Fang W, Jiang X, Luo H, Geng J (2018) Synthesis of graphene/SiO2@polypyrrole nanocomposites and their application for Cr(VI) removal in aqueous solution. Chemosphere 197:594–602. https://doi.org/10.1016/j.chemosphere.2017.12.163

Freundlich HMF (1906) Uber Die Adsorption in Losungen. Z Phys Chem 57:385–470

Ghaedi M, Ansari A, Habibi MH, Asghari AR (2014) Removal of malachite green from aqueous solution by zinc oxide nanoparticle loaded on activated carbon: kinetics and isotherm study. J Ind Eng Chem 20:17–28. https://doi.org/10.1016/j.jiec.2013.04.031

Ghaemi N, Daraei P (2016) Enhancement in copper ion removal by PPy@Al_2O_3 polymeric nanocomposite membrane. J Ind Eng Chem 40:26–33. https://doi.org/10.1016/j.jiec.2016.05.027

Ghorai S, Sarkar A, Raoufi M, Panda AB, Schönherr H, Pal S (2014) Enhanced removal of methylene blue and methyl violet dyes from aqueous solution using a nanocomposite of hydrolyzedpolyacrylamide grafted xanthan gum and incorporated nanosilica. ACS Appl Mater Interfaces 6(7):4766–4777. https://doi.org/10.1021/am4055657

Ghosh S, Maiyalagan T, Basu RN (2016) Nanostructured conducting polymers for energy applications: towards a sustainable platform. Nanoscale 8(13):6921–6947. https://doi.org/10.1039/c5nr08803h

Gong J, Liu T, Wang X, Hu X, Zhang L (2011) Efficient removal of heavy metal ions from aqueous systems with the assembly of anisotropic layered double hydroxide nanocrystals@carbonnanosphere. Environ Sci Technol 45:6181–6187. https://doi.org/10.1021/es200668q

Gu ZJ, Ye JR, Song W, Shen Q (2014) Synthesis of polyaniline nanotubes with controlled rectangular or square pore shape. Mater Lett 121:12–14. https://doi.org/10.1016/j.matlet.2014.01.133

Hackett AJ, Malmström J, Travas-Sejdic J (2017) Functionalization of conducting polymers for biointerface applications. Prog Polym Sci 70:18–33. https://doi.org/10.1016/j.progpolymsci.2017.03.004

Hall KR, Eagleton LC, Acrivos A, Vermeulen T (1966) Pore and solid-diffusion kinetics in fixed-bed adsorption under constant-pattern conditions. Ind Eng Chem Fundam 5:212–223. https://doi.org/10.1021/i160018a011

Hanif Z, Lee S, Qasim GH, Ardiningsih I, Kim JA, Seon J, Han S, Hong S, Yoon MH (2016) Polypyrrole multilayer-laminated cellulose for large-scale repeatable mercury ion removal. J Mater Chem A 4(32):12425–12433. https://doi.org/10.1039/c6ta01219a

Harijan DK, Chandra V (2016) Polyaniline functionalized graphene sheets for treatment of toxic hexavalent chromium. J Environ Chem Eng 4(3):3006–3012. https://doi.org/10.1016/j.jece.2016.06.014

He S, Zhang F, Cheng S, Wang W (2016) Synthesis of sodium acrylate and acrylamide copolymer/GO hydrogels and their effective adsorption for Pb^{2+} and Cd^{2+}. ACS Sustain Chem Eng 4:3948–3959. https://doi.org/10.1021/acssuschemeng.6b00796

Ho YS (2006) Second order kinetic model for the sorption of cadmium onto tree fern: a comparison of linear and nonlinear methods. Water Res 40:119–125. https://doi.org/10.1016/j.watres.2005.10.040

Ho YS, McKay G (1999) Pseudo second order model for sorption processes. Process Biochem 34:451–465. https://doi.org/10.1016/S0032-9592(98)00112-5

Holmes AL, Wise SS, Sandwick SJ, Wise JP (2006) The clastogenic effects of chronic exposure to particulate and soluble Cr(VI) in human lung cells. Mutat Res/Genet Toxicol Environ Mutagen 610(1–2):8–13

Hua Y, Clark S, Ren J, Sreejayan N (2012) Molecular mechanisms of chromium in alleviating insulin resistance. J Nutr Biochem 23(4):313–319. https://doi.org/10.1016/j.jnutbio.2011.11.001

Huang J, Kaner RB (2004) Nanofiber formation in the chemical polymerization of aniline: a mechanistic study. Angew Chem Int Ed 43:5817–5821. https://doi.org/10.1002/anie.200460616

Huang Y, Chen Q, Deng M, Japenga J, Li T, Yang X, He Z (2018) Heavy metal pollution and health risk assessment of agricultural soils in a typical peri-urban area in southeast China. J Environ Manag 207:159–168. https://doi.org/10.1016/j.jenvman.2017.10.072

Jaishankar M, Tseten T, Anbalagan N, Mathew BB, Beeregowda KN (2014) Toxicity, mechanism and health effects of some heavy metals. Interdiscip Toxicol 7(2):60–72. https://doi.org/10.2478/intox-2014-0009

Javadian H, Taghavi M (2014) Application of novel Polypyrrole/thiol-functionalized zeolite Beta/MCM-41 type mesoporous silica nanocomposite for adsorption of Hg2+ from aqueous solution and industrial wastewater: kinetic, isotherm and thermodynamic studies. Appl Surf Sci 289:487–494. https://doi.org/10.1016/j.apsusc.2013.11.020

Jia YF, Xiao B, Thomas KM (2002) Adsorption of metal ions on nitrogen surface functional groups in activated carbons. Langmuir 18(2):470–478. https://doi.org/10.1021/la011161z

Karthik R, Meenakshi S (2014) Synthesis, characterization and Cr (VI) uptake studies of polypyrrole functionalized chitin. Synth Met 198:181–187. https://doi.org/10.1016/j.synthmet.2014.10.012

Kera NH, Bhaumik M, Ballav N, Pillay K, Ray SS, Maity A (2016) Selective removal of Cr (VI) from aqueous solution by polypyrrole/2,5-diaminobenzene sulfonic acid composite. J Colloid Interface Sci 476:144–157. https://doi.org/10.1016/j.jcis.2016.05.011

Kera NH, Bhaumik M, Pillay K, Ray SS, Maity A (2017) Selective removal of toxic Cr (VI) from aqueous solution by adsorption combined with reduction at a magnetic nanocomposite surface. J Colloid Interface Sci 503:214–228. https://doi.org/10.1016/j.jcis.2017.05.018

Kim Y, Lee YJ (2014) Characterization of mercury sorption on hydroxylapatite: batch studies and microscopic evidence for adsorption. J Colloid Interface Sci 430:193–199. https://doi.org/10.1016/j.jcis.2014.05.028

Klapstein SJ, O'Driscoll NJ (2018) Methylmercury biogeochemistry in freshwater ecosystems: a review focusing on DOM and photodemethylation. Bull Environ Contam Toxicol 100 (1):14–25. https://doi.org/10.1007/s00128-017-2236-x

Kumar PA, Chakraborty S, Ray M (2008) Removal and recovery of chromium from wastewater using short chain polyaniline synthesized on jute fiber. Chem Eng J 141:130–140. https://doi.org/10.1016/j.cej.2007.11.004

Kumar KY, Muralidhara HB, Nayaka YA, Balasubramanyam J, Hanumanthappa H (2013) Low-cost synthesis of metal oxide nanoparticles and their application in adsorption of commercial dye and heavy metal ion in aqueous solution. Powder Technol 246:125–136. https://doi.org/10.1016/j.powtec.2013.05.017

Langmuir I (1918) The adsorption of gases on plane surfaces of glass, mica and platinum. J Am Chem Soc 40:1361–1403. https://doi.org/10.1021/ja02242a004

Legergren S (1898) About the theory of so-called adsorption of soluble substances. K Sven Vetenskapsakad Handl 24:1–39

Lei H, Wei H, Ho H, Liao K, Chien L (2015) Relationship between risk factors for infertility in women and lead, cadmium, and arsenic blood levels: a cross-sectional study from Taiwan. BMC Public Health 15:1220. https://doi.org/10.1186/s12889-015-2564-x

Li N, Bai R, Liu C (2005) Enhanced and selective adsorption of mercury ions on chitosan beads grafted with polyacrylamide via surface-initiated atom transfer radical polymerization. Langmuir 21:11780–11787. https://doi.org/10.1021/la051551b

Li Q, Sun L, Zhang Y, Qian Y, Zhai J (2011) Characteristics of equilibrium, kinetics studies for adsorption of Hg (II) and Cr (VI) by polyaniline/humic acid composite. Desalination 266 (1–3):188–194. https://doi.org/10.1016/j.desal.2010.08.025

Li R, Liu L, Yang F (2013) Preparation of polyaniline/reduced graphene oxide nanocomposite and its application in adsorption of aqueous Hg (II). Chem Eng J 229:460–468. https://doi.org/10.1016/j.cej.2013.05.089

Li R, Liu L, Yang F (2014) Removal of aqueous Hg (II) and Cr (VI) using phytic acid doped polyaniline/cellulose acetate composite membrane. J Hazard Mater 280:20–30. https://doi.org/10.1016/j.jhazmat.2014.07.052

Li X, Forouzandeh F, Fürstenhaupt T, Banham D, Feng F, Ye S, Kwok DY, Birss V (2018) New insights into the surface properties of hard-templated ordered mesoporous carbons. Carbon 127:707–717. https://doi.org/10.1016/j.carbon.2017.11.049

Liu Q, Zhong LB, Zhao QB, Frear C, Zheng YM (2015) Synthesis of Fe_3O_4/polyacrylonitrile composite electrospun nanofiber mat for effective adsorption of tetracycline. ACS Appl Mater Interfaces 7:14573–14583. https://doi.org/10.1021/acsami.5b04598

Malkoc E, Nuhoglu Y (2006) Fixed bed studies for the sorption of chromium(VI) onto tea factory waste. Chem Eng Sci 61:4363–4372. https://doi.org/10.1016/j.ces.2006.02.005

Meena RAA, Sathishkumar P, Ameen F, Yusoff ARM, Gu FL (2018) Heavy metal pollution in immobile and mobile components of lentic ecosystems-a review. Environ Sci Pollut Res 25 (5):4134–4148. https://doi.org/10.1007/s11356-017-0966-2

Meng A, Xing J, Li Z, Li Q (2015) Cr-doped ZnO nanoparticles: synthesis, characterization, adsorption property, and recyclability. ACS Appl Mater Interfaces 7:27449–27457. https://doi.org/10.1021/acsami.5b09366

Moutsatsou P, Coopman K, Smith MB, Georgiadou S (2015) Conductive PANI fibers and determining factors for the electrospinning window. Polymer 77:143–151. https://doi.org/10.1016/j.polymer.2015.08.039

Muliwa AM, Leswifi TY, Onyango MS, Maity A (2016) Magnetic adsorption separation (MAS) process: an alternative method of extracting Cr (VI) from aqueous solution using polypyrrole coated Fe_3O_4 nanocomposites. Sep Sci Technol 158:250–258. https://doi.org/10.1016/j.seppur.2015.12.021

Ng LY, Mohammad AW, Leo CP, Hilal N (2013) Polymeric membranes incorporated with metal/metal oxide nanoparticles: a comprehensive review. Desalination 308:15–33. https://doi.org/10.1016/j.desal.2010.11.033

Nguyen DN, Yoon H (2016) Recent advances in nanostructured conducting polymers: from synthesis to practical applications. Polymers 8(4):118. https://doi.org/10.3390/polym8040118

Nguyen TA, Ngo HH, Guo WS, Zhang J, Liang S, Yue QY, Li Q, Nguyen TV (2013) Applicability of agricultural waste and by-products for adsorptive removal of heavy metals from wastewater. Bioresour Technol 148:574–585. https://doi.org/10.1016/j.biortech.2013.08.124

Onyango MS, Leswifi TYL, Ochieng A, Kucher D, Otieno FO, Matsuda H (2009) Breakthrough analysis for water defluoridation using surface-tailored zeolite in a fixed bed column. Ind Eng Chem Res 48:931–937. https://doi.org/10.1021/ie0715963

Oveisi F, Nikazar M, Razzaghi MH, Mirrahimi MA, Jafarzadeh MT (2017) Effective removal of mercury from aqueous solution using thiol-functionalized magnetic nanoparticles. Environ Nanotechnol Monit Manage 7:130–138. https://doi.org/10.1016/j.enmm.2017.01.004

Pan B, Li Z, Zhang Y, Xu J, Chen L, Dong H, Zhang W (2014) Acid and organic resistant nano-hydrated zirconium oxide (HZO)/polystyrene hybrid adsorbent for arsenic removal from water. Chem Eng J 248:290–296. https://doi.org/10.1016/j.cej.2014.02.093

Paşka OM, Păcurariu C, Muntean SG (2014) Kinetic and thermodynamic studies on methylene blue biosorption using corn-husk. RSC Adv 4:62621–62630. https://doi.org/10.1039/C4RA10504D

Patra AS, Ghorai S, Sarkar D, Das R, Sarkar S, Pal S (2017) Anionically functionalized guar gum embedded with silica nanoparticles: an efficient nanocomposite adsorbent for rapid adsorptive removal of toxic cationic dyes and metal ions. Bioresour Technol 225:367–376. https://doi.org/10.1016/j.biortech.2016.11.093

Patra DK, Pradhan C, Patra HK (2018) An in situ study of growth of Lemongrass *Cymbopogon flexuosus* (Nees ex Steud.) W.Watson on varying concentration of chromium (Cr^{+6}) on soil and its bioaccumulation: perspectives on phytoremediation potential and phytostabilisation of chromium toxicity. Chemosphere 193:793–799. https://doi.org/10.1016/j.chemosphere.2017.11.062

Peng W, Li H, Liu Y, Song S (2017) A review on heavy metal ions adsorption from water by graphene oxide and its composites. J Mol Liq 230:496–504. https://doi.org/10.1016/j.molliq.2017.01.064

Qiu B, Xu C, Sun D, Yi H, Guo J, Zhang X, Qu H, Guerrero M, Wang X, Noel N, Luo Z (2014) Polyaniline coated ethyl cellulose with improved hexavalent chromium removal. ACS Sustain Chem Eng 2(8):2070–2080. https://doi.org/10.1021/sc5003209

Reed BE, Matsumoto MR (1993) Modeling cadmium adsorption by activated carbon using the Langmuir and Freundlich isotherm expressions. Sep Sci Technol 28(13–14):2179–2195. https://doi.org/10.1080/01496399308016742

Reeve PJ, Fallowfield HJ (2018) Natural and surfactant modified zeolites: a review of their applications for water remediation with a focus on surfactant desorption and toxicity towards microorganisms. J Environ Manag 205:253–261. https://doi.org/10.1016/j.jenvman.2017.09.077

Roghani M, Nakhli SA, Aghajani M, Rostami MH, Borghei SM (2016) Adsorption and oxidation study on arsenite removal from aqueous solutions by polyaniline/polyvinyl alcohol composite. J Water Process Eng 14:101–107. https://doi.org/10.1016/j.jwpe.2016.10.012

Salam MA, Gabal MA, Obaid AY (2012) Preparation and characterization of magnetic multi-walled carbon nanotubes/ferrite nanocomposite and its application for the removal of aniline from aqueous solution. Synth Met 161:2651–2658. https://doi.org/10.1016/j.synthmet.2011.09.038

Saldaña-Robles A, Saldaña-Robles N, Saldaña-Robles AL, Damian-Ascencio C, Rangel-Hernández VH, Guerra-Sanchez R (2017) Arsenic removal from aqueous solutions and the

impact of humic and fulvic acids. J Clean Prod 159:425–431. https://doi.org/10.1016/j.jclepro.2017.05.074

Santhosh C, Velmurugan V, Jacob G, Jeong SK, Grace AN, Bhatnagar A (2016) Role of nanomaterials in water treatment applications: a review. Chem Eng J 306:1116–1137. https://doi.org/10.1016/j.cej.2016.08.053

Setshedi KZ, Bhaumik M, Songwane S, Onyango MS, Maity A (2013) Exfoliated polypyrrole-organically modified montmorillonite clay nanocomposite as apotential adsorbent for Cr (VI) removal. Chem Eng J 222:186–197. https://doi.org/10.1016/j.cej.2013.02.061

Setshedi KZ, Bhaumik M, Onyango MS, Maity A (2014) Breakthrough studies for Cr(VI) sorption from aqueous solution using exfoliated polypyrrole-organically modified montmorillonite clay nanocomposite. J Ind Eng Chem 20:2208–2216. https://doi.org/10.1016/j.jiec.2013.09.052

Setshedi KZ, Bhaumik M, Onyango MS, Maity A (2015) High-performance towards Cr (VI) removal using multi-active sites of polypyrrole–graphene oxide nanocomposites: batch and column studies. Chem Eng J 262:921–931. https://doi.org/10.1016/j.cej.2014.10.034

Shafiabadi M, Dashti A, Tayebi HA (2016) Removal of Hg (II) from aqueous solution using polypyrrole/SBA-15 nanocomposite: experimental and modeling. Synth Met 212:154–160. https://doi.org/10.1016/j.synthmet.2015.12.020

Shahid M, Shamshad S, Rafiq M, Khalid S, Bibi I, Niazi NK, Dumat C, Rashid MI (2017) Chromium speciation, bioavailability, uptake, toxicity and detoxification in soil-plant system: a review. Chemosphere 178:513–533. https://doi.org/10.1016/j.chemosphere.2017.03.074

Sommer SK, Zakharov LN, Pluth MD (2015) Design, synthesis, and characterization of hybrid metal–ligand hydrogen-bonded (MLHB) supramolecular architectures. Inorg Chem 54 (4):1912–1918. https://doi.org/10.1021/ic502802f

Sud D, Mahajan G, Kaur MP (2008) Agricultural waste material as potential adsorbent for sequestering heavy metal ions from aqueous solutions–a review. Bioresour Technol 99 (14):6017–6027. https://doi.org/10.1016/j.biortech.2007.11.064

Suksabye P, Thiravetyan P, Nakbanpotec W (2008) Column study of chromium(VI) adsorption from electroplating industry by coconut coir pith. J Hazard Mater 160:56–62. https://doi.org/10.1016/j.jhazmat.2008.02.083

Syversen T, Kaur P (2012) The toxicology of mercury and its compounds. J Trace Elem Med Biol 26(4):215–226. https://doi.org/10.1016/j.jtemb.2012.02.004

Tang L, Fang Y, Pang Y, Zeng G, Wang J, Zhou Y, Deng Y, Yang G, Cai Y, Chen J (2014) Synergistic adsorption and reduction of hexavalent chromium using highly uniform polyaniline–magnetic mesoporous silica composite. Chem Eng J 254:302–312. https://doi.org/10.1016/j.cej.2014.05.119

Tang Y, Hu T, Zeng Y, Zhou Q, Peng Y (2015) Effective adsorption of cationic dyes by lignin sulfonate polymer based on simple emulsion polymerization: isotherm and kinetic studies. RSC Adv 5:3757–3766. https://doi.org/10.1039/c4ra12229a

Thomas HC (1944) Heterogeneous ion exchange in a flowing system. J Am Chem Soc 66:1664–1666. https://doi.org/10.1021/ja01238a017

Uddin MK (2017) A review on the adsorption of heavy metals by clay minerals, with special focus on the past decade. Chem Eng J 308:438–462. https://doi.org/10.1016/j.cej.2016.09.029

Vörösmarty CJ, McIntyre PB, Gessner MO, Dudgeon D, Prusevich A, Green P, Glidden S, Bunn SE, Sullivan CA, Liermann CR, Davies PM (2010) Global threats to human water security and river biodiversity. Nature 467(7315):555–561. https://doi.org/10.1038/nature09440

Walters CR, Somerset VS, Leaner JJ, Nel JM (2011) A review of mercury pollution in South Africa: current status. J Environ Sci Health A Tox Hazard Subst Environ Eng 46(10):1129–1137. https://doi.org/10.1080/10934529.2011.590729

Wang J, Chan S, Carlson RR, Luo Y, Ge G, Ries RS, Heath JR, Tseng HR (2004) Electrochemically fabricated polyaniline nanoframework electrode junctions that function as resistive sensors. Nano Lett 4(9):1693–1697. https://doi.org/10.1021/nl049114p

Wang J, Deng B, Chen H, Wang X, Zheng J (2009) Removal of aqueous Hg (II) by polyaniline: sorption characteristics and mechanisms. Environ Sci Technol 43(14):5223–5228. https://doi.org/10.1021/es803710k

Wang Y, Zou B, Gao T, Wu X, Lou S, Zhou S (2012) Synthesis of orange-like Fe_3O_4/PPy composite microspheres and their excellent Cr(VI) ion removal properties. J Mater Chem 22:9034–9040. https://doi.org/10.1039/c2jm30440f

Wang X, Liu W, Tian J, Zhao Z, Hao P, Kang X, Sang Y, Liu H (2014a) Cr(VI), Pb(II), Cd (II) adsorption properties of nanostructured BiOBr microspheres and their application in a continuous filtering removal device for heavy metal ions. J Mater Chem A 2:2599–2608. https://doi.org/10.1039/C3TA14519K

Wang J, Zhang K, Zhao L (2014b) Sono-assisted synthesis of nanostructured polyaniline for adsorption of aqueous Cr(VI): effect of protonic acids. Chem Eng J 239:123–131. https://doi.org/10.1016/j.cej.2013.11.006

Wang H, Yuan X, Wu Y, Chen X, Leng L, Wang H, Li H, Zeng G (2015) Facile synthesis of polypyrrole decorated reduced graphene oxide–Fe_3O_4 magnetic composites and its application for the Cr(VI) removal. Chem Eng J 262:597–606. https://doi.org/10.1016/j.cej.2014.10.020

Weber WJ, Morris JC (1963) Kinetics of adsorption on carbon from solution. J San Eng DivASCE 89:31–59

Wong S, Ngadi N, Inuwa IM, Hassan O (2018) Recent advances in applications of activated carbon from biowaste for wastewater treatment: a short review. J Clean Prod 175:361–375. https://doi.org/10.1016/j.jclepro.2017.12.059

Xiong C, Jia Q, Chen X, Wang G, Yao C (2013) Optimization of polyacrylonitrile-2-aminothiazole resin synthesis, characterization, and its adsorption performance and mechanism for removal of Hg(II) from aqueous solutions. Ind Eng Chem Res 52:4978–4986. https://doi.org/10.1021/ie3033312

Xu H, Xu Y, Chen Y (2011) Absorption of eriochrome blue black on polyaniline/attapulgite nanocomposites. Adv Mater Res 194–196:488–491. https://doi.org/10.4028/www.scientific.net/AMR.194-196.488

Yan W, Han J (2007) Synthesis and formation mechanism study of rectangular-sectioned polypyrrole micro/nanotubules. Polymer 48(23):6782–6790. https://doi.org/10.1016/j.polymer.2007.09.026

Yan Y, Yu Z, Huang YW, Yuan WX, Wei ZX (2007) Helical polyaniline nanofibers induced by chiral dopants by a polymerization process. Adv Mater 19(20):3353–3357. https://doi.org/10.1002/adma.200700846

Yao W, Ni T, Chen S, Li H, Lu Y (2014) Graphene/Fe_3O_4@ polypyrrole nanocomposites as a synergistic adsorbent for Cr (VI) ion removal. Compos Sci Technol 99:15–22. https://doi.org/10.1016/j.compscitech.2014.05.007

Yin H, Kong M, Gu X, Chen H (2017) Removal of arsenic from water by porous charred granulated attapulgite-supported hydrated iron oxide in bath and column modes. J Clean Prod 166:88–97. https://doi.org/10.1016/j.jclepro.2017.08.026

Yoon YH, Nelson JH (1984) Application of gas adsorption kinetics. I. A theoretical model for respirator catridge service time. Am Ind Hyg Assoc J 45(8):509–516. https://doi.org/10.1080/15298668491400197

Yu XY, Xu RX, Gao C, Luo T, Jia Y, Liu JH, Huang XJ (2012) Novel 3D hierarchical cotton-candy-like CuO: surfactant-free solvothermal synthesis and application in As(III) removal. ACS Appl Mater Interfaces 4(4):1954–1962. https://doi.org/10.1021/am201663d

Zaidi NS, Sohaili J, Muda K, Sillanpää M (2014) Magnetic field application and its potential in water and wastewater treatment systems. Sep Purif Rev 43(3):206–240. https://doi.org/10.1080/15422119.2013.794148

Zare EN, Motahari A, Sillanpää M (2018) Nanoadsorbents based on conducting polymer nanocomposites with main focus on polyaniline and its derivatives for removal of heavy metal ions/dyes: a review. Environ Res 162:173–195. https://doi.org/10.1016/j.envres.2017.12.025

Zhang JX, Ou LL (2013) Kinetic, isotherm and thermodynamic studies of the adsorption of crystal violet by activated carbon from peanut shells. Water Sci Technol 67(4):737–744. https://doi.org/10.2166/wst.2012.605

Zhang X, Zhang J, Song W, Liu Z (2006) Controllable synthesis of conducting polypyrrole nanostructures. J Phys Chem B 110(3):1158–1165. https://doi.org/10.1021/jp054335k

Zhang Y, Li Q, Sun L, Tang R, Zhai J (2010) High efficient removal of mercury from aqueous solution by polyaniline/humic acid nanocomposite. J Hazard Mater 175(1–3):404–409. https://doi.org/10.1016/j.jhazmat.2009.10.019

Zhang M, Song L, Jiang H, Li S, Shao Y, Yang J, Li J (2017) Biomass based hydrogel as an adsorbent for the fast removal of heavy metal ions from aqueous solutions. J Mater Chem A 5:3434–3446. https://doi.org/10.1039/c6ta10513k

Zhang X, Fang X, Li J, Pan S, Sun X, Shen J, Han W, Wang L, Zhao S (2018) Developing new adsorptive membrane by modification of support layer with iron oxide microspheres for arsenic removal. J Colloid Interface Sci 514:760–768. https://doi.org/10.1016/j.jcis.2018.01.002

Zhou G, Liu C, Tang Y, Luo S, Zeng Z, Liu Y, Xu R, Chu L (2015) Sponge-like polysiloxane-graphene oxide gel as a highly efficient and renewable adsorbent for lead and cadmium metals removal from wastewater. Chem Eng J 280:275–282. https://doi.org/10.1016/j.cej.2015.06.041

Chapter 6
Biological Effects of Green-Synthesized Metal Nanoparticles: A Mechanistic View of Antibacterial Activity and Cytotoxicity

Suresh K. Verma, Ealisha Jha, Pritam Kumar Panda, Arun Thirumurugan, and Mrutyunjay Suar

Contents

Abstract Recent advancements in nanotechnology have pushed the boundary of nanomaterial studies and their applications so far that almost each and every aspect of science is looking for their application based on them. The extensive studies and industrial applications have raised demand for nanomaterial in leaps and bounds. To fulfill the demand, new strategies for their synthesis and industrial preparation have been discovered and applied. However, the logarithmic expansion of production of nanomaterials, especially metal and metal oxide nanomaterials, has slowly raised the issue of their toxicity and biocompatibility with respect to ecosystems and human

S. K. Verma (✉) · M. Suar (✉)
School of Biotechnology, KIIT University, Bhubaneswar, India

E. Jha
Department of Physics and Physical Oceanography, Memorial University of Newfoundland, St. John's, NL, Canada

P. K. Panda
Division of Pediatrics, Hematology and Oncology, University of Freiburg, Freiburg, Germany

A. Thirumurugan
Advanced Materials Laboratory, Department of Mechanical Engineering, University of Chile, Santiago, Chile

Mu. Naushad et al. (eds.), *Advanced Nanostructured Materials for Environmental Remediation*, Environmental Chemistry for a Sustainable World 25,
https://doi.org/10.1007/978-3-030-04477-0_6

health. Traditional synthesis of nanomaterials by chemical and physical synthesis procedures has been reported to impose higher toxicity on both ecosystems and human health. There are regular quests for new methods to discover biocompatible nanomaterials. In view of the above facts, green synthesis of nanomaterials, using biological agents, has been shown to be a solution to this issue. However, to address this issue, discussion about their detailed biological effects is urgently needed. To illuminate these concerns, this chapter provides a brief review of the current strategies for green synthesis of nanomaterials, especially focusing on metal and metal oxide nanoparticles and their detail mechanisms of biological effects in view of their antibacterial efficacy and cytotoxicity.

Keywords Green synthesis · Metal oxide nanoparticles · Antibacterial activity · Cytotoxicity

6.1 Introduction

The term "green synthesis" refers to an eco-friendly way of synthesizing nanoparticles (NPs). It includes all procedures that produce no waste or that produce only biodegradable waste. Moreover, such synthesis procedures involve chemicals derived from biological entities for the fabrication of nanoparticles. Paul Anastas and John Warner described the term "green chemistry" on the basis of 12 principles, which include prevention of production of harmful waste, incorporation of all materials' usability in the final product, use of methods showing no toxicity or only low toxicity to human health, design of nanoparticles according to desired properties without compromising the toxicity aspect, use of only minimal and innocuous auxiliary substances, energy efficiency, biodegradability, and pollution prevention. Different synthesis methods that have been recognized as green synthesis methods are high-energy ball milling (HEBM), biological routes of synthesis, and synthesis using biological agents. The biological agents or biomolecules involved are identified on the basis of their derived sources such as plants, bacteria, or other microorganisms.

A plant contains various therapeutic compounds, which can be exploited as traditional medicines. Because of their enormous diversity, plants have an extensive range of applications in various fields such as agriculture, pharmaceutics, and industry. Recent reports have suggested the use of plants in the production of nanoparticles, which are regarded as having advantages such as safe handling, biodegradable waste, and easy availability. Moreover, a wide range of biomolecules (terpenoids, alkaloids, flavonoids, phenols, quinines, tannins, etc.) present in different plants are recognized to arbitrate the synthesis of nanoparticles.

Mittal et al. (2013) and other groups have studied the utility of biomolecules from plant extracts in the reduction of metal ions to nanoparticles in the green synthesis process. This biogenic reduction of metal ions is fast and easily conductible at room conditions. Moreover, plant extract–regulated synthesis of nanoparticles is

environmentally friendly. The reducing agents comprise various water-soluble plant metabolites (e.g., alkaloids, phenolic compounds, and terpenoids) and coenzymes. Silver (Ag), gold (Au), and zinc (Zn) nanoparticles are the main targets of plant-based synthesis. Moreover, the use of plant-derived biomolecules provides an option for controlled synthesis of nanoparticles.

As part of this, biogenic methods engaging biological microorganisms have arisen as a viable substitute for physical methods and chemical synthetic procedures. It is a well-recognized fact that microorganisms such as yeast, bacteria, and fungi can play significant roles in reduction of metal ions, leading to remediation of toxic metals (Mandal et al. 2006). Some bacteria secrete diffusible and small redox compounds that can reduce iron (Fe^{3+}) oxides and can assist as electron shuttles. Hydroquinones released by microorganisms are evidently capable of reducing ions to nanoparticles. However, one drawback of this procedure is the slow rate of generation of nanoparticles.

Green synthesis of nanoparticles has been emphasized because of their biocompatibility and eco-friendly nature. Their biocompatibility can be evaluated, along with their cytotoxicity behavior, by use of different in vitro and in vivo model systems. The biocompatibility of green-synthesized nanoparticles is due to the presence of biological moieties present on the surface of the nanoparticles (Verma and Stellacci 2010). On exposure, these biomolecules interact with the biomolecules present on the cell surface, resulting in a less harmful interaction than that seen with chemically synthesized nanoparticles, which may have harmful chemicals on their surface. The multi-utility of nanomaterials can be estimated on the basis of their extensive use in catalysis (Astruc et al. 2005), magnet cooling (Lee et al. 2011b), optical and recording devices (Zijlstra et al. 2009), purification of enzymes and other biological materials (Cao et al. 2012), water purification (Porada et al. 2008), and targeted drug delivery (Cho et al. 2008). However, this extensive use can be viewed negatively on the basis of the associated threats to health and environment safety. Green synthesis offers potential solutions to these threats. The biocompatibilities of the nanoparticles have been studies in vivo and in vitro, using different models. In vitro analysis includes the interaction of nanoparticles with cell lines. This approach to analysis is an economical tool for evaluation of the toxicity of nanomaterials. A benefit of using this tool includes detailed description of the effects of nanomaterials on objective cells in the absence of their secondary effects, allowing possibilities for exploration of the primary mechanism of toxicity. Moreover, it also explores the probability of improving the design of nanomaterials for in vivo animal studies. On the basis of the objectives of toxicity studies and the targeted tissue, many cell lines have been chosen in the past for studying cellular toxicity. They include A549 (a lung cancer–derived cell line), HCT116 (a colon cancer cell line), RAW264.7 (a macrophage cell line), U87 (astrocytoma cells), HEK293T (a kidney cell line), and fibroblast cell lines. The results of the effects of nanomaterial interactions on them are listed in Table 6.1.

The mechanism of the cytotoxicity of nanoparticles to cell lines can be defined in three steps: the nanoparticles get attached to the surface of the cell membrane through ionic interaction, leading to internalization of these particles. This, in turn,

Table 6.1 Studies on effects of nanoparticle interactions with different cell lines

Nanomaterial	Cell lines	Toxicity effects	Reference
Titanium oxide	Human lung cells	Oxidative stress ↑	Bhattacharya et al. (2009)
		DNA adduct formation	
		Cytotoxicity ↑	
Iron oxide	Rat mesenchymal stem cells	Cell viability ↓	Delcroix et al. (2009)
Iron oxide	Murine macrophage cells	Cell viability ↓	Jeng and Swanson (2006)
Iron oxide	Human macrophages	Cell viability ↓	Naqvi et al. (2010)
Zinc oxide	Human hepatocyte HEK293 cell line	Cell viability ↓	Guan et al. (2012)
		Oxidative stress	
		Mitochondrial damage	
Zinc oxide	Human cervix carcinoma cell line (HEp-2)	DNA damage	Osman et al. (2010)
		Cell viability ↓	
Zinc oxide	Human colon carcinoma cells	Oxidative stress ↑	De Berardis et al. (2010)
		Cell viability ↓	
		Inflammatory biomarkers	
Aluminum oxide	Human brain microvascular endothelial cells	Cell viability ↓	Chen (2008)
		Mitochondrial function ↓	
		Oxidative stress ↑	
Aluminum oxide	Mammalian cells	No significant toxic effect on cell viability	Radziun et al. (2011)
Aluminum oxide	Human mesenchymal stem cells	Cell viability ↓	Alshatwi et al. (2012)
Copper oxide	Human lung epithelial cells	Cell viability ↓	Ahamed et al. (2010)
		Lactate dehydrogenase ↑	
		Lipid peroxidation ↑	

produces secondary effects such as genotoxic abnormalities and reactive oxygen species (ROS) generation. The attachment of the nanoparticle highly depends on the charge present on its surface, and this fact is utilized by researchers to determine the right choice for biocompatible nanoparticle synthesis. Internalization as a result of interaction proceeds by physiological processes such as endocytosis. After internalization of the nanoparticle, its secondary physiological effects can induce cytotoxicity in the cells, which includes phenomena such as lipid metabolism alteration, osteosis, and alteration of ROS.

In vivo cytotoxicity evaluation can be done with a whole-animal model. Researchers have utilized various whole-animal models such as *Caenorhabditis elegans*, mouse, and zebrafish models to determine the toxicity of nanoparticles. The selection of the model depends on genetic similarity to humans, making them a potential candidate to mimic the effects on human cells. Among all of these models, the zebrafish model has recently

Table 6.2 Studies on cytotoxic effects of nanoparticles in a zebrafish model

Nanomaterial	Size and shape	Zebrafish line	Toxicity effect	Reference
Copper oxide	Spherical, 21 nm	Transgenic (nacre/fli1: EGFP) zebrafish	Inhibition of vasculogenesis	Chang et al. (2015)
TiO_2	Spherical, <25 nm	Gene expression of zebrafish embryos	Circadian rhythm gene (s) deregulated by nanoparticles	Jovanović et al. (2011)
CuO, ZnO, NiO, and Co_3O_4	Spherical, 10–50 nm	hsp70:GFP transgenic zebrafish larvae	CuO, ZnO, and NiO may augment expression of hsp70:GFP in transgenic zebrafish larvae	Lin et al. (2011)

been gaining popularity. Several studies have been done to explore and determine the toxic effect of nanoparticles on the zebrafish model, as listed in Table 6.2.

This review describes the use of different biological agents for green synthesis of nanomaterials, focusing on Ag-NPs and ZnO-NPs. It then provides mechanistic detail about their antibacterial activities and cytotoxicity with respect to in vitro and in vivo models such as different mammalian cell lines and embryonic zebrafish.

6.2 Green Synthesis of Metal and Metal Oxide NPs

Green synthesis of two types of metal and metal oxide nanoparticles—Ag-NPs and ZnO-NPs—has been achieved by use of different techniques (Fig. 6.1). The selection of methodology depends on the type of approach for the synthesis. The two most common approaches for any type of nanoparticle synthesis are (1) a top-down approach and (2) a bottom-up approach.

The top-down approach refers to the breaking down of bulk material to a nanosize, using external physical forces. This approach is considered a green method when there is no use of any harmful chemical to catalyze the process. A common example of green methodology with a top-down approach is the HEBM method. HEBM uses high mechanical energy to grind bulk molecules into smaller ones; hence, there is no use of any harmful chemicals. To minimize heat production due to frictional forces, a low revolutions-per-minute (rpm) count and an inert environment are used. Numerous studies have described the use of this method for the synthesis and bulk production of metal and metal oxide nanoparticles such as ZnO-NPs and TiO_2-NPs. It has been shown to be superior to other reported methods in terms of simplicity, reliability, and reproducibility, with application to any class of materials (Badapanda et al. 2015; Murty and Ranganathan 1998). In

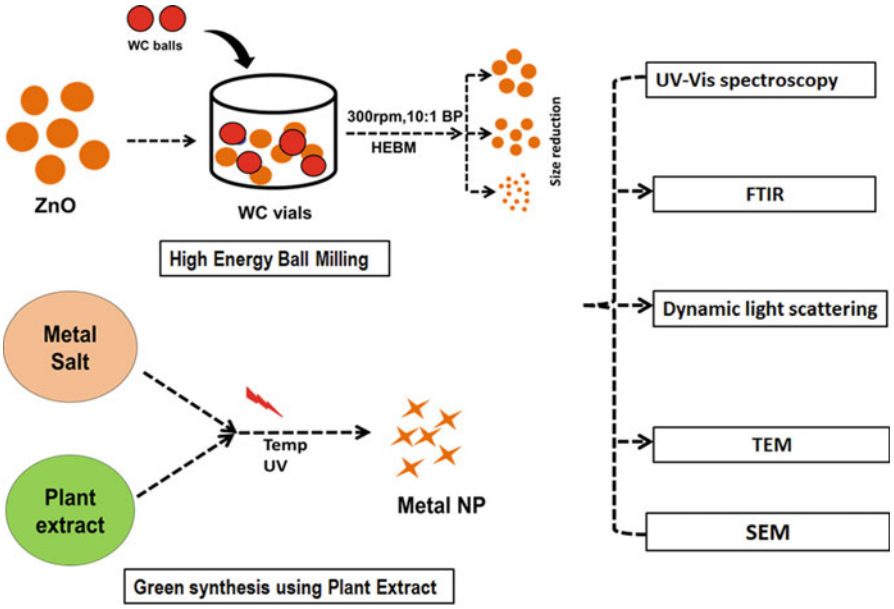

Fig. 6.1 Green methodologies for synthesis of metal and metal oxide nanoparticles (*NPs*). *FTIR* Fourier transform infrared spectroscopy, *HEBM* high-energy ball milling, *SEM* scanning electron microscopy, *TEM* transmission electron microscopy, *Temp* temperature, *UV* ultraviolet, *Vis* visible light

addition, it induces morphological and structural changes such as core–shell intrinsic defects (Parashar et al. 2012) with chemical reactions that are rare at normal room temperature. Muñoz et al. (2007) reported the production of iron nanoparticles, using HEBM. Giri et al. (2007) described the benefits of using HEBM for the production of ZnO-NPs. Similarly, silicon nanoparticles have been synthesized using HEBM for enhancement of optical properties (Goyal and Soni 2018).

Though the top-down approach has provided a good option for production of nanomaterials by use of green synthesis, the purity is a matter of concern. To solve this problem, bottom-up approach strategies are used. The bottom-up approach involves the formation of desired nanoparticles by use of chemical reactions. This approach is considered a green method when the chemicals used are derived from biological sources such as plants and microbes. In this quest, many plant and microbial sources have been used in the last few decades to extract biomolecules for production of nanoparticles. With regard to Ag-NPs and ZnO-NPs, a number of researchers have investigated the utility of many plant and microbial extracts for the synthesis of these nanoparticles. For Ag-NP synthesis, silver nitrate is incubated with plant extracts chosen from different parts of plants and subjected to exposure to

Table 6.3 Studies on green synthesis of silver nanoparticles

Plant	Size (nm)	Reference
Plectranthus amboinicus	88	Fu and Fu (2015)
Vitex trifolia L.	30	Elumalai et al. (2015a)
Aspalathus linearis	1–8	Park and Maaza (2015)
Anisochilus carnosus	20–40	Anbuvannan et al. (2015a)
Coffee	4.6	Fatimah et al. (2016)
Mimosa pudica	2.71	Fatimah et al. (2016)
Ocimum basilicum L. var. *purpurascens*	50	Abdul et al. (2014)
Citrus aurantifolia	50	Çolak and Karaköse (2017)
Black tea	19.3	Hassan et al. (2016)
Azadirachta indica	28	Madan et al. (2016)
Zingiber officinale	23–26	Anbuvannan et al. (2015b)
Moringa oleifera	6–20	Elumalai et al. (2015b)
Trifolium pratense	100–190	Dobrucka and Długaszewska (2016)
Aloe vera	8–18	Ali et al. (2016)
Nephelium lappaceum L.	25–40	Karnan and Selvakumar (2016)
Lobelia leschenaultiana	40	Banumathi et al. (2016)
Carica papaya	11–26	Sharma (2016)
Polygala tenuifolia	33.03–73.48	Nagajyothi et al. (2015)
Anchusa italica	8, 14	Azizi et al. (2016)
Jacaranda mimosifolia	2–4	Sharma et al. (2016)

physical agents such as temperature, or radiation for the formation of the nanoparticles. The roles of plant extracts hereby have been recognized as reducing and capping agents. Different biomolecules present inside the extracts have been reported for synthesis of nanoparticles. The plant materials used for these processes are carefully chosen on the basis of plant parts and medicinal usage (Table 6.3). Numerous reports have described green synthesis of Ag-NPs with use of plant extracts such as *Acalypha indica* leaf (Krishnaraj et al. 2010), *Jatropha curcas* seeds (Bar et al. 2009b), *Chenopodium album* leaf (Dwivedi and Gopal 2010), banana peel (Bankar et al. 2009), *Ocimum tenuiflorum*, *Syzygium cumini*, *Trianthema decandra*, *Rosa rugosa* (Dubey et al. 2010), *Centella asiatica*, *Solanum trilobatum* roots, mulberry leaves (Awwad et al. 2012), *Olea europaea* leaves (Awwad and Salem 2012), *Arbutus unedo* leaves (Kouvaris et al. 2012), *Ficus benghalensis* leaves (Saxena et al. 2012), and *Citrus sinensis* leaves (Logeswari et al. 2015).

Plant extracts have also been reported for the synthesis of ZnO nanoparticles. *Trifolium pratense* flowers have been used to synthesize ZnO-NPs in the presence of phenolic acids, anthocyanins, and small amounts of carotene, tannins, essential oils, and vitamin C (Dobrucka and Długaszewska 2015). ZnO-NPs with a size range of 8–18 nm and variable shapes have been reported to be synthesized with

Table 6.4 Studies on green synthesis of zinc oxide nanoparticles from plants

Plant	Size (nm)	Reference
Azadirachta indica	50–100	Poopathi et al. (2015)
Aloe vera	15–20	Dinesh et al. (2015)
Emblica officinalis	10–20	Ramesh et al. (2015)
Parthenium hysterophorus L.	40–50	Parashar et al. (2009)
Cinnamomum camphora	15–19	Huang et al. (2007)
Camellia sinensis	30–40	Loo et al. (2012)
Diopyros kaki	10–20	Song and Kim (2008)
Jatropha curcas (latex)	15–500	Bar et al. (2009a)
Jatropha curcas (seed)	55–60	Bar et al. (2009b)
Cinnamomum camphora (dried leaf)	55–60	Huang et al. (2007)
Pineapple (leaf extract)	15–500	Emeka et al. (2014)
Persimmon (leaf extract)	15–500	Song and Kim (2008)
Ginkgo (leaf extract)	30–40	Song and Kim (2009)
Magnolia (leaf extract)	30–40	Song et al. (2009)
Pelargonium graveolens (leaf extract)	55–60	Shankar et al. (2003)
Phoma glomerata	10–20	Gade et al. (2013)
Macrotyloma uniflorum	10–20	Vidhu et al. (2011)
Anacardium occidentale	55–60	Mukunthan and Balaji (2012)
Hibiscus rosa sinensis	55–60	Philip (2010)
Mimusops elengi L.	55–60	Prakasha et al. (2013)

the use of *Aloe barbadensis* leaf extract (Ali et al. 2016). Similarly, *Euphorbia prolifera* leaf extract has been used as a reducing and stabilizing agent to form ZnO-NPs (Momeni et al. 2016). Spherical ZnO-NPs 25–40 nm in size have been synthesized from rambutan (*Nephelium lappaceum* L.) peel extract (Karnan and Selvakumar 2016). The milk latex of *Carica papaya* has been reported to possess useful properties for the synthesis of ZnO-NPs. Extracts of other plants such as *Azadirachta indica* (Elumalai and Velmurugan 2015), *Polygala tenuifolia*, *Vitex negundo*, *Anchusa italica*, *Jacaranda mimosifolia*, *Heritiera fomes*, and *Sonneratia apetala* have also played roles as reducing and stabilizing agents in the formation of ZnO-NPs. A short summary can be viewed in Table 6.4.

The available information about green synthesis of nanoparticles with use of plant extracts is elaborated with each new discovery. The basic mechanism of the synthesis lies in the fact that the plant extract contains biomolecules such as proteins, DNA, and saccharides, and other molecules such as flavonoids and carotenoids, which act as reducing and capping agents. In brief, the formation of nanoparticles after the reaction setup can be sketched as:

$$\text{Metal Salts} + \text{Biomolecules} \rightarrow \text{Metal NPs} + \text{By-products}$$

A similar concept has been applied in use of microbes for synthesis of nanoparticles. The biomolecules released by bacterial strains in a culture medium

Table 6.5 Studies on biosynthesis of metal nanoparticles (*NPs*) from bacteria

Bacterial strain	Nanoparticles	Size (nm)	Reference
Bacillus subtilis	Au-NPs	5–25	Lengke et al. (2007)
Lactobacillus sp.	Au-NPs	20–50	Nair and Pradeep (2002)
Pseudomonas aeruginosa	Au-NPs	15–30	Husseiny et al. (2007)
Escherichia coli	Au-NPs	20–25	Deplanche and Macaskie (2008)
Klebsiella pneumoniae	Au-NPs	35–65	Nangia et al. (2009)
Pseudomonas stutzeri	Ag-NPs	100–200	Joerger et al. (2000)
Lactobacillus sp.	Ag-NPs	15–30	Fu et al. (2006)
Morganella sp.	Ag-NPs	20–21	Parikh et al. (2008)
Bacillus subtilis	Ag-NPs	5–50	Saifuddin and Wong (2009)
Bacillus indicus	Ag-NPs	2.5–13.3	Shivaji et al. (2011)
Pseudomonas antarctica	Ag-NPs	3–33	Shivaji et al. (2011)
Salmonella typhimurium	Au-NPs	20–40	Khodashenas and Ghorbani (2014)
Pseudomonas fluorescens	Ag-NPs	80–85	Silambarasan and Jayanthi (2013)
Salmonella typhimurium	Ag-NPs	85–110	Khodashenas and Ghorbani (2014)
Rhodobacter sphaeroides	CdS-NPs	6–7	Bai et al. (2009)
Streptomyces sp.	MnO-NPs, ZnO-NPs	10–20	Waghmare et al. (2011)
Desulfovibrio desulfuricans	Pd-NPs	40–50	Yong et al. (2002)
Bacillus thuringiensis	Ag-NPs	20–30	Verma et al. (2017c)
Staphylococcus aureus	Ag-NPs	30–40	Verma et al. (2017c)
Salmonella typhimurium	Ag-NPs	40–50	Verma et al. (2017c)

have been used for the formation of nanoparticles. Numerous studies in the last few years have shown that biomolecules released in the supernatant of the culture medium used for culturing the bacterial strains can be used for synthesis of metal and metal oxide nanoparticles such as Ag-NPs and ZnO-NPs. A brief overview of these studies is given in Table 6.5.

6.3 Biological Effects of Metal and Metal Oxide NPs

Extensive usage of metal and metal oxide nanoparticles has raised concerns about their effect on biological systems. In view of concerns related to biocompatibility, green-synthesized nanoparticles have been evaluated for their effects on biological systems in terms of both beneficial and toxic aspects. As far as beneficial effects are concerned, green-synthesized metal nanoparticles have been studied for their antibacterial activities against pathogenic as well as nonpathogenic strains. The

approach of green synthesis has been taken to enhance the antibacterial activity of metal nanoparticles such as Ag-NPs, Au-NPs, and ZnO-NPs. On the same platform, it is mandatory for synthesized nanoparticles to have less cytotoxicity to human cells in order to have clinical applicability. However, their toxic effects with high usage and accumulation can sometimes be overlooked. Moreover, these toxic effects can have implications for environmental aspects and can potentially spread to other biotic factors in the ecosystem.

6.3.1 Antibacterial Effects of Green-Synthesized Metal and Metal Oxide NPs (Ag-NPs and ZnO-NPs)

Recent studies have shown that metal and metal oxide nanoparticles, especially Ag-NPs and ZnO-NPs, have high antibacterial efficacy against bacterial strains such as *Escherichia coli* and *Staphylococcus aureus*. With advancement of green synthesis technology, the quest to increase their efficacy is in progress. Ag-NPs synthesized from green methodology have been shown to have antibacterial effects on almost every strain; this property of Ag-NPs has made them applicable for clinical purposes. Many products in the market nowadays are available with Ag-NPs. Ag-NPs synthesized from different plant and bacterial sources have shown significant antibacterial efficacy against different bacterial strains. Nanoparticles synthesized from banana peel by Bisauriya et al. have been shown to have antibacterial effects (Bisauriya et al. 2018). Similarly, many groups have reported green synthesis of Ag-NPs with antibacterial efficacy from *Aloe vera* extract (Kumar et al. 2015), *Prosopis farcta* (Miri et al. 2015), *Cocos nucifera* (Mariselvam et al. 2014), etc.

6.3.1.1 Mechanism of Antibacterial Activity

The antibacterial mechanism of action of Ag-NPs has been defined by many groups; however, the exact mechanism is still unknown, as the different groups have defined the mechanism from different perspectives. Many different groups have determined the antibacterial effect by using different experimental techniques such as well diffusion assays or growth curve analysis. As shown in Figs. 6.2 and 6.3, analyses of zones of inhibition against different bacterial cultures exhibited by nanoparticles have been demonstrated by different groups, e.g., Verma et al. (2017a, 2017b). Durán et al. (2010) evaluated the comparative action of silver ions and silver nanoparticles in terms of their antibacterial activities. Their report mainly suggested that silver ions inactivate bacteria by reacting with the thiol groups of proteins. This emphasis was due to the fact that silver ions weakened DNA replication by affecting respiratory chain enzymes and inhibiting oxidative phosphorylation, leading to abnormalities in membrane permeability. Marambio-Jones and Hoek (2010) discussed the mechanism of antibacterial activities of Ag-NPs with three

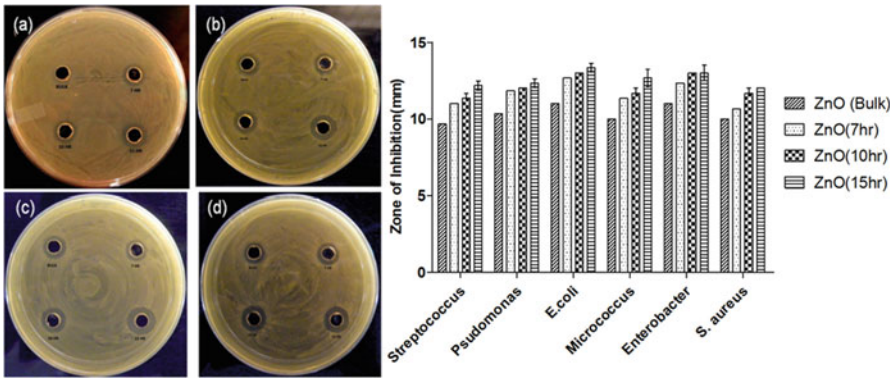

Fig. 6.2 (**a**–**d**) Zones of inhibition formed by zinc oxide nanoparticles (*NPs*) against the Gram-negative bacteria (**a**) *Escherichia coli* and (**b**) *Pseudomonas*, and against the Gram-positive bacteria (**c**) *Staphylococcus aureus* and (**d**) *Micrococcus.* **e** Bar graph representing the zones of inhibition formed by ZnO-NPs against Gram-positive and Gram-negative bacteria. The zones of inhibition against both types of bacteria increased with a reduction in the size of the NPs. Each bar in the graph represents the mean ± the standard error of the mean (Verma et al. 2017a)

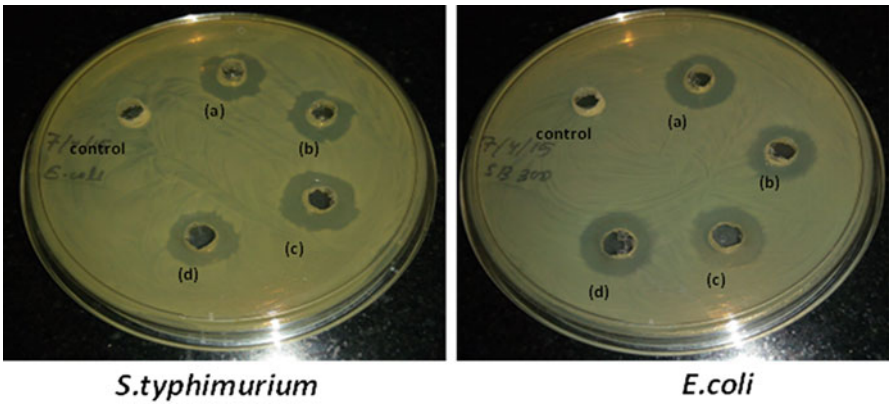

Fig. 6.3 Zones of inhibition formed by different biogenic silver nanoparticles against two bacterial strains (*Salmonella typhimurium* and *Escherichia coli*), as determined by well diffusion assays (Verma et al. 2017b)

conceivable mechanisms: (1) free silver ion uptake followed by disturbance of adenosine triphosphate (ATP) production and DNA replication, (2) oxidative stress generation through induction of ROS by silver nanoparticles and silver ions, and (3) cell membrane damage by silver nanoparticles.

However, the majority of authors have emphasized the perspective of cell damage and oxidative stress induction as major causes of the antibacterial activity of Ag-NPs. Mirzajani et al. (2011) analyzed variations of the peptidoglycan structure in *S. aureus* cells after Ag-NP treatment for disruption of the bacterial cell wall.

McQuillan et al. (2012) described the primary mechanism of Ag-NP action on cell membrane suspension. Kon and Rai (2013) revealed that Ag-NP action also depends on the type of bacterial strain because of the variations in cell wall composition. This revelation was supported by the findings of Kim et al. (2007), who equated the effects of Ag-NPs on *E. coli* and *S. aureus*. Reidy et al. (2013) and Cao and Liu (2010) proposed another important aspect of antibacterial action, describing involvement of the electrochemical proton gradient through respiratory processes that act as the driving force for ATP synthesis in bacteria.

Ag-NPs have been speculated to interrupt the energy source for all reactions, leading to cell death due to unable cell adhesion and proliferation. Manke et al. (2013) described the role of oxidative stress induction by Ag-NPs as a function of cellular factors such as size, particle surface, and composition. Moreover, the mechanism suggested was oriented toward cellular responses such as nanoparticle–cell interactions, mitochondrial respiration, and immune cell activation for ROS-mediated damage. Kim et al. (2011) validated these descriptions in *S. aureus* and *E. coli*, and described that ROS generation leads to increased permeability in the membrane, generating protein breaks and inactivation of enzymes such as lactate dehydrogenase. During their investigation, they found larger amounts of protein leakage through the *E. coli* membrane than through the *S. aureus* membrane, signifying a difference in antibacterial effectiveness against the Gram-positive *S. aureus* compared with the Gram-negative *E. coli*. The difference was attributed to differences in the thickness of the peptidoglycan layer in *S. aureus* and *E. coli.* In view of these studies, it can be explained that the mechanism of antibacterial activity of Ag-NPs varies depending on parameters and factors. A common mechanism is shown in Fig. 6.4. The nanoparticles first get attached to the surface, depending on the nature of the nanoparticles, decided by the coating factors. Followed by attachment, they interact with the cell membrane via different proteins and lipids, leading to their internalization, as well as induction of membrane damage due to action of ROS induced by them. The internalized nanoparticles then interfere with the cellular physiology of the bacteria (e.g., by interaction with respiratory mechanisms and cell wall development processes) and cause their destruction with the help of ROS generated by them. Though this description seems to be complete, the complete profile of the proteins and biomolecules that interact with the Ag-NPs during the course of this mechanism still seems to be incomplete. Further research is needed to fully understand the mechanism in detail.

Like Ag-NPs, ZnO-NPs synthesized by green methodology have been described as having strong antibacterial activity. The mechanism described by different researchers is somewhat similar to the basic mechanism described for Ag-NPs; however, the detail varies in respect of the fact that a ZnO-NP has an extra oxygen atom, which can enhance the oxidative stress phenomenon. Dobrucka and Długaszewska (2016) explained the antibacterial activity of ZnO-NPs, synthesized from *T. pratense*, against *E. coli*, *S. aureus*, and *Pseudomonas aeruginosa* 6749. The synthesized ZnO-NPs were reported to show improved antibacterial activity against *P. aeruginosa* as compared with gentamicin. Elumalai et al. (2015a) described antimicrobial activity of ZnO-NPs against *Bacillus subtilis*, *S. aureus*, *Proteus*

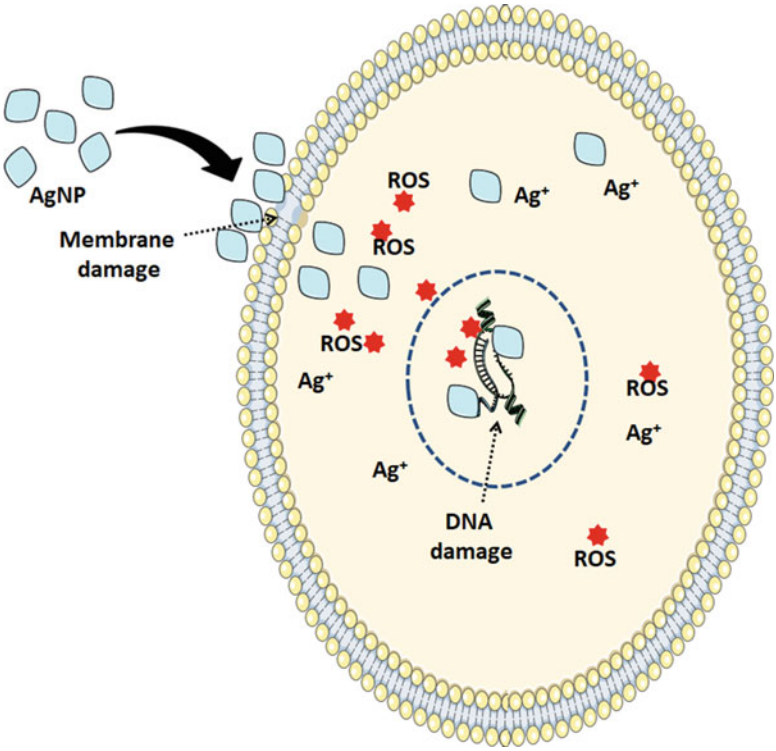

Fig. 6.4 Mechanism of antibacterial activity of silver nanoparticles (*NPs*). *ROS* reactive oxygen species

mirabilis, *P. aeruginosa*, and *E. coli* in a dose-dependent manner. The most probable mechanism of antibacterial activity is disruption of cell wall permeability. It was stated that the Zn^{+} ions are internalized into the bacterial cell by splitting the cell wall. As a consequence, the cytoplasmic fluid gets leaked from the cell, leading to the death of the cell or bacterium (Raghupathi et al. 2011). Another mechanism described by researchers is the involvement of generation of ROS such as O^{2-} and H_2O_2 at the surface of ZnO-NPs. The transference of electrons from the valence band to the conduction band in exposed ZnO nanoparticles creates a hydroxyl group, which reacts with the holes generated in the valence band and absorbs water. Moreover, generation of superoxide radical anions (O^{2-}) occurs as a result of the entrapment of electrons in the conduction band by O_2 (Baek et al. 2017). These molecular mechanisms, however, do not describe the phenomenon taking place inside the bacterial cells. A detailed mechanism showing the involvement of biomolecule interaction of ZnO has recently been discussed by (Verma et al. 2017a). It was stated that two probable mechanisms can be specified for the antibacterial action of ZnO-NPs: (1) generation of increased levels of ROS (Schneider et al. 2010); and (2) attachment of nanoparticles on the bacterial surface, leading to disruption of

cellular function. It was argued that the improved charge density and zeta potential increase size-dependent ZnO-NP interaction with proteins related to bacterial membrane proteins, thereby disturbing the membrane permeability. The augmented permeability increases size-dependent accumulation of ZnO-NPs inside the cytoplasm, altering physiological processes and causing disorganization of the cell. The interaction and accumulation are accompanied by ROS and alterations in the membrane potential of the bacterial cell. The phenomenon significantly differs between Gram-positive and Gram-negative bacterial strains. In Gram-positive bacteria such as *Micrococcus luteus*, attachment of ZnO-NPs takes place through secY alpha helix barrel proteins, leading to internalization inside the cytoplasm, whereas in Gram-negative bacterial such as *E. coli*, the phenomenon is carried out with the help of beta barrel proteins and other proteins such as bamB, bamC, bamD, and bamE. The internalized nanoparticles induce oxidative stress by interacting with consequential proteins. In *M. luteus* (a Gram-positive bacteria), ZnO-NPs directly impact the functionality of sodA protein. When sodA interrelates with ZnO-NPs, which consist of oxygen vacancies, these oxygen vacancies are further filled by the oxygen relesed from water molecules with enhanced generation of ROS. In the case of the Gram-negative bacteria *E. coli*, ZnO-NPs interact with dnaK, creating hyperosmotic pressure and leading to activation of soxR protein. The vacant oxygen of the ZnO-NP gets recognised by oxyR protein and transferred to sodC, leading to enhancement of ROS in the cytoplasm. The collective effect of these factors has been reported to destabilize the cellular functionality, promoting cell lysis. The detailed mechanism can be viewed through the schematic presentation shown in Fig. 6.5.

6.3.2 *Cytotoxicity of Green-Synthesized Metal and Metal Oxide NPs (Ag-NPs and ZnO-NPs)*

The cytotoxicity of a nanoparticle is defined as the induction of abnormal cell activities, leading to cell death by their exposure. Determination of cytotoxicity has been considered an important parameter for proposing any nanomaterial for clinical applications. To determine the cytotoxicity of an engineered nanoparticle, different biological models are used nowadays. They have been defined as in vitro and in vivo evaluation procedures. In vitro evaluation has been described as determination of cytotoxicity (or, conversely, biocompatibility) by use of mammalian cell lines as a model, while in vivo evaluation describes cytotoxicity determination in live models such as the mouse, rat, or zebrafish. Ag-NPs and ZnO-NPs have been reported to exhibit cytotoxicity apart from their antibacterial efficacy. A number of studies have described the cytotoxic effects of Ag-NPs on neuronal cells (Hussain et al. 2006), rat liver cells (Hussain et al. 2005), murine stem cells (Braydich-Stolle et al. 2005), and human lung epithelial cells (Lam et al. 2004). The basic mechanism of Ag-NP toxicity has been understood for a long time; however, a detailed

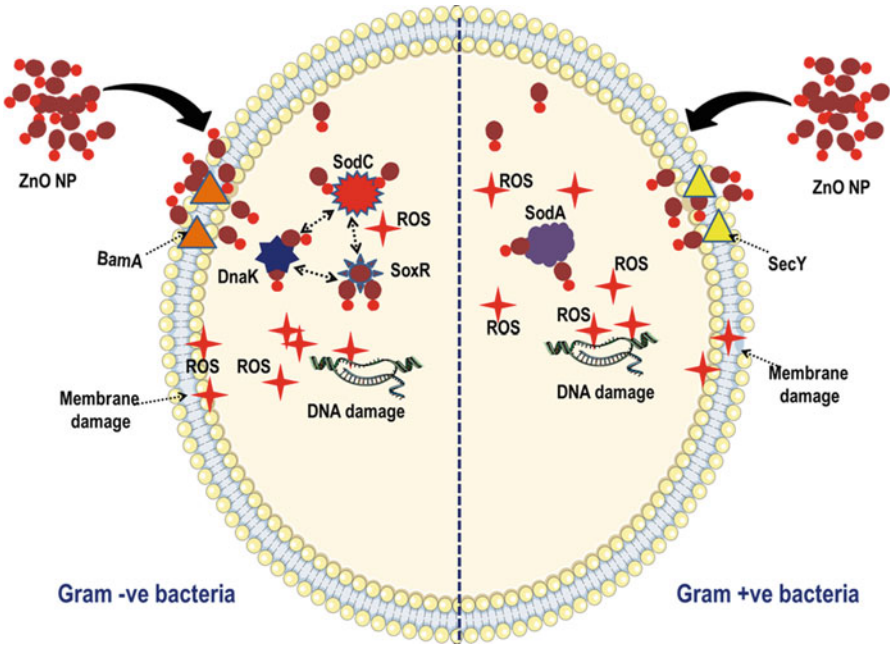

Fig. 6.5 Mechanism of antibacterial activity of zinc oxide nanoparticles (*NPs*) against Gram-positive (*+ve*) and Gram-negative (*−ve*) bacterial strains. *ROS* reactive oxygen species

explanation is still lacking. Ag-NPs that get internalized inside a cell through permeation of the cell membrane increase the levels of intracellular Ag^+, leading to cytotoxic and genotoxic effects carried out through the interruption of cell transport (Choi and Hu 2008). Internalization of Ag-NPs has been reported to depend on their size. Smaller Ag-NPs penetrate cell walls and membranes, while larger Ag-NPs get internalized through the endosomal pathway (Xia et al. 2006). With regard to these basic mechanisms, the whole processes have been defined by many researchers. The mechanisms have been described in terms of three major cellular phenomena happening during their exposure: (1) oxidative stress generation, (2) DNA damage, and (3) changes in immunological factors such as cytokine production. Uptake of Ag-NPs can induce generation of ROS at higher levels, which results in oxidative stress and genotoxic effects. Induction of ROS proceeds toward disruption of flux of ions and electrons across the mitochondrial membrane, leading to either apoptosis or necrosis (AshaRani et al. 2009; Arora et al. 2008). The ROS induction, however, varies according to the physiochemical properties of the Ag-NPs.

As far as genotoxicity induced by Ag-NPs is concerned, the toxic effects are induced by DNA damage, as shown in the case of IMR90 human lung fibroblasts and U251 human glioblastoma cells, increasing ROS production, or diminishing energy production through depletion of ATP generation (Hsin et al. 2008). Moreover, direct DNA damage has also been reported to be caused by Ag-NPs themselves

(Cha et al. 2008; Kumari et al. 2009). Direct damage has been shown in the case of mouse embryonic and fibroblast cells, where the damage was due to the effects of increased expression in DNA repair proteins (Rad51 and H2AX) and dysregulation of p53 (Ahamed et al. 2008). Apart from this, the mechanism of Ag-NP cytotoxicity has also been reported to be due to changes in immunological responses. Ag-NPs have been reported to elicit both stimulatory and suppressive effects on the production of cytokines associated with the inflammatory response, which were found to be dependent on physiological parameters such as size, dose, and cell types. Reports have described enhanced production of proinflammatory response mediators (tumor necrosis factor (TNF)-α, macrophage inflammatory protein (MIP)-2, and interleukin (IL)-1β) (Carlson et al. 2008) and increases in IL-1β, IL-6, IL-8, and TNF-α in human epidermal cells (Greulich et al. 2009).

Though in vitro studies have provided detailed information, in vivo studies have verified the toxicity of Ag-NPs with regard to their exposure and organism basis. Acute effects of Ag-NPs on the circulatory system, due to their ingestion or inhalation, have been reported (Sung et al. 2009). Mice exposed to Ag-NPs have shown platelet aggregation (Shrivastava et al. 2009). Ag-NPs have been shown to be accumulated in the mouse liver after exposure (Takenaka et al. 2001). Histopathological analysis of the liver and bile duct have revealed vacuolization and hepatic focal necrosis, hyperplasia of bile ducts, increased infiltration of inflammatory cells, and dilation of central veins (Kim et al. 2008). At the gene level, the genes responsible for apoptosis and inflammation pathways have also been found to be in upregulation on Ag-NP exposure (Cha et al. 2008). Toxicity of Ag-NPs has also been reported in an embryonic zebrafish model. The heart rate, mortality rate, and hatching rate were reported to be significantly affected by exposure to Ag-NPs, in a dose-dependent manner (Verma et al. 2018). Changes in morphology such as abnormal organ formation, pericardial edema, and slow development have also been reported (Verma et al. 2018).

In brief, the mechanism of toxicity of Ag-NPs has been defined with respect to both in vitro and in vivo models; however, the detailed understanding has come mostly from in vitro studies. In vivo studies have illuminated the detail, but it needs to be explored in more intensive and molecular ways.

Similarly, the cytotoxic effects of ZnO-NPs have also been a matter of discussion with regard to extensive studies and industrial production of them. The toxicity of ZnO-NPs has been discussed in the frames of both in vitro and in vivo studies. Knowledge about toxicity in in vitro models has been obtained on a large scale in each and every type of cell line. The cytotoxicity of Ag-NPs and ZnO-NPs has been determined by different groups, by measuring morphological changes as well as survivability in different cell lines and in vivo models such as zebrafish, as shown in Figs. 6.6 and 6.7. Cytotoxicity screening in BEAS-2B cells and RAW264.7 murine macrophages has shown induction of intracellular Ca^{2+} flux, lowering of the mitochondrial membrane potential, and loss of membrane integrity.

Uptake has been reported to occur via the lysosomal pathway (Verma et al. 2018). Similarly, A549 cell exposure to ZnO-NPs has revealed induced toxicity through ROS generation, oxidative stress, and activation of caspase-3 and caspase-9 in a

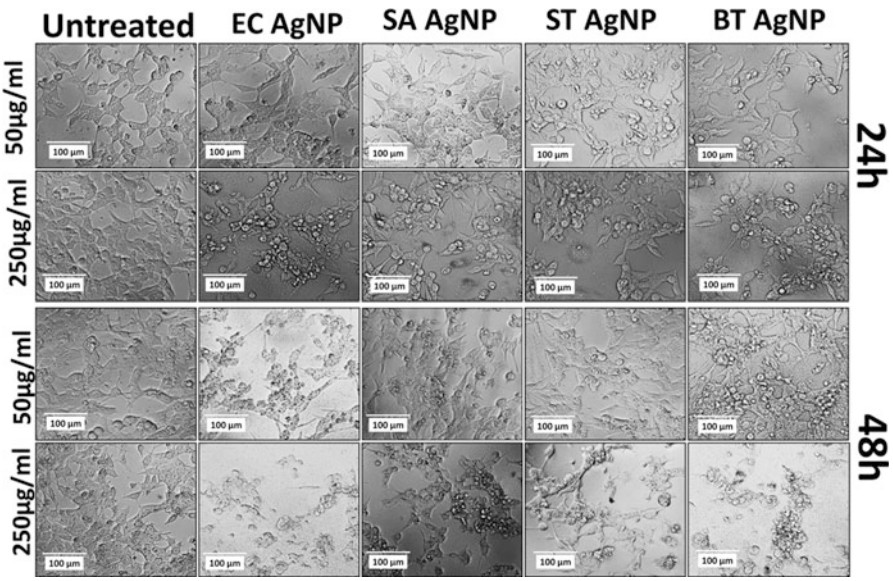

Fig. 6.6 Cytotoxicity of silver nanoparticles (*NPs*): morphology analysis of HCT116 colon cancer cells in the presence of 50 µg/ml and 250 µg/ml concentrations of Ag-NPs after treatment for 24 h and 48 h (Verma et al. 2017b). *BT Bacillus thuringiensis*, *EC Escherichia coli*, *SA Staphylococcus aureus*, *ST Salmonella typhimurium*

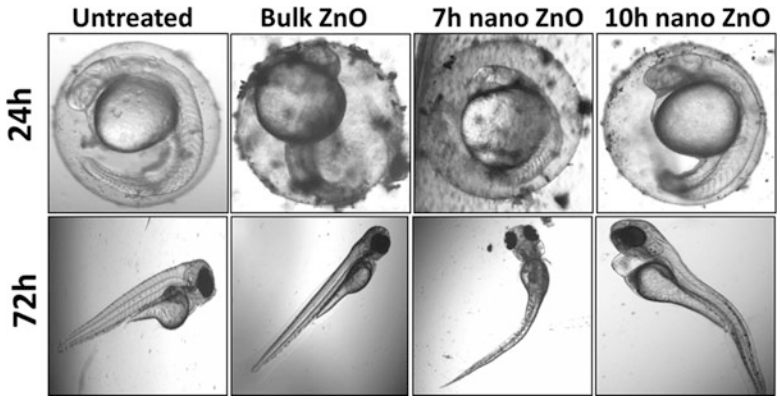

Fig. 6.7 Morphological analysis of zebrafish embryos exposed to 50 µg/ml of zinc oxide nanoparticles (*NPs*) at different times postfertilization. Significant accumulation of bulk ZnO and ZnO-NPs was observed at 24 h. At 10 h, embryos exposed to ZnO-NPs showed acute effects, with pericardial edema and notochord bending (Verma et al. 2017d)

dose- and time-dependent manner (Ahamed et al. 2011). Moreover, proteins such as bax and bc2 have been found to be upregulated and downregulated with significant effects on cells. Exposure of colon cells such as HCT116, HaCaT, and CaCo2 to ZnO has also shown significant toxicity. The immediate effects leading to cell death

included oxidative stress, decreased viability, decreased glutathione, depolarization of the inner mitochondrial membrane, apoptosis, and IL-8 release (De Berardis et al. 2010). In H1355 cells, these NPs were found to induce lactate dehydrogenase (LDH) release, depolarization of the mitochondrial membrane potential, and caspase-3 activation. In conclusion, ZnO nanorods induced apoptosis involving p53, survivin, bax/bcl-2, and caspase pathways. Thus, in view of the reports available, the mechanism of in vitro toxicity of ZnO-NPs can be sketched as a phenomenon induced by accumulation and internalization of ZnO-NPs inside cells, leading to interaction with cell membranes and their disruption. The internalized ZnO-NPs interact with the cytoplasmic content and produce oxidative stress, which, in turn, dysregulates the functionality of proteins related to cellular functions. The oxidative stress that is generated also affects the nuclear bodies, causing genotoxic effects such as DNA damage and cell cycle arrest. The detailed mechanism can be viewed in Fig. 6.8.

With respect to in vivo studies, many reports have been published showing toxicity of ZnO-NPs in in vivo models such as the mouse and zebrafish. However, a detailed understanding of in vivo toxicity is yet to be established. Intraperitoneal administration of ZnO-NPs (2.5 g/kg of body weight (bw)) was shown to result in their accumulation in the liver, spleen, lung, kidney, and heart (Li et al. 2012), while oral administration in the same dose caused their accumulation in the liver, spleen, lung, and kidney (Li et al. 2012). Dermal exposure has shown significant effects on the skin of mice (Tso et al. 2010). Moreover, toxic effects of ZnO-NPs have also been reported in zebrafish embryos. Significant changes in the hatching rate, mortality rate, and heart rate were reported, with exhibition of malfunctioned organ development (Verma et al. 2017d). Acute effects have also been observed, such as pericardial edema and notochord bending. Recent studies have shown that these effects are caused by interaction of ZnO-NPs with cell function proteins, influencing their enzymatic function and cellular physiological activities such as ROS

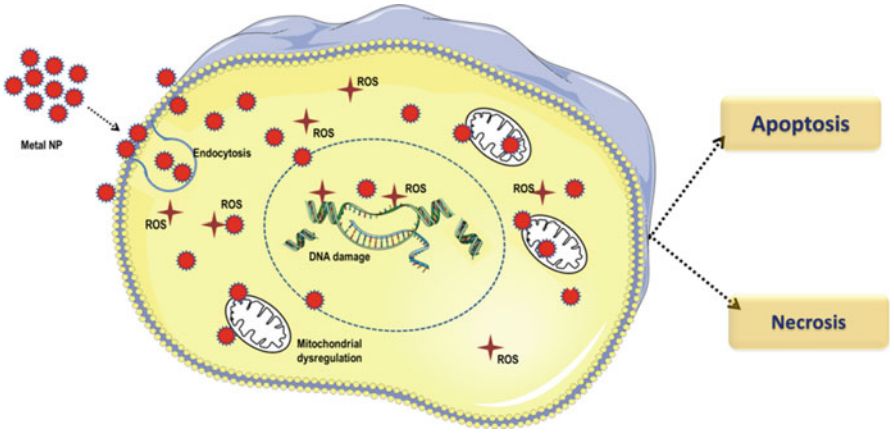

Fig. 6.8 Mechanism of cytotoxicity of metal nanoparticles (*NPs*). *ROS* reactive oxygen species

regulation, apoptosis, and necrosis. In view of these reports, the in vivo toxicity can be described as an effect of dysregulated expression of ROS production, leading to greater apoptosis and other cell death–related phenomena.

6.4 Conclusion

Advancements in nanotechnology have drawn interest from the whole scientific community toward the implications in different aspects. The involvement of industry has increased the production of nanomaterials, especially metal and metal oxide nanoparticles, in leaps and bounds. This extensive production has drawn the attention of the community toward biocompatible and green synthesis of these nanoparticles, which has been achieved by the use of different approaches such as high-energy ball milling, and plant and biological agent extraction methodology. With the help of these approaches, many metal and metal oxide nanoparticles such as silver and zinc oxide nanoparticles (Ag-NPs and ZnO-NPs) have been synthesized. These green-synthesized nanoparticles have been found to exhibit significant beneficial and harmful biological effects. Their beneficial effects include antibacterial effects, and their harmful effects include toxic effects on humans and the environment. Green-synthesized nanoparticles have been shown to be beneficial in respect of their high antibacterial efficacy with biocompatibility on the same platform. Detail mechanistic study has been conducted in both respects. Antibacterial activities of metal and metal oxide nanoparticles such as Ag-NPs and ZnO-NPs has been shown in respect of elucidation of the mechanism. The basic mechanism that has been elucidated involves production of oxidative stress, followed by their internalization and cell membrane interaction. Moreover, these nanoparticles have been shown to exhibit a molecular interaction with the nucleus as well as cell proteins, constituting a effective cause of the antibacterial phenomenon. Apart from their antibacterial activities, the cytotoxicity of these nanoparticles has been a matter of concern, which has been studied in mechanistic detail in both in vitro and in vivo models. In vitro model studies have been able to illustrate the mechanism of cytotoxicity in detail; however, in vivo studies are still in progress for a clear illustration of the mechanism. Future studies will be aimed at explanation and further exploration of the mechanisms in both clinical and environmental aspects.

References

Abdul H, Sivaraj R, Venckatesh R (2014) Green synthesis and characterization of zinc oxide nanoparticles from *Ocimum basilicum* L. var. *purpurascens* Benth.-Lamiaceae leaf extract. Mater Lett 131:16–18. https://doi.org/10.1016/j.matlet.2014.05.033

Ahamed M, Karns M, Goodson M, Rowe J, Hussain SM, Schlager JJ, Hong YL (2008) DNA damage response to different surface chemistry of silver nanoparticles in mammalian cells. Toxicol Appl Pharmacol 233:404–410. https://doi.org/10.1016/j.taap.2008.09.015

Ahamed M, Siddiqui M, Akhtar M, Ahmad I, Pant A, Alhadlaq H (2010) Genotoxic potential of copper oxide nanoparticles in human lung epithelial cells. Biochem Biophys Res Commun 296:578–583. https://doi.org/10.1016/j.bbrc.2010.04.156

Ahamed M, Akhtar MJ, Raja M, Ahmad I, Siddiqui MKJ, AlSalhi MS, Alrokayan SA (2011) ZnO nanorod–induced apoptosis in human alveolar adenocarcinoma cells via p53, survivin and bax/bcl-2 pathways: role of oxidative stress. Nanomed Nanotechnol Biol Med 7:904–913. https://doi.org/10.1016/j.nano.2011.04.011

Ali K et al (2016) Aloe vera extract functionalized zinc oxide nanoparticles as nanoantibiotics against multi-drug resistant clinical bacterial isolates. J Colloid Interface Sci 472:145–156

Alshatwi AA, Vaiyapuri Subbarayan P, Ramesh E, Al-Hazzani AA, Alsaif MA, Alwarthan AA (2012) Al_2O_3 nanoparticles induce mitochondria-mediated cell death and upregulate the expression of signaling genes in human mesenchymal stem cells. J Biochem Mol Toxicol 26:469–476. https://doi.org/10.1002/jbt.21448

Anbuvannan M, Ramesh M, Viruthagiri G, Shanmugam N (2015a) *Anisochilus carnosus* leaf extract mediated synthesis of zinc oxide nanoparticles for antibacterial and photocatalytic activities. Mater Sci Semicond Process 39:621–628. https://doi.org/10.1016/j.mssp.2015.06.005

Anbuvannan M, Ramesh M, Viruthagiri G, Shanmugam N, Kannadasan N (2015b) Synthesis, characterization and photocatalytic activity of ZnO nanoparticles prepared by biological method. Spectrochim Acta – Part A Mol Biomol Spectrosc 143:304–308. https://doi.org/10.1016/j.saa.2015.01.124

Arora S, Jain J, Rajwade JM, Paknikar KM (2008) Cellular responses induced by silver nanoparticles: in vitro studies. Toxicol Lett 179:93–100. https://doi.org/10.1016/j.toxlet.2008.04.009

AshaRani P, Mun G, Hande M, Valiyaveettil S (2009) Cytotoxicity and genotoxicity of silver nanoparticles in human cells. ACS Nano 3:279–290

Astruc D, Lu F, Aranzaes JR (2005) Nanoparticles as recyclable catalysts: the frontier between homogeneous and heterogeneous catalysis. Angew Chem – Int Ed 44:7852–7872. https://doi.org/10.1002/anie.200500766

Awwad A, Salem N (2012) Green synthesis of silver nanoparticles by mulberry leaves extract. Nanosci Nanotechnol 2:125–128

Awwad AM, Salem NM, Abdeen AO (2012) Biosynthesis of silver nanoparticles using *Olea europaea* leaves extract and its antibacterial activity. Nanosci Nanotechnol 2:164–170

Azizi S, Mohamad R, Bahadoran A, Bayat S, Rahim RA, Ariff A, Saad WZ (2016) Effect of annealing temperature on antimicrobial and structural properties of bio-synthesized zinc oxide nanoparticles using flower extract of *Anchusa italica*. J Photochem Photobiol B Biol 161:441–449. https://doi.org/10.1016/j.jphotobiol.2016.06.007

Badapanda T et al (2015) Optical and dielectric study of strontium modified barium zirconium titanate ceramic prepared by high energy ball milling. J Alloys Compd 645:586–596

Baek S, Joo SH, Kumar N, Toborek M (2017) Antibacterial effect and toxicity pathways of industrial and sunscreen ZnO nanoparticles on *Escherichia coli*. J Environ Chem Eng 5:3024–3032. https://doi.org/10.1016/j.jece.2017.06.009

Bai H, Zhang Z, Guo Y, Jia W (2009) Biological synthesis of size-controlled cadmium sulfide nanoparticles using immobilized *Rhodobacter sphaeroides*. Nanoscale Res Lett 4:717–723. https://doi.org/10.1007/s11671-009-9303-0

Bankar A, Joshi B, Kumar AR, Zinjarde S (2009) Banana peel extract mediated novel route for synthesis of silver nanoparticles. Colloid Surf A Physicochem Eng Asp 368:58–63

Banumathi B, Malaikozhundan B, Vaseeharan B (2016) In vitro acaricidal activity of ethnoveterinary plants and green synthesis of zinc oxide nanoparticles against *Rhipicephalus* (*Boophilus*) *microplus*. Vet Parasitol 216:93–100. https://doi.org/10.1016/j.vetpar.2015.12.003

Bar H, Bhui DK, Sahoo GP, Sarkar P, De SP, Misra A (2009a) Green synthesis of silver nanoparticles using latex of *Jatropha curcas*. Colloids Surf A Physicochem Eng Asp 339:134–139

Bar H et al (2009b) Green synthesis of silver nanoparticles using seed extract of Jatropha curcas. Colloids Surfaces A Physicochem Eng Asp 348:212–216

Bhattacharya K, Davoren M, Boertz J, Schins RP, Hoffmann E, Dopp E (2009) Titanium dioxide nanoparticles induce oxidative stress and DNA-adduct formation but not DNA-breakage in human lung cells. Part Fibre Toxicol 6:17. https://doi.org/10.1186/1743-8977-6-17

Bisauriya R, Verma D, Goswami YC (2018) Optically important ZnS semiconductor nanoparticles synthesized using organic waste banana peel extract and their characterization. J Mater Sci Mater Electron 29:1868–1876. https://doi.org/10.1007/s10854-017-8097-6

Braydich-Stolle L, Hussain S, Schlager JJ, Hofmann MC (2005) In vitro cytotoxicity of nanoparticles in mammalian germline stem cells. Toxicol Sci 88:412–419. https://doi.org/10.1093/toxsci/kfi256

Cao H, Liu X (2010) Silver nanoparticles–modified films versus biomedical device–associated infections. Wiley Interdiscip Rev Nanomed Nanobiotechnol 2:670–684. https://doi.org/10.1002/wnan.113

Cao M, Li Z, Wang J, Ge W, Yue T, Li R, Colvin VL, Yu WW (2012) Food related applications of magnetic iron oxide nanoparticles: enzyme immobilization, protein purification, and food analysis. Trends Food Sci Technol 27:47–56. https://doi.org/10.1016/j.tifs.2012.04.003

Carlson C, Hussein SM, Schrand AM, Braydich-Stolle LK, Hess KL, Jones RL, Schlager JJ (2008) Unique cellular interaction of silver nanoparticles: size-dependent generation of reactive oxygen species. J Phys Chem B 112:13608–13619. https://doi.org/10.1021/jp712087m

Cha K, Hong HW, Choi YG, Lee MJ, Park JH, Chae HK, Ryu G, Myung H (2008) Comparison of acute responses of mice livers to short-term exposure to nano-sized or micro-sized silver particles. Biotechnol Lett 30:1893–1899. https://doi.org/10.1007/s10529-008-9786-2

Chang J, Ichihara G, Shimada Y, Tada-Oikawa S, Kuroyanagi J, Zhang B, Suzuki Y, Sehsah R, Kato M, Tanaka T, Ichihara S (2015) Copper oxide nanoparticles reduce vasculogenesis in transgenic zebrafish through down-regulation of vascular endothelial growth factor expression and induction of apoptosis. J Nanosci Nanotechnol 15:2140–2147. https://doi.org/10.1166/jnn.2015.9762

Chen L (2008) Manufactured aluminum oxide nanoparticles decrease expression of tight junction proteins in brain vasculature. J Neuroimmune Pharmacol 3:286–295. https://doi.org/10.1007/s11481-008-9131-5.Manufactured

Cho K, Wang X, Nie S, Chen ZGSD (2008) Therapeutic nanoparticles for drug delivery in cancer. Clin Cancer Res 14:1310–1316

Choi O, Hu Z (2008) Size dependent and reactive oxygen species related nanosilver toxicity to nitrifying bacteria. Environ Sci Technol 42:4583–4588. https://doi.org/10.1021/es703238h

Çolak H, Karaköse E (2017) Green synthesis and characterization of nanostructured ZnO thin films using *Citrus aurantifolia* (lemon) peel extract by spin-coating method. J Alloys Compd 690:658–662. https://doi.org/10.1016/j.jallcom.2016.08.090

De Berardis B, Civitelli G, Condello M, Lista P, Pozzi R, Arancia G, Meschini S (2010) Exposure to ZnO nanoparticles induces oxidative stress and cytotoxicity in human colon carcinoma cells. Toxicol Appl Pharmacol 246(3):116–127. https://doi.org/10.1016/j.taap.2010.04.012

Delcroix GJR, Jacquart M, Lemaire L, Sindji L, Franconi F, Le Jeune JJ, Montero-Menei CN (2009) Mesenchymal and neural stem cells labeled with HEDP-coated SPIO nanoparticles: in vitro characterization and migration potential in rat brain. Brain Res 1255:18–31. https://doi.org/10.1016/j.brainres.2008.12.013

Deplanche K, Macaskie LE (2008) Biorecovery of gold by *Escherichia coli* and *Desulfovibrio desulfuricans*. Biotechnol Bioeng 99:1055–1064. https://doi.org/10.1002/bit.21688

Dinesh D, Murugan K, Madhiyazhagan P, Panneerselvam C, Mahesh Kumar P, Nicoletti M, Jiang W, Benelli G, Chandramohan B, Suresh U (2015) Mosquitocidal and antibacterial activity of green-synthesized silver nanoparticles from *Aloe vera* extracts: towards an effective tool

against the malaria vector *Anopheles stephensi*? Parasitol Res 114:1519–1529. https://doi.org/10.1007/s00436-015-4336-z

Dobrucka R, Długaszewska J (2015) Biosynthesis and antibacterial activity of ZnO nanoparticles using *Trifolium pratense* flower extract. Saudi J Biol Sci 517:523. https://doi.org/10.1016/j.sjbs.2015.05.016

Dobrucka R, Długaszewska J (2016) Biosynthesis and antibacterial activity of ZnO nanoparticles using *Trifolium pratense* flower extract. Saudi J Biol Sci 23:517–523. https://doi.org/10.1016/j.sjbs.2015.05.016

Dubey SP, Lahtinen M, Sillanpaa M (2010) Green synthesis and characterization of silver and gold nanoparticles using leaf extract of *Rosa rugosa*. Colloid Surf A Physicochem Eng Asp. 364:34–41

Durán N, Marcato PD, Conti RD, Alves OL, Costa FTM, Brocchi M (2010) Potential use of silver nanoparticles on pathogenic bacteria, their toxicity and possible mechanisms of action. J Braz Chem Soc 21:949–959. https://doi.org/10.1590/S0103-50532010000600002

Dwivedi AD, Gopal K (2010) Biosynthesis of silver and gold nanoparticles using *Chenopodium album* leaf extract. Colloids Surfaces A Physicochem Eng Asp 369:27–33

Elumalai K, Velmurugan S (2015) Green synthesis, characterization and antimicrobial activities of zinc oxide nanoparticles from the leaf extract of *Azadirachta indica* (L.). Appl Surf Sci 345:329–336

Elumalai K, Velmurugan S, Ravi S, Kathiravan V, Adaikala Raj G (2015a) Bio-approach: plant mediated synthesis of ZnO nanoparticles and their catalytic reduction of methylene blue and antimicrobial activity. Adv Powder Technol 26:1639–1651. https://doi.org/10.1016/j.apt.2015.09.008

Elumalai K, Velmurugan S, Ravi S, Kathiravan V, Ashokkumar S (2015b) Green synthesis of zinc oxide nanoparticles using *Moringa oleifera* leaf extract and evaluation of its antimicrobial activity. Spectrochim Acta – Part A Mol Biomol Spectrosc 143:158–164. https://doi.org/10.1016/j.saa.2015.02.011

Emeka EE, Ojiefoh OC, Aleruchi C, Hassan LA, Christiana OM, Rebecca M, Dare EO, Temitope AE (2014) Evaluation of antibacterial activities of silver nanoparticles green-synthesized using pineapple leaf (*Ananas comosus*). Micron 57:1–5. https://doi.org/10.1016/j.micron.2013.09.003

Fatimah I, Pradita RY, Nurfalinda A (2016) Plant extract mediated of ZnO nanoparticles by using ethanol extract of *Mimosa pudica* leaves and coffee powder. Procedia Eng 148:43–48. https://doi.org/10.1016/j.proeng.2016.06.483

Fu L, Fu Z (2015) *Plectranthus amboinicus* leaf extract–assisted biosynthesis of ZnO nanoparticles and their photocatalytic activity. Ceram Int 41:2492–2496. https://doi.org/10.1016/j.ceramint.2014.10.069

Fu M, Li Q, Sun D, Lu Y, He N, Deng X, Wang H, Huang J (2006) Rapid preparation process of silver nanoparticles by bioreduction and their characterizations. Chinese J Chem Eng 14:114–117. https://doi.org/10.1016/S1004-9541(06)60046-3

Gade A, Gaikwad S, Duran N, Rai M (2013) Green synthesis of silver nanoparticles by *Phoma glomerata*. Micron 59:52–59. https://doi.org/10.1016/j.micron.2013.12.005

Giri PK et al (2007) Correlation between microstructure and optical properties of ZnO nanoparticles synthesized by ball milling. J Appl Phys 102:1–8

Goyal A, Soni PR (2018) Functionally graded nanocrystalline silicon powders by mechanical alloying. Mater Lett 214:111–114

Greulich C, Kittler S, Epple M, Muhr G, Koller M (2009) Studies on the biocompatibility and the interaction of silver nanoparticles with human mesenchymal stem cells (hMSCs). Langenbecks Arch Surg 394(3):495–502. https://doi.org/10.1007/s00423-009-0472-1

Guan R, Kang T, Lu F, Zhang Z, Shen H, Liu M (2012) Cytotoxicity, oxidative stress, and genotoxicity in human hepatocyte and embryonic kidney cells exposed to ZnO nanoparticles. Nanoscale Res Lett 7:602. https://doi.org/10.1186/1556-276X-7-602

Hassan SSM, Abdel-Shafy HI, Mansour MSM (2016) Removal of pharmaceutical compounds from urine via chemical coagulation by green synthesized ZnO-nanoparticles followed by microfiltration for safe reuse. Arab J Chem. https://doi.org/10.1016/j.arabjc.2016.04.009

Hsin YH, Chen CF, Huang S, Shih TS, Lai PS, Chueh PJ (2008) The apoptotic effect of nanosilver is mediated by a ROS- and JNK-dependent mechanism involving the mitochondrial pathway in NIH3T3 cells. Toxicol Lett 179:130–139. https://doi.org/10.1016/j.toxlet.2008.04.015

Huang J, Li Q, Sun D, Lu Y, Su Y, Yang X, Wang H, Wang Y, Shao W, He N, Hong J, Chen C (2007) Biosynthesis of silver and gold nanoparticles by novel sundried *Cinnamomum camphora* leaf. Nanotechnology 18:105104. https://doi.org/10.1088/0957-4484/18/10/105104

Hussain SM, Hess KL, Gearhart JM, Geiss KT, Schlager JJ (2005) In vitro toxicity of nanoparticles in BRL 3A rat liver cells. Toxicol Vitr 19:975–983. https://doi.org/10.1016/j.tiv.2005.06.034

Hussain SM, Javorina AK, Schrand AM, Duhart HMHM, Ali SF, Schlager JJ (2006) The interaction of manganese nanoparticles with PC-12 cells induces dopamine depletion. Toxicol Sci 92:456–463. https://doi.org/10.1093/toxsci/kfl020

Husseiny MI, El-Aziz MA, Badr Y, Mahmond MA (2007) Biosynthesis of gold nanoparticles using *Pseudomonas aeruginosa*. Spectrochim Acta A 67:1003–1006

Jeng HA, Swanson J (2006) Toxicity of metal oxide nanoparticles in mammalian cells. J Env Sci Heal A Tox Hazard Subst Env Eng 41:2699–2711. https://doi.org/10.1080/10934520600966177

Joerger R, Klaus T, Granqvist CG (2000) Biologically produced silver–carbon composite materials for optically functional thin-film coatings. Adv Mater 12:407–409. https://doi.org/10.1002/(SICI)1521-4095(200003)12:6<407::AID-ADMA407>3.0.CO;2-O

Jovanović B, Ji T, Palić D (2011) Gene expression of zebrafish embryos exposed to titanium dioxide nanoparticles and hydroxylated fullerenes. Ecotoxicol Environ Saf 74:1518–1525. https://doi.org/10.1016/j.ecoenv.2011.04.012

Karnan T, Selvakumar SAS (2016) Biosynthesis of ZnO nanoparticles using rambutan (*Nephelium lappaceum* L.) peel extract and their photocatalytic activity on methyl orange dye. J Mol Struct 1125:358–365

Khodashenas B, Ghorbani HR (2014) Synthesis of silver nanoparticles with different shapes. Arab J Chem. https://doi.org/10.1016/j.arabjc.2014.12.014

Kim JS, Kuk E, Yu KN, Kim JH, Park SJ, Lee HJ, Kim SH, Park YK, Park YH, Hwang CY, Kim YK, Lee YS, Jeong DH, Cho MH (2007) Antimicrobial effects of silver nanoparticles. Nanomedicine 3(1):95–101. https://doi.org/10.1016/j.nano.2006.12.001

Kim YS, Kim JS, Cho HS, Rha DS, Kim JM, Park JD, Choi BS, Lim R, Chang HK, Chung YH, Kwon IH, Jeong J, Han BS, Yu IJ (2008) Twenty-eight-day oral toxicity, genotoxicity, and gender-related tissue distribution of silver nanoparticles in Sprague–Dawley rats. Inhal Toxicol 20:575–583. https://doi.org/10.1080/08958370701874663

Kim SH, Lee HS, Ryu DS, Choi SJ, Lee DS (2011) Antibacterial activity of silver-nanoparticles against *Staphylococcus aureus* and *Escherichia coli*. Korean J Microbiol Biotechnol 39:77–85

Kon K, Rai M (2013) Metallic nanoparticles: mechanism of antibacterial action and influencing factors. J Comp Clin Pathol Res 2:160–174

Kouvaris P et al (2012) Green synthesis and characterization of silver nanoparticles produced using *Arbutus Unedo* leaf extract. Mater Lett 76:18–20

Krishnaraj C et al (2010) Synthesis of silver nanoparticles using *Acalypha indica* leaf extracts and its antimicrobial activity against water borne pathogens. Colloids Surf B Biointerfaces 76:50–56

Kumar PPNV, Shameem U, Kollu P, Kalyani RL, Pammi SVN (2015) Green synthesis of copper oxide nanoparticles using *Aloe vera* leaf extract and its antibacterial activity against fish bacterial pathogens. BioNanoScience 5:135–139. https://doi.org/10.1007/s12668-015-0171-z

Kumari M, Mukherjee A, Chandrasekaran N (2009) Genotoxicity of silver nanoparticles in *Allium cepa*. Sci Total Environ 407:5243–5246. https://doi.org/10.1016/j.scitotenv.2009.06.024

Lam C-W, James JT, McCluskey R, Hunter RL (2004) Pulmonary toxicity of single-wall carbon nanotubes in mice 7 and 90 days after intratracheal instillation. Toxicol Sci 77:126–134. https://doi.org/10.1093/toxsci/kfg243

Lee JH, Jang JT, Choi JS, Moon SH, Noh SH, Kim JW, Kim JG, Kim IS, Park KI, Cheon J (2011) Exchange-coupled magnetic nanoparticles for efficient heat induction. Nat Nanotechnol 6:418–422. https://doi.org/10.1038/nnano.2011.95

Lengke MF, Fleet ME, Southam G (2007) Biosynthesis of silver nanoparticles by filamentous cyanobacteria from a silver(I) nitrate complex. Langmuir 23:2694–2699. https://doi.org/10.1021/la0613124

Li CH, Shen CC, Cheng YW, Huang SH, Wu CC, Kao CC, Liao JW, Kang JJ (2012) Organ biodistribution, clearance, and genotoxicity of orally administered zinc oxide nanoparticles in mice. Nanotoxicology 6:746–756. https://doi.org/10.3109/17435390.2011.620717

Lin S, Zhao Y, Xia T, Meng H, Ji Z, Liu R, George S, Xiong S, Wang X, Zhang H, Pokhrel S, Mädler L, Damoiseaux R, Lin S, Nel AE (2011) High content screening in zebrafish speeds up hazard ranking of transition metal oxide nanoparticles. ACS Nano 5:7284–7295. https://doi.org/10.1021/nn202116p

Logeswari P, Silambarasan S, Abraham J (2015) Synthesis of silver nanoparticles using plants extract and analysis of their antimicrobial property. J Saudi Chem Soc 19:311–317

Loo YY, Chieng BW, Nishibuchi M, Radu S (2012) Synthesis of silver nanoparticles by using tea leaf extract from *Camellia sinensis*. Int J Nanomedicine 7:4263–4267

Madan HR, Sharma SC, Udayabhanu SD, Vidya YS, Nagabhushana H, Rajanaik H, Anantharaju KS, Prashantha SC, Sadananda Maiya P (2016) Facile green fabrication of nanostructure ZnO plates, bullets, flower, prismatic tip, closed pine cone: their antibacterial, antioxidant, photoluminescent and photocatalytic properties. Spectrochim Acta – Part A Mol Biomol Spectrosc 152:404–416. https://doi.org/10.1016/j.saa.2015.07.067

Mandal D, Bolander M, Mukhopadhyay D, Sarkar G, Mukherjee P (2006) The use of microorganisms for the formation of metal nanoparticles and their application. Appl Microbiol Biotechnol 69:485–492. https://doi.org/10.1007/s00253-005-0179-3

Manke A, Wang L, Rojanasakul Y (2013) Mechanisms of nanoparticle-induced oxidative stress and toxicity. Biomed Res Int 2013:1–15 942916. https://doi.org/10.1155/2013/942916

Marambio-Jones C, Hoek EMV (2010) A review of the antibacterial effects of silver nanomaterials and potential implications for human health and the environment. J Nanopart Res 12:1531–1551. https://doi.org/10.1007/s11051-010-9900-y

Mariselvam R, Ranjitsingh AJA, Usha Raja Nanthini A, Kalirajan K, Padmalatha C, Mosae Selvakumar P (2014) Green synthesis of silver nanoparticles from the extract of the inflorescence of *Cocos nucifera* (family: Arecaceae) for enhanced antibacterial activity. Spectrochim Acta – Part A Mol Biomol Spectrosc 129:537–541. https://doi.org/10.1016/j.saa.2014.03.066

McQuillan JS, Groenaga Infante H, Stokes E, Shaw AM (2012) Silver nanoparticle enhanced silver ion stress response in *Escherichia coli* K12. Nanotoxicology 6:857–866. https://doi.org/10.3109/17435390.2011.626532

Miri A, Sarani M, Rezazade Bazaz M, Darroudi M (2015) Plant-mediated biosynthesis of silver nanoparticles using *Prosopis farcta* extract and its antibacterial properties. Spectrochim Acta – Part A Mol Biomol Spectrosc 141:287–291. https://doi.org/10.1016/j.saa.2015.01.024

Mirzajani F, Ghassempour A, Aliahmadi A, Ali Esmaeili M (2011) Antibacterial effect of silver nanoparticles on *Staphylococcus aureus*. Res Microbiol 162:542–549. https://doi.org/10.1016/j.resmic.2011.04.009

Mittal AK, Kaler A, Mulay AV, Banerjee UC (2013) Synthesis of gold nanoparticles using whole cells of *Geotrichum candidum*. J Nanopart 2013:150414. https://doi.org/10.1155/2013/150414

Momeni SS, Nasrollahzadeh M, Rustaiyan A (2016) Green synthesis of the cu/ZnO nanoparticles mediated by Euphorbia prolifera leaf extract and investigation of their catalytic activity. J Colloid Interface Sci 472:173–179

Mukunthan KS, Balaji S (2012) Cashew apple juice (*Anacardium occidentale* L.) speeds up the synthesis of silver nanoparticles. Int J Green Nanotechnol 4(2):71–79. https://doi.org/10.1080/19430892.2012.676900

Muñoz JE, Cervantes J, Esparza R, Rosas G (2007) Iron nanoparticles produced by high-energy ball milling. J Nanopart Res 9:945–950

Murty BS, Ranganathan S (1998) Novel materials synthesis by mechanical alloying/milling. Metall Rev 43:101–141

Nagajyothi PC, Cha SJ, Yang IJ, Sreekanth TVM, Kim KJ, Shin HM (2015) Antioxidant and anti-inflammatory activities of zinc oxide nanoparticles synthesized using *Polygala tenuifolia* root extract. J Photochem Photobiol B-Biology 146:10–17. https://doi.org/10.1016/j.jphotobiol.2015.02.008

Nair B, Pradeep T (2002) Coalescence of nanoclusters and formation of submicron crystallites assisted by *Lactobacillus* strains. Cryst Growth Des 2:293–298. https://doi.org/10.1021/cg0255164

Nangia Y, Wangoo N, Goyal N, Shekhawat G, Suri CR (2009) A novel bacterial isolate *Stenotrophomonas maltophilia* as living factory for synthesis of gold nanoparticles. Microb Cell Factories 8:39. https://doi.org/10.1186/1475-2859-8-39

Naqvi S, Samim M, Abdin MZ, Ahmed FJ, Maitra AN, Prashant CK, Dinda AK (2010) Concentration-dependent toxicity of iron oxide nanoparticles mediated by increased oxidative stress. Int J Nanomedicine 5:983–989. https://doi.org/10.2147/IJN.S13244

Osman IF, Baumgartner A, Cemeli E, Fletcher JN, Anderson D (2010) Genotoxicity and cytotoxicity of zinc oxide and titanium dioxide in HEp-2 cells. Nanomedicine 5:1193–1203. https://doi.org/10.2217/nnm.10.52

Parashar V, Parashar R, Sharma B, Pandey AC (2009) Parthenium leaf extract mediated synthesis of silver nanoparticles: a novel approach towards weed utilization. Dig J Nanomater Biost 4:45–50

Parashar SKS, Murty BS, Repp S, Weber S, Erdem E (2012) Investigation of intrinsic defects in core-shell structured ZnO nanocrystals. J Appl Phys 111

Parikh RY, Singh S, Prasad BLV, Patole MS, Sastry M, Schouche YS (2008) Extracellular synthesis of crystalline silver nanoparticles and molecular evidence of silver resistance from *Morganella* sp.: towards understanding biochemical synthesis mechanism. Chembiochem 9:1415–1422. https://doi.org/10.1002/cbic.200700592

Park E, Maaza M (2015) Green synthesis of ZnO nanoparticles by *Aspalathus linearis*: structural & optical properties. J Alloys Compd 646:425–430. https://doi.org/10.1016/j.jallcom.2015.05.242

Philip D (2010) Green synthesis of gold and silver nanoparticles using *Hibiscus rosa sinensis*. Phys E 42:1417–1424. https://doi.org/10.1016/j.physe.2009.11.081

Poopathi S, De Britto LJ, Praba VL, Mani C, Praveen M (2015) Synthesis of silver nanoparticles from *Azadirachta indica*—a most effective method for mosquito control. Environ Sci Pollut Res 22:2956–2963. https://doi.org/10.1007/s11356-014-3560-x

Porada S, Sales BB, Hamelers HVM, Biesheuvel PM, Kar S, Bindal RC, Tewari PK, Shannon MA, Bohn PW, Elimelech M, Georgiadis JG, Marinas BJ, Mayes AM, Fornasiero F, Park HG, Holt JK, Stadermann M, Grigoropoulos CP, Noy A, Bakajin O, Humplik T, Lee J, O'hern SC, Fellman BA, Baig MA, Hassan SF, Atieh MA, Rahman F, Laoui T, Karnik R, Savage N, Diallo MS, Majumder M, Chopra N, Andrews R, Hinds BJ (2008) Nanomaterials and water purification: opportunities and challenges. Nature 7:1613–1618

Prakasha P, Gnanaprakasama P, Emmanuela R, Arokiyarajb S, Saravananc M (2013) Green synthesis of silver nanoparticles from leaf extract of *Mimusops elengi*, Linn. for enhanced antibacterial activity against multi drug resistant clinical isolates. Colloids Surfaces B Biointerfaces 108:255–259

Radziun E, Dudkiewicz Wilczyńska J, Książek I, Nowak K, Anuszewska EL, Kunicki A, Olszyna A, Zabkowski T (2011) Assessment of the cytotoxicity of aluminium oxide nanoparticles on selected mammalian cells. Toxicol In Vitro 25(8):1694–1700. https://doi.org/10.1016/j.tiv.2011.07.010

Raghupathi KR, Koodali RT, Manna AC (2011) Size-dependent bacterial growth inhibition and mechanism of antibacterial activity of zinc oxide nanoparticles. Langmuir Acs J Surfaces Colloids 27:4020–4028

Ramesh P, Kokila T, Geetha D (2015) Plant mediated green synthesis and antibacterial activity of silver nanoparticles using *Emblica officinalis* fruit extract. Spectrochim Acta A Mol Biomol Spectrosc 142:339–343. https://doi.org/10.1016/j.saa.2015.01.062

Reidy B, Haase A, Luch A, Dawson KA, Lynch I (2013) Mechanisms of silver nanoparticle release, transformation and toxicity: a critical review of current knowledge and recommendations for future studies and applications. Materials (Basel) 6:2295–2350. https://doi.org/10.3390/ma6062295

Saifuddin N, Wong CW, Nur Yasumira A (2009) Rapid biosynthesis of silver nanoparticles using culture supernatant of bacteria with microwave irradiation. E-J Chem 6:61–70. https://doi.org/10.1155/2009/734264

Saxena A, Tripathi R, Zafar F, Singh P (2012) Green synthesis of silver nanoparticles using aqueous solution of *Ficus benghalensis* leaf extract and characterization of their antimicrobial activity. Mater Lett 67:91–94

Schneider JJ, Hoffmann RC, Engstler J, Klyszcz A, Erdem E, Jakes P, Eichel RA, Pitta-Bauermann-L, Bill J (2010) Synthesis, characterization, defect chemistry, and FET properties of microwave-derived nanoscaled zinc oxide. Chem Mater 22:2203–2212. https://doi.org/10.1021/cm902300q

Shankar SS, Ahmad A, Sastry M (2003) *Geranium* leaf assisted biosynthesis of silver nanoparticles. Biotechnol Prog 19:1627–1631. https://doi.org/10.1021/bp034070w

Sharma SC (2016) ZnO nano-flowers from *Carica papaya* milk: degradation of alizarin red-S dye and antibacterial activity against *Pseudomonas aeruginosa* and *Staphylococcus aureus*. Optik (Stuttg) 127:6498–6512. https://doi.org/10.1016/j.ijleo.2016.04.036

Sharma D, Sabela MI, Kanchi S, Mdluli PS, Singh G, Stenström TA, Bisetty K (2016) Biosynthesis of ZnO nanoparticles using *Jacaranda mimosifolia* flowers extract: synergistic antibacterial activity and molecular simulated facet specific adsorption studies. J Photochem Photobiol B Biol 162:199–207. https://doi.org/10.1016/j.jphotobiol.2016.06.043

Shivaji S, Madhu S, Singh S (2011) Extracellular synthesis of antibacterial silver nanoparticles using psychrophilic bacteria. Process Biochem 46:1800–1807. https://doi.org/10.1016/j.procbio.2011.06.008

Shrivastava S, Bera T, Singh SK, Singh G, Ramachandrarao P, Dash D (2009) Characterization of antiplatelet properties of silver nanoparticles. ACS Nano 3:1357–1364. https://doi.org/10.1021/nn900277t

Silambarasan S, Jayanthi A (2013) Biosynthesis of silver nanoparticles using *Pseudomonas fluorescens*. Res J Biotechnol 8:71–75

Song JY, Kim BS (2008) Biological synthesis of bimetallic Au/Ag nanoparticles using persimmon (*Diopyros kaki*) leaf extract. Korean J Chem Eng 25:808–811. https://doi.org/10.1007/s11814-008-0133-z

Song JY, Kim BS (2010) Rapid biological synthesis of silver nanoparticles using plant leaf extracts. Bioprocess Biosyst Eng 32(1):79–84. https://doi.org/10.1007/s00449-008-0224-6

Song JY, Jang HK, Kim BS (2009) Biological synthesis of gold nanoparticles using *Magnolia kobus* and *Diopyros kaki* leaf extracts. Process Biochem 44:1133–1138. https://doi.org/10.1016/j.procbio.2009.06.005

Sung JH, Ji JH, Park JD, Yoon JU, Kim DS, Jeon KS, Song MY, Jeong J, Han BS, Han JH, Chung YH, Chang HK, Lee JH, Cho MH, Kelman BJ, Yu IJ (2009) Subchronic inhalation toxicity of silver nanoparticles. Toxicol Sci 108:452–461

Takenaka S, Karg E, Roth C, Schulz H, Ziesenis A, Heinzmann U, Schramel P, Heyder J (2001) Pulmonary and systemic distribution of inhaled ultrafine silver particles in rats. Environ Health Perspect 109:547–551. https://doi.org/10.1289/ehp.01109s4547

Tso C, Zhung C, Shih Y, Tseng Y-M, Wu S, Doong R (2010) Stability of metal oxide nanoparticles in aqueous solutions. Water Sci Technol 61:127–133. https://doi.org/10.2166/wst.2010.787

Verma A, Stellacci F (2010) Effect of surface properties on nanoparticle–cell interactions. Small 6:12–21. https://doi.org/10.1002/smll.200901158

Verma SK, Jha E, Panda PK, Das JK, Thirumurugan A, Suar M, Parashar S (2017) Molecular aspects of core–shell intrinsic defect induced enhanced antibacterial activity of ZnO nanocrystals. Nanomedicine 13:43–68. https://doi.org/10.2217/nnm-2017-0237

Verma SK, Jha E, Sahoo B, Panda PK, Thirumurugan A, Parashar SKS, Suar M (2017b) Mechanistic insight into the rapid one-step facile biofabrication of antibacterial silver nanoparticles from bacterial release and their biogenicity and concentration-dependent in vitro cytotoxicity to colon cells. RSC Adv 7:40034–40045. https://doi.org/10.1039/c7ra05943d

Verma SK, Jha E, Sahoo B, Panda PK, Thirumurugan A, Parashar SKS, Suar M (2017c) Mechanistic insight into the rapid one-step facile biofabrication of antibacterial silver nanoparticles from bacterial release and their biogenicity and concentration-dependent in vitro cytotoxicity to colon cells. RSC Adv 7:40034–40045. https://doi.org/10.1039/C7RA05943D

Verma SK, Panda PK, Jha E, Suar M, Parashar SKS (2017d) Altered physiochemical properties in industrially synthesized ZnO nanoparticles regulate oxidative stress; induce in vivo cytotoxicity in embryonic zebrafish by apoptosis. Sci Rep 7:13909. https://doi.org/10.1038/s41598-017-14039-y

Verma SK, Jha E, Panda PK, Mishra A, Thirumurugan A, Das B, Parashar SKS, Suar M (2018) Rapid novel facile biosynthesized silver nanoparticles from bacterial release induce biogenicity and concentration dependent in vivo cytotoxicity with embryonic zebrafish-A mechanistic insight. Toxicol Sci 161:125–138. https://doi.org/10.1093/toxsci/kfx204

Vidhu VK, Aromal SA, Philip D (2011) Green synthesis of silver nanoparticles using *Macrotyloma uniflorum*. Spectrochim Acta – Part A Mol Biomol Spectrosc 83:392–397. https://doi.org/10.1016/j.saa.2011.08.051

Waghmare SS, Deshmukh AM, Kulkarni SW, Oswaldo LA (2011) Biosynthesis and characterization of manganese and zinc nanoparticles. Univers J Environ Res Technol 1:64–69

Xia T, Kovochich M, Brant J, Hotze M, Sempf J, Oberley T, Sioutas C, Yeh JI, Wiesner MR, Nel AE (2006) Comparison of the abilities of ambient and manufactured nanoparticles to induce cellular toxicity according to an oxidative stress paradigm. Nano Lett 6:1794–1807. https://doi.org/10.1021/nl061025k

Yong P, Rowson NA, Farr JPG, Harris IR, Macaskie LE (2002) Bioreduction and biocrystallization of palladium by *Desulfovibrio desulfuricans* NCIMB 8307. Biotechnol Bioeng 80:369–379. https://doi.org/10.1002/bit.10369

Zijlstra P, Chon JWM, Gu M (2009) Five-dimensional optical recording mediated by surface plasmons in gold nanorods. Nature 459:410–413. https://doi.org/10.1038/nature08053

Chapter 7
Surface Plasmon-Based Nanomaterials as Photocatalyst

Mohammad Ehtisham Khan and Moo Hwan Cho

Contents

Abstract In recent era, plasmonic photocatalysts have facilitated rapid progress in improving the photocatalytic efficiency under visible light irradiation, increasing the prospect of using sunlight for environmental and energy applications, such as wastewater treatment, water splitting, and carbon dioxide reduction. Plasmonic photocatalysis makes use of noble metal NPs dispersed in semiconductor photocatalysts and has two prominent features, a Schottky junction and localized SPR effect. With the advances in fundamental and experimental studies on plasmon-mediated photocatalysis, the rational design and synthesis of metal/semiconductor and carbon-based hybrid nanostructures as photocatalysts have been realized. This chapter highlights a recently reported and easy methodology for the fabrication of SPR-based materials and its real developments in plasmon-mediated photocatalytic mechanisms, such as Schottky junctions, direct electron transfer, enhanced local electric field, plasmon resonant energy transfer, and scattering and heating effects. In addition, this chapter also summarizes the factors, size, shape, geometry, loading, and composition of plasmonic metal, as well as the nanostructure and properties of

M. E. Khan (✉) · M. H. Cho (✉)
Department of Chemical Engineering and Technology, BCC, Jazan University, Jazan, Saudi Arabia

Mu. Naushad et al. (eds.), *Advanced Nanostructured Materials for Environmental Remediation*, Environmental Chemistry for a Sustainable World 25,
https://doi.org/10.1007/978-3-030-04477-0_7

semiconductors that mainly affect the photodegradation of dyes. Finally, a perspective on future directions within this rich field of research is provided.

Keywords Metal nanoparticles · Au and Ag · Surface plasmon resonance · Visible light · Photocatalysis · Water treatment

7.1 Introduction

Visible light sources are a clean, renewable, and abundant energy alternative to fossil fuels (Liu et al. 2011). In addition to direct light-to-electricity conversion, photocatalysis provides an alternative method for storing energy in chemical bonds that can be released later without producing harmful by-products (Zeitler 2009). This is a kind of green chemical synthesis because of its abundance and environment-friendly nature. Considerable efforts have been made to use visible light as a driving force for chemical synthesis processes. Nevertheless, the potential applications of photochemical reactions have been limited by the inability of most organic molecules to absorb light in the visible range of the spectrum (Lang et al. 2014). Consequently, recent reviews on general organic photocatalysis highlighted the design of highly efficient photocatalysts to bring significant progress in an easy, scalable, and biogenic synthesis (Lang et al. 2014; Daniel and Astruc 2004; Wang et al. 2012a). Plasmonic photocatalysis has recently come into focus as a very promising technology for the high-performance photodegradation of harmful dyes (Wang et al. 2012a; Nan Zhang et al. 2012; Linic et al. 2011). This process involves the dispersal of noble metal nanoparticles (mostly Au and Ag, tens to hundreds of nanometers in size) into semiconductor photocatalysts and obtain drastic enhancement of photoreactivity under the visible light irradiation (Linic et al. 2011; Yu et al. 2011; Nan Zhang et al. 2014). Extensive work has been made to develop effective photocatalysts for the degradation of organic harmful pollutants (Ahmad et al. 2015). Dyes are generally toxic, carcinogenic, and harmful with adverse effects on human and animal health (Nan Zhang et al. 2012; Jian Long Wang and Xu 2012). Most dyes are recycled because their release into the aquatic and marine environments could be a source of severe ecological pollution (Chong et al. 2010; Yu et al. 2010). Different kinds of dyes have many applications in numerous industries, including, plastic, paper, rubber, furniture, textile, concrete, and medicine (Yu et al. 2010). Among the industries, the textile industry is the main consumer of toxic dyes. Approximately 10% of the dyes used in industry are liquidated directly into the atmosphere as a pollutant, which is ecologically unsafe and esthetically unacceptable (Lettmann et al. 2001). Based on several studies, SPR-based nanomaterials have promising applications in dye degradation for wastewater treatment. At present, the most extensively studied nanomaterials for wastewater treatment mainly include zerovalent metal nanoparticles/nanostructures and carbon-based metal nanostructures. (Mingkui Wang et al. 2010).

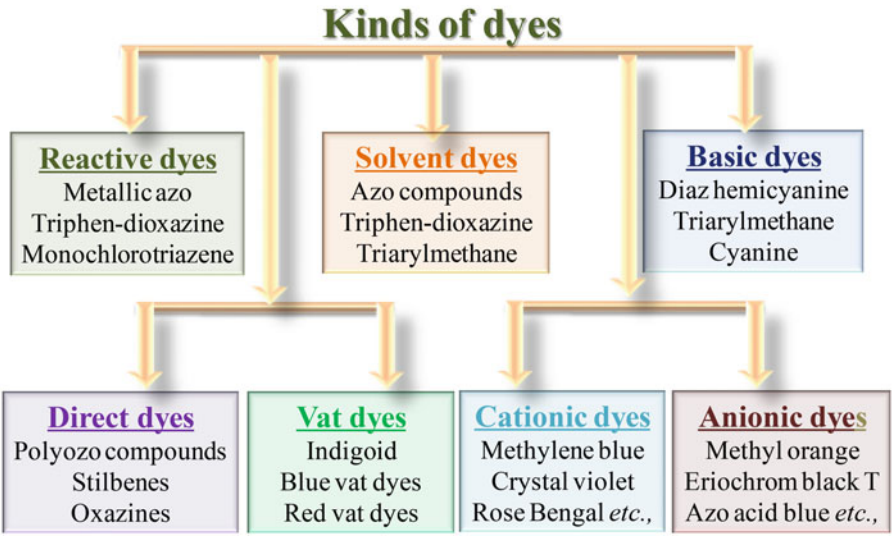

Fig. 7.1 Different category of dyes and its derivatives

Figure 7.1 represents the different categories of dyes that are openly released as waste in aqueous streams from several industries (Camarero et al. 2003; William IV et al. 2008). The direct release of enormous amounts of toxic dyes is unavoidable because the individual textile industry consumes immense amounts of water and dyes are not consumed completely by the fibers during the dyeing procedure (Muhd Julkapli et al. 2014; Jie et al. 2013). These high concentrations of dyes in effluents interfere with the dispersion of visible light in water, causing interference to photosynthesis and a decrease in gas solubility. Furthermore, artificial dyes, which contain an aromatic ring in their structure, are noxious and carcinogenic compounds (Salleh et al. 2011; He et al. 2011). Photocatalytic reactions can be classified into two types: homogeneous and heterogeneous photocatalysis. The most prominent features of the photocatalytic system are the required band gap, suitable morphology, high surface area, stability, reusability, and special SPR effect. This chapter focuses on the recent progress in the fabrication, decoration/anchoring, modification, and water treatment applications of SPR-based effect of metal NPs as photocatalysts, which provides perspectives on future water treatment developments.

7.2 Metal (Au and Ag) Nanoparticles

Noble metals, such as gold (Au), silver (Ag), platinum (Pt), and palladium (Pd), have been assessed for potential visible light applications. Particular attention on Au and AgNPs has been studied widely because of their unique optical and electronic properties together with their many applications in electronics, photonics, catalysis,

and nano-biotechnology (Daniel and Astruc 2004; Burda et al. 2005). AuNPs have also attracted remarkable attention for both heterogeneous and homogeneous visible light-induced catalysis (Haruta 2005). Recently, the localized surface plasmon resonance (LSPR) effect of nanostructured materials, e.g., Ag and AuNPs, has been applied successfully to photocatalysis under visible light irradiation and shown to be quite promising. Therefore, the present chapter deals selectively with plasmonic nanogold photocatalysis with the main focus on the following (Hashmi and Hutchings 2006):

(i) Basic concepts of the SPR effect of metal NPs.
(ii) Metal NP-based plasmonic photocatalyst preparation methods.
(iii) Recent developments in the efficient Au- and AgNP-based plasmonic photocatalysis.
(iv) Application of plasmonic photocatalysis to energy conversion processes that are driven by visible light.
(v) Possible reaction mechanisms of SPR-enhanced photocatalytic activity: In conclusion, the challenges and probable future applications will be highlighted.

7.3 Surface Plasmon Resonance Effect

Mie's theory defines the special SPR as the resonant photon-induced coherent oscillation of charges at the metal–dielectric interface that are recognized when the photon frequency matches the natural frequency of the metal surface electrons oscillating against the restoring force of their positive nuclei (Sarina et al. 2013).

When the wavelength of incident light is in the range of the SPR absorption of noble metal NPs, the electrons are excited by SPR to the conduction band (Fuku et al. 2013). For example, the resonance energy of AuNPs usually occurs in the visible range ($\lambda = 530$ nm, depending on the size, shape, and diffraction index of the medium of AuNPs). The interaction between the resonant photons and the surface electrons results in a high absorption coefficient of photons in resonance with the plasmon excitation and capacitive coupling between clusters of plasmonic AuNPs. Figure 7.2 presents the process of the displacement of electron density. The columbic restoring force that is caused by oscillations in the NP is established, and the resonance between the oscillations and incident light is known as SPR (Kelly et al. 2003).

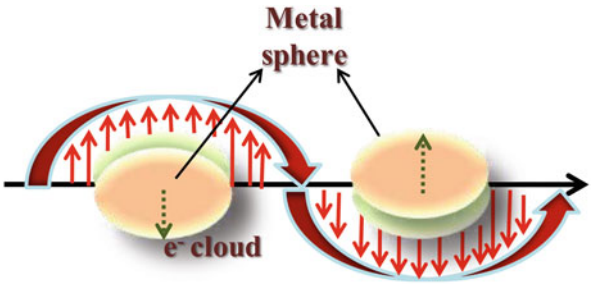

Fig. 7.2 Schematic diagram of SPR in small spherical metallic NPs under visible light irradiation

Mayer et al. described the basis of the SPR effect in a review (Link and El-Sayed 2000) and provided detailed illustrations of the mechanisms of the plasmonic enhancement to photocatalysis. This review provided a better understanding of the physical principles of the special effect of SPR and hence with only brief introduction. When small spherical metallic NPs are under visible light irradiation, the number of electrons decreases on one side of the NPs and increases on the other side. This causes a redistribution of charge density. The redistributed charge density produces an electric field inside and outside the metal NPs with a direction that is opposite to that of the electric field of the light, as shown clearly in Fig. 7.1.

7.4 Basic Concepts and Beneficial Effects of SPR

The basic concept of special SPR effect is comprised of the following. A collective oscillation of free electrons in metal NPs is driven by the electromagnetic field of incident light, in which the metallic NPs absorb visible and infrared light in particular regions. For example, Au and AgNPs show a strong photoabsorption band of visible light because of their surface plasmon, which displays maxima at approximately $\lambda = 530$ and $\lambda = 400$ nm, respectively (Khan et al. 2015a, b, c). On the other hand, nanostructured AgNPs are oxidized easily, whereas AuNPs are more chemically stable in the presence of oxygen (Rayalu et al. 2013).

Recently, we successfully introduced this unique property to the new field of plasmonic photocatalysts to catalyze organic reactions and water splitting (Khan et al. 2015a, b, c). Plasmonic photocatalysis offers a new opportunity to solve the limited efficiency of photocatalysts and photovoltaic devices. In these reactions, nanostructured plasmonic metals are combined frequently with a semiconductor-based material (e.g., SnO_2, TiO_2, WO_3, and CeO_2, namely, plasmonic photocatalysts), and the catalytic activity and efficiency are enhanced greatly by the SPR effect that improves the solar-energy-conversion efficiency in the following aspects (Khan et al. 2015a, b, c, 2016; Nayak et al. 2017):

(i) Near-field enhancement of localized plasmon
(ii) Increase of the scattering effect
(iii) Excitation of e^-/h^+ pairs in the semiconductor due to the plasmonic energy transfer from the metal to the semiconductor

Figure 7.3 shows the special beneficial effects of plasmonic catalyst under visible light irradiation. Plasmonic photocatalysis has attracted recent attention as a hopeful technology for the high-performance photocatalytic degradation of harmful dyes (Kochuveedu et al. 2013; Wang et al. 2012a), (Nan Zhang et al. 2012; Linic et al. 2011). This involves the distribution of noble metal nanoparticles (generally Au and AgNPs) into semiconductor photocatalysts and obtains strong enhancement of the photoreactivity under a broad range of visible light. The use of noble metal nanoparticles has numerous benefits in the field of photocatalysis.

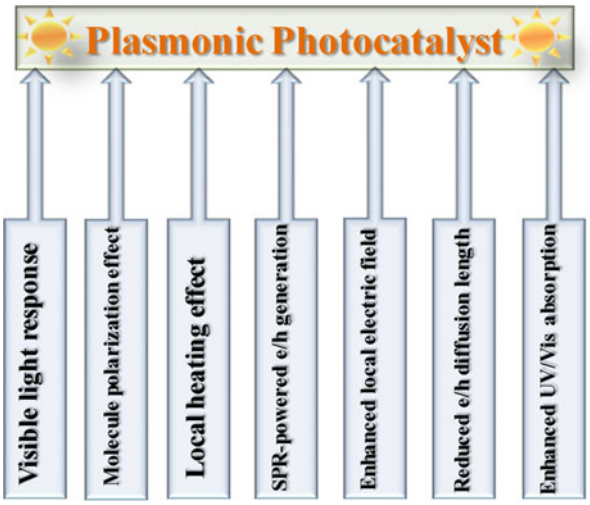

Fig. 7.3 Major special beneficial effects of SPR for improved photocatalysis

Compared to the common semiconductor photocatalysis, plasmonic photocatalysis has two distinct features: Schottky junction and localized surface plasmon resonance; each feature benefits photocatalysis in a different way. For example, a Schottky junction results from the contact of a noble metal and semiconductor. This builds up an internal electric field in a region inside the photocatalyst but close to the metal/semiconductor interface. This would force the electrons and holes to move in different directions once they are formed inside or near the Schottky junction (Wang et al. 2012b). In addition, the metal fraction provides a quick lane for charge transfer, and its surface acts as a charge-trapping center to host more active sites for photoreactions. The Schottky junction and the fast lane charge transfer work together to reduce electron–hole recombination charge (Chang et al. 2007; Xuming Zhang et al. 2013).

7.5 Preparation Methods of Metal NPs as Photocatalysts

Various sets of chemical, physical, and biological methods for the preparation of plasmonic photocatalysts are available. Examples include chemical reduction, physical vapor deposition, hydrothermal, and electrochemically active biofilm-assisted synthesis methods for the fabrication of plasmonic photocatalysts (Zhu et al. 2010; Hou and Cronin 2013; Wang et al. 2012a; Khan et al. 2015a, b, c). A series of synthesis methods have been adopted for the fabrication of metal NPs that would be ideally controllable in terms of their shape, size, morphology, cost, environmental friendliness, and high product yield with fewer waste products (Fig. 7.4).

Metal nanoparticles show a high abundance of surface plasmon excitation. For example, Au and AgNPs have attracted considerable attention because of the spatial

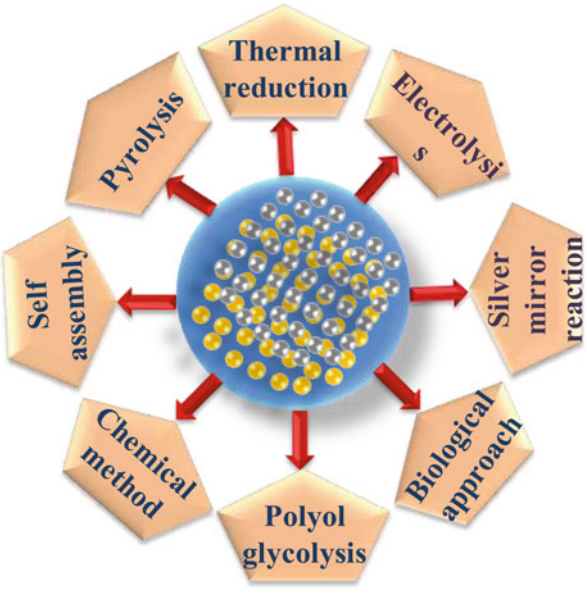

Fig. 7.4 Several preparation methods for the metal nanoparticles

SPR effect in the visible spectrum range, which can be used in numerous environmental remediation applications (Sun and Xia 2002; Jian Zhang et al. 2009). The surface plasmon properties of metal NPs are dependent on their shape, size, and morphology. The specific morphology of metal NPs is a noteworthy concern that affects their special plasmonic behavior (Gramotnev and Bozhevolnyi 2010). Several methods have been used for the fabrication of metal NPs with a controlled size and shape. The metal precursor is mixed with a reducing agent in the presence of a stabilizing agent that is used to control the size and shape of metal NPs. Similarly, $AgNO_3$ (silver nitrate), as a precursor, can be used because of its low cost and high abundance. More than a few reducing agents, such as sodium citrate, sodium borohydride, and electrochemically developed biofilms are used to reduce the metal ions present in solution to metal, metal oxide/Ag nanocomposites. On the other hand, in most cases, stabilizing/capping agents are introduced to manage and stabilize the morphology of the resulting metal NPs. Despite this, in photochemical synthesis, a variation of light treatment methods is assumed to produce metal NPs. Light-mediated synthesis has been applied to the fabrication of NPs, e.g., laser ablation or direct laser irradiation of an aqueous solution of metal salt precursor in the presence of a surfactant to make an accurate shape, size, and distribution of metal NPs, where the light source works as a reducing agent (Yee et al. 1999; Lim et al. 2006; Sharma et al. 2009).

The biological route is considered a green and sustainable methodology that has attracted substantial attention because of its potential to address the energy and environmentally related issues. The development/growth of biofilms using microorganisms is a biological approach for the fabrication of different kinds of metal nanoparticles and nanocomposites (Kalathil et al. 2011). Bio-electrochemical

systems (BESs) use microorganisms as a catalyst in electrochemical reactions. The best recognized BES is the microbial fuel cell (MFC), which can be used in metal-consuming microorganisms to transform the chemical energy of the substrates dissolved in wastewater to electrical energy. BESs can be used for power generation from wastewater, power-driven electricity production, bioremediation, and biosensing applications. In recent times, mixed culture-developed biofilms were reported to be a biogenic reducing tool for the synthesis of NPs (Au, Ag, and Cys − Ag) and metal-graphene nanocomposites (Khan et al. 2012, 2013, 2015a, b, c). The main benefit of these procedures is that the mixed culture-developed biofilms are used as the reducing tool that does not involve an exterior energy contribution, toxic chemicals, or expensive solvents. In addition, the reactions occur at room temperature, which makes the formation of nanoparticles/nanocomposites highly efficient.

7.6 Effect of Plasmonic Resonance in Photocatalysis

7.6.1 Plasmonic Resonance Mechanisms

In highly conductive nanocomposites, free electrons are confined locally. When the as-fabricated nanomaterials are irradiated with electromagnetic energy at the plasma frequency, the spatial electron density redistributes and produces an electric field. Concurrently, a columbic restoring force of the positively charged surface nuclei is present and induces collective oscillations of the charges in the particle, which are similar to an oscillating spring after stretch and release (Warren and Thimsen 2012). Such oscillations of electrons and electromagnetic fields are defined as localized surface plasmons. In the state of localized surface plasmonic resonance (LSPR) induced by the radiation of a specific LSPR wavelength, the free electrons will oscillate with the maximum amplitude. LSPR is characterized by a buildup of intense, spatially nonhomogeneous oscillating electrical fields in the vicinity of the nanostructure (Linic et al. 2011). In such a way, the energy of incident radiation is transferred to the plasmonic particles. The LSPR profile can be tuned by tailoring several parameters, such as their nano-size, shape, interparticle distance, and nature of the surrounding medium (Linic et al. 2011; Clavero 2014; Liz-Marzán 2006; Kale et al. 2013).

The fundamental principle in the photocatalytic degradation of dyes or pollutants is when the metal nanoparticles, as a catalyst, are irradiated with photons with an energy greater than or equal to their band-gap energy (E_g), an electron (e^--cb) is excited from the valence band to the conduction band, which leaves a hole (h^+-vb). The excited electrons and holes then migrate to the surface of another state. The rate of charge recombination is inhibited frequently by a scavenger or another doped material, which can easily trap the electrons or holes. Accordingly, better crystalline nanostructure materials with fewer defects can minimize the trapping states and charge recombination sites, which results in improved efficiency in the use of the

photogenerated transporters for the desired photoreactions. For higher photocatalytic efficiency, the electron–hole pairs should be separated well, and the charges should be transferred rapidly across the surface/interface to impede recombination (Linic et al. 2015).

7.7 Photocatalytic Dye Decomposition Processes

Photocatalysis can be used for the degradation of environmentally harmful dyes, photocatalytic hydrogen evolution, and photosynthesis of useful chemicals. The basic mechanisms of nano-semiconductor-based photocatalysis comprise photochemical processes of visible light absorption, electron-hole pair generation, separation, and free charge carrier-induced redox reactions. This is beneficial for a wide range of applications, such as wastewater treatment, air purification, water splitting, and the self-cleaning of surfaces (Linic et al. 2015).

Table 7.1 lists the performances of novel plasmonic nanocomposites with graphene sheets as base materials. Numerous studies have chosen organic dyes as the pollutant because the degradation process can be examined simply through the variations in the photoabsorption of the responding or degrading solution.

Table 7.1 Comparative results of photocatalytic dye degradation performances using different nanostructures

Nanocomposites	Dye as pollutant	Light source	Degradation result	References
Au-graphene	Methylene blue	($\lambda > 420$ nm)	64%	Khan et al.
Ag-graphene	Methylene blue and Congo red	($\lambda > 420$ nm)	65% and 90%	Khan et al.
Pt-graphene/TiO_2	Methylene blue	(8 W, $\lambda > 420$ nm)	93%	S.yYe et al.
Graphene-gold	Methylene blue, RhB and orange II	($\lambda > 420$ nm)	88.6%, 27.6%, and 8.5%	Zhao et al.
Pt-Pd-graphene	Basic fuchsin and indigo carmine dyes	($\lambda > 420$ nm)	70% and 65%	Kurt et al.
Pt/graphene	Rhodamine B and methylene blue	8 W, halogen lamp	70% and 82%	Oh et al.
Au@TiO_2-graphene	Acid blue 92	125 W mercury lamp	72% and 43%	Setayesh et al.
		($\lambda > 574$ nm)		
Au@TiO_2/graphene	2,4-dichlorophenol (2,4-DCP)	($\lambda > 420$ nm)	78%	Shi et al.
Ag-Au on graphene sheets	4-nitrophenol	($\lambda > 420$ nm)	97.38%	Dhole et al.
Au–Pd-reduced graphene oxide	2-chlorophenol	Sunlight	100%	Yamauchi et al.

7.7.1 Photochemical Mechanism

Photocatalysis can be applied effectively to the photodegradation of environmentally harmful matter, photocatalytic hydrogen evolution, and photosynthesis of useful chemicals. The emerging technologies have attracted considerable research interest. The basic mechanisms of nano-semiconductor-based photocatalysis involve the photochemical processes of light absorption, electron-hole pair generation, and the separation and free charge carrier-induced redox reactions, as shown in Fig. 7.5.

Metal/semiconductor hybrid structures are usually employed for plasmonic photocatalysis applications. There are some insightful review addressing the mechanisms (Hou and Cronin 2013; Jiang et al. 2014). The charge-transfer mechanism also affects the photochemical selectivity of LSPR-mediated photocatalysis (Xuming Zhang et al. 2013). In a study of the SPR-mediated oxidation of p-aminothiophenol (PATP), when Au nanoparticles were used as a catalyst, the LSPR-mediated oxidation of PATP yielded p,p-dimercaptobenzene (DMAB). On the other hand, no DMAB evolution was detected when the AuNPs were loaded onto a metal oxide (TiO_2 NPs) under LSPR spectral irradiation, as the hot electrons were injected from the AuNPs to the conduction band (CB) of TiO_2 NPs. When UV illumination was introduced, p-nitrophenol (PNTP) formed from PATP in a single step, which was attributed to electron transfer from the UV-excited TiO_2 to AuNPs. Interestingly, when the UV illumination was stopped, the PNTP molecules were reduced further to DMAB. This suggests that the charge-transfer mechanism may play an important role in LSPR-mediated photocatalysis to manipulate the reaction activity, product formation, and selectivity (Hou and Cronin 2013; Jiang et al. 2014).

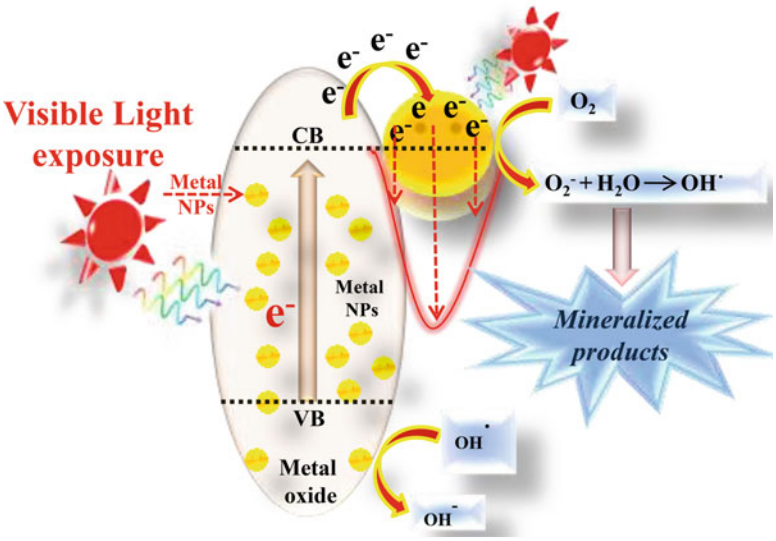

Fig. 7.5 Schematic diagram of plasmonic-mediated photocatalysis under visible light irradiation

The photodegradation of organic pollutants by semiconductor-based photocatalysts is an economical, clean, and effective means for water and air purification. In typical aqueous solution-based photocatalytic reactions, upon photoexcitation, either the photogenerated energetic charge carriers will react with the solvent to form highly reactive radicals that can break the chemical bonds of the organic pollutants or the charge carriers will be transferred directly to the reactants adsorbed on the surface of the catalysts to induce photochemical transformations. Either way, the organic pollutants are degraded photocatalytically into short-chain molecules or eventually into CO_2 and H_2O. The photocatalytic reactions are strongly dependent on the absolute surface area, light absorption properties, energy band level, and charge separation potential of the photocatalyst. The beneficial surface plasmonic effect on photocatalysis has been proven. Upon plasmonic excitation, the elevated field increases the rate of energetic charge carrier generation, resulting in a higher probability of redox reactions (Ni et al. 2007; Priebe et al. 2015). Efforts have been made for better morphology control, more suitable energy coupling, and novel hybrid structures to achieve higher efficiency and better stability of the catalyst. Many studies chose organic dyes as the representative pollutant because the degradation process can be monitored simply through changes in the photoabsorption of the reacting solution.

7.8 Conclusion

This study reviewed the recent developments of plasmon-enhanced photocatalysis, particularly on the three major functions of the plasmonic effect, i.e., (i) light absorption, (ii) hot electron injection, and (iii) near-field enhancement. The plasmon-based mechanisms and their photonic effects showed that the plasmon effect is a very promising strategy to improve the photocatalytic performance of metal/metal oxides. Significant advances have been made to extend the technology for practical applications. In the future, constant research should address the following concerns:

1. Although the plasmonic enhancement has been found to be useful for photocatalysis applications, considerable effort is needed to develop the material and architecture for optimization.
2. The photostability and chemical stability of plasmonic materials are not up to the work particularly when complicated morphologies with high structural energies are required. While many studies have reported more robustness of the plasmonic materials, the exchange between protection and efficiency needs to be addressed.
3. Bare Au and AgNPs are effective but expensive. Low-cost plasmonic metals with carbon-based materials, such as Ag-graphene/*g*-C_3N_4 or Au-graphene/*g*-C_3N_4, should be fabricated using easy and scalable methodologies.

4. The limited understanding of the interaction between plasmonic materials and electrolyte in plasmonic effects hinders the development of novel, effective materials.

Acknowledgment This study was supported by the Priority Research Centers Program by Basic Science Research Program (Grant No: 2015R1D1A3A03018029) through the National Research Foundation of Korea (NRF) funded by the Korean Ministry of Education.

References

Ahmad A, Mohd-Setapar SH, Chuong CS, Khatoon A, Wani WA, Kumar R et al (2015) Recent advances in new generation dye removal technologies: novel search for approaches to reprocess wastewater. RSC Adv 5(39):30801–30818. https://doi.org/10.1039/C4RA16959J

Burda C, Chen X, Narayanan R, El-Sayed MA (2005) Chemistry and properties of nanocrystals of different shapes. Chem Rev 105(4):1025–1102. https://doi.org/10.1021/cr030063a

Camarero L, Peche R, Merino JM, Rodríguez E (2003) Photo-assisted oxidation of indigocarmine in an acid medium. Environ Eng Sci 20(4):281–287. https://doi.org/10.1089/109287503322148555

Chang DE, Sørensen AS, Demler EA, Lukin MD (2007) A single-photon transistor using nanoscale surface plasmons. Nat Phys 3(11):807. https://doi.org/10.1038/nphys708

Chong MN, Jin B, Chow CW, Saint C (2010) Recent developments in photocatalytic water treatment technology: a review. Water Res 44(10):2997–3027. https://doi.org/10.1016/j.watres.2010.02.039

Clavero C (2014) Plasmon-induced hot-electron generation at nanoparticle/metal-oxide interfaces for photovoltaic and photocatalytic devices. Nat Photonics 8(2):95. https://doi.org/10.1038/nphoton.2013.238

Daniel M-C, Astruc D (2004) Gold nanoparticles: assembly, supramolecular chemistry, quantum-size-related properties, and applications toward biology, catalysis, and nanotechnology. Chem Rev 104(1):293–346. https://doi.org/10.1021/cr030698+

Fuku K, Hayashi R, Takakura S, Kamegawa T, Mori K, Yamashita H (2013) The synthesis of size- and color-controlled silver nanoparticles by using microwave heating and their enhanced catalytic activity by localized surface Plasmon resonance. Angew Chem Int Ed 52 (29):7446–7450. https://doi.org/10.1002/anie.201301652

Gramotnev DK, Bozhevolnyi SI (2010) Plasmonics beyond the diffraction limit. Nat Photonics 4 (2):83. https://doi.org/10.1038/nphoton.2009.282

Haruta M (2005) Catalysis: gold rush. Nature 437(7062):1098. https://doi.org/10.1038/4371098a

Hashmi ASK, Hutchings GJ (2006) Gold catalysis. Angew Chem Int Ed 45(47):7896–7936. https://doi.org/10.1002/anie.200602454

He L, Freeman HS, Lu L, Zhang S (2011) Spectroscopic study of anthraquinone dye/amphiphile systems in binary aqueous/organic solvent mixtures. Dyes Pigments 91(3):389–395. https://doi.org/10.1016/j.dyepig.2011.05.010

Hou W, Cronin SB (2013) A review of surface plasmon resonance-enhanced photocatalysis. Adv Funct Mater 23(13):1612–1619. https://doi.org/10.1002/adfm.201202148

Jiang R, Li B, Fang C, Wang J (2014) Metal/semiconductor hybrid nanostructures for plasmon-enhanced applications. Adv Mater 26(31):5274–5309. https://doi.org/10.1002/adma.201400203

Jie R, Guo G, Zhao W, An S (2013) Preparation and photocatalytic degradation of methyl orange of nano-powder TiO_2 by hydrothermal method supported on activated carbon. J Synth Cryst 42:2144–2149. https://doi.org/10.1002/jctb.4391

Kalathil S, Lee J, Cho MH (2011) Electrochemically active biofilm-mediated synthesis of silver nanoparticles in water. Green Chem 13(6):1482–1485. https://doi.org/10.1039/C1GC15309A

Kale MJ, Avanesian T, Christopher P (2013) Direct photocatalysis by plasmonic nanostructures. ACS Catal 4(1):116–128. https://doi.org/10.1021/cs400993w

Kelly KL, Coronado E, Zhao LL, Schatz GC (2003) The optical properties of metal nanoparticles: the influence of size, shape, and dielectric environment. ACS Publications DOI: https://doi.org/10.1021/jp026731y

Khan MM, Kalathil S, Lee J-T, Cho M-H (2012) Synthesis of cysteine capped silver nanoparticles by electrochemically active biofilm and their antibacterial activities. Bull Kor Chem Soc 33 (8):2592–2596. https://doi.org/10.5012/bkcs.2012.33.8.2592

Khan MM, Kalathil S, Han TH, Lee J, Cho MH (2013) Positively charged gold nanoparticles synthesized by electrochemically active biofilm—a biogenic approach. J Nanosci Nanotechnol 13(9):6079–6085. https://doi.org/10.1166/jnn.2013.7666

Khan MM, Ansari SA, Khan ME, Ansari MO, Min B-K, Cho MH (2015a) Visible light-induced enhanced photoelectrochemical and photocatalytic studies of gold decorated SnO_2 nanostructures. New J Chem 39(4):2758–2766. https://doi.org/10.1039/C4NJ02245A

Khan ME, Khan MM, Cho MH (2015b) Green synthesis, photocatalytic and photoelectrochemical performance of an Au–Graphene nanocomposite. RSC Adv 5(34):26897–26904. https://doi.org/10.1039/C5RA01864A

Khan ME, Khan MM, Cho MH (2015c) Biogenic synthesis of a Ag–graphene nanocomposite with efficient photocatalytic degradation, electrical conductivity and photoelectrochemical performance. New J Chem 39(10):8121–8129. https://doi.org/10.1039/C5NJ01320H

Khan ME, Khan MM, Cho MH (2016) Fabrication of WO_3 nanorods on graphene nanosheets for improved visible light-induced photocapacitive and photocatalytic performance. RSC Adv 6 (25):20824–20833. https://doi.org/10.1039/C5RA24575C

Kochuveedu ST, Jang YH, Kim DH (2013) A study on the mechanism for the interaction of light with noble metal-metal oxide semiconductor nanostructures for various photophysical applications. Chem Soc Rev 42(21):8467–8493. https://doi.org/10.1039/C3CS60043B

Lang X, Chen X, Zhao J (2014) Heterogeneous visible light photocatalysis for selective organic transformations. Chem Soc Rev 43(1):473–486. https://doi.org/10.1039/C3CS60188A

Lettmann C, Hinrichs H, Maier WF (2001) Combinatorial discovery of new photocatalysts for water purification with visible light. Angew Chem Int Ed 40(17):3160–3164. https://doi.org/10.1002/1521-3773(20010903)40:17<3160::AID-ANIE3160>3.0.CO;2-Z

Lim P, Liu R, She P, Hung C, Shih H (2006) Synthesis of Ag nanospheres particles in ethylene glycol by electrochemical-assisted polyol process. Chem Phys Lett 420(4–6):304–308. https://doi.org/10.1016/j.cplett.2005.12.075

Linic S, Christopher P, Ingram DB (2011) Plasmonic-metal nanostructures for efficient conversion of solar to chemical energy. Nat Mater 10(12):911. https://doi.org/10.1038/nmat3151

Linic S, Aslam U, Boerigter C, Morabito M (2015) Photochemical transformations on plasmonic metal nanoparticles. Nat Mater 14(6):567. https://doi.org/10.1038/nmat4281

Link S, El-Sayed MA (2000) Shape and size dependence of radiative, non-radiative and photothermal properties of gold nanocrystals. Int Rev Phys Chem 19(3):409–453. https://doi.org/10.1080/01442350050034180

Liu Z, Hou W, Pavaskar P, Aykol M, Cronin SB (2011) Plasmon resonant enhancement of photocatalytic water splitting under visible illumination. Nano Lett 11(3):1111–1116. https://doi.org/10.1021/nl104005n

Liz-Marzán LM (2006) Tailoring surface plasmons through the morphology and assembly of metal nanoparticles. Langmuir 22(1):32–41. https://doi.org/10.1021/la0513353

Muhd Julkapli N, Bagheri S, Bee Abd Hamid S (2014) Recent advances in heterogeneous photocatalytic decolorization of synthetic dyes. Sci World J 2014. https://doi.org/10.1155/2014/692307

Nayak AK, Das AK, Pradhan D (2017) High performance solid-state asymmetric supercapacitor using green synthesized graphene–WO_3 nanowires nanocomposite. ACS Sustain Chem Eng 5 (11):10128–10138. https://doi.org/10.1021/acssuschemeng.7b02135

Ni M, Leung MK, Leung DY, Sumathy K (2007) A review and recent developments in photocatalytic water-splitting using TiO_2 for hydrogen production. Renew Sust Energ Rev 11 (3):401–425. https://doi.org/10.1016/j.rser.2005.01.009

Priebe JB, Radnik J r, Lennox AJ, Pohl M-M, Karnahl M, Hollmann D et al (2015) Solar hydrogen production by plasmonic Au–TiO_2 catalysts: impact of synthesis protocol and TiO_2 phase on charge transfer efficiency and H2 evolution rates. ACS Catal 5(4):2137–2148. https://doi.org/10.1021/cs5018375

Rayalu SS, Jose D, Joshi MV, Mangrulkar PA, Shrestha K, Klabunde K (2013) Photocatalytic water splitting on Au/TiO_2 nanocomposites synthesized through various routes: enhancement in photocatalytic activity due to SPR effect. Appl Catal B Environ 142:684–693. https://doi.org/10.1016/j.apcatb.2013.05.057

Salleh MAM, Mahmoud DK, Karim WAWA, Idris A (2011) Cationic and anionic dye adsorption by agricultural solid wastes: a comprehensive review. Desalination 280(1–3):1–13. https://doi.org/10.1016/j.desal.2011.07.019

Sarina S, Waclawik ER, Zhu H (2013) Photocatalysis on supported gold and silver nanoparticles under ultraviolet and visible light irradiation. Green Chem 15(7):1814–1833. https://doi.org/10.1039/C3GC40450A

Sharma VK, Yngard RA, Lin Y (2009) Silver nanoparticles: green synthesis and their antimicrobial activities. Adv Colloid Interf Sci 145(1–2):83–96. https://doi.org/10.1016/j.cis.2008.09.002

Sun Y, Xia Y (2002) Shape-controlled synthesis of gold and silver nanoparticles. Science 298 (5601):2176–2179. https://doi.org/10.1126/science.1077229

Wang JL, Xu LJ (2012) Advanced oxidation processes for wastewater treatment: formation of hydroxyl radical and application. Crit Rev Environ Sci Technol 42(3):251–325. https://doi.org/10.1080/10643389.2010.507698

Wang M, Chamberland N, Breau L, Moser J-E, Humphry-Baker R, Marsan B et al (2010) An organic redox electrolyte to rival triiodide/iodide in dye-sensitized solar cells. Nat Chem 2 (5):385. https://doi.org/10.1038/nchem.610

Wang P, Huang B, Dai Y, Whangbo M-H (2012a) Plasmonic photocatalysts: harvesting visible light with noble metal nanoparticles. Phys Chem Chem Phys 14(28):9813–9825. https://doi.org/10.1039/C2CP40823F

Wang Z, Liu J, Chen W (2012b) Plasmonic Ag/AgBr nanohybrid: synergistic effect of SPR with photographic sensitivity for enhanced photocatalytic activity and stability. Dalton Trans 41 (16):4866–4870. https://doi.org/10.1039/C2DT12089E

Warren SC, Thimsen E (2012) Plasmonic solar water splitting. Energy Environ Sci 5 (1):5133–5146. https://doi.org/10.1039/C1EE02875H

William L IV, Kostedt I, Ismail AA, Mazyck DW (2008) Impact of heat treatment and composition of ZnO−TiO_2 nanoparticles for photocatalytic oxidation of an azo dye. Ind Eng Chem Res 47 (5):1483–1487. https://doi.org/10.1021/ie071255p

Yee C, Scotti M, Ulman A, White H, Rafailovich M, Sokolov J (1999) One-phase synthesis of thiol-functionalized platinum nanoparticles. Langmuir 15(13):4314–4316. https://doi.org/10.1021/la9814283

Yu J, Zhang J, Jaroniec M (2010) Preparation and enhanced visible-light photocatalytic H 2-production activity of CdS quantum dots-sensitized $Zn_{1-x}Cd_xS$ solid solution. Green Chem 12(9):1611–1614. https://doi.org/10.1039/C0GC00236D

Yu J, Ma T, Liu G, Cheng B (2011) Enhanced photocatalytic activity of bimodal mesoporous titania powders by C_{60} modification. Dalton Trans 40(25):6635–6644. https://doi.org/10.1039/C1DT10274E

Zeitler K (2009) Photoredox catalysis with visible light. Angew Chem Int Ed 48(52):9785–9789. https://doi.org/10.1002/anie.200904056

Zhang J, Li S, Wu J, Schatz GC, Mirkin CA (2009) Plasmon-mediated synthesis of silver triangular bipyramids. Angew Chem 121(42):7927–7931. https://doi.org/10.1002/ange.200903380

Zhang N, Liu S, Xu Y-J (2012) Recent progress on metal core@semiconductor shell nanocomposites as a promising type of photocatalyst. Nanoscale 4(7):2227–2238. https://doi.org/10.1039/C2NR00009A

Zhang X, Chen YL, Liu R-S, Tsai DP (2013) Plasmonic photocatalysis. Rep Prog Phys 76 (4):046401. https://doi.org/10.1088/0034-4885/76/4/046401

Zhang N, Ciriminna R, Pagliaro M, Xu Y-J (2014) Nanochemistry-derived Bi_2WO_6 nanostructures: towards production of sustainable chemicals and fuels induced by visible light. Chem Soc Rev 43(15):5276–5287. https://doi.org/10.1039/C4CS00056K

Zhu H, Ke X, Yang X, Sarina S, Liu H (2010) Reduction of nitroaromatic compounds on supported gold nanoparticles by visible and ultraviolet light. Angew Chem 122(50):9851–9855. https://doi.org/10.1002/ange.201003908

Chapter 8
Polymer-Based Magnetic Nanocomposites for the Removal of Highly Toxic Hexavalent Chromium from Aqueous Solutions

Mpitloane J. Hato, Thabiso C. Maponya, Kabelo E. Ramohlola, Kwena D. Modibane, Arjun Maity, Gobeng R. Monama, Katlego Makgopa, and Abdulhakeem Bello

Contents

M. J. Hato (✉)
Department of Chemistry, School of Physical and Mineral Sciences, University of Limpopo (Turfloop), Polokwane, South Africa

Department of Environmental Sciences, College of Agriculture and Environmental Sciences, University of South Africa (UNISA), Pretoria, South Africa
e-mail: mpitloane.hato@ul.ac.za

T. C. Maponya
Department of Chemistry, School of Physical and Mineral Sciences, University of Limpopo (Turfloop), Polokwane, South Africa

DST/CSIR Innovation Centre, National Centre for Nanostructured Materials, CSIR Material Science and Manufacturing, Pretoria, South Africa

K. E. Ramohlola · K. D. Modibane (✉) · G. R. Monama
Department of Chemistry, School of Physical and Mineral Sciences, University of Limpopo (Turfloop), Polokwane, South Africa
e-mail: kwena.modibane@ul.ac.za

A. Maity
Department of Applied Chemistry, University of Johannesburg, Johannesburg, South Africa

DST/CSIR National Center for Nanostructured Materials, Council for Scientific and Industrial Research (CSIR), Pretoria, South Africa

Mu. Naushad et al. (eds.), *Advanced Nanostructured Materials for Environmental Remediation*, Environmental Chemistry for a Sustainable World 25,
https://doi.org/10.1007/978-3-030-04477-0_8

Abstract This review paper focuses on the use of iron oxide nanocomposites for the removal of hexavalent chromium, Cr(VI), from wastewater. Cr(VI) is very toxic and carcinogenic as compared to Cr(III) and can cause health defects such as liver, lung and kidney damage. It is mostly expelled from untreated or partially treated effluents from mining operation, electroplating and water cooling activities. As a result, these activities produce effluents with higher concentration levels of Cr (VI) than the acceptable discharge limits of 0.1 and 0.05 mg/L in inland surface water and drinking water, respectively, as regulated by the World Health Organisation (WHO). This review paper summarises the performance of different water treatment technologies studied on the last decade. Adsorption technology has emerged as an attractive method for Cr(VI) removal from industrial wastewater amongst the mentioned methods. Hence, the adsorption isotherms and kinetics models are also discussed in this review paper. The factors such as the effect of solution pH, temperature, initial Cr(VI) concentration, adsorbent dosage and other coexisting ions are also briefly discussed. In this review, magnetic polymers reveal good result than other techniques used in water treatment because of its high surface area (surface/volume ratio). It is suggested that these may be used in the future at large-scale water purification. It is also found that the polymer rich with amino groups (polypyrrole and polyaniline) enhanced Cr (VI) removal efficiency. From the results, it is evident that more attention needs to be paid on the industrial application of the technologies which were successful in the laboratory scale. In the future, combination of both copolymers may be the best option for treatment of wastewater.

Keywords Water purification · Nanotechnology · Magnetic nanoparticles · Polypyrrole · Polyaniline

K. Makgopa (✉)
Department of Chemistry, Faculty of Science, Tshwane University of Technology (Acardia Campus), Pretoria, South Africa
e-mail: makgopak@tut.ac.za

A. Bello
Department of Materials Science and Engineering, African University of Science and Technology (AUST), Abuja, Nigeria

8.1 Introduction

8.1.1 Background of Water Pollution

The detoxification of noxious pollutants from wastewater is vital due to the dangerous effects that they impose on the health of human beings, terrestrial and aquatic organisms. Due to growth in population, there is a need to produce more basic needs such as food, shelter, clothing and electricity and provide safe drinking water to meet the increasing population demand. During production of the above-mentioned basic needs, there is discharge of toxic waste (generated during production activities) which results in polluting the existing water systems (Barrera-Díaz et al. 2012). There are various pollutants such as biological, organic and inorganic (depending on the source) (Barrera-Díaz et al. 2012; Kera et al. 2017); hence, the next section fully discusses different types of pollutants that can be found in the water streams.

8.1.2 Water Pollutants

A water pollutant is a material that is present in water systems and is harmful to living organisms, even when it exists in trace amounts. The effect of these materials can either be acute or chronic through their bioaccumulation nature in the environment. Different types of water pollutants include (Cui et al. 2015; Kanchi 2014; M'Bareck et al. 2006).

- Pathogens – these are viruses and bacteria.
- Macroscopic pollutants – these include all the garbage, i.e. plastics, broken glass, empty aluminium containers, etc.
- Organic pollutants – such as dyes, chlorinated solvents and phenolic compounds.
- Inorganic pollutants – phosphates, nitrates and heavy metals.

8.1.2.1 Pathogens and Macroscopic Pollutants

Pathogens can be bacteria, protozoa or viruses. For example, bacteria are commonly found in water system and start to be harmful if their number increases above safe levels.

The well-known pathogenic bacteria are *Escherichia coli* and coliform bacteria. The presence of *E.coli* bacteria in water systems is mostly associated with human and animal waste, which normally comes from poor management of sewage systems (Narayan 2010; Li et al. 2008a, b). Macroscopic pollutants are noticeable objects found in waterways, which have been thrown or disposed illegally directly, washed off by rain or blown by wind into water systems (Bielefeldt et al. 2009). Materials such as nurdles (small plastic pellets), pieces of wood, metals from shipwrecks and

shipping containers form part of macroscopic pollutants and can be managed. However, urgent removal of these pollutants is necessary, to avoid disruption of aquatic systems and environmental contamination upon their chemical breakdown.

8.1.2.2 Organic Pollutants

Organic pollutants are usually those materials that contain aromatic rings in their structure. The existence of various organic pollutants such as dyes, chlorinated and aliphatic compounds (including chlorobenzene and carbon tetrachloride) and phenolic compounds (nitrophenol and chlorophenol) is of critical concern (Angelidaki and Sanders 2004). Dyes from textile, paper, pigment and plastic industries cause decolouration of water, which can negatively impact aquatic life by tempering with the photosynthetic process (Zhou et al. 2015; Srinivasan and Viraraghavan 2010). For example, methylene blue dye is very harmful to humans and can cause burning sensation, nausea, vomiting and mental confusion after ingestion (Mahdavinia and Massoumi 2012). Hence, nanocomposites are used to remove and decompose dyes from wastewater. For example, Ameen et al. 2012 reported on the degradation of Rose Benga (RB) dye by polyaniline-reduced graphene nanocomposites, which was prepared by chemical oxidative polymerization. The authors investigated the photocatalytic activity of the prepared nanocomposites under light irradiation. Chlorinated and phenolic compounds are mostly used in pesticides, detergents, fertilisers, solvents industries, etc. Chlorinated compounds have a tendency to form toxic by-products, e.g. trichloromethane, when they are in contact with organic matter (Rafatullah et al. 2010; Tran et al. 2015).

8.1.2.3 Inorganic Pollutants

Agricultural activities are the main source for inorganic pollutants such as phosphates, nitrates and sulphates. They usually enter water systems through surface water run-off (Chowdhury and Viraraghavan 2009; Bhatnagar and Sillanpää 2011). Nitrates and phosphates in drinking water usually originate from fertilisers or from animal or human wastes. Their concentrations in water tend to be highest in areas of intensive agriculture or where there is a high density of septic system (Bhatnagar and M. Sillanpää 2011; Blaney et al. 2007; Tyagi et al. 2018). Sulphates normally are present at some level in all private water systems. Sulphates occur naturally as a result of leaching from sulphur deposits in the earth. It has a secondary drinking water standard of 250 mg/L because it may impart a bitter taste to the water at this level (Zhang et al. 2017). The general sources of heavy metals are weathering of rocks (due to their abundance in nature) and mining industries (as a result of mineral process of metal ores) (Dou et al. 2017). Water pollution caused by toxic heavy metals including nickel, cadmium, lead, mercury, chromium, arsenic and copper is a major global concern, owing to their acute toxicity and enduring accumulation

(Duruibe et al. 2007). Unlike other organic pollutants, heavy metals are problematic since they are mutagenic and carcinogenic and are not biodegradable. They can bio-accumulate in living tissues and become concentrated throughout the food chain (Sounthararajah et al. 2015). Some of the health effects include kidney, liver and lung damages which are caused by ingestion of lead, cadmium and chromium. Nickel metal may result in various adverse effects such as allergic reaction resulting in contact dermatitis if exposure is prolonged (Horst et al. 2016). Arsenic is known to cause skin lesions, hyperkeratosis and cancer (Duruibe et al. 2007; Sounthararajah et al. 2015). Its sources include agricultural use of arsenical herbicides, pesticides and crop desiccants (Tirtom et al. 2012; Yoon et al. 2016). Another issue associated with heavy metals is their ability to exist as different species which are environmentally stable and having high mobility (Badruddoza et al. 2013; Choppala et al. 2018). For example, chromium exists in various oxidation states ranging from Cr(II) to Cr (VI). In aqueous environment the most stable oxidation states of chromium are Cr (III) and Cr(VI) (Kunhikrishnan et al. 2017).

Cr(III) Speciation

Cr(III) species is less toxic compared to the Cr(VI) species. It can serve as an essential micronutrients for human, plant and animal metabolism at trace levels (Shahid et al. 2017). One of the functions of Cr(III) is to break down glucose and fats; hence, it is contained in some supplements used for weight loss and performance enhancement (Wang et al. 2013; Hu et al. 2016). Cr(III) is less soluble and immobile as compared to Cr(VI) and can be easily removed from wastewater by chemical precipitation (Kotaśâ and Stasicka 2000; Zhao et al. 2010). The decrease in the solubility of Cr(III) species is due to the complexation of OH^- ligands (Pattnaik and Equeenuddin 2016). In aqueous solution, Cr(III) species complexes with hydroxides and exists as $Cr(OH)_3$. At lower pH and in the presence of H_2O and H^+ (Fig. 8.1), Cr(III) exists as hexaaquachromium (3+) ($Cr(H_2O)_6^{3+}$). The deprotonation of $Cr(H_2O)_6^{3+}$ reaction is represented in Eq. 8.1 (Wang et al. 2013; Hu et al. 2016):

$$Cr(OH)_2(H_2O)_4^{+} + H_2O \leftrightarrow Cr(OH)_3.aq + H_3O^{+} \tag{8.1}$$

At increased pH values, $Cr(OH)_3.aq$ displays amphoteric behaviour and is converted to soluble tetraoxo complex through the following reaction in Eq. 8.2:

$$Cr(OH)_3.(s) + 2H_2O \leftrightarrow Cr(OH)_4^{-} + H_3O^{+} \tag{8.2}$$

Moreover, Cr(III) is a hard acid, which forms hexacoordinate octahedral complexes with various ligands including water, ammonia and organic ligands containing nitrogen and oxygen donor atoms (Pattnaik and Equeenuddin 2016).

Cr(VI) Speciation

Hexavalent chromium (Cr(VI)) species is considered the most toxic stable form of Cr that exists in aqueous solution (Jin et al. 2016). Species of Cr(VI) is known to be more soluble and mobile in the environment as compared to Cr(III). The strong oxidising ability of Cr(VI) makes it carcinogenic, since it can easily diffuse through membrane cell and oxidise biological molecules (Shahid et al. 2017; Bhaumik et al. 2014a, b; Dhal et al. 2013). In water, Cr(VI) is present as oxyanions which are $HCrO_4^-$, $Cr_2O_7^{2-}$ and CrO_4^{2-} depending on the pH of the aqueous solution, the redox potential and Cr(VI) concentration as indicated by Fig. 8.1 (Hao et al. 2013). At lower pH values between 2 and 6.5, the prevailing species of Cr(VI) is $HCrO_4^-$. As the pH value 6.5 increases, $HCrO_4^-$ gets converted into CrO_4^{2-} and $Cr_2O_7^{2-}$ (Wang et al. 2014). The deprotonation reactions that form these Cr(VI) species are represented in Eqs. 8.3, 8.4 and 8.5:

$$H_2CrO_4 \leftrightarrow H^+ + HCrO_4^- \tag{8.3}$$

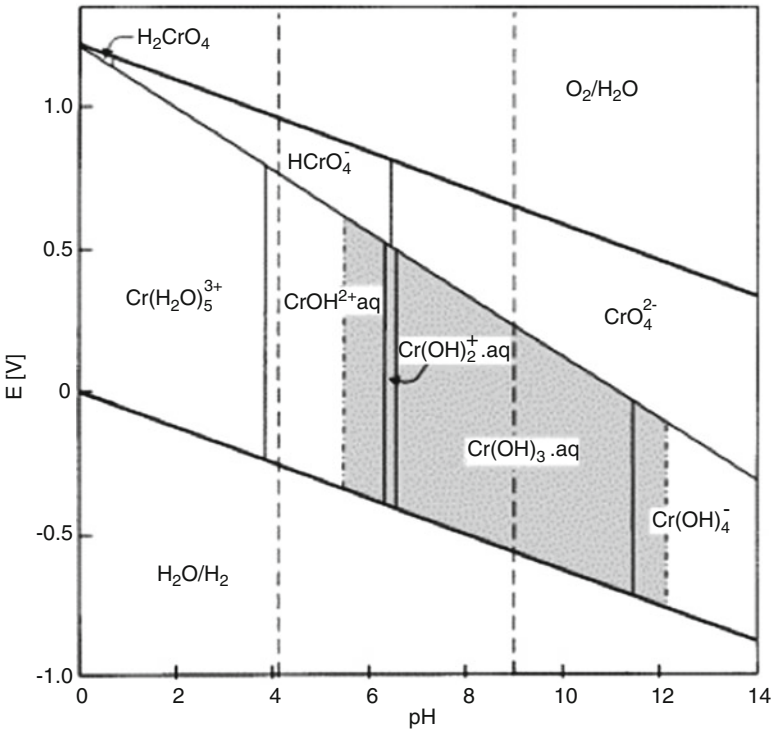

Fig. 8.1 The Eh-pH diagram of Cr-O-H system (Kotasâ and Z. Stasicka 2000)

$$HCrO_4^- \leftrightarrow H^+ + CrO_4^{2-} \tag{8.4}$$

$$2HCrO_4^- \leftrightarrow Cr_2O_7^{2-} + H_2O \tag{8.5}$$

In acidic aqueous environment, Cr(VI) species display a very high potential redox that is between 1.33 and 1.38 V. This indicates that it is a strong oxidising agent that may be unstable in the presence of electron donors, resulting to its reduction to Cr (III) as represented by Eq. 8.6 (Hu et al. 2016):

$$HCrO_4^- + 7H^+ + 3e^- \leftrightarrow Cr^{3+} + 4H_2O \tag{8.6}$$

Since the reduction of $HCrO_4^-$ is accompanied by proton consumption, decrease in acidity reduces the formal potential (Barrera-Díaz et al. 2012).

8.1.3 Health and Environmental Effects of Cr(VI)

Chromium is placed on the top of the priority list of toxic pollutants by the United States Environmental Protection Agency (US-EPA 1990). According to the Agency for Toxic Substances and Disease Registry, it is the 7th amongst the top 20 list of lethal substances (Kunhikrishnan et al. 2017). The carcinogenic nature of hexavalent chromium compounds was recognised first in the late nineteenth century when nasal tumours were detected in Scottish chrome pigment workers (Sun et al. 2015). Cr (VI) species are of global concern because they can be freely adsorbed by marine animals and enter the human food chains, therefore, posing health hazards to consumers (Mitra et al. 2011). The readily uptake of Cr(VI) by mammalian and bacterial cells is through sulphate transport systems which is due to the structural similarities of Cr(VI) species to SO_4^{2-} (Edebali and Pehlivan 2010). Hexavalent Cr species causes cancer and mutation by damaging the DNA-protein cross-links and also by causing single-strand breaks in living cells (Patra et al. 2010). The other environmental hazard caused by Cr(VI) include soil pollution. The presence of high concentration of Cr(VI) in the soil cause disruptions in number, type, health and activity of soil organisms, thus destroying the natural soil enzymes that help maintain good soil quality (Zhao et al. 2010). Therefore, there is a need to remove this toxic heavy metal pollutant from industrial wastewater prior to release into the environment.

8.2 Water Treatment Methods

There are several methods that have been implemented to remove Cr(VI) species from industrial wastewater are shown in Fig. 8.2. For instance, membranes are susceptible to fouling which is triggered by rejected colloids, chemicals and

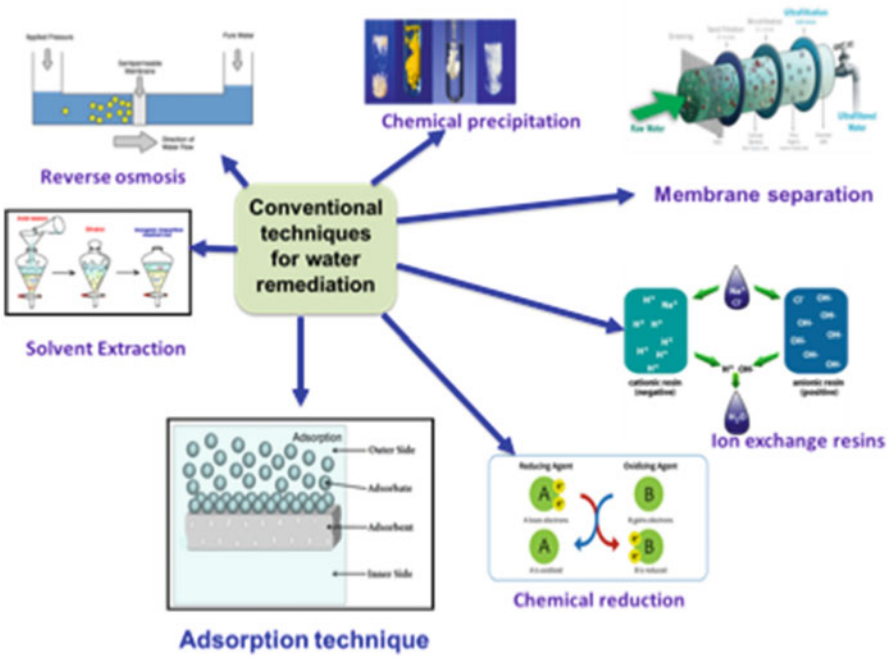

Fig. 8.2 Different water treatment methods for Cr(VI) removal from wastewater

microbes. This fouling drawback results in higher energy and clean-up costs and continuous replacement of membranes (Lytle et al. 1998; Kim and Van Der Bruggen 2010). Reverse osmosis has been reported to be efficient in heavy metals removal; however, it utilises high energy because its operation requires high pressure and limited pH range (Goh et al. 2015; Das et al. 2006; Rad et al. 2009). Chemical precipitation involves a reaction amongst a chemical precipitant and heavy metal ions, which yields an insoluble suspension that can be separated from water through sedimentation or filtration (Zhu et al. 2013). However, it cannot be directly applied for the removal of Cr(VI) species, since Cr(VI) is very soluble in aqueous solution (Sun et al. 2015; Patra et al. 2010; Rad et al. 2009). Chemical coagulation has been reported to be efficient in the removal of Cr(VI) by adding chemical coagulants such as aluminium or iron salts (Adeleye et al. 2016). These chemical coagulants are added in order to overcome the repulsive forces between particles. The types of coagulants may be inorganic electrolytes, organic polymers or synthetic polyelectrolytes (Zhu et al. 2013). Chemical precipitation and coagulation are expensive methods, since they involve the use of luxurious chemical reagents. They also require cautious control and monitoring of the systems to avoid adding excess chemicals. The systems may be affected by amphoteric nature of other compounds due to the presence of multiple metal species, resulting in poor treatment. The major challenge of both coagulation and precipitation is the production of large amounts of sludge that is generally harmful owing to the presence of toxic heavy metals

removed (Zhu et al. 2013; Adeleye et al. 2016). Biological reduction of Cr(VI) has also been reported, wherein enzymes and microorganisms are used to reduce it to less toxic Cr(III). The drawbacks associated with this process include low activity, production and stability of the enzymes (Akbal and Camc 2011). Adsorption technology has emerged as an attractive method for Cr(VI) removal from industrial wastewater amongst the mentioned methods. This process has advantages such as high efficiency, ease operation and low cost depending on the type of adsorbent chosen (Thatoi et al. 2014; Ali 2016).

8.3 Adsorption Technology

Adsorption process involves the accumulation or adherence of gas, liquid or dissolved solid molecules on the surface of a solid (Wang et al. 2015a, b). This process occurs when the adsorbate (molecule or ion that is being adsorbed) attaches itself on the surface of the adsorbent (material that provides surface for adsorption) via physical attachment or chemical bonding (Scheme 8.1) (Wang et al. 2015a, b; Yan et al. 2015). Consequently, the process of adsorption is regarded as a mass transfer system (diffusion, migration and convection), typically from a liquid or gaseous phase to solid phase. During adsorption process, there is movement of adsorbate molecules from bulk solution to the active sites available on the surface of the adsorbent. Based on the adsorption mechanism, there could be different interactions such as van der Waals, Columbic and Lewis acid-base (Foo and Hameed 2010; Milonjić et al. 2007; González et al. 2016). Adsorbents are distinguished by active sites which are able to interact with particles from bulk solution as a result of their specific electronic and spatial properties (Hintermeyer et al. 2008). Adsorption active sites may have the same or different energy, depending on the type of material surface. Due to its principle, the concept of adsorption has been gaining interest for application in various applications such as hydrogen storage (Worch 2012) sensing (Monama et al. 2018), CO_2 capture (Xia et al. 2010), water treatment (Jeppua and Clement 2012) and biomedical field (drugs delivery) (Zare et al. 2015). The opposite of adsorption is called desorption, which is the release of adsorbed species from the adsorbent surface, back into the bulk solution (Hintermeyer et al. 2008).

Recently, adsorption technique is mostly applied in wastewater remediation for the removal of toxic pollutants, due to its simplicity and cost effective (Akbarzadeh et al. 2012). The efficiency of the adsorbents is optimised through batch mode, and then if the adsorption process shows a high removal efficiency, it can be explored for column adsorption studies (Zhao et al. 2011). The column adsorption technique is mostly important for industrial-scale adsorption processes. It is a continuous flow adsorption process in which an adsorbent is arranged in a fixed bed and is in turn operated in adsorption and regeneration mode (Ali 2014). Factors that affect the adsorption process in wastewater treatment include (Kera et al. 2017; González et al. 2016; Zhao et al. 2011):

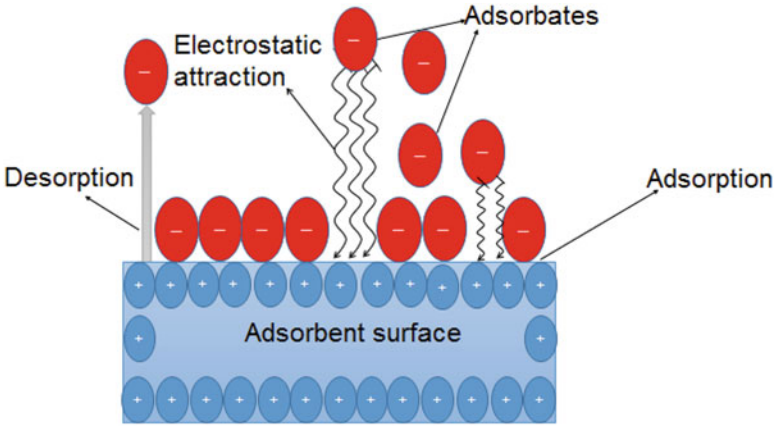

Scheme 8.1 Summary of the concept of adsorption

- Charge of the adsorbent and adsorbate (cationic, anionic or neutral)
- pH of the aqueous solution
- The temperature of the solution
- The concentration of the adsorbate
- The dosage of the adsorbent
- The surface area of the adsorbent

During adsorption, the interaction between an adsorbent and adsorbate often reaches equilibrium. The point of equilibrium is reached if the pollutant comes into contact with the adsorbent surface and gets adsorbed, and then after sometime, the amount of pollutant adsorbed becomes saturated (Zhao et al. 2011).

8.3.1 Equilibrium Adsorption Isotherms

Equilibrium relationship between an adsorbate and adsorbent is referred to as adsorption isotherm, which is described as the relationship between the quantity of pollutant adsorbed on the adsorbent surface and that remaining in solution at constant temperature (Montagnaro and Balsamo 2014). Equilibrium adsorption isotherms are vital for adsorption systems as they assist in predicting adsorption parameters. These parameters can be used qualitatively and quantitatively to compare the behaviour of adsorbents for different adsorption systems of varying experimental conditions (Yan et al. 2015). They are essential for optimising adsorption mechanisms, expressing the surface characteristics and adsorption capacities of adsorbents (Yan et al. 2015; Montagnaro and Balsamo 2014). Various adsorption isotherm models to evaluate adsorption data include Langmuir, Freundlich, Dubinin-Kaganer-Radushkevich, Harkin-Jura and Temkin model. The most commonly used

models in literature for adsorption are the Freundlich and Langmuir isotherms (Zhao et al. 2011; Montagnaro and Balsamo 2014). The efficiency of the adsorbent can be predicted by computing the parameter values of these isotherm models.

8.3.1.1 Langmuir Isotherm Model

The Langmuir isotherm model was initially established to explain gas-solid phase adsorption onto the surface of the activated carbon (Wang et al. 2015a, b). This model is now applied to quantify and differentiate the performance of various adsorbents (Yan et al. 2015; Asgari et al. 2014). The model's theory assumes a monolayer surface coverage of the adsorbate onto an adsorbent surface where all the adsorption active sites have the same energy [El-khaiary 2008; Allen et al. 2003). The adsorbed layer is regarded to be one molecule in thickness, with adsorption occurring at constant temperature only at fixed number of localised sites, which are equal and having adsorbed molecules which can no longer interact or have steric hindrance between them, even if they occupy adjacent sites (Yan et al. 2015). Graphically, the Langmuir isotherm model is characterised by a plateau, at which an equilibrium saturation point is reached. At this point, no further adsorption can occur once the adsorbate molecules or ions have occupied the available adsorption active site (Thatoi et al. 2014; Yan et al. 2015; El-khaiary 2008). The mathematical representation of the Langmuir isotherm model is represented by Eq. 8.7:

$$\frac{q_e}{q_m} = \frac{K_L C_e}{1 + K_L C_e} \tag{8.7}$$

where q_e (mg/g) and q_m (mg/g) represent the equilibrium adsorption capacity and maximum adsorption capacity of the adsorbent, C_e (mg/L) denotes the final equilibrium concentration of the adsorbate in the aqueous solution and K_L (L/mg) is the Langmuir constant that relates to the energy of adsorption (Yan et al. 2015). The linear form of the Langmuir isotherm is in Eq. 8.8:

$$\frac{Ce}{qe} = \frac{1}{q_m K_L} + \frac{Ce}{qm} \tag{8.8}$$

The isothermal models are transformed to linear forms and linear regression in order to estimate the adsorption model parameters. The linear forms of these equation models can be easily applied to the adsorption (Wang et al. 2015a, b). Another important parameter is the dimensionless Langmuir constant, known as separation factor (R_L), which can be deduced from Eq. 8.9:

$$R_L = \frac{1}{1 + K_L C_0} \tag{8.9}$$

where C_o (mg/L) represents the initial concentration of the adsorbate. The R_L value is used to determine if the adsorption process is favoured or unflavoured. In simple terms, the nature of adsorption process is favoured if $0 < R_L < 1$, unflavoured if $R_L > 1$, linear for $R_L = 1$ and irreversible for $R_L = 0$ (Yan et al. 2015).

8.3.1.2 Freundlich Isotherm Model

The Freundlich isotherm model is the ancient known relation used to describe nonideal and reversible adsorption, not limited to the emergence of monolayer adsorption. Its development was initially for the adsorption of animal charcoal. The results demonstrated that the ratio of the adsorbed material onto a given mass of adsorbent to the solute was changing at different concentrations of the solution (Yan et al. 2015). The Freundlich isotherm model can be applied to multilayer adsorption that has non-uniform dispersal of adsorption heat and affinities over the heterogeneous surface (Montagnaro and Balsamo 2014). In context, the model assumes that the amount of adsorbed molecules is added for all active sites having distinct bond energy, with the stronger binding sites being occupied first. The system is continuous until the adsorption process is complete and adsorption energy decreases exponentially (Yan et al. 2015; El-khaiary 2008). The Freundlich isotherm model is represented by Eq. 8.10:

$$q_e = K_F C_e^{1/n} \tag{8.10}$$

where K_F denotes the Freundlich adsorption constant (mg/g)(L/g)^n and 1/n is associated with the determination of adsorption intensity (El-khaiary 2008). This multilayer adsorption model does not have the linear transformations and therefore was linearised by taking the logarithm of both sides of empirical equation as shown in Eq. 8.11 (Montagnaro and Balsamo 2014):

$$\ln qe = lnK_F + \frac{1}{n} lnC_e \tag{8.11}$$

Currently, Freundlich isotherm model is commonly used in heterogeneous systems for organic compounds, activated carbon or molecular sieves having exceedingly interactive species. The adsorption intensity or surface heterogeneity is measured with slope values ranging between 0 and 1. The surface of the adsorbent becomes more heterogeneous if the adsorption intensity value approaches zero. If the $1/n$ value is above on, it indicates cooperative adsorption and implies chemisorption below a unity value. The Freundlich model correlates well with Langmuir model at adequate concentrations. At lower concentrations, it deviates from Henry's Law, by not reducing to linear isotherm, and this is due to lack of fundamental basics of thermodynamics (Montagnaro and M. Balsamo 2014; El-khaiary 2008).

8.3.1.3 Thermodynamics Parameters

In overall, thermodynamics simply defines the changes of matter as a function of state variables such as pressure, temperature and chemical composition (Vi and Belton 1976). Therefore, adsorption process can be referred to as the simple adjustment in the state of adsorbate, i.e.:

$$C \rightarrow C_{ads} \Delta G^{\circ} \tag{8.12}$$

where C (mg/L) is the molar concentration of the adsorbate in bulk solution, C_{ads} (mg/L) represents the adsorbed concentration at time and ΔG° (kJ/mol) describes the change in effective free energy of adsorption (Hirth and Rice 1980). The adsorption process is favoured if ΔG° decreases with an increase in the adsorbate concentration, and therefore ΔG° can be described by Eq. 8.13, respectively (Liu and Liu 2008):

$$\Delta G^{0} = -RT \ln K_{eq} \tag{8.13}$$

where equilibrium constant K_{eq} (L/mol) represents the ratio of equilibrium concentration of adsorbed molecules to that remaining in bulk solution, T (K) represents the absolute temperature and R (J/mol.K) is the gas constant. The values of ΔG° can be calculated using the K_{eq} values obtained from the adsorption isotherm data of different experimental temperatures (Hirth and Rice 1980; Kara et al. 2015). Since ΔG° is a function of the change in enthalpy (ΔH° (kJ/mol)) of adsorption and change in entropy (ΔS° (kJ/mol)), it can be written as in Eq. 8.14:

$$\Delta G^{0} = \Delta H^{0} - \Delta T^{0} \tag{8.14}$$

A combination of Eqs. 8.13 and 8.14 reduces to Eq. 8.15:

$$\ln K_{eq} = \frac{\Delta S^{0}}{R} - \frac{\Delta H^{0}}{RT} \tag{8.15}$$

It is shown from Eq. 8.15 that both (ΔH°) and (ΔS°) can be deduced experimentally from a plot of $\ln K_{eq}$ against $1/T$, where the slope denotes enthalpy change and entropy change is represented by the intercept (Hirth and Rice 1980).

8.3.2 Adsorption Kinetics

Adsorption rate for the removal of contaminants from solid/liquid systems is complex subject as compared to the theoretical analysis of adsorption equilibrium (Jeppua and Clement 2012). The adsorption equilibrium takes into account only the final distributions of the pollutants amongst the solid and aqueous phases,

independent of adsorbate transportation and capturing steps which are involved in the sorption process that are time-dependent (Ali 2014). Predicting the rate at which pollutants move from bulk solution to the surface of the adsorbent is an essential factor used for determining the efficiency of adsorption process. There are various endeavours which have been implemented to formulate general mathematical expressions that can be applied to sufficiently describe the kinetics of adsorption in such systems (Bisinella et al. 2016). Generally, the rate at which pollutants are adsorbed to the adsorbent surface is dependent on both the actual attachment of the pollutants onto the available adsorptive sites (described by the equivalent kinetic and equilibrium constant parameters) and their mass transfer towards these active sites represented by analogous diffusion coefficient (Plazinski et al. 2009). Kinetics study of solid/liquid schemes are carried out under batch mode of adsorption, and data obtained from the remaining concentration of adsorbate in solution is fitted to an appropriate kinetic model. The most commonly applied adsorption models are pseudo-first and pseudo-second order (Tripathi and Tabor 2016). However, it is recognised that the overall rate of adsorption on a porous solid may be explained by three consecutive steps mechanism, i.e. (Miyake et al. 2013):

- External mass transport, which is the flow of the adsorbate through the liquid phase adjoining the adsorbent particles
- Intraparticle diffusion, which represents the distribution within the adsorbent particle and can result from either pore or surface or a mixture of the two
- Surface reaction that refers to adsorption rate at the interior sites

Many adsorption systems have the surface reaction step being the fastest process and the intraparticle or film diffusion being the rate determining step (Miyake et al. 2013; Yao and Chen 2017).

8.3.2.1 Pseudo-First-Order Model

The introduction of the first empirical rate equation was presented by Lagergren during the end of the nineteenth century (Vi and Belton 1976). His rate equation was developed for kinetics studies of oxalic and malonic acids adsorption onto charcoal (Bisinella et al. 2016). The first order or Lagergren equation is regarded as first order with respect to concentration of adsorbate, and solid-liquid adsorption systems are regarded as the pseudo-first-order equation (Ofomaja 2010). The mathematical expression of the model is represented by Eq. 8.16 (Marczewski et al. 2010; Eris and Azizian 2017):

$$\frac{dq_t}{dt} = k_1(q_e - q_t) \tag{8.16}$$

where q_t (mg/g) describes the amount of molecules or ions adsorbed at specified time of adsorption, q_e (mg/g) is the amount adsorbed at equilibrium state per unit mass of

the adsorbent and k_1 (1/min) represents the pseudo-first-order rate coefficient. The linearised form of the equation is obtained by integrating the empirical equation using the boundary condition q(t = 0) = 0, and it reduces to Eq. 8.17 (Ofomaja 2010; Marczewski 2010):

$$\ln (q_e - q_t) = lnq_e - k_1 t \tag{8.17}$$

The parameters q_e and k_1 are normally calculated from the generally accepted linear regression procedure, constructed from the above empirical equation. The rate coefficient, k_1, is an important parameter since it determines how fast the equilibrium can be reached within the reaction scheme. The increase in the value of k_1 means that the time required for the system to reach equilibrium is less and the value is maintained (Bisinella et al. 2016; Ofomaja 2010).

8.3.2.2 Pseudo-Second-Order Model

Second-order and pseudo-second models are the most commonly used kinetics mathematical expression whereby second order is concentration dependent and pseudo-second-order reaction is adsorption dependent. These models are represented in Eq. 8.18 (Ofomaja 2010):

$$\frac{dq_t}{dt} = k_2 (q_e - q_t)^2 \tag{8.18}$$

where k_2 (g/mg·min) is the rate coefficient for second-order models. Its integrated form is represented by Eq. 8.19 and is widely used in its linear form due to the simplicity to approximate equilibrium adsorption (Azizian and Fallah 2010):

$$\frac{t}{q_t} = \frac{1}{k_2 q_t^2} + \frac{1}{q_e} t \tag{8.19}$$

The earliest usage of the second-order equations was reported by Ritchie in 1974, followed by Blanchard in 1984; however, Ho is the well-known dynamic promoter of the equation (Haerifar and Azizian 2013). The pseudo-second-order equation was well demonstrated theoretically by Eris and Azizian (2017) and revealed that if the concentration changes significantly during experiment, it will show some properties of Langmuir rate equation. Rendering to a theoretical study that was shown by Azizian, the pseudo-second-order model rate coefficient (k_2) is a complex function of the initial solute concentration (Azizian and Fallah 2010). Some scientists proved, using statistical rate theory, that the second-order rate equation can be able to approximate the behaviour of adsorption kinetics that involves intensely heterogeneous solids (Ofomaja 2010; Haerifar and Azizian 2013).

8.3.2.3 Intraparticle Diffusion Model

Ballav et al. (2012) discussed the application of intraparticle diffusion (IPD) model, which is given in three various forms as follows:

- Adsorption amount, q_t, at a certain time is plotted against the square root of time ($t^{0.5}$) to obtain a straight line curve which is forcefully passing through the origin.
- Multi-linearity is taken into account in the plot of q_t against $t^{0.5}$; thus, two or three steps are involved in the entire procedure. Hence, the initial occurring step is external surface adsorption or instantaneous adsorption. The second step involves gradual adsorption, which controls intraparticle diffusion. The final step is equilibration, where solutes migrate gradually from bigger pores to micropores causing a slow adsorption rate.
- q_t is plotted against $t^{0.5}$ to obtain a straight line but does not necessarily pass through the origin; that is, there is an intercept (Yao and Chen 2017; Marczewski 2010).

The most commonly used intraparticle diffusion equation for adsorption system is specified by Weber and Morris as given in Eq. 8.20:

$$q_t = k_i t^{0.5} + C \tag{8.20}$$

where k_i (mg g^{-1} min$^{-0.5}$) denotes the intraparticle diffusion rate constant and C is the y-intercept which is obtainable through extrapolating the linear portion of the plot of q_t against $t^{0.5}$, and it provides ideas about extent of the boundary layer thickness (Yao and Chen 2017; Wu et al. 2009; Doke and Khan 2017).

8.4 Adsorbents for Cr(VI) Removal

In adsorption technology, the most important aspects to be considered are the choice and design of the adsorbent material. The selection of the appropriate adsorbent material is mainly based on the properties such as surface area, the presence of active sites, selectivity, stability, ability to be recovered after use and the rapidness of the adsorption process (Soleimani and Siahpoosh 2015; Chauke et al. 2015). Conventional adsorbents that have been utilised for the removal of heavy metals especially Cr(VI) include activated carbon, biosorbents and low-cost adsorbents such as fly ash, clay, zeolites, polymers and lignin by-products (Haerifar and Azizian 2013; Marczewski 2010; Wu et al. 2009). The challenges associated with some of these adsorbents include low adsorption capacities, inadequate chemical stability, long intraparticle diffusion distance, separation and recovery of adsorbent following remediation (Soleimani and Siahpoosh 2015; Chauke et al. 2015; Qu et al. 2013). Table 8.1 shows some of the adsorbents that have been reported for Cr

Table 8.1 Adsorbents for Cr(VI) adsorption

Adsorbents	Adsorption capacity (mg/g)	Initial concentration (mg/L)	References
Activated carbon	151.51	100	Wu et al. (2009)
Biomass	4.7	5	Karthik and Meenakshi (2014)
Natural clay	9.9	100	Dileepa Chathuranga et al. (2013)
Fly ash	4.35	50	Akar et al. (2009)
Polymers	3.4–485	100	Gupta and Ali (2004)

(VI) adsorption (Marczewski 2010; Qu et al. 2013; Karthik and Meenakshi 2014; Dileepa Chathuranga et al. 2013; Akar et al. 2009). Amongst these adsorbents, polymers have shown to have a range of highest adsorption capacity for Cr (VI) removal from wastewater.

8.5 Background of Polymers

Polymers are macromolecules made up of repeating units named monomers, which are clasped together by covalent bonds. These materials normally have higher molecular weight. The types of polymers that exist include biopolymers, which refer to the naturally occurring ones and synthetic polymers which are resulting from chemical reactions of monomers. Naturally existing polymers include proteins, cellulose, latex and starch (Mahmud et al. 2016). Synthetic polymers are usually manufactured on a large scale for commercialisation owing to their interesting properties which have a diverse range of applications. For instance, polymers such as polyethylene (PE), polystyrene (PS) and polypropylene (PP) are used as packaging materials due to their exceptional mechanical properties such as tensile and tear strength (Mahmud et al. 2016; Siracusa and Dalla 2008). The process in which polymers are formed is called polymerisation which involves the linkage of a reactive intermediate. This process is governed by the nature of the intermediate and can be classified according to the following (Wang et al. 2010; Pitsikalls 2013):

- Radical polymerisation – in which a radical is responsible for the initiation step and the process propagates via a reactive carbon radical.
- Cationic polymerisation – in this type of process, an acid is an initiator, and the process propagates a reactive site carbocation.
- Anionic polymerisation – in which a nucleophile initiates the process and the reaction proceeds through a reactive carbo-anion.
- Coordination catalytic polymerisation – in which the activator is a transition metal complex and the reaction proceeds via site reactive terminal catalytic complex.

8.5.1 Conducting Polymers

Conducting polymers (CPs) are types of synthetic polymers possessing conjugated π-electron (they have C=C alternating bonds) backbone which exhibit uncommon electronic properties such as low energy optical transition and ionisation potentials as well as high electron affinities (Akar et al. 2009). The conductivity of these polymers arises due to their easiness of being oxidised or reduced as compared to conventional polymers. The two ways of the process of doping in CPs are simplified by Eqs. 8.21 and 8.22:

$$\mathrm{Cp} \rightarrow \mathrm{Cp}^{\mathrm{n}+}\left(\mathrm{A}^{-}\right)_{\mathrm{n}} + \mathrm{ne}^{-} \quad (p-\text{doping}) \tag{8.21}$$

$$\mathrm{Cp} + \mathrm{ne}^{-} \rightarrow \left(\mathrm{C}^{+}\right)_{\mathrm{n}}\mathrm{Cp}^{\mathrm{n}-} \quad (n-\text{doping}) \tag{8.22}$$

The p-doping is when the polymer gets oxidised with (counter) anions, whereas n-doping is when the polymer is reduced with (counter) cations. In general, the discharge reactions are the reverse of the mentioned equations, and some CPs, especially polythiophene, can undergo both doping processes (Hutchinson 2013). Various factors that affect the conductivity of conducting polymers include the polaron length, conjugation length, overall chain length as well as the charge transfer between adjacent molecules (Snook et al. 2011; Stenger-Smith 1998; Gerard et al. 2002). The commonly known conducting polymers and their structures are listed in Fig. 8.3, respectively.

The inherent properties of conducting polymers include the combination of both electrical characteristics of the metals and attractive features of polymers such as

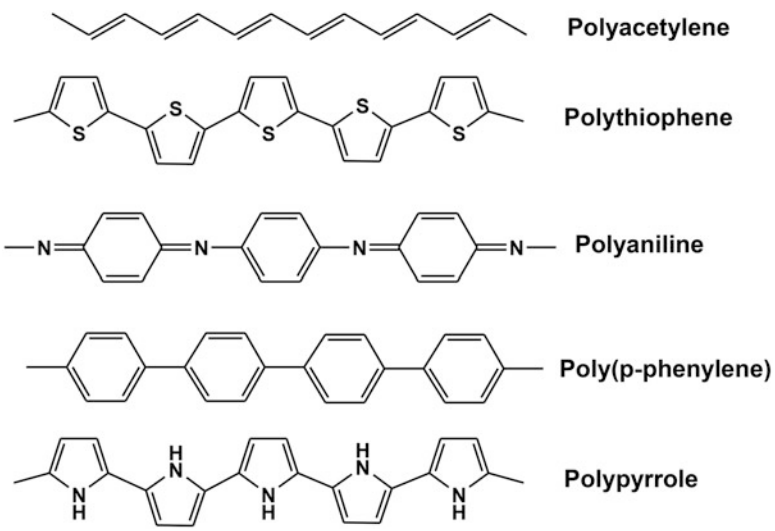

Fig. 8.3 Molecular structures of various conducting polymers

resist chemical attack and corrosion resistance, lighter weight, greater workability and their cost effective synthesis (Snook et al. 2011; Gerard et al. 2002). Owing to these interesting properties, conducting polymers have gained attention for various industrial applications including biosensors (Brooke et al. 2017; Monama et al. 2018), energy storage devices (i.e. supercapacitors, batteries and solar cells) (Hutchinson 2013; Ziadan 2012), corrosion inhibitors, biomedical engineering (Ates 2013) as well as wastewater treatment (Fan and J. Maier 2006; Hao et al. 2013). More research is being done on the removal of Cr(VI) and its reduction to less toxic Cr(III) that involves its complexation with conducting polymers (Ravichandran et al. 2010; Bhaumik et al. 2015). Based on the results arising from these studies, conducting polymers have been used in the analysis of other toxic heavy metals present in the environment (Bhaumik et al. 2015). Amongst these conducting polymers, polypyrrole (PPy) and polyaniline (PANI) are the most popular polymers used in water purification technologies (Dhal et al. 2013; Wang et al. 2015a, b; Krishnani et al. 2013). This is owing to their high stability in ambient conditions, wide range of tunable conductivity as well as incredible electroactivity. As a result, other researchers have given their attention to chemical reactions and physical interactions occurring between conducting polymers and toxic heavy metal ions (Bhaumik et al. 2015; Olad and Nabavi 2007; Bhaumik et al. 2012).

8.5.1.1 Polypyrrole

Polypyrrole (PPy) has received greater attention in a wide range of application due to its ease synthesis, adequate electrical conductivity, good biocompatibility, interesting electronic and redox properties, environmental friendliness, low cost and easiness synthesis. Other advantageous properties of PPy that are essential for other technological includes thermal stability and biodegradation in composition with biodegradable polymers (Brooke et al. 2017). For adsorption purpose, PPy contains cationic nitrogen atoms that can effectively adsorb heavy metals. And some of the counterions are included into the growing polymer chain to maintain charge neutrality. The incorporated ions can help to facilitate metal adsorption through ion exchange which is a proper aspect for water treatment (Bhaumik et al. 2012, 2016).

Polypyrrole was first synthesised in the 1916, and it showed high electrical conductivity as compared to all other polymers (Wang et al. 2015a, b). As a result, it gained popularity for application in various fields such as biosensor, gas sensors, adsorption, wires and electrolytic capacitors (Wang et al. 2010; Ziadan 2012). For application in Cr(VI) adsorption, PPy was reported focusing on its derivatives and composites for detoxification of Cr(VI) from aqueous phase (Ates 2013). The authors further synthesised PPy and carbon black alloy, which additional increased Cr(VI) adsorption capacity (Wang et al. 2011). Bhaumik et al. (2012) synthesised PPy-PANI nanofibers with the maximum adsorption capacity of 227 mg/g at pH 2 and 25 °C for 100 mg/L Cr(VI) solution. Kera and co-workers (Bilal et al. 2015; Zhao et al. 2015) prepared PPy/DABSA and PPy-mPD via in situ chemical polymerisation. They obtained maximum adsorption capacities of 303 and 526 mg/g at

pH and 25 °C for 100 mg/L Cr(VI) solution, respectively. Ballav et al. (2012) reported PPy-glycine composite for Cr(VI) removal, which had the Langmuir maximum adsorption capacity of 217.39 mg/g for 100 mg/L Cr(VI) at pH 2 and 25 °C. Li et al. (2012) synthesised PPy-GO composite with the maximum adsorption capacity of 497.1 mg/g for a 0.2 mg/L of Cr(VI) at pH 3 and 25 °C. The two commonly used methods for preparing PPy are oxidative chemical and electrochemical polymerisation (Ballav et al. 2012).

Chemical Polymerisation

Chemical polymerisation is the simplest polymerisation process which is faster and does not require specialised instrumentation. This process involves oxidative polymerisation of pyrrole monomer to polypyrrole, which occurs through a one electron oxidation of pyrrole to a radical cation. The resultant radical couples with another radical forms 2,2-'bipyrrole, which continues coupling and forming longer PPy chain as shown by the Scheme 8.2 (Li et al. 2012; Wang et al. 2001; Kumar et al. 2015a, b).

Chemical oxidative polymerisation results in bulk quantities of PPy, which is obtainable in fine powder form. This process is achievable through oxidative polymerisation of pyrrole monomer with a suitable chemical oxidant and can be in aqueous or nonaqueous solvents or via chemical vapour deposition. However, using chemical polymerisation restricts the amount of counterions that may be

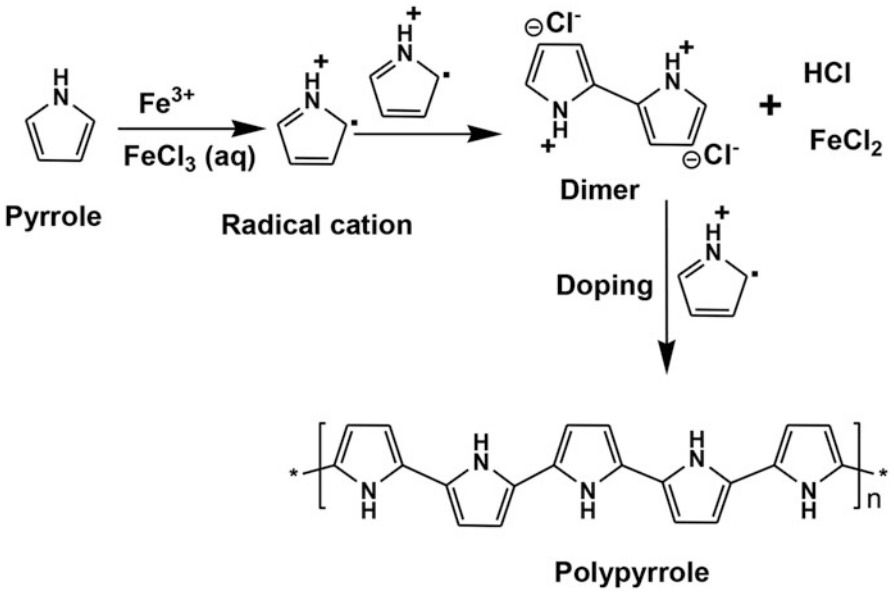

Scheme 8.2 Chemical polymerisation of pyrrole monomer

incorporated, and this restricts the range of conducting polymers that can be produced. The process is seemingly a common and beneficial tool for the synthesis of conductive polymer composites and dispersed particles in aqueous media (Kausaite-minkstimiene et al. 2015). The regularly used chemical oxidants for the preparation of CPs in aqueous phase, during this process, are $(NH_4)_2S_2O_7$ and $FeCl_3$ (Tan and Ghandi 2013). The suitable chemical oxidant for chemical polymerisation has been identified as iron (III) chloride, whereas water is regarded as the ideal solvent in terms of appropriate conductivity characteristics (Ansari 2006). The overall stoichiometry resulting from chemical polymerisation of PPy with ferric chloride oxidant is shown in Scheme 8.2. In the chemical polymerisation of pyrrole, charge neutrality over the polymer backbone is sustained by anions introduced onto the polymer from the reaction solution. The anions are typically from the chemical or reduced product of the oxidant. For instance, if $FeCl_3$ or Cl_2 are utilised as oxidants, then Cl^- ion is blend in as counterion (Kausaite-minkstimiene et al. 2015).

Electrochemical Polymerisation

The electrochemical polymerisation involves making electroactive/conductive films, wherein CPs are deposited on conductive substrates (Tan and Ghandi 2013; Lange et al. 2008). This method is very flexible and offers a facile way of varying film properties by merely changing the electrolysis conditions such as electrode potential, current density, solvent and electrolyte in a controlled way. The electrochemical polymerisation mechanism (Scheme 8.3) comprises a variety of steps, which are listed below (Gerard et al. 2002):

- Forming a radical cation by oxidising a monomer
- Dimerisation of radical cations through proton loss that yields a neutral dimer
- Oxidising the dimer to form its radical cation
- Reaction between dimer radical cation and additional radical cation

Electrochemical polymerisation process can be performed by applying techniques such as (i) galvanostat (i.e. applying constant current), (ii) potentiostat (using constant voltage) or (iii) cyclic voltammetry (changing the voltage) (Stenger-Smith 1998; Lange et al. 2008). This method of preparing CPs is complex, and the type of polymer film can be affected by a variety of factors such as nature and concentration of monomer/electrolyte, cell conditions, the solvent, electrode, applied potential and temperature as well as pH.

The electrochemical process is advantageous since the thickness of the film can be controlled by charge passing through the electrochemical cell during film growth (Tan and Ghandi 2013). However, the disadvantages of this method include difficulty in preparing large quantity of polymer, since the polymerisation is performed on the surface of the electrode. Another drawback is that PPy prepared electrochemically is often insoluble in common organic solvents as well as in water (Wang et al. 2001).

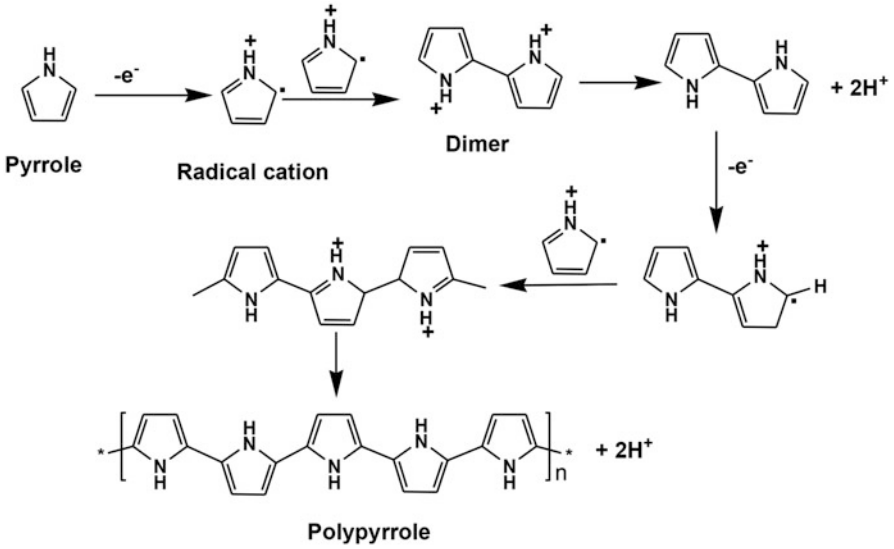

Scheme 8.3 Electrochemical polymerisation of pyrrole monomer

8.5.1.2 Polyaniline

Polyaniline (PANI) and its derivative (polyphenylenediamines) have attained greater attention in the study of conducting polymers owing to their exceptional electrical property which has widespread potential applications (Bhaumik et al. 2016). The three isomers of phenylenediamines are originating from the addition of amino group onto the *ortho*-, *para*- and *meta*-positions of the aniline (Brezoi 2010). Phenylenediamines or "amino anilines" can undergo similar oxidation pathways as aniline and form corresponding oligomers and polymers. Same as PANI and PPy, these polymers can simply be synthesised by oxidative chemical or electrochemical polymerisation method. Due to the lower conductivity as compared to polyaniline, they are ranked amongst non-conductors (Fonner et al. 2008). And since electrical conductivity is not the only important parameter, phenylenediamines have been used extensively (Fonner et al. 2008). Polyphenylenediamine (PPD) have been used for heavy metal ion adsorption owing to their abundant amine/imino functional groups in the conjugated structure which facilitate more metal adsorption through chelation or redox reaction as compared with polyaniline (Li et al. 2005; Stejskal 2015). Consequently, more research work has been dedicated to their application in wastewater remediation due to their robust adsorbability, rapid adsorption rate and cost effectiveness than traditional adsorbents such as the activated carbon, clays and zeolites (Stejskal 2015). However, PPD and PPy are amorphous in nature which resulted in low surface area and hard to recover in solution. In order to overcome these drawbacks, nanotechnology may be employed.

8.6 Nanotechnology

Nanotechnology is a scientific discipline that covers a variety of technologies that are performed at a nanometre scale. These technologies include the design, production and application of devices, structures and systems by manipulating the size and shape at a scale between 1 and 100 nm (Cui et al. 2015; Akbarzadeh et al. 2012). Different forms of nanomaterials produced include nanowires, nanotubes, films, particles and quantum dots. These are by far the smallest structures that have been developed by humans (Kong et al. 2013). Nanotechnology has been applied in various areas such as energy for hydrogen production and storage (Amer et al. 2013; Anjum et al. 2016) medicine for drug delivery and tissue engineering (Ramohlola et al. 2017, 2018), cosmetics (Ochubiojo et al. 2012) and in water treatment for catalysis (Shi et al. 2010) and adsorption (Ssneha 2014). Based on a wide range of applications, nanoscale offers material with ideal properties such as high specific surface area, enhanced catalytic properties, antimicrobial activity, high conductivity, high sensitivity and stability (Tuan et al. 2015). For adsorption process, the inherent properties provided by nanomaterials include tuneable surface chemistry, easy reuse, superparamagnetic and short intraparticle distance (Chauke et al. 2015). The development and application of nanotechnology for water treatment has since been at the heart of water research.

8.7 Nanomaterials for Water Treatment

Nanomaterials for water treatment encompasses both organic and inorganic forms and are classified according to their surface and physical properties depending on the treatment method that is being implemented (Cui et al. 2015). These nanomaterials include nano-adsorbents, nano-catalysts, nano-sensors and nano-membranes (Chen et al. 2014). Nano-catalysts are mainly used for reduction or degradation of contaminants (Kong et al. 2013; Brame et al. 2011; Zhang et al. 2016). Nano-sensors are used for the detection of pollutants in water, through emission of light (Vellaichamy et al. 2017). Nano-membranes are used for filtration of wastewater leaving the pollutants on the surface of the membrane and water passing through (Debnath et al. 2015; Li et al. 2011). For adsorption technology, well-studied nano-adsorbents include carbon-based nano-adsorbents, metal oxides, metallic nanoparticles, nanoclays and nanofibers (Cui et al. 2015).

8.7.1 Carbon-Based Nano-adsorbents

Carbon-based nanomaterials are mainly composed of carbon atom, and these include single-walled carbon nanotubes (SWNT), graphene (G), graphene oxide (GO) and

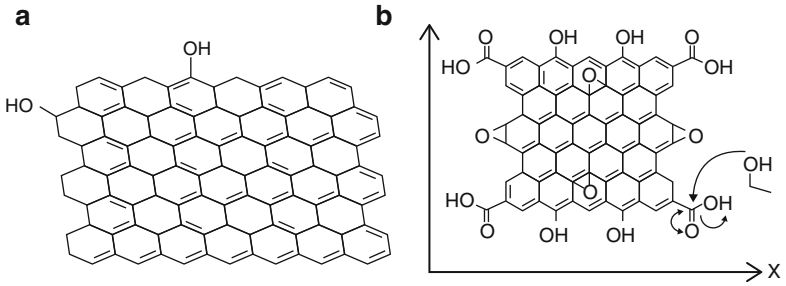

Fig. 8.4 Structural arrangements of (**a**) graphene (Kumar et al. 2017) and (**b**) graphene oxide (Maktedar et al. 2014)

multi-walled carbon nanotubes (MWNT) (Zhu et al. 2013; Wu et al. 2014a, b). These materials have become attractive due to their excellent characteristics which include high surface area and the ability to inhibit bacterial growth upon contact with the cells (Zinadini et al. 2014; Smith and Rodrigues 2015). Carbon nanomaterials are rarely used in their pure form. They can be dispersed in polymers or be doped with metallic nanoparticles. Functionalisation of carbon-based nanomaterials offers the following characteristics: improvement in the hydrophilicity of the materials leading to better dispersion in aqueous solutions and improve the surface charge of the nanomaterial to increase the electrostatic interaction between the adsorbate and the adsorbent (Wu et al. 2014a, b). Graphene is a 2D carbon sheet of carbon atoms bonded through sp^2 hybridisation as shown in the Fig. 8.4(a) (Hegab and Zou 2015). The unique properties of graphene amongst others include high mechanical strength, thermal and electrical conductivity, flexibility and excellent electronic properties (Chen et al. 2014; Luo et al. 2013).

GO is a single layer carbon nanomaterial produced by oxidation of graphite layer (Kong et al. 2013). Various functional groups that forms part of GO the structure includes hydroxyl, carboxyl, carbonyl and epoxy groups (Chen et al. 2014; Kuilla et al. 2010). Figure 8.4(b) represents the structure of GO, with hydroxyl and carboxyl functional groups (Hummers and Offeman 1958) which increases the adsorption of heavy metal. The attraction of GO is due to its excellent properties such as light weight, chemical stability, mechanical strength, its two basal planes for maximum adsorption of heavy metals and easy to synthesise (Kong et al. 2013). Carbon nanotubes (CNT) are small, concentric cylinders of rolled-up graphene sheets as shown in Fig. 8.5. Their walls behave as basal plane of graphite, while their edge plane and tube ends are the electrochemically active sites (Sreeprasad et al. 2011).

The unique features of CNT which contribute to high removal capacities include fibrous shape with high aspect ratio, large external surface area and well-developed mesopores (Chauke et al. 2015; Li et al. 2015a, b). CNT aggregates have high affinity towards organic pollutants due to the interstitial spaces and grooves, which are high adsorption energy sites for organic molecules (Chauke et al. 2015).

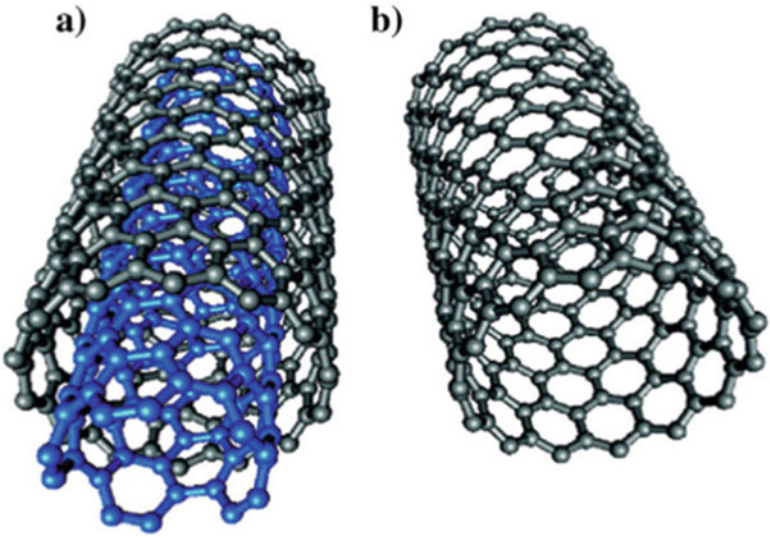

Fig. 8.5 The structural difference between (**a**) multi-walled carbon nanotube and (**b**) single-walled carbon nanotube (Santhosh et al. 2016)

However, single-walled CNT have poor dispersion ability and difficulty in separation; hence, they are being modified to multi-walled CNT (Kong et al. 2013). The difference between single-walled carbon nanotubes (SWNTs) and multi-walled carbon nanotubes (MWNTs) is the number of layers they possess (Cui et al. 2015).

8.7.2 Nanoclays and Nano-fibres

Clays are hydrous aluminium-silicate-bearing minerals with layered sheet structure held together by van der Waals forces (Khobragade et al. 2016). Adsorption of metal onto the structure of clay minerals can occur on three types of crystalline surfaces, which are a hydroxyl, oxygen and particles edges. The oxygen plane is associated with the silica tetrahedral layer, the hydroxyl plane is associated with alumina octahedral plane and the irregular lattice structure forms particle edges (Cui et al. 2015; Khobragade et al. 2016). The commonly reported clays for nanocomposite formation include montmorillonite, laponite and sepiolite and the others (Gupta et al. 2011; Soleimani and Siahpoosh 2016). Montmorillonite has attained much attention because of its abundance and has high exchange capacity (Shirsath et al. 2011). Introduction of nanoclays on adsorbents such as polymers and hydrogels provides the nanocomposite formed with inherent properties which includes good mechanical and thermal strength (Gupta et al. 2011; Patel et al. 2006). Their porous structure and ion-exchange properties provide high adsorption capacities for the removal of

pollutants from wastewater (Srinivasan and Viraraghavan 2010; Soleimani and Siahpoosh 2016).

Nanofibers can be prepared from different adsorbents such as polymers, metal oxides and also membranes. The mostly used method for the preparation of different nanofibers is electrospinning (Akbarzadeh et al. 2012; Kong et al. 2013). The nanoscale diameter of the nanofibers makes them efficient as they lead to high surface area (Shahid et al. 2017). Different nanofibers such as PPy nanofibers (Pillai and Ray 2012), PANI nanofibers (Krishnani et al. 2013), sodium titanate nanofibers (Duruibe et al. 2007) and chitosan/polymethylmethacrylate (PMMA) fibrous membrane (Srinivasan 2011) have been reported for wastewater treatment.

8.7.3 Metal Oxide and Metallic Nanoparticles

Metal oxide nanoparticles and metallic nanoparticles have gained popularity in water treatment due to their outstanding performance and cost effectiveness for removal of pollutants from wastewater. Metallic and metal oxide nanoparticles are inorganic nanoparticles which are prepared from non-metals and metals. Various methods for synthesising these materials include sol-gel method (Al_2O_3 and TiO_2) (Chen et al. 2014), reduction of metal salts ($AgNO_3$, $FeCl_2$ and $KMnO_4$) with reducing agents such as sodium borohydrate ($NaBH_4$) and hydrazine (Brame et al. 2011; Salem et al. 2016). Xu et al. (2012) followed precipitation method for synthesis of NiO and Fe_3O_4. The nanoparticles of metal oxides are characterised by high BET surface area, minimum environmental impacts and less solubility (Duruibe et al. 2007; Kong et al. 2013). Metallic and metal oxide nanoparticles which are mostly used include titanium oxides (TiO_2), ferric oxides, nanosized zero-valent iron (Fe°), manganese oxide (MnO_2), magnesium oxides (MgO), cerium oxides (Ce_2O_4) and aluminium oxides (Al_2O_3) (Chen et al. 2014). Various studies have suggested that metallic and metal oxide nanoparticles have considerable adsorption affinity towards heavy metal pollutants such as chromium, arsenic, cadmium, uranium and other contaminants like organic and phosphates with regard to high capacity and selectivity (Kong et al. 2013; Chen et al. 2014). For application in water treatment, metal oxide and metallic nanoparticles have been widely used to form composites with materials such as polymers (Akbarzadeh et al. 2012), carbonaceous materials (Smith and Rodrigues 2015), membranes (Kim and Van Der Bruggen 2010) and clays (Gupta et al. 2011) to improve their dispersion stability (Wu et al. 2014a, b). In metal oxides, the adsorption process is controlled by the complexation between dissolved metals and oxygen. The first step is the fast adsorption of metal ions on the external surface of the metals oxides. The second step is the rate-liming intraparticle diffusion taking place along the micropore walls. At a nanoscale, metal oxides possess high adsorption capacity and fast kinetics, due to high specific surface area, short intraparticle diffusion distance and large number of active sites (Rad et al. 2009; Chauke et al. 2015).

8.7.4 Magnetic Iron Oxide Nanoparticles

The use of iron oxide for wastewater remediation has gained much interest over the years, due to its natural occurrence and its simple synthesis (Li et al. 2015a, b; Zhang et al. 2015; Rasmussen and Muhling 2018). A number of studies have suggested that iron oxide is cost effective and eco-friendly material to be utilised in the adsorption of toxic heavy metals (Eslami et al. 2018). Various phases of iron oxide that exist in nature include magnetic magnetite (Fe_3O_4), maghemite (γ-Fe_2O_3) and hydrous ferric oxides (HFO) and non-magnetic hematite (α-Fe_2O_3) and goethite (α-FeOOH) (Chen et al. 2014; Ward et al. 2018; Xu et al. 2012). The most extensively used iron oxide forms are magnetite and maghemite due to their low toxicity, good magnetic property and cheaper price. In addition to their inherent properties, these magnetic iron oxide forms can easily undergo surface chemical modification, which results in improved capacity for the removal of heavy metals from wastewater (Ward et al. 2018). Maghemite is the oxidised form of magnetite which has a cubic crystal structure that is similar to the inverse spinel crystal structure of magnetite (Zare et al. 2015; Anjum et al. 2016). Its synthesis mostly involves co-precipitation of iron salts in the presence of a base. Magnetite is formed from a mixture of iron oxides (FeO and·Fe_2O_3), which resulted in an inverse spinel crystal structure. The structure of the inverse spinel consists of half of the Fe^{3+} in a tetrahedral coordination, the other half and Fe^{2+} ions are in octahedral coordination (Anjum et al. 2016). Due to their high specific area and superparamagnetic properties, magnetite and maghemite have gained extensive application in water research for the removal of toxic heavy metals and other pollutants from wastewater (Rad et al. 2009; Ward et al. 2018; Ilankoon 2014; Xu et al. 2012).

8.8 Magnetic Nanocomposites

Magnetic nanocomposites have been extensively explored for the removal of various pollutants from wastewater. This is because these materials combine the exceptional physical or chemical features such as greater density of active sites per unit mass owing to their superior specific surface area and super paramagnetic property for easy separation. Additionally, magnetic nanomaterials display larger surface free energy, resulting in enhanced surface reactivity. Taking the benefits of these size-dependent effects, modern wastewater purification methods can be significantly developed with the introduction of magnetic nanocomposites into systems (Chen et al. 2014). Different PPy-based magnetic nanocomposites for the removal of toxic Cr(VI) from wastewater have been reported in literature.

Ballav et al. (2014) synthesised Fe_3O_4@glycine-PPy nanocomposite via in situ oxidative polymerisation. The maximum adsorption capacity obtained from Langmuir was 238 mg/g for 25 °C temperature at pH 2, initial Cr(VI) concentration

of 200 mg/L and adsorbent dose of 100 mg. Wang et al. (2015a, b) reported a PPy-decorated Fe_3O_4/rGO nanocomposite which had the Langmuir maximum adsorption capacity of 180.8 mg/g at pH of 3 and 25 °C for 48.4 mg/L initial concentration of Cr(VI) solution and 250 mg adsorbent dose. PPy/γ-Fe_2O_3 nanocomposites were reported by Chávez-Guajardo et al. (2015) wherein the maximum adsorption capacity was obtained to be 208.8 mg/g. The synthesis involved in situ chemical polymerisation of pyrrole monomer in the presence γ-Fe_2O_3 nanoparticles. Kera et al. (2016) chemically oxidised pyrrole and aniline monomers in the presence of Fe_3O_4, to form PPy-PANI/Fe_3O_4 nanocomposite. They obtained the maximum adsorption capacity of the nanocomposite to be 303 mg/g for 100 mg/L of Cr(VI) solution at a pH 2 and 25 °C with a dose 50 mg adsorbent dose. Wang et al. (2017) prepared PmPD/rGO/NFO nanocomposite via in situ oxidative polymerisation of mPD monomer in the presence of rGO/NF. They obtained maximum adsorption capacity 502.5 mg/g at pH 3, dose of 10 mg and 25 °C temperature for Cr(VI) initial concentration of 50 mg/L. Bhaumik et al. (2011) chemically oxidised pyrrole monomer in the presence of Fe_3O_4 to prepare PPy-Fe_3O_4 via in situ polymerisation. The prepared PPy-Fe_3O_4 (100 mg) nanocomposite had the Langmuir maximum adsorption capacity of 169.59 mg/g for 200 mg/L Cr(VI) solution at pH 2 and 25 °C. The above literature shows that magnetic polymer-based nanocomposite has activity against toxic Cr (VI) (Table 8.2).

8.9 Conclusions

This review article covers the recent studies done for the aqueous hexavalent chromium removal using polymer-based nanocomposites. Adsorption technology has been identified as the most promising treatment method due to its ease operation and low cost. This review explained the principle behind adsorption technology and some of the important parameters such as solution pH, temperature and concentration, adsorbent dose and the effect of contact time. Two isotherm models, which are Langmuir and Freundlich models, have been explained in terms of how they are used to determine the maximum adsorption capacity of an adsorbent. It was seen that the optimum pH value for chromium (VI) adsorption onto iron oxide nanocomposites are within the range of 2–3. The choice of adsorbent is very vital, and this review emphasised the importance of using magnetic nanomaterials for Cr(VI) removal due to their high surface area and easy separation from aqueous solution after adsorption. Different nanosorbents that have been reported in literature include CNTs, GO, nanoclays and polymer-based magnetic nanocomposites. The surveyed literature demonstrated that amino functionalised magnetic polymer (polypyrrole and polyaniline) nanocomposites are efficient for the removal of Cr(VI) from wastewater. In the future, combination of both copolymers may be the best option for treatment of wastewater. From the results, it is evident that more attention needs to be paid on adsorption experiments with actual industrial wastewaters, as they are

Table 8.2 Adsorption capacity of Fe_3O_4 nanocomposite for removal Cr(VI)

Composites	Q_{max} (mg/g)	pH	Material dose (mg	Concentration (mg/L)	References
Fe_3O_4- chitin/MWCNT	11.3	2	40	50	Salam (2017)
Magnetic-MWCNT	14.28	5	5	11.5	Salam (2017)
Magnetic-activated carbon	2.8	5	5	11.5	Bayazit and Kerkez (2014)
Fe_3O_4/CTAB	18.5	4	12	100	Elfeky et al. (2017)
Fe_3O_4-GO	31.8	3	50	50	Hou et al. (2016)
Fe_3O_4-chitosan	46	4	50	100	Li et al. (2008a, b)
EDA- F_3O_4	32.15	2.5	50	50	Zhao et al. (2010)
Magnetic-β-cyclodextrin-chitosan/GO	67.66	3	100	50	Li et al. (2013)
$FeNi_3/TiO_2$	76.335	3	500	0.5	Shekari et al. (2017)
Fe_3O_4@C@MgAl-LDH	152	6	20	100	Kumar et al. (2015a, b)
EDA/GMA-Fe_3O_4@SiO_2@cellulose	171.5	2	20	150	Sun et al. (2014)
PPy/Fe_3O_4	169.4	2	100	200	Chávez-guajardo et al. (2015)
MnO_2/Fe_3O_4/o-MWCNTs	186.9	2	50	300	Luo and Wei (2013)
PANI-magnetic mesoporous silica	193.85	2	8	100	Tang et al. (2010)
Fe_3O_4/PPy microspheres	209.2	2	20	50	Liu et al. (2011)
Magnetic poly-(MA-DVB) microspheres	231.8	3	200	150	Wang et al. (2012a, b, c)
Fe_3O_4@gly-PPy NCs	238	2	100	200	Ballav et al. (2012)
Fe/CMK-3	256.86	5	10	100	Hu et al. (2012)
PPy-decorated Fe_3O_4/rGO	293.3	3	250	48.4	Wang et al. (2015a, b)
PPy-PANI/Fe_3O_4	303	2	50	100	Wang et al. (2012a, b, c)
Fe_3O_4 (PAA coated and amino functionalized)	370.37	2	625	500	Gao et al. (2015)
Magnetic zeolite-PPy	344.83	2	100	300	Mthombeni et al. (2015a, b)
PANI/Fe^0 nanofibers	434.78	2	10	100	Bhaumik et al. (2015)
Fe_3O_4-Polyethylenimine/poly (glycidyl methacrylate)	492	2	100	150	Sun et al. (2014)

more complex solutions consisting of different ions and the performance of adsorbent may be considerably different from the performance in the laboratory prepared from single ion solution. By taking all the facts into consideration, we can conclude that magnetic polymer-based nanomaterials are potentially useful nanosorbents for the removal of hexavalent chromium from aqueous solution; however, more work is still required to develop the systems to be applied in industrial scale.

Acknowledgements KDM and MJH would like to thank the National Research Foundation (NRF) (Grant Nos. 99166 and 99278), University of Limpopo (Research Development Grants R202 and R232) and Sasol Inzalo Foundation, South Africa, for the financial support.

Conflict of Interest We declare there are no conflicts of interest.

References

Adeleye AS, Conway JR, Garner K, Huang Y, Su Y, Keller AA (2016) Engineered nanomaterials for water treatment and remediation: costs, benefits and applicability. Chem Eng J 286:640–662

Akar ST, Yetimoglu Y, Gedikbey T (2009) Removal of chromium (VI) ions from aqueous solutions by using Turkish montmorillonite clay: effect of activation and modification. Desalination 244:97–108

Akbal F, Camc S (2011) Copper, chromium and nickel removal from metal plating wastewater by electrocoagulation. Desalination 269:214–222

Akbarzadeh A, Samiei M, Davaran S (2012) Magnetic nanoparticles: preparation, physical properties, and applications in biomedicine. Nanoscale Res Lett 7:144

Ali I (2014) Water treatment by adsorption columns: evaluation at ground level. Sep Purif Rev 43:175–205

Ali MEA (2016) Synthesis and adsorption properties of chitosan-CDTA-GO nanocomposite for removal of hexavalent chromium from aqueous solutions. Arab J Chem. https://doi.org/10.1016/j.arabjc.2016.09.010

Allen SJ, Gan Q, Matthews R, Johnson PA (2003) Comparison of optimised isotherm models for basic dye adsorption by kudzu. Bioresour Technol 88:143–152

Ameen S, Seo H, Akhtar MS, Shik H (2012) Novel graphene/polyaniline nanocomposites and its photocatalytic activity toward the degradation of rose Bengal dye. Chem Eng J 210:220–228

Amer I, Young DA, Vosloo HCM (2013) Chemical oxidative polymerization of m-phenylenediamine and its derivatives using aluminium triflate as a co-catalyst. Eur Polym J 49(10):3251–3260

Angelidaki I, Sanders W (2004) Assessment of the anaerobic biodegradability of macropollutants. Rev Environ Sci Biotechnol 3:117–129

Anjum M, Miandad R, Waqas M, Gehany F, Barakat MA (2016) Remediation of wastewater using various nano-materials. Arab J Chem. https://doi.org/10.1016/j.arabjc.2016.10.004

Ansari R (2006) Polypyrrole conducting electroactive polymers: synthesis and stability studies. J Chem 3:186–201

Asgari M, Anisi H, Mohammadi H, Sadighi S (2014) Designing a commercial scale pressure swing adsorber for hydrogen purification. Pet Coal 56:552–561

Ates M (2013) A review study of (bio) sensor systems based on conducting polymers. Mater Sci Eng C 33:1853–1859

Azizian S, Fallah RN (2010) A new empirical rate equation for adsorption kinetics at solid/solution interface. Appl Surf Sci 256:5153–5156

Badruddoza AZM, Shawon ZBZ, Rahman MT, Hao KW, Hidajat K, Uddin MS (2013) Ionically modified magnetic nanomaterials for arsenic and chromium removal from water. Chem Eng J 225:607–615

Ballav N, Maity A, Mishra SB (2012) High efficient removal of chromium(VI) using glycine doped polypyrrole adsorbent from aqueous solution. Chem Eng J 198–199:536–546

Ballav N, Choi HJ, Mishra SB, Maity A (2014) Synthesis, characterization of Fe_3O_4@glycine doped polypyrrole magnetic nanocomposites and their potential performance to remove toxic Cr (VI). J Ind Eng Chem 20:4085–4093

Barrera-Díaz CE, Lugo-Lugo V, Bilyeu B (2012) A review of chemical, electrochemical and biological methods for aqueous Cr(VI) reduction. J Hazard Mater 223–224:1–12

Bayazit SS, Kerkez Ö (2014) Hexavalent chromium adsorption on superparamagnetic multi-wall carbon nanotubes and activated carbon composites. Chem Eng Res Des 92:2725–2733

Bhatnagar A, Sillanpää M (2011) A review of emerging adsorbents for nitrate removal from water. Chem Eng J 168:493–504

Bhaumik M, Maity A, Srinivasu VV, Onyango MS (2011) Enhanced removal of Cr(VI) from aqueous solution using polypyrrole/Fe_3O_4 magnetic nanocomposite. J Hazard Mater 190:381–390

Bhaumik M, Maity A, Srinivasu VV, Onyango MS (2012) Removal of hexavalent chromium from aqueous solution using polypyrrole-polyaniline nanofibers. Chem Eng J 181–182:323–333

Bhaumik M, Choi HJ, Seopela MP, Mccrindle RI, Maity A (2014a) Highly effective removal of toxic Cr (VI) from wastewater using sulfuric acid-modified avocado seed. Ind Eng Chem Res 53:1214–1224

Bhaumik M, Choi HJ, McCrindle RI, Maity A (2014b) Composite nanofibers prepared from metallic iron nanoparticles and polyaniline: high performance for water treatment applications. J Colloid Interface Sci 425:75–82

Bhaumik M, McCrindle RI, Maity A (2015) Enhanced adsorptive degradation of Congo red in aqueous solutions using polyaniline/Fe^0 composite nanofibers. Chem Eng J 260:716–729

Bhaumik M, Agarwal S, Gupta VK, Maity A (2016) Enhanced removal of Cr(VI) from aqueous solutions using polypyrrole wrapped oxidized MWCNTs nanocomposites adsorbent. J Colloid Interface Sci 470:257–267

Bielefeldt AR, Kowalski K, Summers RS (2009) Bacterial treatment effectiveness of point-of-use ceramic water filters. Water Res 43:3559–3565

Bilal S, Perveen F, Shah AA (2015) Chemical synthesis of polypyrrole doped with dodecyl benzene sulfonic acid. J Sci Innov Res 4:33–42

Bisinella F, Módenes AN, Borba CE, Ribeiro C, Espinoza-Quiñones FR, Bergamasco R, Pereira NC (2016) Monolayer–multilayer adsorption phenomenological model: kinetics, equilibrium and thermodynamics. Chem Eng J 284:1328–1341

Blaney LM, Cinar S, SenGupta AK (2007) Hybrid anion exchanger for trace phosphate removal from water and wastewater. Water Res 41:1603–1613

Brame J, Li Q, Alvarez PJJ (2011) Nanotechnology-enabled water treatment and reuse: emerging opportunities and challenges for developing countries. Trends Food Sci Technol 22:618–624

Brezoi D (2010) Polypyrrole films prepared by chemical oxidation of pyrrole in aqueous $FeCl_3$ solution. J Sci Arts 1:53–58

Brooke R, Cottis P, Talemi P, Fabretto M, Murphy P, Evans D (2017) Recent advances in the synthesis of conducting polymers from the vapour phase. Prog Mater Sci 86:127–146

Chauke VP, Maity A, Chetty A (2015) High-performance towards removal of toxic hexavalent chromium from aqueous solution using graphene oxide-alpha cyclodextrin-polypyrrole nanocomposites. J Mol Liq 211:71–77

Chávez-guajardo AE, Medina-llamas JC, Maqueira L, Andrade CAS, Alves KGB, De Melo CP (2015) Efficient removal of Cr (VI) and Cu (II) ions from aqueous media by use of polypyrrole/maghemite and polyaniline/maghemite magnetic nanocomposites. Chem Eng J 281:826–836

Chen J, Hong X, Xie Q, Li D, Zhang Q (2014) Sepiolite fiber oriented-polypyrrole nanofibers for efficient chromium(VI) removal from aqueous solution. J Chem Eng Data 59:2275–2282

Choppala G, Kunhikrishnan A, Seshadri B, Hee J, Bush R, Bolan N (2018) Comparative sorption of chromium species as in fl uenced by pH, surface charge and organic matter content in contaminated soils. J Geochem Explor 184:255–260
Chowdhury P, Viraraghavan T (2009) Sonochemical degradation of chlorinated organic compounds, phenolic compounds and organic dyes – a review. Sci Total Environ 407:2474–2492
Cui L, Wang Y, Gao L, Hu L, Yan L, Wei Q, Du B (2015) EDTA functionalized magnetic graphene oxide for removal of Pb (II), Hg (II) and Cu (II) in water treatment: adsorption mechanism and separation property. Chem Eng J 281:1–10
Das C, Patel P, De S, Dasgupta S (2006) Treatment of tanning effluent using nanofiltration followed by reverse osmosis. Sep Purif Technol 50:291–299
Debnath S, Ballav N, Nyoni H, Maity A, Pillay K (2015) Optimization and mechanism elucidation of the catalytic photo-degradation of the dyes Eosin Yellow (EY) and Naphthol blue black (NBB) by a polyaniline-coated titanium dioxide nanocomposite. Appl Catal B Environ 163:330–342
Dhal B, Thatoi HN, Das NN, Pandey BD (2013) Chemical and microbial remediation of hexavalent chromium from contaminated soil and mining/metallurgical solid waste: a review. J Hazard Mater 250–251:272–291
Dileepa Chathuranga PK, Priyantha N, Iqbal SS, Mohomed Iqbal MC (2013) Biosorption of Cr(III) and Cr(VI) species from aqueous solution by Cabomba caroliniana: kinetic and equilibrium study. Environ Earth Sci 70:661–671
Doke KM, Khan EM (2017) Equilibrium, kinetic and diffusion mechanism of Cr(VI) adsorption onto activated carbon derived from wood apple shell. Arab J Chem 10:S252–S260
Dou W, Zhou Z, Jiang LM, Jiang A, Huang R, Tian X, Zhang W, Chen D (2017) Sulfate removal from wastewater using ettringite precipitation: magnesium ion inhibition and process optimization. J Environ Manag 196:518–526
Duruibe JO, Ogwuegbu MOC, Egwurugwu JN (2007) Heavy metal pollution and human biotoxic effects. Int J Phys Sci 2:112–118
Edebali S, Pehlivan E (2010) Evaluation of Amberlite IRA96 and Dowex 1×8 ion-exchange resins for the removal of Cr(VI) from aqueous solution. Chem Eng J 161:161–166
Elfeky SA, Mahmoud SE, Youssef AF (2017) Applications of CTAB modified magnetic nanoparticles for removal of chromium (VI) from contaminated water. J Adv Res 8:435–443
El-khaiary MI (2008) Least-squares regression of adsorption equilibrium data: comparing the options. J Hazard Mater 158:73–87
EPA (Environmental Protection Agency) (1990) Environmental pollution control alternatives. EPA/625/5-90 /025; EPA/625/4-89/023, Cincinnati, US
Eris S, Azizian S (2017) Analysis of adsorption kinetics at solid/solution interface using a hyperbolic tangent model. J Mol Liq 231:523–527
Eslami A, Arai S, Miura M, Mackizadeh MA (2018) Metallogeny of the peridotite-hosted magnetite ores of the Nain ophiolite, Central Iran: implications for Fe concentration processes during multi-episodic serpentinization. Ore Geol Rev. https://doi.org/10.1016/j.oregeorev.2018.03.020
Fan L, Maier J (2006) High-performance polypyrrole electrode materials for redox supercapacitors. Electrochem Commun 8:937–940
Fonner JM, Forciniti L, Nguyen H, Byrne JD, Kou Y, Syeda-Nawaz J, Schmidt CE (2008) Biocompatibility implications of polypyrrole synthesis techniques. Biomed Mater 3:34124
Foo KY, Hameed BH (2010) Insights into the modeling of adsorption isotherm systems. Chem Eng J 156:2–10
Gao F, Gu H, Wang H, Wang X, Xiang B, Guo Z (2015) Magnetic amine-functionalized polyacrylic acid-nanomagnetite for hexavalent chromium removal from polluted water. RSC Adv 5:60208–60219
Gerard M, Chaubey A, Malhotra BD (2002) Application of conducting polymers to biosensors. Biosens Bioelectron 17:345–359
Goh PS, Ng BC, Lau WJ, Ismail AF (2015) Inorganic nanomaterials in polymeric ultrafiltration membranes for water treatment. Sep Purif Rev 44:216–249
González O, Bayarri B, Aceña J, Pérez S, Barceló D (2016) Treatment technologies for wastewater reuse: fate of contaminants of emerging concern. In: Fatta-Kassinos D et al (eds) Advanced

treatment technologies for urban wastewater reuse, The handbook of environmental chemistry, pp 5–38. https://doi.org/10.1007/698_2015_363
Gupta VK, Ali I (2004) Removal of lead and chromium from wastewater using bagasse fly ash – a sugar industry waste. J Colloid Interface Sci 271:321–328
Gupta VK, Agarwal S, Saleh TA (2011) Chromium removal by combining the magnetic properties of iron oxide with adsorption properties of carbon nanotubes. Water Res 45:2207–2212
Haerifar M, Azizian S (2013) An exponential kinetic model for adsorption at solid/solution interface. Chem Eng J 215–216:65–71
Hao J, Meng X, Mulchandani A (2013) Hexavalent chromium removal mechanism using conducting polymers. J Hazard Mater 252–253:99–106
Hegab HM, Zou L (2015) Graphene oxide-assisted membranes: fabrication and potential applications in desalination and water purification. J Membr Sci 484:95–106
Hintermeyer BH, Lacour NA, Padilla AP, Tavani EL (2008) Separation of the chromium (iii) present in a tanning wastewater by means of precipitation, reverse osmosis and adsorption. Lat Am Appl Res 71:63–71
Hirth JP, Rice JR (1980) On the thermodynamics of adsorption at interfaces as it influences decohesion. Metall Trans A 11:1501–1511
Horst MF, Alvarez M, Lassalle VL (2016) Removal of heavy metals from wastewater using magnetic nanocomposites: analysis of the experimental conditions. Sep Sci Technol 51:550–563
Hou T, Kong L, Guo X, Wu Y, Wang F, Wen Y, Yang H (2016) Magnetic ferrous-doped graphene for improving Cr(VI) removal. Mater Res Express 3. https://doi.org/10.1088/2053-1591/3/4/045006
Hu L, Dang S, Yang X, Dai J (2012) Synthesis of recyclable catalyst–sorbent Fe/CMK-3 for dry oxidation of phenol. Microporous Mesoporous Mater 147:188–193
Hu L, Cai Y, Jiang G (2016) Chemosphere occurrence and speciation of polymeric chromium (III), monomeric chromium (III) and chromium (VI) in environmental samples. Chemosphere 156:14–20
Hummers WS, Offeman RE (1958) Preparation of graphitic oxide. J Am Chem Soc 80:1339–1339
Hutchinson RA (2013) Radical polymerization kinetics. In: Reference module in chemistry, molecular sciences and chemical engineering, pp 1–14. https://doi.org/10.1016/B978-0-12-409547-2.05416-0
Ilankoon N (2014) Use of iron oxide magnetic nanosorbents for Cr (VI) removal from aqueous solutions: a review. Int J Eng Res Appl 4:55–63
Jeppua GP, Clement TP (2012) A modified Langmuir-Freundlich isotherm model for simulating pH-dependent adsorption effects. J Contam Hydrol 129–130:46–53
Jin W, Du H, Zheng S, Zhang Y (2016) Electrochimica acta electrochemical processes for the environmental remediation of toxic Cr (VI): a review industrial fields Cr (VI) discharge/tons. Electrochim Acta 191:1044–1055
Kanchi S (2014) Nanotechnology for water treatment. J Environ Anal Chem 1:10–12
Kara A, Demirbel E, Tekin N, Osman B, Beşirli N (2015) Magnetic vinylphenyl boronic acid microparticles for Cr(VI) adsorption: kinetic, isotherm and thermodynamic studies. J Hazard Mater 286:612–623
Karthik R, Meenakshi S (2014) Removal of hexavalent chromium ions using polyaniline/silica gel composite. J Water Process Eng 1:37–45
Kausaite-minkstimiene A, Mazeiko V, Ramanaviciene A (2015) Evaluation of err56chemical synthesis of polypyrrole particles. Colloids Surfaces A Physicochem Eng Asp 483:224–231
Kera NH, Bhaumik M, Ballav N, Pillay K, Ray SS, Maity A (2016) Selective removal of Cr (VI) from aqueous solution by polypyrrole/2,5-diaminobenzene sulfonic acid composite. J Colloid Interface Sci 476:144–157
Kera NH, Bhaumik M, Pillay K, Ray SS, Maity A (2017) Selective removal of toxic Cr(VI) from aqueous solution by adsorption combined with reduction at a magnetic nanocomposite surface. J Colloid Interface Sci 503:214–228
Khobragade PS, Hansora DP, Naik JB, Chatterjee A (2016) Flame retarding performance of elastomeric nanocomposites: a review. Polym Degrad Stab 130:194–244

Kim J, Van Der Bruggen B (2010) The use of nanoparticles in polymeric and ceramic membrane structures: review of manufacturing procedures and performance improvement for water treatment. Environ Pollut 158:2335–2349

Kong Y, Li W, Wang Z, Yao C, Tao Y (2013) Electrochemistry communications electrosorption behavior of copper ions with poly (mphenylenediamine) paper electrode. Electrochem Commun 26:59–62

Kotasâ J, Stasicka Z (2000) Chromium occurrence in the environment and methods of its speciation. Environ Pollut 107:263–283

Krishnani KK, Srinives S, Mohapatra BC, Boddu VM, Hao J, Meng X, Mulchandani A (2013) Hexavalent chromium removal mechanism using conducting polymers. J Hazard Mater 252–253:99–106

Kuilla T, Bhadra S, Yao D, Kim NH, Bose S, Lee JH (2010) Recent advances in graphene based polymer composites. Prog Polym Sci 35:1350–1375

Kumar P, Gill K, Kumar S, Ganguly SK, Jain SL (2015a) Magnetic Fe_3O_4@MgAl–LDH composite grafted with cobalt phthalocyanine as an efficient heterogeneous catalyst for the oxidation of mercaptans. J Mol Catal A Chem 401:48–54

Kumar R, Singh S, Yadav BC (2015b) Conducting polymers: synthesis, properties and applications. Int Adv Res J Sci Eng Technol 2:110–124

Kumar V, Kim K-H, Park J-W, Hong J, Kumar S (2017) Review Graphene and its nanocomposites as a platform for environmental applications. Chem Eng J 315:210–232

Kunhikrishnan A, Choppala G, Seshadri B, Wijesekara H, Bolan NS, Mbene K, Kim W (2017) Impact of wastewater derived dissolved organic carbon on reduction, mobility, and bioavailability of As (V) and Cr (VI) in contaminated soils. J Environ Manag 186:183–191

Lange U, Roznyatovskaya NV, Mirsky VM (2008) Review article conducting polymers in chemical sensors and arrays. Anal Chim Acta 4:1–26

Li X, Duan W, Huang M, Rodriguez LNJ (2005) Electrocopolymerization of meta -phenylenediamine and ortho -phenetidine. React Funct Polym 62:261–270

Li G, Jiang Y, Huang K, Ding P, Chen J (2008a) Preparation and properties of magnetite Fe_3O_4-chitosan nanoparticles. J Alloys Compd 466:451–456

Li Q, Mahendra S, Lyon DY, Brunet L, Liga MV, Li D, Alvarez PJJ (2008b) Antimicrobial nanomaterials for water disinfection and microbial control: potentiaapplications and implications. Water Res 42:4591–4602

Li M, Wang Q, Shi X, Hornak LA, Wu N (2011) Detection of mercury(II) by quantum dot/DNA/gold nanoparticle ensemble based nanosensor via nanometal surface energy transfer. Anal Chem 83:7061–7065

Li S, Lu X, Xue Y, Lei J, Zheng T, Wang C (2012) Fabrication of polypyrrole/graphene oxide composite nanosheets and their applications for Cr(VI) removal in aqueous solution. PLoS One 7:1–7

Li L, Fan L, Sun M, Qiu H, Li X, Duan H, Luo C (2013) Adsorbent for chromium removal based on graphene oxide functionalized with magnetic cyclodextrin-chitosan. Colloids Surf B: Biointerfaces 107:76–83

Li F, Jiang X, Zhao J, Zhang S (2015a) Graphene oxide: a promising nanomaterial for energy and environmental applications. Nano Energy 16:488–515

Li Z, Li T, An L, Fu P, Gao C, Zhang Z (2015b) Highly efficient chromium (VI) adsorption with nanofibrous filter paper prepared through electrospinning chitosan/polymethylmethacrylate composite. Carbohydr Polym 137:119–126

Liu Y, Liu Y (2008) Biosorption isotherms, kinetics and thermodynamics. Sep Purif Technol 61:229–242

Liu B, Zhang W, Yang F, Feng H, Yang X (2011) Facile method for synthesis of Fe_3O_4@Polymer microspheres and their application as magnetic support for loading metal nanoparticles. J Phys Chem C 115:15875–15884

Luo C, Wei R (2013) Adsorption behavior of MnO_2 functionalized multi-walled carbon nanotubes for the removal of cadmium from aqueous solutions. Chem Eng J 225:406–415

Luo C, Tian Z, Yang B, Zhang L, Yan S (2013) Manganese dioxide/iron oxide/acid oxidized multi-walled carbon nanotube magnetic nanocomposite for enhanced hexavalent chromium removal. Chem Eng J 234:266–275

Lytle CM, Lytle FW, Yang N, Qian J, Hansen D, Zayed A, Terry N (1998) Reduction of Cr(VI) to Cr(III) by wetland plants: potential for in situ heavy metal detoxification. Environ Sci Technol 32:3087–3093

M'Bareck CO, Nguyen QT, Alexandre S, Zimmerlin I (2006) Fabrication of ion-exchange ultra-filtration membranes for water treatment. I. Semi-interpenetrating polymer networks of polysulfone and poly(acrylic acid). J Membr Sci 278:10–18

Mahdavinia GR, Massoumi B (2012) Effect of sodium montmorillonite nanoclay on the water absorbency and cationic dye removal of carrageenan-based nanocomposite superabsorbents. J Polym Res 19:9947

Mahmud HNME, Huq AO, Yahya RB (2016) Removal of heavy metal ions from wastewater/aqueous solution by polypyrrole-based adsorbents: a Review. RSC Adv 6:14778–14791

Maktedar SS, Mehetre SS, Singh M, Kale RK (2014) Ultrasound irradiation: a robust approach for direct functionalization of graphene oxide with thermal and antimicrobial aspects. Ultrason Sonochem 21:1407–1416

Marczewski AW (2010) Application of mixed order rate equations to adsorption of methylene blue on mesoporous carbons. Appl Surf Sci 256:5145–5152

Marczewski AW, Winter S, Sternik D (2010) Studies of adsorption equilibria and kinetics in the systems: aqueous solution of dyes – mesoporous carbons. Appl Surf Sci 256:5164–5170

Milonjić SK (2007) Short communication a consideration of the correct calculation of thermodynamic parameters of adsorption. J Serb Chem Soc 72:1363–1367

Mitra P, Sarkar D, Chakrabarti S, Dutta BK (2011) Reduction of hexa-valent chromium with zero-valent iron: batch kinetic studies and rate model. Chem Eng J 171:54–60

Miyake Y, Ishida H, Tanaka S, Kolev SD (2013) Theoretical analysis of the pseudo-second order kinetic model of adsorption. Application to the adsorption of Ag (I) to mesoporous silica microspheres functionalized with thiol groups. Chem Eng J 218:350–357

Monama GR, Mdluli SB, Mashao G, Makhafola MD, Ramohlola KE, Molapo KM, Hato MJ, Makgopa K, Iwuoha EI, Modibane KD (2018) Palladium deposition on copper (II) phthalocyanine/metal organic framework composite and electrocatalytic activity of the modified electrode towards the hydrogen evolution reaction. Renew Energy 119:62–72

Montagnaro F, Balsamo M (2014) Deeper insights into fractal concepts applied to liquid-phase adsorption dynamics. Fuel Process Technol 128:412–416

Mthombeni NH, Onyango MS, Aoyi O (2015a) Adsorption of hexavalent chromium onto magnetic natural zeolite-polymer composite. J Taiwan Inst Chem Eng 50:242–251

Mthombeni N, Mbakop S, Onyango M (2015b) Magnetic zeolite-polymer composite as an adsorbent for the remediation of wastewaters containing vanadium. Int J Environ Sci Dev 6:602–605

Narayan R (2010) Use of nanomaterials in water purification. Mater Today 13:44–46

Ochubiojo M, Chinwude I, Ibanga E, Ifianyi S (2012) Nanotechnology in drug delivery. In: Recent advances in novel drug carrier systems. https://doi.org/10.5772/51384

Ofomaja AE (2010) Intraparticle diffusion process for lead (II) biosorption onto mansonia wood sawdust. Bioresour Technol 101:5868–5876

Olad A, Nabavi R (2007) Application of polyaniline for the reduction of toxic Cr(VI) in water. J Hazard Mater 147:845–851

Patel HA, SomanI RS, Bajaj HC, Jasra RV (2006) Nanoclays for polymer nanocomposites, paints, inks, greases and cosmetics formulations, drug delivery vehicle and waste water treatment. Bull Mater Sci 29:133–145

Patra RC, Malik S, Beer M, Megharaj M, Naidu R (2010) Molecular characterization of chromium (VI) reducing potential in Gram positive bacteria isolated from contaminated sites. Soil Biol Biochem 42:1857–1863

Pattnaik BK, Equeenuddin SM (2016) Potentially toxic metal contamination and enzyme activities in soil around chromite mines at Sukinda Ultramafic Complex, India. J Geochem Explor 168:127–136

Pillai SK, Ray SS (2012) Chitosan-based nanocomposites. Nat Polym 2:33–68

Pitsikalls M (2013) Ionic polymerization. In: Reference module in chemistry, molecular sciences and chemical engineering, pp 1–19. https://doi.org/10.1016/B978-0-12-409547-2.05419-6

Plazinski W, Rudzinski W, Plazinska A (2009) Theoretical models of sorption kinetics including a surface reaction mechanism: a review. Adv Colloid Interf Sci 152:2–13

Qu X, Alvarez PJJ, Li Q (2013) Applications of nanotechnology in water and wastewater treatment. Water Res 47:3931–3946

Rad SAM, Mirbagheri SA, Mohammadi T (2009) Using reverse osmosis membrane for chromium removal from aqueous solution. World Acad Sci Eng Technol 3:505–509

Rafatullah M, Sulaiman O, Hashim R, Ahmad A (2010) Adsorption of methylene blue on low-cost adsorbents: a review. J Hazard Mater 177:70–80

Ramohlola KE, Masikini M, Mdluli SB, Monama GR, Hato MJ, Molapo KM, Iwuoha EI, Modibane KD (2017) Electrocatalytic hydrogen evolution reaction of metal organic frameworks decorated with poly(3-aminobenzoic acid). Electrochim Acta 246:1174–1182

Ramohlola KE, Monana GR, Hato MJ, Modibane KD, Molapo KM, Masikini M, Mduli SB, Iwuoha EI (2018) Polyaniline-metal organic framework nanocomposite as an efficient electrocatalyst for hydrogen evolution reaction. Compos Part B Eng 137:129–139

Rasmussen B, Muhling JR (2018) Making magnetite late again: evidence for widespread magnetite growth by thermal decomposition of siderite in Hamersley banded iron formations. Precambrian Res 306:64–93

Ravichandran R, Sundarrajan S, Venugopal JR, Mukherjee S, Ramakrishna S (2010) Applications of conducting polymers and their issues in biomedical engineering. J R Soc Interface:1–21. https://doi.org/10.1098/rsif.2010.0120

Salam MA (2017) Preparation and characterization of chitin/magnetite/multiwalled carbon nanotubes magnetic nanocomposite for toxic hexavalent chromium removal from solution. J Mol Liq 233:197–202

Salem MA, Elsharkawy RG, Hablas MF (2016) Adsorption of brilliant green dye by polyaniline/silver nanocomposite: kinetic, equilibrium, and thermodynamic studies. Eur Polym J 75:577–590

Santhosh C, Velmurugan V, Jacob G, Jeong SK, Grace AN, Bhatnagar A (2016) Role of nanomaterials in water treatment applications: a review. Chem Eng J 306:1116–1137

Shahid M, Shamshad S, Rafiq M, Khalid S, Bibi I, Niazi NK, Dumat C, Rashid MI (2017) Chromium speciation, bioavailability, uptake, toxicity and detoxification in soil-plant system: a review. Chemosphere 178:513–533

Shekari H, Sayadi MH, Rezaei MR, Allahresani A (2017) Synthesis of nickel ferrite/titanium oxide magnetic nanocomposite and its use to remove hexavalent chromium from aqueous solutions. Surf Interfaces 8:199–205

Shi J, Votruba AR, Farokhzad OC, Langer R (2010) Nanotechnology in drug delivery and tissue engineering: From discovery to applications. Nano Lett 10:3223–3230

Shirsath SR, Hage AP, Zhou M, Sonawane SH, Ashokkumar M (2011) Ultrasound assisted preparation of nanoclay Bentonite-FeCo nanocomposite hybrid hydrogel: a potential responsive sorbent for removal of organic pollutant from water. Desalination 281:429–437

Siracusa V, Dalla M (2008) Biodegradable polymers for food packaging: a review. Trends Food Sci Technol 19:634–643

Smith SC, Rodrigues DF (2015) Carbon-based nanomaterials for removal of chemical and biological contaminants from water: a review of mechanisms and applications. Carbon N Y 91:122–143

Snook GA, Kao P, Best AS (2011) Conducting-polymer-based supercapacitor devices and electrodes. J Power Sources 196:1–12

Soleimani M, Siahpoosh ZH (2015) Ghezeljeh nanoclay as a new natural adsorbent for the removal of copper and mercury ions: equilibrium, kinetics and thermodynamics studies. Chin J Chem Eng 23:1819–1833

Soleimani M, Siahpoosh ZH (2016) Journal of the Taiwan Institute of Chemical Engineers Determination of Cu (II) in water and food samples by Na^+-cloisite nanoclay as a new adsorbent: equilibrium, kinetic and thermodynamic studies. J Taiwan Inst Chem Eng 59:413–423

Sounthararajah DP, Loganathan P, Kandasamy J, Vigneswaran S (2015) Adsorptive removal of heavy metals from water using sodium titanate nanofibres loaded onto GAC in fixed-bed columns. J Hazard Mater 287:306–316

Sreeprasad TS, Maliyekkal SM, Lisha KP, Pradeep T (2011) Reduced graphene oxide-metal/metal oxide composites: facile synthesis and application in water purification. J Hazard Mater 186:921–931

Srinivasan R (2011) Advances in application of natural clay and its composites in removal of biological, organic, and inorganic contaminants from drinking water. Adv Mater Sci Eng 2011:1–17

Srinivasan A, Viraraghavan T (2010) Decolorization of dye wastewaters by biosorbents: a review. J Environ Manag 91:1915–1929

Ssneha B (2014) Application of nanotechnology in dentistry. Res J Pharm Technol 7:81–83

Stejskal J (2015) Polymers of phenylenediamines. Prog Polym Sci 41:1–31

Stenger-Smith JD (1998) Intrinsically electrically conducting polymers. synthesis, characterization, their applications. Proq Polym Sci 23:57–79

Sun X, Yang L, Li Q, Zhao J, Li X, Wang X, Liu H (2014) Amino-functionalized magnetic cellulose nanocomposite as adsorbent for removal of Cr(VI): synthesis and adsorption studies. Chem Eng J 241:175–183

Sun X, Yang L, Xing H, Zhao J, Li X, Huang Y, Liu H (2015) Synthesis of polyethylenimine-functionalized poly(glycidyl methacrylate) magnetic microspheres and their excellent Cr (VI) ion removal properties. Chem Eng J 234:1–10

Tan Y, Ghandi K (2013) Kinetics and mechanism of pyrrole chemical polymerization. Synth Met 175:183–191

Tang L, Fang Y, Pang Y, Zeng G, Wang J, Zhou Y, Deng Y, Yang G, Cai Y, Chen J (2010) Synergistic adsorption and reduction of hexavalent chromium using highly uniform polyaniline–magnetic mesoporous silica composite. Chem Eng J 254:302–1375

Thatoi H, Das S, Mishra J, Rath BP, Das N (2014) Bacterial chromate reductase, a potential enzyme for bioremediation of hexavalent chromium: a review. J Environ Manag 146:383–399

Tirtom VN, Dinçer A, Becerik S, Aydemir T, Çelik A (2012) Comparative adsorption of Ni(II) and Cd(II) ions on epichlorohydrin crosslinked chitosan-clay composite beads in aqueous solution. Chem Eng J 197:379–386

Tran VS, Hao H, Guo W, Zhang J, Liang S, Ton-that C (2015) Bioresource technology typical low cost biosorbents for adsorptive removal of specific organic pollutants from water. Bioresour Technol 182:353–363

Tripathi S, Tabor RF (2016) Modeling two-rate adsorption kinetics: two-site, two-species, bilayer and rearrangement and rearrangement adsorption processes. J Colloid Interface Sci 476:119–131

Tuan TN, Chung S, Lee JK, Lee J (2015) Improvement of water softening efficiency in capacitive deionization by ultra purification process of reduced graphene oxide. Curr Appl Phys 15:1397–1401

Tyagi S, Rawtani D, Khatri N, Tharmavaram M (2018) Strategies for nitrate removal from aqueous environment using nanotechnology: a review. J Water Process Eng 21:84–95

Vellaichamy B, Periakaruppan P, Nagulan B (2017) Reduction of Cr^{6+} from wastewater using a novel in situ-synthesized PANI/MnO_2/TiO_2 nanocomposite: renewable, selective, stable, and synergistic catalysis. ACS Sustain Chem Eng 5:9313–9324

Vi G, Belton GR (1976) Langmuir adsorption, the Gibbs adsorption isotherm, and interfacial kinetics in liquid metal systems. Metall Trans B 7:35–42
Wang LX, Li XG, Yang YL (2001) Preparation, properties and applications of polypyrroles. React Funct Polym 47:125–139
Wang J, Xu Y, Wang J, Du X, Xiao F, Li J (2010) High charge/discharge rate polypyrrole films prepared by pulse current polymerization. Synth Met 160:1826–1831
Wang J, Xu Y, Wang J, Du X (2011) Toward a high specific power and high stability polypyrrole supercapacitors. Synth Met 161:1141–1144
Wang Q, Guan Y, Liu X, Yang M, Ren X (2012a) Micron-sized magnetic polymer microspheres for adsorption and separation of Cr(VI) from aqueous solution. Chin J Chem Eng 20:105–110
Wang Q, Guan Y, Liu X, Ren X, Yang M (2012b) High-capacity adsorption of hexavalent chromium from aqueous solution using magnetic microspheres by surface dendrimer graft modification. J Colloid Interface Sci 375:160–166
Wang Y, Zou B, Gao T, Wu X, Lou S, Zhou S (2012c) Synthesis of orange-like Fe_3O_4/PPy composite microspheres and their excellent Cr(VI) ion removal properties. J Mater Chem 22:9034
Wang J, Pan K, He Q, Cao B (2013) Polyacrylonitrile/polypyrrole core/shell nanofiber mat for the removal of hexavalent chromium from aqueous solution. J Hazard Mater 244–245:121–129
Wang J, Zhang K, Zhao L (2014) Sono-assisted synthesis of nanostructured polyaniline for adsorption of aqueous Cr (VI): effect of protonic acids. Chem Eng J 239:123–131
Wang H, Yuan X, Wu Y, Chen X, Leng L, Wang H, Li H, Zeng G (2015a) Facile synthesis of polypyrrole decorated reduced graphene oxide-Fe_3O_4 magnetic composites and its application for the Cr(VI) removal. Chem Eng J 262:597–606
Wang K, Qiu G, Cao H, Jin R (2015b) Removal of chromium(VI) from aqueous solutions using Fe_3O_4 magnetic polymer microspheres functionalized with amino groups. Materials (Basel) 8:8378–8391
Wang W, Cai K, Wu X, Shao X, Yang X (2017) A novel poly(m-phenylenediamine)/reduced graphene oxide/nickel ferrite magnetic adsorbent with excellent removal ability of dyes and Cr (VI). J Alloys Compd 722:532–543. https://doi.org/10.1016/j.jallcom.2017.06.069
Ward LA, Holwell DA, Barry TL, Blanks DE, Graham SD (2018) The use of magnetite as a geochemical indicator in the exploration for magmatic Ni-Cu-PGE sulfide deposits: a case study from Munali, Zambia. J Geochem Explor 188:172–184
Worch E (2012) Adsorption technology in water treatment fundamentals, processes, and modeling. © 2012 Walter de Gruyter GmbH & Co. KG, Berlin/Boston. ISBN 978-3-11-024022-1
Wu F, Tseng R, Juang R (2009) Initial behavior of intraparticle diffusion model used in the description of adsorption kinetics. Chem Eng J 153:1–8
Wu H, Tang B, Wu P (2014a) Development of novel SiO_2-GO nanohybrid/polysulfone membrane with enhanced performance. J Membr Sci 451:94–102
Wu JJ, Lee HW, You JH, Kau YC, Liu SJ (2014b) Adsorption of silver ions on polypyrrole embedded electrospun nanofibrous polyethersulfone membranes. J Colloid Interface Sci 420:145–151
Xia L, Wei Z, Wan M (2010) Conducting polymer nanostructures and their application in biosensors. J Colloid Interface Sci 341:1–11
Xu P, Zeng GM, Huang DL, Feng CL, Hu S, Zhao MH, Lai C, Wei Z, Huang C, Xie GX, Liu ZF (2012) Use of iron oxide nanomaterials in wastewater treatment: a review. Sci Total Environ 424:1–10
Yan F, Chub Y, Zhang K, Zhang F, Bhandari N, Ruana G, Dai Z, Liu Y, Zhang Z, Kana AT, Tomson MB (2015) Determination of adsorption isotherm parameters with correlated errors by measurement error models. Chem Eng J 281:921–930
Yao C, Chen T (2017) A film-diffusion-based adsorption kinetic equation and its application. Chem Eng Res Des 119:87–92
Yoon Y, Park WK, Hwang TM, Yoon DH, Yang WS, Kang JW (2016) Comparative evaluation of magnetite-graphene oxide and magnetite-reduced graphene oxide composite for As(III) and As (V) removal. J Hazard Mater 304:196–204

Zare EN, Lakouraj MM, Ramezani A (2015) Effective adsorption of heavy metal cations by superparamagnetic poly(aniline-*co*-m- phenylenediamine)@Fe_3O_4 nanocomposite. Adv Polym Technol 34:1–11

Zhang H, Huang F, Liu D-L, Shi P (2015) Highly efficient removal of Cr(VI) from wastewater via adsorption with novel magnetic Fe_3O_4@C@MgAl-layered double-hydroxide. Chin Chem Lett 26:1137–1143

Zhang Y, Wu B, Xu H, Liu H, Wang M, He Y, Pan B (2016) Nanomaterials-enabled water and wastewater treatment. NanoImpact 3–4:22–39

Zhang L, Liu J, Guo X (2017) Investigation on mechanism of phosphate removal on carbonized sludge adsorbent. J Environ Sci 64:335–344

Zhao YG, Shen HY, Pan SD, Hu MQ (2010) Synthesis, characterization and properties of ethylenediamine-functionalized Fe_3O_4 magnetic polymers for removal of Cr(VI) in wastewater. J Hazard Mater 182:295–302

Zhao X, Lv L, Pan B, Zhang W, Zhang S, Zhang Q (2011) Polymer-supported nanocomposites for environmental application: a review. Chem Eng J 170:381–394

Zhao J, Li Z, Wang J, Li Q, Wang X (2015) Capsular polypyrrole hollow nanofibers: an efficient recyclable adsorbent for hexavalent chromium removal. J Mater Chem A 3:15124–15132

Zhou Y, Zhang L, Cheng Z (2015) Removal of organic pollutants from aqueous solution using agricultural wastes: a review. J Mol Liq 212:739–762

Zhu J, Wei S, Chen M, Gu H, Rapole SB, Pallavkar S, Hoa TC, Hoppera J, Guo Z (2013) Magnetic nanocomposites for environmental remediation. Adv Powder Technol 24:459–467

Ziadan KM (2012) Conducting polymers application. In: New polymers for special applications. InTech, pp 3–24. https://doi.org/10.5772/76437

Zinadini S, Zinatizadeh AA, Rahimi M, Vatanpour V, Zangeneh H (2014) Preparation of a novel antifouling mixed matrix PES membrane by embedding graphene oxide nanoplates. J Membr Sci 453:292–301

Chapter 9
Nanomaterials as an Immobilizing Platform for Enzymatic Glucose Biosensors

Devaraj Manoj and J. Santhanalakshmi

Contents

Abstract The development of new and innovative matrices for the immobilization of enzymes has attracted remarkable attention, given the increased demand for electrochemical biosensors. Advances in nanomaterials have enabled the design of immobilization matrices for enzymes that can directly improve the sensitivity of enzymatic biosensors at the electrode interface owing to their distinguished structural and physiochemical properties. The enzymes are attached to the electrode surface by either electrostatic or covalent attachment, but retaining the enzyme functionality for a prolonged time at the electrode interface is highly challenging in the implementation of various real-time monitoring devices. This chapter provides an overview of recent developments in electrochemical glucose biosensors based on various nanomaterials. Furthermore, more efficient nanomaterials as electrochemical platforms for electrochemical glucose biosensors are discussed in detail.

D. Manoj (✉)
Department of Physical Chemistry, University of Madras, Chennai, India

Present Address: Key laboratory of Material Chemistry for Energy Conversion and Storage, Ministry of Education, School of Chemistry and Chemical Engineering, Huazhong University of Science and Technology, Wuhan, China

J. Santhanalakshmi
Department of Physical Chemistry, University of Madras, Chennai, India

Mu. Naushad et al. (eds.), *Advanced Nanostructured Materials for Environmental Remediation*, Environmental Chemistry for a Sustainable World 25,
https://doi.org/10.1007/978-3-030-04477-0_9

Keywords Biosensor · Glucose · Modified electrode · Enzymatic · Nanomaterials

9.1 Introduction

Determination of potential molecules in biological systems such as nucleic acids, enzymes, and proteins is of great importance for understanding of their physiological functions and also for development of modern health care diagnostics. These biological molecules are involved in numerous functions in the human body, which include storage, transmission, and transportation of small molecules, and regulation of physiological activities (Paleček and Bartošík 2012; Kirsch et al. 2013). The practice of using devices for both preclinical studies and clinical diagnostics started over a decade ago. However, many promising devices are never commercialized or are even withdrawn from the market because of their inconvenient operational conditions, causing irritation during tedious sampling procedures. Moreover, they may not produce reproducible and comprehensive results and hence cannot be applicable for long-term use and user friendliness. Therefore, from the user's point of view, the device should be user friendly and widely usable for practical implementations.

A sensor is a device that can convert physical, chemical, or biological changes into a measurable signal. It consists of three major components: a recognition element, a transducer, and a signal processor. The recognition element provides a response from specific/selective binding with the target analytes, and the transducer produces a signal from the binding event. The signal processor then receives that signal from the transducer, and it gets amplified into a readable digital unit. The ideal challenge in the development of sensors is to provide a fast response time, reliable, portable, highly selective, and sensitive determination of biomolecules at low cost. Among the broad range of various analytical techniques, electrochemical sensors, which are considered a subclass of chemical sensors, have been extensively studied and proved to be a cost-effective method for selective and sensitive determination of species involved in food, health care, and environmental applications (Turner 2013; Kimmel et al. 2012; Wang 2008). One well-known example of an electrochemical sensor is the portable blood glucose strip. This sensor technology is based on an electrochemical technique using disposable screen-printed electrodes, and has generated over 5 billion dollars per year (da Silva et al. 2017; Yamanaka et al. 2016; Wang 2008). The transducer (working electrode) processes the changes in the electrical signal upon interaction with the recognition element (enzyme, proteins, antibodies), which is directly proportional to the concentration of the analyte. The binding with the analyte results in ionic discharge, and it can be measured in the form of voltage or current, using suitable transducers. Herein, electrochemical reactions take place at the electrode–electrolyte interface and electron transfer reactions occur between these phases. There are many reported electrochemical techniques. Among them, cyclic voltammetry (CV) and linear sweep voltammetry (LSV) are mostly used to investigate the nature of the electrochemical process. Differential pulse voltammetry (DPV) or square wave voltammetry (SQV) and amperometric techniques are widely used to quantify analytes for electrochemical sensors.

Electrochemical biosensing for determination of various biomolecules is usually performed either using conventional metal electrodes such as Au, Pt, or Cu, or using a glassy carbon electrode (GCE). These conventional electrodes have numerous disadvantages, which include poor sensitivity, poor stability, low reproducibility, long response times, and a high operating potential for electron transfer reactions (Dai et al. 2006; Park et al. 2012; Toghill and Compton 2010). Therefore, there is a huge demand for development of electrode materials that can overcome the disadvantages of conventional electrodes and also provide high electron transfer rates with highly selective and sensitive responses for determination of electrochemical analytes.

In this context, nanomaterials have gained significant attention because of their potential applications in the chemical, textile, and electronic industries, and also for widespread applications in drug delivery and medical diagnostics (Willner et al. 1996; Xiao et al. 2003; Rubianes and Rivas 2007). The introduction of nanomaterials in science has created evolutionary developments and extensive technological applications, especially in electrochemical biosensors (Crespilho et al. 2006; Shan et al. 2007). In general, the properties of nanomaterials are highly dependent on increased relative surface area and also the dominance of quantum effects. When the size of matter is reduced to the nanoscale (10^{-9}), quantum effects can dominate, and these can significantly enhance optical, magnetic, and conducting properties. An increase in surface area results in an increase in chemical reactivity, making nanomaterials an effective electrode platform in electrochemical sensors (Niemeyer 2001; Katz et al. 2004; Privett et al. 2010). For these reasons, numerous research efforts have been put into electrochemical biosensors in the past few years and have been especially focused on introducing new nanomaterials into modified electrodes (Katz and Willner 2004; Le Goff et al. 2011; Ohara et al. 1994; Teo et al. 2013; Wang 2001; Zhu et al. 2015). Unique target binding characteristics can be achieved for great selectivity, high specificity, high sensitivity, stability, and a fast response time.

The field of research on electrochemical sensors/biosensors is large and is advancing rapidly; therefore, this chapter will acquaint readers with the most recently developed nanomaterials, as an electrochemical electrode platform can be deployed for determination of glucose (Besteman et al. 2003). An overview of GOx molecule were immobilized over different nanomaterials based electrodes were presented, and the performance of the modified electrodes—in terms of linear range, sensitivity, and detection limits—is also addressed.

9.2 Enzymatic Electrochemical Sensing: Evolution of Glucose Biosensors

The evolution of glucose electrochemical biosensors is an excellent example of how innovative breakthroughs have created a biomedical field that is now widespread in all areas of life. Clarks and Lyons (1962) were the first to demonstrate quantitative indirect measurement of glucose by oxygen consumption in an enzyme-catalyzed

reaction using an electrochemical oxygen electrode coupled with glucose oxidase (GOx). Later, Updike and Hicks (1967) proposed an enzyme electrode based on this principle by coupling a polyacrylamide gel membrane with GOx for fast and quantitative determination of glucose.

$$\mathrm{GOx} + \mathrm{glucose} + \mathrm{O_2} \rightarrow \mathrm{gluconic\ \ acid} + \mathrm{H_2O_2} \tag{9.1}$$

In the early 1980s, significant and considerable efforts were focused on development of mediator-based enzymatic sensors (second generation) using oxygen replacement. GOx does not directly transfer electrons to electrodes, because of the presence of a thick protein layer surrounding its flavin adenine dinucleotide (FAD) redox center. Therefore, utilization of an artificial mediator is able to tailor the electrical contact between the redox center of GOx and the electrode surface. In general, mediators are redox active molecules (e.g., ferrocene, ferrocyanide, quinones), which are able to undergo fast and redox reactions by shuttling of electrons between the redox center and the active site of the enzyme. Ohara et al. (1994) developed implantable enzymatic glucose sensor devices using a flexible polymer with an osmium complex; hence, communication between GOx and the redox couple is fast and efficient.

$$\mathrm{GOx} + \mathrm{GOx(FAD)} \rightarrow \mathrm{gluconic\ \ acid} + \mathrm{GOx(FADH_2)} \tag{9.2}$$

$$\mathrm{GOx(FADH_2)} + 2\mathrm{M(ox)} + 2\mathrm{e^-} \rightarrow \mathrm{GOx(FADH_2)} + 2\mathrm{M(red)} + 2\mathrm{H} \tag{9.3}$$

$$2\mathrm{M(red)} \rightarrow 2\mathrm{M(ox)} + 2\mathrm{e^-} \tag{9.4}$$

Subsequently, the elimination of the mediator has been focused on the development of electrochemical glucose biosensors to lower fabrication costs and complexity while increasing the durability of the glucose sensor. The third-generation glucose sensor enables direct electron transfer between the redox center of the enzyme and the electrode surface, leading to very high sensitivity and reproducibility without using artificial redox mediators. The research on third-generation electrochemical biosensors has been significantly advanced with the introduction of nanomaterials.

$$\mathrm{GOx(FAD)} + \mathrm{glucose} \rightarrow \mathrm{GOx(FADH_2)} + \mathrm{gluconic\ \ acid} \tag{9.5}$$

$$\mathrm{GOx(FADH_2)} + 2\mathrm{e^-} \rightarrow \mathrm{GOx(FAD)} + 2\mathrm{H^+} \tag{9.6}$$

To generate efficient electrochemical responses for the GOx enzyme, different immobilization strategies are utilized, as represented in Scheme 9.1.

9.3 Nanomaterial-Based Glucose Biosensors

The nanomaterials most commonly used as electrode platforms (Scheme 9.2) for immobilization of enzymes are:

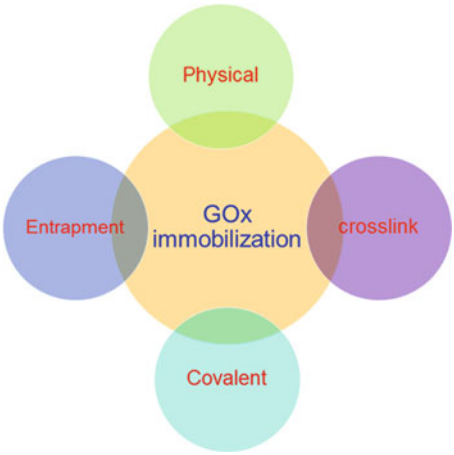

Scheme 9.1 Strategies for immobilization of glucose oxidase (*GOx*) in electrode modification

Scheme 9.2 Representation of various nanomaterial over glucose oxidase (*GOx*)

- Metal (Au, Cu, Pd, etc.) nanostructures
- Metal oxide (Fe_2O_3, ZnO, TiO_2, etc.) nanomaterials
- Carbon nanotubes (single-walled, multiwalled)
- Graphene (graphene oxide, reduced graphene oxide)
- Hybrid materials

A detailed review of various nanomaterial-modified electrodes for glucose biosensors is given in the following sections.

9.3.1 Metal Nanoparticle–Based Glucose Oxidase Biosensors

Metal nanoparticles such as Au, Cu, Pt, and Pd, as electrochemical platforms for sensors and biosensors, have made a significant impact in biomedical applications owing to their high electrocatalytic properties. Nanomaterial-based modified electrodes have been recognized as potential materials because of their easier preparation and fabrication process, high biocompatibility, high chemical stability, large surface area, and also improved sensitivity and selectivity for signal amplifications (Murray 2008). These metal nanomaterials are very helpful in decreasing overpotential and thus provide a wide linear range and low detection limits (Sardar et al. 2009; Katz et al. 2004).

Gold (Au) nanoparticles have been considered as a potential material and possess distinct physical and chemical properties (nonreactivity), making them an excellent electrode platform for fabrication of novel electrochemical sensors and biosensors. These superior properties of Au nanoparticles create advantages over other metals; hence, the shape and size of the particles can be easily tuned for the surrounding chemical environment (Saha et al. 2012). Au nanoparticles act as an efficient host substrate for immobilization of GOx and thus exhibit higher affinity for GOx by maintaining the enzyme activity against denaturation. Hence, many forms of Au-based nanostructures have been developed for electrochemical sensors and biosensors. For example, nanoparticles, nanorods, nanochains, nanocorals, nanowire arrays, urchin-like structures, and porous and nanoporous-based electrodes are employed for successful electrochemical glucose biosensors. Sharma et al. (2012) developed a glucose biosensor by coupling of GOx with amino-functionalized Au nanoparticles. The fabricated biosensor exhibited a wide linear concentration range from 1–5 mM and high sensitivity of 47.2 $\mu A\ mM^{-1}\ cm^{-2}$. Si et al. (2011) and Qiu et al. (2012) investigated covalent immobilization of GOx on high-density Au nanostructures, which provided a greater response to glucose. Xiao et al. (2014) designed a nanoporous Au electrode for an electrochemical glucose biosensor using three-dimensional (3D) bicontinuous nanostructures. The modified electrode was constructed by covalent immobilization of GOx though glutaraldehyde cross-coupling; hence, a more stable current response was obtained. It was found that the sensor had excellent selectivity and anti-interference ability for glucose oxidation. To increase the linear range of glucose oxidation, GOx was immobilized over a conducting polymer nanocomposite. Haghighi and Tabrizi (2013) established GOx immobilization over surface-oxidized films of polypyrrole and Au nanoparticles. The modified electrode demonstrated an excellent biocompatible scaffold for GOx immobilization with a wide linear range of glucose concentrations from 1 mM to 8 mM.

Platinum nanoparticle–based electrochemical sensors and biosensors have been widely employed because of their favorable electrocatalytic properties. Therefore, many recent studies have been focused on fabrication of a Pt-based electrochemical platform for direct immobilization of GOx, because it maintains satisfactory stability and activity of the enzyme. Ren et al. (2012) designed Pt nanocube to enhance the

electrocatalytic activity of glucose. The electrode was fabricated by covalent linking of GOx with chitosan immobilized on the surface of Pt nanocubes, and it showed good performance for analysis of glucose, with a wide linear range of 1 μM–5 mM, good sensitivity (35.92 μA mM^{-1} cm^{-2}), and a low detection limit (0.5 μM). More recently, Wang et al. (2017) prepared Pt nanoparticles assembled on a stannic sulfide nanoflake (Pt@SnS_2), which provided solid support for immobilization of GOx; hence, direct electron transfer of GOx was achieved. The behavior of the modified electrode displayed good bioactivity and large surface coverage for high loading of enzymes; therefore, the Pt@SnS_2 modified electrode showed a linear range of 0.1–12 mM and a detection limit of 2.5 μM.

The development of a cost-effective electrochemical platform is of great interest to replace the utilization of precious noble metals such as Au and Pt. In this regard, the prospect of a palladium (Pd)–based electrochemical platform has drawn immense attention from researchers because of the high earth abundance of palladium in comparison with noble metals. Li et al. (2011b) explored the fabrication of n-alkylamine-stabilized Pd nanoparticles for immobilization of GOx. Higher stability, higher enzyme activity, and a better detection limit of the modified electrode were achieved using hydrophobic nanomaterial. The sensitivity and selectivity for GOx have been drastically increased by use of these modified electrodes (Table 9.1).

9.3.2 *Use of Metal Oxides as Platforms for Enzymatic Glucose Biosensors*

The exploration of metal oxide nanomaterials has fueled research on electrochemical biosensors because of their low cost, high conductivity, biocompatibility, hydrophilicity, and uniform porosity, which enhances impregnation of enzymes (Hahn et al. 2012; Pachauri et al. 2010; Pauliukaite et al. 2010). A variety of metal oxide nanomaterials have been employed for electrochemical glucose biosensors: zinc oxide (ZnO), iron oxide (Fe_2O_3), titanium dioxide (TiO_2), manganese oxide (MnO), copper oxide (CuO), etc. A few selected electrochemical sensors based on GOx and metal oxide nanoparticles are highlighted below.

Nor et al. (2017) developed an Fe_2O_3 magnetic nanoparticle–based electrochemical immobilization platform for a GOx-based amperometric glucose biosensor. The modified electrode presented high sensitivity of about 175 μA mM^{-1} cm^{-2} and a lower detection limit of 7 μM. It has been shown that fabricated amperometric biosensors with the advantages of simple fabrication, low cost, and disposable electrodes can be employed for analytical applications. Yang et al. (2014) designed tetragonal columnar-shaped TiO_2 (TCS-TiO_2) nanorods, using a facile route with thermal decomposition of Ti and NH_4Cl powders at 400 °C. The obtained TiO_2

Table 9.1 Comparison of various noble metal nanoparticle–based enzymatic glucose biosensors

Electrodes	Linear range	Sensitivity	LOD (μM)	Reference
Chitosan/GOD/Au nanoplate/GCE	2–20 mM	49.5 μA mM^{-1} cm^{-2}	200	Zhang et al. (2011a)
Nf/GOD/Pt-NC/PB-Au/GCE	0.003–1.1 mM	2.77 mA M^{-1}	1.0	Wang et al. (2011c)
GOx-(H30-SO_3H)/Au/GCE	0.2–20 mM	–	12	Sun et al. (2013)
GOx/PPyAA/Au/GCE	1–18 mM	0.42 μA mM^{-1} cm^{-2}	50	Şenel and Nergiz (2012)
GOx/Th/GN/GCE	0.5–6.0 mM	43.2 μA mM^{-1} cm^{-2}	9.6	Shervedani et al. (2016)
GOx/Au/GCE	2.5–32.5 μM	–	0.32	Qiu et al. (2012)
GOx/Au-NP/PANI composite	0.1–150 mM	–	–	Mazeiko et al. (2013)
GOx/OOPPy-nano-Au/GCE	1–8 mM	0.217 μA mM^{-1}	500	Haghighi and Tabrizi (2013)
GOx/Pd@IL-meso-carbon/GCE	0.5–10.5 mM	–	190	Haghighi et al. (2014)
GOx/nano-Pt/Au monolayer	0.1–50 μM	0.29 nA μM^{-1}	0.01	Li et al. (2011a)
GOx-PoPD/Pt-NP/$PVF^+ClO_4^-$/Pt	0.06–9.64 mM	17.40 μA mM^{-1} cm^{-2}	0.018	Turkmen et al. 2014
CS-GA-GOx/Pt-NP/Au	0.001–5.3 mM	102 μA mM^{-1} cm^{-2}	0.0001	Tan et al. (2010)
CHIT/GOx@Pt-NC/Pt	0.001–8 mM	35.92 μA mM^{-1} cm^{-2}	0.0005	Ren et al. (2012)
GOx/Pt/OMC/Au	0.05–3.70 mM	12.10 μA mM^{-1} cm^{-2}	0.05	Jiang et al. (2011)
GOx/Pd-HCNF/GCE	0.06–6 mM	13 mA M^{-1} cm^{-2}	30	Jia et al. (2013)
Pd/CS-GR/GCE	0.001–1	31.2 μA mM^{-1} cm^{-2}	0.2	Zeng et al. (2011)
C18-Pd-NP-GOx/GC	0.003–8 mM	70.8 μA mM^{-1} cm^{-2}	3	Li et al. (2011a, b, c, d, e)
GOx-Au-NP/ESM	0.008–0.96 mM	–	3.50	Zheng et al. (2011)

C18 octadecylamine, *CHIT* chitosan, *CS* chitosan, *ESM* eggshell membrane, *GA* glutaraldehyde, *GC* glassy carbon, *GCE* glassy carbon electrode, *GN* graphene nanosheet, *GOD* glucose oxidase, *GOx* glucose oxidase, *GR* graphene, *HCNF* helical carbon nanofiber, *IL* ionic liquid, *LOD* lower limit of detection, *meso* mesoporous, *NC* nanocluster, *Nf* Nafion, *NP* nanoparticle, *OMC* ordered mesoporous carbon, *OOPPy* overoxidized polypyrrole, *PANI* polyaniline, *PB* Prussian blue, *PoPD* poly(o-phenylenediamine), *PPyAA* poly(3-pyrrol-1-ylpropanoic acid), *$PVF^+ClO_4^-$* polyvinylferrocenium perchlorate matrix

nanorods were dispersed with chitosan for immobilization of GOx for determination of glucose. The GOx/TCS-TiO_2/chitosan modified electrodes exhibited excellent selectivity, good reproducibility, and acceptable operational stability. Zhai et al. (2011) prepared GOx adsorbed onto nanostructured ZnO-modified indium tin oxide (ITO) electrodes for direct electron transfer of GOx on the electrode surface. The GOx immobilized onto the ZnO nanostructured electrode demonstrated higher current signals with reversible redox peaks for an FAD/$FADH_2$ redox probe. The modified electrode exhibited a wide linear range from 0.1 mM to 9 mM, a limit of detection of about 1.94 μM, and an apparently low Michaelis–Menten constant (K_M) of 3.12 mM. Zhang et al. (2013) fabricated a GCE electrode with MnO_2 nanowires and GOx on the electrode surface for glucose oxidation. The electrode behavior was examined, and it was shown that the GOx retained its bioactivity with improved performance for each additional glucose concentration. The biosensor demonstrated excellent selectivity, high sensitivity, and good stability. Pradhan et al. (2010) designed high-performance and flexible GOx biosensors based on ZnO nanowires (NWs) coated on an gold-coated polyester (PET) substrate. The GOx/ZnO-NWs/Au/PET biocomposite electrodes exhibited good electrocatalytic performance for glucose concentrations with a fast response time, high sensitivity of 19.5 μA mM^{-1} cm^{-2}, and a low K_M of 1.57 mM (Table 9.2).

Table 9.2 Comparison of various metal oxide nanoparticle–based enzymatic glucose biosensors

Electrodes	Linear range	Sensitivity (μA mM^{-1} cm^{-2})	LOD (μM)	Reference
Unhybridized TiO_2 nanoarray	0.05–0.65 mM	199.61	3.8	Wang et al. (2014)
Alginate-CuO-GOD	4–35 mM	30.443	1.6	Buk et al. (2017)
GOx/NiO-doped ZnO NR/Pt	0.5–8 mM	61.78	25	Chu et al. (2012)
ZnO nanoterapod	0.01–5.9 mM	23.43	10	Lei et al. (2010)
ZnO nanorod	0.01–0.7 mM	25.7	10	Yang et al. (2010)
GOx/ZnO-NW/graphite	0.03–1.52 mM	17	9	Gallay et al. (2016)
GOx/ZnO-NW/Au/PET	0.2–2 mM	19.5	<50	Pradhan et al. (2010)
Linker-mediated GOx/ZnO NW	–	17.72	0.02	Jung and Lim (2013)
GOx/ZnO-NW/paper	0–15 mM	8.24	59.5	Li et al. (2015)
Nf/GOD/CuO/GCE	1–170 μM	246	0.91	Li et al. (2011c)
ZnO/ZnS-MAA-GOx	3.51–24.1 mM	–	0.23	Sung et al. (2012)

GCE glassy carbon electrode, *GOD* glucose oxidase, *GOx* glucose oxidase, *LOD* lower limit of detection, *MAA* mercapto-acetic acid, *Nf* Nafion, *NR* nanorod, *NW* nanowire, *PET* polyester

9.3.3 Use of Carbon Nanotubes in Electrochemical Glucose Biosensors

Advanced engineering materials such as SiC, Si_3N_4, and Al_2O_3 possess interesting properties such as high stiffness and excellent thermostability, which are advantageous for development of numerous devices. However, devices made from these materials mainly suffer from a highly brittle nature, which restricts their use in many applications, especially in flexible electronic devices. In this context, researchers have developed a freestanding, transparent, highly conductive nanomaterial with outstanding mechanical strength, known as carbon nanotubes (CNTs). CNTs were first observed by Sumio Iijima. CNTs have a tube-like structure created by curling (like paper) or rolling up into cylinders; their diameter is typically in the nanometer range, and they contain sp^2 hybridized carbon. The nanotube can be closed or open, and the length can be several hundred times the width. Depending on the number of concentric rolled sheets forming the cylinders, they can be divided into two general categories: single-walled CNTs (SWCNTs—made from a single rolled graphene sheet) or multiwalled CNTs (MWCNTs—made from two or more rolled graphene sheets). SWCNTs have a typical diameter of 1–2 nm, while that of MWCNTs is typically 2–25 nm. The interlayer distance in MWCNTs is approximately 3.3 Å, which is close to the distance between the graphene layers in graphite. CNTs have assumed an important role in the context of nanomaterials because of their novel chemical and physical properties. They are mechanically very strong and flexible, and they can conduct electricity extremely well. All of these remarkable properties make CNTs effective transducers for a wide range of potential applications in electrochemical sensors/biosensors. CNTs can overcome most of the disadvantages of conventional electrodes owing to their high conductivity, fast electron transfer rate, and ability to minimize possible interference species; hence, a highly sensitive and selective electrochemical platform for determination of analytes can be achieved (Ghica et al. 2009; Barsan and Brett 2009). Selected studies using CNTs as electrochemical platforms for immobilization of GOx-based glucose biosensors, reported after 2010, are discussed below.

Periasamy et al. (2011) investigated the direct electrochemistry of GOx in gelatin-functionalized MWCNTs (GCNTs) for use in an amperometric glucose biosensor. A free amino ($–NH_2$) group in the GOx molecule was covalently linked with an aldehyde (–CHO) group in glutaraldehyde (GAD). The GCNT/GOx/GAD modified electrode exhibited two well-defined redox peaks, which were attributed to the presence of an FAD/$FADH_2$ redox couple. Also, the modified biocomposite electrode displayed a steady amperometric response to glucose in a linear concentration range of 6.30 mM–20.09 mM, and sensitivity of 2.47 μA mM^{-1} cm^{-2}. Gutierrez et al. (2012) reported use of GOx as a dispersing agent for MWCNTs. The interactions between MWCNTs and GOx created more efficient electron transfer pathways to the GCE electrode; hence, it exhibited excellent biocatalytic activity and high sensitivity to glucose. Subsequently, Wooten et al. (2014) demonstrated the direct electron transfer ability and enzymatic activity of GOx

and chitosan in a matrix. Once glucose was added to a solution containing 0.1 M phosphate buffer, the enzymatically active GOx(FAD) molecules were converted to the reduced form of the enzyme ($GOx(FADH_2)$), which was subsequently oxidized by O_2, producing H_2O_2.

$$GOx(FAD) + \text{glucose} \rightarrow GOx(FADH_2) \tag{9.7}$$

$$GOx(FADH_2) + O_2 \rightarrow GOx(FAD) + H_2O_2 \tag{9.8}$$

More recently, Muguruma et al. (2015) compared the electrochemical response for GOx with two different types of SWCNTs: metallic SWCNTs (m-SWCNTs) and semiconducting SWCNTs (s-SWCNTs). It was found that in the presence of GOx in an O_2-saturated medium, the electrochemical response of the m-SWCNT/GOx electrode was two times greater than that of the s-SWCNT/GOx electrode. In contrast, under N_2 saturated conditions, the response of the s-SWCNT/GOx electrode was retained whereas the electrochemical response of the m-SWCNT/GOx electrode was significantly diminished. This indicates that direct electron transfer (DET) proceeded with the s-SWCNT/GOx electrode, whereas the m-SWCNT/GOx electrode was dominated by the hydrogen peroxide route. For biosensors with the GDH enzyme, the response with the s-SWCNT/GDH electrode was four times greater than that with the m-SWCNT/GDH electrode.

9.3.4 Graphene-Based Glucose Biosensors

Recently, a great deal of attention has been paid to the implementation of graphene-based electrochemical devices by both the experimental and theoretical scientific communities. Graphene, a new class of two-dimensional (2D) carbon nanostructure, has a single atomic layer of sp^2 carbon atoms. This unique nanostructure holds great promise for potential applications in nanoelectronics, sensors, nanocomposites, batteries, supercapacitors, and hydrogen storage (Brownson et al. 2012a). The utilization of graphene-based sensors is of huge interest because of their flexible nature, high conductivity, and large surface area (Chua and Pumera 2013; Brownson and Banks 2010, 2011; Brownson et al. 2012b). However, a lack of functional groups on the surface of graphene sheets has been a major obstacle to exploiting most of their potential electrochemical applications (Table 9.3).

Moon et al. (2010) established synthesis of graphene oxide (GO) through chemical oxidation of graphite to hydrophilic graphite oxide, using an ultrasonication method. GO is highly hydrophilic with good dispersibility in water owing to the presence of oxygen and carboxyl and epoxy functional groups. It can be easily exfoliated into single layers or a few layers of graphite by chemical oxidation. GO was mainly prepared by oxidation of natural graphite powder, using Hummer's method. To a stirring reaction mixture containing 50 mL of sulfuric acid, 2 g of $NaNO_3$ and 2 g of graphite powder were added slowly, one after the other, to avoid

Table 9.3 Comparison of various carbon nanomaterial–based enzymatic glucose biosensors

Electrodes	Linear range	Sensitivity ($\mu A\ mM^{-1}\ cm^{-2}$)	LOD (μM)	Reference
GOD/PPy-graphene	2–40 μM	–	3	Alwarappan et al. (2010)
N-doped graphene	0.1–1.1 mM		–	Wang et al. (2010)
Nylon 6,6/4-MWCNT/PBIBA	0.01–2 mM	–	9	Uzun et al. (2014)
Gelatin-CNT/GOx/GAD	6.30–20.09 mM	2.47	–	Periasamy et al. (2011)
GR-CoPc/GOx	0.01–14.8 mM	5.09	1.6	Mani et al. (2014)
Graphene-GOD/Au	2–14 mM	21.9	0.04	Hui et al. (2013)
GOx-PVA-MWCNT	0.1–20 mM	8.67	0.00015	Gupta et al. (2016)
GOx/NH_2-TiO_2-CNT	1.8–266 μM	223	0.44	Tasviri et al. (2011)
GOx/meso-HAP/MWCNT/GCE	0.01–15.2 mM	57	2	Li et al. (2012)
RGO/GOx	0.1–27 mM	1.85	–	Unnikrishnan et al. (2013)
GOx/ERGO/poly-L-lysine	0.25–5 mM	–	–	Hua et al. (2012)
GOx/graphene/Nf	0.5–14 mM	–	30	Zhang et al. (2012)
GOx/graphene	0.1–10 mM	3	10	Wu et al. (2010)

CNT carbon nanotube, *CoPc* cobalt phthalocyanine, *ERGO* electrochemically reduced graphene oxide, *GAD* glutaraldehyde, *GCE* glassy carbon electrode, *GOD* glucose oxidase, *GOx* glucose oxidase, *GR* graphene, *LOD* lower limit of detection, *meso-HAP* mesoporous hydroxyapatite, *MWCNT* multiwalled carbon nanotube, *Nf* Nafion, *PBIBA* poly-4-(4,7-di(thiophen-2-yl)-1H-benzo[d]imidazol-2-yl)benzaldehyde, *PPy* polypyrrole, *PVA* polyvinyl alcohol, *RGO* reduced graphene oxide

agglomeration. With the reaction temperature kept below 10 °C in an ice bath, 6 g of $KMnO_4$ was gently added to the vigorously stirred reaction mixture to avoid overheating caused by the exothermic reaction. After 2 h the ice bath was removed, the reaction temperature was raised to 35 °C, and the mixture was allowed to stir continuously for 12 h. The resulting dense paste was subsequently diluted with 50 mL of Milli-Q water and refluxed at 98 °C for 30 min, then another 150 mL of Milli-Q water followed by 10 mL of H_2O_2 (30%) were added slowly under vigorous stirring until the solid color changed from brown to yellow. The solid GO was isolated by centrifugation, washed multiple times (pH neutral) with Milli-Q water, and finally dried under a vacuum.

Thus, enormous efforts and attention have been devoted to the production of GO because of its considerable promise for possible applications in electrochemical biosensors. In the following section, a few selected electrochemical glucose sensors based on GO are discussed.

Liu et al. (2010) demonstrated highly efficient electrochemical GOx-based sensors that can be covalently linked using carboxyl (–COOH) groups of GO sheets and an amino ($–NH_2$) group of GOx. The modified electrodes exhibited a broad linear range up to 28 mM glucose with high reproducibility and good storage stability, suggesting that the sensors could be applicable in health care clinics. Liu et al. (2011) established graphene oxide and GOx nanostructures through self-assembly of GOx and graphene oxide platelets by electrostatic interaction. A glucose biosensor was constructed by deposition of the resultant nanostructures on the surface of a glassy carbon (GC) electrode. It was found that the biosensor exhibited a good response to glucose over a linear range from 2 mM to 22 mM, and the detection limit was about 20 μM. Ping et al. (2011) reported immobilization of GOx on electrochemically reduced GO, which was deposited over an ionic liquid/screen-printed modified electrode. The modified electrode provided high sensitivity and a greater linear range for glucose concentrations. Mani et al. (2013) demonstrated a simple electrochemical route for fabrication of GOx on chemically reduced GO. A well-resolved redox peak was observed for GOx, corresponding to the FAD/$FADH_2$ redox couple. The mediator-free response of the biosensor exhibited a wide linear range, a fast electron transfer rate, high selectivity, and good stability. Zhang et al. (2014) investigated the structure of a GOx electrode modified with reduced GO sheets with different defect density, layers, and oxygen concentrations. The resulting electrode exhibited excellent electrocatalytic activities and performance for glucose. Shamsipur and Tabrizi (2014) achieved direct electron transfer of GOx, using electrochemically reduced GO, for enzymatic glucose sensing. The glucose was determined by a decrease in the peak current due to the reduction of dissolved oxygen. The biosensor exhibited good reproducibility and stability, and was selective for determination of glucose, with high sensitivity (Table 9.4).

9.3.5 Use of Hybrid Materials in Glucose Oxidase Biosensors

To achieve high enzyme loading and provide high electrocatalytic activity of modified electrodes, the electrodes can be designed using combinations of transition metal nanoparticles/metal oxides/carbon-based nanomaterials, which have been extensively utilized in electrochemical platforms for electrochemical biosensors. These hybrid nanocomposites increase their surface area, conductivity, and electrocatalytic activity toward the analyte, while lowering the overpotential. There are numerous reports available on these hybrid nanocomposite–based electrochemical glucose biosensors.

Shan et al. (2010) observed a prominent electrochemical response for glucose obtained by immobilizing GOx in thin films of chitosan deposited over a graphene/Au nanoparticle nanocomposite electrode. Zhai et al. (2013) designed a highly sensitive glucose enzyme sensor based on Pt nanoparticles with polyaniline hydrogel heterostructures. The glucose enzyme sensor exhibited unprecedented high sensitivity of 96.1 μA mM^{-1} cm^{-2}, with a wide linear range of 0.01–8 mM and a low

Table 9.4 Comparison of various hybrid material–based enzymatic glucose biosensors

Electrodes	Linear range	Sensitivity	LOD (μM)	Reference
GOx/TiO_2/FePc-CNT	0.05–4 mM	8.25 μA mM^{-1} cm^{-2}	30	Cui et al. (2013)
ERGO-MWCNT/GOx/Nf	0.01–6.5 mM	7.95 μA mM^{-1} cm^{-2}	4.7	Mani et al. (2013)
nPt-RGO-NCe-GOx	Up to 120 μM	66.2 μA mM^{-1} cm^{-2}	1.3	Chaturvedi et al. (2014)
GO/Pt-black/GOx	0.001–2 mM	78 μA mM^{-1} cm^{-2}	–	Shi et al. (2012)
GR-MWCNT/Au-NP	10 μM–2 mM	0.695 μA mM^{-1} cm^{-2}	4.1	Devasenathipathy et al. (2015)
PANI/PAA-GOx	Up to 1.1 mM	29.9 μA mM^{-1} cm^{-2}	60	Homma et al. (2014)
GOx/RGO/Pd-Pt-NP	2–12 mM	24 μA mM^{-1} cm^{-2}	1	Hossain and Park (2014)
Gr/PANI/Au-NP/GOD	Up to 8 mM	20.32 μA mM^{-1} cm^{-2}	100	Kong et al. (2014)
GOx/Pt/Fe_yO_x-MWCNT/CS	0.006–6.2 mM	–	2	Li et al. (2010)
(Con-A/GOD)/Pt_{nano}-CNT-CS/GCE	0.0012–2.0 mM	41.9 μA mM^{-1} cm^{-2}	0.4	Li et al. (2011e)
Gr/pyrene functionalized GOx	0.2–40 mM	–	154	Liu et al. (2013)
GOx/r-GO-Ag	0.5–12.5 mM	3.84 μA mM^{-1} cm^{-2}	160	Palanisamy et al. (2014)
Nf/graphene/GOx/Au	2–14 mM	21.9 μA mM^{-1} cm^{-2}	40	Hui et al. (2013)
RGO/PAMAM/Ag/GOx/CS	0.032–1.89 mM	75.72 μA mM^{-1} cm^{-2}	4.5	Luo et al. (2012)
RGO/ZnO/GOx	0.02–6.24 mM	18.97 μA mM^{-1} cm^{-2}	20	Palanisamy et al. (2012)
GOx/graphene-CNT	2–8 mM	19.31 μA mM^{-1} cm^{-2}	500	Terse-Thakoor et al. (2015)
GOx/graphene/PANI/Au-NP	4–1.12 mM	–	0.6	Xu et al. (2014)
GOx/PPMH/GC electrode	0.02–48 mM	–	80	Oztekin et al. (2011)
GOx/Au-NP/graphene/MWCNT	0.3–2.1 mM	29.72 mA M^{-1} cm^{-2}	4.8	Yu et al. (2014)
GOx/H_2BpybcBr$_2$/TiO_2/FTO	0.153–1.3 mM	1.25 μA mM^{-1}	51	Zhu et al. (2009)
GOx/meso-carbon/Au-NP	0.05–20 mM	4.34 μA mM^{-1}	–	Wang et al. (2011b)
GOx/graphene oxide/PB	0.1–13.5 mM	15.82 μA mM^{-1} cm^{-2}	0.343	Zhang et al. (2011b)
GOx/graphene/CdS nanocrystals	2–16 mM	1.76 μA mM^{-1} cm^{-2}	700	Wang et al. (2011a)

(continued)

Table 9.4 (continued)

Electrodes	Linear range	Sensitivity	LOD (μM)	Reference
GOx/Pt/meso-silica	0.001–26 mM	–	0.8	Li et al. (2011d)
GOx/Pt/MWCNT/polyaniline	0.003–8.2 mM	16.1 μA mM^{-1}	1	Zhong et al. (2011)
GOx/Ni^{2+}/MgFe LDH	1–20 mM	1.995 μA mM^{-1}	120	Xu et al. (2011)
GOx/con-A/Pt/CNT	0.001–2 mM	41.9 μA mM^{-1} cm^{-2}	0.4	Li et al. (2011a, b, c, d, e)

CNT carbon nanotube, *con-A* concanavalin A, *CS* chitosan, *ERGO* electrochemically reduced graphene oxide, *FePc* iron phthalocyanine, Fe_yO_x iron oxide, *FTO* fluorine-doped tin oxide, *GC* glassy carbon, *GCE* glassy carbon electrode, *GO* graphene oxide, *GOD* glucose oxidase, *GOx* glucose oxidase, *GR* graphene, *Gr* graphene, $H_2BpybcBr_2$ 1,1′-bis(4-carboxybenzyl)-4,4′-bipyridium bromide, *LDH* layered double hydroxide, *LOD* lower limit of detection, *meso* mesoporous, *MWCNT* multiwalled carbon nanotube, *NCe* nanoceria, *Nf* Nafion, *NP* nanoparticle, *nPt* nanoplatinum, *PAA* poly(acrylic acid), *PAMAM* polyamidoamine, *PANI* polyaniline, *PB* Prussian blue, *PPMH* poly-1,10-phenanthroline, Pt_{nano} Pt nanoparticles, *r-GO* reduced graphene oxide, *RGO* reduced graphene oxide

detection limit of 0.7 μM. The higher sensitivity was reported to be due to the presence of a conducting polymer hydrogel on Pt nanoparticles, which provided an electronically continuous 3D path for efficient electron transfer of GOx. Baby et al. (2010) demonstrated immobilization of GOx over Pt/Au nanoparticles utilized for dispersion of graphene. The Au/Pt nanoparticles acted as spaces, which eliminated the restacking of graphene; thus, there was an increase in the electroactive surface area. The modified electrode decreased the overpotential for the determination of glucose, with an excellent detection limit of 1 μM and reasonable selectivity with high anti-interference ability and good stability. Mani et al. (2013) studied direct electrochemistry of GOx immobilized over an electrochemically reduced GO-MWCNT/GC electrode. A higher peak current (2.1-fold) was observed for the hybrid modified electrode in comparison with pristine MWCNTs, demonstrating that the hybrid biocomposite film modified electrode exhibited fast electron transfer between GOx and the modified electrode surface. Jang et al. (2012) assessed adsorption of GOx at a TiO_2–graphene nanocomposite electrode and observed a greater response of the glucose biosensor at the fabricated electrode, which was found to be linear for glucose concentrations ranging up to 8 mM. It was estimated that the modified electrode showed a superior response for glucose when compared with pure TiO_2 and graphene nanosheets. Razmi and Mohammad-Rezaei (2013) studied GOx on a graphene quantum dot–modified carbon ceramic electrode. The modified electrode was reported to have higher performance in the presence of glucose, which was due to a high surface area to volume ratio, biocompatibility of the graphene quantum dot, high porosity, and high abundance of hydrophilic edges, which created higher catalytic active sites with a large absorption capability of the enzymes on electrode surface.

On the basis of the reported literature, it is concluded that electrode materials containing hybrid materials will show prominent electrochemical responses for glucose oxidation.

9.4 Conclusion

This chapter has described the history and evolution of enzymatic glucose biosensors. In comparison with conventional electrodes, utilization of nanomaterials offers a superior electrochemical platform for immobilization of enzymes in glucose biosensors. The performance of various nanomaterial-based glucose biosensors in practical applications is well established, but the development of fast-response and highly reproducible glucose biosensors for use in complicated real samples should be seriously addressed.

References

Alwarappan S, Liu C, Kumar A, Li C-Z (2010) Enzyme-doped graphene nanosheets for enhanced glucose biosensing. J Phys Chem C 114:12920–12924

Baby TT, Aravind SJ, Arockiadoss T, Rakhi RB, Ramaprabhu S (2010) Metal decorated graphene nanosheets as immobilization matrix for amperometric glucose biosensor. Sensors Actuators B Chem 145:71–77. https://doi.org/10.1016/j.snb.2009.11.022

Barsan MM, Brett CMA (2009) A new modified conducting carbon composite electrode as sensor for ascorbate and biosensor for glucose. Bioelectrochemistry 76:135–140. https://doi.org/10.1016/j.bioelechem.2009.03.004

Besteman K, Lee J-O, Wiertz FGM, Heering HA, Dekker C (2003) Enzyme-coated carbon nanotubes as single-molecule biosensors. Nano Lett 3:727–730. https://doi.org/10.1021/nl034139u

Brownson DAC, Banks CE (2010) Graphene electrochemistry: an overview of potential applications. Analyst 135:2768–2778. https://doi.org/10.1039/c0an00590h

Brownson DAC, Banks CE (2011) Graphene electrochemistry: fabricating amperometric biosensors. Analyst 136:2084–2089. https://doi.org/10.1039/c0an00875c

Brownson DAC, Kampouris DK, Banks CE (2012a) Graphene electrochemistry: fundamental concepts through to prominent applications. Chem Soc Rev 41:6944–6976. https://doi.org/10.1039/c2cs35105f

Brownson DAC, Foster CW, Banks CE (2012b) The electrochemical performance of graphene modified electrodes: an analytical perspective. Analyst 137:1815–1823. https://doi.org/10.1039/c2an16279b

Buk V, Emregul E, Emregul KC (2017) Alginate copper oxide nano-biocomposite as a novel material for amperometric glucose biosensing. Mater Sci Eng C Mater Biol Appl 74:307–314. https://doi.org/10.1016/j.msec.2016.12.003

Chaturvedi P, Vanegas DC, Taguchi M, Burrs SL, Sharma P, McLamore ES (2014) A nanoceria–platinum–graphene nanocomposite for electrochemical biosensing. Biosens Bioelectron 58:179–185. https://doi.org/10.1016/j.bios.2014.02.021

Chu X, Zhu X, Dong Y, Chen T, Ye M, Sun W (2012) An amperometric glucose biosensor based on the immobilization of glucose oxidase on the platinum electrode modified with NiO doped ZnO nanorods. J Electroanal Chem 676:20–26. https://doi.org/10.1016/j.jelechem.2012.04.009

Chua CK, Pumera M (2013) Covalent chemistry on graphene. Chem Soc Rev 42:3222–3233. https://doi.org/10.1039/c2cs35474h

Clark LC, Lyons C (1962) Electrode systems for continuous monitoring in cardiovascular surgery. Ann N Y Acad Sci 102:29–45. https://doi.org/10.1111/j.1749-6632.1962.tb13623.x

Crespilho FN, Ghica ME, Florescu M, Nart FC, Oliveira ON Jr, Brett CMA (2006) A strategy for enzyme immobilization on layer-by-layer dendrimer–gold nanoparticle electrocatalytic membrane incorporating redox mediator. Electrochem Commun 8:1655–1670. https://doi.org/10.1016/j.elecom.2006.07.032

Cui H-F, Zhang K, Zhang Y-F, Sun Y-L, Wang J, Zhang W-D, Luong JHT (2013) Immobilization of glucose oxidase into a nanoporous TiO_2 film layered on metallophthalocyanine modified vertically-aligned carbon nanotubes for efficient direct electron transfer. Biosens Bioelectron 46:113–118. https://doi.org/10.1016/j.bios.2013.02.029

da Silva ETSG, Souto DEP, Barragan JTC, de F. Giarola J, de Moraes ACM, Kubota LT (2017) Electrochemical biosensors in point-of-care devices: recent advances and future trends. ChemElectroChem 4:778–794. https://doi.org/10.1002/celc.201600758

Dai X, Wildgoose GG, Salter C, Crossley A, Compton RG (2006) Electroanalysis using macro-, micro-, and nanochemical architectures on electrode surfaces. Bulk surface modification of glassy carbon microspheres with gold nanoparticles and their electrical wiring using carbon nanotubes. Anal Chem 78:6102–6108. https://doi.org/10.1021/ac060582o

Devasenathipathy R, Mani V, Chen S-M, Huang S-T, Huang T-T, Lin C-M, Hwa K-Y, Chen T-Y, Chen B-J (2015) Glucose biosensor based on glucose oxidase immobilized at gold nanoparticles decorated graphene-carbon nanotubes. Enzym Microb Technol 78:40–45. https://doi.org/10.1016/j.enzmictec.2015.06.006

Gallay P, Tosi E, Madrid R, Tirado M, Comedi D (2016) Glucose biosensor based on functionalized ZnO nanowire/graphite films dispersed on a Pt electrode. Nanotechnology 27:425501. https://doi.org/10.1088/0957-4484/27/42/425501

Ghica ME, Pauliukaite R, Fatibello-Filho O, Brett CMA (2009) Application of functionalised carbon nanotubes immobilised into chitosan films in amperometric enzyme biosensors. Sensors Actuators B Chem 142:308–315. https://doi.org/10.1016/j.snb.2009.08.012

Gupta S, Prabha CR, Murthy CN (2016) Functionalized multi-walled carbon nanotubes/polyvinyl alcohol membrane coated glassy carbon electrode for efficient enzyme immobilization and glucose sensing. J Environ Chem Eng 4:3734–3740. https://doi.org/10.1016/j.jece.2016.08.021

Gutierrez F, Rubianes MD, Rivas GA (2012) Dispersion of multi-wall carbon nanotubes in glucose oxidase: characterization and analytical applications for glucose biosensing. Sensors Actuators B Chem 161:191–197. https://doi.org/10.1016/j.snb.2011.10.010

Haghighi B, Tabrizi MA (2013) Direct electron transfer from glucose oxidase immobilized on an overoxidized polypyrrole film decorated with Au nanoparticles. Colloids Surf B Biointerfaces 103:566–571. https://doi.org/10.1016/j.colsurfb.2012.11.010

Haghighi B, Karimi B, Tavahodi M, Behzadneia H (2014) Electrochemical behavior of glucose oxidase immobilized on Pd-nanoparticles decorated ionic liquid derived fibrillated mesoporous carbon. Electroanalysis 26:2010–2016. https://doi.org/10.1002/elan.201400266

Hahn Y-B, Ahmad R, Tripathy N (2012) Chemical and biological sensors based on metal oxide nanostructures. Chem Commun (Camb) 48:10369–10385. https://doi.org/10.1039/c2cc34706g

Homma T, Sumita D, Kondo M, Kuwahara T, Shimomura M (2014) Amperometric glucose sensing with polyaniline/poly(acrylic acid) composite film bearing covalently-immobilized glucose oxidase: a novel method combining enzymatic glucose oxidation and cathodic O_2 reduction. J Electroanal Chem 712:119–123. https://doi.org/10.1016/j.jelechem.2013.11.009

Hossain MF, Park JY (2014) Amperometric glucose biosensor based on Pt–Pd nanoparticles supported by reduced graphene oxide and integrated with glucose oxidase. Electroanalysis 26:940–951. https://doi.org/10.1002/elan.201400018

Hua L, Wu X, Wang R (2012) Glucose sensor based on an electrochemical reduced graphene oxide-poly(L-lysine) composite film modified GC electrode. Analyst 137:5716–5719. https://doi.org/10.1039/c2an35612k

Hui J, Cui J, Xu G, Adeloju SB, Wu Y (2013) Direct electrochemistry of glucose oxidase based on Nafion–graphene–GOD modified gold electrode and application to glucose detection. Mater Lett 108:88–91. https://doi.org/10.1016/j.matlet.2013.06.097

Jang HD, Kim SK, Chang H, Roh K-M, Choi J-W, Huang J (2012) A glucose biosensor based on TiO_2–graphene composite. Biosens Bioelectron 38:184–188. https://doi.org/10.1016/j.bios.2012.05.033

Jia X, Hu G, Nitze F, Barzegar HR, Sharifi T, Tai C-W, Wågberg T (2013) Synthesis of palladium/helical carbon nanofiber hybrid nanostructures and their application for hydrogen peroxide and glucose detection. ACS Appl Mater Interfaces 5:12017–12022. https://doi.org/10.1021/am4037383

Jiang X, Wu Y, Mao X, Cui X, Zhu L (2011) Amperometric glucose biosensor based on integration of glucose oxidase with platinum nanoparticles/ordered mesoporous carbon nanocomposite. Sensors Actuators B Chem 153:158–163. https://doi.org/10.1016/j.snb.2010.10.023

Jung J, Lim S (2013) ZnO nanowire–based glucose biosensors with different coupling agents. Appl Surf Sci 265:24–29. https://doi.org/10.1016/j.apsusc.2012.10.069

Katz E, Willner I (2004) Integrated nanoparticle–biomolecule hybrid systems: synthesis, properties, and applications. Angew Chem Int Ed Engl 43:6042–6108. https://doi.org/10.1002/anie.200400651

Katz E, Willner I, Wang J (2004) Electroanalytical and bioelectroanalytical systems based on metal and semiconductor nanoparticles. Electroanalysis 16:19–44. https://doi.org/10.1002/elan.200302930

Kimmel DW, LeBlanc G, Meschievitz ME, Cliffel DE (2012) Electrochemical sensors and biosensors. Anal Chem 84:685–707. https://doi.org/10.1021/ac202878q

Kirsch J, Siltanen C, Zhou Q, Revzin A, Simonian A (2013) Biosensor technology: recent advances in threat agent detection and medicine. Chem Soc Rev 42:8733–8768. https://doi.org/10.1039/c3cs60141b

Kong F-Y, Gu S-X, Li W-W, Chen T-T, Xu Q, Wang W (2014) A paper disk equipped with graphene/polyaniline/Au nanoparticles/glucose oxidase biocomposite modified screen-printed electrode: toward whole blood glucose determination. Biosens Bioelectron 56:77–82. https://doi.org/10.1016/j.bios.2013.12.067

Le Goff A, Holzinger M, Cosnier S (2011) Enzymatic biosensors based on SWCNT-conducting polymer electrodes. Analyst 136:1279–1287. https://doi.org/10.1039/c0an00904k

Lei Y, Yan X, Luo N, Song Y, Zhang Y (2010) ZnO nanotetrapod network as the adsorption layer for the improvement of glucose detection via multiterminal electron-exchange. Colloids Surf A Physicochem Eng Asp 361:169–173. https://doi.org/10.1016/j.colsurfa.2010.03.029

Li J, Yuan R, Chai Y, Che X (2010) Fabrication of a novel glucose biosensor based on Pt nanoparticles–decorated iron oxide–multiwall carbon nanotubes magnetic composite. J Mol Catal B Enzym 66:8–14. https://doi.org/10.1016/j.molcatb.2010.03.005

Li J, Yu J, Wei X, Liu R (2011a) A sensitive and selective biosensor activated by tailor-designed platinum nanoparticles electrodeposited onto a gold microelectrode. J Solid State Electrochem 15:1129–1137. https://doi.org/10.1007/s10008-010-1178-6

Li Z, Wang X, Wen G, Shuang S, Dong C, Paau MC, Choi MMF (2011b) Application of hydrophobic palladium nanoparticles for the development of electrochemical glucose biosensor. Biosens Bioelectron 26:4619–4623. https://doi.org/10.1016/j.bios.2011.04.057

Li Y, Wei Y, Shi G, Xian Y, Jin L (2011c) Facile synthesis of leaf-like CuO nanoparticles and their application on glucose biosensor. Electroanalysis 23:497–502. https://doi.org/10.1002/elan.201000343

Li H, He J, Zhao Y, Wu D, Cai Y, Wei Q, Yang M (2011d) Immobilization of glucose oxidase and platinum on mesoporous silica nanoparticles for the fabrication of glucose biosensor. Electrochim Acta 56:2960–2965. https://doi.org/10.1016/j.electacta.2010.12.098

Li W, Yuan R, Chai Y, Zhong H, Wang Y (2011e) Study of the biosensor based on platinum nanoparticles supported on carbon nanotubes and sugar–lectin biospecific interactions for the determination of glucose. Electrochim Acta 56:4203–4208. https://doi.org/10.1016/j.electacta.2011.01.095

Li J, Kuang D, Feng Y, Zhang F, Liu M (2012) Glucose biosensor based on glucose oxidase immobilized on a nanofilm composed of mesoporous hydroxyapatite, titanium dioxide, and modified with multi-walled carbon nanotubes. Microchim Acta 176:73–80. https://doi.org/10.1007/s00604-011-0693-1

Li X, Zhao C, Liu X (2015) A paper-based microfluidic biosensor integrating zinc oxide nanowires for electrochemical glucose detection. Microsyst Nanoeng 1:19606 https://doi.org/10.1038/micronano.2015.14

Liu Y, Yu D, Zeng C, Miao Z, Dai L (2010) Biocompatible graphene oxide–based glucose biosensors. Langmuir 26:6158–6160. https://doi.org/10.1021/la100886x

Liu S, Tian J, Wang L, Luo Y, Lu W, Sun X (2011) Self-assembled graphene platelet–glucose oxidase nanostructures for glucose biosensing. Biosens Bioelectron 26:4491–4496. https://doi.org/10.1016/j.bios.2011.05.008

Liu J, Kong N, Li A, Luo X, Cui L, Wang R, Feng S (2013) Graphene bridged enzyme electrodes for glucose biosensing application. Analyst 138:2567–2575. https://doi.org/10.1039/c3an36929c

Luo Z, Yuwen L, Han Y, Tian J, Zhu X, Weng L, Wang L (2012) Reduced graphene oxide/PAMAM–silver nanoparticles nanocomposite modified electrode for direct electrochemistry of glucose oxidase and glucose sensing. Biosens Bioelectron 36:179–185. https://doi.org/10.1016/j.bios.2012.04.009

Mani V, Devadas B, Chen S-M (2013) Direct electrochemistry of glucose oxidase at electrochemically reduced graphene oxide–multiwalled carbon nanotubes hybrid material modified electrode for glucose biosensor. Biosens Bioelectron 41:309–315. https://doi.org/10.1016/j.bios.2012.08.045

Mani V, Devasenathipathy R, Chen S-M, Huang S-T, Vasantha VS (2014) Immobilization of glucose oxidase on graphene and cobalt phthalocyanine composite and its application for the determination of glucose. Enzym Microb Technol 66:60–66. https://doi.org/10.1016/j.enzmictec.2014.08.009

Mazeiko V, Kausaite-Minkstimiene A, Ramanaviciene A, Balevicius Z, Ramanavicius A (2013) Gold nanoparticle and conducting polymer-polyaniline-based nanocomposites for glucose biosensor design. Sensors Actuators B Chem 189:187–193. https://doi.org/10.1016/j.snb.2013.03.140

Mohamad Nor N, Abdul Razak K, Lockman Z (2017) Physical and electrochemical properties of iron oxide nanoparticles–modified electrode for amperometric glucose detection. Electrochim Acta 248:160–168. https://doi.org/10.1016/j.electacta.2017.07.097

Moon IK, Lee J, Ruoff RS, Lee H (2010) Reduced graphene oxide by chemical graphitization. Nat Commun 1:73. https://doi.org/10.1038/ncomms1067

Muguruma H, Hoshino T, Nowaki K (2015) Electronically type-sorted carbon nanotube–based electrochemical biosensors with glucose oxidase and dehydrogenase. ACS Appl Mater Interfaces 7:584–592. https://doi.org/10.1021/am506758u

Murray RW (2008) Nanoelectrochemistry: metal nanoparticles, nanoelectrodes, and nanopores. Chem Rev 108:2688–2720. https://doi.org/10.1021/cr068077e

Niemeyer CM (2001) Nanoparticles, proteins, and nucleic acids: biotechnology meets materials science. Angew Chem Int Ed 40:4128–4158

Ohara TJ, Rajagopalan R, Heller A (1994) "Wired" enzyme electrodes for amperometric determination of glucose or lactate in the presence of interfering substances. Anal Chem 66:2451–2457

Oztekin Y, Ramanaviciene A, Yazicigil Z, Solak AO, Ramanavicius A (2011) Direct electron transfer from glucose oxidase immobilized on polyphenanthroline-modified glassy carbon electrode. Biosens Bioelectron 26:2541–2546. https://doi.org/10.1016/j.bios.2010.11.001

Pachauri V, Vlandas A, Kern K, Balasubramanian K (2010) Site-specific self-assembled liquid-gated ZnO nanowire transistors for sensing applications. Small 6:589–594. https://doi.org/10.1002/smll.200900876

Palanisamy S, Karuppiah C, Chen S-M (2014) Direct electrochemistry and electrocatalysis of glucose oxidase immobilized on reduced graphene oxide and silver nanoparticles

nanocomposite modified electrode. Colloids Surf B Biointerfaces 114:164–169. https://doi.org/10.1016/j.colsurfb.2013.10.006
Palanisamy S, Vilian ATE, Chen S-M (2012) Direct electrochemistry of glucose oxidase at reduced Graphene oxide/zinc oxide composite modified electrode for glucose sensor. Int J Electrochem Sci 7:2153–2163
Paleček E, Bartošík M (2012) Electrochemistry of nucleic acids. Chem Rev 112:3427–3481. https://doi.org/10.1021/cr200303p
Park S, Kim HC, Chung TD (2012) Electrochemical analysis based on nanoporous structures. Analyst 137:3891–3903. https://doi.org/10.1039/c2an35294j
Pauliukaite R, Ghica ME, Fatibello-Filho O, Brett CMA (2010) Electrochemical impedance studies of chitosan-modified electrodes for application in electrochemical sensors and biosensors. Electrochim Acta 55:6239–6247. https://doi.org/10.1016/j.electacta.2009.09.055
Periasamy AP, Chang Y-J, Chen S-M (2011) Amperometric glucose sensor based on glucose oxidase immobilized on gelatin-multiwalled carbon nanotube modified glassy carbon electrode. Bioelectrochemistry 80:114–120. https://doi.org/10.1016/j.bioelechem.2010.06.009
Ping J, Wang Y, Fan K, Wu J, Ying Y (2011) Direct electrochemical reduction of graphene oxide on ionic liquid doped screen-printed electrode and its electrochemical biosensing application. Biosens Bioelectron 28:204–209. https://doi.org/10.1016/j.bios.2011.07.018
Pradhan D, Niroui F, Leung KT (2010) High-performance, flexible enzymatic glucose biosensor based on ZnO nanowires supported on a gold-coated polyester substrate. ACS Appl Mater Interfaces 2:2409–2412. https://doi.org/10.1021/am100413u
Privett BJ, Shin JH, Schoenfisch MH (2010) Electrochemical sensors. Anal Chem 82:4723–4741. https://doi.org/10.1021/ac101075n
Qiu C, Wang X, Liu X, Hou S, Ma H (2012) Direct electrochemistry of glucose oxidase immobilized on nanostructured gold thin films and its application to bioelectrochemical glucose sensor. Electrochim Acta 67:140–146. https://doi.org/10.1016/j.electacta.2012.02.011
Razmi H, Mohammad-Rezaei R (2013) Graphene quantum dots as a new substrate for immobilization and direct electrochemistry of glucose oxidase: application to sensitive glucose determination. Biosens Bioelectron 41:498–504. https://doi.org/10.1016/j.bios.2012.09.009
Ren J, Shi W, Li K, Ma Z (2012) Ultrasensitive platinum nanocubes enhanced amperometric glucose biosensor based on chitosan and nafion film. Sensors Actuators B Chem 163:115–120. https://doi.org/10.1016/j.snb.2012.01.017
Rubianes MD, Rivas GA (2007) Dispersion of multi-wall carbon nanotubes in polyethylenimine: a new alternative for preparing electrochemical sensors. Electrochem Commun 9:480–484. https://doi.org/10.1016/j.elecom.2006.08.057
Saha K, Agasti SS, Kim C, Li X, Rotello VM (2012) Gold nanoparticles in chemical and biological sensing. Chem Rev 112:2739–2779. https://doi.org/10.1021/cr2001178
Sardar R, Funston AM, Mulvaney P, Murray RW (2009) Gold nanoparticles: past, present, and future. Langmuir 25:13840–13851. https://doi.org/10.1021/la9019475
Şenel M, Nergiz C (2012) Novel amperometric glucose biosensor based on covalent immobilization of glucose oxidase on poly(pyrrole propylic acid)/Au nanocomposite. Curr Appl Phys 12:1118–1124. https://doi.org/10.1016/j.cap.2012.02.004
Shamsipur M, Tabrizi MA (2014) Achieving direct electrochemistry of glucose oxidase by one step electrochemical reduction of graphene oxide and its use in glucose sensing. Mater Sci Eng C Mater Biol Appl 45:103–108. https://doi.org/10.1016/j.msec.2014.09.002
Shan D, Zhu M, Xue H, Cosnier S (2007) Development of amperometric biosensor for glucose based on a novel attractive enzyme immobilization matrix: calcium carbonate nanoparticles. Biosens Bioelectron 22:1612–1617. https://doi.org/10.1016/j.bios.2006.07.019
Shan C, Yang H, Han D, Zhang Q, Ivaska A, Niu L (2010) Graphene/AuNPs/chitosan nanocomposites film for glucose biosensing. Biosens Bioelectron 25:1070–1074. https://doi.org/10.1016/j.bios.2009.09.024
Sharma S, Gupta N, Srivastava S (2012) Modulating electron transfer properties of gold nanoparticles for efficient biosensing. Biosens Bioelectron 37:30–37. https://doi.org/10.1016/j.bios.2012.04.027

Shervedani RK, Amini A, Sadeghi N (2016) Electrografting of thionine diazonium cation onto the graphene edges and decorating with Au nano-dendrites or glucose oxidase: characterization and electrocatalytic applications. Biosens Bioelectron 77:478–485. https://doi.org/10.1016/j.bios.2015.09.062

Shi J, Zhang H, Snyder A, M-x W, Xie J, Marshall Porterfield D, Stanciu LA (2012) An aqueous media based approach for the preparation of a biosensor platform composed of graphene oxide and Pt-black. Biosens Bioelectron 38:314–320. https://doi.org/10.1016/j.bios.2012.06.007

Si P, Kannan P, Guo L, Son H, Kim D-H (2011) Highly stable and sensitive glucose biosensor based on covalently assembled high density Au nanostructures. Biosens Bioelectron 26:3845–3851. https://doi.org/10.1016/j.bios.2011.02.044

Sun C, Chen X, Han Q, Zhou M, Mao C, Zhu Q, Shen J (2013) Fabrication of glucose biosensor for whole blood based on Au/hyperbranched polyester nanoparticles multilayers by antibiofouling and self-assembly technique. Anal Chim Acta 776:17–23. https://doi.org/10.1016/j.aca.2013.03.032

Sung Y-M, Noh K, Kwak W-C, Kim TG (2012) Enhanced glucose detection using enzyme-immobilized ZnO/ZnS core/sheath nanowires. Sensors Actuators B Chem 161:453–459. https://doi.org/10.1016/j.snb.2011.10.061

Tan Y, Deng W, Chen C, Xie Q, Lei L, Li Y, Fang Z, Ma M, Chen J, Yao S (2010) Immobilization of enzymes at high load/activity by aqueous electrodeposition of enzyme-tethered chitosan for highly sensitive amperometric biosensing. Biosens Bioelectron 25:2644–2650. https://doi.org/10.1016/j.bios.2010.04.040

Tasviri M, Rafiee-Pour H-A, Ghourchian H, Gholami MR (2011) Amine functionalized TiO_2–carbon nanotube composite: synthesis, characterization and application to glucose biosensing. Appl Nanosci 1:189–195. https://doi.org/10.1007/s13204-011-0025-0

Teo WZ, Ambrosi A, Pumera M (2013) Direct electrochemistry of copper oxide nanoparticles in alkaline media. Electrochem Commun 28:51–53. https://doi.org/10.1016/j.elecom.2012.12.006

Terse-Thakoor T, Komori K, Ramnani P, Lee I, Mulchandani A (2015) Electrochemically functionalized seamless three-dimensional graphene-carbon nanotube hybrid for direct electron transfer of glucose oxidase and bioelectrocatalysis. Langmuir 31:13054–13061. https://doi.org/10.1021/acs.langmuir.5b03273

Toghill KE, Compton RG (2010) Electrochemical non-enzymatic glucose sensors: a perspective and an evaluation. Int J Electrochem Sci 5:1246–1301

Turkmen E, Bas SZ, Gulce H, Yildiz S (2014) Glucose biosensor based on immobilization of glucose oxidase in electropolymerized poly(o-phenylenediamine) film on platinum nanoparticles–polyvinylferrocenium modified electrode. Electrochim Acta 123:93–102. https://doi.org/10.1016/j.electacta.2013.12.189

Turner APF (2013) Biosensors: sense and sensibility. Chem Soc Rev 42:3184–3196. https://doi.org/10.1039/c3cs35528d

Unnikrishnan B, Palanisamy S, Chen S-M (2013) A simple electrochemical approach to fabricate a glucose biosensor based on graphene-glucose oxidase biocomposite. Biosens Bioelectron 39:70–75. https://doi.org/10.1016/j.bios.2012.06.045

Updike SJ, Hicks GP (1967) The enzyme electrode. Nature 214:986–988

Uzun SD, Kayaci F, Uyar T, Timur S, Toppare L (2014) Bioactive surface design based on functional composite electrospun nanofibers for biomolecule immobilization and biosensor applications. ACS Appl Mater Interfaces 6:5235–5243. https://doi.org/10.1021/am5005927

Wang J (2001) Glucose biosensors: 40 years of advances and challenges. Electroanalysis 13 (12):983–988

Wang J (2008) Electrochemical glucose biosensors. Chem Rev 108:814–825. https://doi.org/10.1021/cr068123a

Wang Y, Shao Y, Matson DW, Li J, Lin Y (2010) Nitrogen-doped graphene and its application in electrochemical biosensing. ACS Nano 4:1790–1798. https://doi.org/10.1021/nn100315s

Wang K, Liu Q, Guan Q-M, Wu J, Li H-N, Yan J-J (2011a) Enhanced direct electrochemistry of glucose oxidase and biosensing for glucose via synergy effect of graphene and CdS nanocrystals. Biosens Bioelectron 26:2252–2257. https://doi.org/10.1016/j.bios.2010.09.043

Wang L, Bai J, Bo X, Zhang X, Guo L (2011b) A novel glucose sensor based on ordered mesoporous carbon–Au nanoparticles nanocomposites. Talanta 83:1386–1139

Wang C, Chen S, Xiang Y, Li W, Zhong X, Che X, Li J (2011c) Glucose biosensor based on the highly efficient immobilization of glucose oxidase on Prussian blue–gold nanocomposite films. J Mol Catal B Enzym 69:1–7. https://doi.org/10.1016/j.molcatb.2010.12.002

Wang W, Xie Y, Wang Y, Du H, Xia C, Tian F (2014) Glucose biosensor based on glucose oxidase immobilized on unhybridized titanium dioxide nanotube arrays. Microchim Acta 181:381–387. https://doi.org/10.1007/s00604-013-1121-5

Wang L, Li J, Pan Y, Min L, Zhang Y, Hu X, Yang Z (2017) Platinum nanoparticle–assembled nanoflake-like tin disulfide for enzyme-based amperometric sensing of glucose. Microchim Acta 184:2357–2363. https://doi.org/10.1007/s00604-017-2209-0

Willner I, Heleg-Shabtai V, Blonder R, Katz E, Tao G (1996) Electrical wiring of glucose oxidase by reconstitution of FAD-modified monolayers assembled onto Au-electrodes. J Am Chem Soc 118:10321–10322

Wooten M, Karra S, Zhang M, Gorski W (2014) On the direct electron transfer, sensing, and enzyme activity in the glucose oxidase/carbon nanotubes system. Anal Chem 86:752–757. https://doi.org/10.1021/ac403250w

Wu P, Shao Q, Hu Y, Jin J, Yin Y, Zhang H, Cai C (2010) Direct electrochemistry of glucose oxidase assembled on graphene and application to glucose detection. Electrochim Acta 55:8606–8614. https://doi.org/10.1016/j.electacta.2010.07.079

Xiao Y, Patolsky F, Katz E, Hainfeld JF, Willner I (2003) "Plugging into enzymes": nanowiring of redox enzymes by a gold nanoparticle. Science 299:1877–1899. https://doi.org/10.1126/science.1080664

Xiao X, Ulstrup J, Li H, Wang M'e, Zhang J, Si P (2014) Tabri gold assembly of glucose oxidase for electrochemical biosensing. Electrochim Acta 130:559–567. https://doi.org/10.1016/j.electacta.2014.02.146

Xu Y, Liu X, Ding Y, Luo L, Wang Y, Zhang Y, Xu Y (2011) Preparation and electrochemical investigation of a nano-structured material Ni^{2+}/MgFe layered double hydroxide as a glucose biosensor. Appl Clay Sci 52:322–327. https://doi.org/10.1016/j.clay.2011.03.011

Xu Q, Gu S-X, Jin L, Y-e Z, Yang Z, Wang W, Hu X (2014) Graphene/polyaniline/gold nanoparticles nanocomposite for the direct electron transfer of glucose oxidase and glucose biosensing. Sensors Actuators B Chem 190:562–569. https://doi.org/10.1016/j.snb.2013.09.049

Yamanaka K, Vestergaard M'dC, Tamiya E (2016) Printable electrochemical biosensors: a focus on screen-printed electrodes and their application. Sensors (Basel) 16:1761. https://doi.org/10.3390/s16101761

Yang Z, Ye Z, Zhao B, Zong X, Wang P (2010) A rapid response time and highly sensitive amperometric glucose biosensor based on ZnO nanorod via citric acid–assisted annealing route. Physica E 42:1830–1833. https://doi.org/10.1016/j.physe.2010.02.001

Yang Z, Tang Y, Li J, Zhang Y, Hu X (2014) Facile synthesis of tetragonal columnar-shaped TiO_2 nanorods for the construction of sensitive electrochemical glucose biosensor. Biosens Bioelectron 54:528–533. https://doi.org/10.1016/j.bios.2013.11.043

Yu Y, Chen Z, He S, Zhang B, Li X, Yao M (2014) Direct electron transfer of glucose oxidase and biosensing for glucose based on PDDA-capped gold nanoparticle modified graphene/multi-walled carbon nanotubes electrode. Biosens Bioelectron 52:147–152. https://doi.org/10.1016/j.bios.2013.08.043

Zeng Q, Cheng J-S, Liu X-F, Bai H-T, Jiang J-H (2011) Palladium nanoparticle/chitosan-grafted graphene nanocomposites for construction of a glucose biosensor. Biosens Bioelectron 26:3456–3463. https://doi.org/10.1016/j.bios.2011.01.024

Zhai Y, Zhai S, Chen G, Zhang K, Yue Q, Wang L, Liu J, Jia J (2011) Effects of morphology of nanostructured ZnO on direct electrochemistry and biosensing properties of glucose oxidase. J Electroanal Chem 656:198–205. https://doi.org/10.1016/j.jelechem.2010.11.020

Zhai D, Liu B, Shi Y, Pan L, Wang Y, Li W, Zhang R, Yu G (2013) Highly sensitive glucose sensor based on Pt nanoparticle/polyaniline hydrogel heterostructures. ACS Nano 7:3540–3546. https://doi.org/10.1021/nn400482d

Zhang Y, Chang G, Liu S, Lu W, Tian J, Sun X (2011a) A new preparation of Au nanoplates and their application for glucose sensing. Biosens Bioelectron 28:344–348. https://doi.org/10.1016/j.bios.2011.07.041

Zhang Y, Sun X, Zhu L, Shen H, Jia N (2011b) Electrochemical sensing based on graphene oxide/Prussian blue hybrid film modified electrode. Electrochim Acta 56:1239–1245

Zhang Y, Fan Y, Wang S, Tan Y, Shen X, Shi Z (2012) Facile fabrication of a graphene-based electrochemical biosensor for glucose detection. Chin J Chem 30:1163–1167. https://doi.org/10.1002/cjoc.201100452

Zhang L, Yuan S-m, Yang L-m, Fang Z, Zhao G-c (2013) An enzymatic glucose biosensor based on a glassy carbon electrode modified with manganese dioxide nanowires. Microchim Acta 180:627–633. https://doi.org/10.1007/s00604-013-0968-9

Zhang X, Liao Q, Chu M, Liu S, Zhang Y (2014) Structure effect on graphene-modified enzyme electrode glucose sensors. Biosens Bioelectron 52:281–287. https://doi.org/10.1016/j.bios.2013.07.022

Zheng B, Xie S, Qian L, Yuan H, Xiao D, Choi MMF (2011) Gold nanoparticles–coated eggshell membrane with immobilized glucose oxidase for fabrication of glucose biosensor. Sensors Actuators B Chem 152:49–55. https://doi.org/10.1016/j.snb.2010.09.051

Zhong H, Yuan R, Chai Y, Li W, Zhong X, Zhang Y (2011) In situ chemo-synthesized multi-wall carbon nanotube–conductive polyaniline nanocomposites: characterization and application for a glucose amperometric biosensor. Talanta 85:104–111. https://doi.org/10.1016/j.talanta.2011.03.040

Zhu LY, Yu G, Wang XQ, Xu D (2009) Preparation and characterization of TiO_2 fiber with a facile polyorganotitanium precursor method. J Colloid Interface Sci 336:438–442. https://doi.org/10.1016/j.jcis.2009.03.077

Zhu C, Yang G, Li H, Du D, Lin Y (2015) Electrochemical sensors and biosensors based on nanomaterials and nanostructures. Anal Chem 87:230–249. https://doi.org/10.1021/ac5039863

Chapter 10
Innovations in Antimicrobial Engineered Nanomaterials

Marcela P. Bernardo, Francys K. V. Moreira, Luiz H. C. Mattoso, and Sebastian Raja

Contents

Abstract The threat caused by drug-resistant pathogens represents a great concern to several economic sectors. This issue has intensified the development of more efficient antimicrobial products that could be safe not only for medical, pharmaceutical, water disinfection and food applications but also for reduced environmental impact. Nanotechnology now emerges as a powerful tool for scientists and engineers to develop engineered nanomaterials with remarkable antimicrobial activity. The potential of engineered nanomaterials is now certain to benefit different areas, such as medicine, food, pharmaceutical, and agriculture, once higher antimicrobial

M. P. Bernardo
Department of Chemistry, Federal University of São Carlos, São Carlos, SP, Brazil

National Nanotechnology Laboratory for Agribusiness, Embrapa Instrumentação, São Carlos, SP, Brazil

F. K. V. Moreira
Department of Materials Engineering – DEMa, Federal University of São Carlos – UFSCar, São Carlos, SP, Brazil

National Nanotechnology Laboratory for Agribusiness, Embrapa Instrumentação, São Carlos, SP, Brazil
e-mail: moreira.fkv@dema.ufscar.br

L. H. C. Mattoso · S. Raja (✉)
National Nanotechnology Laboratory for Agribusiness, Embrapa Instrumentação, São Carlos, SP, Brazil

Mu. Naushad et al. (eds.), *Advanced Nanostructured Materials for Environmental Remediation*, Environmental Chemistry for a Sustainable World 25,
https://doi.org/10.1007/978-3-030-04477-0_10

effectiveness implies in reduced content of antimicrobial compounds, thereby reducing cytotoxicity effects as well as environmental impact to different forms of life. This chapter summarizes the most recent achievements on antimicrobial engineered nanomaterials intended for better medicine, cosmetics, environmental, and food applications with emphasis on (i) new silver-based hybrid nanomaterials, (ii) new bioinspired antimicrobial nanoparticles, (iii) new antimicrobial nanostructures derived from layered minerals, (iv) recent developments on antimicrobial polymer nanocomposites, and finally (v) some recent trends in nanotechnological antimicrobial products available at the European market. The remarkable importance of antimicrobial engineered nanomaterials emerges from the combination of different nanomaterials so that main advantages of each are built together into new, revolutionary systems capable of solving the pathogen infection issue.

Keywords Pathogen infestation · Biocidal effect · Antimicrobial agent · Nanomaterials · Nanosilver · Carbon nanotubes · Layered double hydroxides · Polymer nanocomposites · Antibacterial consumer goods · Nanoscience

10.1 Introduction

Infection by pathogenic microorganisms represents a worldwide health concern for several economic sectors (Raghunath and Perumal 2017). Clinical area and food industry have invested enormously in technologies for preventing pathogens contamination, but such investments have raised year by year due to the emergence of multidrug-resistant microorganisms (Raghunath and Perumal 2017; Hajipour et al. 2012). There has been intense development of highly effective antimicrobial products for medical, pharmaceutical, water disinfection, and food applications which could also be safe for human health (Salam et al. 2017; Sharma et al. 2017).

Nanotechnology is a multidisciplinary field that has leveraged various economic sectors, such as electronics, catalysis, medicine, and tissue engineering, among others (Alsaleh and Brown 2018). The main concept guiding nanotechnology is the design of materials whose properties are a consequence of a very high surface reactivity due to the greater number of atoms that can interact both physically and chemically with their surroundings (Shevlin et al. 2018). "Nanoeffects" are particularly achieved in nanomaterials with very large surface area-to-volume ratio. According to the European Commission Directive, nanomaterials are "natural, incidental or manufactured materials containing particles, in an unbound state or as an aggregate or as an agglomerate and where, for 50% or more of the particles in the number size distribution, one or more external dimensions is in the size range 1 nm – 100 nm" (European Commission 2015). Nanotechnology has now been applied in the development of nanostructures with remarkable antimicrobial activity (Rajendran et al. 2018; Hoseinzadeh et al. 2017; Raghunath and Perumal 2017).

This chapter presents the recent advances on antimicrobial engineered nanomaterials (ENMs) for medicine, cosmetics, environmental, and food

applications. In the medical and pharmaceutical fields, the use of nanotechnology allows much better antimicrobial effects on bacteria that tend to infect wounds, since they can easily penetrate the wound through the body fluids. Also, nanomaterials may be applied as drug delivery systems, bringing innovation of dosage forms with improved therapeutic effects and physicochemical characteristics of the antimicrobial substances. For water decontamination, antimicrobial nanomaterials exhibit potential to replace or enhance conventional disinfection methods, while not producing harmful products. For food applications, the inclusion of antimicrobial nanomaterials in the package material is effective for food protection against common foodborne pathogens, especially under visible or UV light depending of the antimicrobial agent.

The principal scientific achievements in the last 5 years concerning silver-based nanomaterials, organic nanoparticles, antimicrobial layered clays, and polymer nanocomposites are summarized. Recent patenting trends in antimicrobial nanomaterials are also presented to point out their technological potential in everyday consumer products.

10.2 Antimicrobial Silver-Based Nanomaterials

Silver (Ag) is one the oldest antimicrobial substances known to be used by man. The antimicrobial activity of silver was exploited by most ancient civilizations for water disinfection, food conservation, and treatment of wounds (McGillicuddy et al. 2017; Chernousova and Epple 2013). Since then, silver has been used as an active principle either in its ionic (Ag^+ ions), complexed (Ag salts), or colloidal nanoparticulate (Ag nanoparticles, AgNPs) states for countless decades (Bilal et al. 2017).

The mechanism behind the silver antimicrobial activity has been discussed in excellent reviews (Noronha et al. 2017; Chernousova and Epple 2013). In brief, it requires the oxidation of metallic silver to Ag^+ ions, which further bind electrostatically to structural N– and S– groups of proteins and other biomolecules present in the microbial cell membrane, leading to its lysis. Ag^+ ions can also penetrate the microbial cell through several ways and interfere on the ribosomes and DNA dynamics by reactive oxygen species (ROS), also leading to cell death (Durán et al. 2016), as illustrated in Fig. 10.1. There are mechanistic differences between Ag^+ ions and very small AgNPs (size <10 nm), but for most silver-based materials, the ending active species is the Ag^+ ion (Noronha et al. 2017; Chernousova and Epple 2013).

AgNPs have been extensively used for their antibacterial activity; nevertheless the intense agglomeration effects in AgNPs are still a challenge hampering their successful practical applications (Wei et al. 2015). One feasible alternative is the use of material supports to prevent AgNP agglomeration, for instance, nanoporous silica (0D), carbon nanotubes (1D), clay minerals (2D), and zeolites (3D). Currently, nanotechnology has tiled the way for developing silver-based ENMs with stabilized

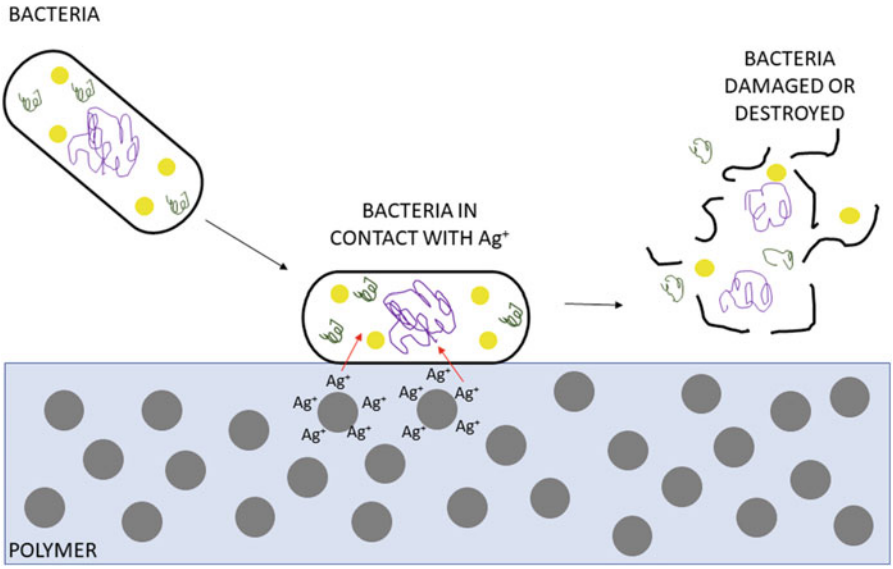

Fig. 10.1 Schematics of silver (Ag^+) antibacterial effect leading to destruction or damage of the genetic material and causing weakened protection, structure, and integrity of the bacterial cell membrane

AgNPs and remarkable antimicrobial activity against several microorganisms, including viruses. Table 10.1 summarizes some of these recent developments.

Carbon nanotubes (CNTs) are one of the most promising engineered nanomaterials for Ag support. Recently, Xia et al. (2018) synthesized AgNPs (6–10 nm) encapsulated into tip open carbon nanotubes (CNTs) using a new glucose-assisted method. The AgNP-CNT hybrid loaded with 4 wt. % Ag exhibited higher antibacterial activity against *Escherichia coli* than AgNPs supported onto active carbon and on CNTs obtained by wet impregnation, which was mainly attributed to the better dispersion of the AgNPs inside the CNT tunnels.

Another important application of CNT-supported AgNPs is the removal of microorganisms from drinking water. Salam et al. (2017) synthesized CNT/polypyrrole hybrids via oxidative polymerization of pyrrole with silver nitrate, leading to nanocomposites loaded with 80 wt.% AgNPs, which were further used for water disinfection in a column filter test. The CNT/polypyrrole/AgNP nanocomposites effectively inactivated the *Escherichia coli* and *Staphylococcus aureus* cells by nearly 100 wt.%.

Aani et al. (2017) developed multiwalled carbon nanotubes (MWCNTs) coated with 10 wt.% and 20 wt.% AgNPs via microwave treatments, which were incorporated into polyethersulfone (PES) ultrafiltration (UF) membranes. The membranes were effective against *Escherichia coli* and *Staphylococcus aureus*, being the biocidal effect attributed to the release of Ag^+ ions because there was no contact between the AgNPs and the bacteria.

Table 10.1 Recent developments of selected Ag-based ENMs

Nanomaterial	Silver form	Ag loading	Target microorganism	Potential application	References
Single-wall carbon nanotubes (CNTs)	AgNP	4 wt.%	*Escherichia coli*	Biomedicine	Xia et al. (2018)
Nanoporous SiO_2/poplar propolis	AgNP	0.5–0.6 mmol/g	*Escherichia coli*, *Staphylococcus aureus*, *Candida albicans*	Biomedicine	Popova et al. (2018)
Monodispersed SiO_2 particles	AgNP	294 mg/L	Bacteriophage MS2 and murine norovirus (MNV)	Water disinfection	Park et al. (2018)
Multiwalled carbon nanotubes (MWCNTs)	AgNP	10 wt.% and 20 wt.%	*Escherichia coli*, *Staphylococcus aureus*	Water disinfection	Aani et al. (2017)
SiO_2 particles	AgNP	Not provided	*Staphylococcus aureus*	Cellulosic fabric	Panwar et al. (2018)
Single-wall carbon nanotubes (CNTs)/polypyrrole	AgNP	80 wt.%	*Escherichia coli*, *Staphylococcus aureus*	Water disinfection	Salam et al. (2017)
Zeolite A (ZA), faujasite NaX (ZX), and analcime (ANA)	Ag^+ ions	0.16 wt.%	*Staphylococcus aureus*, *Pseudomonas aeruginosa*, *Candida albicans*, *Aspergillus niger*	Additives for consumer products	Youssef et al. (2017)
SiO_2 particles	AgNP	33–22 wt.%	*Staphylococcus aureus*, *Escherichia coli*	Surgical implants	Priebe et al. (2017)
SiO_2 particles	AgNP	Not provided	*Staphylococcus aureus*, *Escherichia coli*, *Candida albicans*	Kevlar® fabric coating	Balagna et al. (2017)
Multiwalled carbon nanotubes (MWCNTs)	AgNP	Not provided	Polio-, Noro-, and Coxsackie viruses	Water disinfection	Kim et al. (2016)

Kim et al. (2016) prepared a nanofilter based on MWCNTs decorated with 20-nm-sized AgNPs using ethylene glycol as a reducing agent. The nanofilter was tested for removal of nanosized viruses (Polio-, Noro-, and Coxsackie viruses), *Escherichia coli*, and *Staphylococcus aureus* from water. The MWCNT/AgNP nanofilter could also be used for other biological separation processes.

Nanosilica has also been used as a material support for AgNPs. Spherical nanoporous MCM-41 and SBA-15 silicas were decorated with AgNPs (5–15 nm)

by direct and post-synthesis approaches, with AgNPs impregnated into the channels and external surface of the silica. This inorganic hybrid nanomaterial was further loaded with propolis extract at 15–17 wt.%. The resulting multifunctional material presented a synergistic effect between the AgNPs and the propolis compounds in terms of antibacterial activity against *Escherichia coli*, *Staphylococcus aureus*, and *Candida albicans* (Popova et al. 2018).

Panwar et al. (2018) applied amine-, thiol-, and epoxy-functionalized AgNP/SiO_2 Janus particles on cotton fabric. The AgNPs were produced by chemical reduction, while the AgNP/SiO_2 Janus particles were synthesized by the Pickering emulsion method at low temperature and further used to impregnate epoxy-treated cotton fabrics. The AgNP/SiO_2 Janus particles showed higher antimicrobial activity than the pure AgNPs due to the non-agglomerated state of the AgNPs in the former. The epoxy-functionalized cotton fabrics treated with AgNP/SiO_2 Janus particles presented high antibacterial effect against *Staphylococcus aureus*. Such a biocidal effect persisted even after several washing cycles.

Balagna et al. (2017) used a co-sputtering process to coat Kevlar® plain woven fabrics intended for inflatable modulus uses with AgNP/SiO_2 hybrid nanomaterial. The coating did not avoid *Staphylococcus aureus*, *Escherichia coli*, and *Candida albicans* proliferation, but it significantly reduced the adhesion of these microorganisms on the Kevlar® fabric surface. The SiO_2 nanomaterial acted specifically in the controlled release of the Ag^+ ions.

Priebe et al. (2017) synthesized AgNP/SiO_2 nanorattles by a microemulsion technique intending antibacterial orthopedic implant applications. The AgNP/SiO_2 nanorattles exhibited strong antibacterial effect against *S. aureus* and *E. coli*, but they did not affect the viability of phagocytic cells. Further, they did not induce inflammation and did not impair immune responses.

Ag-decorated nanosilica has also been developed for water disinfection purposes. Park et al. (2018) impregnated monodispersed amine-functionalized silica (d = 400 nm) with 30-nm-diameter AgNPs to prevent their aggregation and facilitate their recovery after use. The major antiviral effects against two viruses, bacteriophage MS2 and MNV, were attributed only to the AgNPs impregnated in the silica core. The AgNP-silica hybrid induced large virus reduction at the first few hours (~ 6 h), but this antiviral effect gradually reduced over time, which was ascribed to the amount of Ag^+ ions released from the AgNPs.

An important group of ENMs for silver immobilization that must be emphasized are the aluminosilicates. Clays and zeolite structures exhibit large ion exchange capacity, leading to successful separation and ion exchange process applications. For example, Youssef et al. (2017) impregnated the Zeolite A (ZA), faujasite NaX (ZX), and analcime (ANA) previously synthesized by a microwave technique with Ag^+ ions using the ion exchange route. The Ag-treated zeolites inhibited the growth of *S. aureus*, *Pseudomonas aeruginosa*, *Candida albicans*, and *Aspergillus niger.* The zeolites presenting large specific area also presented the large Ag^+ loading, thereby resulting in the highest antimicrobial efficiency.

10.3 Antimicrobial Organic Nanoparticles

Biopolymer-based antimicrobial nanoparticles are a promising class of ENMs for microbial proliferation control. For instance, some protein and polysaccharide nanoparticles have been associated with antimicrobial agents for improved antimicrobial release rate and biocidal effectiveness toward several pathogens (Perinelli et al. 2018; Arora et al. 2016). Such functional biopolymer nanostructures have attracted enormous interest due to their biodegradability, biocompatibility, nontoxic, and non-immunogenic properties. Additionally, most of these biopolymers are approved as a GRAS (generally recognized as safe) by the FDA (Food and Drug Administration) which is remarkable advantage especially for medicine and food applications (Arora et al. 2016).

Table 10.2 lists recent achievements on biopolymer-based antimicrobial ENMs. The overall strategy in most of these reports consisted in elaborating a biopolymer solution containing the antimicrobial agent, which is further added to a precipitating medium under controlled conditions (temperature, pH, injection rate) to obtain ENMs having narrow particle size distribution.

Starch is a polysaccharide made up of D-glucose units connected by α-type glycosidic linkages. Starch is a water-soluble, abundant, fully biodegradable, and cheap biopolymer. Starch can also assume thermoplastic behavior so that it can be shaped by melt-processing techniques into films, bottles, etc. Due to its versatility, starch has been used in the development of several antimicrobial ENMs.

Jung et al. (2018) synthetized 7-nm-sized AgNPs using a sonochemical method using starch as a stabilizing agent. The complexed AgNP-starch ENM was combined with chitosan, another promising polysaccharide, to form coatings on papers. The functional papers exhibited inhibitory effect against *E. coli* and *S. aureus* with antimicrobial effect dependent on the AgNP-starch concentration, thereby demonstrating potential for food packaging and other applications.

Starch nanoparticles (SNPs) have been considered as promising ENMs for controlled antimicrobial agent delivery. Qiu et al. (2017) encapsulated menthone, oregano, cinnamon, lavender, and citra essential oils into SNPs with size ranging from 93 to 113 nm for applications in food, cosmetics, as well as pathogen control in general. The encapsulation efficiency was 87%, and the essential oil-loaded SNPs inhibited the growth of *Escherichia coli* and *Staphylococcus aureus*. The antimicrobial effect of the essential oils was prolongated due to the encapsulation with starch. Ismail and Gopinath (2017) encapsulated penicillin and streptomycin into starch nanoparticles. The SNPs were prepared by the microemulsion nanoprecipitation method using alkaline urea solution as a solvent and ethanol as a precipitation batch. *The antibiotic-loaded SNPs successfully inhibited the growth of Streptococcus pyogenes and Escherichia coli*. Previously, Alzate et al. (2016) exploited sodium trimetaphosphate (STMP)-cross-linked SNPs as a nanocarrier for potassium sorbate, a widely used food preservative. Native and acetylated starches were used in the study. The potassium sorbate-loaded cross-linked SNPs were effective against *E. coli* and *S. aureus* growth. The encapsulation of the potassium sorbate in the

Table 10.2 Recent biopolymer-based antimicrobial ENMs

Biopolymer	Antimicrobial agent	Target microorganism	Application	References
Fungal chitosan nanoparticles	Fungal chitosan	*Staphylococcus aureus*, *Listeria monocytogenes*, *Pseudomonas aeruginosa*, *Salmonella* ssp., *Escherichia coli*	Food preservation	Melo et al. (2018)
Chitosan/ alginate nanoparticles	Nisin	*Listeria monocytogenes*	Beef preservation	Zimet et al. (2018)
Chitosan nanoparticles	Levofloxacin	*Pseudomonas aeruginosa*, *Staphylococcus aureus*	Ocular infection treatment	Ameeduzzafar et al. (2018)
Chitosan nanoparticles	Spiramycin	*Toxoplasma gondii*	Toxoplasmosis treatment	Etewa et al. (2018)
Alginate coating	ZnO nanoparticles	*Staphylococcus aureus*	Water disinfection	Motshekga et al. (2018)
Starch-chitosan	AgNP	*Escherichia coli*, *Staphylococcus aureus*	Paper coating	Jung et al. (2018)
Starch nanoparticle	Menthone, oregano, cinnamon, lavender, and citra essential oils	*Escherichia coli*, *Staphylococcus aureus*	Food preservation, cosmetics	Qiu et al. (2017)
Chitosan nanoparticles	Triclosan	*Pseudomonas aeruginosa*, *Escherichia coli*, *Staphylococcus aureus*, *Candida albicans*	Wound treatment	De Marchi et al. (2017)
Starch nanoparticle	Penicillin, streptomycin	*Streptococcus pyogenes*, *Escherichia coli*	Medicine, pharmaceuticals	Ismail and Gopinath (2017)
Zein coating	Au nanoparticles	*Bacillus pumilus*, *Bacillus*, *Shigella sonnei*, *Pseudomonas aeruginosa*, *Aedes aegypti* larvae	Biofilm and *Aedes aegypti* mosquitoes control	Suganya et al. (2017)
Starch nanoparticles	Potassium sorbate	*Escherichia coli*, *Staphylococcus aureus*	Food preservation	Alzate et al. (2016)
Gelatin nanoparticles	Moxifloxacin	*Bacillus subtilis*, *Staphylococcus aureus*	Eye infection therapy	Mahor et al. (2016)
Chitosan-coated alginate nanoparticles	Daptomycin	*Methicillin-susceptible Staphylococcus aureus*, *S. epidermidis*, *Staphylococcus capitis*, *Staphylococcus hominis*, *Staphylococcus lugdunensis*,	Endophthalmitis therapy	Costa et al. (2015)

(continued)

Table 10.2 (continued)

Biopolymer	Antimicrobial agent	Target microorganism	Application	References
		Staphylococcus haemolyticus, *Staphylococcus warneri*		
Zein nanoparticles	Thymol, carvacrol	*Listeria monocytogenes*, *Staphylococcus aureus*, *Escherichia coli*, *Salmonella enterica subsp. enterica serovar. typhimurium*	Food preservation	Da Rosa et al. (2015)
Sodium caseinate	Thymol	*Listeria monocytogenes*	Food preservation	Pan et al. (2014)
Starch nanoparticles	Au nanoparticles	*Escherichia coli*, *Enterobacter aerogenes*, *Pseudomonas aeruginosa*, *Staphylococcus epidermidis*, *Enterococcus durans*, *Streptococcus bovis*	Textile fibers, film surfaces	Pender et al. (2013)

SNPs enabled the controlled release and higher stability of the antimicrobial compound.

Chitosan is a polysaccharide composed of randomly distributed β-(1 → 4)-linked D-glucosamine and N-acetyl-D-glucosamine units (Aider 2010). Chitosan has been applied in the food, cosmetic, biomedical, and agricultural fields due to its low toxicity, biodegradability, and biocompatibility (Ma et al. 2017, Aider 2010). Currently, there are many antimicrobial ENMs based on chitosan, also because chitosan has intrinsic antimicrobial activity (Ma et al. 2017). Melo et al. (2018) tested chitosan nanoparticles as coating for table grapes. The chitosan nanoparticles were prepared by ionotropic gelation and displayed minimal inhibitory concentration (MIC) from 2 to 3 g L^{-1} tested for *S. aureus*, *Listeria monocytogenes*, *Pseudomonas aeruginosa*, *Salmonella* ssp., and *E. coli*. Zimet et al. (2018) loaded nisin, a 34-amino acid lantibiotic, into chitosan nanoparticles synthesized by ionotropic gelation. The chitosan nanoparticles presented diameter of 66 nm and nisin encapsulation efficiency of 36% and prolongated the shelf life of beef when stored at 4 °C.

Chitosan nanoparticles have also been tested for medical applications. Ameeduzzafar et al. (2018) encapsulated levofloxacin, a synthetic third-generation fluoroquinolone, into chitosan nanoparticles (150–300 nm). The antibacterial chitosan nanoparticles were prepared by ionotropic gelation and achieved levofloxacin encapsulation efficiency of 56–76%. The levofloxacin-loaded chitosan nanoparticles were also effective against *Pseudomonas aeruginosa and S. aureus*, but they were nontoxic as ocular dosage. Chitosan nanoparticles prepared by ionotropic gelation were also loaded with spiramycin to treat acute and chronic toxoplasmosis in mice. The spiramycin-loaded chitosan nanoparticles presented

superior antibacterial effect than pure spiramycin against *Toxoplasma gondii* infection (Etewa et al. 2018).

Alginic acid is a biodegradable linear polysaccharide extracted from brown seaweed. Alginate is plentifully available, and it has also been used in the development of antimicrobial ENMs. Motshekga et al. (2018) used sodium alginate (the alginic acid salty form) beads to encapsulate ZnO nanoparticles supported in bentonite. The alginate beads were obtained using $CaCl_2$ solution as a precipitation medium. The alginate beads containing ZnO were effective for water disinfection once they were capable of inhibiting *S. aureus* growth both in natural and synthetic water over 1 min. Praphakar et al. (2017) used sodium alginate-g-allylamine-mannose copolymer nanoparticles to encapsulate rifampicin, an antituberculosis drug. The nanoparticles had size of about 300 nm, excellent drug encapsulation and release performances, and strong antimicrobial activity against *Mycobacterium tuberculosis* but, at the same time, low cytotoxicity for VERO cells. Costa et al. (2015) prepared chitosan-coated alginate nanoparticles sized at about 400 nm and used them as a nanocarrier for daptomycin intended for endophthalmitis therapy. The antimicrobial potential of daptomycin was preserved after encapsulation, revealing good potential against methicillin-susceptible *S. aureus*, *S. epidermidis*, *Staphylococcus capitis*, *Staphylococcus hominis*, *Staphylococcus lugdunensis*, *Staphylococcus haemolyticus*, and *Staphylococcus warneri*. This daptomycin-loaded nanocarrier exhibited a promising potential for the therapy of methicillin-resistant *Staphylococcus aureus* (MRSA) bacterial endophthalmitis.

Some proteins have also been applied in the development of antimicrobial ENMs. Suganya et al. (2017) developed gold nanoparticles (50–80 nm) coated with zein and evaluated their antimicrobial properties against *Bacillus pumilus*, *Shigella sonnei*, *Pseudomonas aeruginosa*, and instar larvae of *Aedes aegypti*, the major dengue and Zika virus vector. The zein-coated AuNPs presented high antibacterial and antibiofilm properties and the capability of controlling the *A. aegypti* larva population growth. Da Rosa et al. (2015) encapsulated thymol and carvacrol into zein nanoparticles and evaluated the stability of the antimicrobial ENMs over storage, which presented high antimicrobial activity against gram-positive bacterium *Listeria monocytogenes* and *S. aureus*. Mahor et al. (2016) synthesized gelatin nanoparticles by a desolvation method using glutaraldehyde as a cross-linking agent. The gelatin nanoparticles were loaded with moxifloxacin, reaching an encapsulation efficiency of 57%. MGP1 considerably inhibited the *S. aureus* growth in comparison to the commercial MoxiGram® eye drop solution. The moxifloxacin-loaded gelatin nanoparticles were also stable, thereby being promising for the development of eye infection treatment market products. Pan et al. (2014) used sodium caseinate, a bovine milk protein, to encapsulate 1% w/v thymol using a high homogenization treatment. The thymol-loaded sodium caseinate nanoparticles were tested against *Listeria monocytogenes* inoculated into milk samples and presented high antibacterial activity regarding media with different fat contents.

Overall, biopolymer-based ENMs offer a feasible, eco-friendly, and nontoxic way to encapsulate antimicrobial agents to further improve their compatibility with biological environments as well as to improve the release rate of the antimicrobial

agent at specific sites with minimal efficiency loss and toxic side effects, which is particularly favorable for medical and food applications.

10.4 Antimicrobial Layered Nanomaterials

One of the biggest challenges for the successful application of antimicrobials agents is the control of the delivery mechanism. The revolutionary development of nanomedicines has emerged as one of the most prominent research areas in biomedical sciences. This interdisciplinary technology is a combination both of traditional medical technology and nanotechnology with the particular exploitation of the ENMs.

Bioinorganic nanohybrids have been of great interest due to their role both as reservoirs and delivery carriers of functional biomolecules, which is useful for safe, targeted, and controlled delivery systems. Numerous types of inorganic nanoparticles are of potential interest in this context, including metal nanoparticles, metal oxides and quantum dots, iron oxides and other magnetic nanoparticles, mesoporous silica, carbon-based nanomaterials, and nanoclays. Layered materials, such as some clay minerals, have been subjected to intense research not only due to their eco-friendly, biodegradable, and biocompatible aspects but also due to the role that these materials play in the development of drug delivery carriers in pharmaceutical formulations, contributing to the effect of the drug activity by increasing or decreasing the bioavailability of drug after administration (Ryu et al. 2010; Wang and Zhang 2012; Djebbi et al. 2016a, 2016b).

Montmorillonite (MMT) $[(Na,Ca)_{0.33}\ (Al,Mg)_2(Si_4\ O_{10})(OH)_2{\cdot}nH_2O]$ is a layered clay mineral composed of two silica tetrahedral sheets and one central octahedral sheet of aluminum, bonded to oxygen atoms common to the two sheet surfaces. MMT is well-known for its large cation exchange capacity. Similarly to MMT, layered double hydroxides (LDHs) are known as anionic clays due to their structure, which is based on cationic brucite-like layers and exchangeable interlayer anions, represented by the general formula: $[M^{2+}{}_{1-x}M_x{}^{3+}(OH)_2]^{x+}\ (A^{n-})_{x/n}{\cdot}yH_2O$, where M^{2+} are bivalent cations, M^{3+} are trivalent cations, A^{n-} is a charge-balancing anion, and x is the molar ratio $(M^{3+}/(M^{3+}+M^{2+}))$ ranging from 0.1 to 0.5. Due to anion-exchangeable properties, LDHs can form bioinorganic hybrids with various anionic drugs (Ryu et al. 2010). Additionally, MMT and LDH have been explored to achieve a good combination between antimicrobial biomolecules and inorganic moieties such as vermiculite, palygorskite, kaolin, bentonite, and zeolite (Rytwo et al. 2011).

The mechanisms involved in the clay-antimicrobial agent interaction include strong and weak molecular bonding, predominantly hydrogen bonding, dipole-dipole interaction, ion dipole interaction, covalent bonding, ion pairing, ion-π interaction, and ion exchange mechanism (Jayrajsinh et al. 2017). Cohen et al.

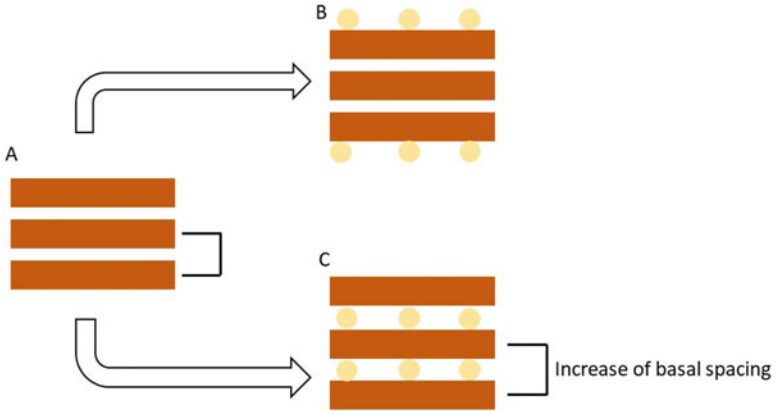

Fig. 10.2 Interactions between antimicrobial agents and layered nanomaterials. (**a**) Layered material (**b**) adsorption of the antimicrobial agent on the external layered nanomaterial surface; (**c**) intercalation of the antimicrobial agent molecules within the nanomaterial interlayer region with increase of the basal spacing

(2005) found that cation exchange and secondary organophilic adsorption are the main mechanisms in the berberine (a powerful antimicrobial compound) adsorption on MMT, while the mechanism for intercalation of antibiotics in LDHs occurs via topotactic mechanism, and the interaction between the layers and the antimicrobial agent is mainly through electrostatic interaction (Wang and Zhang 2012) (Fig. 10.2).

According to Häffner et al. (2017), the mechanism related to the microorganism membrane-antimicrobial agent-loaded LDH interaction depends mainly on particle size. With decreasing LDH crystal size, membrane binding and anionic lipid extraction is accentuated, making small LDH nanoparticles more effective for cell membrane disruption than larger ones, translating into size-dependent synergistic effects with the antimicrobial agent. Other authors have found that the larger the amount of antimicrobial agent, the size, and z-potential of the loaded nanoparticles, the higher the antimicrobial activity (Wu et al. 2011).

Antimicrobial biohybrids (inorganic layered material + antimicrobial agent) have been applied in diverse fields. The self-controlled release property of LDHs based upon antifoulant intercalated into LDH matrices creates new opportunities for the preparation and application in the field of long-acting antifouling coatings (Sun et al. 2016). The well-known ion exchange property was used for immobilization of the active agent on the inorganic matrix of Zn-Al and Mg-Al-LDHs. Both antibiotic anions (benzoate, succinate, benzylpenicillin, and ticarcillin) and paeonolsilate presented successfully antifouling activity against *Micrococcus lysodeikticus* and *Micrococcus* and *Ulva* spores. Kinetic studies showed that the temperature control is essential to guarantee the release of the antimicrobial agent and thus the antifouling activity (Wang and Zhang 2012; Sun et al. 2016; Yang et al. 2017).

Other important application of biohybrids is as a drug carrier. For layered materials, the intercalation of the antimicrobial agent is the main purpose because

it offers protection against adverse external conditions and may provide the release at specific target sites. However, the activity of the antimicrobial agent must be preserved after the intercalation process. Numerous studies have been focused on strategies able to preserve the activity of the antimicrobial agent and guarantee the intercalation effect. Thermal treatment of montmorillonite revealed that the largest amount of intercalated gentamicin, an antimicrobial agent, is achieved at 50 °C and presented the highest inhibitory effect against *E. coli* (Rapacz-Kmita et al. 2017). The pH effect was also evaluated in relation to the adsorption of tetracycline (TC) and minocycline (MC) in montmorillonite, which was high under acidic conditions and decreased with the increasing pH. The inhibitory effect shown by MC and TC was slightly reduced after intercalation, but the TC-MMT and MC-MMT yet inhibited *E. coli* growth (Parolo et al. 2010).

Effective intercalation of the antimicrobial agents ampicillin and nalidixic acid in Mg-Al-LDH was achieved by the ion exchange method. The nanohybrids were effective in the releasing of the antimicrobial agents at appropriated medium, making these nanohybrids very promising antimicrobial ENMs (Trikeriotis and Ghanotakis 2007). Cefazolin, a cephalosporin antibacterial class agent, was intercalated in Zn-Al-LDH by ion exchange and stabilized by electrostatic interaction. The activity against *S. aureus* increased when the cefazolin was combined with the Mg-Al-LDH with respect to the cefazolin pure. Comparable results were achieved when berberine was adsorbed in Mg-Al-LDH, with high destructive effect against *S. aureus*, *Pseudomonas aeruginosa*, and *Bacillus subtilis* (Ryu et al. 2010; Djebbi et al. 2016b).

Other possible manner for obtaining LDH-based antimicrobial biohybrids is through the so-called coprecipitation route. Zn-Al-LDH intercalated with berberine was able to cause high cytotoxicity and inhibitory effects on *S. aureus*, *Pseudomonas aeruginosa*, and *Bacillus subtilis* (Djebbi et al. 2016a). Mg-Al-LDH intercalated with cinnamic acid was also obtained by coprecipitation to be used against *Phytophthora capsici*, a fungus responsible for important crop diseases. The Mg-Al-LDH-cinnamic acid biohybrid was able to inhibit the growth of the fungus and contributed to green protection of crops and agricultural products (Park et al. 2010).

Silver is a well-known broad-spectrum antimicrobial agent, which encourages its application in different fields, as water and air purification, food production, cosmetics, clothing, and numerous household products. Silver may be available at different nanostructured forms such as stabilized silver salts, silver-dendrimer, polymer and metal oxide composites, silver-impregnated zeolites, and activated carbon materials (Bugatti et al. 2011).

Das et al. (2011) synthetized an AgNP/graphene (GrO) hybrid nanomaterial. The GrO induced a binding capability that usually lacks in AgNPs and enhanced the antimicrobial activity of the nanomaterial, which was effective against *E. coli* and *Pseudomonas aeruginosa*. Ag-[Mg-Al]-LDH coatings exhibit excellent and durable antimicrobial activities against both gram-negative (*E. coli* and *P. Aeruginosa*) and gram-positive (*B. Subtilis* and *S. Aureus*) bacteria (Chen et al. 2012). The combination of silver with MMT was also evaluated and exhibited a combination of accelerated and diffusion-controlled antimicrobial activity, with long-term impact, where MMT provided a physically stable surface for nucleation of the AgNPs and

Table 10.3 Recent achievements on nanolayered antimicrobial ENMs

Antimicrobial agent	Layered ENM	Target microorganism	Application	References
Silver	Graphene oxide	*Escherichia coli*; *Pseudomonas aeruginosa*	Antimicrobial applications	Das et al. (2011)
Silver	MMT	*E. coli*	Antimicrobial applications	Girase et al. (2011)
Silver	LDH	*E. coli*; *P. aeruginosa*; *B. subtilis*; *S. aureus*	Antimicrobial applications	Chen et al. (2012)
Gramicidin; amphotericin B; ampicillin; nalidixic acid	LDH	–	Controlled release systems	Trikeriotis and Ghanotakis (2007)
Cinnamic acid	LDH	*Phytophthora capsici*	Green pesticide	Park et al. (2010)
Tetracycline	MMT	*Helicobacter pylori*	System to act against gastroretentive infection	Iannuccelli et al. (2015)
Tetracycline	MMT	*E. coli*	Formulation of topical products	Parolo et al. (2010)
Sodium paeonolsilate	LDH	*Ulva* sp.	Antifouling coatings	Yang et al. (2017)
Tetradecyl tributyl phosphonium bromide	MMT Vermiculite (VER) and palygorskite Kaolin	*E. coli*; *Staphylococci aureus*	Controlled release systems	Wu et al. (2011)
Sodium paeonolsilate	LDH	*Ulva* sp.	Antifouling agent	Sun et al. (2016)
Cephalosporin	LDH	*S. aureus*	Controlled release systems	Ryu et al. (2010)
Silver+TiO_2	MMT	*E. coli*	decontamination	Wu et al. (2010)
Berberine	LDH	*S. aureus*; *P. aeruginosa*; *B. subtilis*	Controlled release systems	Djebbi et al. (2016b)
Gentamicin	LDH	–	Controlled release systems	Carja et al. (2007)
Berberine	LDH	*S. aureus*; *P. aeruginosa*; *B. subtilis*	Controlled release systems	Djebbi et al. (2016a)
Benzoate; succinate; benzylpenicillin; ticarcillin	LDH	*Micrococcus lysodeikticus*	Antifouling agent	Wang and Zhang (2012)

effectiveness activity against *E. coli*. (Girase et al. 2011). Table 10.3 summarizes the main achievements in the field of nanolayered materials and antimicrobial agents.

Therefore, lamellar systems are effective inorganic matrices for antimicrobial agent protection against chemical and environmental degradation. They are eco-friendly and biocompatible and may be used in several applications once they are efficient delivery systems.

10.5 Antimicrobial Polymer Nanocomposites

The combination of antimicrobial compounds and nanoclays is a suitable approach to control and avoid microorganism contamination. However, other combinations, especially those between nanocomposites and polymers, also allow the exploitation of antimicrobial structures for application in many other areas. The use of bionanocomposites is expected to minimize environmental problems accompanying conventional antimicrobial agents by reducing their residual toxicity, increasing their efficiency and selectivity, and prolonging their lifetime. Furthermore, physical polymer properties may be enhanced by the addition of nanoparticles. For example, the addition of carvacrol-loaded MMT to methyl cellulose polymer films increased the thickness and opacity; however the presence of carvacrol, an antimicrobial agent, decreased these parameters. Additionally, the MMT concentration also controlled the amount of carvacrol released from the nanocomposite films. The antimicrobial nanocomposites were effective against *E. coli* and *S. aureus* (Tunç and Duman 2011). Thus, several bio-nanostructures can be useful to provide active and/or smart properties for polymers applicable in the food packaging sector (Fig. 10.3).

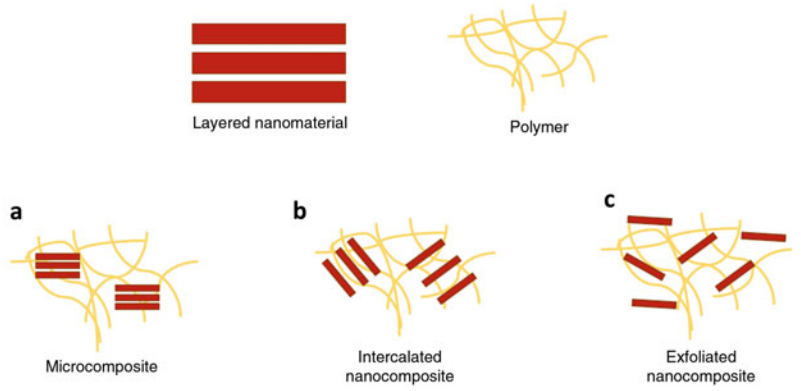

Fig. 10.3 Schematic diagram illustrating the possible interactions between polymers and layered nanomaterials. (**a**) Microcomposite: the polymer is unable to be intercalated within the layered nanomaterial. (**b**) Intercalated structure: the polymer is intercalated within the layers of the nanomaterials without delamination. (**c**) Delaminated structure: all the layers are completely dispersed within the polymer matrix

Chitosan is a bacteriostatic and fungistatic biopolymer, which is an adequate property for food preservation. MMT has been added to chitosan films as a nanofiller for enhanced mechanical properties and water vapor permeability. The presence of plasticizer, such as glycerol, improved the chitosan intercalation within the MMT galleries and enhanced the physical properties of the chitosan bionanocomposites. Moreover, the chitosan-MMT bionanocomposites were effective in the inhibition of *Listeria monocytogenes* and *S. aureus* (Lavorgna et al. 2010; Rhim et al. 2006).

Starch is a biodegradable and biocompatible polymer, which presents poor mechanical properties and high water affinity. The inclusion of Na-MMT did not impart antimicrobial activity to starch films; however properties including tensile strength and gas barrier were improved. The addition of AgNPs and potassium sorbate in the Na-MMT/starch nanocomposites at proper concentrations presented antimicrobial activity against *S. aureus*, *E. coli*, *Candida albicans*, and *Aspergillus niger*, respectively. The addition of MMT to the starch film delayed the release rate of the antimicrobial agents and enabled the film to retain its antimicrobial properties suitably over storage (Barzegar et al. 2014; Abreu et al. 2015; Heydari et al. 2013). All nanocomposites cited above are suitable for food packaging applications.

Wound healing has evolved from the ancient times, and it is still necessary to restore the integrity of the tissues. An ideal wound dressing should allow gaseous exchange while acting as a barrier against microorganisms. Wound dressing materials should be nontoxic, nonallergenic, nonadherent, and easily removed without trauma. A material that requires minimal processing and possesses antimicrobial properties is also required (Jayakumar et al. 2011).

Polycaprolactone (PCL) is a biodegradable and easy processable polymer enabling the production of tissue ingrowth with appropriate pore size and the controlled delivery of drugs contained within their matrix (Woodruff and Hutmacher 2010). Nanohybrids based on ZnAl-LDH intercalated with antimicrobially active benzoate derivatives, 2,4-dichlorobenzoate (BzDC), p-hydroxybenzoate, and o-hydroxybenzoate, were dispersed in PCL. Exfoliated and microcomposite structures were obtained depending on the kind of interaction between the antimicrobial-ZnAl-LDH and the PCL matrix. The release of the antimicrobial agents occurred over a long time interval, and the amount released depended on the antimicrobial anion/LDH layer interaction extent, the dispersion degree, and amount of LDH in the nanocomposite. Also, the antimicrobial/LDH/PCL nanocomposites were able to inhibit the *Saccharomyces cerevisiae* growth by 40% in comparison with the medium without antimicrobial agent (Bugatti et al. 2011; Costantino et al. 2009).

The use of biohybrids based on Zn-Al-LDH and benzoate derivatives was also evaluated in pectin films. The mechanical, thermal, and barrier properties of the pectin film were improved for all antimicrobial-intercalated Zn-Al-LDHs; however, the enhancement extent depended on the LDH interaction with the pectin matrix. After exposure of the antimicrobial-intercalated Zn-Al-LDHs/pectin films to air for 12 months, there was no contamination; therefore, these bionanocomposites may be suitable for wound dressing applications (Gorrasi et al. 2012).

Antibiotics such as tetracycline, doxorubicin, 5-fluorouracil, vancomycin, and sodium fusidate were intercalated in Mg-Al-LDH by the ion exchange process. The

obtained nanohybrids were dispersed in poly(lactide-co-glycolic acid) (PLGA) films. The films reduced the burst antibiotic release phase and released effective amounts of antibiotics continuously over weeks. Additionally, the antibiotic-Mg-Al-LDH/PLGA bionanocomposites films inhibited the *S. epidermidis* growth. These films could be applied at sites that require long-term antibiotic exposure as required for wound dressing, due to the ability to maintain the release of the antibiotic in a non-degraded state over long time period (Chakraborti et al. 2012).

AgNPs were also used in combination with polymer and layered materials for different applications. Kanmani and Rhim (2014) combined gelatin, MMT, and AgNPs to obtain nanocomposite films with minor elongation at break and strong antibacterial activity against foodborne pathogens for food packaging usages. Similar antimicrobial behavior was obtained when chitosan was used as the polymer matrix, where the nanocomposite (chitosan + silver) was more effective as a biocidal ENM than other pure nanoparticles. Interestingly, the mechanical properties and water vapor barrier were increased for all nanocomposites (Trikeriotis and Ghanotakis 2007). Incoronato et al. (2010) found that the silver antimicrobial activity may be inhibited by association with polymers. The nanohybrid formed by MMT and silver (Ag-MMT) was embedded in agar, zein, and PCL. The Ag-MMT nanoparticles embedded in agar exhibited antimicrobial activity against selected spoilage microorganisms, but no antimicrobial effects were recorded for zein and PCL. Other nanocomposite and application developments are summarized in Table 10.4.

Bionanocomposites appear to have a very bright future as biofunctional materials for a wide range of applications.

10.6 Recent Patenting Trends in Antimicrobial ENMs

There has also been intense development of antimicrobial processes and products based on nanotechnology, as attested by the increasing number of patents filled worldwide. A search on the European Patent Office website (Espacenet) using the keywords “nano” and “antimicrobial” retrieves 952 filled documents in the worldwide database. Table 10.5 lists the principal countries responsible for the filled patents. China is so far the leading country on antimicrobial nanotechnologies, followed by South Korea, the United States, and Japan. Among the total of 952 patents, 482 relate to silver, while chitosan, antibiotics in general, essential oils, and other antimicrobial substances relate to the remaining documents.

Currently, antimicrobial ENMs are present in various everyday products including filters, clothes, wound dressings, kitchen tools, personal care products, etc. The Nanodatabase (http://nanodb.dk/), which is an inventory of products created from nanotechnology that are available at the European market, records currently 3037 products of which 51 and 129 are related to the antimicrobial and antibacterial functions, respectively. However, 539 products relate to silver, which suggests that silver-based ENMs have been used in a broader context.

Table 10.4 Recent achievements in antimicrobial polymer nanocomposites

Antimicrobial agent	Layered structure	Polymer	Target microorganism	Application field	References
Silver	MMT	Agar, zein; PCL	*Pseudomonas* spp.	Active packaging	Incoronato et al. (2010)
Tetracycline; doxorubicin; 5-fluorouracil; vancomycin; sodium fusidate; antisense oligonucleotides	LDH	PLGA	*S. epidermidis*	Medical field	Chakraborti et al. (2012)
κ-Carrageenan; locust bean gum	MMT	κ-Carrageenan, locust bean gum	*L. monocytogenes*	Active packaging	Martins et al. (2013)
Potassium sorbate	MMT	Starch	*A. niger*	Active packaging	Barzegar et al. (2014)
MMT and starch	MMT	Starch	*E. coli*; *S. aureus*	Active packaging	Heydari et al. (2013)
Benzoate; 2,4- dichlorobenzoate, p-hydroxybenzoate; o-hydroxybenzoate	LDH	Pectin	*Room microorganisms*	Active packaging	Gorrasi et al. (2012)
Ciprofloxacin	MMT	Gelatin	*Biocompatibility with cells*	Wound dressing	Kevadiya et al. (2014)
Silver	MMT	Gelatin	*E. coli*; *L. monocytogenes*	Active packaging	Kanmani and Rhim (2014)
Silver; quaternary ammonium salt	MTT	Starch	*S. aureus*; *E. coli*; *C. albicans*	Active packaging	Abreu et al. (2015)
Benzoate; 2,4- dichlorobenzoate, p-hydroxybenzoate; o-hydroxybenzoate	LDH	PCL	*S. cerevisiae*	Active packaging	Costantino et al. (2009)
Carvacrol	MMT	Methyl cellulose	*E. coli*; *S. aureus*	Active packaging	Tunç and Duman (2011)

Table 10.5 Leading countries in antimicrobial nanotechnology patent filling

Country	Number of filled patents[a]
China	621
Republic of Korea	142
United States	46
Japan	19
Germany	9
Spain	9
Canada	6
United Kingdom	5
Others	95

[a]Search conducted using the keywords "nano" and "antimicrobial" in both title and abstract of documents

Table 10.6 Number of products containing nanosilver registered in the Nanodatabase (http://nanodb.dk/) per category of application

Category	Number of products
Health and fitness	402
Food and beverages	46
Home and garden	53
Appliances	19
Goods for children	18
Electronic and computers	4
Automotive	4

Table 10.7 Number of products containing nanosilver registered at the Nanodatabase (http://nanodb.dk/) per country of origin

Country	Number of products
United States	234
Germany	40
Poland	25
Republic of Korea	20
Belgium	15
Canada	14
Australia	11
France	8

Table 10.6 lists the silver-based products registered on the Nanodatabase per category of application. Products intended for health and fitness usages have been the main uses of nanosilver possibly due to its antimicrobial activity.

Table 10.7 lists the silver-based products registered at the Nanodatabase per country of origin. Differently from the patenting trend shown in Table 10.5, the United States is the leading country in enabling silver-based nanotechnological products to the European commercial market.

Overall, the technological potential of antimicrobial ENMs to improve the microbial safety of different consumer goods is clear, as there are a huge market and consumers favorable to absorb such products. In specific, there is plenty of room for the development and innovation of antimicrobial ENMs containing antimicrobial

substances other than nanosilver. The worldwide concern about the nanotoxicological effects of antimicrobial ENMs on the human health and the environment may drive further developments toward effective antimicrobial nanomaterials based on safe, nontoxic substances such as plant essential oils, antimicrobial biopolymers, etc.

10.7 Conclusion

The antimicrobial ENMs described in this chapter denote that nanotechnology is now fully applied for the development of nanosystems with remarkable antimicrobial activity. Recent scientific achievements demonstrate the enhancement of antibacterial activity when classical antimicrobial agents are combined with nanostructures. Improved antibacterial effects are now confirmed to imply in reduced amounts of antimicrobial agents which is further positive for medical, food, environmental, cosmetics, and agricultural applications. Besides, the combination of antimicrobials in general with different nanolayer materials provides a great and efficient route for the delivery of antimicrobial agents to specific targets with the use of antifouling agents and controlled/slow release of the antimicrobial compound. The use of polymers extends the applications of antimicrobial ENMs to a new, broader range. Therefore, antimicrobial ENMs improve the polymer properties and provide the polymer with an antimicrobial character, which is very helpful for preventing the proliferation of pathogenic microorganisms as well as extending product shelf life. Effective antimicrobial wound dressing technologies with minor side effects have also been developed. It is of paramount importance to conduct toxicological analyses on all new antimicrobial ENMs in a postconsumer scenario in order to guarantee minimal impact to environment and life.

Acknowledgments Authors thank Embrapa, DEMa/UFSCar, FAPESP, CNPq, FAPESP (Proc. No. 2015/00094-0; Proc. No. 2017/22017-3), MCTI/SISNANO, and REDEAGRONANO for the financial support.

References

Aani SA, Gomez V, Wright CJ, Hilal N (2017) Fabrication of antibacterial mixed matrix nanocomposite membranes using hybrid nanostructure of silver coated multi-walled carbon nanotubes. Chem Eng J 326:721–736. https://doi.org/10.1016/j.cej.2017.06.029

Abreu AS, Oliveira M, Rodrigues De SA, Cerqueira MA, Vicente AA, Machado AV (2015) Antimicrobial nanostructured starch based films for packaging. Carbohydr Polym 129:127–134. https://doi.org/10.1016/j.carbpol.2015.04.021

Aider M (2010) Chitosan application for active bio-based films production and potential in the food industry. Review LWT Food Sci Technol 43(6):837–842. https://doi.org/10.1016/j.lwt.2010.01.021

Alsaleh NB, Brown JM (2018) Immune responses to engineered nanomaterials: current understanding and challenges. Curr Opin Toxicol 10:8–14. https://doi.org/10.1016/j.cotox.2017.11.011

Alzate P, Zalduendo PM, Gerschenson L, Flores SK (2016) Micro and nanoparticles of native and modified cassava starches as carriers of the antimicrobial potassium sorbate. Starch/Stärke 68:1038–1047. https://doi.org/10.1002/star.2016000981038

Ameeduzzafar, Imam SS, Bukhari SNA, Ahmad J, Ali A (2018) Formulation and optimization of levofloxacin loaded chitosan nanoparticle for ocular delivery: in-vitro characterization, ocular tolerance and antibacterial activity. Int J Biol Macromol 108:650–659. https://doi.org/10.1016/j.ijbiomac.2017.11.170

Arora D, Sharma N, Sharma V, Abrol V, Shankar R, Jaglan S (2016) An update on polysaccharide-based nanomaterials for antimicrobial applications. Appl Microbiol Biotechnol 100:2603–2615. https://doi.org/10.1007/s00253-016-7315-0

Balagna C, Irfan M, Perero S, Miola M, Maina G, Santella D, Simone A (2017) Characterization of antibacterial silver nanocluster/silica composite coating on high performance Kevlar® textile. Surf Coat Technol 321:438–447. https://doi.org/10.1016/j.surfcoat.2017.05.009

Barzegar H, Azizi MH, Barzegar M, Hamidi-Esfahani Z (2014) Effect of potassium sorbate on antimicrobial and physical properties of starch-clay nanocomposite films. Carbohydr Polym 110:26–31. https://doi.org/10.1016/j.carbpol.2014.03.092

Bilal M, Rasheed T, Muhammad H, Iqbal N, Hu H, Zhang X (2017) Silver nanoparticles: biosynthesis and antimicrobial potentialities. Int J Antimicrob Agents 49:137–152. https://doi.org/10.3923/ijp.2017.832.845

Bugatti V, Gorrasi G, Montanari F, Nocchetti M, Tammaro L, Vittoria V (2011) Modified layered double hydroxides in polycaprolactone as a tunable delivery system: In vitro release of antimicrobial benzoate derivatives. Appl Clay Sci 52:1–2. https://doi.org/10.1016/j.clay.2011.01.025

Carja G, Niiyama H, Ciobanu G, Aida T (2007) Towards new drugs formulations: Gentamicin-anionic clay as nanohybrids. Mater Sci Eng C 27:1129–1132. https://doi.org/10.1016/j.msec.2006.07.017

Chakraborti M, Jackson JK, Plackett D, Gilchrist SE, Burt HM (2012) The application of layered double hydroxide clay (LDH)-poly(lactide-co- glycolic acid) (PLGA) film composites for the controlled release of antibiotics. J Mater Sci Mater Med 23(7):1705–1713. https://doi.org/10.1007/s10856-012-4638-y

Chen C, Gunawan P, Lou XW, Xu R (2012) Silver nanoparticles deposited layered double hydroxide nanoporous coatings with excellent antimicrobial activities. Adv Funct Mater 22 (4):780–787. https://doi.org/10.1002/adfm.201102333

Chernousova S, Epple M (2013) Silver as antibacterial agent: ion, nanoparticle, and metal. Angew Chem Int Ed 52:1636–1653. https://doi.org/10.1002/anie.201205923

Cohen E, Joseph T, Lapides I, Yariv S (2005) The adsorption of berberine by montmorillonite and thermo-XRD analysis of the organo-clay complex. Clay Miner 40(2):223–232. https://doi.org/10.1180/0009855054020168

Costa JR, Silva NC, Sarmento B, Pintado M (2015) Potential chitosan-coated alginate nanoparticles for ocular delivery of daptomycin. Eur J Clin Microbiol Infect Dis 34(6):1255–1262. https://doi.org/10.1007/s10096-015-2344-7

Costantino U, Bugatti V, Gorrasi G, Montanari F, Nocchetti M, Tammaro L, Vittoria V (2009) New polymeric composites based on poly(ε-caprolactone) and layered double hydroxides containing antimicrobial species. ACS Appl Mater Interfaces 1(3):668–677. https://doi.org/10.1021/am8001988

Da Rosa CG, Maciel MVOB, de Carvalho SB, de Melo APZ, Jummes B, da Silva T, Martelli SM, Villetti MA, Bertoldi FC, Barreto PLM (2015) Characterization and evaluation of physicochemical and antimicrobial properties of zein nanoparticles loaded with phenolics monoterpenes. Colloids Surf A Physicochem Eng Asp 481:337–344. https://doi.org/10.1016/j.colsurfa.2015.05.019

Das MR, Sarma RK, Saikia R, Kale VS, Shelke MV, Sengupta P (2011) Synthesis of silver nanoparticles in an aqueous suspension of graphene oxide sheets and its antimicrobial activity. Colloids Surf B Biointerfaces 83(1):16–22. https://doi.org/10.1016/j.colsurfb.2010.10.033

De Marchi JGB, Jornada DS, Silva FK, Freitas AL, Fuentefria AM, Pohlmann AR, Guterres SS (2017) Triclosan resistance reversion by encapsulation in chitosan-coated-nanocapsule containing α-bisabolol as core: development of wound dressing. Int J Nanomedicine 12:7855–7868. https://doi.org/10.2147/IJN.S143324

Djebbi MA, Elabed A, Bouaziz Z, Sadiki M, Elabed S, Namour P, Jaffrezic-Renault N, Amara ABH (2016a) Delivery system for berberine chloride based on the nanocarrier ZnAl-layered double hydroxide: physicochemical characterization, release behavior and evaluation of antibacterial potential. Int J Pharm 515:1–2. https://doi.org/10.1016/j.ijpharm.2016.09.089

Djebbi MA, Bouaziz Z, Elabed A, Sadiki M, Elabed S, Namour P, Jaffrezic-Renault N, Amara ABH (2016b) Preparation and optimization of a drug delivery system based on berberine chloride-immobilized MgAl hydrotalcite. Int J Pharm 506:1–2. https://doi.org/10.1016/j.ijpharm.2016.04.048

Durán N, Durán M, de Jesus MB, Seabra AB, Fávaro WJ, Nakazato G (2016) Silver nanoparticles: a new view on mechanistic aspects on antimicrobial activity. Nanomedicine 12(3):789–799. https://doi.org/10.1016/j.nano.2015.11.016

Etewa SE, El-Maaty DAA, Hamza RS, Metwaly AS, Sarhan MH, Abdel-Rahman SA, Fathy GM, El-Shafey MA (2018) Assessment of spiramycin-loaded chitosan nanoparticles treatment on acute and chronic toxoplasmosis in mice. J Parasit Dis 42(1):102–113. https://doi.org/10.1007/s12639-017-0973-8

European Commission (2015) Definition – nanomaterials – environment – European Commission. online. European Commission available at: http://ec.europa.eu/environment/chemicals/nanotech/faq/definition_en.htm

Girase B, Depan D, Shah JS, Xu W, Misra RDK (2011) Silver-clay nanohybrid structure for effective and diffusion-controlled antimicrobial activity. Mater Sci Eng C 31(8):1759–1766. https://doi.org/10.1016/j.msec.2011.08.007

Gorrasi G, Bugatti V, Vittoria V (2012) Pectins filled with LDH-antimicrobial molecules: preparation, characterization and physical properties. Carbohydr Polym 89(1):132–137. https://doi.org/10.1016/j.carbpol.2012.02.061

Häffner SM, Nyström L, Nordström R, Xu ZP, Davoudi M, Schmidtchen S, Malmsten M (2017) Membrane interactions and antimicrobial effects of layered double hydroxide nanoparticles. Phys Chem Chem Phys 19(35):23832–23842. https://doi.org/10.1039/C7CP02701J

Hajipour ML, Fromm KM, Ashkarran AA, de Aberasturi DJ, de Larramendi IR, Rojo T, Serpoonshan V, Parak W, Mahmoundi M (2012) Antibacterial properties of nanoparticles. Trends Biotechnol 30(10). https://doi.org/10.1016/j.tibtech.2012.06.004

Heydari A, Alemzadeh I, Vossoughi M (2013) Functional properties of biodegradable corn starch nanocomposites for food packaging applications. Mater Des 50:954–961. https://doi.org/10.1016/j.matdes.2013.03.084

Hoseinzadeh E, Makhdoumi P, Taha P, Hossini H, Stelling J, Kamal MA, Ashraf GM (2017) A review on nano-antimicrobials: metal nanoparticles, methods and mechanisms. Curr Drug Metab 18(2):120–128. https://doi.org/10.2174/1389200217666161201111146

Iannuccelli V, Maretti E, Montorsi M, Rustichelli C, Sacchetti F, Leo E (2015) Gastroretentive montmorillonite-tetracycline nanoclay for the treatment of Helicobacter pylori infection. Int J Pharm 493:1–2. https://doi.org/10.1016/j.ijpharm.2015.06.049

Incoronato AL, Buonocore GG, Conte A, Lavorgna M, Del Nobile MA (2010) Active systems based on silver-montmorillonite nanoparticles embedded into bio-based polymer matrices for packaging applications. J Food Prot 73(12):2256. https://doi.org/10.4315/0362-028X-73.12.2256

Ismail NS, Gopinath SCB (2017) Enhanced antibacterial effect by antibiotic loaded starch nanoparticle. J Assoc Arab Uni Basic Appl Sci 24:136–140. https://doi.org/10.1016/j.jaubas.2016.10.005

Jayakumar R, Prabaharan M, Sudheesh Kumar PT, Nair SV, Tamura H (2011) Biomaterials based on chitin and chitosan in wound dressing applications. Biotechnol Adv 29(3):322–337. https://doi.org/10.1016/j.biotechadv.2011.01.005

Jayrajsinh S, Shankar G, Agrawal YK, Bakre L (2017) Montmorillonite nanoclay as a multifaceted drug-delivery carrier: a review. J Drug Deliv Sci Technol 39:200–209. https://doi.org/10.1016/j.jddst.2017.03.023

Jung J, Kasi G, Seo J (2018) Development of functional antimicrobial papers using chitosan/starch-silver nanoparticles. Int J Biol Macromol 112:530–553. https://doi.org/10.1016/j.ijbiomac.2018.01.155

Kanmani P, Rhim JW (2014) Physical, mechanical and antimicrobial properties of gelatin based active nanocomposite films containing AgNPs and nanoclay. Food Hydrocoll 35:644–652. https://doi.org/10.1016/j.foodhyd.2013.08.011

Kevadiya BD, Rajkumar S, Bajaj HC, Chettiar SS, Gosai K, Brahmbhatt H, Bhatt AS, Barvaliya YK, Dave GS, Kothari RK (2014) Biodegradable gelatin-ciprofloxacin-montmorillonite composite hydrogels for controlled drug release and wound dressing application. Colloids Surf B Biointerfaces 122:175–183. https://doi.org/10.1016/j.colsurfb.2014.06.051

Kim JP, Kim JH, Kim J, Lee SN, Park H (2016) A nanofilter composed of carbon nanotube-silver composites for virus removal and antibacterial activity improvement. J Environ Sci 42:275–283. https://doi.org/10.1016/j.jes.2014.11.017

Lavorgna M, Piscitelli F, Mangiacapra P, Buonocore GG (2010) Study of the combined effect of both clay and glycerol plasticizer on the properties of chitosan films. Carbohydr Polym 82(2):291–298. https://doi.org/10.1016/j.carbpol.2010.04.054

Ma Z, Garrido-Maestu A, Jeong KC (2017) Application, mode of action, and in vivo activity of chitosan and its micro and nanoparticles as antimicrobial agents: a review. Carbohydr Polym 176:257–265. https://doi.org/10.1016/j.carbpol.2017.08.08

Mahor A, Prajapati SK, Verma A, Gupta R, Iyer AK, Kesharwani P (2016) Moxifloxacin loaded gelatin nanoparticles for ocular delivery: formulation and in-vitro, in-vivo evaluation. J Colloid Interface Sci 483:132–138. https://doi.org/10.1016/j.jcis.2016.08.018

Martins JT, Bourbon AI, Pinheiro AC, Souza BWS, Cerqueira MA, Vicente AA (2013) Biocomposite films based on κ-carrageenan/locust bean gum blends and clays: physical and antimicrobial properties. Food Bioprocess Technol 6(8):2081–2092. https://doi.org/10.1007/s11947-012-0851-4

Melo NFCB, Soares BLM, Diniz KM, Leal CF, Canto D, Flores MAP, Tavares-Filho JHC, Galembeck A, Stamford TLM, Stamford-Arnaud TM, Stamford TCM (2018) Effects of fungal chitosan nanoparticles as eco-friendly edible coatings on the quality of postharvest table grapes. Postharvest Biol Technol 139:56–66. https://doi.org/10.1016/j.postharvbio.2018.01.014

Motshekga SC, Ray SS, Maity A (2018) Synthesis and characterization of alginate beads encapsulated zinc oxide nanoparticles for bacteria disinfection in water. J Colloid Interface Sci 512:686–692. https://doi.org/10.1016/j.jcis.2017.10.098

Noronha VT, Paula JÁ, Durán G, Galembeck A, Cogo-Müller K, Franz-Montan M, Durán N (2017) Silver nanoparticles in dentistry. Dent Mater 33:1110–1116. https://doi.org/10.1016/j.dental.2017.07.002

Pan K, Chen H, Davidson PM, Zhong Q (2014) Thymol nanoencapsulated by sodium caseinate: physical and antilisterial properties. J Agric Food Chem 62:1649–1657. https://doi.org/10.1021/jf4055402

Panwar K, Jassal M, Agrawal AK (2018) Readily dispersible antimicrobial Ag – SiO_2 Janus particles and their application on cellulosic fabric. Carbohydr Polym 187(2018):43–50. https://doi.org/10.1016/j.carbpol.2018.01.076

Park M, Lee CII, Seo YJ, Woo SR, Shin D, Choi J (2010) Hybridization of the natural antibiotic, cinnamic acid, with layered double hydroxides (LDH) as green pesticide. Environ Sci Pollut Res 17(1):203–209. https://doi.org/10.1007/s11356-009-0235-0

Park S, Ko Y, Jung H, Lee C, Woo K, Ko G (2018) Disinfection of waterborne viruses using silver nanoparticle-decorated silica hybrid composites in water environments. Sci Total Environ 625:477–485. https://doi.org/10.1016/j.scitotenv.2017.12.318

Parolo ME, Avena MJ, Pettinari G, Zajonkovsky I, Valles JM, Baschini MT (2010) Antimicrobial properties of tetracycline and minocycline-montmorillonites. Appl Clay Sci 49(3):194. https://doi.org/10.1016/j.clay.2010.05.005

Pender DS, Vangala LM, Badwaik VD, Willis CB, Aguilar ZP, Sangoi TN, Paripelly R, Dakshinamurt R (2013) Bactericidal activity of starch-encapsulated gold nanoparticles. Front Biosci 18:993–1002

Perinelli DR, Fagioli L, Campana R, Lam JKW, Baffone W, Palmieri GF, Casettari L, Bonacucina G (2018) Chitosan-based nanosystems and their exploited antimicrobial activity. Eur J Pharm Sci 117:8–20. https://doi.org/10.1016/j.ejps.2018.01.046

Popova M, Lazarova H, Trusheva B, Popova M, Bankova V, Mihály J, Najdenski H, Tsvetkova I, Szegedi A (2018) Nanostructured silver silica materials as potential propolis carriers. Microporous Mesoporous Mater 263:28–33. https://doi.org/10.1016/j.micromeso.2017.11.043

Praphakar RA, Munusamy MA, Alarfaj AA, Suresh Kumar S, Rajan M (2017) Zn^{2+} cross-linked sodium alginate-g-allylamine-mannose polymeric nanocarrier of rifampicin for macrophage targeting tuberculosis nanotherapy. New J Chem 41(19):11324–11334. https://doi.org/10.1039/c7nj01808h

Priebe M, Widmer J, Löwa NS, Abram S-L, Mottas I, Woischnig A-K, Brunetto PS, Khanna N, Bourquin C, Fromm KM (2017) Antimicrobial silver-filled silica nanorattles with low immunotoxicity in dendritic cells. Nanomedicine 13:11–22. https://doi.org/10.1016/j.nano.2016.08.002

Qiu C, Chang R, Yang J, Ge S, Xiong L, Zhao M, Li M, Sun Q (2017) Preparation and characterization of essential oil-loaded starch nanoparticles formed by short glucan chains. Food Chem 221:1426–1433. https://doi.org/10.1016/j.foodchem.2016.11.009

Raghunath A, Perumal E (2017) Metal oxide nanoparticles as antimicrobial agents: a promise for the future. Int J Antimicrob Agents 49:137–152. https://doi.org/10.1016/j.ijantimicag.2016.11.011

Rajendran NK, Kumar SSD, Houreld NN, Abrahamse H (2018) A review on nanoparticle based treatment for wound healing. J Drug Deliv Sci Technol 44:421–430. https://doi.org/10.1016/j.jddst.2018.01.009

Rapacz-Kmita A, Bućko MM, Stodolak-Zych E, Mikołajczyk M, Dudek P, Trybus M (2017) Characterisation, in vitro release study, and antibacterial activity of montmorillonite-gentamicin complex material. Mater Sci Eng C 70:471–478. https://doi.org/10.1016/j.msec.2016.09.031

Rhim JW, Hong SI, Park HM, Ng PKW (2006) Preparation and characterization of chitosan-based nanocomposite films with antimicrobial activity. J Agric Food Chem 54(16):5814–5822. https://doi.org/10.1021/jf060658h

Rytwo G, Varman H, Bluvshtein N, König TN, Mendelovits A, Sandler A (2011) Adsorption of berberine on commercial minerals. Appl Clay Sci 51(1–2):43–50. https://doi.org/10.1016/j.clay.2010.10.031

Ryu SJ, Jung H, Oh JM, Lee JK, Choy JH (2010) Layered double hydroxide as novel antibacterial drug delivery system. J Phys Chem Solids 71(4):685–688. https://doi.org/10.1016/j.jpcs.2009.12.066

Salam MA, Obaid AY, El-Shishtawy RM, Mohamed SA (2017) Synthesis of nanocomposites of polypyrrole/carbon nanotubes/silver nano particles and their application in water disinfection. RSC Adv 7:16878–16884. https://doi.org/10.1039/c7ra01033h

Sharma C, Dhiman R, Rokana N, Panwar H (2017) Nanotechnology: An updated resource for food packaging. Front Microbiol 8:1735. https://doi.org/10.3389/fmicb.2017.01735

Shevlin D, O'Brien N, Cummins E (2018) Silver engineered nanoparticles in freshwater systems–likely fate and behaviour through natural attenuation processes. Sci Total Environ 621:1033–1046. https://doi.org/10.1016/j.scitotenv.2017.10.123

Suganya P, Vaseeharan B, Vijayakumar S, Balan B, Govindarajan M, Alharbi NS, Kadaikunnan S, Khaled JM, Benelli G (2017) Biopolymer zein-coated gold nanoparticles: synthesis, antibacterial potential, toxicity and histopathological effects against the Zika virus vector Aedes aegypti. J Photochem Photobiol B Biol 173:404–411. https://doi.org/10.1016/j.jphotobiol.2017.06.004

Sun Z, Gu L, Zheng J, Zhang J, Wang L, Xu F, Lin C (2016) A controlled release strategy of antifouling agent in coating based on intercalated layered double hydroxides. Mater Lett 172:105–108. https://doi.org/10.1016/j.matlet.2016.02.151

Trikeriotis M, Ghanotakis DF (2007) Intercalation of hydrophilic and hydrophobic antibiotics in layered double hydroxides. Int J Pharm 332(1–2):176–184. https://doi.org/10.1016/j.ijpharm.2006.09.031

Tunç S, Duman O (2011) Preparation of active antimicrobial methyl cellulose/carvacrol/montmorillonite nanocomposite films and investigation of carvacrol release. LWT – Food Sci Technol 44(2):465–472. https://doi.org/10.1016/j.lwt.2010.08.018

Wang Y, Zhang D (2012) Synthesis, characterization, and controlled release antibacterial behavior of antibiotic intercalated Mg-Al layered double hydroxides. Mater Res Bull 47(11):3185–3194. https://doi.org/10.1016/j.materresbull.2012.08.029

Wei L, Lu J, Xu H, Patel A, Chen Z-S, Chen G (2015) Silver nanoparticles: synthesis, properties, and therapeutic applications. Drug Discov Today 20(5). https://doi.org/10.1016/j.drudis.2014.11.014

Woodruff MA, Hutmacher DW (2010) The return of a forgotten polymer – polycaprolactone in the 21st century. Prog Polym Sci 35(10):1217–1256. https://doi.org/10.1016/j.progpolymsci.2010.04.002

Wu TS, Wang KX, Li GD, Sun SY, Sun J, Chen JS (2010) Montmorillonite-supported Ag/TiO2 nanoparticles: an efficient visible-light bacteria photodegradation material. ACS Appl Mater Interfaces 2(2):544–550. https://doi.org/10.1021/am900743d

Wu T, Xie A, Tan S, Cai X (2011) Antimicrobial effects of quaternary phosphonium salt intercalated clay minerals on Escherichia coli and Staphylococci aureus. Colloids Surf B Biointerfaces 86(1):232–236. https://doi.org/10.1016/j.colsurfb.2011.04.009

Xia L, Xu M, Cheng G, Yang L, Guo Y, Li D, Fang D, Zhang Q, Liu H (2018) Facile construction of Ag nanoparticles encapsulated into carbon nanotubes with robust antibacterial activity. Carbon 130:775–781. https://doi.org/10.1016/j.carbon.2018.01.073

Yang M, Lianghua G, Bin Y, Li W, Sun Z, Zheng J, Zhang J, Hou J (2017) Antifouling composites with self-adaptive controlled release based on an active compound intercalated into layered double hydroxides. Appl Surf Sci 426:185–193. https://doi.org/10.1016/j.apsusc.2017.07.207

Youssef HF, Abdel-Aziz MS, Fouda FK (2017) Evaluation of antimicrobial activity of different silver-exchanged nano and micronized zeolites prepared by microwave technique. J Porous Mater 24(4):947–957. https://doi.org/10.1007/s10934-016-0334-5

Zimet P, Mombrú AW, Faccio R, Brugnini G, Miraballes I, Rufo C, Pardo H (2018) Optimization and characterization of nisin-loaded alginate-chitosan nanoparticles with antimicrobial activity in lean beef. LWT Food Sci Technol 91:107–116. https://doi.org/10.1016/j.lwt.2018.01.015

Chapter 11
Exploitation of Nanoparticles as Photocatalysts for Clean and Environmental Applications

Vignesh Kumaravel and Sivaraman Somasundaram

Contents

Abstract Semiconductor photocatalysis is one of the most promising tools to address energy crisis, global warming, and environmental pollution. Owing to its exceptional physicochemical properties and biocompatibility, TiO_2 nanoparticles are commonly used as photocatalysts. TiO_2 is a benchmark photocatalyst, and it can be used for dye-sensitized solar cells, water splitting to produce hydrogen, air purification, self-cleaning surfaces, disinfection of microbes, carbon dioxide conversion, NO_x removal, and degradation of various organic pollutants under UV/visible/UV-visible/solar light irradiation. This book chapter covers the basic

V. Kumaravel (✉)
Department of Environmental Science, School of Science, Institute of Technology Sligo, Sligo, Republic of Ireland
e-mail: Kumaravel.Vignesh@itsligo.ie

S. Somasundaram (✉)
Department of Chemistry, Kongju National University, Gongju, Republic of Korea
e-mail: sivaraman79@kongju.ac.kr

Mu. Naushad et al. (eds.), *Advanced Nanostructured Materials for Environmental Remediation*, Environmental Chemistry for a Sustainable World 25,
https://doi.org/10.1007/978-3-030-04477-0_11

principles, mechanism, and environmental applications of TiO_2 nanoparticles. The photo-reactor designs (lab scale and pilot scale) and operational challenges are described briefly. In addition to that, energy production of TiO_2 using photovoltaics and photoelectrochemical methods is also discussed briefly.

Keywords Nanoparticles · Photocatalysis · Energy · Environment · Solar light · Pollutants · Microorganisms · Self-cleaning

11.1 Introduction to Photocatalysts

Photocatalyst is a material that can stimulate the rate of a chemical reaction under light irradiation. A photocatalyst must be stable under light, chemically inert, economically cheap, and nontoxic. The photochemistry of nanoparticles is one of the most significant research areas in the recent decades (Henglein 1997; Zhang et al. 1998). The unique physicochemical characteristics of these nanoparticles could be the primary reason for this interest. Semiconductor nanoparticles are commonly used as photocatalysts owing to their appropriate bandgap energy. The redox potential of H_2O/•OH couple ($OH^- => •OH + e^-$; $E^0 = -2.8$ V) should exist within the bandgap energy of the semiconductor (Hoffmann et al. 1995). Titanium dioxide (TiO_2), graphite-like carbon nitride (g-C_3N_4), and cadmium sulfide (CdS) are the three main pillars of semiconductor photocatalysis research. TiO_2 is the most extensively used photocatalyst because of its biocompatibility, nontoxicity, bandgap energy, light absorption efficiency, and photostability (Hoffman et al. 1992; Howe 1998; Aruna and Patil 1996; Malato et al. 2009; Coronado et al. 2013; Chen and Mao 2007).

11.2 Application of TiO_2 Nanoparticles in Photocatalysis

The application of TiO_2 nanoparticles as photocatalyst was first discovered in 1956 (Kato and Mashio 1956; Fujishima and Honda 1972; Hashimoto et al. 2005). The number of research articles in TiO_2 (first-generation photocatalyst) was continuously increased during the 1990s. During the 2000s, many researchers explored visible light-active semiconductor photocatalysts (second-generation photocatalyst) especially metal-/nonmetal-doped TiO_2 (Asahi et al. 2001). Visible light-active semiconductor nanocomposites with multiple features were also explored in the recent decades (third-generation photocatalysts) (Fresno et al. 2014). The photoreduction and photooxidation mechanisms of TiO_2 nanoparticles are schematically displayed in Fig. 11.1. When TiO_2 is irradiated with light energy higher than the bandgap energy, electrons and holes are generated in the conduction band (CB) and valance band (VB) of TiO_2, respectively. The photo-generated electrons and holes further react with surface-adsorbed oxygen (O_2) and water (H_2O) to form reactive oxygen

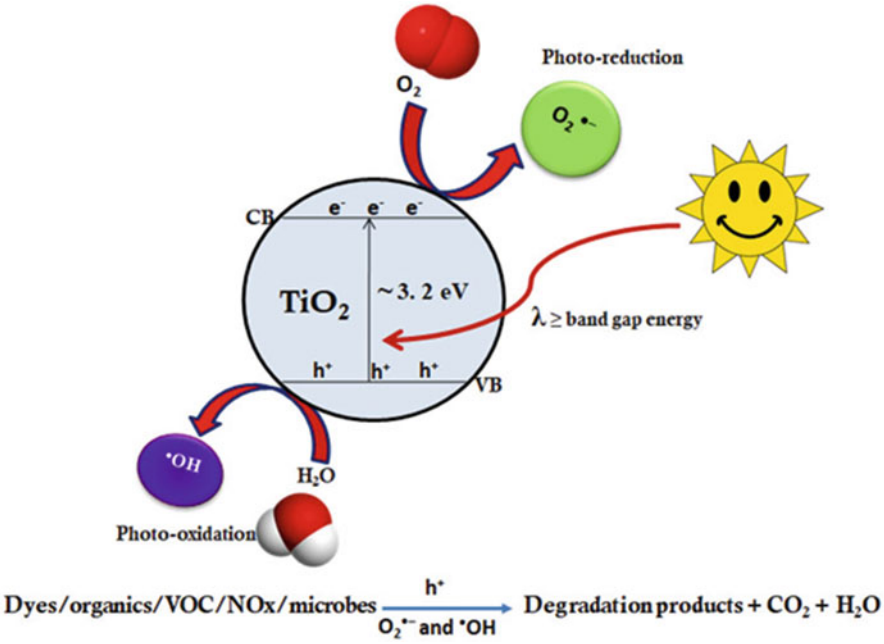

Fig. 11.1 Schematic of photoreduction and photooxidation mechanism on the TiO_2 surface for the degradation of dyes/organics/VOC/NOx/microbes under light irradiation

species (ROS). The photo-generated electrons and holes have a short lifetime, and hence they should be utilized quickly to avoid the charge-carrier recombination at the surface/bulk.

Interfacial recombination/charge transfer and trapping are the important photochemical reactions. The formation of all ROS from O_2 to H_2O during semiconductor photocatalysis is schematically shown in Fig. 11.2. ROS such as $^{\bullet}OH$, H_2O_2, $O_2^{\bullet-}$, and O_2^{1} would be produced from the stepwise photooxidation of H_2O. Likewise, $O_2^{\bullet-}$, H_2O_2, and $^{\bullet}OH$ would be created from the stepwise photoreduction of O_2. The organic pollutants/dyes/air contaminants/dirt/microbes/volatile organic carbon (VOC)/NOx/Sox are completely degraded and mineralized by the repetitive attack of ROS. The size of nanoparticles is more essential to achieve the maximum efficiency. Photocatalysis is a surface phenomenon. Consequently, the photo-induced charge-carrier recombination processes are strongly influenced by the surface area and nanoparticle size. The surface recombination is faster than the interfacial charge-carrier transfer process when the photo-generated holes and electrons are nearer to the surface.

The efforts are still in progress to enhance the reactivity, selectivity, and photocatalytic activity of TiO_2 by focusing on the features such as crystal facet engineering, phase transition, dimensions, etc. (Liu et al. 2011; Xu et al. 2013). In this fashion, the introduction of disorder on TiO_2 through hydrogenation or calcination with sodium borohydride (called as black TiO_2) was reported to shift the

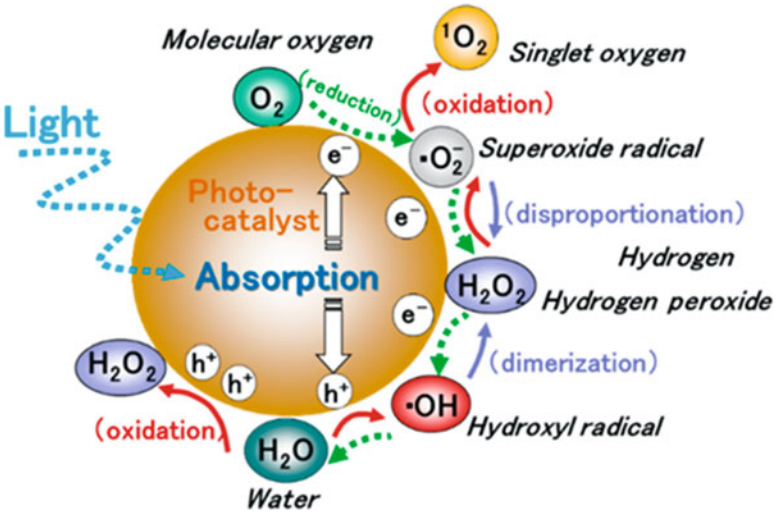

Fig. 11.2 Schematic of reactive oxygen species (ROS) generation from oxygen (O_2) and water (H_2O) during semiconductor photocatalysis. (Reprinted from Nosaka and Nosaka (2017) with permission from the American Chemical Society)

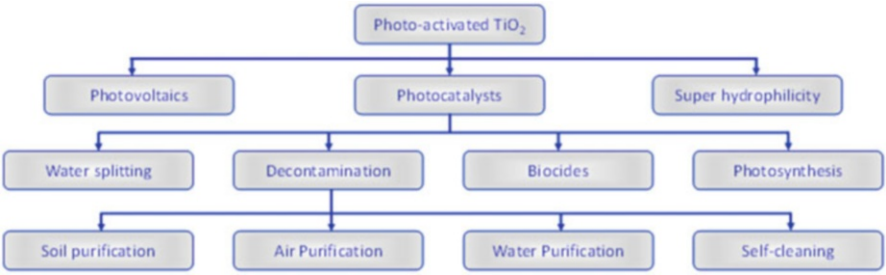

Fig. 11.3 Schematic for the applications of TiO_2 nanoparticles. (Modified from Lan et al. (2013) with permission from Elsevier)

absorption edge of TiO_2 to the visible region. The lattice disorder creates new energy levels between the VB and CB of TiO_2. The black TiO_2 nanoparticles enrich the photocatalytic activity via strong light absorption and effective electron-hole separation (Ullattil et al. 2018).

The various applications of TiO_2 nanoparticles are schematically displayed in Fig. 11.3 (Hashimoto et al. 2005; Wold 1993; Konstantinou and Albanis 2004; Carp et al. 2004; Blake et al. 1999; Fujishima et al. 2000; Grätzel 1999; Grätzel 2001; Fox and Dulay 1993; Heller 1995; Chen and Mao 2007; Kočí et al. 2008).

TiO_2 nanoparticles have been widely used in pigments, paints, papers, plastics, printing inks, toothpastes, foods, and medicines. Since from the ancient time, both rutile and anatase TiO_2 have been commercially utilized as white pigments due to their reflectance properties. Anatase is being employed as building pigments since

1916; on the other hand, rutile was introduced in 1940 as pigments to enhance the opacity and durability. TiO_2 nanoparticles are also utilized in sunscreens due to its high refractive index. In recent review literatures (Bora and Mewada 2017; Hassan et al. 2016; Nosaka and Nosaka 2017; Reddy et al. 2017; Wenderich and Mul 2016; Zhang et al. 2016), the mechanisms and photocatalytic applications have been discussed in detail. Though the TiO_2 nanoparticles are used for various applications, its energy- and environment-related applications are much important in the current scenario.

11.3 Energy-Related Applications: Sunlight to Fuels

We are continuously forced to change our fossil energy sources due to environmental and socioeconomic concerns. Governments and researchers are primarily interested to find the alternative energy sources to maintain sustainability of the ecosystem. In this circumstance, the research on renewable energy sources like solar, wind, rain, tides, and biomass have received much attention. Among them, inexhaustible solar energy is more popular due to its renewability and sustainability.

11.3.1 Photovoltaics

Under an applied electric field, the photo-induced electron and hole can be easily separated from TiO_2 nanoparticles. Based on this mechanism, different types of TiO_2 photovoltaic solar cells have been reported since 1972 (Carp et al. 2004; Grätzel 1999, 2001, 2005; O'Regan and Grätzel 1991; Baran et al. 2017; Gu et al. 2017; Kobosko et al. 2017). The schematic of Grätzel photovoltaic cell is shown in Fig. 11.4 (Grätzel 1999).

The electrons are received by the photo-anode from the photosensitized dye under light irradiation. The redox mediator species in the electrolyte are regenerated by the photoreduction of electrons circulated through an external circuit at the cathode. A solar-to-energy conversion efficiency of 10% was obtained (Grätzel 1999; Nazeeruddin et al. 1993), while it is still lower than that of conventional silicon-based photovoltaic cells (~20%).

11.3.2 Water Splitting and H_2 Production

In 1972, Fujishima and Honda (1972) discovered that TiO_2 nanoparticles can split the water into H_2 and O_2 via photoelectrochemical (PEC) approach. Since then, intensive research works have been performed (Pi et al. 2017; Peng et al. 2017; Liu et al. 2017b); in this area the mechanism of TiO_2 water splitting was reviewed in

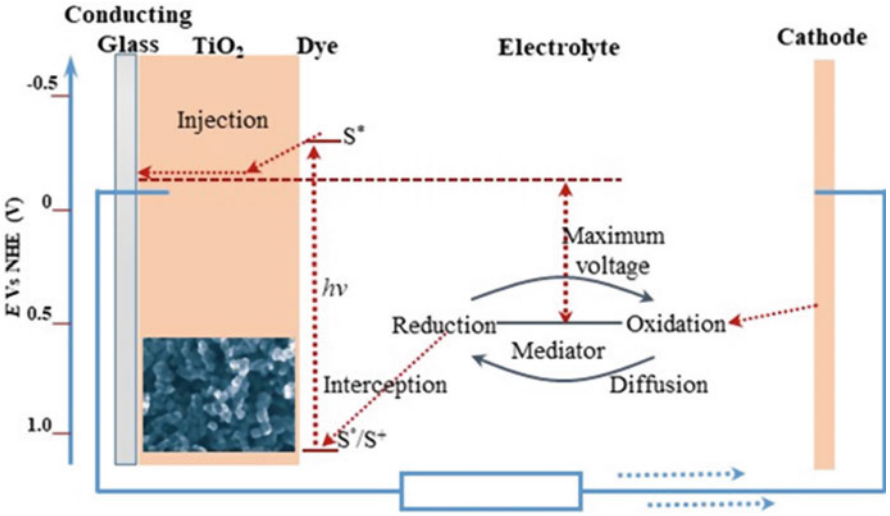

Fig. 11.4 Schematic and mechanism of dye-sensitized solar cell (Inset: SEM image of TiO_2 photoanode). (Modified from Lan et al. (2013) with permission from Elsevier)

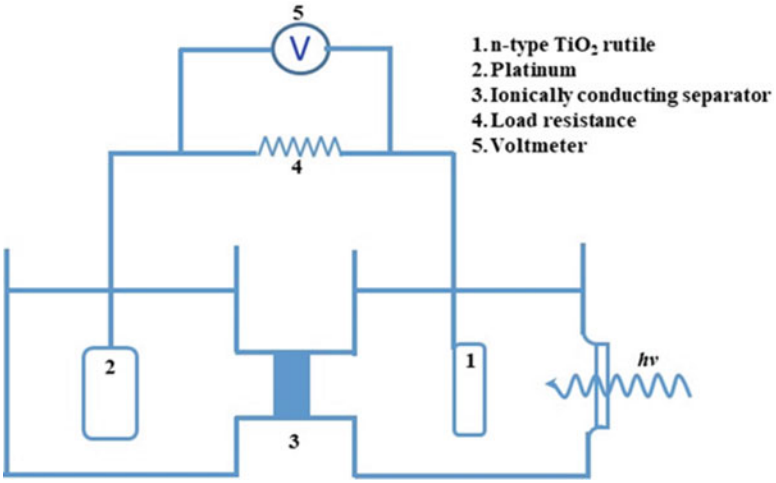

Fig. 11.5 Schematic of TiO_2 PEC cell for water splitting. (Modified from Lan et al. (2013) with permission from Elsevier)

detail (Ni et al. 2007; Navarro et al. 2009). The schematic of PEC water splitting using TiO_2 is shown in Fig. 11.5. TiO_2 electrode was connected to a platinum black counter electrode through an electrical load, and it was exposed to UV light irradiation. A flow of photocurrent from the platinum counter electrode to the

TiO_2 electrode through an external circuit was observed when the TiO_2 surface was irradiated with light ($\lambda < 415$ nm). The current direction revealed that photoreduction (hydrogen evolution) was occurred at the Pt electrode and the photooxidation (oxygen evolution) was transpired at the TiO_2 electrode.

This research evidenced (Fujishima and Honda 1972) the possibilities of water splitting on TiO_2 surface into O_2 and H_2 under UV-visible light irradiation according to the following equations:

$$H_2O + 2h^+ \rightarrow \frac{1}{2}O_2 \uparrow + 2H^+ \tag{11.1}$$

$$2H^+ + 2e^- \rightarrow H_2 \uparrow \tag{11.2}$$

The overall photocatalytic reaction is

$$H_2O + h\nu \rightarrow \frac{1}{2}O_2 \uparrow + H_2 \uparrow \tag{11.3}$$

Generally anatase TiO_2 nanoparticles have higher water splitting efficiency as compared to rutile nanoparticles. This may be ascribed to the high reduction potential of photo-generated electron in anatase (Ohno et al. 2012). A two-compartment PEC cell with cation exchange membrane and electro donors (bromide ions) was reported in 1998 (Fujihara et al. 1998). A novel low-cost visible light-assisted PEC cell using two photosystems was examined by Grätzel (2001). The first photosystem was a nanocrystalline metal oxide thin-film (WO_2 and Fe_2O_3) electrode, and the second photosystem was a dye-sensitized nanocrystalline TiO_2 cell. Maeda and Domen (2010) reported an effective Z-scheme system using $Pt/ZrO_2/TaON$ and Pt/WO_3 nanocomposites. A quantum yield of 6.3% was achieved by the Z-scheme system under visible light irradiation. Less energy is required to operate the PEC with two semiconductors as compared to the single semiconductor system. Additionally, H_2 and O_2 evolution occurs separately, and this hampers the reverse reaction. Nozik (1977) proved that water splitting could be done without external potential. The incorporation of noble metals could enhance the photoactivity of TiO_2. The second-component incorporation is called as co-catalyst. It is important to note that some of the active components such as noble metals can catalyze the reaction between O_2 and H_2 to produce water again in spite of water splitting. An efficient and durable photocatalyst is necessary to implement the photocatalytic water splitting. Also, the selection of appropriate co-catalyst may control the photocatalytic activity.

Though some photocatalysts like $NiO/NaTaO_3$:La (QY = 56% at 270 nm) attained high photonic efficiency, the water splitting efficiency of pure water is not sufficient (Kato et al. 2003). Because water oxidation is a multistep reaction, which involves four electrons and needs the reaction of two hydroxyl radicals to produce one hydrogen peroxide molecule.

$$2OH\cdot \rightarrow H_2O_2\cdot \rightarrow H_2O + \frac{1}{2}O_2 \tag{11.4}$$

The recombination of O_2 and H_2 can be avoided with the help of electron donors or sacrificial agents (methanol or triethanolamine or sodium sulfide/sodium sulfite). The photo-induced holes are easily scavenged by the sacrificial agents to avoid the electron-hole recombination (Hernández-Alonso et al. 2009). Patsoura and his coworkers (2007) reported a one-step approach for water purification and hydrogen production using wastewater as sacrificial agent. Ohno et al. (2012) carried out a long-term investigation on the stability of GaN:ZnO. They found that the photoactivity was not changed for the first 3 months, but it was significantly reduced (almost half of the efficiency) after 6 months. The loss of co-catalyst and the hydrolysis of nitride were the main reasons for the poor efficiency. Tüysüz and Chan (2013) prepared an amorphous and nanocrystalline $Na_2Ta_2O_6$ photocatalyst with porous matrix for the water splitting. These nanocrystalline photocatalysts showed promising activity without any co-catalysts. In addition, novel electron mediators such as the redox $[Co(bpy)_3]^{3+/2+}$ and $[Co(phen)_3]^{3+/2+}$ coupled with $Ru/SrTiO_3$:Rh and $BiVO_4$ photocatalysts (Z-scheme photocatalysts) were examined for overall water splitting under visible light irradiation. Likewise, Park et al. (2012) used stainless steel as cathode for hydrogen production in order to reduce the cost. Ryu et al. (2007) and Abdi et al. (2013) studied visible light-assisted water splitting using CdS nanoparticles and Bi_2S_3 dispersed in zeolite-Y. To improve the efficiency and minimize the unknown flaws between visible light absorption and suitable redox capability, it is suggested to use solid solutions and heterojunctions with tunable electronic structures. For a profitable solar-to-energy conversion and to utilize the natural solar light, the photocatalysts should be developed with absorption capability over 600 nm.

11.4 Environment-Related Applications

The developed and developing countries are facing a tremendous environmental pollution by the industrialization and consumerization. These issues are associated with the remediation of hazardous wastes and polluted groundwaters and the control of toxic air contaminants. Owing to address such significant problems, governments and funding agencies allocate a major portion of their grants toward renewable energy production and environmental remediation research. Photocatalysis using TiO_2 nanoparticles is an environmentally benign method to address air, water, and soil pollution with the help of inexhaustible solar energy (Hoffmann et al. 1995; Wold 1993). Photocatalysis will be executed on the basis of photoreduction, photo-oxidation, photo-sterilization, and photo-induced super-hydrophilicity (self-cleaning surface) reactions (Hoffmann et al. 1995; Fujishima and Honda 1972; Fox and Dulay 1993). Several research articles and reviews have been published on the mechanism and fundamental for all these phenomena.

11.4.1 Air Purification

Most of the environmental air problems such as global warming, climate change, stratospheric ozone depletion, and air quality degradation are caused by the atmospheric emissions from domestic and industrial activities. Photocatalytic process may significantly reduce their impact even at low concentrations as compared to other conventional air treatment methods (such as adsorption, filtration, or combustion). The application of photocatalytic systems for air purification is more attractive (Mamaghani et al. 2017; Nie et al. 2018) for the industries though the scientific reports are considerably higher for the photocatalytic water purification (Paz 2010). Photocatalysis is an appropriate technology to degrade most of the air pollutants including organic (simple alkanes, alkenes, alkynes, aromatics, alcohols, aldehydes, ethers, or ketones), organic halogenated (trichloroethylene, tetrachloroethylene, dichloroacetic acid, or trichloromethane), and organic/inorganic compounds with heteroatoms (H_2S, SO_x, alkyl sulfides, NO_x, amines) at the laboratory scale. Incorporation of TiO_2 nanoparticles in building materials (such as tiles, paints, bricks) substantially decreases the concentration of airborne pollutants such as CO_2, NO_2, and volatile organic compounds (VOCs).

11.4.1.1 Removal of CO_2

In 1979 (Inoue et al. 1979), the photoreduction of CO_2 in water into formic acid, formaldehyde, methanol, and methane was first reported using TiO_2 nanoparticles. Since then, the research was focused on photoreduction of CO_2 by TiO_2 under UV (Anpo et al. 1997; Wu et al. 2005; Dimitrijevic et al. 2011) or visible light (Wu and Chiou 2008; Woolerton et al. 2010) irradiation. Methane and/or methanol was generally produced as a by-product of this process (Low et al. 2017). Owing to minimize the photo-induced electron-hole recombination and enhance the efficiency of CO_2 photoreduction, the surface of TiO_2 is deposited with metals such as Cu, Pt, and Pd (Hirano et al. 1992; Ishitani et al. 1993; Yui et al. 2011). The mechanism of CO_2 photoreduction on metal-doped TiO_2 is schematically expressed in Fig. 11.6.

The mechanism of photocatalytic CO_2 transformation to methoxyl radical over TiO_2 surface in the presence of dissociated/bound water is schematically shown in Fig. 11.7.

The O=C=O bond cleavage initiates the electron transfer and absorption of hydrogen atoms for formate ion production. Subsequent electron/proton transfer leads to methoxyl radical formation which further reduces to methane on TiO_2 surfaces.

Kwak et al. (2015) studied the photoreduction of CO_2 using Ni-doped TiO_2 under UV light irradiation. The photocatalytic CO_2 reduction experiments were carried out in a circulated liquid photo-reactor (Fig. 11.8). The highest CH_4 yield was achieved by TiO_2 with 0.1 mol % of Ni. This is attributed to the high surface area and electron-hole separation via the formation of new energy levels by Ni dopant.

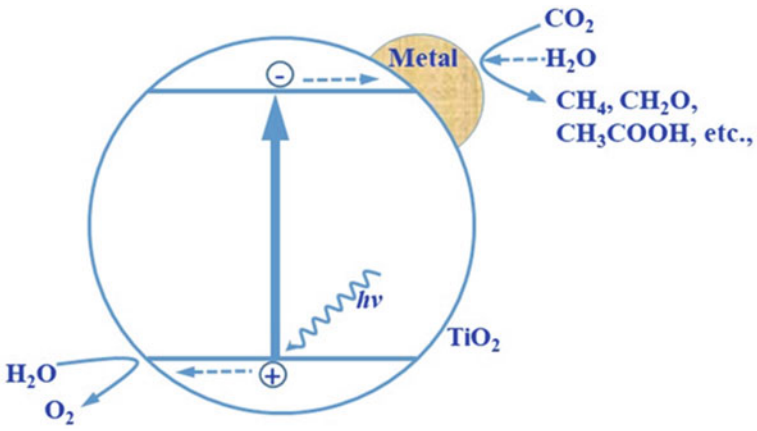

Fig. 11.6 Schematic for the mechanism of CO_2 photoreduction on metal-doped TiO_2. (Modified from Linsebigler and Lu (1995) with permission from the American Chemical Society)

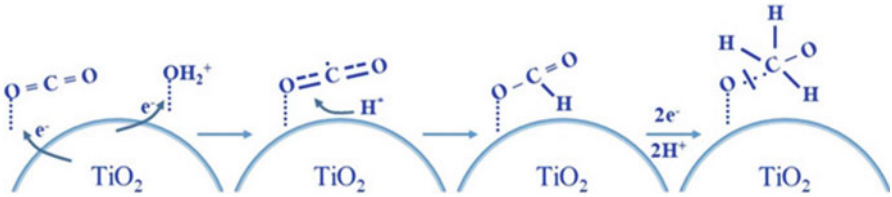

Fig. 11.7 Schematic for the mechanism of photocatalytic CO_2 transformation to methoxyl radical over the TiO_2 surface in the presence of dissociated/bound water. (Modified from Dimitrijevic et al. (2011) with permission from the American Chemical Society)

11.4.1.2 Removal of NO_x

To confirm the photocatalytic removal of NO_x at ambient conditions and at large scale, NO_x concentration was observed over different periods (Chen and Chu 2011; Papailias et al. 2017; Yao et al. 2017). The oxidation NO_2 to nitrate ions will occur very slowly under normal atmospheric conditions. TiO_2 nanoparticles catalyze the photooxidation of NO_2 and NO into nitrate ions in air using hydroxyl and superoxide radicals (Dalton et al. 2002).

$$NO_2 + \cdot OH \rightarrow H^+ + NO_3^- \tag{11.5}$$

$$NO + \cdot O_2^- \rightarrow NO_3^- \tag{11.6}$$

Since then, the less harmful nitrate ions can be either removed by rainfall or soaked into concretes forming stable compounds as weak nitric acid and incorporated to the nitrogen cycle by plants and microorganisms (Chen and Poon 2009; Hüsken et al. 2009; Skalska et al. 2010). To retard the catalytic poison and increase

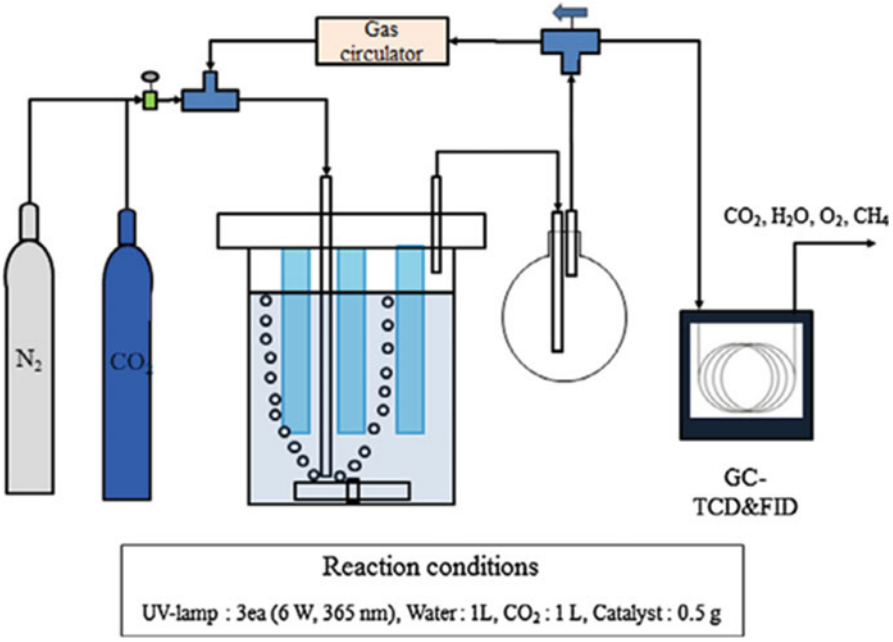

Fig. 11.8 Schematic of experimental setup for the photoreduction of CO_2 in a circulated liquid photo-reactor. (Reprinted from Kwak et al. (2015) with permission from Elsevier)

the catalyst lifetime, alkaline additives with high O_2 and NO_3^- adsorption capacity were incorporated (Ichiura et al. 2003). Nevertheless, the gaseous nitrous acid formation (Langridge et al. 2009) and nanoparticle inhalation are harmful to the health (Lee et al. 2010).

11.4.1.3 Removal of Volatile Organic Compounds (VOCs) and Others

The hazardous volatile organic compounds (VOCs) are released into the environment by human and industrial activities. They cause serious health issues to all living systems. VOCs can be effectively degraded by the TiO_2 nanoparticles (Ji et al. 2017; Qian et al. 2017). The degradation of benzene and other persistent VOCs was demonstrated by N- and Pt-doped TiO_2 ($Pt/TiO_{2-x}N_x$) under visible light irradiation (Li et al. 2008). The interfacial electron transfer was enhanced by the N doping and Pt incorporation. Ethylbenzene, *o*-xylene, *m*-xylene, and *p*-xylene were successfully removed at indoor air levels in an annular reactor using N-TiO_2 (Li et al. 2008). The superior photocatalytic activity was attained by low stream flow rate and low hydraulic diameter in the reactor. Likewise, N-TiO_2/zeolite composite was studied for the removal of toluene (Wei et al. 2010). VOCs such as trichloroethylene, isooctane, acetone, methanol, methyl ethyl ketone, *t*-butyl methyl ether, dimethoxymethane, and methylene chloride can be abated by TiO_2 nanoparticles

with a high conversion yield of ~90% (Alberici and Jardim 1997). Studies revealed that a high potential is required for industrial process vents and indoor air treatments for the removal of VOCs. Kemme et al. (1999) executed a large-scale study to moderate VOCs and nitroglycerine from solvent multi-base propellant production at Radford Army Ammunition Plant (Virginia, USA) using photocatalytic oxidation technology.

11.4.2 Water/Soil Purification

The water and soil pollution is caused by the persistent organic pollutants (POPs) and endocrine-disrupting compounds (EDCs) released from domestic and industrial activities (like pharmaceuticals, agrochemicals, polymers, and automobile industries). Existing conventional water treatment technologies (physical, chemical, or biological) are not effective for the removal of toxic pollutants, and the operation cost is considerably high (Kasprzyk-Hordern et al. 2003; Benotti et al. 2009). Besides, the usage of conventional technologies is regulated by EU directives such as 85/337/EEC, 91/271/EEC, 76/464/EEC, 2010/75/EU, and 2006/118/EC due to their ineffectiveness and incomplete biodegradation of the waste products (Fagan et al. 2016).

Semiconductor photocatalysis can degrade a wide range of POPs (sources from pharmaceuticals, steroids, antibiotics, phthalates, disinfectants, pesticides, fragrances, preservatives, and additives) and EDCs (such as polycyclic aromatic hydrocarbons, alkylphenols, bisphenol A, organotins, dyes, surfactants, pesticides, volatile organic compounds, heavy metals, natural and synthetic estrogenic chemicals, and heavy metals). The utilization of TiO_2 for the degradation of various toxic contaminants has been highlighted in several publications (Alrousan et al. 2012; Ahmed et al. 2011; Teh and Mohamed 2011; Prieto-Rodriguez et al. 2012a, b; Chong et al. 2010; Chatterjee and Dasgupta 2005; Qu et al. 2013; Kabra et al. 2004; Rizzo et al. 2009; Ali and Kim 2018; Mahadik et al. 2017; Vignesh et al. 2014a). Table 11.1 summarizes the key findings on the photodegradation of various organic pollutants using TiO_2 nanoparticles.

The use of immobilized TiO_2 for the photodegradation of 15 selected CECs in a simulated and real effluent wastewater under solar irradiation was studied by Miranda-Garcia et al. (2011). TiO_2 was immobilized on borosilicate glass support to overcome the recovery of nanoparticles for recycling. The efficiency of TiO_2 was still maintained after five recycles for the simulated water system. For the real effluents, the complete photodegradation was achieved by immobilized TiO_2 in a shorter duration as compared to TiO_2 suspension. Carbamazepine (CBZ) is a derivative of dibenzazepine used primarily in the treatment of epilepsy and relief of neuralgia and psychotic disorders. It was found to be a stable contaminant, hazardous to aquatic life, and not easily degraded in the treatment plants (Jelic et al. 2011). Haroune et al. (2014) found that CBZ and its three important metabolites were effectively degraded using TiO_2 under solar irradiation. TiO_2

Table 11.1 A summary of photocatalysts used for the degradation of various pollutants

S. no.	Photocatalyst	Pollutants (CECs and EDCs)	Remarks	References
1	P25 TiO_2 on FTO glass	Amino acids and derivatives	The degradation products and amino acids were decomposed into NO^{3-}, NH^{4+}, and CO_2	Hidake et al. (1997)
2	P25 TiO_2 on Ti plate	Imidacloprid	Apparent rate constant for PEC was higher than the normal photocatalysis	Philippidis et al. (2009)
3	TiO_2 thin films	Rose bengal dye	PEC oxidation was faster than the normal photocatalytic oxidation with TiO_2 concentration below 0.3%	Li et al. (2000)
4		Remazol Brilliant Orange 3R dye	The dye degradation rate was improved in the presence of chloride electrolyte	Zanoni et al. (2003)
5		Simulated tannery effluent	100% dye decolorization, surfactant removal, and Cr (VI) reduction	Paschoal et al. (2009a)
6		Disperse dyes from a textile industry	89% of dye decolorization with 69% of COD removal and 50% TOC reduction	Paschoal et al. (2009b)
7		Indigo carmine dye	The authors applied controlled current instead of the constant potential in PEC oxidation	Guaraldo et al. (2011)
8		Metallophtalocyanine (reactive turquoise blue 15 dye)	95% of mineralization and 69% of copper removal	Osugi et al. (2005)
9	TiO_2 NTs	Bisphenol A	100% of degradation and mineralization of bisphenol A was attained	Brungnera et al. (2010)
10		Ofloxacin	100% degradation of 40 mg/L ofloxacin was achieved with 70% of COD removal	Li et al. (2014)
11		Triclosan	The authors identified that intermediates formed during PEC were more toxic and stable than triclosan	Liu et al. (2013)
12	TiO_2 NTs and wormhole-shaped TiO_2 electrode	Alachlor (herbicide)	TiO_2 NTs electrode showed superior performance than wormhole-shaped TiO_2 electrode	Xin et al. (2011)
13	TiO_2 nanostructured electrode	Chlortetracycline and carbamazepine	The factors that influence the pollutant degradation, kinetics, and by-products were analyzed in detail	Daghrir et al. (2012a, 2013)

(continued)

Table 11.1 (continued)

S. no.	Photocatalyst	Pollutants (CECs and EDCs)	Remarks	References
14	TiO_2 NTs decorated with Sb_2S_3 particles	Arianor Tyrian Purple® dye (ATP)	TiO_2/Sb_2S_3 showed strong photoabsorption in the visible light region ($\lambda < 740$ nm)	Bessegato et al. (2014)
15	TiO_2 NTs decorated with Pt nanoparticles	Acid red 29	100% of dye decolorization with 92% mineralization was achieved by Pt-TiO_2	Almeida and Zanoni (2014)
16	TiO_2 NTs decorated with Pd nanocrystallites	Diclofenac	Pd/TiO_2 NTs displayed maximum photovoltage, photocurrent density, and electron density	Cheng et al. (2013)
17	TiO_2 NTs modified with molecular imprinted polymer (MIP)	Tetracycline hydrochloride (TC)	The adsorption capacity of TC was improved by MIP. The PEC activity of MIP-TiO_2 was1.2 times higher than that of TiO_2	Lu et al. (2008)
18	N-doped TiO_2	Chlortetracycline (CTC)	Bandgap energy was shifted from 3.2 to 2.3 eV after N-doping. 100% degradation of CTC with 92% TOC removal was achieved	Daghrir et al. (2012b, 2014)
19	B-doped TiO_2 NTs	Acid Yellow 1 dye (AY1)	The light absorption of TiO_2 NTs was enhanced by B-doping. B-TiO_2 NTs showed high photocurrent and PEC response	Bessegato et al. (2015a)
20	W-doped TiO_2 NTs	Rh-B dye	W-TiO_2 NTs exhibited best PEC efficiency than pure TiO_2 NTs	Gong et al. (2013)
21	Cr-doped TiO_2 NTs	p-Nitrophenol (PNP)	PEC efficiency of Cr-TiO_2 NTs was quite stable after recycling	Yang et al. (2014)
22	N-/Zr-doped TiO_2 NTs	4,4′-Dibromobiphenyl	Co-doped TiO_2 showed the highest PEC efficiency than the single metal-doped TiO_2	Liu et al. (2010)
23	ZnO nanorods embedded in TiO_2 NTs	Methyl orange dye	Bandgap energy was shifted from 3.34 eV (TiO_2 NTs) to 3.03 eV (ZnO/TiO_2 NTs)	Zhang et al. (2008)
24	TiO_2 nanobelts (NBs) decorated with Au nanoparticles	Tetrabromobisphenol A (TBBPA)	The TiO_2 NBs/Au nanocomposites showed maximum efficiency as compared to pure TiO_2 NBs under irradiation of simulated solar light and visible light; after five cycles, the PEC efficiency decreased only 8%	Chen et al. (2014)

Modified from Bessegato et al. (2015b) with permission from Springer Nature

nanoparticles were also employed in the photodegradation of tamoxifen and gemfibrozil drugs under near-UV light irradiation (Yurdakal et al. 2007). The photodegradation of lindane, an organochlorine pesticide, was reported by Senthilnathan and Philip (2010) using N-doped TiO_2 nanoparticles. N-doped TiO_2 showed maximum efficiency when compared to other metal ion-doped TiO_2. 2,4-Dichlorophenoxyacetic acid is a well-known herbicide and found in the surface and groundwater from agricultural runoffs. Anatase and rutile forms of pure-, Fe-, and N-doped TiO_2 nanoparticles were studied for the degradation of numerous phenoxy acid herbicides. The results showed that N-doped TiO_2 anatase exhibited the best efficiency than undoped and Fe-doped TiO_2. The photocatalytic efficiency is influenced by the molecular structure of herbicide and its interaction with the ROS (Šojić et al. 2010). Mamane et al. (2014) employed N-doped TiO_2 thin films on glass slide surface to enhance the photodegradation of various chemical and biological pollutants. Wang et al. (2013) explored the photocatalytic activity of C-, N-, and S-doped TiO_2 under visible light irradiation. Approximately, 68% of CBZ was photodegraded over 120 min using C-N-S-TiO_2.

Various TiO_2 photocatalysts were found to be active for the degradation of bisphenol A including nitrogen-carbon co-doped TiO_2 (Wang and Lim 2010) and nitrogen-doped TiO_2 hollow spheres (Subagio et al. 2010) under LED light irradiation. The photocatalytic performance of metal-doped TiO_2 was 90% higher than that of bare TiO_2. The use of light-emitting diodes has several benefits like energy efficiency, flexibility, and extended lifetime. The degradation of bisphenol A in water favors at the neutral pH and blue LED (465 nm) light irradiation. Nitrogen-doped TiO_2 supported on activated carbon (N-TiO_2/AC) nanocomposites also exhibited high adsorption and photodegradation of bisphenol A under solar light irradiation. The photocatalytic activity of CuO/Pb_2O_3 was reported (Kamaraj et al. 2018) for the degradation of rose bengal dye under visible light irradiation. The photocatalytic activity of the nanocomposite was two times higher than that of CuO or Pb_2O_3. Ananpattarachai and Kajitvichyanukul (2015) reported the degradation of dichlorodiphenyltrichloroethane (DDT) under UV and visible light irradiation using N-doped TiO_2. The efficiency under visible light was six times higher than that of UV light for the complete DDT photodegradation. Atrazine (an herbicidal pollutant found in soil and water) was studied for the photodegradation using metalloporphyrins supported on TiO_2 under visible light. Four different metalloporphyrin systems were studied by Granados-Oliveros (2009) for the photodegradation efficiency against atrazine. Copper (II) tetra (4-carboxyphenol) porphyrin (TcPPCu(II))/TiO_2 displayed maximum efficiency (82% of atrazine removal) as compared to other photocatalysts during 1 h. NF co-doped TiO_2 was also studied for the degradation of atrazine under visible and solar light irradiation (Barndõk et al. 2013; Andersen et al. 2013). Studies are also being carried out to detect the presence of hormones and steroids in wastewater (Ying et al. 2002; Aris et al. 2014; Vega-Morales et al. 2010). Several investigations have been conducted for the removal of steroids from various water sources using TiO_2 photocatalysts under UV and solar irradiation (Oliveira et al. 2015; Dimitroula et al. 2012; Silva et al. 2012; Sun et al. 2010; Puma et al. 2008; Pan et al. 2014; Mueses et al. 2013;

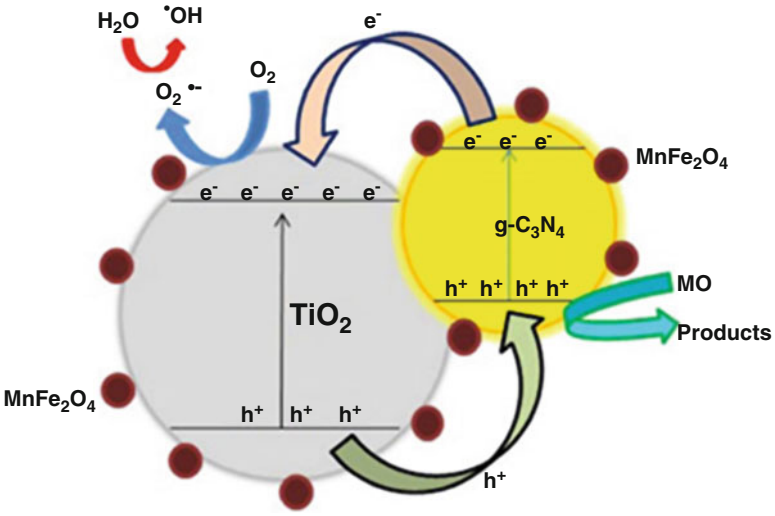

Fig. 11.9 The schematic of photo-generated electron-hole separation process on $MnFe_2O_4$/g-C_3N_4/TiO_2 under simulated solar light irradiation. (Reprinted from Vignesh et al. (2014b) with permission from Elsevier)

Wang et al. 2015). For the remediation of 17βα-ethinylestradiol from aqueous solution under solar light irradiation, two systems such as heterogeneous photocatalysis (HP) and electrochemically assisted heterogeneous photocatalysis (EHP) were studied using TiO_2/WO_3 electrodes (Oliveira et al. 2015). Among them EHP system was found to be highly effective.

Metal vanadates such as silver vanadate (Ag_3VO_4), cadmium vanadate (CdV_2O_6), and strontium vanadate ($Sr_3(VO_4)_2$) were used with TiO_2 to study the photocatalytic degradation of fast green (FG) dye under visible light irradiation (Vignesh et al. 2013). Approximately, 89% of FG (5 μM) photodegradation with 72% of COD reduction and 66% of TOC removal were achieved using TiO_2-Ag_3VO_4 during 180 min of visible light irradiation. The maximum efficiency of TiO_2-Ag_3VO_4 is ascribed to the effective electron-hole separation/migration on the nanocomposite surface. Magnetically separable $MnFe_2O_4$/g-C_3N_4/TiO_2 was examined for the photodegradation of methyl orange under simulated solar light irradiation (Vignesh et al. 2014b). The nanocomposite showed maximum efficiency as compared to TiO_2, g-C_3N_4, $MnFe_2O_4$, and $MnFe_2O_4$/g-C_3N_4. This is attributed to the effective electron-hole separation and strong visible light absorption. The photo-generated electron-hole separation process on the nanocomposite is displayed in Fig. 11.9.

The effects of different operational parameters were already highlighted in many books and review articles. The primary factors that influence the photocatalytic water and soil treatment are pH, kinetics, cost, low-oxygen solubility, and low light absorption in turbid waters (Vidal et al. 1999). Currently, researchers are interested to use the combination of photocatalysis and biological water treatment technology to

enhance the efficiency toward non-biodegradable water-soluble pollutants. The initial pollutant concentration, flow rate, nature of catalyst, reactor design, light intensity, and wavelength distribution are the key factors to determine the efficiency and selectivity of a photocatalytic system. The effect of temperature is ignorable; however, high temperature may affect the lamp efficacy, favor the electron-hole recombination, and hinder the adsorption of pollutants at the active sites. Hence, all the operational parameters must be optimized first at the laboratory scale.

11.4.3 Degradation of Microorganisms and Cyanotoxins

Since Egyptian era, disinfection of water using solar power is being known; however, the first scientific report was published during 1870. The water purification technology was developed only a century later in 1980. Earlier to the photocatalysis technology, the physicochemical methods such as adsorption, ultracentrifugation, chlorine, chlorine dioxide, ozone, and ultraviolet radiation were used to purify the wastewater. Due to the low cost and the wide range of availability, chloride is broadly used to purify the drinking water. However, chlorine can also form toxic substance like trihalomethanes, and chlorine is found to be inactive to some microorganisms. Solar light-assisted semiconductor photocatalysis is one of the promising technologies to disinfect the microorganism in a sustainable way. The microorganisms are completely destroyed by the ROS produced from semiconductor photocatalysis (Li et al. 2013; Liu et al. 2017a; Miao et al. 2017).

The photocatalytic disinfection was initially reported by Matsunaga et al. (1985) using platinum-loaded TiO_2 (TiO_2/Pt) to inactivate *Lactobacillus acidophilus*, *Saccharomyces cerevisiae*, and *Escherichia coli* (10^3 cells/mL) under UV light irradiation during 60–120 min. After this invention, this technology has been studied extensively for a broad spectrum of microorganism such as bacteria, virus, fungi, algae, protozoa, and cancer cells. Single and pure cultures of *Escherichia coli* are used as a model target microorganisms for several investigations, and the important key findings are shown in Table 11.2.

The photocatalytic disinfection mechanism of bacteria proceeds through the following steps: (i) cell membrane damage, (ii) the leakage of internal bacterial components from the damaged sites, and (iii) photocatalytic oxidation of the leaked cell fragments by the ROS (Ganguly et al. 2018). Studies demonstrated that various microbes like *Staphylococcus aureus*, *Bacillus subtilis*, *Escherichia coli*, *Salmonella typhimurium*, and *Micrococcus lylae* were effectively disinfected by pure and doped TiO_2 photocatalysts (nitrogen (Dunnil et al. 2011), nitrogen-silver (Fisher et al. 2013; Ashkarran et al. 2014), nitrogen-copper (Fisher et al. 2013), sulfur (Yu et al. 2005), carbon (Shao et al. 2009), copper (Yadav et al. 2014), and graphene nanosheet (Cao et al. 2013)-doped TiO_2). Inactivation of *Staphylococcus aureus* by carbon-doped TiO_2 anatase-brookite heterojunction (80/20 ratio) under visible light irradiation was studied by Etacheri et al. (2013). The effects of N- and S-dopants (doping and co-doping) on TiO_2 for *Escherichia coli* disinfection was studied by Pulgarin's

Table 11.2 A summary of photocatalysts used for the degradation of various microorganisms

S. no.	Photocatalyst	Examined microorganism	Conditions	% degradation	References
1	TiO_2	*Escherichia coli 103 CFU* mL^{-1}	Two-compartment reactor with 50 mL volume, UV light source (450 W Xe-Hg arc lamp), and + 1 V external potential	The presence of Cl^- and SO_4^{2-} ions resulted in 99.9% *E. coli* inactivation in 45 and 60 min, respectively	Selcuk (2010)
2		*Escherichia coli* 9.0 × 106 *CFU* mL^{-1}	UV-LED array light source (λ_{max} = 365 nm), 0.1 $NaNO_3$ solution was supporting electrolyte and additional 1.0 mM NaBr, applied potential of +0.30 V	100% within 1.57 s	Li et al. (2013)
3		*Escherichia coli* 9.0 × 106 *CFU* mL^{-1}	UV-LED, +0.1 $NaNO_3$ solution was supporting electrolyte and additional 1.0 mM NaBr or NaCl, applied potential of +0.30 V vs. Ag/AgCl	100% within 1.57 s	Li et al. (2013)
4		*Escherichia coli 107 CFU* mL^{-1}	Flow reactor operated in a recycling mode at a flow rate of 100 mL min^{-1}, 3.0 V, UVA irradiation	95% within 25 min	Christensen et al. (2003)
5		*Escherichia coli 107 CFU* mL^{-1}	UV and visible irradiation, 0.10 M $NaNO_3$ electrolyte, and applied potential +0.40 V	99.97% within 10 min 100% within 180 min	Liu et al. (2014)
6		*Microcystin aeruginosa 50 g* L^{-1}	Chloride concentration higher than 0.010 mol L^{-1}, pH 4, and current density 30 mA cm^{-2}, UV (λ = 315–400 nm) irradiation	100% within 150 min	Fraga et al. (2009)
7	TiO_2 NTs	*Escherichia coli 106 CFU* mL^{-1}	UV light illumination (30 W, intensity 3 mW cm^{-2}) in 0.01% NaCl (pH 5.2) and under an anodic potential of +3.0 V SCE	100% within 10 min	Baram et al. (2009)
8		*Escherichia coli BW25113* and *Escherichia coli K-12*	Reactor with 100 μL under constant applied potential of +1.0 V and	100% within 180 s	Nie et al. (2014a)

			illuminated by a UV light-emitting diode array (λ 365 nm)		
9		*Mycobacterium fortuitum 2.0 × 106 CFU mL^{-1}; Mycobacterium chelonae 6.0 × 108 CFU mL^{-1}; Mycobacterium abscessus 1.0 × 104 CFU mL^{-1}*	0.05 M Na_2SO_4 (pH 6), applied potential of +1.5 V vs. Ag/AgCl	99.98%, 99.93% and 100% within 360 min, respectively	Brugner et al. (2013a, b)
10	TiO_2/Ti	*Enterococcus faecalis and Escherichia coli 107 CFU mL^{-1}*	Simulated solar radiation (UV-A and UV-B radiation λ < 280 nm) in the presence of 1% (w/v) Na_2SO_4, potential applied +10 V	6.2 log reduction within 15 min	Venieri et al. (2012)
11		*Escherichia coli and Enterococcus faecalis*	Simulated solar irradiation xenon ozone-free lamp 150 W, 1% (w/v) Na_2SO_4 aqueous solution +2.0 V	6 orders of magnitude within 15 min	Venieri et al. (2013)
12	TiO_2/Fe	*Escherichia coli*	Bias potential +3.0 V, reactor of 0.5 L, UV lamp (8 W UV black light lamps, λ = 370 nm)	99.5% within 25 min	Egerton et al. (2006)
13	TiO_2/Pt	*Lactobacillus acidophilus, Saccharomyces cerevisiae, and Escherichia coli 10^3 CFU mL^{-1}*	Metal-halide lamp	100% within 60–120 min	Matsunaga et al. (1985)
14	Ti/TiO_2 P25	*Escherichia coli XL^{-1} blue 103 CFU mL^{-1}*	Supporting electrolyte 0.1 mol L^{-1} Na_2SO_4 (pH 5.6), bias potential +1.0 V, UVA 365 nm irradiation	100% within 3 h	Philippidis et al. (2010)
15	Ti/TiO_2-Ag and Ti/TiO_2NTs	*Mycobacterium kansasii; Mycobacterium avium 7.5 × 104 CFU mL^{-1}*	0.05 M Na_2SO_4 (pH 6), applied potential of +1.5 V vs. Ag/AgCl, UV irradiation	100% within 3 min	Brugnera et al. (2013a, b)
16	Ti/TiO_2-Ag NTs	*Mycobacterium smegmatis*	UV and visible irradiation, 0.05 M Na_2SO_4 (pH 6), applied potential of +1.5 V vs. Ag/AgCl	100% within 3 min 99.96% within 30 min	Brugnera et al. (2013a)
17	TiO_2-Ag NTs	*Mycobacterium smegmatis 5.1 × 10^3 CFU mL^{-1}*	UV irradiation, 0.05 M Na_2SO_4 (pH 6), applied potential of + 1.5 V	100% within 3 min	Brugnera et al. (2012)

(continued)

Table 11.2 (continued)

S. no.	Photocatalyst	Examined microorganism	Conditions	% degradation	References
18	N-doped carbonaceous / TiO_2	*Escherichia coli K-12107 CFU* mL^{-1}	Potential bias of +1.0 V and a light intensity of 15 mV cm-2 in 0.2 M $NaNO_3$, reactor of 50 mL	100% within 30 min	Nie et al. (2014b)
19	Ag-TiO_2/G Cu-TiO_2/G	*Escherichia coli*	Potential applied +3 V, KCl 0.1 M solution, UV 254 nm irradiation	89.7%; 67.8% within 30 min, using Ag-TiO_2/G and $CuTiO_2$/G, respectively	Rahmawati et al. (2010)
20	Ag-TiO_2/ ACF	*Penicillium expansum*	Light intensity 2.3 mW cm-2 ($\lambda = 254$ nm), bias voltage 66.7 V	1.8 log reduction within 300 min	Ye et al. (2010)
21	TiO_2 coated onto on indium trioxide	*MS-2 bacteriophage*	Black light blue irradiation ($\lambda = 300$–420 nm), 20 mM phosphate buffer at pH 7.1, and potential bias 2.0 V	99% within 109 min	Cho et al. (2011)

Modified from Bessegato et al. (2015b) with permission from Springer Nature

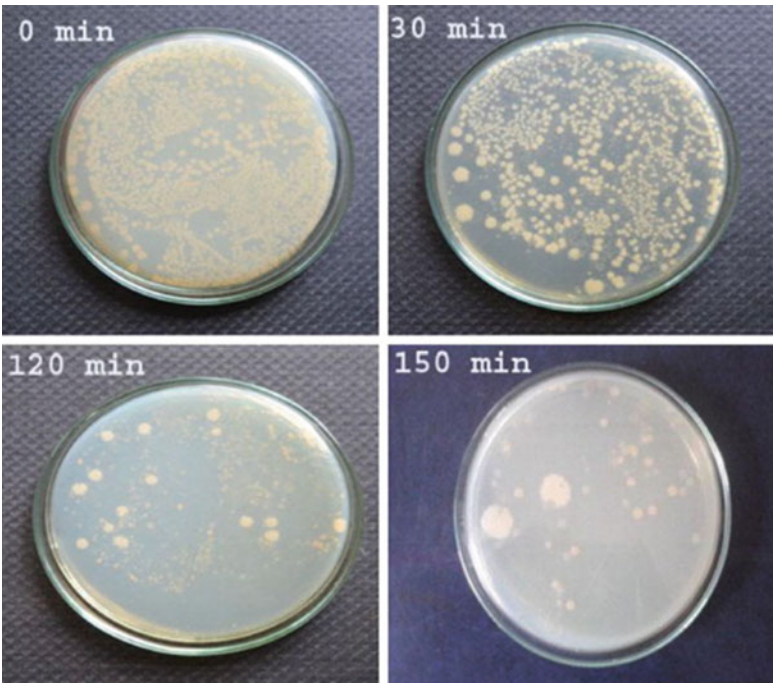

Fig. 11.10 Photographs for the inactivation of *P. aeruginosa* at various irradiation times using CdS-$CuWO_4$-TiO_2. (Vignesh et al. (2014a) with permission from Elsevier)

group (Rengifo-Herrera et al. 2008, 2009a, b). They found that the nature of the dopant, surface hydroxylation, nature of light source, and the particle size of photocatalyst are the key factors for the maximum generation of ROS.

Visible light-driven photocatalytic disinfection of various gram-negative and gram-positive bacteria (*E. coli*, *Staphylococcus aureus*, and *Enterococcus faecalis*) and fungi (*Candida albicans*, *Aspergillus niger*) was studied by Mitoraj et al. (2007) using carbon-doped and Pt-modified TiO_2 in both suspension and immobilized reactors. Likewise, S-doped TiO_2 was proposed for the destruction of gram-positive bacterium *Micrococcus lylae* (Yu et al. (2005)) using a 100 W tungsten-halogen lamp with a 420 nm UV cutoff glass filter. 96.7% destruction was achieved during 1-h treatment in a slurry photo-reactor using S-doped TiO_2 nanoparticles. The photocatalytic inactivation of *Pseudomonas aeruginosa* was studied using cadmium sulfide (CdS)- and copper tungstate ($CuWO_4$)-modified TiO_2 nanoparticles under visible light (Vignesh et al. 2014a). The photographs for the inactivation of *P. aeruginosa* at various irradiation times are shown in Fig. 11.10. Most of the bacterial species were inactivated by CdS-$CuWO_4$-TiO_2 during 150 min of irradiation time. The high bactericidal activity of CdS-$CuWO_4$-TiO_2 is attributed to repetitive attack of ROS and the effective binding of metal ions (Cd, Cu, and Ti) with the bacterial cell wall, suggesting the cell membrane damage.

Table 11.3 A summary of microorganisms studied for the photocatalytic disinfection using TiO_2

Gram-positive bacteria	Gram-negative bacteria	Virus	Fungal species
Bacillus anthracis	*Salmonella typhimurium*	*Astrovirus*	*Aspergillus niger*
Bacillus cereus	*Acinetobacter baumannii*	*Bacteriophage T4*	*Candida albicans*
Bacillus pumilus	*Acinetobacter calcoaceticus*	*Feline calicivirus*	*Diaporthe actinidiae*
Bacillus subtilis	*Bacteroides*	*Hepatitis B*	*Fusarium anthophilum*
Clostridium perfringens	*Coliform bacteria*	*Herpes simplex*	*Fusarium equiseti*
Deinococcus radiophilus	*Enterobacter cloacae*	*Influenza virus*	*Fusarium oxysporum*
Enterococcus faecalis	*Fragilis*	*MS2 phage*	*Fusarium solani*
Enterococcus faecium	*Klebsiella pneumoniae*	*Poliovirus*	*Fusarium verticillioides*
Enterococcus hirae	*Legionella pneumophila*	*Rotavirus*	*Penicillium expansum*
Lactobacillus acidophilus	*Pseudomonas aeruginosa*		*Penicillium chrysogenum*
Lactobacillus helveticus	*Pseudomonas putida*		*Saccharomyces cerevisiae*
Listeria monocytogenes	*Pseudomonas stutzeri*		
Lylae	*Salmonella enterica*		
Micrococcus luteus	*Serratia marcescens*		
Micrococcus luteus	*Shigella flexneri*		
Streptococcus aureus	*Vibrio cholerae*		
Streptococcus pyogenes	*Vibrio parahaemolyticus*		
Streptococcus faecalis			
Streptococcus mutans			

Modified by from Coronado et al. (2013) with permission from Springer Nature

The photocatalysts such as Zr-doping (Swetha et al. 2010), and C-doping (Liu et al. 2006) of TiO_2 were studied for their efficiency to inactivate *Pseudomonas aeruginosa* (Swetha et al. 2010) and *Escherichia coli* (Liu et al. 2006) under visible light irradiation. Recently, a broad range of microorganisms (including bacteria, virus, and fungi) were surveyed by Markowska-Szczupal et al. (2011) and Paspaltsis et al. (2006) for the photocatalytic activity of TiO_2 as mentioned in Table 11.3.

Though the hydroxyl radical (•OH) is accounted for the photocatalytic degradation of bacteria, the role of H_2O_2 and $O_2^{\bullet -}$ is not ignorable. A plausible photocatalytic mechanism for the bacteria degradation is demonstrated in Fig. 11.11. A positive hole and an electron are generated in the VB and CB of a semiconductor during the light irradiation. It will further react with the surface oxygen/water to produce ROS such as $O_2^{\bullet -}$, $^1O_2$, •OH, H_2O_2, and $HO_2^{\bullet}$. The microorganism is degraded through cell wall damage by the ROS. The self-defense mechanism of microbes is overwhelmed by the repetitive attack of ROS. Due to the

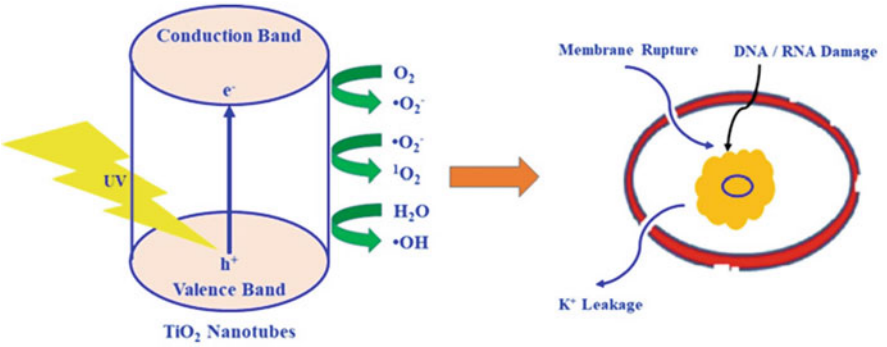

Fig. 11.11 The proposed photocatalysis mechanism of bacterial degradation. (Modified from Podporska-Carroll et al. (2015) with permission from Elsevier)

different composition, structure, and cell wall thickness, the photocatalytic disinfection of fungi is considerably weaker than the bacteria (Malato et al. 2009).

Photocatalytic degradation of cancer cells is more difficult as compared to other microorganisms because they are structurally complex and eukaryotic. Nevertheless, photocatalysis stimulates the apoptosis of cancer cells through an unknown mechanism. TiO_2-mediated destruction of brain cancer cells without damaging nearby healthy cells was reported by Rozhkova et al. (2009). Viruses are much smaller in size (0.01–0.3 μm) when compared to bacteria. Hence, the degradation rate of virus is greater than the bacteria. The complexity and cell wall thickness determine the efficiency of a photocatalyst. The rate of photocatalytic activity is in the following order (Coronado et al. 2013): *viruses* > *E. coli* > *other gram-negative bacteria* > *other coliforms* > *Enterococcus species* > *gram-positive bacteria* > *endospores* > *yeasts* > *filamentous fungi.*

Cyanotoxins are the secondary metabolites that are produced by some cyanobacteria under the favorable conditions of light and nutrients. They also cause many harmful effects to living being and the environment. Various metal-doped TiO_2 nanoparticles including N-doped (Choi et al. 2007; Graham et al. 2010), immobilized TiO_2 (Antoniou et al. 2008), NF co-doped (Pelaez et al. 2010, 2011, 2012; Zhao et al. 2014), graphene oxide-modified (Fotiou et a. 2013), Rh-doped (Graham et al. 2010), Pt-doped (Graham et al. 2010), and carbon-doped (Graham et al. 2010) TiO_2 were examined for the degradation of cyanotoxins in particularly microcystin-LR (MC-LR) under visible light irradiation.

11.4.4 Photocatalysts for Active Surfaces

Under light irradiation, surfaces coated with certain semiconductor nanoparticles showed wettability by means of lowering the water contact angle (WCA) on those coated surfaces. This is called as photo-induced super-hydrophilicity. TiO_2

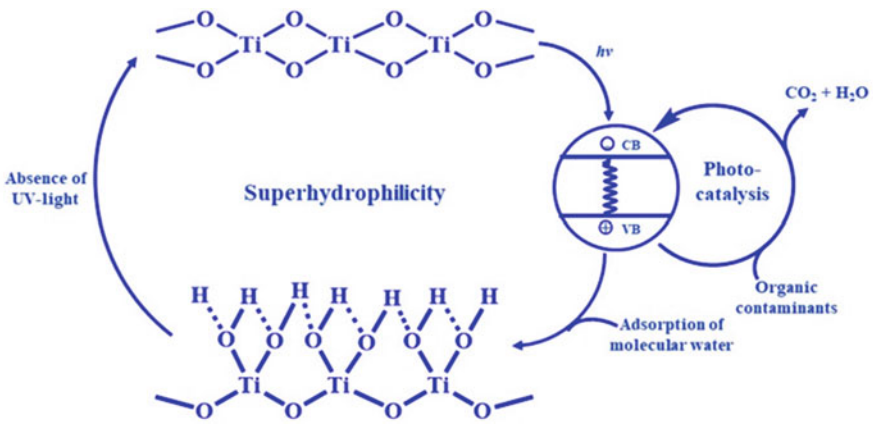

Fig. 11.12 Schematic for the mechanism of photo-induced hydrophilicity (Modified from Zhang et al. (2012) with permission from the Royal Society of Chemistry)

nanoparticle-coated surfaces exhibited self-cleaning, antimicrobial, and antifogging properties. Since from the past few decades, photocatalytic self-cleaning surfaces have received much attention with a research focus from the laboratory to commercial market. A combination of three mechanisms is generally being accepted for the photo-induced super-hydrophilicity such as (a) generation of surface vacancies (b) photo-induced Ti-OH reformation, and (c) photocatalytic removal of pollutants and dirt (Fig. 11.12, Zhang et al. 2012).

Several factors influence the super-hydrophilicity such as surface roughness, surface defects, residual tensile stress, and crystallographic facet. TiO_2 nanoparticles with self-cleaning action have been used in many features such as windows, walls, roofs, vehicles, fabrics, antifogging glass, antibacterial surfaces, and building materials. The applications of self-cleaning surfaces are summarized in Table 11.4.

11.5 Operational Challenges and Future Perspectives

Although the nanoparticle photocatalysis has gained substantial achievement over the past decades, this technology still has significant operational challenges as listed below:

11.5.1 Photo-Reactors

Photodegradation of dyes or water contaminants is commonly carried out in an immersion-type photo-reactor. The photographs and schematic of immersion-type photo-reactor (HEBER: HIPR-Compact-P-8/125/250/400) are illustrated in

Table 11.4 A summary of the applications of photo-induced self-cleaning surfaces

Substrate	Property	Application	References
Tile	Self-cleaning	Kitchens, bathroom, roofs, and walls	Benedix et al. (2000), Bondioli et al. (2009), and Xie and Lin (2007)
Metal	Self-cleaning	Self-cleaning steel for automobile bodies, hospital equipments, aluminum panels, kitchens	Fallet et al. (2001), Nazeri et al. (1997), Yu et al. (2003), and Fernandez et al. (1995)
Glass	Self-cleaning	Windows, tunnel and road-lighting cover glass, greenhouse glasses, and vehicles	Wang et al. (1997), Parkin and Palgrave (2005)
	Antifogging	Vehicle mirrors, road mirrors, interior mirrors	Wang et al. (1997), Watanabe et al. (1999), and Takata et al. (2005)
Plastic/ polycarbonate	Self-cleaning	Automotive industry and buildings	Fateh et al. (2011), Carneiro et al. (2007), and Yaghoubi et al. (2010)
Textile/fiber/ cotton	Self-cleaning anti-odor	Household appliances, interior furnishing, and protective clothing and regular clothing	Qi et al. (2006), Tung and Daoud (2009, 2011)
	Antibacterial	Hospital, health departmental garments and uniforms	Tung and Daoud (2009)

Modified from Zhang et al. (2012) Energy and Environmental Science 5(6):7491–7507 with permission from the Royal Society of Chemistry

Fig. 11.13. The dye solution with required amount of TiO_2 nanoparticles is taken in the cylindrical glass vessel, which is surrounded by a quartz water jacket to keep a constant temperature during the experiments. pH of the reaction mixture is adjusted using dilute sulfuric acid (H_2SO_4) or sodium hydroxide (NaOH). Air is bubbled continuously into the aqueous suspension using an air pump to provide a constant source of dissolved O_2. Before light irradiation, the suspension is initially stirred in dark for 30 min to ensure an adsorption-desorption equilibrium. Xenon (Xe) arc lamp or tungsten (W) lamp is used as the light irradiation source. The dye samples are analyzed regularly from the reaction mixture at a specified time interval. TiO_2 nanoparticles are removed by centrifugation (400 rpm for 10 min) or filtration (using a Millipore filter with pore size of 0.2 μm). The concentration of dye is evaluated by a UV-vis spectrophotometer at the corresponding λ_{max}.

11.5.2 Pilot Plant and Scale-Up

Most of the research works have been executed at the laboratory scale. There are few studies that have been performed at the piolet scale. For instance, photo-reactors such as packed bed, parabolic trough, fixed/fluidized bed, inclined plate, corrugated plate, and falling film were employed (Daghrir et al. 2012b) for the degradation of

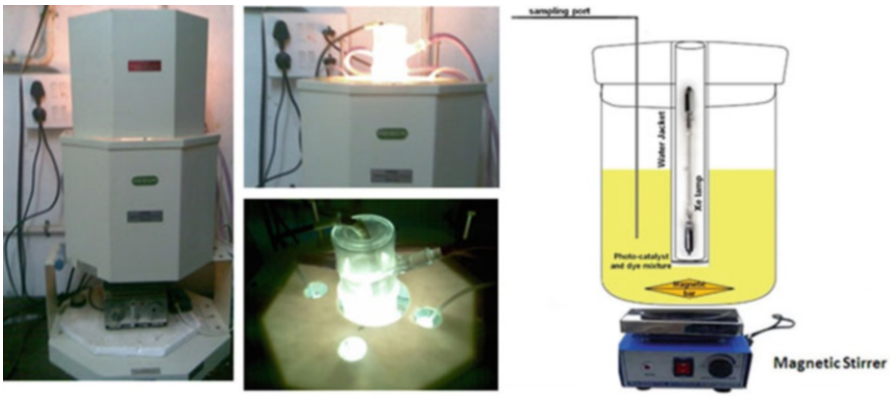

Fig. 11.13 The photographs and schematic of the immersion-type photo-reactor

various pollutants. Despite the promising results at the laboratory scale, more developments are required in the future for the degradation of persistent organic pollutants (other than dyes) and the treatment of real effluents (such as municipal and industrial effluents). Few research works reported for the photocatalytic degradation of real effluents such as wastewater from oil field (Christensen et al. 2003) and textile industry (Paschoal et al. 2009b; Baram et al. 2009). Sacco et al. studied the photocatalytic treatment of municipal wastewater using a pilot-scale packed-bed photo-reactor (Fig. 11.14) under visible/solar light irradiation. Nitrogen (N)-doped TiO_2 immobilized on polystyrene (PS) was used as photocatalyst. A solar compound triangular collector (CTC) was used to concentrate the solar light. *E.coli* in the municipal wastewater was successfully inactivated by the N-TiO_2/PS under direct solar light irradiation.

11.5.3 Cost and Energy

While selecting a cost-effective technology for the wastewater treatment, the factors such as effluent condition before/after treatment, robustness of the system, regulations, cost, and electric energy requirement (Bolton et al. 2001) should be considered. The use of photovoltaic materials with photocatalytic systems is an ideal solution to reduce the cost in terms of electricity demand and maintenance. A combination of photocatalysis with other sustainable technologies may be beneficial to achieve maximum efficiency in industrial effluent degradation. The photostability of nanoparticles is an important parameter that needs to be considered when commercializing the photocatalyst (Herrmann 2010). Moreover, the partially degraded contaminants block the active sites of the photocatalyst. This is attributed to the strong adsorption of intermediates on the active sites of a photocatalyst, indicating photocatalyst deactivation. Several efforts have been made to regenerate and reuse

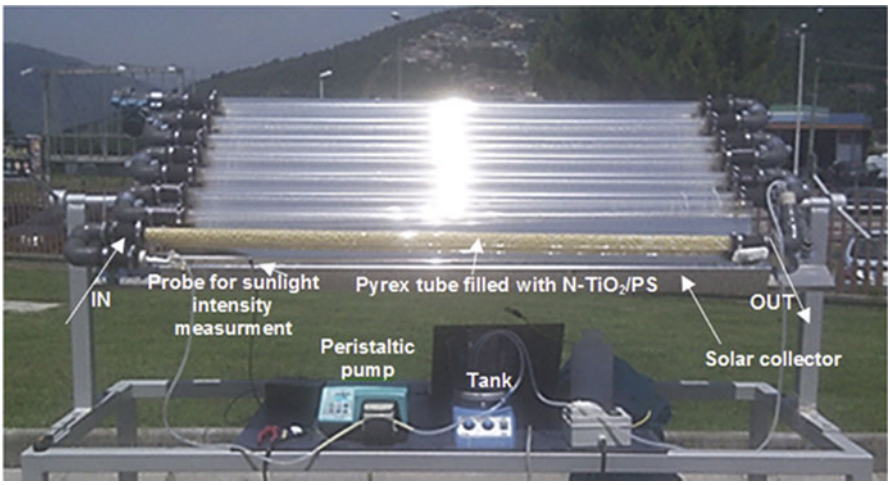

Fig. 11.14 Schematic of pilot-scale packed-bed solar photo-reactor. (Reprinted from Sacco et al. (2018) with permission from Elsevier)

the photocatalyst. Calcination (< 400 °C) in air (Pillai and Sahle–Demessie 2002), sonication with water and methanol (Shang et al. 2002), and irradiation with UV light in the presence of humid air (Ameen and Raupp 1999) or H_2O_2 (Piera et al. 2002) are the reported techniques to regenerate a photocatalyst surface.

Inspired by the structure and functionality of biological systems, recent studies are focused on the design of photoactive devices. For example, to imitate the photosynthesis of leaves, devices with hierarchical structure of leaves are developed by the researchers. In these artificial systems, chlorophyll (the natural pigment) is replaced by inorganic photocatalyst (Zhou et al. 2010). These biomimetic devices are known as "artificial leafs" (Nocera 2012; Cox et al. 2013).

11.6 Summary

Photocatalysis using TiO_2 nanoparticles is one of the eco-friendly technologies for inexhaustible solar energy conversion. The significant perspectives of TiO_2 nanoparticles for clean energy production and environmental remediation are summarized briefly in this chapter. We could mineralize the POPs, disinfect microbes (bacteria, virus, fungi), purify water/air, and produce energy (in the form of hydrogen) using TiO_2 photocatalysis. TiO_2-based products such as self-cleaning windows, paints, building materials, and portable depollution system are already commercialized in the market. The development of novel photocatalytic materials (2D materials, perovskites, etc.) with enhanced efficiency is one of the hot research areas in the recent years. Most of the research works in photocatalysis are carried out at the laboratory scale using high-intensity artificial lamps. Future research works should

be focused on the pilot-scale studies and commercialization of novel photocatalytic materials for various applications under natural solar light.

Acknowledgments Sivaraman Somasundaram is grateful to the Energy Technology Development Program of the Korea Institute of Energy Technology Evaluation and Planning (KETEP) for the financial support from the Ministry of Trade Industry & Energy, Republic of Korea (No.20163010012200).

References

Abdi A, Denoyelle A, Commenges-Bernole N, Trari M (2013) Photocatalytic hydrogen evolution on new mesoporous material Bi_2S_3/Y-zeolite. Int J Hydrog Energy 38(5):2070–2078. https://doi.org/10.1016/j.ijhydene.2012.11.085

Ahmed S, Rasul MG, Brown R, Hashib MA (2011) Influence of parameters on the heterogeneous photocatalytic degradation of pesticides and phenolic contaminants in wastewater: a short review. J Environ Manag 92(3):311–330. https://doi.org/10.1016/j.jenvman.2010.08.028

Alberici RM, Jardim WF (1997) Photocatalytic destruction of VOCs in the gas-phase using titanium dioxide. Appl Catal B Environ 14(1–2):55–68. https://doi.org/10.1016/S0926-3373(97)00012-X

Ali I, Kim J-O (2018) Visible-light-assisted photocatalytic activity of bismuth-TiO2 nanotube composites for chromium reduction and dye degradation. Chemosphere 207:285–292. https://doi.org/10.1016/j.chemosphere.2018.05.075

Almeida LC, Zanoni MV (2014) Decoration of Ti/TiO2 nanotubes with Pt nanoparticles for enhanced UV-Vis light absorption in photoelectrocatalytic process. J Braz Chem Soc 25 (3):579–588. https://doi.org/10.5935/0103-5053.20140034

Alrousan DM, Polo-López MI, Dunlop PS, Fernández-Ibáñez P, Byrne JA (2012) Solar photocatalytic disinfection of water with immobilised titanium dioxide in re-circulating flow CPC reactors. Appl Catal B Environ 128:126–134. https://doi.org/10.1016/j.apcatb.2012.07.038

Ameen MM, Raupp GB (1999) Reversible catalyst deactivation in the photocatalytic oxidation of diluteo-xylene in air. J Catal 184(1):112–122. https://doi.org/10.1006/jcat.1999.2442

Ananpattarachai J, Kajitvichyanukul P (2015) Photocatalytic degradation of p, p′-DDT under UV and visible light using interstitial N-doped TiO_2. J Environ Sci Health B 50(4):247–260. https://doi.org/10.1080/03601234.2015.999592

Andersen J, Pelaez M, Guay L, Zhang Z, O'Shea K, Dionysiou DD (2013) NF-TiO_2 photocatalysis of amitrole and atrazine with addition of oxidants under simulated solar light: emerging synergies, degradation intermediates, and reusable attributes. J Hazard Mater 260:569–575. https://doi.org/10.1016/j.jhazmat.2013.05.056

Anpo M, Yamashita H, Ichihashi Y, Fujii Y, Honda M (1997) Photocatalytic reduction of CO_2 with H_2O on titanium oxides anchored within micropores of zeolites: effects of the structure of the active sites and the addition of Pt. J Phys Chem B 101(14):2632–2636. https://doi.org/10.1021/jp962696h

Antoniou MG, Shoemaker JA, Armah A, Dionysiou DD (2008) LC/MS/MS structure elucidation of reaction intermediates formed during the TiO_2 photocatalysis of microcystin-LR. Toxicon 51 (6):1103–1118. https://doi.org/10.1016/j.toxicon.2008.01.018

Aris AZ, Shamsuddin AS, Praveena SM (2014) Occurrence of 17α-ethynylestradiol (EE2) in the environment and effect on exposed biota: a review. Environ Int 69:104–119. https://doi.org/10.1016/j.envint.2014.04.011

Aruna ST, Patil KC (1996) Synthesis and properties of nanosized titania. J Mater Synth Process 4 (3):175–180

Asahi RY, Morikawa TA, Ohwaki T, Aoki K, Taga Y (2001) Visible-light photocatalysis in nitrogen-doped titanium oxides. Science 293(5528):269–271. https://doi.org/10.1126/science.1061051

Ashkarran AA, Hamidinezhad H, Haddadi H, Mahmoudi M (2014) Double-doped TiO_2 nanoparticles as an efficient visible-light-active photocatalyst and antibacterial agent under solar simulated light. Appl Surf Sci 301:338–345. https://doi.org/10.1016/j.apsusc.2014.02.074

Baram N, Starosvetsky D, Starosvetsky J, Epshtein M, Armon R, Ein-Eli Y (2009) Enhanced inactivation of E. coli bacteria using immobilized porous TiO_2 photoelectrocatalysis. Electrochim Acta 54(12):3381–3386. https://doi.org/10.1016/j.electacta.2008.12.033

Baran D et al (2017) Reducing the efficiency–stability–cost gap of organic photovoltaics with highly efficient and stable small molecule acceptor ternary solar cells. Nat Mater 16:363. https://doi.org/10.1038/nmat4797

Barndõk H, Peláez M, Han C, Platten WE, Campo P, Hermosilla D, Blanco A, Dionysiou DD (2013) Photocatalytic degradation of contaminants of concern with composite NF-TiO_2 films under visible and solar light. Environ Sci Pollut Res 20(6):3582–3591. https://doi.org/10.1007/s11356-013-1550-z

Benedix R, Dehn F, Quaas J, Orgass M (2000) Application of titanium dioxide photocatalysis to create self-cleaning building materials. Lacer 5:157–168

Benotti MJ, Trenholm RA, Vanderford BJ, Holady JC, Stanford BD, Snyder SA (2009) Pharmaceuticals and endocrine disrupting compounds in US drinking water. Environ Sci Technol 43 (3):597–603. https://doi.org/10.1021/es801845a

Bessegato GG, Cardoso JC, da Silva BF, Zanoni MV (2014) Enhanced photoabsorption properties of composites of Ti/TiO_2 nanotubes decorated by Sb_2S_3 and improvement of degradation of hair dye. J Photochem Photobiol A Chem 276:96–103. https://doi.org/10.1016/j.jphotochem.2013.12.001

Bessegato GG, Cardoso JC, Zanoni MV (2015a) Enhanced photoelectrocatalytic degradation of an acid dye with boron-doped TiO_2 nanotube anodes. Catal Today 240:100–106. https://doi.org/10.1016/j.cattod.2014.03.073

Bessegato GG, Guaraldo TT, de Brito JF, Brugnera MF, Zanoni MV (2015b) Achievements and trends in photoelectrocatalysis: from environmental to energy applications. Electrocatalysis 6 (5):415–441. https://doi.org/10.1007/s12678-015-0259-9

Blake DM, Maness PC, Huang Z, Wolfrum EJ, Huang J, Jacoby WA (1999) Application of the photocatalytic chemistry of titanium dioxide to disinfection and the killing of cancer cells. Sep Purif Methods 28(1):1–50. https://doi.org/10.1080/03602549909351643

Bolton JR, Bircher KG, Tumas W, Tolman CA (2001) Figures-of-merit for the technical development and application of advanced oxidation technologies for both electric-and solar-driven systems (IUPAC Technical Report). Pure Appl Chem 73(4):627–637. https://doi.org/10.1351/pac200173040627

Bondioli F, Taurino R, Ferrari AM (2009) Functionalization of ceramic tile surface by sol–gel technique. J Colloid Interface Sci 334(2):195–201. https://doi.org/10.1016/j.jcis.2009.02.054

Bora LV, Mewada RK (2017) Visible/solar light active photocatalysts for organic effluent treatment: Fundamentals, mechanisms and parametric review. Renew Sust Energ Rev 76:1393–1421. https://doi.org/10.1016/j.rser.2017.01.130

Brugnera MF, Rajeshwar K, Cardoso JC, Zanoni MV (2010) Bisphenol A removal from wastewater using self-organized TIO_2 nanotubular array electrodes. Chemosphere 78(5):569–575. https://doi.org/10.1016/j.chemosphere.2009.10.058

Brugnera MF, Miyata M, Zocolo GJ, Leite CQ, Zanoni MV (2012) Inactivation and disposal of by-products from Mycobacterium smegmatis by photoelectrocatalytic oxidation using Ti/TiO_2-Ag nanotube electrodes. Electrochim Acta 85:33–41. https://doi.org/10.1016/j.electacta.2012.08.116

Brugnera MF, Miyata M, Leite CQ, Zanoni MV (2013a) Silver ion release from electrodes of nanotubes of TiO_2 impregnated with Ag nanoparticles applied in photoelectrocatalytic

disinfection. J Photochem Photobiol A Chem 278:1–8. https://doi.org/10.1016/j.jphotochem.2013.12.020

Brugnera MF, Miyata M, Zocolo GJ, Leite CQ, Zanoni MV (2013b) A photoelectrocatalytic process that disinfects water contaminated with Mycobacterium kansasii and Mycobacterium avium. Water Res 47(17):6596–6605. https://doi.org/10.1016/j.watres.2013.08.027

Cao B, Cao S, Dong P, Gao J, Wang J (2013) High antibacterial activity of ultrafine TiO_2/graphene sheets nanocomposites under visible light irradiation. Mater Lett 93:349–352. https://doi.org/10.1016/j.matlet.2012.11.136

Carneiro JO, Teixeira V, Portinha A, Magalhaes A, Coutinho P, Tavares CJ, Newton R (2007) Iron-doped photocatalytic TiO2 sputtered coatings on plastics for self-cleaning applications. Mater Sci Eng B 138(2):144–150. https://doi.org/10.1016/j.mseb.2005.08.130

Carp O, Huisman CL, Reller A (2004) Photoinduced reactivity of titanium dioxide. Prog Solid State Chem 32(1–2):33–177. https://doi.org/10.1016/j.progsolidstchem.2004.08.001

Chatterjee D, Dasgupta S (2005) Visible light induced photocatalytic degradation of organic pollutants. J Photochem Photobiol C: Photochem Rev 6(2–3):186–205. https://doi.org/10.1016/j.jphotochemrev.2005.09.001

Chen M, Chu JW (2011) NOx Photocatalytic degradation on active concrete road surface—from experiment to real-scale application. J Clean Prod 19(11):1266–1272. https://doi.org/10.1016/j.jclepro.2011.03.001

Chen X, Mao SS (2007) Titanium dioxide nanomaterials: synthesis, properties, modifications, and applications. Chem Rev 107(7):2891–2959. https://doi.org/10.1021/cr0500535

Chen J, Poon CS (2009) Photocatalytic construction and building materials: from fundamentals to applications. Build Environ 44(9):1899–1906. https://doi.org/10.1016/j.buildenv.2009.01.002

Chen Q, Liu H, Xin Y, Cheng X (2014) Coupling immobilized TiO_2 nanobelts and Au nanoparticles for enhanced photocatalytic and photoelectrocatalytic activity and mechanism insights. Chem Eng J 241:145–154. https://doi.org/10.1016/j.cej.2013.12.028

Cheng X, Liu H, Chen Q, Li J, Wang P (2013) Preparation and characterization of palladium nanocrystallite decorated TiO_2 nano-tubes photoelectrode and its enhanced photocatalytic efficiency for degradation of diclofenac. J Hazard Mater 254:141–148. https://doi.org/10.1016/j.jhazmat.2013.03.062

Cho M, Cates EL, Kim JH (2011) Inactivation and surface interactions of MS-2 bacteriophage in a TiO_2 photoelectrocatalytic reactor. Water Res 45(5):2104–2110 https://doi.org/10.1016/j.watres.2010.12.017

Choi H, Antoniou MG, Pelaez M, De la Cruz AA, Shoemaker JA, Dionysiou DD (2007) Mesoporous nitrogen-doped TiO_2 for the photocatalytic destruction of the cyanobacterial toxin microcystin-LR under visible light irradiation. Environ Sci Technol 41(21):7530–7535. https://doi.org/10.1021/es0709122

Chong MN, Jin B, Chow CW, Saint C (2010) Recent developments in photocatalytic water treatment technology: a review. Water Res 44(10):2997–3027. https://doi.org/10.1016/j.watres.2010.02.039

Christensen PA, Curtis TP, Egerton TA, Kosa SA, Tinlin JR (2003) Photoelectrocatalytic and photocatalytic disinfection of E. coli suspensions by titanium dioxide. Appl Catal B Environ 41(4):371–386 https://doi.org/10.1016/S0926-3373(02)00172-8

Coronado JM, Fresno F, Hernández-Alonso MD, Portela R (2013) Design of advanced photocatalytic materials for energy and environmental applications. Springer, London. https://doi.org/10.1007/978-1-4471-5061-9

Cox CR, Winkler MT, Pijpers JJ, Buonassisi T, Nocera DG (2013) Interfaces between water splitting catalysts and buried silicon junctions. Energy Environ Sci 6(2):532–538. https://doi.org/10.1039/C2EE23932A

Daghrir R, Drogui P, Ka I, El Khakani MA (2012a) Photoelectrocatalytic degradation of chlortetracycline using Ti/TiO_2 nanostructured electrodes deposited by means of a pulsed laser deposition process. J Hazard Mater 199:15–24. https://doi.org/10.1016/j.jhazmat.2011.10.022(a)

Daghrir R, Drogui P, Robert D (2012b) Photoelectrocatalytic technologies for environmental applications. J Photochem Photobiol A Chem 238:41–52. https://doi.org/10.1016/j.jphotochem.2012.04.009(b)

Daghrir R, Drogui P, Dimboukou-Mpira A, El Khakani MA (2013) Photoelectrocatalytic degradation of carbamazepine using Ti/TiO2 nanostructured electrodes deposited by means of a pulsed laser deposition process. Chemosphere 93(11):2756–2766. https://doi.org/10.1016/j.chemosphere.2013.09.031

Daghrir R, Drogui P, Delegan N, El Khakani MA (2014) Removal of chlortetracycline from spiked municipal wastewater using a photoelectrocatalytic process operated under sunlight irradiations. Sci Total Environ 466:300–305. https://doi.org/10.1016/j.scitotenv.2013.07.001

Dalton JS, Janes PA, Jones NG, Nicholson JA, Hallam KR, Allen GC (2002) Photocatalytic oxidation of NOx gases using TiO_2: a surface spectroscopic approach. Environ Pollut 120 (2):415–422. https://doi.org/10.1016/S0269-7491(02)00107-0

Dimitrijevic NM, Vijayan BK, Poluektov OG, Rajh T, Gray KA, He H, Zapol P (2011) Role of water and carbonates in photocatalytic transformation of CO_2 to CH_4 on titania. J Am Chem Soc 133(11):3964–3971. https://doi.org/10.1021/ja108791u

Dimitroula H, Daskalaki VM, Frontistis Z, Kondarides DI, Panagiotopoulou P, Xekoukoulotakis NP, Mantzavinos D (2012) Solar photocatalysis for the abatement of emerging micro-contaminants in wastewater: synthesis, characterization and testing of various TiO_2 samples. Appl Catal B Environ 117:283–291. https://doi.org/10.1016/j.apcatb.2012.01.024

Dunnill CW, Ansari Z, Kafizas A, Perni S, Morgan DJ, Wilson M, Parkin IP (2011) Visible light photocatalysts—N-doped TiO 2 by sol–gel, enhanced with surface bound silver nanoparticle islands. J Mater Chem 21(32):11854–11861. https://doi.org/10.1039/C1JM11557J

Egerton TA, Kosa SA, Christensen PA (2006) Photoelectrocatalytic disinfection of E. coli suspensions by iron doped TiO_2. Phys Chem Chem Phys 8(3):398–406. https://doi.org/10.1039/B507516E

Etacheri V, Michlits G, Seery MK, Hinder SJ, Pillai SC (2013) A highly efficient TiO_{2-x} C_x nanoheterojunction photocatalyst for visible light induced antibacterial applications. ACS Appl Mater Interfaces 5(5):1663–1672. https://doi.org/10.1021/am302676a

Fagan R, McCormack DE, Dionysiou DD, Pillai SC (2016) A review of solar and visible light active TiO_2 photocatalysis for treating bacteria, cyanotoxins and contaminants of emerging concern. Mater Sci Semicond Process 42:2–14. https://doi.org/10.1016/j.mssp.2015.07.052

Fallet M, Mahdjoub H, Gautier B, Bauer JP (2001) Electrochemical behaviour of ceramic sol–gel coatings on mild steel. J Non-Cryst Solids 293–295:527–533. https://doi.org/10.1016/S0022-3093(01)00770-0

Fateh R, Ismail AA, Dillert R, Bahnemann DW (2011) Highly active crystalline mesoporous TiO2 films coated onto polycarbonate substrates for self-cleaning applications. J Phys Chem C 115 (21):10405–10411. https://doi.org/10.1021/jp200892z

Fernandez A, Lassaletta G, Jimenez VM, Justo A, Gonzalez-Elipe AR, Herrmann JM, Tahiri H, Ait-Ichou Y (1995) Preparation and characterization of TiO2 photocatalysts supported on various rigid supports (glass, quartz and stainless steel). Comparative studies of photocatalytic activity in water purification. Appl Catal B Environ 7(1–2):49–63 https://doi.org/10.1016/0926-3373(95)00026-7

Fisher MB, Keane DA, Fernandez-Ibanez P, Colreavy J, Hinder SJ, McGuigan KG, Pillai SC (2013) Nitrogen and copper doped solar light active TiO2 photocatalysts for water decontamination. Appl Catal B Environ 130-131:8–13 https://doi.org/10.1016/j.apcatb.2012.10.013

Fotiou T, Triantis TM, Kaloudis T, Pastrana-Martínez LM, Likodimos V, Falaras P, Silva AM, Hiskia A (2013) Photocatalytic Degradation of Microcystin-LR and Off-Odor Compounds in Water under UV-A and Solar Light with a Nanostructured Photocatalyst Based on Reduced Graphene Oxide–TiO2 Composite. Identification of Intermediate Products. Ind Eng Chem Res 52(39):13991–14000. https://doi.org/10.1021/ie400382r

Fox MA, Dulay MT (1993) Heterogeneous photocatalysis. Chem Rev 93(1):341–357 DOI:0009-2665/93/0793-0341

Fraga LE, Anderson MA, Beatriz ML, Paschoal FM, Romão LP, Zanoni MV (2009) Evaluation of the photoelectrocatalytic method for oxidizing chloride and simultaneous removal of microcystin toxins in surface waters. Electrochim Acta 54(7):2069–2076 https://doi.org/10.1016/j.electacta.2008.08.060

Fresno F, Portela R, Suárez S, Coronado JM (2014) Photocatalytic materials: recent achievements and near future trends. J Mater Chem A 2(9):2863–2884. https://doi.org/10.1039/C3TA13793G

Fujihara K, Ohno T, Matsumura M (1998) Splitting of water by electrochemical combination of two photocatalytic reactions on TiO_2 particles. J Chem Soc Faraday Trans 94(24):3705–3709. https://doi.org/10.1039/A806398B

Fujishima A, Honda K (1972) Electrochemical photolysis of water at a semiconductor electrode. Nature 238(5358):37–38. https://doi.org/10.1038/238037a0

Fujishima A, Rao TN, Tryk DA (2000) Titanium dioxide photocatalysis. J Photochem Photobiol C: Photochem Rev 1(1):1–21. https://doi.org/10.1016/S1389-5567(00)00002-2

Ganguly P, Byrne C, Breen A, Pillai SC (2018) Antimicrobial activity of photocatalysts: fundamentals, mechanisms, kinetics and recent advances. Appl Catal B Environ 225:51–75. https://doi.org/10.1016/j.apcatb.2017.11.018

Gong J, Pu W, Yang C, Zhang J (2013) Novel one-step preparation of tungsten loaded TiO2 nanotube arrays with enhanced photoelectrocatalytic activity for pollutant degradation and hydrogen production. Catal Commun 36:89–93. https://doi.org/10.1016/j.catcom.2013.03.009

Graham D, Kisch H, Lawton LA, Robertson PK (2010) The degradation of microcystin-LR using doped visible light absorbing photocatalysts. Chemosphere 78(9):1182–1185. https://doi.org/10.1016/j.chemosphere.2009.12.003

Granados-Oliveros G, Páez-Mozo EA, Ortega FM, Ferronato C, Chovelon JM (2009) Degradation of atrazine using metalloporphyrins supported on TiO_2 under visible light irradiation. Appl Catal B Environ 89(3–4):448–454. https://doi.org/10.1016/j.apcatb.2009.01.001

Grätzel M (1999) Mesoporous oxide junctions and nanostructured solar cells. Curr Opin Colloid Interface Sci 4(4):314–321. https://doi.org/10.1016/S1359-0294(99)90013-4

Grätzel M (2001) Photoelectrochemical cells. Nature 414(6861):338–344. https://doi.org/10.1038/35104607

Grätzel M (2005) Solar energy conversion by dye-sensitized photovoltaic cells. Inorg Chem 44 (20):6841–6851. https://doi.org/10.1021/ic0508371

Gu A, Xiang W, Wang T, Gu S, Zhao X (2017) Enhance photovoltaic performance of tris (2, 2′-bipyridine) cobalt (II)/(III) based dye-sensitized solar cells via modifying TiO2 surface with metal-organic frameworks. Sol Energy 147:126–132. https://doi.org/10.1016/j.solener.2017.03.045

Guaraldo TT, Pulcinelli SH, Zanoni MB (2011) Influence of particle size on the photoactivity of Ti/TiO_2 thin film electrodes, and enhanced photoelectrocatalytic degradation of indigo carmine dye. J Photochem Photobiol A Chem 217(1):259–266. https://doi.org/10.1016/j.jphotochem.2010.10.019

Haroune L, Salaun M, Ménard A, Legault CY, Bellenger JP (2014) Photocatalytic degradation of carbamazepine and three derivatives using TiO_2 and ZnO: Effect of pH, ionic strength, and natural organic matter. Sci Total Environ 475:16–22. https://doi.org/10.1016/j.scitotenv.2013.12.104

Hashimoto K, Irie H, Fujishima A (2005) TiO_2 photocatalysis: a historical overview and future prospects. Jpn J Appl Phys 44(12R):8269–8285. https://doi.org/10.1143/JJAP.44.8269

Hassan M, Zhao Y, Xie B (2016) Employing TiO2 photocatalysis to deal with landfill leachate: current status and development. Chem Eng J 285:264–275. https://doi.org/10.1016/j.cej.2015.09.093

Heller A (1995) Chemistry and applications of photocatalytic oxidation of thin organic films. Acc Chem Res 28(12):503–508 doi:0001-4842/95/0128-0503

Henglein A (1997) Nanoclusters of semiconductors and metals: Colloidal nano-particles of semiconductors and metals: Electronic structure and processes. Ber Bunsenges Phys Chem 101 (11):1562–1572. https://doi.org/10.1002/bbpc.19971011103

Hernández-Alonso MD, Fresno F, Suárez S, Coronado JM (2009) Development of alternative photocatalysts to TiO_2: challenges anda opportunities. Energy Environ Sci 2(12):1231–1257. https://doi.org/10.1039/B907933E

Herrmann JM (2010) Photocatalysis fundamentals revisited to avoid several misconceptions. Appl Catal B Environ 99(3–4):461–468. https://doi.org/10.1016/j.apcatb.2010.05.012

Hidaka H, Shimura T, Ajisaka K, Horikoshi S, Zhao J, Serpone N (1997) Photoelectrochemical decomposition of amino acids on a TiO2/OTE particulate film electrode. J Photochem Photobiol A Chem 109(2):165–170. https://doi.org/10.1016/S1010-6030(97)00137-8

Hirano K, Inoue K, Yatsu T (1992) Photocatalysed reduction of CO_2 in aqueous TiO_2 suspension mixed with copper powder. J Photochem Photobiol A Chem 64(2):255–258 doi: 1010-6030/9285112-8

Hoffman AJ, Mills G, Yee H, Hoffmann MR (1992) Q-sized cadmium sulfide: synthesis, characterization, and efficiency of photoinitiation of polymerization of several vinylic monomers. J Phys Chem 96(13):5546–5552. https://doi.org/10.1021/j100192a067

Hoffmann MR, Martin ST, Choi W, Bahnemann DW (1995) Environmental applications of semiconductor photocatalysis. Chem Rev 95(1):69–96. https://doi.org/10.1021/cr00033a004

Howe RF (1998) Recent developments in photocatalysis. Asia Pac J Chem Eng 6(1–2):55–84. https://doi.org/10.1002/apj.5500060105

Hüsken G, Hunger M, Brouwers HJ (2009) Experimental study of photocatalytic concrete products for air purification. Build Environ 44(12):2463–2474. https://doi.org/10.1016/j.buildenv.2009.04.010

Ichiura H, Kitaoka T, Tanaka H (2003) Photocatalytic oxidation of NOx using composite sheets containing TiO_2 and a metal compound. Chemosphere 51(9):855–860. https://doi.org/10.1016/S0045-6535(03)00049-3

Inoue T, Fujishima A, Konishi S, Honda K (1979) Photoelectrocatalytic reduction of carbon dioxide in aqueous suspensions of semiconductor powders. Nature 277(5698):637–638. https://doi.org/10.1038/277637a0

Ishitani O, Inoue C, Suzuki Y, Ibusuki T (1993) Photocatalytic reduction of carbon dioxide to methane and acetic acid by an aqueous suspension of metal-deposited TiO_2. J Photochem Photobiol A Chem 72(3):269–271. https://doi.org/10.1016/1010-6030(93)80023-3

Jelic A, Gros M, Ginebreda A, Cespedes-Sánchez R, Ventura F, Petrovic M, Barcelo D (2011) Occurrence, partition and removal of pharmaceuticals in sewage water and sludge during wastewater treatment. Water Res 45(3):1165–1176. https://doi.org/10.1016/j.watres.2010.11.010

Ji J et al (2017) Mesoporous TiO2 under VUV irradiation: Enhanced photocatalytic oxidation for VOCs degradation at room temperature. Chem Eng J 327:490–499. https://doi.org/10.1016/j.cej.2017.06.130

Kabra K, Chaudhary R, Sawhney RL (2004) Treatment of hazardous organic and inorganic compounds through aqueous-phase photocatalysis: A review. Ind Eng Chem Res 43 (24):7683–7696. https://doi.org/10.1021/ie0498551

Kamaraj E, Somasundaram S, Balasubramani K, Eswaran MP, Muthuramalingam R, Park S (2018) Facile fabrication of CuO-Pb2O3 nanophotocatalyst for efficient degradation of Rose Bengal dye under visible light irradiation. Appl Surf Sci 433:206–212 https://doi.org/10.1016/j.apsusc.2017.09.139

Kasprzyk-Hordern B, Ziółek M, Nawrocki J (2003) Catalytic ozonation and methods of enhancing molecular ozone reactions in water treatment. Appl Catal B Environ 46(4):639–669 https://doi.org/10.1016/S0926-3373(03)00326-6

Kato S, Mashio F (1956) Autooxidation by TiO_2 as a photocatalyst Abstract Book Annual Meeting Chemical Society of Japan 223

Kato H, Asakura K, Kudo A (2003) Highly efficient water splitting into H_2 and O_2 over lanthanum-doped $NaTaO_3$ photocatalysts with high crystallinity and surface nanostructure. J Am Chem Soc 125(10):3082–3089. https://doi.org/10.1021/ja027751g

Kemme MR, Lateulere M, Maloney SW (1999) Reducing air pollutant emissions from solvent multi-base propellant production. Construction Engineering Research Lab (ARMY), Champaign. http://www.dtic.mil/dtic/tr/fulltext/u2/a367284.pdf

Kobosko SM, Jara DH, Kamat PV (2017) AgInS2–ZnS Quantum Dots: Excited State Interactions with TiO2 and Photovoltaic Performance. ACS Appl Mater Interfaces 9:33379–33388. https://doi.org/10.1021/acsami.6b14604

Kočí K, Obalová L, Lacný Z (2008) Photocatalytic reduction of CO_2 over TiO_2 based catalysts. Chem Pap 62(1):1–9. https://doi.org/10.2478/s11696-007-0072-x

Konstantinou IK, Albanis TA (2004) TiO_2-assisted photocatalytic degradation of azo dyes in aqueous solution: kinetic and mechanistic investigations: a review. Appl Catal B Environ 49 (1):1–4. https://doi.org/10.1016/j.apcatb.2003.11.010

Kwak BS, Vignesh K, Park N-K, Ryu H-J, Baek J-I, Kang M (2015) Methane formation from photoreduction of CO2 with water using TiO2 including Ni ingredient. Fuel 143:570–576. https://doi.org/10.1016/j.fuel.2014.11.066

Lan Y, Lu Y, Ren Z (2013) Mini review on photocatalysis of titanium dioxide nanoparticles and their solar applications. Nano Energy 2(5):1031–1045. https://doi.org/10.1016/j.nanoen.2013.04.002

Langridge JM, Gustafsson RJ, Griffiths PT, Cox RA, Lambert RM, Jones RL (2009) Solar driven nitrous acid formation on building material surfaces containing titanium dioxide: A concern for air quality in urban areas? Atmos Environ 43(32):5128–5131. https://doi.org/10.1016/j.atmosenv.2009.06.046

Lee J, Mahendra S, Alvarez PJ (2010) Nanomaterials in the construction industry: a review of their applications and environmental health and safety considerations. ACS Nano 4(7):3580–3590. https://doi.org/10.1021/nn100866w

Li XZ, Liu HL, Yue PT, Sun YP (2000) Photoelectrocatalytic oxidation of rose bengal in aqueous solution using a Ti/TiO2 mesh electrode. Environ Sci Technol 34(20):4401–4406. https://doi.org/10.1021/es000939k

Li D, Chen Z, Chen Y, Li W, Huang H, He Y, Fu X (2008) A new route for degradation of volatile organic compounds under visible light: Using the bifunctional photocatalyst Pt/TiO_2- xNx in H_2-O_2 atmosphere. Environ Sci Technol 42(6):2130–2135. https://doi.org/10.1021/es702465g

Li A, Zhao X, Liu H, Qu J (2011) Characteristic transformation of humic acid during photoelectrocatalysis process and its subsequent disinfection byproduct formation potential. Water Res 45(18):6131–6140. https://doi.org/10.1016/j.watres.2011.09.012

Li G, Liu X, Zhang H, Wong PK, An T, Zhao H (2013) Comparative studies of photocatalytic and photoelectrocatalytic inactivation of E. coli in presence of halides. Appl Catal B Environ 140:225–232 https://doi.org/10.1016/j.apcatb.2013.04.004

Li R, Williams SE, Li Q, Zhang J, Yang C, Zhou A (2014) Photoelectrocatalytic degradation of ofloxacin using highly ordered TiO_2 nanotube arrays. Electrocatalysis 5(4):379–386. https://doi.org/10.1007/s12678-014-0204-3

Linsebigler AL, Lu G, Yates JT Jr (1995) Photocatalysis on TiO_2 surfaces: principles, mechanisms, and selected results. Chem Rev 95(3):735–758 doi:0009-2665/95/0795-0735

Liu Y, Li J, Qiu X, Burda C (2006) Novel TiO_2 Nanocatalysts for Wastewater Purification-Tapping Energy from the Sun. Water Pract Technol 1(4):wpt2006073. https://doi.org/10.2166/wpt.2006.073

Liu H, Liu G, Shi X (2010) N/Zr-codoped TiO_2 nanotube arrays: fabrication, characterization, and enhanced photocatalytic activity. Colloids Surf A Physicochem Eng Asp 363(1–3):35–40. https://doi.org/10.1016/j.colsurfa.2010.04.010

Liu G, Jimmy CY, Lu GQ, Cheng HM (2011) Crystal facet engineering of semiconductor photocatalysts: motivations, advances and unique properties. Chem Commun 47 (24):6763–6783. https://doi.org/10.1039/C1CC10665A

Liu H, Cao X, Liu G, Wang Y, Zhang N, Li T, Tough R (2013) Photoelectrocatalytic degradation of triclosan on TiO2 nanotube arrays and toxicity change. Chemosphere 93(1):160–165. https://doi.org/10.1016/j.chemosphere.2013.05.018

Liu X, Zhang H, Liu C, Chen J, Li G, An T, Wong PK, Zhao H (2014) UV and visible light photoelectrocatalytic bactericidal performance of 100%{1 1 1} faceted rutile TiO_2 photoanode. Catal Today 224:77–82. https://doi.org/10.1016/j.cattod.2013.09.041

Liu B, Mu L, Han B, Zhang J, Shi H (2017a) Fabrication of TiO2/Ag2O heterostructure with enhanced photocatalytic and antibacterial activities under visible light irradiation. Appl Surf Sci 396:1596–1603. https://doi.org/10.1016/j.apsusc.2016.11.220

Liu K, Wang G, Meng M, Chen S, Li J, Sun X, Yuan H, Sun L, Qin N (2017b) TiO2 nanotube photonic crystal fabricated by two-step anodization method for enhanced photoelectrochemical water splitting. Mater Lett 207:96–99. https://doi.org/10.1016/j.matlet.2017.07.060

Low J, Cheng B, Yu J (2017) Surface modification and enhanced photocatalytic CO2 reduction performance of TiO2: a review. Appl Surf Sci 392:658–686. https://doi.org/10.1016/j.apsusc.2016.09.093

Lu N, Chen S, Wang H, Quan X, Zhao H (2008) Synthesis of molecular imprinted polymer modified TiO_2 nanotube array electrode and their photoelectrocatalytic activity. J Solid State Chem 181(10):2852–2858. https://doi.org/10.1016/j.jssc.2008.07.004

Maeda K, Domen K (2010) Photocatalytic water splitting: recent progress and future challenges. J Phys Chem Lett 1(18):2655–2661. https://doi.org/10.1021/jz1007966

Mahadik MA, An GW, David S, Choi SH, Cho M, Jang JS (2017) Fabrication of A/R-TiO2 composite for enhanced photoelectrochemical performance: solar hydrogen generation and dye degradation. Appl Surf Sci 426:833–843. https://doi.org/10.1016/j.apsusc.2017.07.179

Malato S, Fernández-Ibáñez P, Maldonado MI, Blanco J, Gernjak W (2009) Decontamination and disinfection of water by solar photocatalysis: recent overview and trends. Catal Today 147 (1):1–59. https://doi.org/10.1016/j.cattod.2009.06.018

Mamaghani AH, Haghighat F, Lee C-S (2017) Photocatalytic oxidation technology for indoor environment air purification: the state-of-the-art. Appl Catal B Environ 203:247–269. https://doi.org/10.1016/j.apcatb.2016.10.037

Mamane H, Horovitz I, Lozzi L, Di Camillo D, Avisar D (2014) The role of physical and operational parameters in photocatalysis by N-doped TiO_2 sol–gel thin films. Chem Eng J 257:159–169. https://doi.org/10.1016/j.cej.2014.07.018

Markowska-Szczupak A, Ulfig K, Morawski AW (2011) The application of titanium dioxide for deactivation of bioparticulates: an overview. Catal Today 169(1):249–257. https://doi.org/10.1016/j.cattod.2010.11.055

Matsunaga T, Tomoda R, Nakajima T, Wake H (1985) Photoelectrochemical sterilization of microbial cells by semiconductor powders. FEMS Microbiol Lett 29(1–2):211–214. https://doi.org/10.1111/j.1574-6968.1985.tb00864.x

Miao Y, Xu X, Liu K, Wang N (2017) Preparation of novel Cu/TiO2 mischcrystal composites and antibacterial activities for Escherichia coli under visible light. Ceram Int 43:9658–9663. https://doi.org/10.1016/j.ceramint.2017.04.137

Miranda-García N, Suárez S, Sánchez B, Coronado JM, Malato S, Maldonado MI (2011) Photocatalytic degradation of emerging contaminants in municipal wastewater treatment plant effluents using immobilized TiO_2 in a solar pilot plant. Appl Catal B Environ 103 (3–4):294–301. https://doi.org/10.1016/j.apcatb.2011.01.030

Mitoraj D, Jańczyk A, Strus M, Kisch H, Stochel G, Heczko PB, Macyk W (2007) Visible light inactivation of bacteria and fungi by modified titanium dioxide. Photochem Photobiol Sci 6 (6):642–648. https://doi.org/10.1039/B617043A

Mueses MA, Machuca-Martinez F, Puma GL (2013) Effective quantum yield and reaction rate model for evaluation of photocatalytic degradation of water contaminants in heterogeneous pilot-scale solar photoreactors. Chem Eng J 215:937–947. https://doi.org/10.1016/j.cej.2012.11.076

Navarro Yerga RM, Álvarez Galván MC, Del Valle F, Villoria de la Mano JA, Fierro JL (2009) Water Splitting on Semiconductor Catalysts under Visible-Light Irradiation. Chem Sus Chem 2 (6):471–485. https://doi.org/10.1002/cssc.200900018

Nazeeruddin MK, Kay A, Rodicio I, Humphry-Baker R, Müller E, Liska P, Vlachopoulos N, Grätzel M (1993) Conversion of light to electricity by cis-X_2bis (2,2′-bipyridyl-4,4-′-dicarboxylate) ruthenium (II) charge-transfer sensitizers (X= Cl^-, Br^-, I^-, CN^-, and SCN^-) on nanocrystalline titanium dioxide electrodes. J Am Chem Soc 115(14): 6382–6390. doi:0002-7863/93/1515-63

Nazeri A, Trzaskoma-Paulette PP, Bauer D (1997) Synthesis and properties of cerium and titanium oxide thin coatings for corrosion protection of 304 stainless steel. J Sol-Gel Sci Technol 10 (3):317–331. https://doi.org/10.1023/A:1018381503008

Ni M, Leung MK, Leung DY, Sumathy K (2007) A review and recent developments in photocatalytic water-splitting using TiO_2 for hydrogen production. Renew Sust Energ Rev 11 (3):401–425. https://doi.org/10.1016/j.rser.2005.01.009

Nie X, Li G, Gao M, Sun H, Liu X, Zhao H, Wong PK, An T (2014a) Comparative study on the photoelectrocatalytic inactivation of Escherichia coli K-12 and its mutant Escherichia coli BW25113 using TiO2 nanotubes as a photoanode. Appl Catal B Environ 147:562–570. https://doi.org/10.1016/j.apcatb.2013.09.037

Nie X, Li G, Wong PK, Zhao H, An T (2014b) Synthesis and characterization of N-doped carbonaceous/TiO2 composite photoanodes for visible-light photoelectrocatalytic inactivation of Escherichia coli K-12. Catal Today 230:67–73. https://doi.org/10.1016/j.cattod.2013.09.046

Nie C, Liu L, He R (2018) Pt/TiO2-ZnO in a circuit Photo-electro-catalytically removed HCHO for outstanding indoor air purification. Sep Purif Technol 206:316–323. https://doi.org/10.1016/j.seppur.2018.06.024

Nocera DG (2012) The artificial leaf. Acc Chem Res 45(5):767–776. https://doi.org/10.1021/ar2003013

Nosaka Y, Nosaka AY (2017) Generation and detection of reactive oxygen species in photocatalysis. Chem Rev 117:11302–11336. https://doi.org/10.1021/acs.chemrev.7b00161

Nozik AJ (1977) Photochemical diodes. Appl Phys Lett 30(11):567–570. https://doi.org/10.1063/1.89262

Ohno T, Bai L, Hisatomi T, Maeda K, Domen K (2012) Photocatalytic water splitting using modified GaN: ZnO solid solution under visible light: long-time operation and regeneration of activity. J Am Chem Soc 134(19):8254–8259. https://doi.org/10.1021/ja302479f

Oliveira HG, Ferreira LH, Bertazzoli R, Longo C (2015) Remediation of 17-α-ethinylestradiol aqueous solution by photocatalysis and electrochemically-assisted photocatalysis using TiO_2 and TiO_2/WO_3 electrodes irradiated by a solar simulator. Water Res 72:305–314. https://doi.org/10.1016/j.watres.2014.08.042

O'regan B, Grätzel M (1991) A low-cost, high-efficiency solar cell based on dye-sensitized colloidal TiO2 films. Nature 353(6346):737–740. https://doi.org/10.1038/353737a0

Osugi ME, Umbuzeiro GA, Anderson MA, Zanoni MV (2005) Degradation of metallophtalocyanine dye by combined processes of electrochemistry and photoelectrochemistry. Electrochim Acta 50(25–26):5261–5269. https://doi.org/10.1016/j.electacta.2005.01.058

Pan Z, Stemmler EA, Cho HJ, Fan W, LeBlanc LA, Patterson HH, Amirbahman A (2014) Photocatalytic degradation of 17α-ethinylestradiol (EE2) in the presence of TiO_2-doped zeolite. J Hazard Mater 279:17–25. https://doi.org/10.1016/j.jhazmat.2014.06.040

Papailias I, Todorova N, Giannakopoulou T, Yu J, Dimotikali D, Trapalis C (2017) Photocatalytic activity of modified g-C3N4/TiO2 nanocomposites for NOx removal. Catal Today 280:37–44. https://doi.org/10.1016/j.cattod.2016.06.032

Park H, Bak A, Ahn YY, Choi J, Hoffmannn MR (2012) Photoelectrochemical performance of multi-layered BiOx–TiO_2/Ti electrodes for degradation of phenol and production of molecular hydrogen in water. J Hazard Mater 211:47–54. https://doi.org/10.1016/j.jhazmat.2011.05.009

Parkin IP, Palgrave RG (2005) Self-cleaning coatings. J Mater Chem 15(17):1689–1695. https://doi.org/10.1039/B412803F

Paschoal FM, Anderson MA, Zanoni MV (2009a) Simultaneous removal of chromium and leather dye from simulated tannery effluent by photoelectrochemistry. J Hazard Mater 166(1):531–537. https://doi.org/10.1016/j.jhazmat.2008.11.058

Paschoal FM, Anderson MA, Zanoni MV (2009b) The photoelectrocatalytic oxidative treatment of textile wastewater containing disperse dyes. Desalination 249(3):1350–1355. https://doi.org/10.1016/j.desal.2009.06.024(2009b)

Paspaltsis I, Kotta K, Lagoudaki R, Grigoriadis N, Poulios I, Sklaviadis T (2006) Titanium dioxide photocatalytic inactivation of prions. J Gen Virol 87(10):3125–3130. https://doi.org/10.1099/vir.0.81746-0

Patsoura A, Kondarides DI, Verykios XE (2007) Photocatalytic degradation of organic pollutants with simultaneous production of hydrogen. Catal Today 124(3–4):94–102. https://doi.org/10.1016/j.cattod.2007.03.028

Paz Y (2010) Application of TiO_2 photocatalysis for air treatment: Patents' overview. Appl Catal B Environ 99(3–4):448–460. https://doi.org/10.1016/j.apcatb.2010.05.011

Pelaez M, Falaras P, Likodimos V, Kontos AG, Armah A, O'shea K, Dionysiou DD (2010) Synthesis, structural characterization and evaluation of sol–gel-based NF-TiO_2 films with visible light-photoactivation for the removal of microcystin-LR. Appl Catal B Environ 99(3–4):378–387. https://doi.org/10.1016/j.apcatb.2010.06.017

Pelaez M, Armah A, O'Shea K, Falaras P, Dionysiou DD (2011) Effects of water parameters on the degradation of microcystin-LR under visible light-activated TiO_2 photocatalyst. Water Res 45(12):3787–3796. https://doi.org/10.1016/j.watres.2011.04.036

Pelaez M, Falaras P, Kontos AG, Armah A, O'shea K, Dunlop PS, Byrne JA, Dionysiou DD (2012) A comparative study on the removal of cylindrospermopsin and microcystins from water with NF-TiO_2-P25 composite films with visible and UV–vis light photocatalytic activity. Appl Catal B Environ 121:30–39. https://doi.org/10.1016/j.apcatb.2012.03.010

Peng Y-P, Chen H, Huang C (2017) The synergistic effect of photoelectrochemical (PEC) reactions exemplified by concurrent perfluorooctanoic acid (PFOA) degradation and hydrogen generation over carbon and nitrogen codoped TiO2 nanotube arrays (CN-TNTAs) photoelectrode. Appl Catal B Environ 209:437–446. https://doi.org/10.1016/j.apcatb.2017.02.084

Philippidis N, Sotiropoulos S, Efstathiou A, Poulios I (2009) Photoelectrocatalytic degradation of the insecticide imidacloprid using TiO_2/Ti electrodes. J Photochem Photobiol A Chem 204(2–3):129–136. https://doi.org/10.1016/j.jphotochem.2009.03.007

Philippidis N, Nikolakaki E, Sotiropoulos S, Poulios I (2010) Photoelectrocatalytic inactivation of E. coli XL-1 blue colonies in water. J Chem Technol Biotechnol 85(8):1054–1060. https://doi.org/10.1002/jctb.2394

Pi Y, Li Z, Xu D, Liu J, Li Y, Zhang F, Zhang G, Peng W, Fan X (2017) 1T-Phase MoS2 Nanosheets on TiO2 Nanorod Arrays: 3D Photoanode with Extraordinary Catalytic Performance. ACS Sustain Chem Eng 5:5175–5182. https://doi.org/10.1021/acssuschemeng.7b00518

Piera E, Ayllón JA, Doménech X, Peral J (2002) TiO_2 deactivation during gas-phase photocatalytic oxidation of ethanol. Catal Today 76(2–4):259–270. https://doi.org/10.1016/S0920-5861(02)00224-9

Pillai UR, Sahle–Demessie E (2002) Selective oxidation of alcohols in gas phase using light-activated titanium dioxide. J Catal 211(2):434–444. https://doi.org/10.1006/jcat.2002.3771

Podporska-Carroll J, Panaitescu E, Quilty B, Wang L, Menon L, Pillai SC (2015) Antimicrobial properties of highly efficient photocatalytic TiO_2 nanotubes. Appl Catal B Environ 176–177:70–75. https://doi.org/10.1016/j.apcatb.2015.03.029

Prieto-Rodriguez L, Miralles-Cuevas S, Oller I, Fernández-Ibáñez P, Agüera A, Blanco J, Malato S (2012a) Optimization of mild solar TiO_2 photocatalysis as a tertiary treatment for municipal wastewater treatment plant effluents. Appl Catal B Environ 128:119–125. https://doi.org/10.1016/j.apcatb.2012.03.034(a)

Prieto-Rodriguez L, Miralles-Cuevas S, Oller I, Agüera A, Puma GL, Malato S (2012b) Treatment of emerging contaminants in wastewater treatment plants (WWTP) effluents by solar

photocatalysis using low TiO_2 concentrations. J Hazard Mater 211:131–137. https://doi.org/10.1016/j.jhazmat.2011.09.008 b

Puma GL, Bono A, Krishnaiah D, Collin JG (2008) Preparation of titanium dioxide photocatalyst loaded onto activated carbon support using chemical vapor deposition: a review paper. J Hazard Mater 157(2–3):209–219. https://doi.org/10.1016/j.jhazmat.2008.01.040

Qi K, Daoud WA, Xin JH, Mak CL, Tang W, Cheung WP (2006) Self-cleaning cotton. J Mater Chem 16(47):4567–4574. https://doi.org/10.1039/B610861J

Qian X, Ren M, Yue D, Zhu Y, Han Y, Bian Z, Zhao Y (2017) Mesoporous TiO2 films coated on carbon foam based on waste polyurethane for enhanced photocatalytic oxidation of VOCs. Appl Catal B Environ 212:1–6. https://doi.org/10.1016/j.apcatb.2017.04.059

Qu X, Alvarez PJ, Li Q (2013) Applications of nanotechnology in water and wastewater treatment. Water Res 47(12):3931–3946. https://doi.org/10.1016/j.watres.2012.09.058

Rahmawati F, Kusumaningsih T, Hapsari AM, Hastuti A (2010) Ag and Cu loaded on TiO_2/graphite as a catalyst for Escherichia coli-contaminated water disinfection. Chem Pap 64 (5):557–5565. https://doi.org/10.2478/s11696-010-0036-4

Reddy PVL, Kavitha B, Reddy PAK, Kim K-H (2017) TiO2-based photocatalytic disinfection of microbes in aqueous media: a review. Environ Res 154:296–303. https://doi.org/10.1016/j.envres.2017.01.018

Rengifo-Herrera JA, Mielczarski E, Mielczarski J, Castillo NC, Kiwi J, Pulgarin C (2008) Escherichia coli inactivation by N, S co-doped commercial TiO_2 powders under UV and visible light. Appl Catal B Environ 84(3–4):448–456. https://doi.org/10.1016/j.apcatb.2008.04.030

Rengifo-Herrera JA, Pierzchała K, Sienkiewicz A, Forro L, Kiwi J, Pulgarin C (2009a) Abatement of organics and Escherichia coli by N, S co-doped TiO_2 under UV and visible light. Implications of the formation of singlet oxygen ($^1O_2$) under visible light. Appl Catal B Environ 88 (3–4):398–406. https://doi.org/10.1016/j.apcatb.2008.10.025(a)

Rengifo-Herrera JA, Kiwi J, Pulgarin C (2009b) N, S co-doped and N-doped Degussa P-25 powders with visible light response prepared by mechanical mixing of thiourea and urea. Reactivity towards E. coli inactivation and phenol oxidation. J Photochem Photobiol A Chem 205(2–3):109–115. https://doi.org/10.1016/j.jphotochem.2009.04.015 b

Rizzo L, Meric S, Guida M, Kassinos D, Belgiorno V (2009) Heterogenous photocatalytic degradation kinetics and detoxification of an urban wastewater treatment plant effluent contaminated with pharmaceuticals. Water Res 43(16):4070–4078. https://doi.org/10.1016/j.watres.2009.06.046

Rozhkova EA, Ulasov I, Lai B, Dimitrijevic NM, Lesniak MS, Rajh T (2009) A high-performance nanobio photocatalyst for targeted brain cancer therapy. Nano Lett 9(9):3337–3342. https://doi.org/10.1021/nl901610f

Ryu SY, Balcerski W, Lee TK, Hoffmann MR (2007) Photocatalytic production of hydrogen from water with visible light using hybrid catalysts of CdS attached to microporous and mesoporous silicas. J Phys Chem C 111(49):18195–18203. https://doi.org/10.1021/jp074860e

Sacco O, Vaiano V, Rizzo L, Sannino D (2018) Photocatalytic activity of a visible light active structured photocatalyst developed for municipal wastewater treatment. J Clean Prod 175:38–49. https://doi.org/10.1016/j.jclepro.2017.11.088

Selcuk H (2010) Disinfection and formation of disinfection by-products in a photoelectrocatalytic system. Water Res 44(13):3966–3972. https://doi.org/10.1016/j.watres.2010.04.034

Senthilnathan J, Philip L (2010) Photocatalytic degradation of lindane under UV and visible light using N-doped TiO_2. Chem Eng J 161(1–2):83–92. https://doi.org/10.1016/j.cej.2010.04.034

Shang J, Zhu Y, Du Y, Xu Z (2002) Comparative studies on the deactivation and regeneration of TiO_2 nanoparticles in three photocatalytic oxidation systems: C_7H_{16}, SO_2, and C_7H_{16}–SO_2. J Solid State Chem 166(2):395–399. https://doi.org/10.1006/jssc.2002.9613

Shao GS, Ma TY, Zhang XJ, Ren TZ, Yuan ZY (2009) Phosphorus and nitrogen co-doped titania photocatalysts with a hierarchical meso−/macroporous structure. J Mater Sci 44 (24):6754–6763. https://doi.org/10.1007/s10853-009-3628-z

Silva CP, Otero M, Esteves V (2012) Processes for the elimination of estrogenic steroid hormones from water: a review. Environ Pollut 165:38–58. https://doi.org/10.1016/j.envpol.2012.02.002

Skalska K, Miller JS, Ledakowicz S (2010) Trends in NOx abatement: A review. Sci Total Environ 408(19):3976–3989. https://doi.org/10.1016/j.scitotenv.2010.06.001

Šojić DV, Despotović VN, Abazović ND, Čomor MI, Abramović BF (2010) Photocatalytic degradation of selected herbicides in aqueous suspensions of doped titania under visible light irradiation. J Hazard Mater 179(1–3):49–56. https://doi.org/10.1016/j.jhazmat.2010.02.055

Subagio DP, Srinivasan M, Lim M, Lim TT (2010) Photocatalytic degradation of bisphenol-A by nitrogen-doped TiO_2 hollow sphere in a vis-LED photoreactor. Appl Catal B Environ 95 (3–4):414–422. https://doi.org/10.1016/j.apcatb.2010.01.021

Sun W, Li S, Mai J, Ni J (2010) Initial photocatalytic degradation intermediates/pathways of 17α-ethynylestradiol: Effect of pH and methanol. Chemosphere 81(1):92–99. https://doi.org/10.1016/j.chemosphere.2010.06.051

Swetha S, Santhosh SM, Geetha Balakrishna R (2010) Enhanced Bactericidal Activity of Modified Titania in Sunlight against Pseudomonas aeruginosa, a Water-Borne Pathogen. Photochem Photobiol 86(5):1127–1134. https://doi.org/10.1111/j.1751-1097.2010.00781.x

Takata Y, Hidaka S, Cao JM, Nakamura T, Yamamoto H, Masuda M, Ito T (2005) Effect of surface wettability on boiling and evaporation. Energy 30(2–4):209–220. https://doi.org/10.1016/j.energy.2004.05.004

Teh CM, Mohamed AR (2011) Roles of titanium dioxide and ion-doped titanium dioxide on photocatalytic degradation of organic pollutants (phenolic compounds and dyes) in aqueous solutions: a review. J Alloys Compd 509(5):1648–1660. https://doi.org/10.1016/j.jallcom.2010.10.181

Tung WS, Daoud WA (2009) Effect of wettability and silicone surface modification on the self-cleaning functionalization of wool. J Appl Polym Sci 112(1):235–243. https://doi.org/10.1002/app.29396

Tung WS, Daoud WA (2011) Self-cleaning fibers via nanotechnology: a virtual reality. J Mater Chem 21(22):7858–7869. https://doi.org/10.1039/C0JM03856C

Tüysüz H, Chan CK (2013) Preparation of amorphous and nanocrystalline sodium tantalum oxide photocatalysts with porous matrix structure for overall water splitting. Nano Energy 2 (1):116–123. https://doi.org/10.1016/j.nanoen.2012.08.003

Ullattil SG, Narendranath SB, Pillai SC, Periyat P (2018) Black TiO2 Nanomaterials: A Review of Recent Advances. Chem Eng J 343:708–736. https://doi.org/10.1016/j.cej.2018.01.069

Vega-Morales T, Sosa-Ferrera Z, Santana-Rodríguez JJ (2010) Determination of alkylphenol polyethoxylates, bisphenol-A, 17α-ethynylestradiol and 17β-estradiol and its metabolites in sewage samples by SPE and LC/MS/MS. J Hazard Mater 183(1–3):701–711. https://doi.org/10.1016/j.jhazmat.2010.07.083

Venieri D, Chatzisymeon E, Sofianos SS, Politi E, Xekoukoulotakis NP, Katsaounis A, Mantzavinos D (2012) Removal of faecal indicator pathogens from waters and wastewaters by photoelectrocatalytic oxidation on TiO_2/Ti films under simulated solar radiation. Environ Sci Pollut Res 19(9):3782–3790. https://doi.org/10.1007/s11356-012-0768-5

Venieri D, Chatzisymeon E, Politi E, Sofianos SS, Katsaounis A, Mantzavinos D (2013) Photoelectrocatalytic disinfection of water and wastewater: performance evaluation by qPCR and culture techniques. J Water Health 11(1):21–29. https://doi.org/10.2166/wh.2012.208

Vidal A, Dıaz AI, El Hraiki A, Romero M, Muguruza I, Senhaji F, González J (1999) Solar photocatalysis for detoxification and disinfection of contaminated water: pilot plant studies. Catal Today 54(2–3):283–290. https://doi.org/10.1016/S0920-5861(99)00189-3

Vignesh K, Hariharan R, Rajarajan M, Suganthi A (2013) Visible light assisted photocatalytic activity of TiO2–metal vanadate (M= Sr, Ag and Cd) nanocomposites. Mater Sci Semicond Process 16:1521–1530

Vignesh K, Priyanka R, Hariharan R, Rajarajan M, Suganthi A (2014a) Fabrication of CdS and CuWO4 modified TiO2 nanoparticles and its photocatalytic activity under visible light irradiation. J Ind Eng Chem 20:435–443. https://doi.org/10.1016/j.jiec.2013.04.038

Vignesh K, Suganthi A, Min B-K, Kang M (2014b) Photocatalytic activity of magnetically recoverable MnFe2O4/g-C3N4/TiO2 nanocomposite under simulated solar light irradiation. J Mol Catal A Chem 395:373–383. https://doi.org/10.1016/j.molcata.2014.08.040

Wang X, Lim TT (2010) Solvothermal synthesis of C–N codoped TiO_2 and photocatalytic evaluation for bisphenol A degradation using a visible-light irradiated LED photoreactor. Appl Catal B Environ 100(1–2):355–364 https://doi.org/10.1016/j.apcatb.2010.08.012

Wang R, Hashimoto K, Fujishima A, Chikuni M, Kojima E, Kitamura A, Shimohigoshi M, Watanabe T (1997) Light-induced amphiphilic surfaces. Nature 388(6641):431–432. https://doi.org/10.1038/41233

Wang P, Fane AG, Lim TT (2013) Evaluation of a submerged membrane vis-LED photoreactor (sMPR) for carbamazepine degradation and TiO_2 separation. Chem Eng J 215:240–251 https://doi.org/10.1016/j.cej.2012.10.075

Wang D, Li Y, Puma GL, Wang C, Wang P, Zhang W, Wang Q (2015) Mechanism and experimental study on the photocatalytic performance of Ag/AgCl@ chiral TiO2 nanofibers photocatalyst: The impact of wastewater components. J Hazard Mater 285:277–284 https://doi.org/10.1016/j.jhazmat.2014.10.060

Watanabe T, Nakajima A, Wang R, Minabe M, Koizumi S, Fujishima A, Hashimoto K (1999) Photocatalytic activity and photoinduced hydrophilicity of titanium dioxide coated glass. Thin Solid Films 30;351(1–2):260–263. https://doi.org/10.1016/S0040-6090(99)00205-9

Wei Z, Sun J, Xie Z, Liang M, Chen S (2010) Removal of gaseous toluene by the combination of photocatalytic oxidation under complex light irradiation of UV and visible light and biological process. J Hazard Mater 15;177(1–3):814–821. https://doi.org/10.1016/j.jhazmat.2009.12.106

Wenderich K, Mul G (2016) Methods, mechanism, and applications of photodeposition in photocatalysis: a review. Chem Rev 116:14587–14619. https://doi.org/10.1021/acs.chemrev.6b00327

Wold A (1993) Photocatalytic properties of titanium dioxide (TiO_2). Chem Mater 5(3):280–283. https://doi.org/10.1021/cm00027a008

Woolerton TW, Sheard S, Reisner E, Pierce E, Ragsdale SW, Armstrong FA (2010) Efficient and clean photoreduction of CO_2 to CO by enzyme-modified TiO_2 nanoparticles using visible light. J Am Chem Soc 132(7):2132–2133. https://doi.org/10.1021/ja910091z

Wu JC, Chiou CH (2008) Photoreduction of CO_2 over Ruthenium dye-sensitized TiO_2-based catalysts under concentrated natural sunlight. Catal Commun 9(10):2073–2076. https://doi.org/10.1016/j.catcom.2008.04.004

Wu JC, Lin HM, Lai CL (2005) Photo reduction of CO_2 to methanol using optical-fiber photoreactor. Appl Catal A Gen 296(2):194–200. https://doi.org/10.1016/j.apcata.2005.08.021

Xie TH, Lin J (2007) Origin of photocatalytic deactivation of TiO2 film coated on ceramic substrate. J Phys Chem C 111(27):9968–9974. https://doi.org/10.1021/jp072334h

Xin Y, Liu H, Han L, Zhou Y (2011) Comparative study of photocatalytic and photoelectrocatalytic properties of alachlor using different morphology TiO_2/Ti photoelectrodes. J Hazard Mater 192 (3):1812–1818. https://doi.org/10.1016/j.jhazmat.2011.07.005

Xu H, Ouyang S, Li P, Kako T, Ye J (2013) High-active anatase TiO_2 nanosheets exposed with 95%{100} facets toward efficient H_2 evolution and CO_2 photoreduction. ACS Appl Mater Interfaces 5(4):1348–1354. https://doi.org/10.1021/am302631b

Yadav HM, Otari SV, Koli VB, Mali SS, Hong CK, Pawar SH, Delekar SD (2014) Preparation and characterization of copper-doped anatase TiO_2 nanoparticles with visible light photocatalytic antibacterial activity. J Photochem Photobiol A Chem 280:32–38. https://doi.org/10.1016/j.jphotochem.2014.02.006

Yaghoubi H, Taghavinia N, Alamdari EK (2010) Self cleaning TiO_2 coating on polycarbonate: surface treatment, photocatalytic and nanomechanical properties. Surf Coat Technol 204 (9–10):1562–1568. https://doi.org/10.1016/j.surfcoat.2009.09.085

Yang K, Pu W, Tan Y, Zhang M, Yang C, Zhang J (2014) Enhanced photoelectrocatalytic activity of Cr-doped TiO_2 nanotubes modified with polyaniline. Mater Sci Semicond Process 27:777–784. https://doi.org/10.1016/j.mssp.2014.08.007

Yao X, Zhao R, Chen L, Du J, Tao C, Yang F, Dong L (2017) Selective catalytic reduction of NOx by NH3 over CeO2 supported on TiO2: Comparison of anatase, brookite, and rutile. Appl Catal B Environ 208:82–93. https://doi.org/10.1016/j.apcatb.2017.02.060

Ye SY, Fan ML, Song XL, Luo SC (2010) Enhanced photocatalytic disinfection of P. expansum in cold storage using a TiO_2/ACF film. Int J Food Microbiol 136(3):332–339. https://doi.org/10.1016/j.ijfoodmicro.2009.09.028

Ying GG, Kookana RS, Ru YJ (2002) Occurrence and fate of hormone steroids in the environment. Environ Int 28(6):545–451. https://doi.org/10.1016/S0160-4120(02)00075-2

Yu JC, Ho W, Lin J, Yip H, Wong PK (2003) Photocatalytic activity, antibacterial effect, and photoinduced hydrophilicity of TiO_2 films coated on a stainless steel substrate. Environ Sci Technol 37(10):2296–2301. https://doi.org/10.1021/es0259483

Yu JC, Ho W, Yu J, Yip H, Wong PK, Zhao J (2005) Efficient visible-light-induced photocatalytic disinfection on sulfur-doped nanocrystalline titania. Environ Sci Technol 39(4):1175–1179. https://doi.org/10.1021/es035374h

Yui T, Kan A, Saitoh C, Koike K, Ibusuki T, Ishitani O (2011) Photochemical reduction of CO_2 using TiO_2: effects of organic adsorbates on TiO2 and deposition of Pd onto TiO_2. ACS Appl Mater Interfaces 3(7):2594–2600. https://doi.org/10.1021/am200425y

Yurdakal S, Loddo V, Augugliaro V, Berber H, Palmisano G, Palmisano L (2007) Photodegradation of pharmaceutical drugs in aqueous TiO_2 suspensions: Mechanism and kinetics. Catal Today 129(1–2):9–15. https://doi.org/10.1016/j.cattod.2007.06.044

Zanoni MV, Sene JJ, Anderson MA (2003) Photoelectrocatalytic degradation of Remazol Brilliant Orange 3R on titanium dioxide thin-film electrodes. J Photochem Photobiol A Chem 157 (1):55–63. https://doi.org/10.1016/S1010-6030(02)00320-9

Zhang Z, Wang CC, Zakaria R, Ying JY (1998) Role of particle size in nanocrystalline TiO_2-based photocatalysts. J Phys Chem B 102(52):10871–10878. https://doi.org/10.1021/jp982948+

Zhang Z, Yuan Y, Liang L, Cheng Y, Shi G, Jin L (2008) Preparation and photoelectrocatalytic activity of ZnO nanorods embedded in highly ordered TiO_2 nanotube arrays electrode for azo dye degradation. J Hazard Mater 158(2–3):517–522. https://doi.org/10.1016/j.jhazmat.2008.01.118

Zhang L, Dillert R, Bahnemann D, Vormoor M (2012) Photo-induced hydrophilicity and self-cleaning: models and reality. Energy Environ Sci 5(6):7491–7507. https://doi.org/10.1039/C2EE03390A

Zhang J, Zhang X, Dong S, Zhou X, Dong S (2016) N-doped carbon quantum dots/TiO2 hybrid composites with enhanced visible light driven photocatalytic activity toward dye wastewater degradation and mechanism insight. J Photochem Photobiol A Chem 325:104–110. https://doi.org/10.1016/j.jphotochem.2016.04.012

Zhao C, Pelaez M, Dionysiou DD, Pillai SC, Byrne JA, O'Shea KE (2014) UV and visible light activated TiO2 photocatalysis of 6-hydroxymethyl uracil, a model compound for the potent cyanotoxin cylindrospermopsin. Catal Today 224:70–76. https://doi.org/10.1016/j.cattod.2013.09.042

Zhou H, Li X, Fan T, Osterloh FE, Ding J, Sabio EM, Zhang D, Guo Q (2010) Artificial inorganic leafs for efficient photochemical hydrogen production inspired by natural photosynthesis. Adv Mater 22(9):951–956. https://doi.org/10.1002/adma.200902039

Chapter 12
Nanoparticles: Antimicrobial Applications and Its Prospects

Krishnapriya Madhu Varier, Mounika Gudeppu, Arulvasu Chinnasamy, Sumathi Thangarajan, Jesudas Balasubramanian, Yanmei Li, and Babu Gajendran

Contents

K. M. Varier
Department of Medical Biochemistry, Dr. ALM PGIBMS, University of Madras, Chennai, India

Department of Zoology, University of Madras, Chennai, India

M. Gudeppu · J. Balasubramanian
Department of Pharmacology and Environmental Toxicology, Dr. ALM PGIBMS, University of Madras, Chennai, India

A. Chinnasamy
Department of Zoology, University of Madras, Chennai, India

S. Thangarajan
Department of Medical Biochemistry, Dr. ALM PGIBMS, University of Madras, Chennai, India

Y. Li · B. Gajendran (✉)
Department of Biology and Chemistry, The Key Laboratory of Chemistry for Natural Products of Guizhou Province and Chinese Academy of Sciences, Guizhou, China

State Key Laboratory of Functions and Applications of Medicinal Plants, Guizhou Medical University, Guiyang, China

Mu. Naushad et al. (eds.), *Advanced Nanostructured Materials for Environmental Remediation*, Environmental Chemistry for a Sustainable World 25,
https://doi.org/10.1007/978-3-030-04477-0_12

Abstract Nowadays, nanomaterials [NPs; size, 1–100 nm] have emerged as unique antimicrobial agents. Specially, several classes of antimicrobial NPs and nanosized carriers for antibiotic delivery have proven their efficacy for handling infectious diseases, including antibiotic-resistant ones, in vitro as well as in animal models, which can offer better therapy than classical drugs due to their high surface area-to-volume ratio, resulting in appearance of new mechanical, chemical, electrical, optical, magnetic, electro-optical, and magneto-optical properties, unlike from their bulk properties. Thus, scientifically NPs have been validated to be fascinating in fighting bacteria. In this chapter, we will discuss precise properties of microorganisms and their modifications among each strain specifically. The toxicity mechanisms vary from one stain to another. Even the NP's efficacy to treat against bacteria and drug-resistant bacteria and their defense mechanisms change according to strains in particular composition of cell walls, the enzymic composition, and so on. Thus, we provide an outlook on NPs in the microbial world and mechanism to overcome the drug resistance by tagging antibiotics in NPs and its future prospects for the scientific world.

Keywords Nanoparticles · Antibacterial action · Microbial resistance · NP-assisted drug delivery · Future prospects of NP-assisted therapy

12.1 Introduction

Antibacterial activity is regarded as the ability of the compounds that can kill or reduce the progression of the bacterial growth. Most of the antibacterial agents which are released in the market today are mainly either chemically synthesized or naturally extracted (Nussbaum et al. 2006). Many natural products, such as aminoglycosides, as well as purely synthetic antibiotics like sulfonamides are often used. In broad spectrum, the mediator molecules of the compounds may be either bactericidal (which kill bacteria) or bacteriostatic (slowing down bacterial growth).

There are some essential related terms for studying the antibacterial agents that are mentioned as in the following:

Terms	Explanation
Biocide	A widespread chemical or physical agent which inactivates microorganisms
Bacteriostatic	The property of a specific biocide agent which is able to bacterial multiplication
Bactericidal	A specific term referring to the property by which a biocide is able to kill bacteria
Disinfectants	Products or biocides used to reduce only the number of viable microorganisms on the inanimate objects
Septic	Characterized by the presence of pathogenic microbes in living tissue
Antiseptic	A biocide or product that inhibits the growth of microorganisms in or on living tissue
Aseptic	Free of or using methods to keep free of microorganisms. h. Antibiotics: Naturally occurring or synthetic organic compounds which inhibit or destroy selective bacteria, generally at low concentrations
Sterilization	The process where all the living microorganisms, including bacterial spores, are killed. Sterilization can be achieved by physical, chemical, and physiochemical means
Asepsis	The employment of techniques (such as usage of gloves, air filters, UV rays, etc.) to achieve microbe-free environment

12.1.1 Chemical and Physical Agents for Antimicrobial Action

The chemical and physical agents are the most widespread methods used for controlling microorganism. The physical methods include radiation, heat, and filtration which can destroy or eradicate detrimental microorganisms.

12.1.2 Radiation

Mainly there are two types of radiations, namely, ionizing and non-ionizing. Non-ionizing rays are poorly penetrating low energy rays, while ionizing rays are good penetrating high-energy rays.

Non-ionizing Rays These non-ionizing rays are with wavelength longer than the visible light. Microbicidal wavelength of UV rays lies in the range of 200–280 nm, with 260 nm being the most effective. UV rays generated from a high-pressure mercury vapor lamp produce wavelength that maximally absorbs microorganisms and causes the germicidal effect. UV rays induce formation of thymine–thymine dimers, which ultimately inhibit DNA replication. A nonlethal dose UV ray even

induces mutations in cells. The UV radiation inactivates microorganisms such as bacteria, viruses, and yeast within seconds. Since UV rays don't kill spores, they are considered to be of use in surface disinfection.

Ionizing Rays Ionizing rays, similar to the prior, are of two types, particulate and electromagnetic rays. Electron beams which are particulate in nature produce high-speed electrons by a linear accelerator from a heated cathode, while gamma rays are electromagnetic in nature and are employed to sterilize articles like syringes, gloves, dressing packs, foods, and pharmaceuticals, and sterilization can be achieved in a few seconds. Moreover, the instruments can be switched off.

12.1.3 Heat

Heat is another easier way of sterilization which exerts oxidative effects as well as denaturation and coagulation of proteins. The objects that couldn't withstand elevated temperatures can quiet be sterilized at lower temperatures by extending the interval of exposure. There are two types of heat sterilization – dry and moist heat. The dry heat deeds by protein denaturation, oxidative damage, and toxic effects of higher levels of electrolytes, while the moist heat cracks by coagulation and denaturation of proteins. Moist heat is more effective than dry heat in action as the temperature necessary to exterminate microbe by dry heat is higher than the moist heat. The minimum time required to kill a suspension of organisms at a predetermined temperature in a specified environment is known as thermal death time. In laboratory-scale cultures, a temperature of 121 °C for 15 min is utilized to kill spores. This process is called autoclaving.

12.1.4 Filtration

Filtration as the word sense just separates microbes out instead of killing them. Membrane filters with pore sizes ranging 0.2–0.45 μm are frequently used to eliminate particles from solutions that are non-autoclavable. Numerous applications of filtration contain measuring sizes of viruses, removing bacteria from ingredients of culture media, separating toxins from culture filtrates, counting preparing suspensions of viruses and phages free of bacteria, purifying hydrated fluid, and clarifying fluids. Different types of filters are earthenware filters, membrane filters, sintered glass filters, asbestos filters, as well as air filters. The additional antimicrobial agents are those chemicals which rescind pathogenic bacteria from inert surfaces (Marzieh et al. 2012).

12.2 Biological Inhibitory Mechanisms

Antibacterial properties of drugs and its essential mechanisms behind the process are very important to understand the underlying principles of its inhibitory action. Many of the bactericidal/bacteriostatic antimicrobials used currently are the ones which inhibit DNA, RNA, cell wall, or protein synthesis processes, as a result of the specific mechanistic pathways as described below:

12.2.1 Inhibition of DNA Replication by Quinolones

The processes like DNA synthesis, mRNA transcription, and cell division require the intonation of chromosomal supercoiling over strand breakage catalyzed by topoisomerase and rejoining responses (Gellert et al. 1976; Drlica and Snyder 1978; Espeli and Marians 2004). The synthetic quinolone class of antimicrobials exploits these reactions by targeting DNA–topoisomerase complexes (Sugino et al. 1977; Gellert et al. 1977; Drlica et al. 2008). Quinolones a derivative of nalidixic acid was introduced in the 1960s to treat urinary tract infections, which was a by-product of the synthesis of chloroquine (a quinine; Hooper and Rubnstein 2003). Nalidixic acid and other first-generation quinolones (e.g., oxolinic acid) are hardly used today owing to their toxicity, whereas second (ciprofloxacin)-, third (levofloxacin)-, and fourth (gemifloxacin)-generation quinolone antibiotics (Table 12.1) are widely marketed. These can be classified on the basis of their chemical structure and of qualitative differences between the killing mechanisms they execute (Rubinstein 2001; Hooper and Rubnstein 2003).

12.2.2 The Role of Protein Expression in Quinolone-Mediated Cell Death

The double-stranded DNA breaks caused by topoisomerase inhibition by quinolones induce the DNA stress response (SOS response), where RecA is stimulated by DNA damage and encourages self-cleavage of the lexA repressor protein, persuading the expression of SOS response genes such as DNA repair enzymes (Courcelle and Hanawalt 2003) which enhances the activity of quinolones (except in the case of nalidixic acid) (Howard et al. 1993). The prevention of the activation of the SOS response has also been displayed to decrease the development of drug-resistant mutants by hindering the generation of error-prone DNA polymerases (Criz et al. 2005), horizontal transfer of drug-resistant elements (Guerin et al. 2009), and homologous recombination. Owing to these studies, illuminating the co-treatment with the protein synthesis inhibitor chloramphenicol and quinolones inhibits the ability of quinolones (Beaber et al. 2004)

Table 12.1 Some antibiotic targets and the pathways in which they effect

Drug type	Drug	Derivation	Species range	Primary target	Pathways affected
Rifamycins					
RNA synthesis, inhibitor	Rifamycins, rifampin, and rifapentine	Natural and semisynthetic forms of ansamycins (derived from *S. mediterranei*)	Gram-positive and Gram-negative species and *M. tuberculosis*	DNA-dependent, RNA polymerase	RNA transcription, DNA replication, and SOS response
β-lactams					
Cell wall synthesis, inhibitors	Penicillins (penicillin, ampicillin, oxacillin), cephalosporins (cefazolin, cefoxitin, ceftriaxone, cefepime), and carbapenems (imipenem)	Natural and semisynthetic forms of carbonyl lactam ring-containing azetidinone molecules (from *P. notatum*, *C. acremonium*, and *S. cattleya*)	Aerobic and anaerobic, Gram-positive, and Gram-negative species	Penicillin-binding proteins	Cell wall synthesis, cell, division, autolysin activity (regulated by LytSR–VncRS two-component system), SOS response, TCA cycle, Fe–S cluster synthesis, ROS formation, and envelope and redox-responsive two-component systems

Courtesy to Nature review, Microbiology, 2010: 8: 423–435

12.2.3 Inhibition of Cell Wall Synthesis: Lytic Cell Death

The bacterial cell is sheathed by strata of peptidoglycan (also known as murein), a covalently cross-linked polymer matrix that is composed of peptide-linked β-(1–4)-*N*-acetyl hexosamine. The mechanical strength afforded by this layer of the cell wall is crucial to a bacterium's ability to endure environmental conditions that can alter prevalent osmotic pressures; of note, the degree of peptidoglycan cross-linking compares with the structural integrity of the cell. Maintenance of the peptidoglycan layer is accomplished by the activity of transglycosylases and penicillin-binding proteins (PBPs; also known as transpeptidases), which add disaccharide pentapeptides to encompass the glycan strands of existing peptidoglycan molecules and cross-link adjacent peptide strands of immature peptidoglycan units, respectively (Bugg and Walsh 1992). The treatment with an inhibitor of cell wall syntheses changes induction of cell stress responses, cell shape and size, and ultimately cell lysis. For instance, β-lactams (including penicillins, carbapenems, and cephalosporins) wedge the cross-linking of peptidoglycan units by obstructing the peptide bond formation reaction that is catalyzed by peptidoglycan-binding proteins (PBPs) (Wise and Park 1965; Holtje 1998; Park and Uehara 2008). This inhibition is achieved by penicilloylation of the PBP active site – the β-lactam (containing a cyclic amide ring) is an analogue of the terminal d-alanyl-d-alanine dipeptide of peptidoglycan. Penicilloylation of the PBP active site blocks the hydrolysis of the bond created with the now ring-opened drug, thereby disabling the enzyme (Waxman et al. 1980; Josephine et al. 2004) through autolysis using autolysins. Autolysins are membrane-associated enzymes that break down bonds of peptidoglycan strands. Autolysins have also been displayed to show a part in lytic cell death in bacterial species that contain numerous peptidoglycan hydrolases, such as *E. coli* (Tipper and Strominger 1965). In *E. coli*, a set of putative peptidoglycan hydrolases (lytM domain factors) were shown to be important for rapid ampicillin-mediated lysis (Uehara et al. 2009). The discovery that autolysins contributed to cell death expanded our understanding of lysis and showed that active degradation of the peptidoglycan with inhibition of peptidoglycan synthesis by a β-lactam antibiotic triggers lysis.

12.2.4 Non-lytic Cell Death

Streptococcus pneumoniae lacking peptidoglycan hydrolase activity can still be killed by β-lactams, but at a slower rate than autolysin-active cells, indicating that there is a lysis-independent mode of killing induced by β-lactams (Moreillon et al. 1990; Hoch 2000; Novak et al. 2000). For instance, in *Staphylococcus aureus*, the lytSR two-component system affects cell lysis by modifying autolysin activity (Burnskill and Bayles 1996). lytR triggers the manifestation of *lrgAB*, which was found to impede autolysin activity and thereby lead to antibiotic tolerance. lrgA is similar to bacteriophage holin proteins (Groicher et al. 2000), which control the

access of autolysins to the peptidoglycan layer. Based on this evidence, a supplementary holin-like system, *cidAB*, was uncovered in *S. aureus* and initiated to activate autolysins, representing *S. aureus* more susceptible to β-lactam-mediated killing. Complementation of *cidA* into a *cidA*-null strain inverted the damage of autolysin activity but did not wholly reinstate sensitivity to β-lactams (Rice et al. 2003).

12.2.5 Role of the SOS Response in Cell Death by β-Lactams

The handling with β-lactams leads to variations in cell morphology that are accompanying with the primary drug–PBP interaction. Generally speaking, PBP1 inhibitors source cell elongation and are strong activators of lysis, PBP2 inhibitors change cell shape but do not lyse, and PBP3 inhibitors impact cell division and can persuade filamentation (Spratt 1975). Accordingly, PBP1-binding β-lactams are also the most effective inducers of peptidoglycan hydrolase activity, and PBP2 inhibitors are the least proficient autolysin activators (Kitano and Tomasz 1979).

12.2.6 Inhibition of Protein Synthesis

The mRNA translation process occurs over three sequential phases (initiation, elongation, and termination) that comprise the ribosome and a range of cytoplasmic accessory factors (Garrett 2000). The ribosome is composed of two ribonucleoprotein subunits, the 50S and 30S, which assemble (during the initiation phase) following the formation of a complex between an mRNA transcript, *N*-formylmethionine-charged aminoacyl tRNA, several initiation factors, and a free 30S subunit. Drugs that inhibit protein synthesis are among the biggest classes of antibiotics and can be divided into two subclasses: the 50S inhibitors and 30S inhibitors (Table 12.2). 50S ribosome inhibitors include lincosamides (e.g., clindamycin), macrolides (e.g., erythromycin), streptogramins (e.g., dalfopristin– quinupristin), amphenicols (e.g., chloramphenicol), and oxazolidinones (e.g., linezolid) (Nissen et al. 2000; Katz and Ashley 2005). The 50S ribosome inhibitors work by physically blocking the access of aminoacyl-tRNAs to the ribosome or either initiation of protein translation (as is the case for oxazolidinones) (Patel et al. 2001). Among ribosome inhibitors, the only class that is broadly bactericidal is naturally derived aminoglycosides. Macrolides, streptogramins, spectinomycin, tetracyclines, chloramphenicol, and macrolides are typically bacteriostatic; however, they can be bactericidal in a species- or treatment-specific manner.

Even though antibiotics can be a preventive measure for bacterial growth, to the excitement of the scientific community, they exhibit a phenomenon called microbial resistance. This results in a portent that the microbe develops survival even when antibiotics are administered after a point where which they get mutated itself and

Table 12.2 Antibiotics which affect ribosome machinery

Drug type	Drug	Derivation	Species range	Primary target	Pathways affected
Aminoglycosides and tetracyclines					
Protein synthesis inhibitors	Gentamicin, tobramycin, streptomycin, kanamycin, tetracycline, and doxycycline	Natural and semisynthetic forms of amino sugars (-mycins from *Streptomyces* spp. and -mycins from *Micromonospora* spp.)	Aerobic, Gram-positive and Gram-negative species, and *M. tuberculosis*	30S ribosome	Protein translation (mistranslation by tRNA mismatching), ETC, SOS response, TCA cycle, Fe–S cluster synthesis, ROS formation, and envelope and redox-responsive two-component systems
Macrolides					
Protein synthesis inhibitors	Erythromycin and azithromycin	Natural and semisynthetic forms of 14- and 16-membered lactone rings (from *S. erythraea* and *S. ambofaciens*)	Aerobic and anaerobic, Gram-positive and Gram-negative species	50S ribosome	Protein translation (through inhibition of elongation and translocation steps) and free tRNA depletion

Courtesy to: Nature review, Microbiology, 2010: 8: 423–435

become resistant to those antibiotics which they have come across earlier in its lifetime. Here comes the application of nanoparticles (NPs) as a carrier of antibiotics/a replacement of antibiotics.

12.3 Positive Side: As an Effective Therapeutic Method to Combat Microbial Resistance and Multidrug-Resistant Mutants

Against microbial resistance and multidrug resistance (MDR), numerous NP variants and NP-based materials have been used as a new line of defense (Singh et al. 2014; Cavassin et al. 2015) having different mechanisms for compaction. The complementary advantages of using NPs/nanotechnologies as antibacterial agents compared with traditional antibiotics can be summarized as follows:

1. Overcoming the existing antibiotic resistance mechanisms including the disruption of bacterial membranes and the hindrance of biofilm formation
2. Combatting microbes using multiple mechanisms simultaneously
3. Acting as good carriers of antibiotics (Zhang et al. 2010)

12.3.1 Overcoming the Existing Antibiotic Resistance Mechanisms

Many NPs usually counteract at least any one of the common resistance mechanisms. These possessions are effect of the bactericidal mode of NPs, which bases on their specific physicochemical properties (Chen et al. 2014). The uniquely small size helps NPs to interact with cells due to a larger surface area-to-mass ratio with handy and manageable application, in contrast to traditional antibiotics. Besides the interruption of bacterial membranes, difficulty of biofilm formation is another significant mechanism, as they portray a major measure in the progress of bacterial resistance (Peulen and Wilkinson 2011). The distinctive structure and arrangement of bacterial biofilms deliver protection to the implanted microorganisms, assisting them to escape from most antibiotics. Moreover, bacterial biofilms are "a breeding ground" for regular resistance mutations and the interchange and variation of these mutations among diverse bacterial cells (Khameneh et al. 2016). Studies have revealed that many NPs can prevent or overcome biofilm formation, including Au-based NPs (Yu et al. 2016), NPs, 7 CuO NPs (Miao et al. 2016), Ag-based NPs (Markowska et al. 2013), ZnO Fe3O4 NPs, Mg-based NPs (Lellouche et al. 2012b), NO NPs (Hetrick et al. 2009; Slomberg et al. 2013), and YF NPs (Lellouche et al. 2012a). Better prevention of biofilms is attained by a lesser size and larger surface area-to-

mass ratio, as well as the particle shape of NPs with an extraordinary outcome on biofilm destruction (e.g., NPs with a rodlike shape are more operational than NPs with a spherical shape).

12.3.2 Combatting Microbes Using Multiple Mechanisms Simultaneously

The antimicrobial mechanism of traditional antibiotics is modest owing for bacteria to develop resistance. In disparity to traditional antibiotics, NPs combat microbes via multiple mechanisms that are simultaneously active. The advantage of these simultaneous mechanisms is that even though microbes have multiple mutated genes, Nps can assist so as to reduce the microbial resistance.

12.3.3 Acting as Good Carriers of Antibiotics

NPs not only can combat bacterial and microbial resistance themselves, as mentioned earlier, but also can act as a "medium and carrier" of antibiotics. However, the mechanisms of NP-based drug delivery are different from those presented earlier.

12.3.4 Several Types of NPs Are Currently Used for Drug Delivery

Solid lipid (SL) NPs (Thukral et al. 2014; Naseri et al. 2015), liposomal NPs (Daeihamed et al. 2017), polymer-based NPs, inorganic nanodrug carriers (including magnetic NPs, mesoporous silica NPs, polymer micelles, carbon nanomaterials, and quantum dots), dendrimer NPs (Liu et al. 2015), and terpenoid-based NPs (Abed and Couvreur 2014) are used as a transporter for the supply of antibiotics; the central advantages of NPs associated with conventional distribution systems are as follows:

Size The governable smaller size of NPs is appropriate for accompanying antimicrobial operations and fighting intracellular bacteria (Ranghar 2012). The management of infections caused by intracellular strains with drug resistance is more multifarious using antibiotics (Andrade et al. 2013; Qi et al. 2013) because of antibiotics' reduced membrane transport. Drugs of ordinary size have less influence on intracellular microbes. An improved treatment method using drug-loaded NPs as mediators has been projected to overcome the limitation.

Protection NP carriers can aid to rise the serum levels of antibiotics and shield the drugs from resistance by targeted bacteria. Within NP carriers, drugs are sheltered from harmful chemical reactions so as to maintain the potency of the drugs. Moreover, better efflux and reduced uptake of antibiotics in bacterial cells (such as in *P. aeruginosa* and *E. coli*) are the normal and significant reasons for resistance to traditional antibiotics. However, researchers have proved that numerous NPs can incredulous these mechanisms (Muhling et al. 2009), preventing drug resistance. For example, in the gastrointestinal tract, dendrimers can inhibit P-glycoprotein-mediated efflux (Liu et al. 2015).

Precision and Security NP carriers can minimize systemic side effects and target antibiotics to an infection site. When we use a carrier, we can reduce the side effects (including drug toxicity) and can encourage a high-dose drug absorption at the desired site. NP-based antibacterial drug delivery systems deliver the drug to the site of action and therefore reduce the side effects. Targeted NP-based drug delivery entails of active targeting or passive targeting. Active targeting is achieved through NPs' surface modification, allowing the NP-based drug delivery system to selectively identify precise ligands on the cells at the site of infection, while passive targeting is achieved through improved permeation and retaining at the infection site. Active targeting embraces receptor targeting, temperature targeting, and magnetic targeting (Xiong et al. 2012).

Controllability Controllable sustained discharge of antibiotics can be attained docilely. With a conventional delivery method, the blood drug level is maintained for a short time with the lowest effective dose. As a consequence, frequent dosing is obligatory, which leads to side effects. With the appropriate NP carrier or method of drug release, the blood concentration of the medicine at the infection site can be persistent at the compulsory effective level for a long time, occasioning in good stability, compact frequency of medication, enhanced patient compliance, and condensed patient pain. Along with prolonged drug release (Liu et al. 2016), Nps are effective even by different types of governable stimulatory factors (such as a magnetic field, chemical agents, light, heat, and pH) (Lim et al. 2018; Wu et al. 2016; Baig et al. 2016).

Combination Many drugs can be packaged within the same NP or with assisted constructs to increase the agents' antibacterial properties. The concurrent combination of dissimilar drugs helps in developed efficiency due to the joint action of multiple mechanisms. On the other hand, two or more types of NPs can be used in combination for improved antibacterial effects and prevention of resistance (Liu et al. 2015). Fusion NPs can maximize the powers while diminishing the weaknesses of the individual types of NPs. For example, studies have shown that superior efficacy of in vivo cellular delivery can be achieved by lipid–polymer hybrid NPs compared with delivery without polymeric NPs or by liposomes (Hadinoto et al. 2013), which can effectively and expressively decrease the possibility of the growth of bacterial resistance (Brooks and Brooks 2014). The abovementioned advantages may unite in diverse combinations with different emphases in the process of actual application.

Size The recent studies have revealed that the size of NPs has a great role in its bioactivity. The length and diameter of nanotubes were attuned by the anodic oxidation process parameter by increasing the release time of drug. The TiO2 nanotubes and silica NPs administered synereticaly on the composite films for antibacterial activity resulted that the size of the TiO2 nanotubes basically dogged the amount and machinery of the activity. Smaller NPs having larger specific surface areas resulted in larger permeability to the cell membranes (Gurunathan et al. 2014; Deplanche et al. 2010).

Shape Shape also accounts for antimicrobial activity. NPs interacting with periplasmic enzymes cause varying gradations of bacterial cell damage with respect to the shape of NPs (Cha et al. 2015). A comparison of ZnO NPs with pyramid, plate, and sphere shape showed the arrangement of β-galactosidase (GAL), and shape-specific ZnO NPs produced photocatalytic activity (Prasannakumar et al. 2015). *Pseudomonas desmolyticum* and *S. aureus* were greatly affected with prismatic-shaped Y2O3 NP due to the direct interaction between NPs and the surface of the bacterial cell membrane (Hong et al. 2016). Moreover, cube-shaped AgNPs exhibit stronger antibacterial activity than sphere-shaped and wire-shaped AgNPs with similar diameters, due to the specific surface area and facet reactivity (Actis et al. 2015) having a lesser effect on microbiota susceptibility (Talebian and Sadeghi 2014).

Roughness Roughness also acts as a factor with respect to antibacterial action as the roughness of NPs increases the size and the surface area-to-mass ratio, which promotes the adsorption of bacterial proteins, followed by a reduction in bacterial adhesion (Sukhorukova et al. 2015).

Zeta Potential Recent studies have validated that the zeta potential for NPs has durable influence on bacterial adhesion. The electrostatic attraction among positively charged NPs and the bacterial negatively charged cell membrane has a positive surface charge and is prone to being adsorbed on the bacterial surface and is meticulously connected with bacteria, in contrast to their negatively charged counterparts (Pan et al. 2013), and rises vascular permeability (Maeda 2010), by limiting bacterial attachment through ion exchange (Fang et al. 2015). In comparison with negatively charged and neutral NPs, positively charged counterparts have been believed to enhance ROS production, which leads to interactions between the NPs and the bacterial surface (Arakha et al. 2015).

Doping Modification The NPs used in clinics can be now altered for its aggregation using doping modification techniques allowing NPs to disperse in hydrophilic or aqueous environments. Doping modification is also one of the most operational methods to normalize and regulate the interaction of NPs with bacteria. Lately, the ZnO NPs with Au (gold) combination to form ZnO/Au nanocomposites were administered to improve photocatalytic activity and to enhance ROS generation. These effects are the result of the following factors: an altered ZnO bandwidth, better light absorption owing to the surface plasmon resonance wavelength of Au, enhancement of the photo-induced charge carrier reactivity, and amplified electron transport efficiency and carrier charge separation (He et al. 2014). For instance, ZnO

NPs doped with fluorine generate more ROS than ZnO NPs, resulting in greater damage to bacterial cells (Guo et al. 2015; Podsporka et al. 2017). The ZnO NPs have "O" content at the surface regulating antimicrobial effectiveness against both Gram-positive and Gram-negative bacteria (Mehmood et al. 2015). Nano-TiO2 reduces the formation of biofilms in dental implants, showing greater antimicrobial action. In comparison with unmodified TiO2, nano-TiO2 increases photocatalytic activity, as the doped form can effectively extend the active spectrum to the visible light region by the valence bandwidth elevation and the forbidden bandwidth deprivation (Peng et al. 2010; Sangari et al. 2015).

Environmental Conditions Various environmental conditions displayed significant differences in antimicrobial activity. For example, the temperature of the environment potentially influences the antibacterial activity following its effect on the ROS generation rate. When ZnO NPs are encouraged by temperature, electrons are detained at the active sites. Afterward, the electrons interact with oxygen molecules (O2) for ROS generation, thereby increasing the antimicrobial effectiveness of ZnO NPs. A decrease in the pH increases the rate of dissolute ZnO NPs, which elevated the antimicrobial properties (Saliani et al. 2015). In addition, under acidic conditions, the injury of ability of poly (lactic-*co*-glycolic acid) (PLGA)-poly(l-histidine) (PLH)-poly(ethylene glycol) (PEG)-encapsulated vancomycin deceased selectively. Certain results proposed that protonation of the imidazole groups of PLH selectively under acidic conditions intensely influenced NP surface charge switching. The surfaces of the NPs were charged positively at low pH that becomes beneficial to the interaction with the negatively charged groups of the bacterial cell barrier, prompting multivalent strong electrostatic regulation (Radovic et al. 2012). Another study proposed that the interaction of Ag+ with dissolved oxygen and protons caused an oxidative dissolution mechanism for AgNPs which could activate AgNPs and release many Ag ions, enhancing the antibacterial activity of the AgNPs in acetic acid than in neutral water (Peretyazhko et al. 2014).The culture medium characteristics, such as osmotic pressure and pH, can influence the aggregation, surface charge, and solubility of NPs. Antibacterial tests in five types of media demonstrated that the antimicrobial activity of ZnO NPs is mainly due to free Zn ions and zinc complexes. Furthermore, the medium can supply nutrients to bacteria to improve their tolerance to NPs (Li et al. 2011). Finally, a study has shown that preparation of ZnO NPs under different stirring conditions can affect their antibacterial activity against Gram-positive (*B. subtilis*) and Gram-negative (*E. coli*) bacteria and a fungus (*C. albicans*; Khan et al. 2016).

12.4 Mechanism of Action of Nanoparticles

One key element in the design of a more potent antibacterial system is the understanding of its mode of action. This involves two distinctive steps – the first one is the way the system will behave in the physical or chemical modifications occurring

in environments involving aggregation, dissolution, RedOx photo-reactions, release of adsorbed silver species, adsorption or desorption of ions, molecular species or polymers, or interaction with other nanoparticles or surfaces which can all have an effect on the speciation of silver, modifying this metal availability and impacting the antibacterial effect, while in the second step, the silver-containing species interact with the bacterial cell and lead to the cellular death. This impact trusts on the considered organism, even the synthetic parameters (ligand type, shape, size, washing steps, dispersion, evaluation procedures for bacterial strain used, growth inhibition due to toxicity criterion or full eradication, nature of the test to assess it, presence of light or oxygen, composition of the medium, and so on) (Misra et al. 2012). As many modes of action are hypothesized from experiential observations and condition evaluated, several decontamination pathways analyzed for silver nanoparticles remain unclear to this date. But some of the theorized silver nanoparticle (AGNP) effects are described in detail below followed by gold and metal NPs.

12.4.1 Role of Silver NPs in Antimicrobial Action

The presence of a Ag0 core has intuitively attributed the antimicrobial activity by most researchers. AgNPs incline to accumulate at the bacterial membrane forming aggregates when they are put in connection with bacteria and cause perforations leading to cellular death (Li et al. 2010). However, different sizes (from 1 nm to several hundreds of nm) also interact for the action mechanisms between biological components and AgNP surfaces as the particle size can propose their action mechanism slightly without a secondary species. The AgNPs generate cytotoxic action by inactivating enzymes of bacteria by producing reactive oxygen species (Kim and Ryu 2013). Some other mechanisms give a prevalent role to Ag+ species. Some systems containing initially silver (+1) species release ROS by simple dissolution or ion exchange such as salts (Valentine et al. 1998), zeolites (Sambhy et al. 2006), or ionomers (Dallas et al. 2011), which doesn't happen with metallic Ag0 nanoparticles. Thus the monovalent silver species becomes antibacterial agent keeping NPs as a reservoir. The silver ions possess affinity toward organic most notably thiols with which they form a quasi-covalent bond (Ag–S binding energy being around 65 kcal/mol), amines and phosphates. Affinity of Ag+ for selenol groups is analogous (Han et al. 2001), but these moieties are fairly uncommon in the living world. Furthermore, silver can act as a linking agent between several thiols forming aggregation of the thiol-containing molecules which are irreversible (Parikh et al. 1999). Several molecules (DNA, peptides (membrane-bound or inside the cell), or cofactors) have been recognized as the target of these ions that was observed with the dying bacteria. With contrast to the antibiotics which targets one particular constituent of the bacterial life cycle, Ag+ ions will adsorb voluntarily to any high affinity moiety; thus unlikely many pathways are affected causing the cellular death. A much more probable hypothesis would be that silver binds non-specifically to a wide variety of targets, perturbing simultaneously many aspects of the cell

metabolism and leading to its death. Among all pathways affected, some are very sensitive to little amount of silver species too. This capability to disrupt a large variety of pathways may be one reason explaining the antibacterial action of silver nanoparticles against a very broad spectrum of microorganisms. Park et al. presented that developed ROS were intricated in more than half of the antibacterial activity by comparing Ag+ action in the presence and absence of oxygenic respiration. The release of chemisorbed ions at the surface of the particles along with oxidation was another source of Ag+ ions in nanoparticulate systems (Dobias and Berrier 2013). A percentage of the novel silver salt will remain oxidized comparatively even if a mild reducing agent (such as sodium citrate) is added to the solution by remaining free in solution or bound to the surface of the Ag0 nanoparticles by a group of pending citrate ligands (Henglein 1998).

Chloride is much available in both environmental and biological systems which forms the slightly soluble precipitate AgCl. However, in presence of excess chloride, soluble silver (+1) polychloride species $AgCl_x^{(x-1)-}$ are formed and contribute to the antibacterial activity (Chambers et al. 2013; Levard et al. 2013). The size and shape dependency of the nanoparticle also contributes to the release of Ag+ ions required to dissolve AgNPs (Pal et al. 2007); Zhang et al. 2011). The improved activity occurs due to a larger surface per unit of mass scales like $1/R$ (the number of particles scales like $1/R3$ and the surface like $R2$, with R the radius). These minor NPs reveal more active surface and are thus more prone to dissolution. For analogous reasons, accumulated NPs uncover a smaller amount of surface to the solvent than separated NPs and possess a lesser antibacterial impact (Bae et al. 2010). However, it has been recently validated by Liu et al. that the released Ag+ scale well if the samples were regularized by their exposed surface. Afterward, Xiu et al. showed in 2012 that the substantial parameters to evaluate the activity of silver nanoparticles were the silver released as Ag+ and not the quantity of primary silver added as nanoparticle (Fig. 12.1) to the solution.

The phytosynthesized AgNPs from *Urtica dioica* were explored for its antibacterial activities for a range of pathogenic microorganisms, by Jyoti et al. 2016. The inhibition zone's diameters in millimeter are presented in Fig. 12.2 and Table 12.3. The AgNPs unveiled higher activity than AgNO3 solution and leave extracts which were served as controls. Moreover, the antibacterial activities were found to be augmented with the higher concentration of AgNPs. In present study, zone of inhibition was found to be highest (27 mm) against *S. marcescens* and lowest (18 mm) against *K. pneumoniae*. These findings are in agreement with previous studies that examined antibacterial activity of AgNPs (Ghosh et al. 2012). However, the mechanism of the inhibitory action of the metal nanoparticles on microorganisms is not still clearly known and need further research assistance.

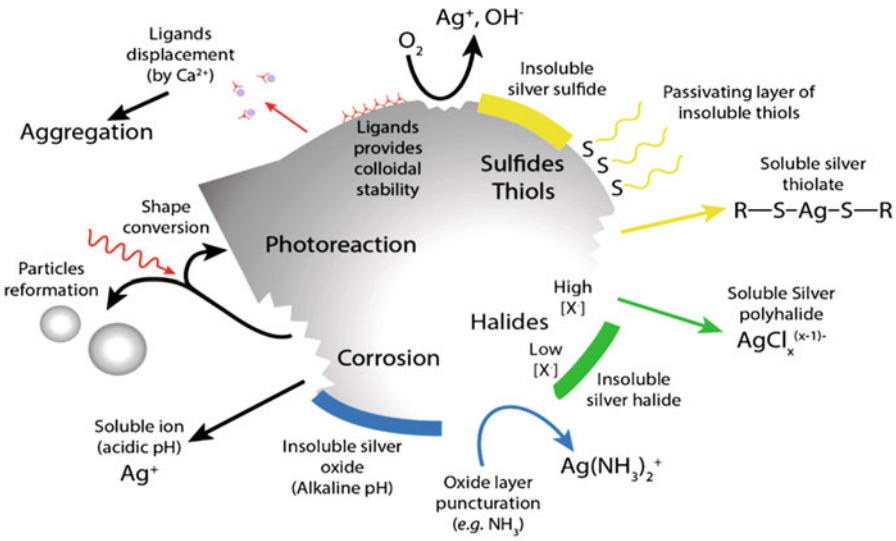

Fig. 12.1 Different methods by which silver nanoparticles react for various physiochemical, biological, and environmental conditions. (Courtesy to Nano today 2015, 10: 339–354)

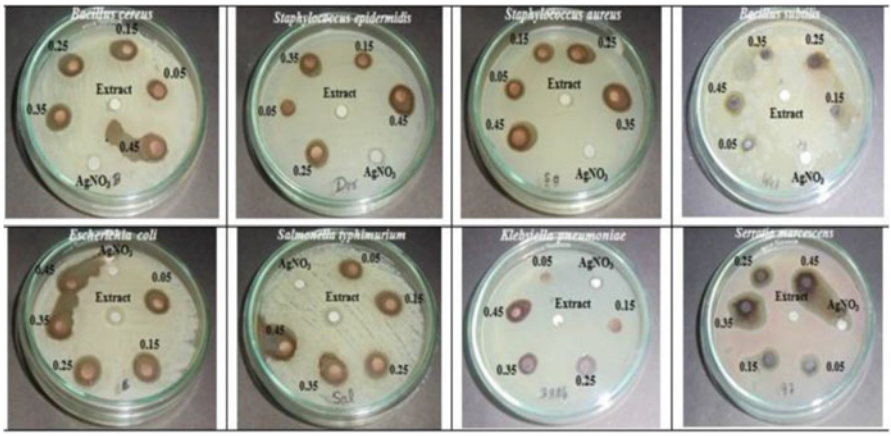

Fig. 12.2 Antibacterial activities of synthesized silver nanoparticles of *Urtica dioica*. (Courtesy to: J of Rad res and app sciences 9(2016): 217–227)

Table 12.3 Inhibition zone of AgNPs, $AgNO_3$, and *Urtica dioica Linn.* leaves extract against Gram-positive and Gram-negative bacteria

		Inhibition zone (mm)				Extract	Ag NO3
Test pathogens	0.05 mg/100 ml	0.15 mg/100 ml	0.25 mg/100 ml	0.35 mg/100 ml	0.45 mg/100 ml	0.45 mg/100 ml	0.45 mg/100 ml
B. cereus	14	15	18	23	24	–	7
S. epidermidis	9	12	14	16	19	7	8
S. aureus	12	16	17	19	21	7	7
B. subtilis	10	12	16	16	25	–	–
E. coli	12	15	16	17	19	98	–
S. typhimurium	14	17	18	19	25	–	7
K. pneumoniae	8	10	13	14	18	7	8
S. marcescens	13	15	16	24	27	–	–

Courtesy to: J of Rad res and app sciences 9(2016): 217–227

12.4.2 Applications of Gold Nanoparticles

Very recently, in the research field , many applications for gold NPs (Au NPs) starting from engineering to medicine, have been attributed (Patra et al. 2015). The biocompatibility of gold nanoparticles made them fit enough to be used in the treatment of arthritis and cancer (Jain et al. 2006) and antimicrobial therapies. Under dark-field light-scattering microscopy, Au NPs can sense endocytosis, tumor metabolites, and receptors in cells (Dykman and Khlebstov 2011). Some Au NP-based diagnostic kits are under clinical trials (Kumar et al. 2015). Green-synthesized Au NPs (Fig. 12.3) have also been used in the development of quantification of blood glucose, biosensors, toxic metals, disease markers, and insecticides (Liu and Lu 2003). Au NPs also have the potential to degrade and detoxify toxic pollutants (Lopez et al. 2004; Hernández et al. 2006). Some other applications have been shown in Fig. 12.4.

For many decades, gold has been used as a treatment in many traditional medicines. Robert Koch first explored the biocidal potential of gold (Glišić and Djuran 2014). Apart from their other applications, due to its ability for the electrostatic flux across membranes, resulting in distorted membranes, the antimicrobial activity of Au NPs has been typically oppressed (Li et al. 2010). Moreover, nanoparticles also improve many gene expressions serving in redox processes leading to microbial death (Nagy et al. 2011) through smaller size, distinctive surface

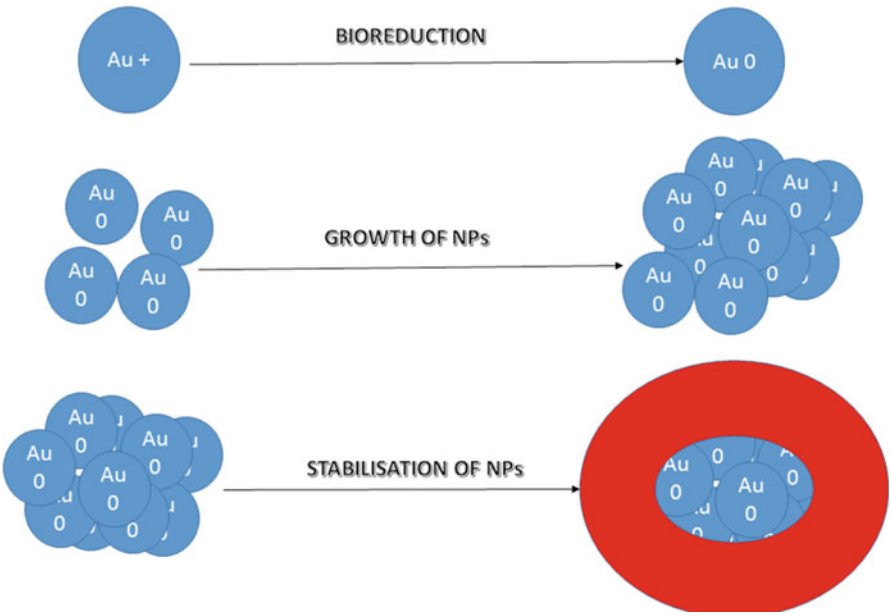

Fig. 12.3 The visual summary of gold nanoparticle synthesis and aggregation of the NPs

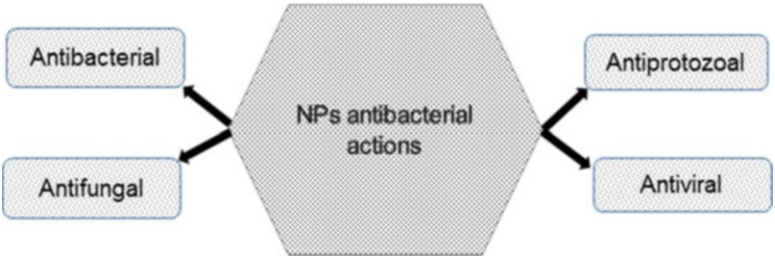

Fig. 12.4 Several antimicrobial actions of nanomaterials

chemistry, photothermic nature, and polyvalences (Gu et al. 2003; Gopinath et al. 2013). The reaction of Au Nps with sulfur- or phosphorus-holding bases leads to inactivation of enzymes (nicotinamide adenine dinucleotide (NADH) dehydrogenases), which interrupt the respiratory chains by high amount of free radical generation causing cell death. Another proposed hypothesis is that these NPs decline the ATPase activities and GNP may also prevent the tRNA binding to ribosomal subunit (Cui et al. 2012). For instance, during leishmaniasis, Au NPs produces an elevated electron numbers by yielding ROS (O − 2 and •OH). These ROS may even abolish DNA and other cellular components of the pathogen. Another possible mechanism is that these Au NPs obstruct the H+ efflux in the transmembrane.

Antimicrobial potential of the many NPs is determined by the size and surface chemistry according to Herdt et al. stating that gold surface attachment leads to DNA degradation (Brayner et al. 2006; Herdt et al. 2006). Moreover, according to Ahmad et al. 2013, a 7 nm Au NPs could confine the H+ transmembrane efflux of the *Candida* species further than the 15 nm Au NPs. Moreover, the antimicrobial activity also differs according to the cell wall composition. This was well evidenced by the Au NPs' highest activity against Gram-negative bacteria than Gram-positive bacteria due to the composition difference as described in earlier section. Other than the cell wall structure of bacteria, surface modification (coating or capping agents), concentration, and purification methods also affect the antibacterial activity (Zhang et al. 2015; Kaviya et al. 2011). The antibacterial activity efficacy of Au NPs can be enhanced by antibiotic coatings especially aminoglycoside antibiotics (Payne et al. 2016). It is very interesting that comparing green-synthesized Au NPs to chemically synthesized Au NPs shows effectual antibacterial activity against certain bacterial strains, which may be due to the synergistic effect of Au NPs and extracts (Mishra et al. 2011).

12.4.3 Metal Oxide NPs

Recently, apart from ZnO used as a wide bandgap semiconductor (3.36 eV), with potential electronic applications (Baxter and Aydil 2005) and a wide range of

nanostructures makes ZnO for nanoscale optoelectronics and piezoelectric nanogenerators (Song et al. 2006). They are used powerfully to fight microorganisms (Sawai et al. 1995). There are some reports (Sawai et al. 1995) considered which reveals by a conductometric method a considerable antibacterial activity of CaO, MgO, and ZnO, which were attributed by the generation of reactive oxygen species on the surface of these oxides. Once ZnO destroys the cell membrane, the ZnONps remain forcefully adsorbed on the dead bacteria surface preventing further antibacterial action continuing to release peroxides into the medium showing high bactericidal efficacy. From the results of another study (Stoimenov et al. 2002), it was being observed that the smaller particle size enhances the activity due to its large surface area-to-volume ratio. The thorough mechanism of ZnONP activity is still under study.

12.4.4 NP for Antifungal Action

Antifungal activity of NPs is less explored compared to antibacterial activity. Gajbhiye et al. (2009) reported efficacy of biosynthesized silver nanoparticles against *P. glomerata*, *P. herbarum*, *Trichoderma* sp., *F. semitectum*, and *C. albicans*. Moreover, they furthermore described the synergistic properties in blend with fluconazole. Jo et al. (2009) deliberated the activity of both nanoparticles and silver ions against two plant pathogenic fungi, *Magnaporthe grisea* and *Bipolaris sorokiniana*. The antifungal activity of NPs in arrangement with dissimilar heterocyclic compounds like thiazolidine, pyrazolo, phthalazine, hydrazide, tetrazolo, and pyridazine derivatives was considered against *C. albicans* and *Aspergillus flavus.* Nasrollahi et al. (2011) investigated antifungal activity of chemically synthesized AgNPs against *C. albicans* and *S. cerevisiae* explaining the potential activity of AgNPs as compared to standard antifungal agents (viz., amphotericin B and fluconazole). Pawan et al. (2012) augmented the potential antifungal activity of chitosan nanoparticles against *R. solani*, *A. flavus*, and *A. alternata* from chickpea seeds. In another study, Tile and Bholay (2012) reported significant activity of AgNPs against *Trichophyton rubrum*, *C. albicans*, and *A. fumigatus*. In an extensive study, Xu et al. (2013) evaluated AgNPs and natamycin against 216 strains of fungi demonstrating higher activity compared to natamycin. One of the possible explanations is destruction of membrane integrity of fungi and inhibition of normal budding process in yeasts (Kim et al. 2009).

12.4.5 Antiviral Activity of NPs

NPs have established marvelous care for its antibacterial activities, but the antiviral properties of metal nanoparticles continue to be an emergent area (Galdiero et al. 2011). The best known examples are West Nile virus, SARS coronavirus,

Hantavirus, monkeypox virus, Nipah virus, Chikungunya virus, Hendra virus, and, last but not least, the threat of pandemic influenza viruses, most recently of avian or swine origin (Howard and Fletcher 2012). Thus, a greater is there to develop a novel unique cure for antiviral agents, which incredulous the issue of antiviral resistance. For instance, AgNPs are developing as one of the remedies for the administration of viral diseases due to their possible antiviral activity that requires maintenance of long-lasting therapeutic regimens or circulating drug concentration. Three key aspects can be extrapolated from the studies conducted so far on the antiviral properties of NPs: (1) NPs have validated antiviral activity against many viruses affecting both prokaryotic (De-Gusseme et al. 2010; Narasimha 2012) and eukaryotic organisms, making them a true broad-spectrum antiviral agent; (2) viral inhibition even relies on the size of NPs (Speshock et al. 2010); and (3) early infection might be the general time frame where NPs exert their antiviral activity imposing the rest of the viral replication cycle (Baram-Pinto et al. 2009; Trefry and Wooley 2013). However, an exact mechanism of NP antiviral activity and a particular phase of infection at which NPs exert antiviral activity have yet to be revealed.

12.5 Limitations of the Current Research

To the surprise, it should be noted here that many antibacterial mechanisms of NPs are still uncertain. For instance, many studies point the antibacterial activity to ROS/oxidative stress, whereas for other NPs, such as MgO NPs, the antibacterial mechanism may not be related with the regulation of metabolism of bacterial strains. Therefore, the antibacterial mechanisms of NPs are substantially relevant in addressing for future research.

The lack of cohesive standards is one limitation of the existing studies on the antibacterial mechanisms of NPs. In particular, different bacterial strains, NP characteristics, and action times were examined in different studies making it difficult to compare antibacterial activity. Thus, no solitary method accomplishes all the situations for procurement evidence about the antibacterial mechanisms of NPs as each type of NPs exhibits distinct antibacterial effects. A complete analysis is often suggested to study the probable antibacterial mechanisms.

Our other limitations are the multifaceted bacterial cell membrane structure and the deficiency of research methods for in vitro studies. Furthermore, in vitro models cannot completely sham the in vivo situation to precisely replicate the cellular body interactions. Therefore, it is intolerable to appraise the antibacterial action of NPs solely through in vitro bacterial cell culture.

Regarding nanoneurotoxicity like crossing of NPs across the bacterial cell membrane, many questions are still unanswered by the research community. The cell membrane of a bacterial is both a barrier and a channel for the movement of substances in and out. In bacterial cell membranes, especially Gram-negative strains

have porins that allow the passage of molecules of around 600 Da molecular weight across the bacterial cell body. Therefore, due to their size, almost the transport of nearly all NPs will be limited. However, certain scholars have projected that porins can facilitate the passage of NPs with thicknesses in the range of 1–9 nm through the bacterial cell membrane. Endocytosis of microorganisms, similar to what is observed for eukaryotic cells, may be measured as additional mechanism of NP movement.

In an era of increasing MDR, NPs are a feasible alternative to antibiotics and seem to have great potential to resolve the difficulty in which bacteria are evolving resistance to numerous antibiotic types, and it is becoming very hard to combat infectious diseases and treat patients, leading to serious mortality.

12.6 Antibiotic-Tagged NPs to Overcome the Current Research Limitations

As mentioned above, the researchers are facing great difficulty in designing an apt NP drug for antimicrobial therapy. Hence, they developed the idea of antibiotic-tagged NPs to reduce the MDR and its side effects. Accordingly Kumar and his coworkers in 2016 analyzed the synergistic effects of AgNPs with eight antibiotics against pathogenic bacteria (Fig. 12.5 and Table 12.4). In many cases, they could analyze that the effects of antibiotics were enhanced. Synergistic interaction of AgNPs and streptomycin showed a minute increase in the inhibition zone against seven pathogenic bacteria in the range 0.1 to 0.9 with the exception of *B. cereus* where a 6.1-fold increase was seen. When combined with kanamycin, amikacin, tetracycline, and cefetaxime, the AgNPs showed comparable synergy (a 0.1–4.4-fold increase). Amoxicillin depicted the highest overall synergistic activity as for *S. marcescens*, while vancomycin with AgNPs revealed synergistic activity against *E. coli*. A greater fold increase in case of inhibition zone was initiated against *S. epidermidis*, *B. subtilis*, and *E. coli* in the existence of a blend of cefepime and AgNPs. *S. epidermidis*, *S. marcescens*, *E. coli*, *S. typhimurium*, *Klebsiella pneumonia*, *S. marcescens*, and *B. subtilis* were found to be subdued in combination of AgNPs and antibiotics, which otherwise indicated a resistant pattern in the manifestation of the antibiotics (vancomycin, cefetaxime, ampicillin, kanamycin, amikacin, cefepime) alone. Thus it could be augmented that AgNPs enhance its efficacy in company of most of the antibiotics, against many drug-resistant bacteria (Fayaz et al. 2010; Ghosh et al. 2012; Singh et al. 2013).

Moreover, this research provides helpful insight into the development of new antibacterial agents. The combination of antibiotics and NPs will make it difficult for pathogenic bacteria to develop resistance which otherwise renders the available antibiotics inefficient; hence, this combination therapy can be further studied to develop new formulation of NPs in synergy with antibiotics.

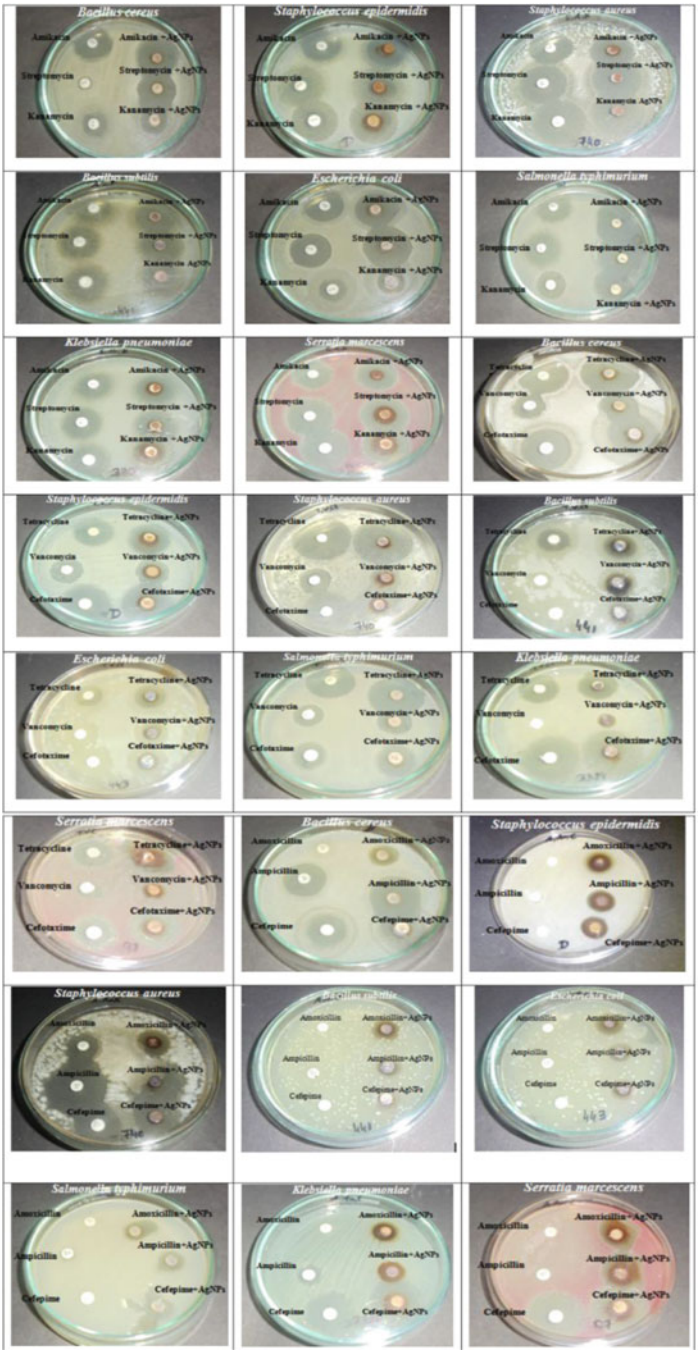

Fig. 12.5 Plates showing the increase in diameter of inhibition zone of antibiotics with AgNPs against pathogenic bacteria

Table 12.4 Inhibition zone (mm) of different antibiotics (with and without AgNPs) against Gram-positive and Gram-negative bacteria

Pathogens						Antibiotics				
		Streptomycin	Amikacin	Kanamycin	Vancomycin	Tetracycline	Ampicillin	Cefepime	Amoxicillin	Cefetaxime
B. cereus	A	09	24	15	19	21	25	22	11	33
	B	24	27	25	26	37	28	30	19	39
	C	6.1	0.3	1.7	0.9	2.1	0.2	0.8	1.9	0.4
S. epidermidis	A	27	26	25	18	22	07	06	06	25
	B	35	31	27	18	30	19	16	16	25
	C	0.7	0.4	0.2	0.0	0.8	6.4	6.1	6.1	0.0
S. aureus	A	27	29	26	13	36	29	1 9	15	24
	B	29	32	29	19	39	29	23	20	28
	C	0.1	0.2	0.2	1.1	0.1	0.0	0.5	0.5	0.4
B. subtilis	A	19	23	19	15	12	06	06	06	06
	B	26	26	23	21	19	13	16	13	14
	C	0.9	0.3	0.5	0.9	1.5	3.7	6.1	3.7	4.4
E. coli	A	23	22	15	06	17	06	06	06	06
	B	27	27	15	20	20	14	13	16	13
	C	0.4	0.5	0.0	10.1	0.4	4.4	3.7	6.1	3.7
S. typhimurium	A	22	24	19	12	28	06	06	06	10
	B	31	32	25	20	31	15	14	14	19
	C	0.9	0.8	0.7	1.8	0.2	5.2	4.4	4.4	2.6
K. pneumoniae	A	18	19	20	06	21	11	23	06	25
	B	21	21	22	12	25	16	28	14	30
	C	0.4	0.2	0.2	0.3	0.4	1.1	0.5	4.4	0.4
S. marcescens	A	22	26	24	11	20	06	27	06	16
	B	27	26	26	11	27	24	27	26	20
	C	0.5	0.0	0.2	0.0	0.8	15.0	0.0	17.8	0.6

Courtesy to: J of Rad res and app sciences 9(2016): 217–227

12.7 Conclusion and Future Prospects

Nanoparticles have manifold applications in numerous fields of science such as electronics, probes, disease diagnostics and treatment, remediation, imaging, and cellular transportation. Various physicochemical methods are being used to synthesize Nps. But, biogenic reduction of the salts to produce NPs is inexpensive, safe, and eco-friendly. Furthermore, NPs of desired morphology and size are also synthesized in massive amounts through this process. Their reduction potential and stability are endorsed to bioactive molecules existing in these biological resources. Among these bio-reductants, plant extracts are more advantageous than biological resources. Therefore, in this prospect, using plant sources for NPs synthesis can open new horizons in the future for antibacterial action as well.

The developing microbial resistance can be ruled out, by many means of many nanomaterials. However, several preclinical and clinical trials are on research levels for better considerations to visualize the restrictions as well as the potential of many nanoparticles to elucidate the antimicrobial mechanisms of these metallo-nanoparticles. Table 12.5 summarizes the potential applications for some nanoparticles that have received some attention in research. Unlike antibiotics that may have only one mechanism of action, nanomaterials can be related to multiple cell processes owing to its potential application in the fight against multidrug-resistant microorganisms. Once explored, it will revolutionize the microbiology world both on laboratory and commercial scale.

Representation of the studied and possible effects of ceria and conventional nanoparticles on a bacterial lipid bilayer and cytoplasm is as follows: (1) damage of the cell wall and peptidoglycan layer caused by direct contact with nanoparticles; (2) release of toxic ions; (3) damage of proton efflux bombs with serious problems on pH regulation and modification of membrane charges; (4) generation of reactive oxygen species (ROS) that can damage biological systems (degrading the cell wall); (5) reactive oxygen species (ROS) degrading DNA, RNA, and proteins that can also interfere in protein synthesis; and (6) low adenosintriphosphat (ATP) production due

Table 12.5 Some nanoparticles with their possible antimicrobial mechanism and current or future applications in health sciences

Nanomaterial	Antimicrobial mechanism	Applications
Silver (Ag)	1, 2, 3, 4, 5, 6	Potable water filters, clothing, medical devices, coatings for washing, refrigerators, food containers
ZnO	2, 4, 5	Antibacterial creams, lotions and ointment, deodorant, self-cleaning glass and ceramics
Cu/CuO	4, 5	Medical devices
TiO_2	1,4, 5	Air purifiers, water treatment systems for organic contaminant degradation, biofouling-resistant surfaces
Al_2O_3	5	Coating surfaces
CeO_2	5	Modify the material to exert antioxidant effects through altered electronic states

to acidification (mechanism 3) and reactive oxygen species (ROS) presence (mechanisms 4 and 5) (Courtesy to: Formatex 2013: 143–154).

References

Abed N, Couvreur P (2014) Nanocarriers for antibiotics: a promising solution to treat intracellular bacterial infections. Int J Antimicrob Agents 43(6):485–496. https://doi.org/10.1016/j.ijantimicag.2014.02.009

Actis L, Srinivasan A, Lopez-Ribot JL, Ramasubramanian AK, Ong JL (2015) Effect of silver nanoparticle geometry on methicillin susceptible and resistant Staphylococcus aureus, and osteoblast viability. J Mater Sci 26(7):215. https://doi.org/10.1007/s10856-015-5538-8

Ahmad T, Wani IA, Lone IH, Ganguly A, Manzoor N, Ahmad A, Ahmed J, Al-Shihri AS (2013) Antifungal Activity of Gold Nanoparticles Prepared by Solvo thermal Method. Mater Res Bull 48(1):12–20. https://doi.org/10.1016/j.materresbull.2012.09.069

Andrade F, Rafael D, Videira M, Ferreira D, Sosnik A, Sarmento B (2013) Nanotechnology and pulmonary delivery to overcome resistance in infectious diseases. Adv Drug Deliv Rev 65 (13–14):1816–1827. https://doi.org/10.1016/j.addr.2013.07.020

Arakha M, Sweta P, Devyani S, Tapan KP, Bairagi CM, Krishna P, Bibekanand M, Suman J (2015) Antimicrobial activity of iron oxide nanoparticle upon modulation of nanoparticle-bacteria interface. Sci Rep 5:14813. https://doi.org/10.1038/srep14813

Bae E, Park H-J, Lee J, Kim Y, Yoon J, Park K, Choi K, Yi J (2010) Repeated-dose toxicity and inflammatory responses in mice by oral administration of silver nanoparticles. Environ Toxicol Pharmacol 30(2):162–168. https://doi.org/10.1016/j.etap.2010.05.004

Baig MS, Ahad A, Aslam M, Imam SS, Aqil M, Ali A (2016) Application of box-Behnken design for preparation of levofloxacin-loaded stearic acid solid lipid nanoparticles for ocular delivery: optimization, in vitro release, ocular tolerance, and antibacterial activity. Int J Biol Macromol 85:258–270. https://doi.org/10.1016/j.ijbiomac.2015.12.077

Baram-Pinto D, Shukla S, Perkas N, Gedanken A, Sarid R (2009) Inhibition of herpes simplex virus type 1 infection by silver nanoparticles capped with mercaptoethane sulfonate. Bioconjug Chem 20:1497–1502. https://doi.org/10.1021/bc900215b

Baxter JB, Aydil ES (2005) Nanowire-based dye-sensitized solar cells. Appl Phys Lett 86:053114. https://doi.org/10.1063/1.1861510

Beaber JW, Hochhut B, Waldor MK (2004) SOS response promotes horizontal dissemination of antibiotic resistance genes. Nature 427:72–74. https://doi.org/10.1038/nature02241

Brayner R, Ferrari-Iliou R, Brivois N, Djediat S, Benedetti MF, Fiévet F (2006) Toxicological impact studies based on Escherichia coli Bacteria in ultrafine ZnO Nanoparticles colloidal medium. Nano Lett 6(4):866–870. https://doi.org/10.1021/nl052326h

Brooks BD, Brooks AE (2014) Therapeutic strategies to combat antibiotic resistance. Adv Drug Deliv Rev 78:14–27. https://doi.org/10.1016/j.addr.2014

Brunskill EW, Bayles KW (1996) Identification and molecular characterization of a putative regulatory locus that affects autolysis in *Staphylococcus aureus*. J Bacteriol 178:611–618

Bugg TD, Walsh CT (1992) Intracellular steps of bacterial cell wall peptidoglycan biosynthesis: enzymology, antibiotics, and antibiotic resistance. Nat Prod Rep 9:199–215. https://doi.org/10.1128/jb.178.3.611-618.1996

Cavassin ED, de Figueiredo LF, Otoch JP, Seckler MM, de Oliveira RA, Franco FF, Marangoni VS, Zucolotto V, Levin AS, Costa SF (2015) Comparison of methods to detect the in vitro activity of silver nanoparticles (AgNP) against multidrug resistant bacteria. J Nanobiotechnol 13:64. https://doi.org/10.1186/s12951-015-0120-6

Cha SH, Hong J, McGuffie M, Yeom B, VanEpps JS, Kotov NA (2015) Shape-dependent biomimetic inhibition of enzyme by nanoparticles and their antibacterial activity. ACS Nano 9(9):9097–9105. https://doi.org/10.1021/acsnano.5b03247

Chambers BA, Afrooz ARMN, Bae S, Aich N, Katz L, Saleh NB, Kirisits MJ (2013) Effects of chloride and ionic strength on physical morphology, dissolution, and bacterial toxicity of silver nanoparticles. Environ Sci Technol 48(1):761–769. https://doi.org/10.1021/es403969x

Chen CW, Hsu CY, Lai SM, Syu WJ, Wang TY, Lai PS (2014) Metal nanobullets for multidrug resistant bacteria and biofilms. Adv Drug Deliv Rev 78:88–104. https://doi.org/10.1016/j.addr.2014.08.004

Cirz RT, Chin JK, Andes DR, de Crécy-Lagard V, Craig WA, Romesberg FE (2005) Inhibition of mutation and combating the evolution of antibiotic resistance. PLoS Biol 3(6):e176. https://doi.org/10.1371/journal.pbio.0030176

Courcelle J, Hanawalt PC (2003) RecA-dependent recovery of arrested DNA replication forks. Annu Rev Genet 37:611–646. https://doi.org/10.1146/annurev.genet.37.110801.142616

Cui Y, Zhao Y, Tian Y, Zhang W Lü X, Jiang X (2012) The molecular mechanism of action of bactericidal gold nanoparticles on *Escherichia coli*. Biomaterials 33(7):2327–2333. https://doi.org/10.1016/j.biomaterials.2011.11.057

Daeihamed M, Dadashzadeh S, Haeri A, Akhlaghi MF (2017) Potential of liposomes for enhancement of oral drug absorption. Curr Drug Deliv Syst 14(2):289–303. https://doi.org/10.2174/1567201813666160115125756

Dallas P, Sharma VK, Zboril R (2011) Silver polymeric nanocomposites as advanced antimicrobial agents: classification, synthetic paths, applications, and perspectives. Adv Colloid Interf Sci 166:119–135. https://doi.org/10.1016/j.cis.2011.05.008

De-Gusseme B, Sintubin L, Baert L, Thibo E, Hennebel T, Vermeulen G, Uyttendaele M, Verstraete W, Boon N (2010) Biogenic silver for disinfection of water contaminated with viruses. Appl Environ Microbiol 76:1082–1087. https://doi.org/10.1128/AEM.02433-09

Deplanche K, Caldelari I, Mikheenko IP, Sargent F, Macaskie LE (2010) Involvement of hydrogenases in the formation of highly catalytic Pd(0) nanoparticles by bioreduction of Pd(II) using Escherichia coli mutant strains. Microbiology 156(9):2630–2640. https://doi.org/10.1099/mic.0.036681-0

Dobias J, Bernier-Latmani R (2013) Silver release from silver nanoparticles in natural waters. Environ Sci Technol 47:4140–4146. https://doi.org/10.1021/es304023p

Drlica K, Snyder M (1978) Superhelical *Escherichia coli* DNA: relaxation by coumermycin. J Mol Biol 120:145–154. https://doi.org/10.1016/0022-2836(78)90061-X

Drlica K, Malik M, Kerns RJ, Zhao X (2008) Quinolone-mediated bacterial death. Antimicrob Agents Chemother 52:385–392. https://doi.org/10.1128/AAC.01617-06

Dykman L, Khlebtsov N (2011) Gold nanoparticles in biology and medicine: recent advances and prospects. Acta Nat 3(2):34–55 https://www.ncbi.nlm.nih.gov/pmc/articles/PMC3347577/

Espeli O, Marians KJ (2004) Untangling intracellular DNA topology. Mol Microbiol 52:925–931. https://doi.org/10.1111/j.1365-2958.2004.04047.x

Fang B, Jiang Y, Nusslein K, Rotello VM, Santore MM (2015) Antimicrobial surfaces containing cationic nanoparticles: how immobilized, clustered, and protruding cationic charge presentation affects killing activity and kinetics. Colloids Surf B 125:255–263. https://doi.org/10.1016/j.colsurfb.2014.10.043

Fayaz AM, Balaji K, Girilal M, Yadav R, Kalaichelvan PT, Venketesan R (2010) Biogenic synthesis of silver nanoparticles and their synergistic effect with antibiotics: a study against gram-positive and gram-negative bacteria. Nanomed Nanotechnol Biol Med 6:103–109. https://doi.org/10.1016/j.nano.2009.04.006

Gajbhiye M, Kesharwani J, Ingle A, Gade A, Rai M (2009) Fungus-mediated synthesis of silver nanoparticles and their activity against pathogenic fungi in combination with fluconazole. Nanomed Nanotechnol Biol Med 5(4):382–386

Galdiero S, Falanga A, Vitiello M, Marra MCV, Galdiero M (2011) Silver nanoparticles as potential antiviral agents molecules. Mol Ther 16:8894–8918. https://doi.org/10.3390/molecules16108894

Garrett RA (2000) The ribosome: structure, function, antibiotics, and cellular interactions. ASM Press, Washington, DC. https://doi.org/10.1128/9781555818142

Gellert M, Mizuuchi K, O'Dea MH, Nash HA (1976) DNA gyrase: an enzyme that introduces superhelical turns into DNA. Proc Natl Acad Sci 73:3872–3876 https://www.ncbi.nlm.nih.gov/pmc/articles/PMC431247/

Gellert M, Mizuuchi K, O'Dea MH, Itoh T, Tomizawa JL (1977) Nalidixic acid resistance: a second genetic character involved in DNA gyrase activity. Proc Natl Acad Sci 74:4772–4776 https://www.ncbi.nlm.nih.gov/pmc/articles/PMC432037/

Ghosh S, Patil S, Ahire M, Kitture R, Kale S, Pardesi K, Cameotra BJ, Dhavale J, Chopade B (2012) Synthesis of silver nanoparticles using *Dioscorea bulbifera* tuber extract and evaluation of its synergistic potential in combination with antimicrobial agents. Int J Nanomedicine 7:483–496. https://doi.org/10.2147/IJN.S24793

Glišić BĐ, Djuran MI (2014) Gold complexes as antimicrobial agents: an overview of different biological activities in relation to the oxidation state of the gold ion and the ligand structure. Dalton Trans 43(16):5950–5969. https://doi.org/10.1039/c4dt00022f

Gopinath K, Gowri S, Arumugam A (2013) Phytosynthesis of silver nanoparticles using *Pterocarpus santalinus* leaf extract and their antibacterial properties. J Nanostruct Chem 3 (1):68. https://doi.org/10.1186/2193-8865-3-68

Groicher KH, Firek BA, Fujimoto DF, Bayles KW (2000) The Staphylococcus aureus lrgAB operon modulates murein hydrolase activity and penicillin tolerance. J Bacteriol 182:1794–1801 https://www.ncbi.nlm.nih.gov/pmc/articles/PMC101860/

Gu H, Ho P, Tong E, Wang L, Xu B (2003) Presenting vancomycin on nanoparticles to enhance antimicrobial activities. Nano Lett 3(9):1261–1263. https://doi.org/10.1021/nl034396z

Guerin E, Cambray G, Sanchez-Alberola N, Campoy S, Erill I, Da Re S, Gonzalez-Zorn B, Barbé J, Ploy MC, Mazel D (2009) The SOS response controls integrin recombination. Science 324:1034. https://doi.org/10.1126/science.1172914

Guo BL, Han P, Guo LC, Cao YQ, Li AD, Kong JZ, Zhai HF, Wu D (2015) The antibacterial activity of ta-doped ZnO nanoparticles. Nanoscale Res Lett 10(1):1047. https://doi.org/10.1186/s11671-015-1047-4

Gurunathan S, Han JW, Kwon DN, Kim JH (2014) Enhanced antibacterial and anti-biofilm activities of silver nanoparticles against gram-negative and gram-positive bacteria. Nanoscale Res Lett 9(1):373. https://doi.org/10.1186/1556-276X-9-373

Hadinoto K, Sundaresan A, Cheow WS (2013) Lipid-polymer hybrid nanoparticles as a new generation therapeutic delivery platform: a review. Eur J Pharm Biopharm 85(3):427–443. https://doi.org/10.1016/j.ejpb.2013.07.002

Han SW, Lee SJ, Kim K (2001) Self-assembled monolayers of aromatic thiol and Selenol on silver: comparative study of Adsorptivity and stability Lang. Langmuir 17(22):6981–6987. https://doi.org/10.1021/la010464q

He W, Kim HK, Wamer WG, Melka D, Callahan JH, Yin JJ (2014) Photogenerated charge carriers and reactive oxygen species in ZnO/au hybrid nanostructures with enhanced photocatalytic and antibacterial activity. J Am Chem Soc 36(2):750–757. https://doi.org/10.1021/ja410800y

Henglein A (1998) Colloidal silver nanoparticles: photochemical preparation and interaction with O_2, CCl_4, and some metal ions. Chem Mater 10(1):444–450. https://doi.org/10.1021/cm970613j

Herdt AR, Drawz SM, Kang Y, Taton TA (2006) DNA dissociation and degradation at gold nanoparticle surfaces. Colloids Surf B Biointerfaces 51(2):130–139. https://doi.org/10.1016/j.colsurfb.2006.06.006

Hernández J, Solla-Gullón J, Herrero E, Aldaz A, Feliu JM (2006) Methanol oxidation on gold nanoparticles in alkaline media: unusual Electrocatalytic activity. Electrochim Acta 52 (4):1662–1669. https://doi.org/10.1016/j.electacta.2006.03.091

Hetrick EM, Shin JH, Paul HS, Schoenfisch MH (2009) Anti-biofilm efficacy of nitric oxide-releasing silica nanoparticles. Biomaterials 30(14):2782–2789. https://doi.org/10.1016/j.biomaterials.2009.01.052

Hoch JA (2000) Two-component and phosphorelay signal transduction. Curr Opin Microbiol 3:165–170. https://doi.org/10.1016/S1369-5274(00)00070-9

Holtje JV (1998) Growth of the stress-bearing and shape maintaining murein sacculus of Escherichia coli. Microbiol Mol Biol Rev 62:181–203 http://mmbr.asm.org/content/62/1/181.long

Hong X, Wen J, Xiong X, Hu Y (2016) Shape effect on the antibacterial activity of silver nanoparticles synthesized via a microwave-assisted method. Environ Sci Pollut Res Int 23 (5):4489–4497. https://doi.org/10.1007/s11356-015-5668

Hooper DC, Rubinstein E (2003) Quinolone antimicrobial agents. ASM Press, Washington, DC. https://doi.org/10.3201/eid1006.040025

Howard CR, Fletcher NF (2012) Emerging virus diseases: can we ever expect the unexpected? Emerg Microbes Infect 1:34–46. https://doi.org/10.1038/emi.2012.47

Howard BM, Pinney RJ, Smith JT (1993) Function of the SOS process in repair of DNA damage induced by modern 4-quinolones. J Pharm Pharmacol 45:658–662. https://doi.org/10.1111/j.2042-7158.1993.tb05673.x

Jain PK, Lee KS, Sayed IH, Sayed MA (2006) Calculated absorption and scattering properties of gold nanoparticles of different size, shape, and composition: applications in biological imaging and biomedicine. J Phys Chem B 110(14):7238–7248. https://doi.org/10.1021/jp057170o

Jo YK, Kim BH, Jung G (2009) Antifungal activity of silver ions and nanoparticles on phytopathogenic fungi. Plan Dis 93:1037–1043. https://doi.org/10.1094/PDIS-93-10-1037

Josephine HR, Kumar I, Pratt RF (2004) The perfect penicillin? Inhibition of a bacterial DD-peptidase by peptidoglycan-mimetic β-lactams. J Am Chem Soc 126:8122–8123. https://doi.org/10.1021/ja048850s

Jyoti K, Baunthiyal M, Singh A (2016) Characterization of silver nanoparticles synthesized using *Urtica dioica* Linn. Leaves and their synergistic effects with antibiotics. J Radiat Res Appl Sci 9 (3):217–227

Katz L, Ashley GW (2005) Translation and protein synthesis: macrolides. Chem Rev 105:499–528. https://doi.org/10.1021/cr030107f

Kaviya S, Santhanalakshmi J, Viswanathan B, Muthumary J, Srinivasan K (2011) Biosynthesis of silver nanoparticles using Citrus sinensis Peel extract and its antibacterial activity. Spectrochim Acta A Mol Biomol Spectrosc 79(3):594–598. https://doi.org/10.1016/j.saa.2011.03.040

Khameneh B, Diab R, Ghazvini K, Fazly Bazzaz BS (2016) Breakthroughs in bacterial resistance mechanisms and the potential ways to combat them. Microb Pathog 95:32–42. https://doi.org/10.1016/j.micpath.2016

Khan MF, Ansari AH, Hameedullah M, Ahmad E, Husain FM, Zia Q, Baig U, Zaheer MR, Alam MM, Khan AM, AlOthman ZA, Ahmad I, Ashraf GM, Aliev G (2016) Sol-gel synthesis of thorn-like ZnO nanoparticles endorsing mechanical stirring effect and their antimicrobial activities: potential role as nano-antibiotics. Sci Rep 6:27689. https://doi.org/10.1038/srep27689

Kim S, Ryu DY (2013) Silver nanoparticle-induced oxidative stress, genotoxicity and apoptosis in cultured cells and animal tissues. J Appl Toxicol 33(2):78–89. https://doi.org/10.1002/jat.2792

Kim KJ, Sung WS, Suh BK, Moon SK, Choi JS, Kim JG, Lee DG (2009) Antifungal activity and mode of action of silver nano-particles on *Candida albicans*. Biometals 22:235–242. https://doi.org/10.1007/s10534-008-9159-2

Kitano K, Tomasz A (1979) Triggering of autolytic cell wall degradation in Escherichia coli by beta-lactam antibiotics. Antimicrob Agents Chemother 16:838–848. https://doi.org/10.1128/AAC.16.6.838

Lellouche J, Friedman A, Gedanken A, Banin E (2012a) Antibacterial and antibiofilm properties of yttrium fluoride nanoparticles. Int J Nanomed 7:5611–5624. https://doi.org/10.2147/IJN.S37075

Lellouche J, Friedman A, Lahmi R, Gedanken A, Banin E (2012b) Antibiofilm surface functionalization of catheters by magnesium fluoride nanoparticles. Int J Nanomed 7:1175–1188. https://doi.org/10.2147/IJN.S26770

Levard C, Mitra S, Yang T, Jew AD, Badireddy AR, Lowry GV, Brown GE (2013) Effect of chloride on the dissolution rate of silver nanoparticles and toxicity to *E coli.* Environ Sci Technol 47(11):5738–5745. https://doi.org/10.1021/es400396f

Li WR, Xie XB, Shi QS, Zeng HY, You-Sheng OY, Chen YB (2010) Antibacterial activity and mechanism of silver nanoparticles on *Escherichia coli*. Appl Microbiol Biotechnol 85 (4):1115–1122. https://doi.org/10.1007/s00253-009-2159-5

Li M, Zhu L, Lin D (2011) Toxicity of ZnO nanoparticles to Escherichia coli: mechanism and the influence of medium components. Environ Sci Technol 45(5):1977–1983. https://doi.org/10.1021/es102624t

Lim EK, Chung BH, Chung SJ (2018) Recent advances in pH-sensitive polymeric nanoparticles for smart drug delivery in cancer therapy. Curr Drug Targets 19(4):300–317. https://doi.org/10.2174/1389450117666160602202339

Liu J, Lu YA (2003) Colorimetric Lead biosensor using DNAzyme-directed assembly of gold nanoparticles. J Am Chem Soc 125(22):6642–6643. https://doi.org/10.1021/ja034775u

Liu Y, Tee JK, Chiu GN (2015) Dendrimers in oral drug delivery application: current explorations, toxicity issues and strategies for improvement. Curr Pharm Des 21(19):2629–2642. https://doi.org/10.2174/1381612821666150416102058

Liu J-L, Zhang W-J, Li X-D, Na Y, Pan W-S, Kong J, Zhang J-S (2016) Sustained-release Genistein from nanostructured lipid carrier suppresses human lens epithelial cell growth. Indian J Ophthalmol 9(5):643–649. https://doi.org/10.18240/ijo.2016.05.01

Lopez N, Janssens T, Clausen B, Xu Y, Mavrikakis M, Bligaard T, Nørskov JK (2004) On the origin of the catalytic activity of gold nanoparticles for low-temperature CO oxidation. J Catal 223(1):232–235. https://doi.org/10.1016/j.jcat.2004.01.001

Maeda H (2010) Tumor-selective delivery of macromolecular drugs via the EPR effect: background and future prospects. Bioconjug Chem 21(5):797–802. https://doi.org/10.1021/bc100070g

Markowska K, Grudniak AM, Wolska KI (2013) Silver nanoparticles as an alternative strategy against bacterial biofilms. Acta Biochim Pol 60(4):523–530 http://www.actabp.pl/pdf/4_2013/523.pdf

Marzieh R, Majid K, Seyed MJ (2012) Bacteriostatic agents. Chapter 11. In: A search for antibacterial agents, pp 119–234. https://doi.org/10.5772/45652

Mehmood S, Rehman MA, Ismail H, Mirza B, Bhatti AS (2015) Significance of postgrowth processing of ZnO nanostructures on antibacterial activity against gram-positive and gram-negative bacteria. Int J Nanomedicine 10:4521–4533. https://doi.org/10.2147/IJN.S83356

Miao L, Wang C, Hou J, Wang P, Ao Y, Li Y, Geng N, Yao Y, Lv B, Yang Y, You G, Xu Y (2016) Aggregation and removal of copper oxide (CuO) nanoparticles in wastewater environment and their effects on the microbial activities of wastewater biofilms. Bioresour Technol 216:537–544. https://doi.org/10.1016/j.biortech.2016.05.082

Mishra A, Tripathy SK, Yun SI (2011) Bio-synthesis of gold and silver nanoparticles from Candida guilliermondii and their antimicrobial effect against pathogenic Bacteria. J Nano Sci Nanotechnol 11(1):243–248. https://doi.org/10.1166/jnn.2011.3265

Misra SK, Dybowska A, Berhanu D, Luoma SN, Valsami Jones E (2012) The complexity of nanoparticle dissolution and its importance in nanotoxicological studies. Sci Total Environ 438:225–232. https://doi.org/10.1016/j.scitotenv.2012.08.066

Moreillon P, Markiewicz Z, Nachman S, Tomasz A (1990) Two bactericidal targets for penicillin in pneumococci: autolysis-dependent and autolysis-independent killing mechanisms. Antimicrob Agents Chemother 34:33–39. https://doi.org/10.1128/AAC.34.1.33

Muhling M, Bradford A, Readman JW, Somerfield PJ, Handy RD (2009) An investigation into the effects of silver nanoparticles on antibiotic resistance of naturally occurring bacteria in an estuarine sediment. Mar Environ Res 68(5):278–283. https://doi.org/10.1016/j.marenvres.2009.07.001

Nagy A, Harrison A, Sabbani S, Munson RS, Dutta PK, Waldman WJ (2011) Silver nanoparticles embedded in zeolite membranes: release of silver ions and mechanism of antibacterial action. Int J Nanomed 6:1833–1852. https://doi.org/10.2147/IJN.S24019

Narasimha G (2012) Antiviral activity of silver nanoparticles synthesized by fungal strain *Aspergillus niger*. J Nanosci Nanotechnol 6(1):18–20 https://www.researchgate.net/publication/222102689

Naseri N, Valizadeh H, Zakeri-Milani P (2015) Solid lipid nanoparticles and nanostructured lipid carriers: structure, preparation and application. Adv Pharm Bull 5(3):305–313. https://doi.org/10.15171/apb.2015.043

Nasrollahi A, Pourshamsian K, Mansourkiaee P (2011) Antifungal activity of silver nanoparticles on some of fungi. Int J Nanomedicine 1:233–239. https://doi.org/10.7508/IJND.2010.03.007

Nissen P, Hansen J, Ban N, Moore PB, Steitz TA (2000) The structural basis of ribosome activity in peptide bond synthesis. Science 289:920–930. https://doi.org/10.1126/science.289.5481.920

Novak R, Charpentier E, Braun JS, Tuomanen E (2000) Signal transduction by a death signal peptide: uncovering the mechanism of bacterial killing by penicillin. Mol Cell Biol 5:49–57. https://doi.org/10.1016/S1097-2765(00)80402-5

Nussbaum VF, Brands M, Hinzen B, Weigand S, Häbich D (2006) Antibacterial natural products in medicinal chemistry – exodus or revival? Angew Chem Int Ed 45:5072–5129. https://doi.org/10.1002/anie.200600350

Patel U, Yong PY, Frank WH, Janet K, Andrew MS, David LP, Michael GK, Ekaterina VB (2001) Oxazolidinones mechanism of action: inhibition of the first peptide bond formation. J Biol Chem 276:37199–37205. https://doi.org/10.1074/jbc.M102966200

Pal S, Tak YK, Song JM (2007) Does the antibacterial activity of silver nanoparticles depend on the shape of the nanoparticle? A study of the gram-negative bacterium *Escherichia coli*. Appl Environ Microbiol 73(6):1712–1720. https://doi.org/10.1128/AEM.02218-06

Pan X, Wang Y, Chen Z, Pan D, Cheng Y, Liu Z, Lin Z, Guan X (2013) Investigation of antibacterial activity and related mechanism of a series of nano-Mg(OH)2. ACS Appl Mater Interfaces 5(3):1137–1142. https://doi.org/10.1021/am302910q

Parikh AN, Gillmor SD, Beers JD, Beardmore KM, Cutts RW, Swanson BI (1999) Characterization of chain molecular assemblies in long-chain, layered silver thiolates: a joint infrared spectroscopy and X-ray diffraction study. J Phys Chem B 103(15):2850–2861. https://doi.org/10.1021/jp983938b

Park JT, UeharaT (2008) How bacteria consume their own exoskeletons (turnover and recycling of cell wall peptidoglycan). Microbiol Mol Biol Rev 72:211–227. https://doi.org/10.1128/MMBR.00027-07

Patra JM, Panda SS, Dhal NK (2015) A review on green synthesis of gold nanoparticles. Int J Pharma Bio Sci 6(3):251–261 http://www.ijpbs.net/cms/php/upload/4537_pdf.pdf

Pawan K, Rajesh T, Ashok C (2012) An in vitro study of the antifungal activity of silver/chitosan nanoformulations against important seed borne pathogens. Int J Sci Technol Res 1(6):83–86

Payne JN, Waghwani HK, Connor MG, Hamilton W, Tockstein S, Moolani H, Chavda F, Badwaik V, Lawrenz MB, Dakshinamurthy R (2016) Novel synthesis of kanamycin conjugated gold nanoparticles with potent antibacterial activity. Front Microbiol 7:634. https://doi.org/10.3389/fmicb.2016.00607

Peng YP, Lo SL, Ou HH, Lai SW (2010) Microwave-assisted hydrothermal synthesis of N-doped titanate nanotubes for visible-light-responsive photocatalysis. J Hazard Mater 183 (1–3):754–758. https://doi.org/10.1016/j.jhazmat.2010.07.090

Peretyazhko TS, Zhang Q, Colvin VL (2014) Size-controlled dissolution of silver nanoparticles at neutral and acidic pH conditions: kinetics and size changes. Environ Sci Technol 48 (20):11954–11961. https://doi.org/10.1021/es5023202

Peulen TO, Wilkinson KJ (2011) Diffusion of nanoparticles in a biofilm. Environ Sci Technol 45 (8):3367–3373. https://doi.org/10.1021/es103450g

Podporska-Carroll J, Myles A, Quilty B, McCormack DE, Fagan R, Hinder SJ, Dionysiou DD, Pillai SC (2017) Antibacterial properties of F-doped ZnO visible light photocatalyst. J Hazard Mater 324:39–47. https://doi.org/10.1016/j.jhazmat.2015.12.038

Prasannakumar JB, Vidya KS, Anantharaju G, Ramgopal H, Nagabhushana SC, Sharma B, Daruka Prasad SC, Prashantha RB, Basavaraj H, Rajanaik KL (2015) Bio-mediated route for the

synthesis of shape tunable Y2O3:Tb3+ nanoparticles: photoluminescence and antibacterial properties. Spectrochim Acta A Mol Biomol Spectrosc 151:131–140. https://doi.org/10.1016/j.saa.2015.06.081

Qi G, Li L, Yu F, Wang H (2013) Vancomycin-modified mesoporous silica nanoparticles for selective recognition and killing of pathogenic gram-positive bacteria over macrophage-like cells. ACS Appl Mater Interfaces 5(21):10874–10881. https://doi.org/10.1021/am403940d

Radovic-Moreno AF, Lu TK, Puscasu VA, Yoon CJ, Langer R, Farokhzad OC (2012) Surface charge-switching polymeric nanoparticles for bacterial cell wall-targeted delivery of antibiotics. ACS Nano 6(5):4279–4287. https://doi.org/10.1021/nn3008383

Ranghar S (2012) Nanoparticle-based drug delivery systems: promising approaches against infections. Braz Arch Biol Technol 57:209–222. https://doi.org/10.1590/S1516-89132013005000011

Rice KC, Brian AF, Jeremy BN, Soo-Jin Y, Toni GP, Kenneth WB (2003) The Staphylococcus aureus cidAB operon: evaluation of its role in regulation of murein hydrolase activity and penicillin tolerance. J Bacteriol 185:2635–2643. https://doi.org/10.1128/JB.185.8.2635-2643.2003

Rubinstein E (2001) History of quinolones and their side effects. Chemotherapy 47(3):3–8. https://doi.org/10.1159/000057838

Saliani M, Jalal R, Kafshdare Goharshadi E (2015) Effects of pH and temperature on antibacterial activity of zinc oxide nanofluid against Escherichia coli O157:H7 and Staphylococcus aureus. Jundish J Microbiol 8(2):e17115. https://doi.org/10.5812/jjm.17115

Sambhy V, MM MB, Peterson BR, Sen A (2006) Silver bromide nanoparticle/polymer composites: dual action tunable antimicrobial materials. J Am Chem Soc 128:9798. https://doi.org/10.1021/ja061442z

Sangari M, Umadevi M, Mayandi J, Pinheiro JP (2015) Photocatalytic degradation and antimicrobial applications of F-doped MWCNTs/ TiO2 composites. Spectrochim Acta A 139:290–295. https://doi.org/10.1016/j.saa.2014.12.061

Sawai J, Igarashi H, Hashimoto A, Kokugan T, Shimizu M (1995) Evaluation of growth inhibitory effect of ceramics powder slurry on Bacteria by conductance method. J Chem Eng Jpn 28:288–293. https://doi.org/10.1252/jcej.28.288

Singh R, Wagh P, Wadhwani S, Gaidhaini S, Kumbhar A, Bellare J, Chopade BA (2013) Synthesis, optimization, and characterization of silver nanoparticles from *Acinetobacter calcoaceticus* and their enhanced antibacterial activity when combined with antibiotics. Int J Nanomedicine 8:4277–4290. https://doi.org/10.2147/IJN.S48913

Singh R, Smitha MS, Singh SP (2014) The role of nanotechnology in combating multi-drug resistant bacteria. J Nanosci Nanotechnol 14(7):4745–4756 https://www.ncbi.nlm.nih.gov/pubmed/24757944

Slomberg DL, Lu Y, Broadnax AD, Hunter RA, Carpenter AW, Schoenfisch MH (2013) Role of size and shape on biofilm eradication for nitric oxide-releasing silica nanoparticles. ACS Appl Mater Interfaces 5(19):9322–9329. https://doi.org/10.1021/am402618w

Song J, Zhou J, Zhong LW (2006) Piezoelectric and semiconducting coupled power generating process of a single ZnO Belt/wire. A Technology for Harvesting Electricity from the environment. Nano Lett 6(8):1656–1662. https://doi.org/10.1021/nl060820v

Speshock JL, Murdock RC, Braydich-Stolle LK, Schrand AM, Hussain SM (2010) Interaction of silver nanoparticles with tacaribe virus. J Nano Biotechnol 8:19. https://doi.org/10.1186/1477-3155-8-19

Spratt BG (1975) Distinct penicillin binding proteins involved in the division, elongation, and shape of Escherichia coli K12. Proc Natl Acad Sci 72:2999–3003 https://www.ncbi.nlm.nih.gov/pmc/articles/PMC432906/

Stoimenov PK, Klinger RL, Marchin GL, Klabunde KJ (2002) Metal Oxide Nanoparticles as Bactericidal Agents. Langmuir 18(17):6679–6686. https://doi.org/10.1021/la0202374

Sugino A, Peebles CL, Kreuzer KN, Cozzarelli NR (1977) Mechanism of action of nalidixic acid: purification of Escherichia coli nalA gene product and its relationship to DNA gyrase and a

novel nicking closing enzyme. Proc Natl Acad Sci 74:4767–4771 https://www.ncbi.nlm.nih.gov/pmc/articles/PMC432036/

Sukhorukova IV, Sheveyko AN, Kiryukhantsev-Korneev PV, Zhitnyak IY, Gloushankova NA, Denisenko EA, Filippovich SY, Ignatov SG, Shtansky DV (2015) Toward bioactive yet antibacterial surfaces. Colloids Surf B 135:158–165. https://doi.org/10.1016/j.colsurfb.2015.06.059

Talebian N, Sadeghi Haddad Zavvare H (2014) Enhanced bactericidal action of SnO2 nanostructures having different morphologies under visible light: influence of surfactant. J Photochem Photobiol B Biol 130:132–139. https://doi.org/10.1016/j.jphotobiol.2013.10.018

Thukral DK, Dumoga S, Mishra AK (2014) Solid lipid nanoparticles: promising therapeutic nanocarriers for drug delivery. Curr Drug Deliv 11(6):771–791. https://doi.org/10.2174/1567201811061412021223335

Tile VA, Bholay AD (2012) Biosynthesis of silver nanoparticles and its antifungal activities. J Environ Res Dev 7:338–345. https://doi.org/10.2147/IJN.S98339

Tipper DJ, Strominger JL (1965) Mechanism of action of penicillins: a proposal based on their structural similarity to acyl-D-alanyl-D-alanine. Proc Natl Acad Sci 54:1133–1141 https://www.ncbi.nlm.nih.gov/pmc/articles/PMC219812/

Trefry JC, Wooley DP (2013) Silver nanoparticles inhibit vaccinia virus infection by preventing viral entry through a micropinocytosis dependent mechanism. J Biomed Nanotechnol 9:1624–1635 https://www.ncbi.nlm.nih.gov/pubmed/23980510

Uehara T, Dinh T, Bernhardt TG (2009) LytM-domain factors are required for daughter cell separation and rapid ampicillin-induced lysis in Escherichia coli. J Bacteriol 191:5094–5107. https://doi.org/10.1128/JB.00505-09

Valentine JS, Wertz DL, Lyons TJ, Liou LL, Goto JJ, Gralla EB (1998) The dark side of dioxygen biochemistry. Curr Opin Chem Biol 2(2):253–226. https://doi.org/10.1016/S1367-5931(98)80067-7

Waxman DJ, Yocum RR, Strominger JL (1980) Penicillins and cephalosporins are active site-directed acylating agents: evidence in support of the substrate analogue hypothesis. Philos Trans R Soc B 289:257–271. https://doi.org/10.1098/rstb.1980.0044

Wise EM, Park JT Jr (1965) Penicillin: its basic site of action as an inhibitor of a peptide cross-linking reaction in cell wall mucopeptide synthesis. Proc Natl Acad Sci 54:75–81 https://www.ncbi.nlm.nih.gov/pmc/articles/PMC285799/

Wu J, Shen Y, Jiang W, Jiang W, Shen Y (2016) Magnetic targeted drug delivery carriers encapsulated with pH-sensitive polymer: synthesis, characterization and in vitro doxorubicin release studies. J Biomater Sci Polym 27(13):1303–1316. https://doi.org/10.1080/09205063.2016.1195159

Xiong MH, Li YJ, Bao Y, Yang XZ, Hu B, Wang J (2012) Bacteria-responsive multifunctional nanogel for targeted antibiotic delivery. Adv Mater 24(46):6175–6180. https://doi.org/10.1002/adma.201202847

Xiu ZM, Zhang QB, Puppala HL, Colvin VL, Alvarez PZ (2012) Negligible particle-specific antibacterial activity of silver nanoparticles. Nano Lett 12(8):4271–4275. https://doi.org/10.1021/nl301934w

Xu Y, Gao C, Li X, He Y, Zhou L, Pang G, Sun S (2013) In vitro antifungal activity of silver nanoparticles against ocular pathogenic filamentous fungi. J Ocul Pharmacol Ther 29:270–274. https://doi.org/10.1089/jop.2012.0155

Yu Q, Li J, Zhang Y, Wang Y, Liu L, Li M (2016) Inhibition of gold nanoparticles (AuNPs) on pathogenic biofilm formation and invasion to host cells. Sci Rep 6:26667. https://doi.org/10.1038/srep26667

Zhang L, Pornpattananangku D, Hu CM, Huang CM (2010) Development of nanoparticles for antimicrobial drug delivery. Curr Med Chem 17(6):585–594. https://doi.org/10.2174/092986710790416290

Zhang W, Yao Y, Sullivan N, Chen Y (2011) Modeling the primary size effects of citrate-coated silver nanoparticles on their ion release kinetics. Environ Sci Technol 45(10):4422–4428. https://doi.org/10.1021/es104205a

Zhang Y, Shareena DTP, Deng H, Yu H (2015) Antimicrobial activity of gold nanoparticles and ionic gold. J Environ Sci Health C 33(3):286–327. https://doi.org/10.1080/10590501.2015.1055161

Chapter 13
Organic and Inorganic Hybrid Diglycidyl/ Tetraglycidyl Epoxy-Containing Nanocoatings on Mild Steel for Corrosion Protection and Antimicrobial Protection

D. Duraibabu and R. Manjumeena

Contents

D. Duraibabu (✉)
The Key Laboratory of Low-Carbon Chemistry & Energy Conservation of Guangdong Province/State Key Laboratory of Optoelectronic Materials and Technologies, School of Materials Science and Engineering, Sun Yat-Sen University, Guangzhou, People's Republic of China

R. Manjumeena
Center for Advanced Studies in Botany, University of Madras, Chennai, India

Mu. Naushad et al. (eds.), *Advanced Nanostructured Materials for Environmental Remediation*, Environmental Chemistry for a Sustainable World 25,
https://doi.org/10.1007/978-3-030-04477-0_13

Abstract Corrosion is constant and continuous deterioration of metal by chemical attack or reaction with its environment. Prevention is more practical and achievable than complete elimination. Protective coatings perform important functions based on the types of coatings/fillers. This review presents an overview of different types of diglycidyl/tetraglycidyl epoxy-containing organic–inorganic hybrid nanocoatings, based on their function, the substances used in coating formulations, and the nanoparticles/nanofillers used for the protection of mild steel surfaces from corrosion and microbial growth, viz., eco-friendly epoxy coatings, epoxy–inorganic compound coatings, epoxy–organic compound coatings, and organic–inorganic hybrid coatings.

Keywords Diglyciyl epoxy · Tetraglycidyl epoxy · Surface modification · Eco-friendly epoxy coating · Inorganic coating · Organic coating · Organic–inorganic hybrid coating · Salt spray · Corrosion conformance · Antimicrobial protection

13.1 Introduction

Epoxy resins are oxirane-containing oligomers, which cure through the reaction of epoxide groups with a suitable curing agent. The first production of epoxy resin occurred simultaneously in Europe and in the USA in the early 1940s. Today, a wide variety of epoxy resins of varying consistency are available. Epoxy resins are unique among all thermoset resins because of several factors: minimum pressure is needed for fabrication of products normally used for thermosetting resins; the degree of cure shrinkage is much lower and hence there is lower residual stress in the cured product than that encountered when vinyl polymerization is used to cure unsaturated polyester resins; use of a wide range of temperatures by judicious selection of curing agents enables good control over the degree of cross-linking; and the availability of the resins ranges from low-viscosity liquids to tack-free solids. Because of these unique characteristics and useful properties of network polymers, epoxy resins are widely used in structural adhesives, surface coatings, engineering composites, and electrical laminates. The chemical structures of difunctional and multifunctional epoxies are shown in Fig. 13.1.

13.2 Corrosion

One very broad definition of corrosion is that it is a natural process of deterioration of metals and alloys in a corrosive environment, which affects those properties of the metal that are intended to be preserved. Corrosion occurs in a wide variety of forms, both in pure metals and in alloys.

Well-known examples of metallic corrosion are rusting of iron and steel, blackening of silver articles, dulling of brass, and fogging of nickel.

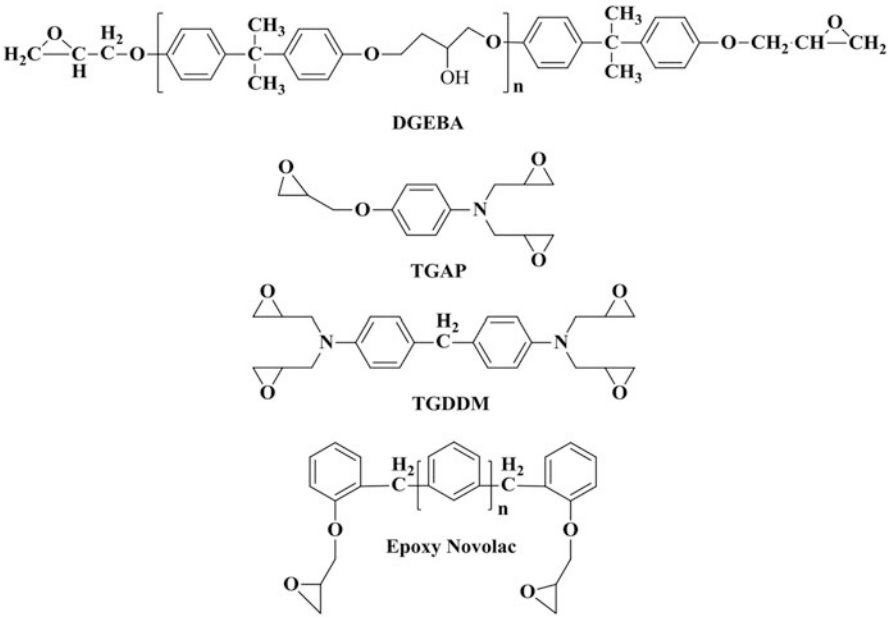

Fig. 13.1 Chemical structures of difunctional and multifunctional epoxies. *DGEBA* diglycidyl ether of bisphenol A, *TGAP* triglycidyl-p-aminophenol, *TGDDM* *N*,*N*′-tetraglycidyl diaminodiphenylmethane

13.2.1 Causes of Corrosion

Corrosion can be caused by:

- Reactivity of metal
- Presence of impurities
- Presence of air, moisture, and gases such as SO_2 and CO_2
- Presence of electrolytes

13.2.2 Importance of Corrosion Research

It has become imperative to give more attention to corrosion, for the following reasons:

- The use of metals is increasing in technological fields.
- The vast development of chemical technology and rapid population growth are leading to increases in pollution of air and water, resulting in a more corrosive environment.

13.3 Surface Preparation

Mild steel (MS) samples (of composition C 0.04%, Si 0.01%, Mn 0.17%, P 0.002%, S 0.005%, Cr 0.04%, Mo 0.03%, Ni 1.31%, Fe balance) were used for our study. The samples were degreased with acetone to remove impurities from the substrate. The samples were then subjected to sandblasting at a pressure of 100 pounds per square inch (psi) through a nozzle to get into the appropriate crevices. The particle size of the sand was 80 meshes. The distance between the substrate and the blaster was maintained at 2 feet, as illustrated in Fig. 13.2. The samples were kept in desiccators for conditioning (Ananda Kumar and Sasikumar 2010; Saravanan et al. 2016).

13.4 Salt Spray Testing

Salt spray corrosion testing was performed using epoxy-coated steel panel samples in a size of 70 mm × 50 mm × 1 mm with and without diagonal scribes on the coated panels, according to the American Society for Testing and Materials (ASTM) B 117 standard. The diagonal scribes on the coated samples were made with the help of a sharp knife for continuous exposure of the base metal in a salt-fog chamber containing a 3.5% NaCl solution used for a salt spray maintained at pH 6.9 and air

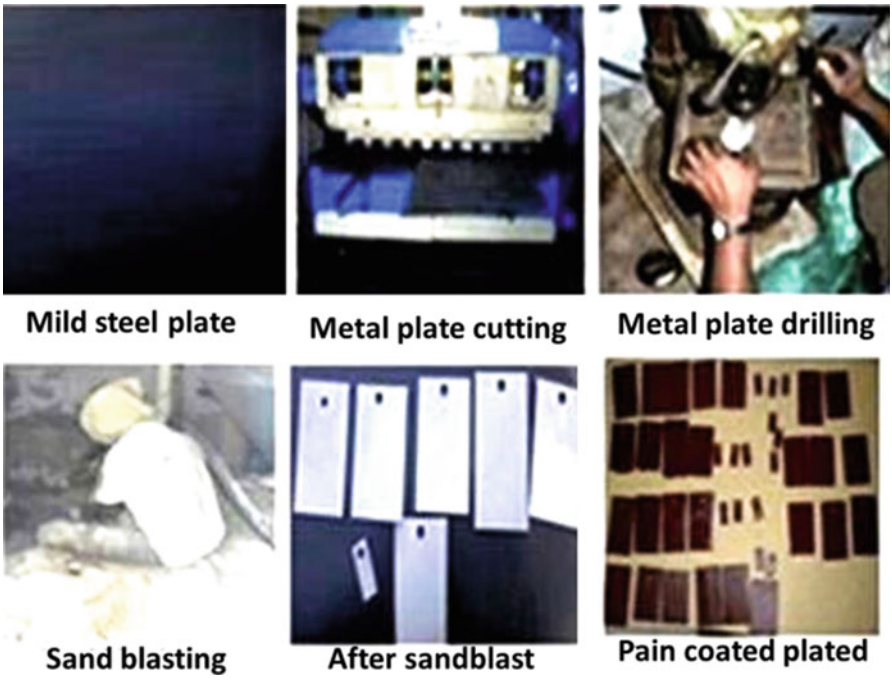

Fig. 13.2 Process used for preparing hybrid coatings (Reproduced from Saravanan et al. 2016, with permission)

pressure of 15 psi. The temperature of the salt spray chamber was kept between 33.8 °C and 35.1 °C, with a day-and-night test time of 1200 h (Fig. 13.3).

Before loading of the test samples and after completion of testing:

(a) The samples were cleaned gently prior to loading.
(b) The samples were then washed gently twice with distilled water to remove unwanted salt deposits from their steel panel surfaces and dried for 1 h.

The test sample panels were then carefully assessed for detection of any rust spots on their steel panel surfaces, and photos were taken using an Olympus 4XWIDE digital camera. The timing of formation of brown rust and blisters was noted (Berndt and Berndt 2003; Ananda Kumar et al. 2006).

13.5 Scope of the Recent Literature

The need for antibacterial properties for marine coating applications has triggered an increase in antimicrobial epoxy coating research in recent years, which is distinctly seen from the increase in the antimicrobial epoxy coatings literature published between the years 2007 and 2018, as presented in Fig. 13.4. Table 13.1 summarizes the recent literature on such coatings.

13.6 Eco-Friendly Epoxy Coatings

There is a growing need to develop eco-friendly processes for corrosion control that does not include any toxic chemical substances. Nanoparticles are prepared by heterogeneous chemical and physical methods, but in general these methods are not environmentally friendly for marine applications, petroleum production and

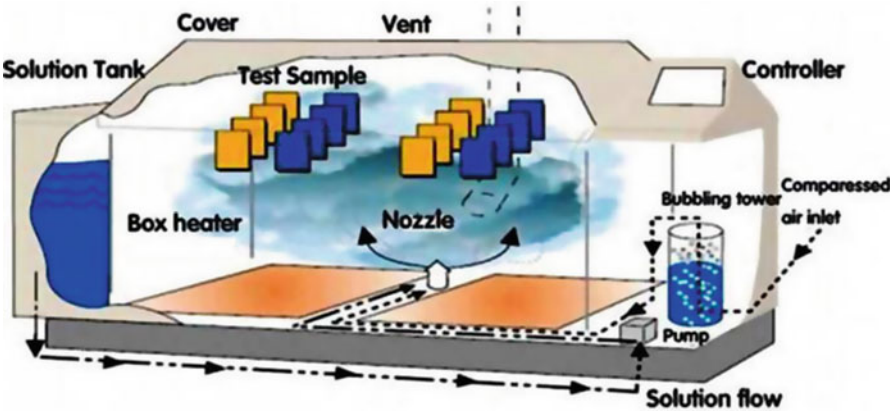

Fig. 13.3 Salt spray test chamber. (Courtesy of http://www.climatictestchambers.com)

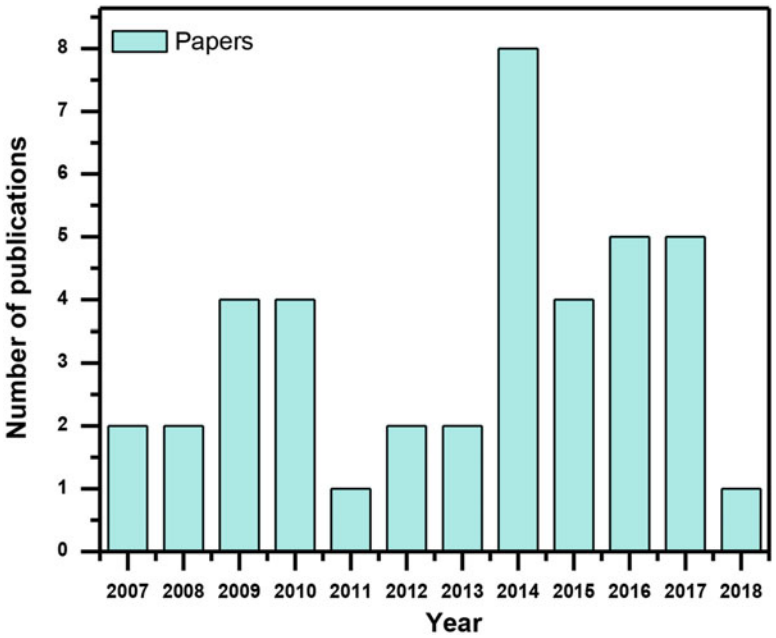

Fig. 13.4 Number of papers on antibacterial epoxy coatings published per year between 2007 and 2018, extracted from the Scopus database (https://www.scopus.com)

Table 13.1 Recent literature on antimicrobial epoxy coatings

Polymer formulation	Application	Reference
DGEBA/F-AgNPs-epoxy	Antibacterial coating	Manjumeena et al. (2016)
DGEBA/TiO_2	Antifouling coating	Saravanan et al. (2016)
DGEBA/BA/SB	Antifouling coating	Saravanan et al. (2016)
Chitosan/epoxy	Antimicrobial coating	Fattah et al. (2016)
Epoxy/Cu_2O	Antimicrobial coating	Ashraf et al. (2016)
Epoxy/glycidyl carbamate	Antifouling coating	Duraibabu et al. (2015)
DGEBA/ECSO/TETA	Antimicrobial coating	Narute et al. 2015
Nano-ZnO/TGBAPB epoxy	Antimicrobial coating	Duraibabu et al. (2014)
HBP-based polyurethanes	Antimicrobial coating	Kumar et al. (2014)
BADGE/DETA	Antibacterial coating	Mondrzyk et al. (2014)
Epoxy/polyamide/nano-ZnO	Anticorrosion coating	Ramezanzadeh et al. (2011)
Metal-containing poly(Schiff) epoxy	Antimicrobial coating	Tansir and Saad Alshehri (2012)
DGEBA/HELA	Antibacterial coating	Sharmin et al. (2010)
EpAcO/BMF	Antimicrobial coating	Zafar et al. (2009a, b)

BA benzoic acid, *BADGE* bisphenol A diglycidyl ether, *BMF* butylated melamine formaldehyde, *DETA* diethylenetriamine, *DGEBA* diglycidyl ether of bisphenol A, *ECSO* epoxidized cottonseed oil, *EpAcO* epoxy-acrylic-oleic acid, *F-AgNPs* surface-functionalized silver nanoparticles, *HBP* hyperbranched polymer, *HELA* linseed amide diol, *SB* sodium benzoate, *TETA* triethylenetetramine, *TGBAPB* tetraglycidyl 1,4′-bis(4-amine-phenoxy)benzene

refining, pipelines, mining, etc. (Yu 2007; Mallick et al. 2005; Liu et al. 2004; Smetuna et al. 2005). To overcome the above disadvantages, there is a need for modifications. Nowadays, green chemistry is of interest and has attracted the attention of academia and industry. Green chemistry using plant (leaf, root, etc.) extracts for synthesis of eco-friendly nanoparticles includes reinforcement with polymers to enhance physical, chemical, electronic, electrical, mechanical, magnetic, thermal, dielectric, optical, and especially biological properties in comparison with the bulk-sized forms of materials (Schmid 1992; Daniel and Astruc 2004).

13.6.1 Green Nanosilver Epoxy Coatings

Manjumeena et al. (2016) described reinforcement with 1, 3, and 5 wt% of surface-functionalized silver nanoparticles (F-AgNPs), synthesized using *Couroupita guianensis* leaf extract, in epoxy resin GY250 representing diglycidyl ether of bisphenol A (DGEBA), with a view toward augmenting the corrosion control property of the epoxy resin and also imparting antimicrobial activity to epoxy coatings on MS. The green-synthesized AgNPs were surface functionalized using 3-aminopropyltri-ethoxysilane to achieve better adhesion and dispersion of the AgNPs in the DGEBA epoxy matrix (Fig. 13.5).

The authors evaluated the corrosion resistance of the coatings by electrochemical impedance spectroscopy (EIS), potentiodynamic polarization (PDP) studies, and cross-scratch testing. Atomic force microscopy (AFM), scanning electron microscopy (SEM), high-resolution transmission electron microscopy (HRTEM), and energy dispersive x-ray spectroscopy (EDX) were utilized to investigate the surface topography, morphology, and elemental composition of the coatings on MS samples. The SEM micrographs of the MS samples coated with systems (a) [coating without F-AgNPs], (b) [coating with 1 wt% F-AgNPs], (c) [coating with 3 wt% F-AgNPs], and (d) [coating with 5 wt% F-AgNPs] prior to the corrosion studies (Fig. 13.6a–d) showed that the surface of the system (a) coated sample was uniform and smooth with no observable cracks.

As the F-AgNP loading into the DGEBA matrix increased to 3 wt% and 5 wt%, the smooth patterns completely disappeared and the surfaces became very rough. This could be attributed to the inevitable occurrence of aggregates. The initial results showed that the corrosion resistance, hardness, and glass transition temperature (T_g) of the DGEBA/F-AgNP coatings were increased at 1 wt% F-AgNPs. One of the

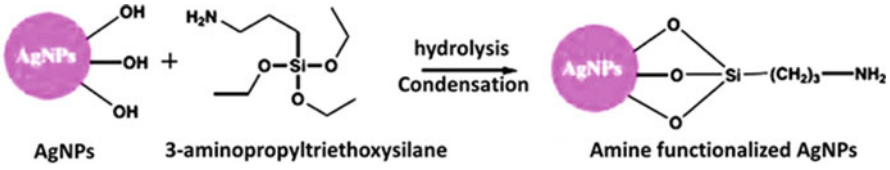

Fig. 13.5 Amine functionalization of silver nanoparticles (*AgNPs*) (Reproduced with permission from Manjumeena et al. 2016)

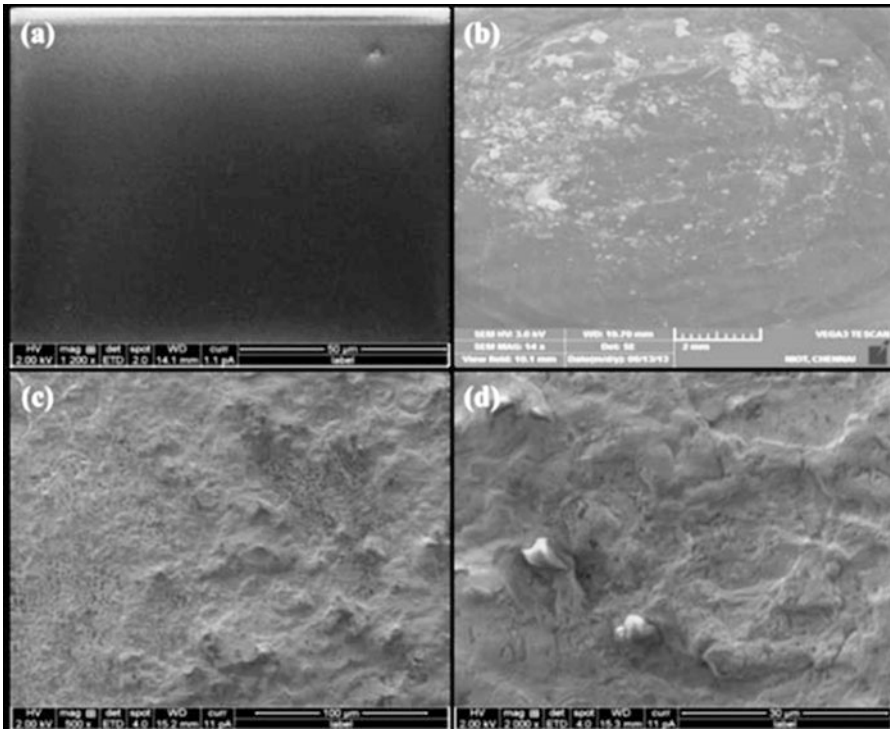

Fig. 13.6 Scanning electron microscopy (*SEM*) images showing the surface morphology of mild steel coated with four different systems before corrosion studies involving 50 days of immersion in a 3.5% NaCl solution (Manjumeena et al. 2016): neat DGEBA (**a**), 1 wt% F-AgNPs/DGEBA (**b**), 3 wt% F-AgNPs/DGEBA (**c**), and 5 wt% F-AgNPs/DGEBA (**d**). *DGEBA* diglycidyl ether of bisphenol A, *F-AgNPs* surface-functionalized silver nanoparticles

reasons could be that the nanoparticles have a large surface area, strong hydrogen bonding through OH groups, and high surface free energy, and thus they tend to be aggregated at higher loading. The polarization response of MS samples coated with systems (a), (b), (c), and (d) studied at 0 days and after 50 days of immersion in a 3.5% NaCl solution (Fig. 13.7a) showed that the polarization responses of coating systems (b) and (c) after 50 days of immersion in NaCl were toward the anodic side, indicating their superior corrosion resistance, whereas the responses of coating systems (a) and (d) were toward the cathodic side.

It is worth noting that the decrease in the corrosion resistance of system (d) was considerably smaller than that of system (a) after 50 days of immersion. This indicated that the corrosive electrolyte could not easily permeate into the coating/metal interface when the coating included F-AgNPs. The lower corrosion resistance of system (d) was attributed to the decrease in cross-linking density between the F-AgNP-epoxy matrix and the tendency of the nanoparticles to form aggregates at high weight percentage loadings (Ramezanzadeh et al. 2011) Also, upon more detailed

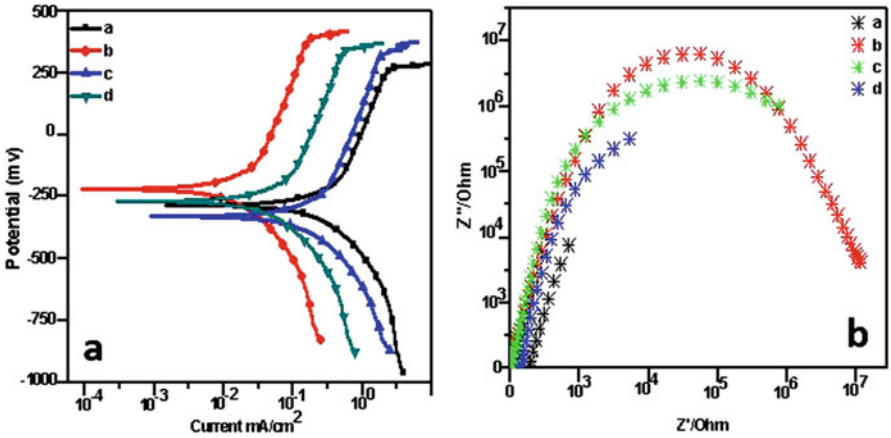

Fig. 13.7 Polarization plot (**a**) and electrochemical impedance spectroscopy Nyquist plot (**b**) of mild steel samples coated with four different coating systems (Manjumeena et al. 2016)

comparison of the Nyquist plots and resistance values for the MS samples coated with systems (a), (b), (c), and (d) at 0 days and after 50 days of immersion in the 3.5% NaCl solution (Fig. 13.7b), it could be observed that the MS sample coated with system (b) exhibited a greater semicircle and relatively higher resistance, even after 50 days of immersion, than the other coating systems (a), (c), and (d). On this basis, the greater semicircle for coating system (b) in the Nyquist plot indicated better corrosion resistance, which may have been explained by the presence of F-AgNPs at a low loading of 1 wt%.

The authors also performed cross-scratch testing and concluded that by the end of 1200 h, no visible corrosion products were seen on the unscratched surface of the coated samples. Corrosion products were seen mainly on the scratched area of the coated samples. Furthermore, the spread of corrosion underneath the coating film was lesser in the system (b) sample than in the system (a), system (c), and system (d) coated samples (Fig. 13.8).

Of all systems studied, system (b) exhibited the maximum corrosion resistance and microbial resistance. The antimicrobial behavior of this epoxy–green nanohybrid coating formulation is noteworthy, as it offers manifold antimicrobial protection to steel surfaces by inhibiting the growth of biofilm-forming bacteria such as *Pseudomonas aeruginosa*, *Bacillus subtilis*, *Escherichia coli* (the most common human pathogen), and *Candida albicans* (the most virulent human pathogenic yeast) (Fig. 13.9).

This dual behavior of corrosion resistance and microbial resistance exhibited by surface-functionalized green nanosilver DGEBA coatings offers environmentally benign solutions by enhancing the corrosion control property of conventional epoxy coatings that are currently in use and imparting antimicrobial activity, leading to better performance and longevity of steel surfaces. A multifunctional feature of these nanocomposite coatings makes them potentially applicable in various areas in high-added-value applications such as smart coatings for corrosion protection and antifouling protection.

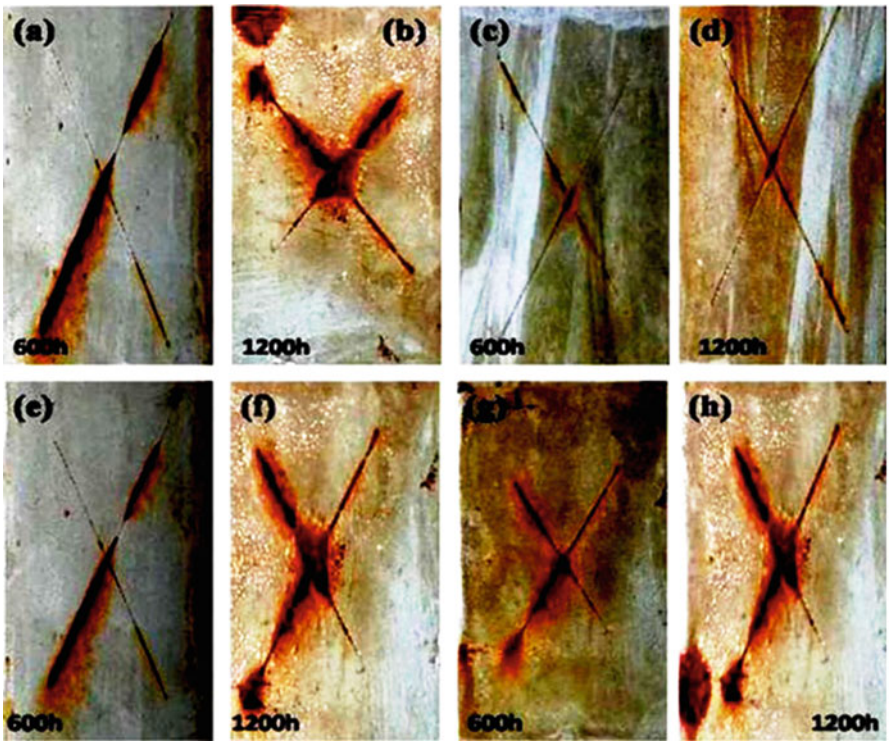

Fig. 13.8 Coated and cross-scratched mild steel samples after 600 h (samples **a**, **c**, **e**, **g**) and after 1200 h (samples **b**, **d**, **f**, **h**): samples with neat DGEBA coating (**a**, **b**); samples with 1 wt% F-AgNP/DGEBA coating (**c**, **d**); samples with 3 wt% F-AgNP/DGEBA coating (**e**, **f**); and samples with 5 wt % F-AgNP/DGEBA coating (**g**, **h**) (Manjumeena et al. 2016). *DGEBA* diglycidyl ether of bisphenol A, *F-AgNP* surface-functionalized silver nanoparticle

13.6.2 Natural Renewable Resource (Chitosan) Epoxy Coatings

Fattah et al. (2016) developed an eco-friendly chitosan/epoxy coating by extracting chitosan (from shrimp shells) (Fig. 13.10) and mixing various weight percentages (between 2 wt% and 20 wt%) of it into epoxy resin, which was then cured with a hardener to form a chitosan/epoxy composite coating.

Chitosan–epoxy composite coatings containing different weight percentages of chitosan were applied to steel panels, which were then exposed to salt spray fog for 500 h (Fig. 13.11).

In Fig. 13.11, different amounts of brown rust spotting can be observed on the steel panels treated with epoxy coating and chitosan–epoxy composite coating. It was found that failure of adhesion of the chitosan–epoxy composite coating during the long exposure to salt spray fog caused an improvement in corrosion resistance in comparison with the neat epoxy coating (Fig. 13.11). This could be attributed to the

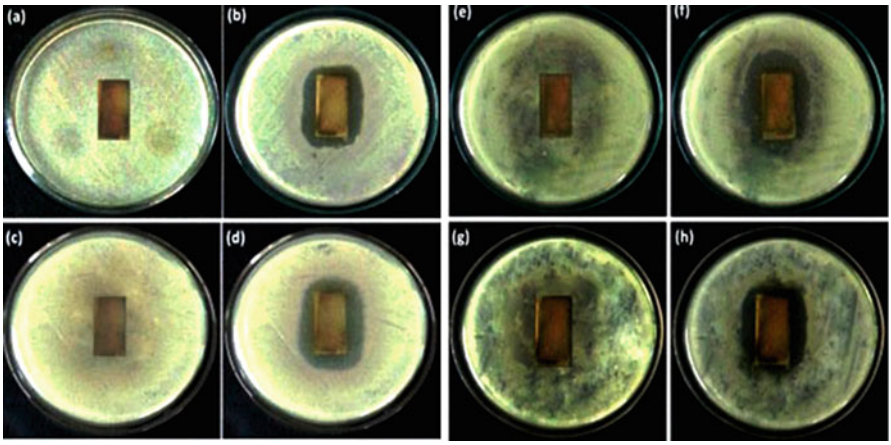

Fig. 13.9 Antimicrobial activity of mild steel samples with epoxy-only coating (samples **a**, **c**, **e**, **g**) and samples with 1 wt% F-AgNP/DGEBA coating (samples **b**, **d**, **f**, **h**): activity against *Pseudomonas aeruginosa* (**a**, **b**); activity against *Bacillus subtilis* (**c**, **d**); activity against *Escherichia coli* (**e**, **f**); and activity against *Candida albicans* (**g**, **h**) (Manjumeena et al. 2016). *DGEBA* diglycidyl ether of bisphenol A, *F-AgNP* surface-functionalized silver nanoparticle

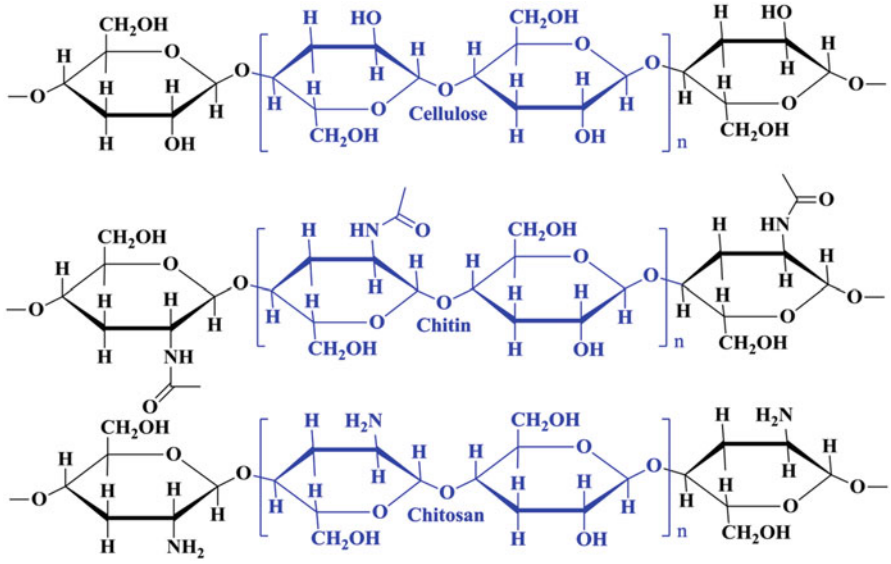

Fig. 13.10 Schematic structures of cellulose, chitin, and chitosan

chitosan, which was effective in reducing rusting during exposure to high humidity and high salt content. Moreover, the nitrogen and oxygen atoms in the structure of chitosan were both strongly adsorbed onto the metal surface and acted to block active corrosion sites.

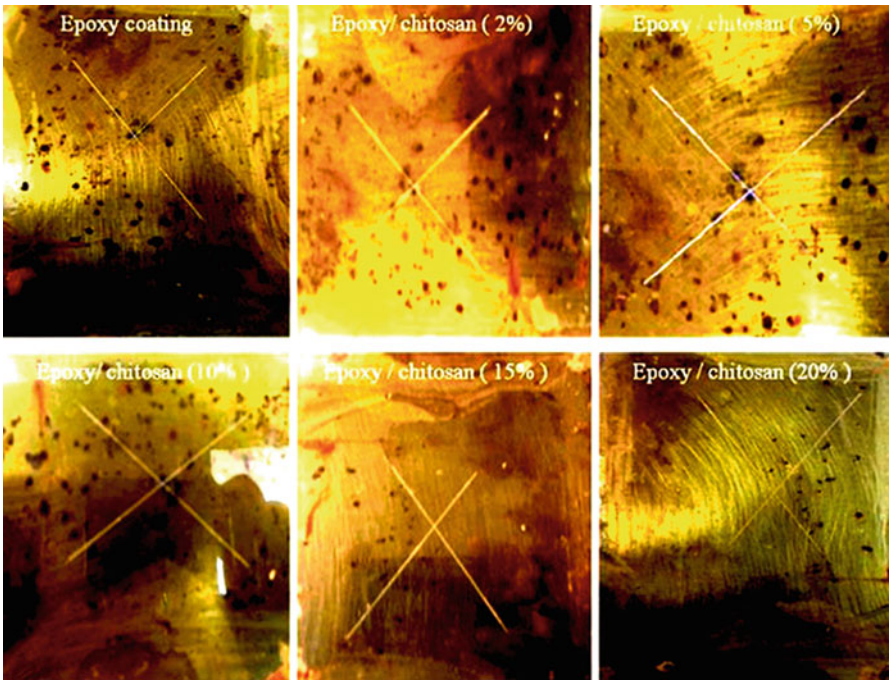

Fig. 13.11 Mild steel samples with epoxy coating (*upper left panel*) and chitosan−epoxy composite coatings containing 2 wt% chitosan (*upper middle panel*), 5 wt% chitosan (*upper right panel*), 10 wt% chitosan (*lower left panel*), 15 wt% chitosan (*lower middle panel*), and 20 wt% chitosan (*lower right panel*) after 500 h of salt spray exposure (Fattah et al. 2016)

The antimicrobial activity of the chitosan–epoxy coatings was analyzed by a solution concentration method. The results indicated that antibacterial activity increased as the content of chitosan increased (Fig. 13.12), which could have occurred because the positively charged chitosan attracted negatively charged bacteria on the surface, leading to emended membrane permeability. This would enhance leakage of intracellular constituents, causing bacterial cell death (Kong et al. 2010; Liu et al. 2004).

The authors evaluated the antimicrobial (Gram-positive and -negative) and antifungal activity of the chitosan/epoxy composite coatings and concluded that the addition of chitosan to the epoxy led to improvements in antimicrobial and antifungal activities.

13.6.3 Unique Nano-ZnO Epoxy Coatings

Duraibabu et al. (2014) successfully developed a unique skeletally modified tetrafunctional epoxy coating for corrosion prevention and antimicrobial protection,

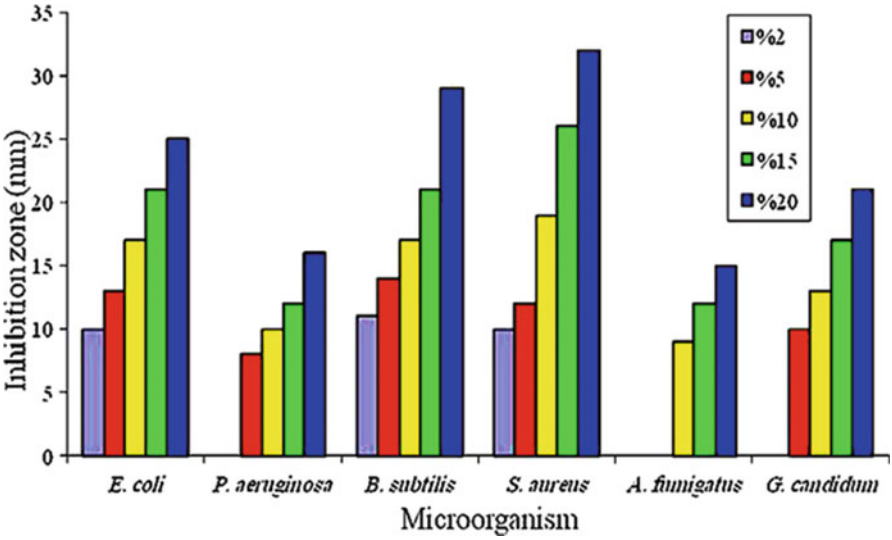

Fig. 13.12 Effects of different loading percentages of chitosan on six tested microorganisms: *Escherichia coli*, *Pseudomonas aeruginosa*, *Bacillus subtilis*, *Staphylococcus aureus*, *Aspergillus fumigatus*, and *Geotrichum candidum* (Fattah et al. 2016)

using tetraglycidyl 1,4′-bis(4-amine-phenoxy)benzene (TGBAPB) epoxy resin and surface-functionalized nano-ZnO (F-ZnO) and nonfunctionalized nano-ZnO (N-ZnO) (Fig. 13.13a). They introduced a reactive NH_2 group onto the surface of the nano-ZnO and achieved a reaction between 3-aminopropyltriethoxysilane and the hydroxyl groups on the nano-ZnO surface. This led to formation of a covalent bond between the F-ZnO and the TGBAPB epoxy resin. It was observed that the Nyquist plots derived from the EIS measurements showed two prominent capacitive loops in the high-frequency region, which were attributed to the high resistance and low capacitance offered by the steel–electrolyte interface of the TGBAPB-F-ZnO and neat TGBAPB coatings. As shown in Fig. 13.13b,the TGBAPB-N-ZnO coating exhibited the least resistance to corrosion in comparison with the TGBAPB-F-ZnO and neat TGBAPB coatings.

The authors confirmed that the formation of a low-frequency diffusion tail in the TGBAPB-N-ZnO coating system in the corrosion process was a diffusion-controlled reaction. They concluded that the order of corrosion resistance was TGBAPB-F-ZnO > TGBAPB > TGBAPB-N-ZnO, and that the reason for the inferior corrosion resistance offered by TGBAPB-N-ZnO coating was the improper dispersion of N-ZnO within the TGBAPB epoxy resin, which would have led to an agglomeration, leading to the entry of corrosive species through the metal coating interface.

The authors undertook an investigation to study and compare the antibacterial activity of TGBAPB-F-ZnO and TGBABP-N-ZnO coatings. The results showed that the sample containing TGBAPB-F-ZnO had a greater zone of inhibition than the control

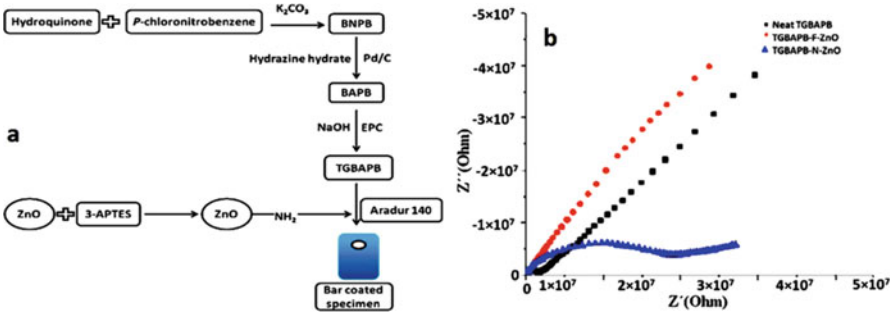

Fig. 13.13 Flowchart of the preparation of TGBAPB-F-ZnO epoxy coatings (**a**) and electrochemical impedance spectroscopy Nyquist plot of neat TGBAPB, TGBAPB-N-ZnO, and TGBAPB-F-ZnO coated systems (**b**) (Duraibabu et al. 2014). *3-APTES* 3-aminopropyltri-ethoxysilane, *BAPB* 4,4′-bis(4-aminophenoxy)biphenyl, *BNPB* 1,4′-bis(4-nitrophenoxy)benzene, *EPC* epichlorohydrin, *F-ZnO* surface-functionalized nano-ZnO, *N-ZnO* nonfunctionalized nano-ZnO, *Pd/C* 10% palladium on activated carbon, *TGBAPB* tetraglycidyl 1,4′-bis(4-amine-phenoxy)benzene

MS sample, TGBAPB-N-ZnO sample, and TGBAPB sample, in which there were no zones of inhibition (Fig. 13.14a–c), indicating their inferior bacterial resistance.

The authors concluded that the surface TGBAPB-F-ZnO coated sample exhibited more effective antibacterial activity against the test bacterium (*E. coli*) than the other two samples coated with TGBAPB-N-ZnO and TGBAPB. They also explained that the antibacterial activity of TGBAPB-F-ZnO could be attributed to the abrasive surface texture due to surface defects. The antibacterial activity of TGBAPB-F-ZnO could be attributed to the better dispersibility and consequent compatibility with the TGBAPB matrix exhibited by F-ZnO.

13.7 Epoxy–Inorganic Compound Coatings

One of the most common methods for improving coating performance can be reduction of the size of the filler and submicron particles to the nanoscale (Allen et al. 2004; Delucchi et al. 2011). With use of nanoparticles (NPs) it has been possible to overcome drawbacks and also incorporate submicron particles with inherent small size and particle morphology (Fernando 2004). The addition of inorganic nanoparticles to an epoxy matrix enhances thermal, mechanical, electrical, corrosion resistance, and antibacterial properties without impairing other properties. Furthermore, the enhancement particularly depends upon the type of material, the size, the shape, and the degrees of dispersion and adhesion to the polymer matrix (Al-Turaif 2010; Omrani et al. 2009). Inorganic nanocomposites possessing greater extent of coating field might be due to their unique physical and chemical properties.

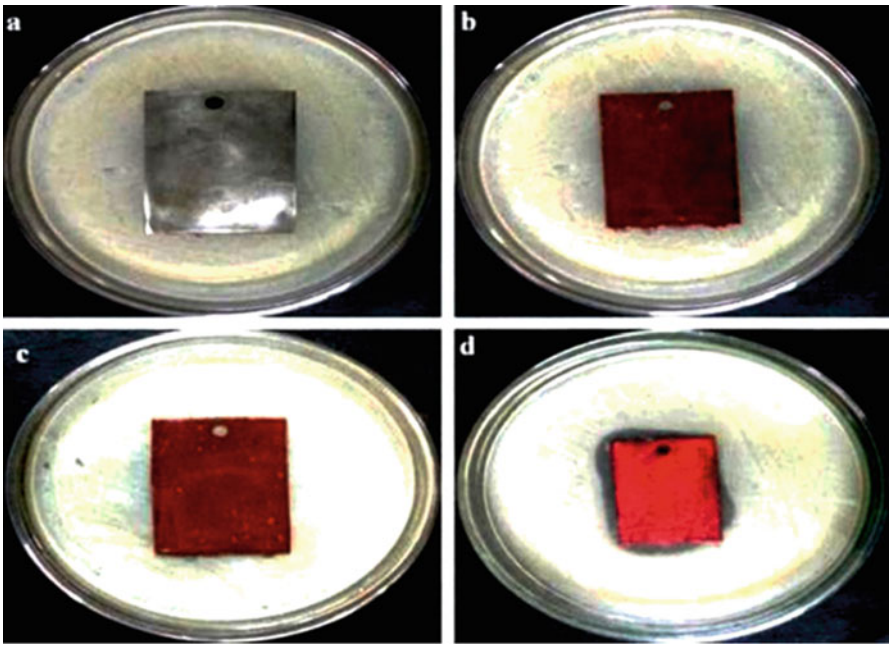

Fig. 13.14 Antibacterial testing against *Escherichia coli* bacteria: control mild steel (**a**), neat TGBAPB (**b**), TGBAPB-N-ZnO (**c**), and TGBAPB-F-ZnO (**d**) (Duraibabu et al. 2014). *F-ZnO* surface-functionalized nano-ZnO, *N-ZnO* nonfunctionalized nano-ZnO, *TGBAPB* tetraglycidyl 1,4′-bis(4-amine-phenoxy)benzene

13.7.1 Cuprous Oxide Epoxy Nanocomposite

Ashraf et al. (2016) synthesized cuprous oxide nanoparticles by the liquid phase chemical method and added different weight percentages (0.1, 0.3, 0.5, 0.7, and 1.0 wt%) to epoxy to produce Cu_2O epoxy nanocomposite coating films. The antimicrobial and antifungal properties of these films were analyzed by means of a disk diffusion method. The zones of inhibition of *Staphylococcus aureus* and *E. coli* showed that they had greater sensitivity to the coated disks. *Klebsiella pneumonia* displayed less sensitivity among the tested bacteria. The best performance was observed with the coating film containing 0.3 wt% of cuprous oxide nanoparticles. It can be concluded that the percentage of biocidal/bacteriostatic activity was closely related to the oxidation state of the Cu_2O nanoparticles. Transmission electron microscopy (TEM) images of Cu_2O-nanoparticle-treated and control (untreated) *S. aureus* bacteria cells showed dark spots inside the cell wall within the cytoplasm of the treated cells, which could possibly be passed into the cells; the pretreatment process allowed exposure of *S. aureus* to the oxygen in the Cu_2O nanoparticles found in the cytoplasm membrane. Even so, the mechanism of the bactericidal action of Cu_2O nanoparticles ion is not fully understood, and it is unclear whether Cu_2O nanoparticles binding to DNA or specific proteins may directly prevent cell

replication or hinder enzymatic function. Although the authors were not able to evaluate the mechanism of action of the Cu_2O epoxy nanocomposite coating film on the bacteria, this work showed that coatings containing Cu_2O epoxy nanocomposites do have an effect on Gram-negative and Gram-positive bacteria.

13.7.2 Metal-Containing Epoxy Coatings

Tansir and Saad Alshehri (2012) developed metal-containing epoxy resin via polycondensation of Schiff base metal complexes with epichlorohydrin (Fig. 13.15).

The polarization corrosion current (I_{corr}) curves of the metal-chelated epoxy resin (Er) coatings Er–Mn(II), Er–Co(II), Er–Ni(II), Er–Cu(II), and Er–Zn(II) in HCl (3.5%), NaOH (3.5%), and NaCl (3.5%) solutions are shown in Fig. 13.16.

In Fig. 13.16 It can be observed that the polarization I_{corr} curves showed higher values in the HCl solution than in the NaOH and NaCl solutions. The Zn(II)-chelated epoxy coating system showed I_{corr} values of 0.482 μA/cm^2 in the NaCl solution, 0.520 μA/cm^2 in the NaOH solution, and 1.02 μA/cm^2 in the HCl solution. This could be because the corrosion resistance property of Er–Zn(II) was much higher than those of the other systems, namely Er–Co(II), Er–Ni(II), and Er–Cu(II). The antimicrobial activity of the systems was evaluated using minimum bactericidal concentration methods against *S. aureus*, *B. subtilis*, *E. coli*, and *P. aeruginosa*. It was found that Er–Cu(II) exhibited greater antimicrobial activity than Er–Co(II) and Er–Ni(II).

The authors concluded from the experimental data that as these coating materials showed better corrosion resistance and antimicrobial activities, they could be used in aerospace vehicles and antimicrobial coating materials for hospitals. In this study the effects of different metal nanoparticles were studied, but the authors could not explain the specific characteristics and mechanisms of action of the different metal nanoparticles, such as their corrosion resistance and antimicrobial properties, and their sizes and dispersion ratios in each type of filler. These characteristics would influence the amount of inorganic material loaded into the polymer and the optimization of the nanofiller and aggregation behavior, which would play important roles in determining the performance of the final composite materials.

13.8 Epoxy–Organic Compound Coatings

In general, epoxy resin cannot behave well in humid conditions, because its hydrophilicity and consequently high water uptake restrict its use for corrosion prevention and antimicrobial protection. Prevention of water uptake by epoxy coatings can be achieved by (1) chemically modifying the backbone with flexible spacers, (2) increasing the molecular weight of the epoxy backbone moiety, (3) decreasing the cross-linking density of the epoxy matrix, and

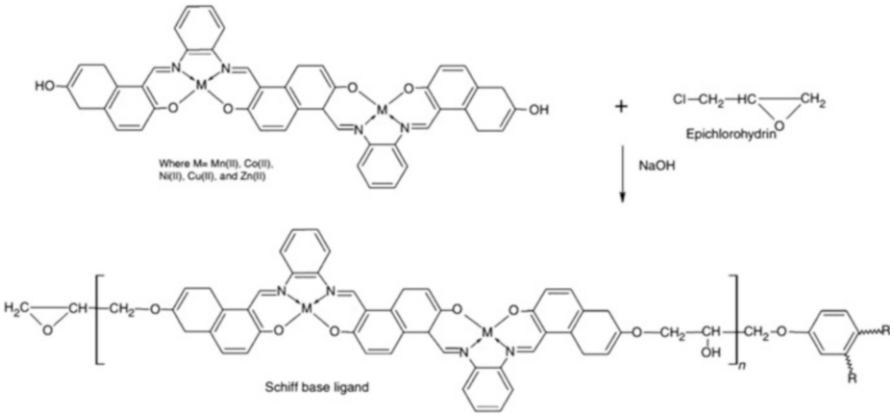

Fig. 13.15 General synthetic route for metal-containing epoxy resins (Tansir and Saad Alshehri 2012)

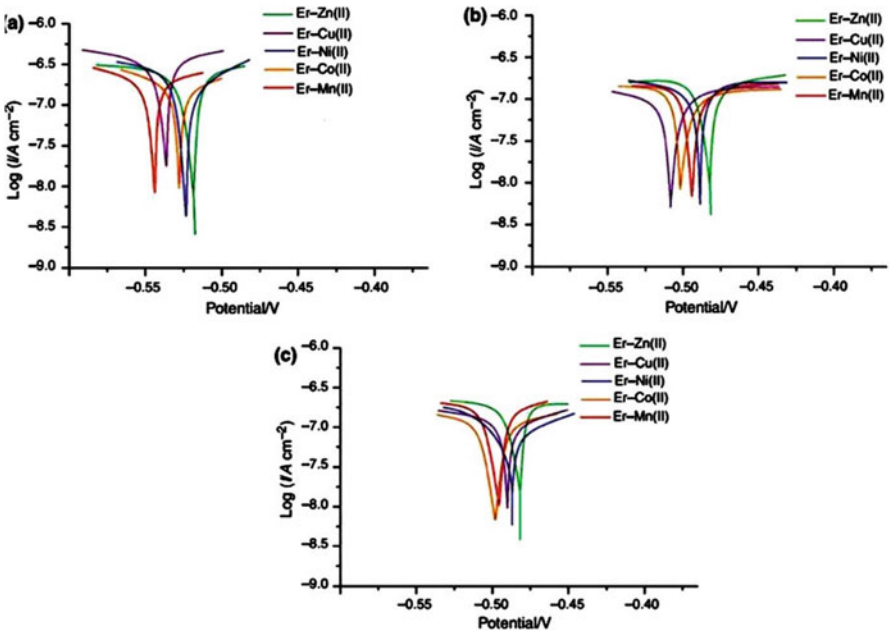

Fig. 13.16 Potentiodynamic polarization curves of chelated epoxy resin (*Er*) in a 3.5% HCl solution (**a**), a 3.5% NaOH solution (**b**), and a 3.5% NaCl solution (**c**) (Tansir and Saad Alshehri 2012)

(4) homogenizing the toughener phase in the epoxy, which has been done with polystyrene, polymethyl-methacrylate, polyether ether ketone, polyether sulfone, polyetherimide, polyurethane (PU) liquid rubber, siloxane-based polymers, hydroxyl-terminated polybutadiene, hydroxyl-functionalized hyperbranched

polymer, polyesters, and liquid elastomers either by chemical reactions or by blending with the epoxy resin (Raghavachar et al. 1999; Sharmin et al. 2010; Ratna 2001; Jin and Park 2008).

13.8.1 ECSO Epoxy Coatings

Narute et al. (2015) synthesized epoxidized cottonseed oil (ECSO), using Prilezhaev epoxidation by sulfuric acid catalysts (Fig. 13.17a), and produced a modified epoxy (ME) resin with commercially available DGEBA and ECSO cured at room temperature using a hardener.

With the addition of different content (Epoxy Resin-10, Epoxy Resin-64, Epoxy Resin-55, and Epoxy Resin-46), system Epoxy Resin-10 showed more uniform corrosion than systems Epoxy Resin-64, Epoxy Resin-55, and Epoxy Resin-46, which showed filiform corrosion, as depicted in Fig. 13.17b. After 30 days of salt spray exposure, an analysis showed that systems Epoxy Resin-55 and Epoxy Resin-46 were more affected by corrosion than systems Epoxy Resin-10 and Epoxy Resin-64. No signs of blistering, loss of gloss, delamination, or failure were observed in the films. Among the different systems, the best performance was observed with 40% ECSO (epoxidized cottonseed oil) content, which showed superior corrosion resistance. The antimicrobial properties of systems Epoxy Resin-10, Epoxy Resin-64, Epoxy Resin-55, and Epoxy Resin-46 were excellent, as shown in Fig. 13.18.

As shown in Fig. 13.18, Epoxy Resin-10 displayed inhibition of fungal/bacteria growth on the film surface. This could have been due to the occurrence of nitrogen atoms in triethylenetetramine (TETA) and quaternary ammonium cations (QACs) in the polymer matrix. In other words, QAC formation could be due to hydrogen bonding between nitrogen lone pairs (TETA) and formation of free hydroxyl (OH) groups. The active OH groups could cause ring opening in the epoxy group (ECSO and DGEBA) resulting in increasing the chain length and molecular weight which would increase antimicrobial activity (Ikeda et al. 1984; Kumar et al. 2014; Mondrzyk et al. 2014).

In this study the investigations of different amounts of ECSO content showed that the lower weight of 40% ECSO content achieved better performance in terms of anticorrosion properties than higher loadings of ECSO. The authors concluded that 40% ECSO content exhibited better corrosion resistance potential in moist environments and low water vapor transmission, which could make this an inexpensive, renewable, and eco-friendly product.

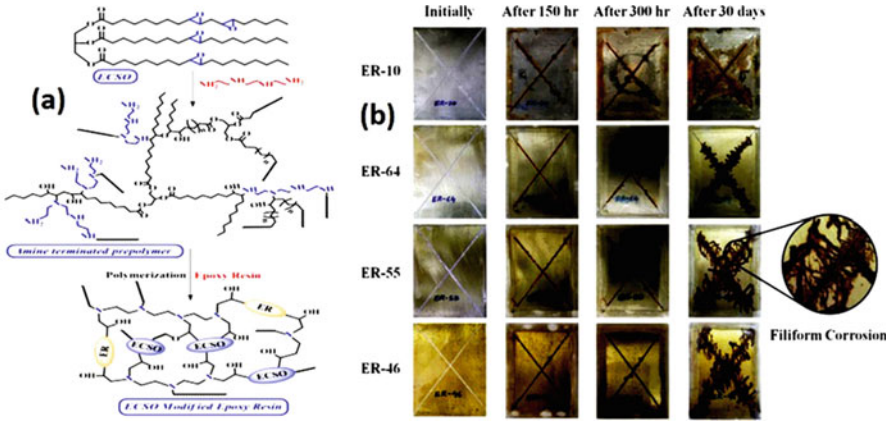

Fig. 13.17 Synthesis of modified epoxy resin with commercially available diglycidyl ether of bisphenol A (*DGEBA*) and epoxidized cottonseed oil (*ECSO*), made using Prilezhaev epoxidation by sulfuric acid catalysts (**a**); and salt spray analysis showing corrosion of panels coated with unmodified and modified epoxy resins (*ERs*) with different content (**b**) (Narute et al. 2015)

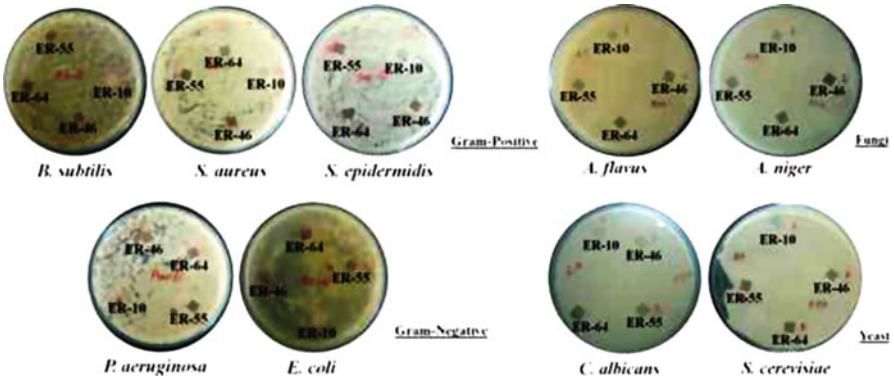

Fig. 13.18 Embedded unmodified and modified epoxy films showing antimicrobial activity against the Gram-positive bacteria *Bacillus subtilis*, *Staphylococcus aureus*, and *Staphylococcus epidermidis*; the Gram-negative bacteria *Pseudomonas aeruginosa* and *Escherichia coli*; the fungi *Aspergillus flavus* and *Aspergillus niger*; and the yeasts *Candida albicans* and *Saccharomyces cerevisiae* (Narute et al. 2015)

13.8.2 Glycidyl Carbamate Epoxy Coatings

Duraibabu et al. (2015) developed and characterized ME and glycidyl carbamate (GC) coatings applied to MS samples to assess the corrosion resistance of these coatings in comparison with a commercially available paint (CAP) by use of PDP and EIS studies. From the polarization responses of coating systems combining hexamethylene diisocyanate (HDI) with GC (HDI-GC), methylene diisocyanate

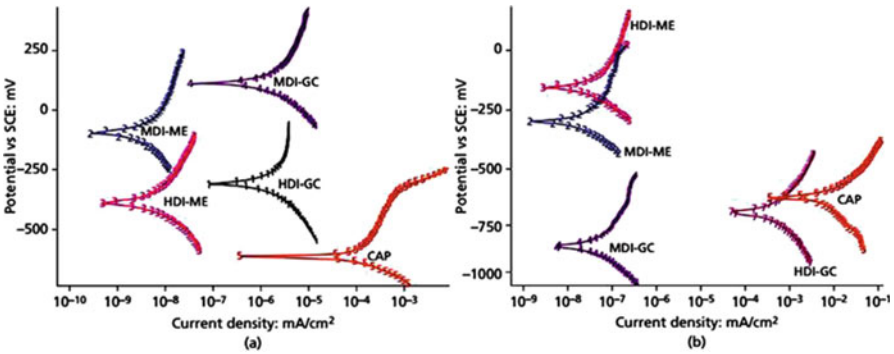

Fig. 13.19 Polarization responses of coating systems HDI-GC, MDI-ME, HDI-ME, MDI-GC, and CAP after 30 min (**a**) and 30 days (**b**) of immersion in a 3.5% sodium chloride solution (Duraibabu et al. 2015). *CAP* commercially available paint, *GC* glycidyl carbamate, *HDI* hexamethylene diisocyanate, *MDI* methylene diisocyanate, *ME* modified epoxy, *SCE* saturated calomel electrode

(MDI) with ME (MDI-ME), HDI-ME, MDI-GC, and CAP—which were studied after 30 min and 30 days of immersion in a 3.5% sodium chloride solution (Fig. 13.19a, b)—the authors made an interesting observation that the ME and GC coatings significantly influenced the corrosion protection behavior. MDI-ME and MDI-GC initially showed a polarization response toward the anodic side and appeared to offer greater corrosion resistance than the other coatings in this study. This may have been due to the presence of aromatic groups in both the DGEBA in MDI-ME and the MDI in MDI-GC, which might have offered chemical resistance to the transit of corrosive species to the metal surface by forming a passive layer (Ananda Kumar and Sankara Narayanan 2002). However, after 30 days of immersion the corrosion resistance offered by these coatings was found to be entirely different. The polarization responses of MDI-ME and HDI-ME (both DGEBA-based coatings) alone were toward the anodic side, indicating superior corrosion resistance, while the other coatings—namely MDI-GC, CAP, and HDI-GC—showed a cathodic response, exhibiting inferior corrosion resistance. The excellent resistance offered by MDI-ME and HDI-ME may also have been explained by the presence of Aradur 140 (polyamidoimidazoline) curative along with DGEBA, which was able to adhere to the metal surface through the π-electrons of the aromatic ring and lone pairs of electrons of nitrogen and sulfur atoms (He et al. 2002). The polarization of the responses of the MDI-GC, CAP, and HDI-GC samples toward the cathodic side may have been explained by the absence of DGEBA, resulting in inferior corrosion resistance. Although polyamidoimidazoline was used as a curing agent for all coating systems (namely HDI-GC, MDI-ME, HDI-ME, and MDI-GC), its effect on corrosion resistance was more apparent with MDI-ME and HDI-ME, which could be attributed to the presence of aromatic rings in MDI-ME and HDI-ME (both are modified DGEBA coatings) and lone pairs of electrons of polyamidoimidazoline together offering a synergistic effect that contributed to enhanced corrosion resistance. Another interesting thing to note is that MDI-GC performed much better than HDI-GC with regard to corrosion resistance,

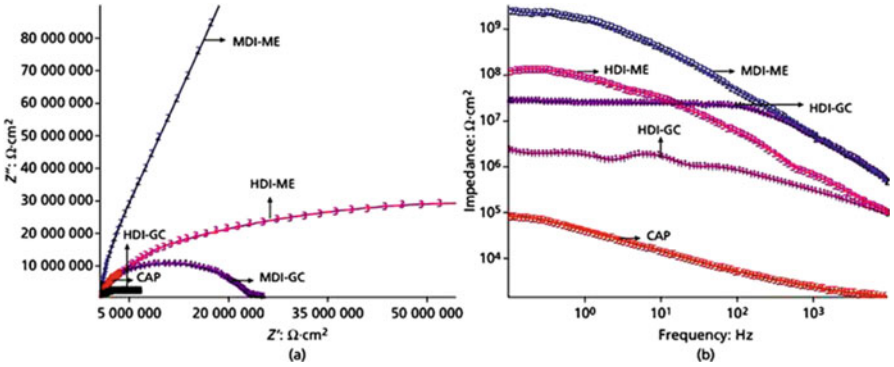

Fig. 13.20 Nyquist plot (**a**) and Bode plot (**b**) of coating systems HDI-GC, MDI-ME, HDI-ME, MDI-GC, and CAP after 30 min and 30 days of immersion in a 3.5% sodium chloride solution (Duraibabu et al. 2015). *CAP* commercially available paint, *GC* glycidyl carbamate, *HDI* hexamethylene diisocyanate, *MDI* methylene diisocyanate, *ME* modified epoxy

indicating the role of the aromatic rings present in MDI in corrosion resistance. The order of corrosion resistance of the different coatings was MDI-ME > HDI-ME > MDI-GC > HDI-GC > CAP. The inferior corrosion resistance observed with HDI-GC and HDI-ME (Fig. 13.19b) was explained by the authors as being due to the absence of additional aromatic rings in these coatings. The CAP coating showed the least corrosion resistance among all coatings studied.

From the Nyquist and Bode plots for the coating systems HDI-GC, MDI-ME, HDI-ME, MDI-GC, and CAP (Fig. 13.20a–b) after 30 min of immersion in NaCl, the authors observed that all of the coating systems were in the range of 109–106 $\Omega \cdot cm^2$, exhibiting the superiority of their corrosion resistance to that of the conventional and commercially available coating. MDI-ME and HDI-ME alone had greater semicircles than those of the other coatings, indicating their excellent corrosion resistance. These findings further supported the results obtained from the Bode plots and PDP study. The phase angle plots of HDI-GC, MDI-ME, HDI-ME, MDI-GC, and CAP (Fig. 13.21a–b) showed that the phase angle values of all coating systems after 30 min of immersion in the electrolyte solution were in the range of 92–12°, indicating capacitive behavior. However, the authors observed that the phase angles for the same coating systems became completely resistive (90–18°) after 30 days of exposure to the electrolyte.

The authors also evaluated the corrosion resistance of the coatings by salt spray testing (Fig. 13.22). At the end of the testing, they observed no visible corrosion products on the surface of the unscratched areas of the coated samples. However, corrosion products were seen on the scratched areas of all coated samples. Furthermore, there was less spreading of the corrosion underneath the coating film on the MDI-ME and HDI-ME samples than on the HDI-GC, MDI-GC, and CAP samples. After removal of the coatings, it was also evident that the MDI-ME and HDI-ME samples looked much brighter than the HDI-GC, MDI-GC, and CAP samples,

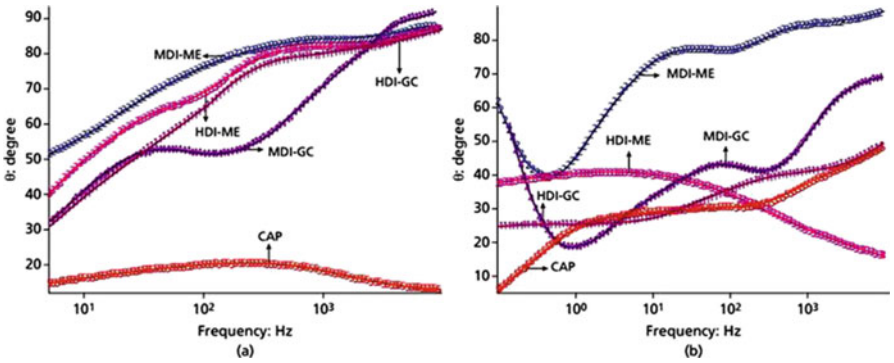

Fig. 13.21 Phase angle plots after 30 min (**a**) and 30 days (**b**) of immersion of coating systems HDI-GC, MDI-ME, HDI-ME, MDI-GC, and CAP in a 3.5% sodium chloride solution (Duraibabu et al. 2015). *CAP* commercially available paint, *GC* glycidyl carbamate, *HDI* hexamethylene diisocyanate, *MDI* methylene diisocyanate, *ME* modified epoxy

indicating their superior corrosion resistance to salt water. The authors noted that the order of corrosion resistance was MDI-ME > HDI-ME > MDI-GC > HDI-GC > CAP.

13.8.3 EpAcO-BMF IPN Coatings

Zafar et al. (2009a, b) prepared a waterborne interpenetrating polymer network (IPN) using epoxy acrylate (EpAc) with oleic acid (epoxy-acrylic-oleic acid (EpAcO)) and butylated melamine formaldehyde (BMF). The corrosion resistance of different systems—EpAcO-BMF-40, EpAcO-BMF-50, and EpAcO-BMF-60—was analyzed by means of (1) distilled water (free from ions), (2) a sodium chloride 3.5% w/v aq. solution, (3) a hydrochloric acid 4% w/v aq. solution, and (4) a sodium hydroxide 5% w/v aq. solution. The chemical resistance test showed better performance of EpAcO-BMF-50 and EpAcO-BMF-60 in all corrosive media, especially in an alkaline environment. In water, EpAcO-BMF-40, EpAcO-BMF-50, and EpAcO-BMF-60 showed good resistance and remained unaffected for 400 h, but a slight loss in gloss was observed for EpAcO-BMF-60 when immersed in a 4% HCl solution or a 3.5% NaCl solution. EpAcO-BMF-40 and EpAcO-BMF-50 exhibited slight losses in gloss after 300 h but remained intact. EpAcO-BMF-60 was completely removed after 192 h. Moreover, EpAcO-BMF-50 and EpAcO-BMF-60 showed poor alkaline resistance in comparison with EpAcO-BMF-40, which remained unaffected after exposure for 384 h. The rates of corrosion of the coatings were 5.5 mils per year (mpy) for EpAcO-BMF-40 and EpAcO-BMF-50 in water, and 4.75 mpy and 4.8 mpy, respectively, in silane media, while EpAcO-BMF-60 showed higher rates of corrosion (5.8 mpy in water and 5.5 mpy in silane media). EpAcO-BMF-40 exhibited a lower corrosion rate (4.5 mpy) than EpAcO-BMF-50 (6.8 mpy) and EpAcO-BMF-60 (8.5 mpy), and in an alkaline medium the corrosion rates were

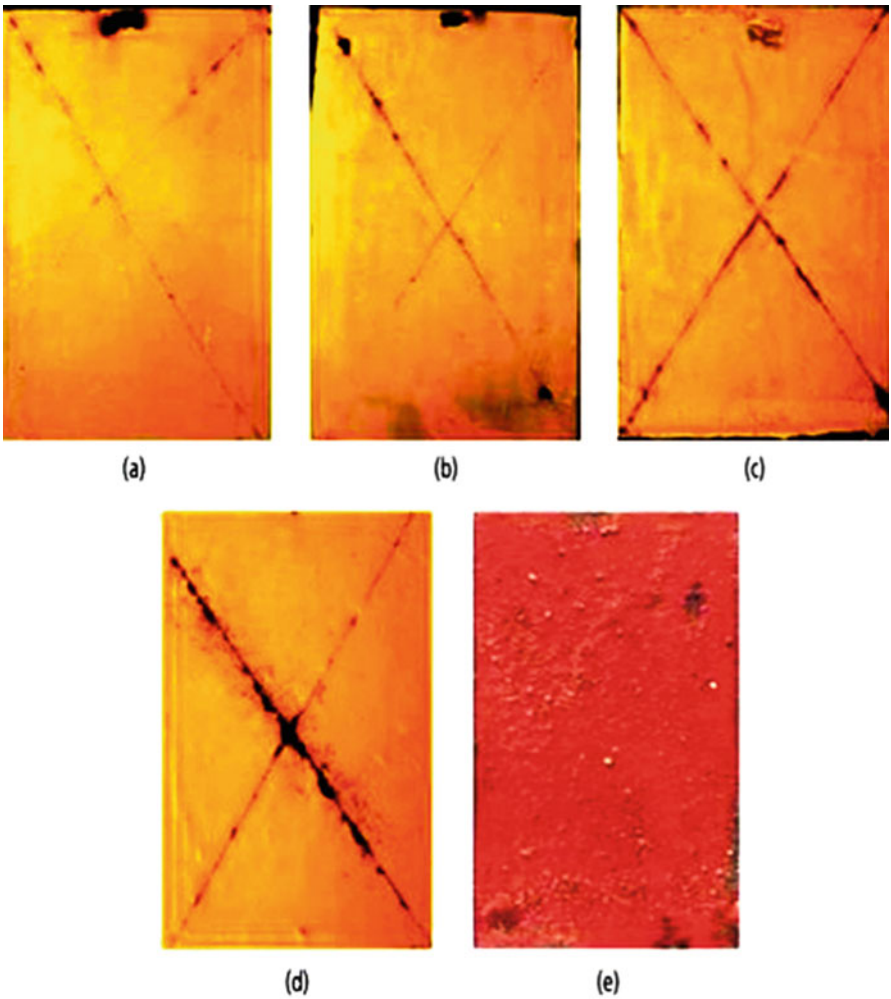

Fig. 13.22 Salt spray testing results after 1000 h of exposure to a 3.5% sodium chloride solution for the coating systems HDI-GC (**a**), MDI-ME (**b**), HDI-ME (**c**), MDI-GC (**d**), and CAP (**e**) (Duraibabu et al. 2015). *CAP* commercially available paint, *GC* glycidyl carbamate, *HDI* hexamethylene diisocyanate, *MDI* methylene diisocyanate, *ME* modified epoxy

5 mpy for EpAcO-BMF-40, 7.8 mpy for EpAcO-BMF-50, and 8.8 mpy for EpAcO-BMF-60. Among all of the systems, EpAcO-BMF-40 showed the best performance in all the media tested, which could have been because this IPN prevented the entrance of corrosive ions. With a 40 wt% loading of BMF, the melamine segments increasing the cross-linking density of the coatings could become highly strained and brittle, and could lose their adhesion. This could provide an easy passage for corrosive ions to penetrate through the coatings, causing damage to the coating framework (Zafar et al. 2009a, b). Furthermore, the authors evaluated the

antimicrobial properties of different systems, namely oxolinic acid (OA), epoxy (Ep), EpAc, and EpAcO-BMF-40. It was assumed that OA, Ep, and EpAc would exhibit no activity against any bacteria. EpAcO showed good activity against *S. aureus* (12 mm), *E. coli* (15 mm), and *Bacillus* (17 mm), while EpAcO-BMF-40 was even more active against *Candida*, *S. aureus*, *E. coli*, and *Bacillus*, showing inhibition zones of 25, 15, 22, and 20 mm, respectively. These results might have been due to the hydroxyl and carboxyl groups in OA and EpAc being bonded together by hydrogen bonding, preventing the type of interaction between the polymer and bacteria that could cause poor antibacterial activity (Wu et al. 2004). On the other hand, EpAcO structures have carboxyl groups, which undergo chemical and physical interaction with microbes and cause inhibition of bacterial growth. In the case of EpAcO-BMF-40, the presence of BMF was found to dramatically improve the bacterial activity of the IPN structure in the system. The bacterial cell wall contains multilayer compounds of peptidoglycan and a lipopolysaccharide (LPS) layer (Nagy et al. 2005). The LPS surface consists of two parts: one is a core of polysaccharides and another includes hydroxyl groups, which interact with IPN structures to form a highly crosslinked structure, resulting in deactivation of the microbes.

In this study a 40 wt% loading of BMF in EpAcO showed excellent film performance; also, the formation of IPNs in the presence of oleic acid imparted flexibility with a higher loading of BMF.

13.9 Organic–Inorganic Hybrid Coatings

Coatings containing inorganic and organic materials have shown much improvement in aging resistance, with no (or with extremely low) volatile organic compound (VOC) emissions, greater resistance to acid and alkali attacks, and amended tolerance of high temperatures that does not produce combustion (Pohrelyuk et al. 2014; Batis et al. 2003; Tkachenko et al. 2012). Furthermore, inorganic fillers can be used to reinforce epoxy resin, which offers integrity and durability of coating performance. The main drawback is that the inorganic nanoparticles cannot be dispersed uniformly in an epoxy coating to fill cavities, causing crack bridging, crack deflection, and crack bowing (Lam and Lau 2006; Shi et al. 2003; Hartwig et al. 2005; Dietsche et al. 2000). Organic materials are commonly used fillers in polymer blends with epoxy resin, which enormously increases the viscosity as well as the molecular weight of the resin, and causes problems particularly during paint formulation. One of the easiest methods used to rectify the above epoxy coating properties is functionalization of nanoparticles with silane coupling agents to form organofunctional groups. The functionalized nanofillers can also prevent epoxy disaggregation during curing, resulting in a homogeneous coating. Similarly, the nanoparticles tend to fill tiny hole defects formed by local shrinkage during curing of the epoxy resin, acting as a bridge and also interconnecting more molecules. Simultaneously, the total free volume is reduced and the cross-linking density is

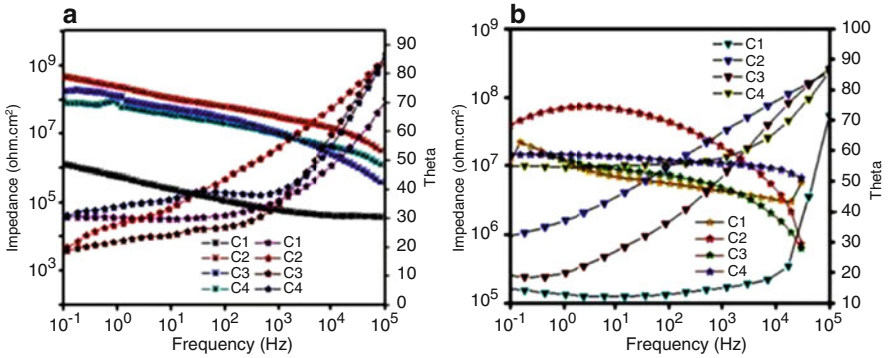

Fig. 13.23 Bode plots of TiO_2-APTES-DGEBA coating systems at 0 days (**a**) and after 30 days of immersion in a 3.5% NaCl solution (**b**) (Saravanan et al. 2016). *APTES* 3-aminopropyltriethoxysilane, *DGEBA* diglycidyl ether of bisphenol A

increased, improving barrier properties against corrosion and antimicrobial activity, and reducing coating blister formation or delamination (Shi et al. 2009; Champ 2000; Chang and Gray 2003; Kim et al. 2004).

13.9.1 Grafted TiO_2 Nanohybrid Coatings

Saravanan et al. (2016) developed organic (epoxy resin) and inorganic (silane) hybrid epoxy coatings from DGEBA epoxy resin with surface-functionalized TiO_2 nanoparticles, using APTES, and studied various weight percentages (1, 3, 5 and 7 wt%). The corrosion resistance of the reinforced grafted TiO_2 with the DGEBA epoxy coatings is presented in Fig. 13.23.

The Bode plots of the TiO_2-APTES-DGEBA coating systems are shown at 0 and 30 days of immersion in a 3.5% NaCl solution. The loading of grafted TiO_2 into the DGEBA epoxy enhanced the impedance value of the 3 wt% loading when compared with neat epoxy, 1 wt%, 5 wt%, and 7 wt%. This may have been due to uniform dispersion throughout the matrix and also increased hydrophobicity of the coating, causing it to repel water and corrosion initiators. Furthermore, the coating with the higher loading of 7 wt% exhibited improper dispersion, forming an aggregation, which indicated decreased corrosion resistance properties. The antimicrobial properties of grafted TiO_2-DGEBA epoxy were examined using *S. aureus* and *P. aeruginosa* bacteria in a zone of inhibition method (Fig. 13.24). The TiO_2 concentration increased the zone of inhibition in all systems because the Ti^{2+} ions on the surface bound to sulfur- and phosphorus-containing biomolecules (DNA), thereby potentially causing cell damage.

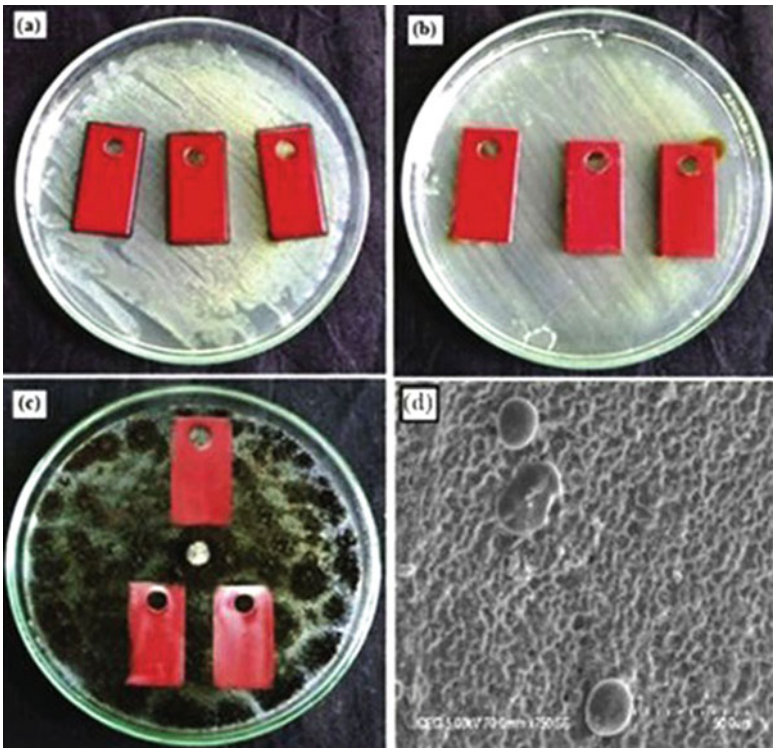

Fig. 13.24 Antimicrobial activities of TiO_2-APTES-DGEBA nanohybrid coatings against *Staphylococcus aureus* (**a**), *Pseudomonas aeruginosa* (**b**), and *Aspergillus niger* (**c**); and scanning electron microscopy image of *S. aureus* after treatment (**d**) (Saravanan et al. 2016). *APTES* 3-aminopropyltri-ethoxysilane, *DGEBA* diglycidyl ether of bisphenol A

13.9.2 Encapsulated Zeolite/Epoxy Nanohybrid Coatings

Saravanan et al. (2015) fabricated nanohybrid coatings using low-toxicity benzoic acid and sodium benzoate with DGEBA epoxy resin. The nanohybrid coatings were made with different weight percentages of 1, 3, 5, 7, and 10 wt% (Fig. 13.25).

It was ascertained that the corrosion potential (E_{corr}) values were decreased by the coatings (C3, C4, C5, C2, C1 (BA systems); C6, C7, C8, C9, and C10 (SB systems)), clearly showing that the cathodic and anodic reactions were controlled by the MS panel coating. The rate of corrosion was decreased from 1.029×10^{-1} mm/y on the uncoated panel to 3.850×10^{-5} mm/y on the C3 (BA system) panel and 9.372×10^{-4} mm/y on the C7 (SB system) panel; these decreases were greater than those seen with the other coating systems C1 (1.384×10^{-2}), C2 (1.228×10^{-3}), C4 (3.043×10^{-3}), and C5 (1.812×10^{-3}). These observations might have been due to the contact between the metal and the electrolyte being restricted by the coatings applied to the MS panels. The maximum

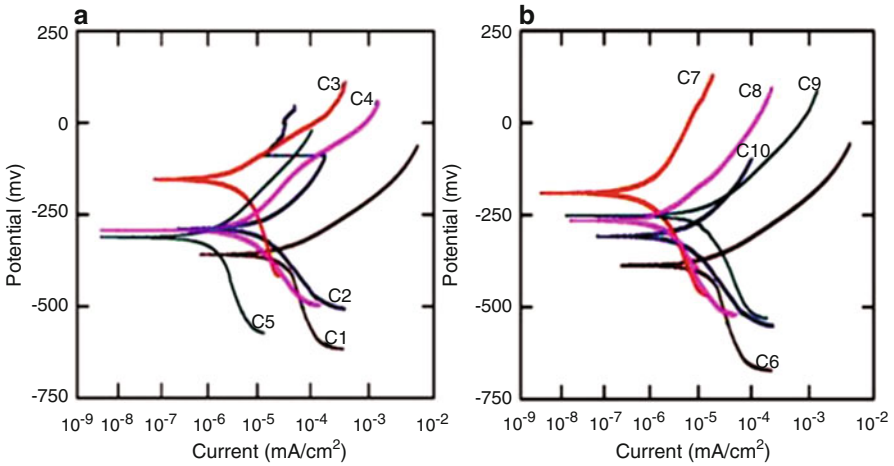

Fig. 13.25 Polarization responses of different epoxy/benzoic acid antifouling coatings (**a**) and epoxy/sodium benzoate antifouling coatings (**b**) after 30 days in a 3.5% NaCl solution (Saravanan et al. 2015)

restriction was shown by the C3 system with BA/epoxy coating and the minimum was shown by the C1 system. This could have been due to a uniform distribution of 5 wt% BA within the C3 epoxy coating, offering a barrier effect through interlinking of more molecules, leading to a defect-free coating. On the other hand, the fast corrosion of the BA/epoxy coating may have been due to the formation of large crystals. Similarly, the maximum restriction of the contact between the metal and the electrolyte was shown by the C7 system with SB/epoxy coating, whereas the minimum restriction was shown by the C6 system. This could have been due to uniform distribution of 3 wt% SB within the C7 epoxy coating, which offered a barrier effect because of the small particle size, giving a defectless coating. Figure 13.26 shows the antibacterial studies of the control system, the neat epoxy matrix, the BA/epoxy system C3 (5 wt%), and the SB/epoxy coating system C7 (3 wt%), showing the greater zones of inhibition achieved by the C3 and C7 systems, owing to the better dispersion and consequent compatibility exhibited by BA and SB with the DGEBA epoxy matrix.

In this study, the low-toxicity biocides BA and SB were separately incorporated into epoxy resin coatings in varying compositions (1, 3, 5, 7, and 10 wt%). The coating incorporating SB 1–3 wt% and the coating incorporating BA 5 wt% exhibited the best corrosion resistance and fouling resistance among all of the systems; further, both BA and SB epoxy coatings can be used for corrosion and fouling protection of the environment.

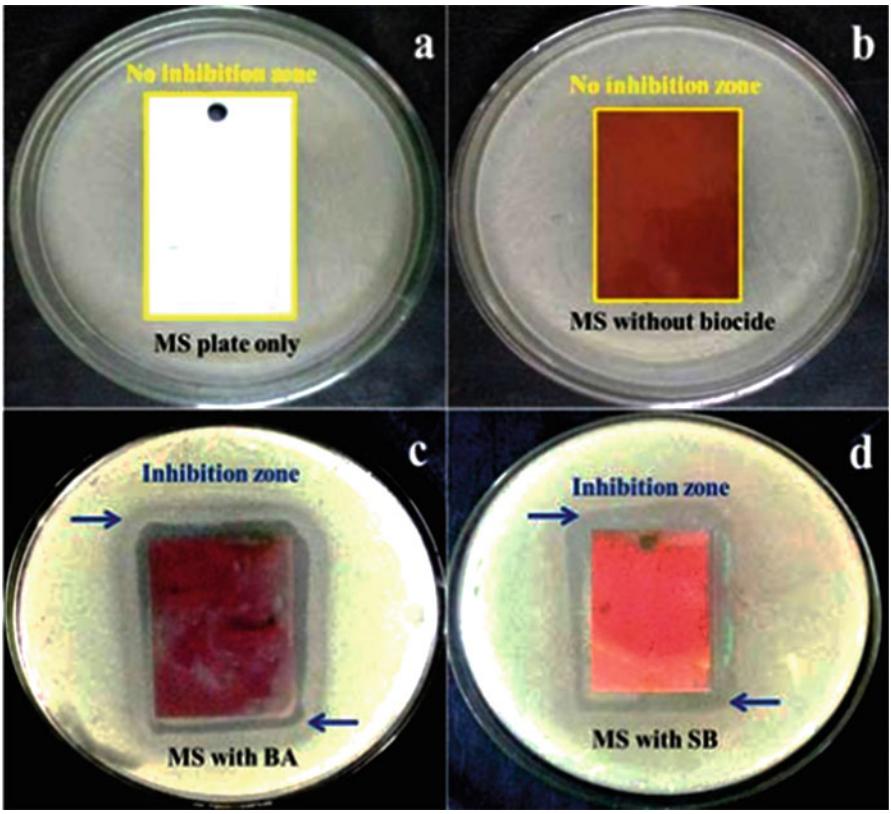

Fig. 13.26 Antibacterial testing against *Escherichia coli* bacteria: control mild steel (*MS*) plate (**a**), neat epoxy coating (**b**), C3 coating (**c**), and C7 coating (**d**) (Saravanan et al. 2015). *BA* benzoic acid, *SB* sodium benzoate

13.10 Conclusion

The application of nanotechnology in corrosion protection of metals has recently gained momentum, as nanoscale materials have unique physical, chemical, and physicochemical properties, which may improve corrosion protection in comparison with the bulk-sized forms of materials. Organic–inorganic nanocomposite materials possess unique properties as new materials and compounds for academic research, as well as for development of innovative industrial applications.

- These nanocomposites combine the unique properties of organic and inorganic components in one material.
- The basic multifunctional feature of these nanocomposite materials makes them potentially applicable in various areas in high-added-value applications such as smart coatings for corrosion protection and abrasion resistance; artificial membranes for ultra- and nanofiltration, pervaporation, and gas separation; catalysts

and nanoscopic reactors; adsorbents of toxic metal ions; biomaterials for osteoreconstructive surgery; and ophthalmic devices with optoelectronic and magnetic properties for telecommunications or information displays.

In the development of these composites, inorganic nanoparticles have a strong tendency to form aggregates; therefore, to improve the dispersion stability and compatibility of inorganic nanofillers with organic solvents or polymer matrices, their surfaces should be modified either by grafting of polymers or by absorption of small molecules, such as silane coupling agents. Surface modification improves the interfacial interactions between the inorganic nanofillers and the polymer matrices, resulting in unique properties such as very high mechanical toughness (even at low loadings of inorganic reinforcements) and other optical, electronic, gas barrier, and flame retardant properties.

13.11 Future Perspectives

Significant work on nanoscale coatings is under way globally in the area of nanocoating, including incorporation of nanoparticles in coating formulations that enhance specific features. Nanotechnology promises to unleash vast potential in the field of coatings. The future of these special coating markets will further expand in different industries such as the marine, building, and defense industries. In the opinion of a great number of experts, nanotechnology has a positive potential not only for economic development, as considerable improvements are also expected with regard to protection of infrastructure and human health. Thus, nanotechnology development may conserve our natural resources and improve the overall performance of corrosion protection and antimicrobial protection of steel surfaces.

References

Abd El-Fattah M, Ashraf M, El S, Ahmed Azzam M, Abdul-Raheim M, Hassan Hefni HH (2016) Improvement of corrosion resistance, antimicrobial activity, mechanical and chemical properties of epoxy coating by loading chitosan as a natural renewable resource. Prog Org Coat 101:288–296. https://doi.org/10.1016/j.porgcoat.2016.09.002

Allen NS, Edge M, Ortega A, Sandoval G, Liauw CM, Verran J, Stratton J, Mclntyre RB (2004) Degradation and stabilization of polymers and coatings: nano versus pigmentary titania particles. Polym Degrad Stab 85(3):927–946. https://doi.org/10.1016/j.polymdegradstab.2003.09.024

Al-Turaif HA (2010) Effect of nano TiO_2 particle size on mechanical properties of cured epoxy resin. Prog Org Coat 69(3):241–246. https://doi.org/10.1016/j.porgcoat.2010.05.011

Ananda Kumar S, Sankara Narayanan TSN (2002) Thermal properties of siliconized epoxy interpenetrating coatings. Prog Org Coat 45(4):323–330. https://doi.org/10.1016/S0300-9440(02)00062-0

Ananda Kumar S, Sasikumar A (2010) Studies on novel silicone/phosphorus/sulphur containing nano-hybrid epoxy anticorrosive and antifouling coatings. Prog Org Coat 68(3):189–200. https://doi.org/10.1016/j.porgcoat.2010.02.005

Ananda Kumar S, Balakrishnan T, Alagar M, Denchev Z (2006) Development and characterization of silicone/phosphorus modified epoxy materials and their application as anticorrosion and antifouling coatings. Prog Org Coat 55(3):207–217. https://doi.org/10.1016/j.porgcoat.2005.10.001

Ashraf ESM, Abd El-Fattah M, Ahmed AM, Dardir MM, Magd Bader M (2016) Synthesis of cuprous oxide epoxy nanocomposite as an environmentally antimicrobial coating. Int J Biol Macromol 89:190–197. https://doi.org/10.1016/j.ijbiomac.2016.04.043

Batis G, Pantazopoulou P, Routoulas A (2003) Corrosion protection investigation of reinforcement by inorganic coating in the presence of alkanolamine-based inhibitor. Cem Concr Compos 25 (3):371–377. https://doi.org/10.1016/S0958-9465(02)00061-6

Berndt ML, Berndt CC (2003) Corrosion: fundamentals, testing, and protection. In: Cramer SD, Covino BS Jr (eds) ASM handbook. ASM International, Materials Park, pp 803–813

Champ M (2000) A review of organotin regulatory strategies, pending actions, related costs and benefits. Sci Total Environ 258(1–2):21–71. https://doi.org/10.1016/S0048-9697(00)00506-4

Chang SI, Gray KA (2003) Chemical composition and Cu complexation characteristics of the extracellular polymeric substances from *Pseudomonas aeruginosa* biofilms. Metal Interact Environ Syst 43(1):529–530

Daniel MC, Astruc D (2004) Gold nanoparticles: assembly, supramolecular chemistry, quantum-size-related properties and applications toward biology, catalysis, and nanotechnology. Chem Rev 104(1):293–346. https://doi.org/10.1021/cr030698+

Delucchi M, Ricotti R, Cerisola G (2011) Influence of micro—and nano—filler on chemico-physical properties of epoxy-based materials. Prog Org Coat 72(1–2):58–64. https://doi.org/10.1016/j.porgcoat.2011.02.018

Dietsche AF, Thomann Y, Thomann R, Mulhaupt R (2000) Translucent acrylic nanocomposites containing anisotropic laminated nanoparticles derived from intercalated layered silicates. J Appl Polym Sci 75(3):396–405. https://doi.org/10.1002/(SICI)1097-4628

Duraibabu D, Ganeshbabu T, Manjumeena R, Ananda Kumar S, Dasan P (2014) Unique coating formulation for corrosion and microbial prevention of mild steel. Prog Org Coat 77(3):657–664. https://doi.org/10.1016/j.porgcoat.2013.12.002

Duraibabu D, Gowripriya R, Saravanan P, Ananda Kumar S (2015) A comparative study on modifed epoxy and glycidyl carbamate coatings for corrosion and fouling prevention. Surface Innov 3(2):127–139. https://doi.org/10.1680/si.13.00025

Fernando RH (2004) Nanomaterial technology applications in coatings. JCT Coatings Tech 1 (5):32–39

Hartwig A, Sebald M, Putz D, Aberle L (2005) Preparation, characterisation and properties of nanocomposites based on epoxy resins—an overview. Macromol Symp 221(1):127–136. https://doi.org/10.1002/masy.200550313

He Z, Rao W, Ren T, Liu W, Xue Q (2002) The tribochemical study of some N-containing heterocyclic compounds as lubricating oil additives. Tribol Lett 13(2):87–93. https://doi.org/10.1023/A:1020100631716

Ikeda T, Tazuke S, Suzuki Y (1984) Biologically active polycations, synthesis and antimicrobial activity of poly(trialkylvinylbenzylammonium chloride)s. Makromol Chem 185:869–876. https://doi.org/10.1002/macp.1984.021850503

Jin FL, Park SJ (2008) Impact-strength improvement of epoxy resins reinforced with a biodegradable polymer. Mater Sci Eng A 478(1–2):402–405. https://doi.org/10.1016/j.msea.2007.05.053

Kim J, Konstantinou I, Albanis T (2004) Worldwide occurrence and effects of antifouling paint booster biocides in the aquatic environment: a review. Environ Int 30(2):235–248

Kong M, Chen XG, Xing K, Park HJ (2010) Antimicrobial properties of chitosan and mode of action: a state of the art review. Int J Food Microbiol 144(1):51–63. https://doi.org/10.1016/j.ijfoodmicro.2010.09.012

Kumar R, Narayan R, Aminabhavi TM, Raju KVSN (2014) Nitrogen rich hyper-branched polyol via $A_3 + B_3$ polycondensation: thermal, mechanical, anti-corrosive and antimicrobial properties of poly (urethane-urea). J Polym Res (21):547. https://doi.org/10.1007/s10965-014-0547-8

Lam K, Lau KT (2006) Localized elastic modulus distribution of nanoclay/epoxy composites by using nanoindentation. Compos Struct 75(1–4):553–558. https://doi.org/10.1016/j.compstruct.2006.04.045

Liu H, Du Y, Wang X, Sun L (2004) Chitosan kills bacteria through cell membrane damage. Int J Food Microbiol 95(2):147–155. https://doi.org/10.1016/j.ijfoodmicro.2004.01.022

Mallick K, Witcombb MJ, Scurrella MS (2005) Self-assembly of silver nanoparticles in a polymer solvent formation of a nanochain through nanoscale soldering. Mater Chem Phys 90 (2–3):221–224. https://doi.org/10.1016/j.matchemphys.2004.10.030

Manjumeena R, Venkatesan R, Duraibabu D, Sudha J, Rajendran N, Kalaichelvan PT (2016) Green nanosilver as reinforcing eco-friendly additive to epoxy coating for augmented anticorrosive and antimicrobial behavior. Silicon 8(2):277–298. https://doi.org/10.1007/s12633-015-9327-2

Mondrzyk A, Fischer J, Ritter H (2014) Antibacterial materials: structure–bioactivity relationship of epoxy–amine resins containing quaternary ammonium compounds covalently attached. Polym Int 63(7):1192–1196. https://doi.org/10.1002/pi.4690

Nagy CM, Fejer SN, Berek L, Malnar J, Viskolcz B (2005) Hydrogen bondings in deoxynivalenol (DON) conformations—a density functional study. J Mol Struct Theochem 726(1–3):55–59. https://doi.org/10.1016/j.theochem.2005.02.079

Narute P, Rajashekhar Rao G, Misra S, Palanisamy A (2015) Modification of cottonseed oil for amine cured epoxy resin: studies on thermo-mechanical, physico-chemical, morphological and antimicrobial properties. Prog Org Coat 88:316–324. https://doi.org/10.1016/j.porgcoat.2015.07.015

Omrani A, Simon LC, Rostami AA (2009) The effects of alumina nanoparticle on the properties of an epoxy resin system. Mater Chem Phys 114(1):145–150. https://doi.org/10.1016/j.matchemphys.2008.08.090

Pohrelyuk IM, Fedirko VM, Tkachuk OV, Proskurnyak RV (2014) Corrosion resistance of titanium alloys with oxynitride coatings in concentrated inorganic acids. Mater Sci 50(2):269–276. https://doi.org/10.1007/s11003-014-9717-4

Raghavachar R, Letasi RJ, Kola PV, Chen Z, Massingill JL (1999) Rubber-toughening epoxy thermosets with epoxidized crambe oil. J Am Oil Chem Soc 76(4):511–516. https://doi.org/10.1007/s11746-999-0033-3

Ramezanzadeh B, Attar MM, Farzam M (2011) A study on the anticorrosion performance of the epoxy–polyamide nanocomposites containing ZnO nanoparticles. Prog Org Coat 72 (3):410–422. https://doi.org/10.1016/j.porgcoat.2011.05.014

Ratna D (2001) Mechanical properties and morphology of epoxidized soyabean-oil-modified epoxy resin. Polym Int 50:179–184. https://doi.org/10.1002/1097-0126

Saravanan P, Aparna S, Ananda Kumar S, Duraibabu D (2015) Studies on biocide encapsulated zeolite–epoxy nano hybrid coatings on mild steel. Curr Bionanotechnol 1(1):37–50. https://doi.org/10.2174/2213529401666150304234007

Saravanan P, Jayamoorthy K, Ananda Kumar S (2016) Design and characterization of non-toxic nano-hybrid coatings for corrosion and fouling resistance. J Sci Adv Mater Devices 1:367–378. https://doi.org/10.1016/j.jsamd.2016.07.001

Schmid G (1992) Large clusters and colloids: metals in the embryonic state. Chem Rev 92 (8):1709–1727. https://doi.org/10.1021/cr00016a002

Sharmin E, Alam MS, Philip RK, Ahmad S (2010) Linseed amide diol/DGEBA epoxy blends for coating applications: preparation, characterization, ageing studies and coating properties. Prog Org Coat 67(2):170–179. https://doi.org/10.1016/j.porgcoat.2009.09.012

Shi G, Zhang MQ, Rong MZ, Wetzel B, Friedrich K (2003) Friction and wear of low nanometer Si_3N_4 filled epoxy composites. Wear 254(7–8):784–796. https://doi.org/10.1016/S0043-1648(03)00190-X

Shi X, Nguyen TA, Suo Z, Liu Y, Avci R (2009) Effect of nanoparticles on the anticorrosion and mechanical properties of epoxy coating. Surf Coat Technol 204(3):237–245. https://doi.org/10.1016/j.surfcoat.2009.06.048

Smetuna AB, Klabunde KJ, Sorensea CM (2005) Synthesis of spherical silver nanoparticles by digestive ripening stabilization with various agents, and their 3-D and 2-D super lattice formation. J Colloid Interface Sci 284(2):521–526. https://doi.org/10.1016/j.jcis.2004.10.038

Tansir A, Saad Alshehri M (2012) Thermal, microbial, and corrosion resistant metal-containing poly(Schiff) epoxy coatings. J Coat Technol Res 9(5):515–523. https://doi.org/10.1007/s11998-011-9393-3

Tkachenko LA, Shaulov AY, Berlin AA (2012) High-temperature protective coatings for carbon fibers. Inorg Mater 48(3):213–221. https://doi.org/10.1134/S0020168512030168

Wu N, Fu L, Su M, Aslam M, Wong K, Dravid VP (2004) Interaction of fatty acid monolayers with cobalt nanoparticles. Nano Lett 4(2):383–386. https://doi.org/10.1021/nl035139x

Yu DG (2007) Formation of colloidal silver nanoparticles stabilized by Na+ poly(γ-glutamic acid)–silver nitrate complex via chemical reduction process. Colloids Surf B: Biointerfaces 59 (2):171–178. https://doi.org/10.1016/j.colsurfb.2007.05.007

Zafar S, Zafar F, Riaz U, Ahmad S (2009a) Synthesis, characterization, and anticorrosive coating properties of waterborne interpenetrating polymer network based on epoxy-acrylic-oleic acid with butylated melamine formaldehyde. J Appl Polym Sci 113(2):827–838. https://doi.org/10.1002/app.29726

Zafar S, Riaz U, Ahmad S (2009b) Water-borne melamine–formaldehyde-cured epoxy–acrylate corrosion resistant coatings. J Appl Polym Sci 107(1):215–222. https://doi.org/10.1002/app.27022

Index

Mu. Naushad et al. (eds.), *Advanced Nanostructured Materials for Environmental Remediation*, Environmental Chemistry for a Sustainable World 25,
https://doi.org/10.1007/978-3-030-04477-0